METAMORPHISM, STRUCTURE AND PETROGENESIS OF THE LINDA VOLCANOGENIC MASSIVE SULPHIDE DEPOSIT, SNOW LAKE, MANITOBA, CANADA

Eva Zaleski

A thesis
submitted to the University of Manitoba
in fulfillment of the requirements for the degree of
Doctor of Philosophy
in Geological Sciences

Winnipeg, Manitoba, Canada

ISBN 0-315-54902-5

Canada

METAMORPHISM, STRUCTURE AND PETROGENESIS OF THE LINDA VOLCANOGENIC MASSIVE SULPHIDE DEPOSIT, SNOW LAKE, MANITOBA, CANADA

BY

EVA ZALESKI

A thesis submitted to the Faculty of Graduate Studies of the University of Manitoba in partial fulfillment of the requirements of the degree of

DOCTOR OF PHILOSOPHY

ABSTRACT

The complex structure and mineralogy of the Linda volcanogenic massive sulphide deposit are the result of polyphase dynamometamorphism superimposed on primary sulphide mineralization and associated hydrothermal alteration. Outcrop mapping and drill-core logging elucidated the 3-dimensional configuration of the deposit. Microstructural and paragenetic relationships, mineral chemistry, and whole-rock geochemistry constrain its petrogenesis and its significance to the structural and metamorphic history of the Snow Lake region.

At the Linda deposit, two discrete zones of Fe-Mg alteration occur in felsic rocks of the stratigraphic footwall. The proximal alteration zone consists mainly of stratabound and stratiform mineralization resulting from the accumulation of chemical sediments in a topographic depression on the down-thrown side of a syn-volcanic fault. The distal alteration zone is hosted by felsic volcanic rocks lower in the stratigraphic sequence and may represent subsurface alteration.

The Linda deposit lies in highly strained overturned rocks on one flank of the Anderson Bay structure, which marks a change in stratigraphic facing direction. The Anderson Bay structure is transected by S_1 and S_2 cleavages. Syn-D_2 porphyroblasts at the Linda deposit record early sinistral S_1/S_2 cleavage vergence; phyllosilicate minerals in the matrix define dextral S_1/S_2 cleavage vergence resulting from late D_2 (or D_3) reactivation of the S_1 cleavage. The reactivation has regional significance.

Metamorphic parageneses at the Linda deposit apparently span three zones of regional metamorphism. The bulk-rock composition of the altered protolith allowed the crystallization of manganiferous garnet, zincian staurolite and F-rich biotite, thus expanding the stability fields of parageneses containing these minerals. A pressure-temperature-time trajectory is recorded by syn-D_1 kyanite and by syn-D_2 amphibolite-facies assemblages, which represent the culmination of metamorphism. Sphalerite geobarometry yields a pressure of about 5 kb; the maximum temperature is limited to about 550°C by the coexistence of margarite + quartz. Sulphide-silicate-oxide equilibria can be modelled in a petrogenetic grid in the SiO_2-Al_2O_3-FeO-MgO-ZnO-K_2O-H_2O-S_2-O_2 system at fixed pressure and temperature. Metamorphic desulphidation of sphalerite released Zn to staurolite and gahnite. The largest massive sulphide body consists of pyrite and calcite, the latter introduced during post-tectonic synmetamorphic metasomatism.

DEDICATION

This thesis is dedicated to my parents,
L. Anne and Witold A. Zaleski,
whose sense of wonder and curiosity
has been part of my upbringing
and inspiration.

ACKNOWLEDGMENTS

I extend my grateful thanks and appreciation to my advisor, Norman Halden, for his encouragement, enthusiasm and excellent advising, and for initiating me in structural geology. To my mentor, Edgar Froese, who proposed the project, provided continual support, and converted me to metamorphic petrology, I extend my thanks. This thesis is presented with esteem and gratitude for the guidance so generously offered by both of my advisors.

Thanks are also due to Terry Gordon for his advice regarding mineral chemistry; to Scott Ercit for instruction in the acquisition of high quality mineral analyses; and to Lee Groat for various counselling sessions and for introducing me to TEX. Discussions with the following people eventually germinated into ideas: Jack Henderson, Jim Franklin, Roger Skirrow, Mariette Henderson, Alan Bailes and Doreen Ames. Alan Galley played devil's advocate with my structural interpretations, a role for which I have much respect. Bob Spark was a willing and able field assistant. Bob Elias, Ray Healy and Jeff Young shared their expertise.

Falconbridge Limited and Minnova Incorporated (formerly Corporation Falconbridge Copper) provided access to drill core and to unpublished company maps and reports. In addition, Minnova Incorporated provided funding for mineral analyses and Falconbridge Limited allowed me the use of their office facilities at Snow Lake. The Geological Survey of Canada provided logistical and laboratory support. NSERC funding was provided through their scholarship program and operating grants.

TABLE OF CONTENTS

List of Figures.

List of Plates.

List of Tables.

PART I

INTRODUCTION

Chapter 1. Introduction.

Chapter 2. Regional Geology.

Chapter 1
Introduction

1.1. Purpose.

The study of dynamometamorphism of metasomatic protoliths in volcanic terranes presents a challenge and, potentially, a catalyst for advances in our understanding of metamorphic, tectonic, volcanic and hydrothermal processes and their interplay. Eskola's formulation of metamorphic facies, and his recognition that the concepts of equilibrium thermodynamics can be applied to Archean rocks, were conceived in the metamorphosed 'pneumatolytic formations' of the Orijärvi region, Finland (Eskola, 1915). Contrary to the general view of the time, that ancient rocks are "utterly complicated and least of all adapted to treatment from this point of view", Eskola observed that mineral parageneses "stand in definite relations to the chemical composition". He also recognized that textural features could be used to identify equilibrium parageneses and, in the case of pseudomorphs, provided a record of the primary and early metamorphic history.

The evolution of ideas regarding the petrogenesis of massive sulphide deposits has had a varied development (*see* Franklin *et al.* (1981) for a brief review). In 1959, the 'Symposium on the Genesis of Massive Sulphide Deposits', sponsored by the Canadian Institute of Mining and Metallurgy (CIM), was dominated by epigenetic models, to the extent that the opening remarks included the statement: "I trust that all would agree that all these deposits have formed either by replacement or sulphide segregation and/or injection" (Gunning, 1959). At the CIM 'Symposium on Strata-bound Sulphides' six years later, a change in emphasis and in interpretation was evident. Broader petrological studies placing massive sulphide deposits in a local and regional context (Moorhouse, 1965), comparisons with occurrences in less deformed and younger terranes (Hutchinson, 1965; Suffel, 1965), and the recognition of systematic asymmetry in the disposition of alteration with respect

to mineralization (Sharpe, 1965; Roscoe, 1965), supported a syngenetic origin for massive sulphide deposits.

The Coronation Mine Project, initiated in 1957 to provide a comprehensive study of Coronation mine in the Flin Flon region (Byers, 1969), was pivotal in the interpretation of alteration as the result of synvolcanic hydrothermal processes directly related to sulphide mineralization (Froese, 1969; Whitmore, 1969). This study also initiated advances in metamorphic petrology, stemming from the recognition that the mineralized altered rocks represented the same metamorphic grade as the enclosing country rocks and, that metamorphic equilibria had involved silicate, sulphide and oxide minerals (*ibid.*). The conceptual framework for modelling silicate-sulphide-oxide equilibria is still evolving (*e.g.* Froese, 1981; 1977; 1971; Hutcheon, 1979; Nesbitt, 1986a; 1986b; 1982; Nesbitt and Kelly, 1980; Tracy and Robinson, 1988) and more case studies are required to expand the range of bulk-rock compositions and metamorphic grades to which the models can be applied.

The construction of geochemical genetic models for massive sulphide deposits received impetus from the discovery of sulphide-precipitating hydrothermal activity on the seafloor (Rona, 1984; Lister, 1980). Comparisons between the physical environments, mineralogy, chemistry and processes observed on the seafloor with those which can be inferred in the geologic record are important elements in many genetic models (*e.g.* Franklin, 1986; Lydon, 1988; Rona, 1988). The observations made on the seafloor and in the geologic record are mutually complementary. Massive sulphide deposits in the geologic record provide access to sections of the subsurface portions of fossilized hydrothermal systems. They likewise record the post-depositional history from the waning of hydrothermal activity to diagenesis and, possibly, to dynamometamorphism.

The Linda volcanogenic massive sulphide deposit is well represented in 3-dimensions by extensive subsurface drilling. In common with deposits in the Snow Lake region and many other ancient deposits, its present-day configuration and mineralogy are the result of dynamometamorphism superimposed on the original hydrothermal deposit. The difficulties encountered in the region, in integrating the various observations into a coherent petrogenetic model, are reminiscent of the problems encountered by the original proponents of syngenetic models for the de-

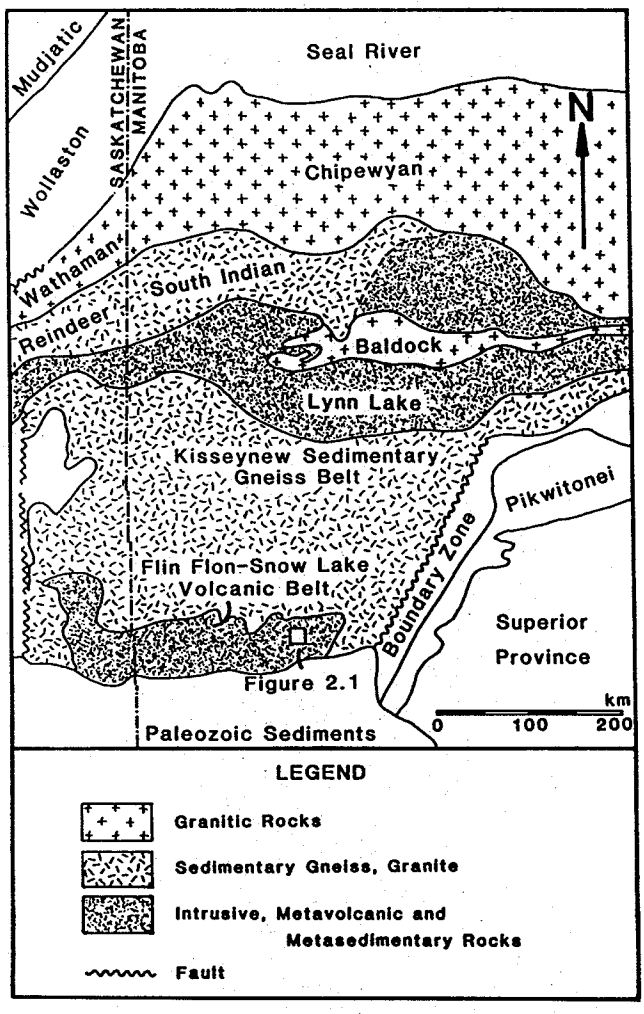

Figure 1.1. Location of the Snow Lake region (Figure 2.1) in the Flin Flon–Snow Lake volcanic belt. Major tectonic subdivisions of Proterozoic age in the Trans-Hudson orogen are ornamented. Adapted from Lenton (1981).

formed and metamorphosed massive sulphide deposits typical of the Precambrian. Specific problems addressed at the Linda deposit include: the structural and stratigraphic relationship to other deposits in the Snow Lake region, the relationship to regional metamorphism, the reconstruction of the synvolcanic setting, and the characterization of the alteration and its relevance to synvolcanic hydrothermal activity. Detailed examination of the Linda deposit provides constraints on the metamorphic, structural and volcanic evolution of the Snow Lake region, many aspects of which are enigmatic.

1.2. Location and Setting.

The Linda volcanogenic massive sulphide deposit is located in the Snow Lake

region, within the Flin Flon–Snow Lake volcanic belt (Figure 1.1). The volcanic belt forms part of the juvenile Proterozoic crustal additions in the Trans-Hudson orogen between the Archean Hearne and Superior provinces (Hoffman, 1988). In the north, the belt is flanked by the Kisseynew metasedimentary gneiss belt and, in the south, overlain by Paleozoic sedimentary rocks. It consists of supracrustal metavolcanic and metasedimentary sequences of Aphebian age, which have undergone dynamic metamorphism and polyphase deformation. Intrusive rocks range from synvolcanic to post-tectonic. Numerous massive sulphide deposits occur in the volcanic belt; in the Snow Lake area, these include the Chisel Lake, Ghost Lake, Lost Lake, Anderson Lake, Stall Lake and Rod mines. The Linda deposit is the largest massive sulphide body in the area (Jeffery, 1982 compared to Table 1 of Walford and Franklin, 1982), but it is mainly pyritic with minor amounts of pyrrhotite, chalcopyrite and sphalerite. It was extensively drilled by Falconbridge Limited and Corporation Falconbridge Copper (now Minnova Incorporated), who provided access to drill core and to unpublished maps and company reports.

1.3. Procedure and Data Accumulation.

Two and a half field seasons were devoted to mapping the surface exposure of the Linda area and logging drill core. Mapping was done on a scale of 1:4800, making use of outcrop maps provided by Falconbridge, air-photo enlargements, and a deteriorated, but functional, cut-and-chained grid. The outcrop is generally sporadic and exposures stripped during previous work on the property were usually obscured by lichen. Stripping new exposures was necessary and the proportion of outcrop on the geological map gives a misleadingly optomistic impression of the actual outcrop control on mapping of lithological units and contacts (Map, in pocket). The massive sulphide deposit and associated alteration zones do not crop out, and the interpretation of surface geology was supplemented by projection of drill-core observations.

Approximately 46 km of core was drilled on the Linda property over a period of more than 20 years (Jeffery, 1982, *unpubl.*). The drill-core logs and cross-sections compiled by Falconbridge geologists were made available. During this study, 7.3 km of core (*i.e.* 16%) was relogged in greater detail than that of the original logging, allowing the independent construction of 3 composite cross-sections of the sulphide

body and alteration zones. Rock fabric/core-axis angles, and projections of drill holes into the composite sections and to surface, were adopted from the sections and maps provided by Falconbridge. The cross-sections are spaced at 275 m and 120 m along-strike (Map, in pocket), intersecting the deposit at intervals along its down-plunge length. The drill core was extensively sampled to obtain a sample suite representative of lithological units, alteration types, protolith types and, in some cases, structural types. This suite was supplemented by surface samples. Petrographic work was done on the entire sample suite, but only geochemical samples are explicitly described (Table A.1). The outermost cross-sections, A-A' and C-C' (in pocket), give the most complete picture of the subsurface geology; 303 samples, collected from these drill holes and from the surface, were selected for analysis of whole-rock geochemistry (Table C.5). Mineral compositions were determined by electron-probe microanalysis in 21 samples representing altered rocks (Table B.3).

Chapter 2
Regional Geology

The geology, structure and metamorphism of the Snow Lake region has been discussed by Bailes *et al.* (1987), Walford and Franklin (1982) and Froese and Moore (1980), and this summary is based mainly on their work.

2.1. Lithology and Stratigraphy.

The Amisk Group was defined to encompass a suite of metavolcanic rocks and overlying volcanogenic metasediments originally consisting of greywacke and shale (Figure 2.1). Probable synvolcanic intrusions include the Sneath Lake and Richard Lake tonalites (Bailes, 1988, 1987, 1986). The Missi Group consists of metamorphosed lithic arenites which were deposited on Amisk Group rocks (Froese and Moore, 1980). In the northern part of the Snow Lake region, the Herblet, Pulver and Squall gneiss domes are composed of granitoid gneisses, compositionally similar to granodiorite or felsic volcanic rocks. Post-tectonic to late tectonic intrusive rocks range from gabbro to granite.

Between the trace of the Anderson Bay structure (*see* 4.1.2. The Anderson Bay Structure) and the McLeod Road thrust fault (Figure 2.1), the Amisk Group forms a northerly facing homoclinal sequence of subaqueously deposited rocks (Bailes *et al.*, 1987). The lower part of the sequence is dominated by pillowed aphyric mafic flows, the upper part by intercalated heterolithic mafic and felsic breccia, and felsic and mafic porphyritic flows. This upper succession hosts most of the massive sulphide deposits and has been subjected to extensive synvolcanic alteration. Detailed stratigraphic mapping has been done locally, but no comprehensive stratigraphy is available for the Snow Lake region. Bailes *et al.* (1987) presented a stratigraphic sequence for the Chisel Lake area, and a generalized correlation with the stratigraphy of Walford and Franklin (1982) for the Anderson and Stall Lakes area.

In the Anderson and Stall Lakes area, the Sneath Lake quartz-phyric tonalite

Figure 2.1. (following page) Geology of the Snow Lake region adapted from Froese and Moore (1980) and Bailes (1988). General structural trends are indicated by the ornamentation, with superimposed traces of F_1 and F_2 fold axes, faults and metamorphic isograds. The area of Figure 2.2 is outlined.

(unit 1, Walford and Franklin, 1982) forms the base of the stratigraphic sequence (Figure 2.2), where it intrudes aphyric mafic flows, and monolithic and heterolithic breccia (Bailes *et al.*, 1987). The interpretation of the tonalite as a synvolcanic intrusion and a potential heat source for hydrothermal activity (Walford and Franklin, 1982) was supported by Bailes (1986) who found that large areas of the intrusion had undergone synvolcanic hydrothermal alteration. The Sneath Lake tonalite is a composite intrusion generally concordant to stratigraphy, but locally shows high-angle contacts to the volcanic stratigraphy of the host rocks (Bailes, 1987). The Richard Lake tonalite (Figure 2.1), which has commonly been assumed to be part of the same body, is discordant and truncates sulphide mineralization near Chisel and Ghost Lakes (Bailes, 1988; 1987; 1986). The trace-element signatures of the two tonalite bodies are distinct and indicate that the intrusions are not comagmatic (Bailes, 1988). The Richard Lake tonalite has a U-Pb zircon age of 1889 +8/-6 Ma (Bailes *et al*, 1988), indistinguishable from a U-Pb zircon age of 1886±1.3 Ma in an Amisk Group rhyolite tuff in the Flin Flon area (Syme *et al*, 1987). The volcanism in the Snow Lake and Flin Flon regions was probably contemporaneous (Bailes *et al*, 1988).

In the vicinity of Anderson and Stall Lakes, the Sneath Lake tonalite is overlain by the Lower Mine Felsic unit (unit 2, Walford and Franklin, 1982), which varies from massive and aphanitic in the lower member, to mainly fragmental in the upper member (Figure 2.2). Toward the Stall Lake mine, this unit thickens slightly and contains possible flows and flow lobes which terminate in fragmental rock, possibly of hyaloclastic origin. Extensive synvolcanic alteration in this unit at the Anderson Lake and Stall Lake mines was interpreted to have resulted from hydrothermal activity in the footwall to the massive sulphide deposits. Quartz-megaphyric felsic rocks constitute the uppermost 100 m of the Lower Mine Felsic unit and form the hanging wall to the Stall Lake and Anderson Lake deposits. Walford and Franklin (1982) suggested that the quartz-megaphyric zone was deposited from a submarine pyroclastic ash flow. In the area of the Rod mine, Coats *et al.* (1970) reported a

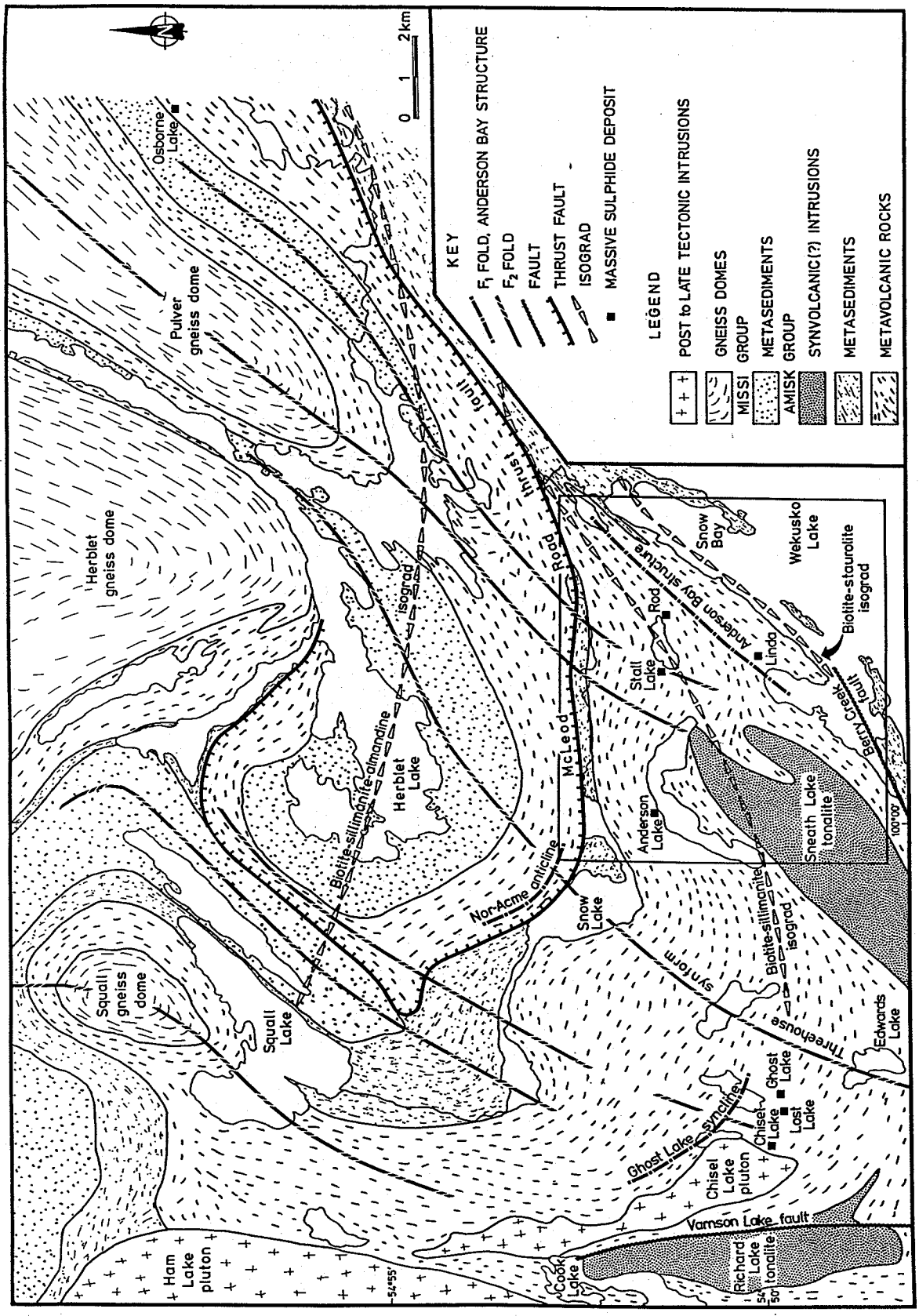
KEY
F1 FOLD, ANDERSON BAY STRUCTURE
F2 FOLD
FAULT
THRUST FAULT
ISOGRAD
MASSIVE SULPHIDE DEPOSIT
LEGEND
POST to LATE TECTONIC INTRUSIONS
GNEISS DOMES
MISSI GROUP
METASEDIMENTS
AMISK GROUP
SYNVOLCANIC(?) INTRUSIONS
METASEDIMENTS
METAVOLCANIC ROCKS
0 1 2km
Osborne Lake
Pulver gneiss dome
Herblet gneiss dome
Squall gneiss dome
Ham Lake pluton
Squall Lake
Herblet Lake
Biotite-sillimanite-almandine isograd
Nor-Acme anticline
McLeod Road
Thrust fault
Snow Lake
Anderson Lake
Stall Lake
Anderson Bay syncline
Snow Bay Road
Wekusko Lake
Linda
Biotite-staurolite isograd
Berry Creek fault
Sneath Lake tonalite
Biotite-sillimanite isograd
synform
Threehouse
Edwards Lake
Ghost Lake synclinal
Chisel Lake pluton
Chisel Lake
Ghost Lake
Lost Lake
Varnson Lake fault
Richard Lake tonalite
Cook Lake
54°55'
54°50'
100°00'

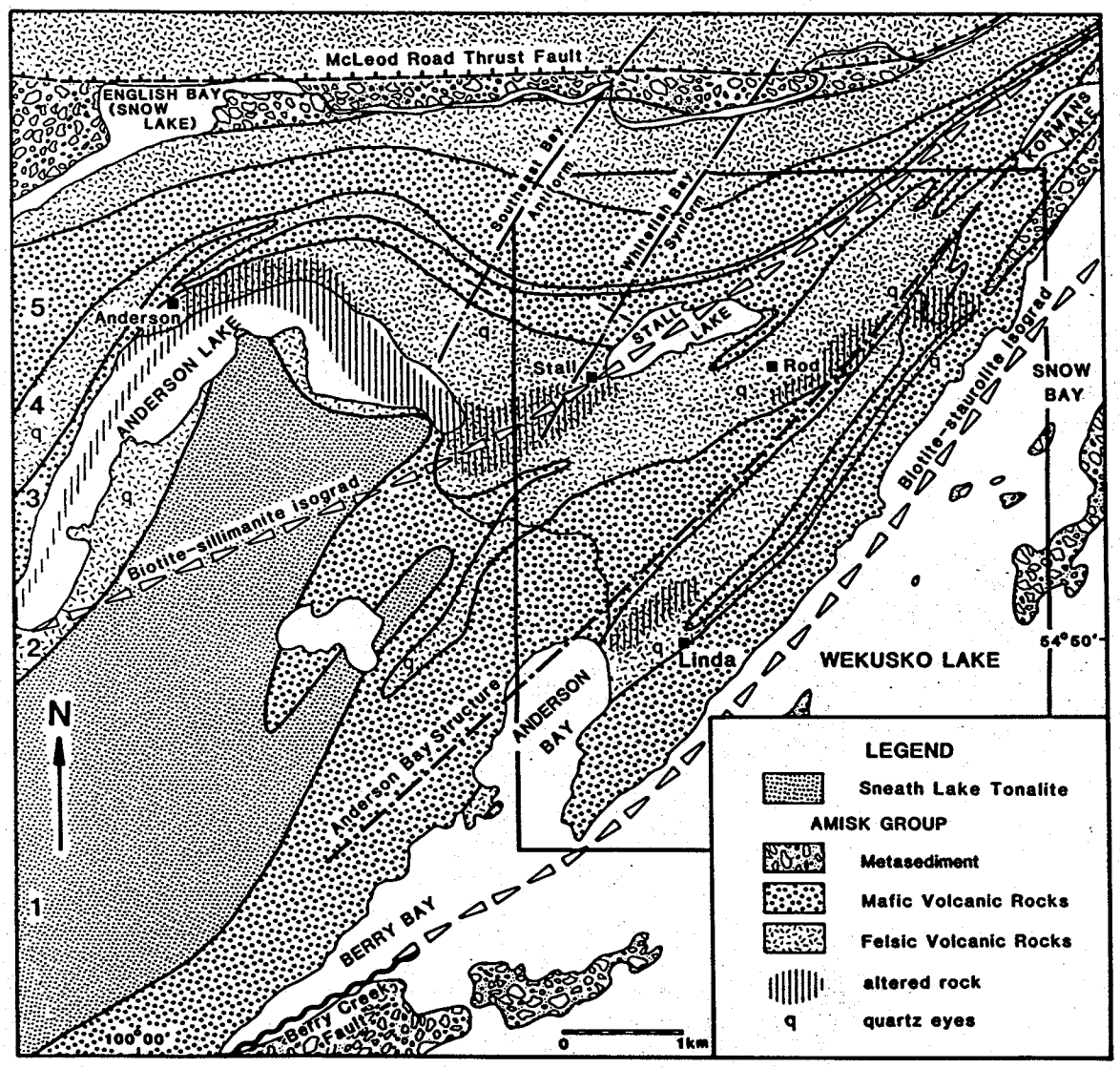

Figure 2.2. Geology of a part of the Snow Lake region in the vicinity of the Linda deposit. Modified from Jeffery (1982), Froese and Moore (1980) and Zaleski (1986). The numbers on the left correspond to the lithological units of Walford and Franklin (1982). The area detailed in Figure 3.1 is outlined.

lesser thickness of rhyolite, overlain by a thick unit (760 m) of quartz-megaphyric felsic rocks (termed 'quartz porphyry' by these authors) hosting the massive sulphide bodies. The quartz-megaphyric rocks grade up-section to coarser felsic pyroclastic rocks.

Overlying the Lower Mine Felsic unit, the Hangingwall Mafic unit (unit 3, Walford and Franklin, 1982) is about 250 m thick between the Anderson Lake and Stall Lake mines, but thins markedly to the west of the Anderson Lake mine. The lowermost member is comprised of andesitic flows, pillow breccias and tuffs, which

thicken to the east. The basal flows are silicified in the vicinity of Stall Lake. The uppermost member consists of basaltic flows and epiclastic rocks. This member directly overlies the andesitic member at the Anderson Lake mine but, to the east, it interfingers with, and terminates within, the Hangingwall Felsic unit (unit 4, *ibid.*).

The Hangingwall Felsic unit (unit 4, Walford and Franklin, 1982) consists of a lower porphyritic rhyolite pyroclastic and flow member, which dominates in the east, and an upper coarsely porphyritic, mainly massive member, which dominates in the west (Figure 2.2). A thin bed of graphitic metasediment lies near the basal contact of the lower member.

The Threehouse Basalt (unit 5, Walford and Franklin, 1982), consisting of porphyritic basalt flows and heterolithic breccias, was reported to be identical in texture and chemical composition to the upper member of the Hangingwall Mafic unit (unit 3).

The Anderson Bay anticline was proposed by Falconbridge geologists (Jeffery, 1982, *unpubl.*) to account for southeasterly facing of the Linda deposit (*see* 2.2. Structure). Quartz-megaphyric felsic rocks host the Anderson Lake, Stall Lake (Walford and Franklin, 1982; Studer, 1982) and Rod deposits (Coats *et al.*, 1970). A similar unit hosting the Linda deposit was mapped continuously around the hinge of the anticline, and correlated directly with the felsic unit hosting the massive sulphide deposits on the northwest limb of the fold (Jeffery, 1982, *unpubl.*). The proposed correlation placed these 4 deposits on approximately the same stratigraphic horizon. However, this stratigraphic continuity was not supported by mapping done during this study (*see* 4.1.2. The Anderson Bay Structure). The Chisel Lake, Ghost Lake and Lost Lake deposits (Figure 2.1) occur higher in the stratigraphic section, at the base of a mafic epiclastic unit equivalent to the Threehouse Basalt (Bailes, 1988; Bailes *et al.*, 1987).

In the Rod mine, Coats *et al.* (1970) reported the presence of a pretectonic, possibly synvolcanic intrusion which, in part, follows the contact between quartz-megaphyric felsic rocks hosting the massive sulphide bodies, and felsic pyroclastic rocks. The intrusion is discordant to foliation in the quartz-phyric rocks and, as interpreted from drill core intersections, truncates sulphide mineralization

(*ibid.*). Amphibolite dykes cut the sulphide zones in the Anderson Lake mine, and were reported to be folded, boudinaged and partly altered to chlorite-garnet and amphibole-magnetite bearing rocks (Walford and Franklin, 1982).

2.2. Structure.

The structural complexity of the Snow Lake region introduces an element of uncertainty into stratigraphic correlations. Three main deformational events were proposed by Froese and Moore (1980). The earliest event produced tight to nearly isoclinal F_1 folds, recognized mainly on the basis of opposing facing directions. Interpretation of the stratigraphic sequence of interlayered felsic and mafic volcanic rocks and the relative stratigraphic position of the massive sulphide occurrences is, in part, contingent on the recognition of F_1 folds. Primary structures indicate northward facing for the succession from Stall Lake to the McLeod Road fault (Figure 2.1). The existence of the Anderson Bay anticline (termed the 'Anderson Bay structure' in this study) was postulated by Falconbridge geologists (Jeffery, 1982, *unpubl.*) to account for a southward facing direction required by the disposition of the sulphide bodies and alteration zones at the Linda deposit. The more northerly trace of the Anderson Lake anticline (F_1), postulated by Gale and Koo (1977) and Froese and Moore (1980), is the result of mistaken identity between the Linda I sulphide occurrence (shown on the maps of the cited authors), a minor stringer zone which does not yield a facing direction (Jeffery, 1982, *unpubl.*), and the Linda II deposit, which is the focus of this study. (Note also that Russell (1957) designated an entirely unrelated F_2 fold, 'Anderson Lake anticline'; this F_2 fold is apparently the continuation of the Southeast Bay antiform south of the McLeod Road thrust fault (Figure 2.2).)

Walford and Franklin (1982) suggested that the Sneath Lake and Richard Lake tonalites (*i.e.* unit 1) may have been structurally thickened by an F_1 fold having an axial trace coincident with the long axis of the intrusions (Figure 2.1). In the Chisel-Morgan Lakes area, Bailes (1986) found some opposed facing directions in volcanogenic sediments flanking opposite margins of the intrusions and evidence of minor folding. However, given the structural complexity, the evidence for F_1 folding was equivocal, and the minor outcrop scale folds are apparently D_2 structures (Bailes, *pers. comm.*, 1987). In the Cook Lake area, Jackson (1983) found no evi-

dence for a fold hinge within the Richard Lake tonalite (which he termed 'quartz monzonite'). On the basis of his mapping and a regional compilation by Falconbridge geologists (Simmons and Stoeterau, 1978, *unpubl.*; cited by Jackson), he proposed the presence of an anticlinal fold consisting of the Anderson Bay anticline in the east, curving around the hinge of the Threehouse synform (*see below*) and tracking north through Cook Lake, *i.e.* not constrained to lie within the tonalite intrusions, but following a similar trace. He attributed this major structure to D_2 deformation and reassigned the Threehouse synform (D_2 of Froese and Moore, 1980) and related structures to D_3.

D_1 fabric elements include an S_1 fabric defined by metamorphic layering, by mineral alignment, and by flattening of primary structures such as clasts and pillows. The S_1 fabric is parallel or subparallel to bedding (S_0), layering and contacts throughout most of the region (Froese and Moore, 1980; Jackson, 1983). F_1 minor folds have been observed in mineralized metasediments in the open pit presently under development at the Chisel Lake mine (Galley, *pers. comm.*, 1988). Amisk metasediments exposed on the shores and islands of Wekusko Lake show numerous, closely spaced changes in facing direction (Froese and Moore, 1980).

Northeasterly trending open flexures of the Threehouse synform, the Southeast Bay antiform and the Whitefish Bay synform (Russell, 1957) were attributed to a second deformational event (Froese and Moore, 1980). The Threehouse syncline, originally mapped by Harrison (1949), was modified by Martin (1966) to the Threehouse synform in recognition of the polyphase structural complexity of the Chisel Lake mine. To the north, flanking the Kisseynew gneiss belt, the D_2 structures have apparently been tightened by subsequent emplacement of gneiss domes (D_3). The flexural folds die out toward the south and recognition of the Threehouse synform in this area seems to depend largely on the apparent curvature of the Sneath Lake and Richard Lake intrusions. This curvature may be exaggerated by the discordant nature of the Richard Lake intrusion.

D_2 minor structures vary in amplitude from decametre-scale F_2 folds to millimetre-scale crenulations (Froese and Moore, 1980). An S_2 axial planar fabric is defined by mineral foliation, particularly of biotite. A pronounced, northeasterly plunging elongation of all sulphide bodies and other primary structures, as well as

a mineral lineation, imparts an L-S tectonite structure to the Snow Lake region. In the Cook Lake area, prolate clasts define a strain ellipsoid with axial ratios of 3.5:1:0.9 (Jackson, 1983). In the vicinity of the Snow Lake townsite, Galley *et al.* (1988) reported that clasts are flattened and stretched with an average ratio of 3:1. Massive sulphide bodies commonly show greater elongations; for example, the lens at Anderson Lake mine has axial ratios of approximately 100:10:1, with the value for longest axis being a minimum estimate (calculated from Walford and Franklin, 1982).

The stretching and mineral lineations were mainly attributed to L_2 fabric development (Froese and Moore, 1980). However, in the Chisel Lake area, a slight angular separation (5–15°) between fragment-elongation directions and S_1/S_2 intersections defined by mica edges was interpreted to indicate that regional elongation should be partly attributed to extension during D_1 deformation. It should be noted that virtually all of the reported mineral lineations and crenulation axes, and most stretching lineations, have been measured in the plane of the S_1 foliation (this study, Froese and Moore, 1980; Galley *et al.*, 1988), and the correct assignment of the prominent linear fabric elements in the area, with respect to D_1 and D_2, is the subject of continuing discussion. Galley (*pers. and written comm.*, 1988) pointed out that the coherent regional orientations of the linear fabrics, the apparent agreement of trends with the axial trace of the Threehouse synform (F_2), and the absence of rotation associated with this structure, supports the assignment of the lineation to D_2. Near the Snow Lake townsite, gold mineralization associated with retrograde alteration in late S_2 shear zones plunges parallel to the regional stretching lineation (Galley *et al.*, 1988). Pronounced rotation of the lineations is only apparent in the vicinity of the gneiss domes (D_3) in the northern part of the Snow Lake region (Froese and Moore, 1980). However, the orientation of the lineations changes from 065°/50° in the vicinity of the Snow Lake townsite (Galley, *written comm.*, 1988), to 023°/35° further south in the Linda area (Zaleski and Halden, 1988), to 020°/14–23° in the Cook Lake area (Jackson, 1983).

The emplacement of the Herblet, Squall and Pulver gneiss domes (Figure 2.1) during D_3 influenced the northern Snow Lake area, adjacent to the Kisseynew gneiss belt (Froese and Moore, 1980). The domes are, in part, localized on F_2 antiformal

crests, with a resultant tightening of the intervening F_2 synforms (*ibid.*).

The McLeod Road thrust fault (Russell, 1957) was postulated to account for older Amisk volcanic rocks overlying younger Amisk and Missi metasediments (Froese and Moore, 1980). The fault was interpreted to be earlier than, or contemporaneous with, D_1. Galley *et al.* (1988) reported that the fault has attentuated and truncated some F_1 fold limbs and was reactivated during D_2, with kinematic indicators showing oblique sinistral movement. In the Crowduck Bay area, immediately northeast of Wekusko Lake, inverted relationships between older and younger rocks led Gordon and Gall (1982) to postulate the presence of an early thrust fault. Froese and Moore (1980) pointed out the difficulty of detecting such features and the possibility of additional cryptic early faulting is problematic.

The Berry Creek fault (Armstrong, 1941) is a late northeasterly trending structure of regional significance, continuous for approximately 40 km from Tramping Lake, near the Paleozoic cover, to the margin of the Kisseynew belt (Bailes, 1971). It forms a topographic lineament west of Wekusko Lake, entering the lake at Berry Bay (Froese and Moore, 1980). The fault has been variously extended to the east, as a single fault or a series of anastomosing splays, in some cases, projected through Anderson Bay and the Linda area (Studer, 1982; Bailes, 1971; Russell, 1957). There is no evidence for a major late displacement in the Linda area; however, recognition may be a problem, as the fault trace would be subparallel to earlier structural trends and to lithological contacts. Prominent topographic lineaments trending northeast from Snow Bay (Figure 2.1) have been proposed as possibly related to the continuation of the Berry Creek fault (Bailes, *pers. comm.*, 1987).

2.3. Metamorphism.

Metamorphic assemblages in the Snow Lake area show a transition from the low-grade volcanic terrane in the south to the high-grade terrane of the Kisseynew gneiss belt to the north (Froese and Moore, 1980; Froese and Gasparrini, 1975). Three reaction isograds delineate the boundaries of 4 metamorphic zones characterized by the assemblages: chlorite-biotite, chlorite-biotite-staurolite, biotite-staurolite-sillimanite and biotite-sillimanite-almandine. The parageneses in muscovite-bearing pelitic rocks were regarded as definitive of metamorphic grade. The common presence of kyanite or kyanite and sillimanite in altered rocks, and of

sillimanite in metasediments, was used to establish metamorphic pressures in excess of the aluminosilicate triple-point. In the Anderson Lake and Stall Lake mines, the occurrence of the isograd assemblage, chlorite-staurolite-kyanite (sillimanite)-biotite-muscovite, was used to constrain the location of the surface trace of the biotite-sillimanite isograd (Figure 2.2).

The discordant relationship of the isograds to the regional structure (Figure 2.1) suggested that peak metamorphic conditions were attained after the occurrence of most of the D_2 deformation (Froese and Moore, 1980). However, the biotite-staurolite isograd partly coincides with the Berry Creek fault and with its possible continuation along the shore of Wekusko Lake. To the northeast of Wekusko Lake, the Crowduck Bay fault also has a northeasterly trace and cuts metamorphic isograds (Gordon, 1981). The biotite-sillimanite isograd and, possibly, the biotite-sillimanite-almandine isograd, apparently display asymmetric sinusoidal traces, consistent with a sinistral strike-slip component, where they cross the McLeod Road thrust fault. This occurs northeast of Snow Bay, nearly along-strike from the prominent topographic lineaments which have been suggested as the possible continuation of the Berry Creek fault. In the vicinity of the gneiss domes, prograde metamorphism continued after gneiss-dome emplacement (D_3), resulting in static crystallization of high grade minerals (Froese and Moore, 1980).

2.4. Alteration.

Altered rocks in the Snow Lake region are characterized by assemblages of metamorphic minerals resulting from regional metamorphism of synvolcanic hydrothermal alteration of Amisk volcanic and subvolcanic rocks (Skirrow, 1987; Trembath, 1986; Bailes, 1986; Jackson, 1983; Walford and Franklin, 1982; Froese and Moore, 1980; Hutcheon, 1979; 1977). The relationships between altered rocks and sulphide mineralization are commonly unclear, due to the superposition of deformation on primary structural and stratigraphic complexity. In many cases, altered rocks contain only minor amounts of stringer or disseminated sulphide minerals, for example, the Joannie and Ram zones (Trembath, 1986) and the Linda I showing (Jeffery, 1982, *unpubl.*). The Anderson Lake and Stall Lake mines are associated with extensive alteration zones (Walford and Franklin, 1982) whereas, in contrast, alteration at the Rod mine is minor (Coats *et al.*, 1970).

Beneath the orebodies at the Anderson Lake mine, the Stall Lake mine, and the Ram deposit, discordant zones of intense alteration cut stratigraphy at an oblique angle (30°), extending down-stratigraphy to intersect a lower, conformable to semi-conformable, alteration zone (Walford and Franklin, 1982). At the Anderson Lake mine, the discordant zone has a core of chlorite-biotite-kyanite schist with an outer zone of less intensely altered staurolitic rhyolite. It is capped by an extensive halo of muscovite schist, which envelops the orebody and the uppermost part of the discordant chloritic alteration (Fleming, *unpubl.*). The lower conformable zone shows vertical zoning from upper staurolitic rhyolite to a lower chlorite-biotite-kyanite schist, and lateral zoning with a decrease in chlorite and an increase in staurolite abundance to the southwest, away from the orebody. The discordant zones were interpreted to be the structurally transposed equivalents of alteration pipes, and the conformable zone, a reservoir horizon of regional extent (Walford and Franklin, 1982). However, the strong deformation in the Snow Lake region has obscured primary relationships and the distinction between conformable and disconformable alteration is commonly tenuous.

In the Edwards Lake area, stratigraphically below the Chisel Lake mine (Figure 2.1), altered rocks are well exposed in a recent burn (Bailes *et al.*, 1987; Skirrow, 1987). Pillowed and massive mafic flows show various degrees of silicification and epidotization, interpreted by Skirrow (1987) as having occurred near a seafloor surface. Semiconcordant zones of silicification and epidotization in mafic breccias grade laterally into Fe-rich alteration characterized by garnet-chlorite±biotite closer to the Chisel Lake mine. These alteration types were proposed to represent deep-seated subsurface hydrothermal activity below, and focussing into, a Chisel Lake footwall alteration pipe (*ibid.*). Williams (1966, 1961) reported quartz, muscovite, staurolite, kyanite, biotite and garnet bearing rocks in the footwall and hanging wall to the Chisel Lake deposit and identified these as metasedimentary intercalations within felsic pyroclastic rocks. He recognized their high quartz and muscovite contents as atypical of pelitic metasediments.

The Chisel Lake mine contains Ca-amphibole-carbonate assemblages in vein material and in retrograde alteration associated with the massive sulphide mineralization, which was interpreted to be of epigenetic origin (Williams, 1966; 1961).

At the Rod mine, Coats *et al.* (1970) reported minor alteration, consisting mainly of a carbonatized network of fractures, which they attributed to remobilization of primary carbonate derived from the volcanic activity. Gold mineralization, in shear zones near the Snow Lake townsite, is associated with carbonatization of wall rock and the precipitation of quartz, albite, ferroan dolomite, oxy-biotite, arsenopyrite, pyrite and pyrrhotite (Galley *et al.*, 1988).

PART II

GEOLOGY OF THE LINDA AREA

Chapter 3. Local Geology of the Linda Area.

Chapter 4. Structural Geology of the Linda Area.

Chapter 5. Proximal and Distal Alteration Zones, and Mineralization.

Chapter 6. Other Types of Alteration.

Chapter 7. Relationships between Textures, Microstructures, Mineralogy and Deformation.

Chapter 8. Reconstruction of the Synvolcanic Hydrothermal System.

Chapter 3
Local Geology of the Linda Area

The sulphide mineralization and alteration associated with the Linda deposit is hosted by Amisk felsic metavolcanic and volcaniclastic rocks with minor intercalated lenses of metasediments. Lithological units strike northeast and dip to the northwest (Map, in pocket; generalized in Figure 3.1). Alteration and disseminated sulphide zones lie to the northwest of the main pyritic body, thus overlying the massive sulphide deposit in the present configuration. This relationship indicates that the Linda deposit is overturned and that stratigraphic facing is to the southeast (*see* 3.2. Facing Direction).

Cross-sections A-A' and C-C' (in pocket; generalized in Figures 3.2 and 3.3), represent vertical sections oriented approximately perpendicular to lithological contacts, tectonic flattening, and the dominant mineral schistosity. The pronounced tectonic lineation lies in the plane of the dominant tectonic fabric, making an angle of approximately 60° with the projection plane of the cross-sections. Thus, the sections are slightly oblique (*i.e.* 30°) to the YZ-section of a generalized strain ellipsoid in which the relationship of the lengths of the principal axes is X>Y>Z (*e.g.* page 170 of Ramsay and Huber, 1980).

3.1. Description of Lithological Units.

The lithological units and their subdivisions represent a compilation of surface mapping (Map, in pocket) and drill-hole logs (Sections A-A' and C-C', in pocket). Surface mapping was done at a scale of 1:4800 and the subsurface cross-sections were prepared at a scale of 1:600. This difference in scale, which entails a difference in the scale of definition of mappable units, has been accommodated by the subdivision of major units, facilitating correlation between surface and subsurface. The subdivisions can be mapped in the subsurface, whereas in most cases, the geological map presents a more generalized picture. Outcrop mapping covered a larger area

and extended higher into the stratigraphic sequence than the subsurface coverage, *i.e.* units 7–9 and unit 11 were not intersected by drilling but were mapped on surface. Massive sulphide (unit 5) and graphitic metasedimentary rocks (unit 3), intersected in drill core, are not exposed at the surface.

The units have a primarily lithological significance; for example, no stratigraphic correlation is implied between units to the northwest, and units to the southeast, of the Anderson Bay structure. For those cases in which lithological changes due to stratigraphic succession are ssuggested, a lithological subdivision of the major unit has been defined, for example, intermediate volcaniclastic rocks (1d) intercalated with felsic volcanic rocks (unit 1) (Sections A-A', C-C', in pocket). Figure 3.4 presents a generalized stratigraphic sequence for the Linda area and summarizes the relationships between the lithological units.

Altered rocks display a spectrum of mineralogical, structural and textural features and range from porphyroblastic schists (units 10d and 10p), which do not preserve evidence of their protolith, to incipient alteration which overprints an identifiable precursor. For cases in which the precursor could be identified, the alteration has been indicated as superimposed on the primary lithology (on maps and cross-sections), and the rocks are designated by the primary unit with an additional descriptor indicating the type of alteration. For example, 4/10p refers to alteration of type 10p superimposed on unit 4. These rocks should not be simply assumed to represent gradations between unaltered and intensely altered rocks, as identification of the precursor is partly dependent on the degree of tectonic overprinting and the susceptibility of the rock to recrystallization, rather than strictly on the degree of chemical alteration. For example, quartz-megaphyric felsic rocks (unit 4) commonly contain recognizable quartz phenocrysts, even when the matrix is intensely altered.

A petrographic code was devised to supplement the designation of hand samples by lithological unit (Appendix A) and as a 'short-hand' notation to facilitate manipulation of the petrographic and geochemical database. The code is based mainly on mineralogical criteria and was used to account for significant variations on scales less than that of mappable units.

Nomenclature of lithological units and subdivisions has been based on megas-

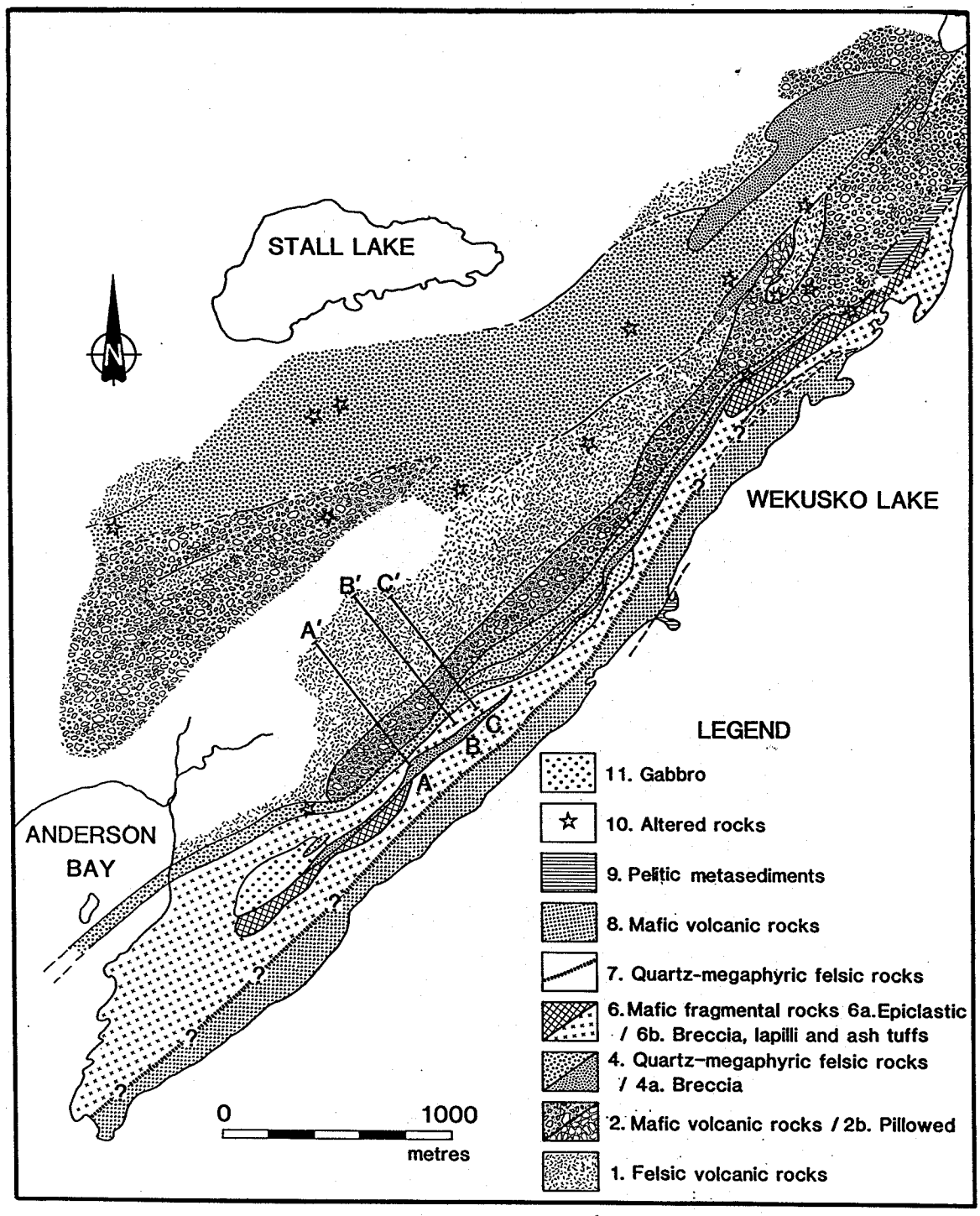

Figure 3.1. Geology of the Linda area generalized from the outcrop map (in pocket). The surface projections of three composite cross-sections are indicated by A-A' (Figure 3.2), B-B' (available on request) and C-C' (Figure 3.3).

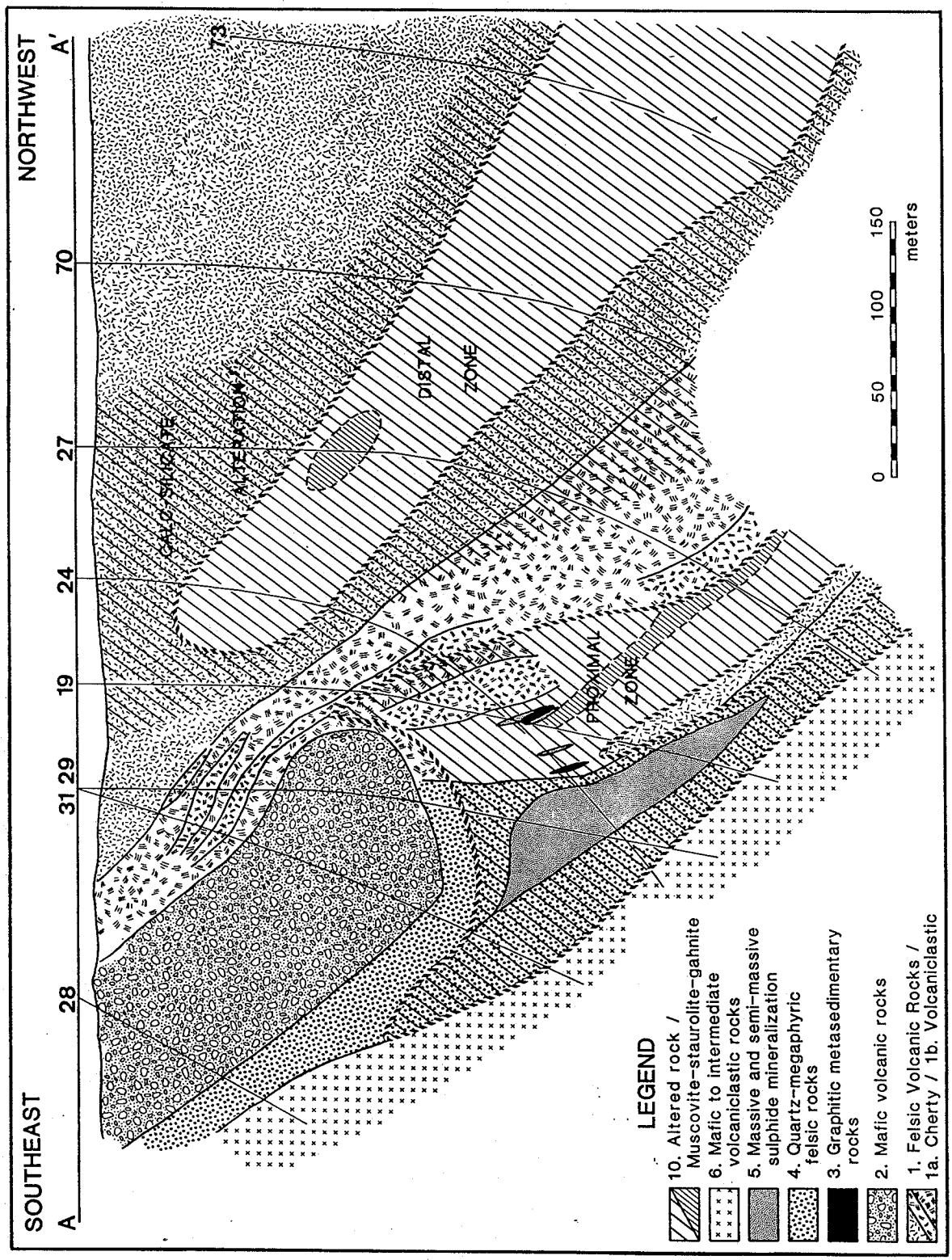

Figure 3.2. Subsurface geology of the Linda deposit in cross-section A-A' (Figure 3.1) looking southwest. Linear structures plunge northeast. Short dashes delineate the proximal and distal alteration zones. Horizontal and vertical scales are equal.

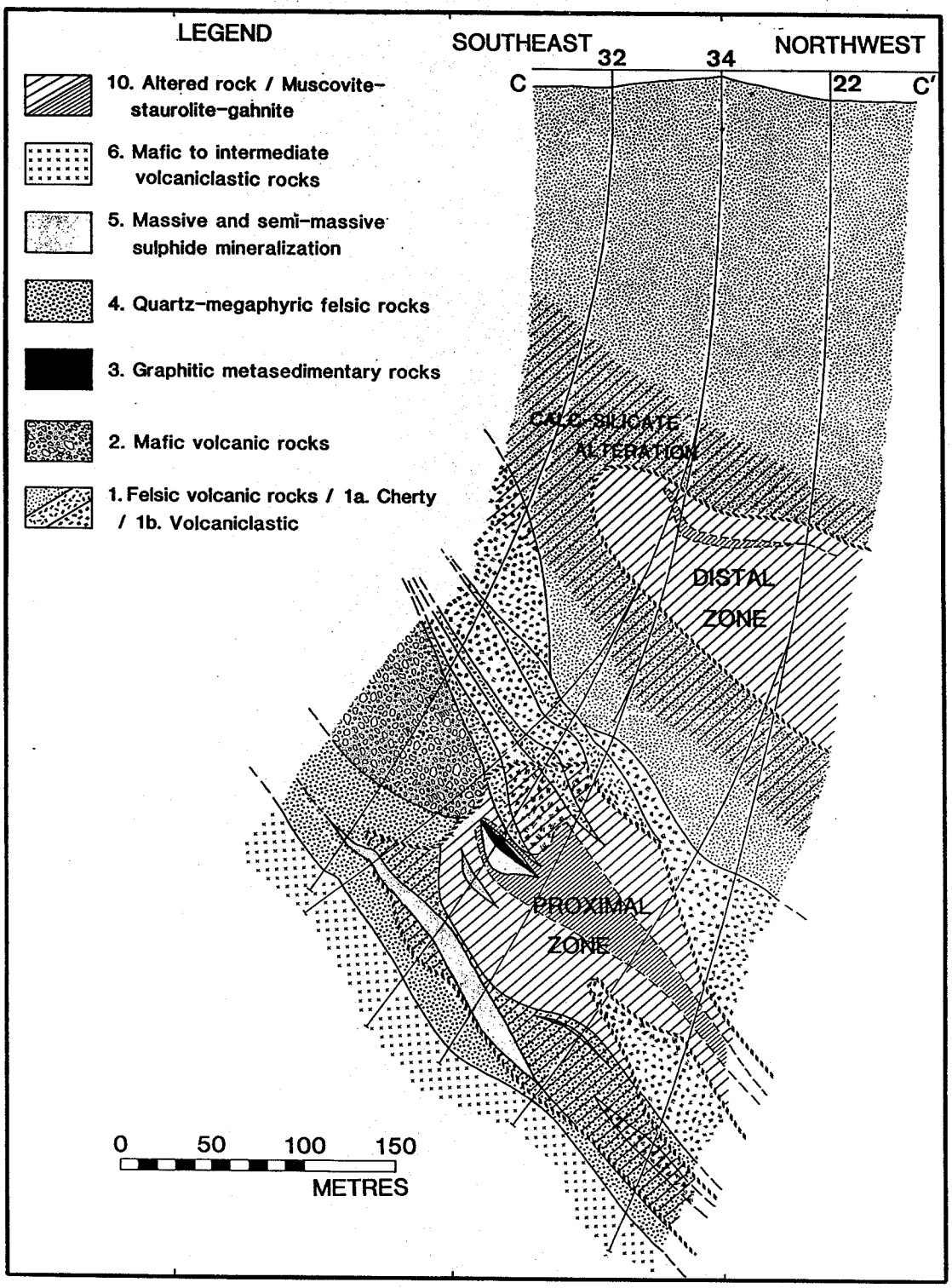

Figure 3.3. Subsurface geology of the Linda deposit in cross-section C-C' (Figure 3.1) looking southwest. Linear structures plunge northeast. Short dashes delineate the proximal and distal alteration zones. Horizontal and vertical scales are equal and the scale is the same as in Figure 3.2.

Generalized Stratigraphy of the Linda Area.

Metaturbidite, metagreywacke (Unit 9)	Rhythmically bedded metasediments
Mafic volcanic rocks (Unit 8)	100 m Fine grained homogeneous, local tuffaceous bedding
Quartz-megaphyric felsic rocks (Unit 7)	0–10 m Bedded, quartz and plagioclase phyric
Mafic to intermediate volcaniclastic rocks (Unit 6)	100 m Breccia, lapilli and crystal tuffs, lower heterolithic breccia contains clasts of Unit 4
Quartz-megaphyric felsic rocks (Unit 4)	20–80 m Quartz and locally plagioclase phyric, hosts massive sulphide (Unit 5) with footwall and hanging wall alteration (4/10p)
Felsic volcanic and volcaniclastic rocks (Unit 1)	Upper 50–200 m volcaniclastic with intercalated massive 'cherty' rhyolite, hosts disseminated sulphide mineralization and proximal alteration zone (10p) Graphitic metasediment (Unit 3) 0–5 m Mafic volcanic rocks (Unit 2) 0–150 m Lower ≤400 m felsic with minor intercalated intermediate to mafic rocks, hosts distal alteration zone (10d) and calc-silicate alteration (1/10c)

Figure 3.4. Generalized stratigraphic succession interpreted for the Linda area southeast of the Anderson Bay structure. The absolute thicknesses of the units are unlikely to have stratigraphic significance.

copic examination of drill core and outcrops, and the designations are intended as informal terms without strict genetic or compositional connotations. All rocks are metamorphosed, but the prefix 'meta' has generally been omitted. The term 'alteration', as used here, implies premetamorphic alteration, unless specified as synmetamorphic, retrograde or, of unknown origin.

Unit 1. Felsic volcanic and volcaniclastic rocks, with minor intermediate to mafic rocks.

Felsic volcanic and volcaniclastic rocks and their altered equivalents were extensively intersected by drilling but are poorly exposed on surface. Unit 1 hosts

the distal and proximal alteration zones (10d and 10p, respectively). The colour of weathered surfaces varies from buff to medium grey, suggesting approximately rhyolitic to dacitic compositions. It is mainly aphanitic (excepting porphyroblastic minerals), but locally contains minor fine ($\leq$2 mm) quartz or plagioclase phenocrysts. In most cases, biotite is the most abundant ferromagnesian mineral, but dacitic varieties commonly contain hornblende. Typically, a metamorphic-segregation fabric is weakly to strongly defined by an anastomosing micaceous layering, consisting of biotite$\pm$muscovite, and also chlorite, garnet, epidote and/or calcite. Micaceous layers, 0.5–5 mm in width, outline lenticular quartzo-feldspathic domains, 2–25 mm in width. The wider micaceous layers tend to be more muscovite-rich and appear to grade into incipiently altered rocks. Tectonic fabrics (S_1 schistosity and S_2 crenulation cleavage; *see* 4. Structural Geology of the Linda Area) are well defined within the micaceous layers and very weak in quartzo-feldspathic domains. Rocks in which the layering is dominated by epidote and/or calcite (1/10c and 1b/10c) define a calc-silicate alteration zone, and also occur locally throughout the unit.

Volcaniclastic rocks (1b) dominate the uppermost (stratigraphically) 50–200 m of the unit and are intercalated with massive 'cherty' felsic rocks (1a), which may represent or, be transitional to, silicified rocks (10s). These upper members host the proximal alteration zone (10p), disseminated sulphide mineralization, minor massive sulphide bodies (unit 5) and graphitic metasediments (unit 3). The volcaniclastic rocks (1b) are mainly monolithologic, containing flattened felsic clasts oriented parallel to the dominant schistosity in a micaceous felsic matrix. They resemble matrix-supported lapillistone or lapilli-tuff (Fisher and Schminke, 1984).

In some cases, metamorphic layering is developed in, or coincident with, the matrix of volcaniclastic rocks, *i.e.* with clasts forming lenticular quartzo-feldspathic domains separated by a fairly uniform thickness of anastomosing matrix. There are many rocks transitional between volcaniclastic rocks and felsic rocks in which primary structures are not discernible. The latter are commonly characterized by diffuse leucocratic domains transected by fine micaceous layering.

A distinctive type of fragmental rock occurs within the proximal alteration zone. It consists of clast-supported breccias (1c or 1c/10p) with interlocking angular fragments of 'cherty' felsic rocks (resembling unit 1a) in an altered and mineralized

matrix.

Within the felsic volcanic rocks, intermediate and minor mafic hornblende-bearing rocks occur as intercalations representing up to 30 m of drill-core intersection. The more mafic varieties are dark green, fine grained homogeneous or, in some cases, recrystallized to aggregates of coarse grained hornblende. Locally, the mafic rocks grade to chlorite schists (possibly retrograde?) with a well developed *S-C* fabric. Intermediate varieties are commonly volcaniclastic, containing cummingtonite-bearing felsic clasts supported in a hornblende-chlorite-bearing matrix. Biotite, garnet and magnetite are common accessory minerals. In some cases, graded bedding is defined by variations in clast size and abundance, with minor occurrences of zones which may be clast-supported.

Hornblende-bearing rocks also occur as enclaves representing 1–10 cm of drill-core intersection, within the typical biotite-layered felsic rocks of unit 1. The enclaves are characterized by radiating sprays and 'bowtie' aggregates of hornblende in an aphanitic felsic matrix which forms a leucocratic halo to the host rock. The halo, in some cases, appears discordant to the biotite layering in the host rock, although the distribution of hornblende defines a weak concordant layering.

Unit 2. Mafic volcanic rocks, with minor intermediate rocks.

Unit 2 encompasses a variety of dark to medium green hornblende-rich rocks. In the immediate proximity of the Linda deposit, a sequence (2a) of approximately 150 m in thickness, terminates laterally and down-dip against the proximal alteration zone. These rocks vary from homogeneous, fine to medium grained, to layered on a 2–25 cm scale, with layering defined by gradational changes in the abundance of plagioclase phenocrysts(?) .5–3 mm in size. The layering is parallel to mineral schistosity and lineation, and commonly deflects around regularly distributed elongate epidotized patches, 0.1–.3 m in thickness and 0.2–1 m in length in the YZ-section of a generalized strain ellipsoid. Locally, the long axes of the epidotized patches have an oblique orientation with respect to the layering. The layering follows a sigmoidal trace around the patches, giving the appearance of rotational strain (*see* Figure 4.1, d).

Within this sequence, there are minor intercalations of apparently volcaniclastic rocks (2e), with felsic clasts flattened parallel to the schistosity of the mafic matrix.

The primary structures are commonly obscured by randomly oriented, medium to coarse grained, hornblende porphyroblasts. Locally, garnet, cummingtonite and magnetite occur as accessory minerals and increase in abundance near contacts with felsic rocks which show evidence of silicification (*see* Unit 10).

A distinctive subdivision (2c) of unit 2 occurs in the northeast of the mapped area where it forms extensive knolls of high relief. In this area, very homogeneous, aphyric mafic rocks are massive except for a mineral lineation defined by fine to medium grained hornblende.

To the northwest of the trace of the Anderson Bay structure, in a poorly exposed area, mafic rocks (2d) consist of pillowed flows and flow breccias intercalated with mainly heterolithic volcanic breccia. The pillowed flows (2b) contain relict plagioclase phenocrysts and hornblende pseudomorphs of euhedral clinopyroxene phenocrysts up to 1 cm in size. The pillows have ameboid shapes; the cores are epidotized and the margins are bleached and carbonatized.

In the northeast, minor volcaniclastic rocks (2e) consist of breccias, lapillistones and tuffs, with graded bedding defined by changes in clast size and abundance, including some clast-supported beds. These rocks are extensively altered, typically containing cummingtonite-magnetite-bearing felsic clasts in a matrix with abundant, medium to coarse grained, garnet-hornblende±cummingtonite±biotite. This subdivision occurs stratigraphically above silicified pillowed flows (2b/10s) which contain a similar mineral assemblage (*see* Plate 6.1, c–d).

Unit 3. Graphitic metasedimentary rocks.

Mineralized graphitic metasediments occur on at least two horizons within the proximal alteration zone, forming lenses 1–5 m thick. The lateral extent is limited, but the metasediments were intersected at intervals along a considerable down-plunge length. The unit is dark, mineralized with pyrite, pyrrhotite, and minor sphalerite, chalcopyrite and arsenopyrite, and commonly associated with minor massive sulphide bodies (unit 5). Thin bedding (0.1–10 mm) is defined by variation in the abundance of very finely divided graphite (*see* Plate 5.2, e). Beds with sparsely disseminated graphite contain abundant kyanite and minor phlogopite porphyroblasts in a schistose margarite-muscovite matrix. They also contain fine ($\leq$1 mm) quartz-crystal clasts. The bedding is folded and crenulation cleavage is well

developed in phyllosilicates (*see* Figure 7.1, Plate 7.1). Unfortunately, the drill core was severely damaged during previous splitting.

Unit 4. Quartz-megaphyric felsic volcanic rocks.

Quartz-megaphyric rocks host the main pyritic body of the Linda deposit and are extensively altered (4/10p) in both the stratigraphic footwall and hanging wall. The thickness of the unit varies from 20–80 m, tending to increase slightly in the proximity of the termination of the mafic volcanic rocks of unit 2. It is laterally continuous throughout most of the mapped area occurring in isolated exposures which commonly show some degree of alteration. To the northwest of the Anderson Bay structure, an extensive area of similar lithology hosts the Rod and Stall Lake mines and shows sporadic alteration.

The unit is characterized by blue quartz phenocrysts, 3–10 mm in diameter (in YZ-sections), which constitute 2–30% of the rock. Relatively unaltered varieties commonly contain 2–20% plagioclase phenocrysts. Variations in phenocryst abundance and size define thick bedding (0.3–3 m), but most primary features are obscured by alteration and by the development of tectonic fabrics. Near the uppermost (stratigraphically) part of the unit, a medium grey, more dacitic rock occurs discontinuously and the quartz-megaphyric rocks show some interleaving with the overlying intermediate rocks (unit 6).

In drill core, the unit is incipiently to intensely altered (4/10p), in many cases, consisting of a muscovite schist with quartz augen, with or without accessory chlorite, biotite, staurolite and kyanite. It typically contains abundant disseminated pyrite in amounts of up to 10% and, in several cases, bedding and bedding-plane contacts are defined by changes in pyrite concentration. Within the unit, there are intercalations of felsic lapillistone and lapilli-tuff which tend to contain lower concentrations of quartz phenocrysts. Felsic clasts are supported in a matrix varying from aphanitic buff-coloured felsic material to an intensely altered muscovite schist. In many cases, the clasts have poorly defined diffuse margins and there is a transition to diffuse quartzo-feldspathic domains of uncertain origin. Less schistose rocks commonly show a layering defined by micaceous segregations similar to that described for unit 1.

On the southeast side of the Anderson Bay structure, the unit is very heteroge-

neous. Surface exposures commonly show carbonatization and calc-silicate mineralogy of unknown genesis (possibly synmetamorphic). Discontinuous thin layering on a centimetre scale is defined by hornblende-epidote-calcite-bearing zones. In some cases, fine ($\leq$5 mm) angular carbonitized domains resemble altered clasts and define layering in association with quartz phenocrysts. These rocks are also associated with zones, .5–10 m in thickness, of coarse grained layered amphibolite and plagioclase-phyric tuffs(?) and lapilli-tuffs which show grading on a 20–50 cm scale.

The uppermost (stratigraphically) 5–30 m of the unit in the northeast consists of volcanic breccia (4a) containing both quartz-megaphyric and aphyric felsic clasts, flattened parallel to the metamorphic-segregation fabric to dimensions of up to 4×25 cm in YZ-sections. The breccias are mainly matrix-supported but with some nearly clast-supported beds. The matrix is felsic to intermediate, containing garnet, biotite, calcite, muscovite and/or hornblende. The clasts commonly show re-entrant angles, possibly resulting from deformation of originally angular shapes.

There is no continuity between quartz-megaphyric felsic rocks to the southeast and to the northwest of the Anderson Bay structure. The unit on the northwest is similar in the occurrence of blue quartz and plagioclase phenocrysts and in sporadic alteration marked by abundant biotite, muscovite, kyanite, staurolite and/or chlorite. However, it is more homogeneous, showing a fairly regular distribution of phenocrysts on outcrop scale and variably developed anastomosing micaceous layering.

Associated volcaniclastic breccias (4a) are matrix-supported and heterolithic, containing clasts of quartz-megaphyric and intermediate rock types, epidotized clasts, white quartz cobbles, and quartz-crystal and plagioclase-crystal clasts in a dark hornblende-biotite-rich matrix. The breccias are poorly sorted, but graded bedding is weakly defined by laterally discontinuous zones with higher abundances of crystal clasts. The lithic clasts are flattened parallel to schistosity, to shapes up to 20 cm long in YZ-sections.

Unit 5. Massive and semi-massive sulphide mineralization.

Massive sulphide bodies were intersected by drilling, but are not exposed on surface. The largest body forms a lens within quartz-megaphyric felsic rocks (unit 4), and lies close to the upper stratigraphic limit of the proximal alteration zone (10p).

Three smaller bodies are associated with disseminated sulphide mineralization lower in the stratigraphic sequence within the proximal zone. All the bodies have flattened elongate shapes generally concordant to bedding and to schistosity. Disseminated sulphide mineralization extends laterally for a considerable distance, particularly along the horizon of the largest sulphide body.

The largest body and, in some cases, parts of the smaller lenses, are dominantly composed of medium to coarse grained, granular pyrite. They are commonly semi-massive, lack penetrative fabrics, and consist of 20–60 % pyrite intergrown with medium to coarse grained, white calcite. Pyrrhotite, chalcopyrite and sphalerite occur locally with pyrite in zones representing 1–15 cm of drill-core intersection. Enclaves of silicate mineralogy are present as zones varying from quartz-augen muscovite schist to semi-massive sulphide containing quartz 'eyes'. Some silicate enclaves of dark colour contain hornblende, epidote, plagioclase and gahnite, and in one case, garnet. These enclaves show fine (thin-section scale) mineralogical zoning along contacts with the pyrite-calcite rocks (*see* 5.6.2. Silicate Enclaves in the Main Massive Sulphide Body). A single occurrence of an enclave characterized by anthophyllite+staurolite+gahnite (sample 24-1131-1; Table A.1) was observed.

The smaller massive sulphide bodies, particularly those associated with graphitic metasediment (unit 3), contain pyrite with accessory pyrrhotite, chalcopyrite and sphalerite, and minor calcite on veinlets and fractures. The contacts of the unit are commonly interleaved with silicate rocks containing quartz, muscovite, margarite, biotite and kyanite.

Unit 6. Mafic to intermediate, mainly volcaniclastic rocks.

Intermediate volcaniclastic rocks overlie the quartz-megaphyric felsic rocks of unit 4 and outcrop over an extensive area on the southeast side of the Anderson Bay structure. Most drill holes ended within the lowermost 50 m of this unit. To the northeast, the base of the unit consists of heterolithic, poorly sorted, volcanic breccia (6a) which contains abundant clasts of the underlying quartz-megaphyric felsic rocks. Other clast types include mafic hornblende-rich rocks, intermediate hornblende-bearing rocks, aphanitic felsic rocks and, in rare cases, quartz-crystal clasts. The clasts range in size from fine lapilli to up to 10 × 30 cm and are supported in a dark hornblende-rich matrix. Weak grading is defined by clast-rich zones.

The bulk of the unit consists of lapillistone, lapilli-tuff and crystal-tuffs (6b) with felsic clasts and plagioclase-crystal clasts. The rocks are matrix-supported with grading defined by variations in clast size and abundance. Some zones attain densities of 40–50 % plagioclase-crystal clasts up to 3 mm in size. Locally, the layering is weakly defined and lenticular. Felsic lithic fragments are mainly less than 1 cm in size but, locally, flattened fragments attain 25 cm in YZ-sections. There is an overall tendency to finer clast sizes higher in the stratigraphic section, grading to a homogeneous fine to medium grained rock near the upper contact. Mineral assemblages vary from cummingtonite-bearing felsic fragments in a hornblende-chlorite-rich matrix, to carbonitized and epidotized fragments in a hornblende-epidote-calcite-bearing matrix. Biotite and garnet are common accessory minerals. Locally, randomly oriented, coarse grained amphibole porphyroblasts obscure primary structures.

Layered amphibolites (6c) of unknown origin occur mainly close to the basal contact with quartz-megaphyric rocks (unit 4). They consist of thin alternating felsic and mafic layers less than 1 cm wide. Hornblende is randomly oriented in coarse grained sheaves confined to mafic chlorite-rich layers.

Unit 7. Quartz-megaphyric felsic volcanic rocks.

A second unit of quartz-megaphyric felsic rocks forms a semi-continuous, poorly exposed, marker horizon higher in the stratigraphy. Its thickness varies along strike from 0–10 m and the possible structural or primary significance of this is unknown. In contrast to the quartz-megaphyric rocks of unit 4, there is no evidence of extensive alteration. Bedding is well defined by varying abundances of quartz phenocrysts, 1–10 mm in diameter, and plagioclase phenocrysts, 0.5–2 mm in diameter, which constitute 5–25 % and 5–15 % of the rock, respectively. These define fairly homogeneous layers, 0.1–1 m in thickness, with abrupt contacts. In some cases, phenocryst fragments are apparently present, as well as minor fine (5 mm) felsic lithic fragments(?). The matrix is aphanitic and felsic, locally with weakly developed micaceous segregations. Biotite, hornblende, chlorite and garnet are common accessory minerals.

Unit 8. Mafic volcanic rocks.

Dark green, fine to medium grained mafic rocks, lithologically similar to the uppermost part of unit 6, overlie quartz-megaphyric rocks (unit 7). The unit is

mainly homogeneous hornblende-rich and, commonly, chloritic, with a moderately developed fissility parallel to mineral schistosity. Locally, it shows thin to medium bedding (0.5–10 cm thick) of tuffaceous sediment, in some cases, with fine ($\leq$2 mm) plagioclase-crystal clasts and possible lithic fragments and, rarely, with a buff-coloured 'cherty' bed. Minor occurrences of epidotized patches up to 0.15×1.5 m are similar to those observed in unit 2. Coarser volcanic breccia and lapilli-tuff form minor intercalations within the main lithology. These typically consist of 5–20% felsic clasts in a mafic matrix, but clast-supported beds, with clast sizes up to 10×40 cm in YZ-section, also occur. To the southeast near Wekusko Lake, some parts of the unit are more heterogeneous. Very poorly exposed coarsely fragmental rocks and felsic rocks, including biotite-garnet dacitic rocks similar to unit 1, and quartz-phyric(?) felsic rocks, are apparently interleaved with mafic rocks.

Unit 9. Metaturbidite and metagreywacke.

Three outcrop areas of metagreywacke occur within the mapped area. Two of these are aligned on a northeasterly trend, suggesting that the metasediment forms an intercalation within metavolcanic rocks. The outcrops are large high relief knolls with thick lichen cover. Prominent weathering concentrations of coarse grained (1–2 cm) staurolite and fine to medium grained (0.5–2 mm) garnet porphyroblasts define rhythmic bedding, 1–5 cm in thickness. Biotite, muscovite and graphite are abundant. Asymmetrical minor folds of 0.5 m amplitude are prevalent. The metasediment is similar in lithology to outcrops of Amisk Group metasediments in the town of Snow Lake.

Another area of metasediment forms a small isolated promontory into Wekusko Lake. The metasediment is quartzo-feldspathic, containing grains of feldspar and blue quartz up to 1 mm in size, with accessory garnet and biotite. Thin to medium bedding ranges from 0.5–10 cm in thickness. In contrast to the more northerly exposures of metasediment, no staurolite porphyroblasts were observed and the sediment composition is more psammitic.

Unit 10. Altered rocks.

This unit encompasses a wide variety of alteration types which are briefly summarized here (*see* 5. Proximal and Distal Alteration Zones, and Mineralization *and* 6. Other Types of Alteration). Two distinct alteration zones have been delineated

in drill core but are not exposed on surface. The zones have been designated 'distal alteration zone' (10d) and 'proximal alteration zone' (10p), with reference to their relative distance from the massive sulphide bodies (unit 5); these terms are not intended to have genetic or lithofacial connotations. The distal zone (10d) occurs in felsic volcanic rocks of unit 1, 200–250 m below (with respect to stratigraphic facing) the largest sulphide body. The proximal zone (10p), in part, occurs in the uppermost part of unit 1, down-dip from the termination of mafic volcanic rocks of unit 2. It is developed mainly in felsic volcaniclastic rocks (1b), 'cherty' felsic rocks (1a) and clast-supported breccias (1c) and, engulfs minor massive sulphide lenses (unit 5) and graphitic metasediment (unit 3). It also occurs in quartz-megaphyric felsic rocks (unit 4), affecting both the hanging wall and footwall to the largest massive sulphide body (unit 5). Both alteration zones extend down-dip beyond the limits of drilling.

Altered rocks within the proximal and distal zones display considerable variation, but are typically quartz-rich chlorite-muscovite schists with various proportions of staurolite, biotite, kyanite, magnetite, garnet, and/or sulphide minerals. Both zones apparently have an irregular core characterized by muscovite-staurolite-gahnite schist (10da, 10pa). Minor occurrences of altered rocks of similar mineralogy are exposed on surface, mainly within quartz-megaphyric felsic rocks (unit 4).

Calc-silicate minerals occur in two types of alteration, distinguished on the basis of textural and structural relations, and paragenesis. Felsic rocks in which micaceous layering is dominated by epidote-biotite±muscovite±calcite (1/10c, 1b/10c), envelop the distal alteration zone (10d) and have isolated occurrences elsewhere (4/10c, 1/10c, 1b/10c). The rocks are characterized by the involvement of calc-silicate minerals in the tectonic fabrics. In contrast, the assemblage Ca-amphibole-epidote-calcite±titanite (10i) occurs in statically crystallized, medium to coarse grained aggregates, generally forming volumetrically minor, discrete drill-core intersections of up to 1.5 m in length. In some cases, the contacts with the host rock are transitional over 1–5 cm and visibly discordant to S_1 layering. This latter type of calc-silicate alteration is usually notably low in sulphide minerals. It occurs sporadically within most units, including calc-silicate altered rocks of the former type (1/10c, 1b/10c, 4/10c).

Dark green mafic schists (10m) containing chlorite±hornblende occur as minor enclaves within the distal zone (10d), or in association with mafic volcanic rocks. These schists may be, at least in part, associated with retrogression.

Epidote-hornblende-calcite alteration of mafic rocks (10e) was encountered in both surface and subsurface exposure. It generally takes the form of epidotized patches as previously described for units 2 and 6.

Quartz veins (10v) constitute a mappable unit only on the more detailed scale used in subsurface cross-sections. They occur in both the proximal and distal alteration zones, as well as in other lithological units and alteration types. They are typically deformed, containing infolded wall-rock inclusions, and have contacts concordant to schistosity or apparently causing the nucleation of asymmetric drag folds in the host rock.

The recognition of possibly silicified and/or feldspathized rocks (10s) is problematic, particularly in drill core. Massive 'cherty' felsic rocks (1a), on the evidence of geochemistry (*see* 11.1.1. Geochemistry of Felsic Rocks and Silicic-Feldspathic Altered Rocks), are albitized and silicified. In some cases, breccias (1c) contain diffuse 'cherty' clasts outlined by fine disseminated sulphide minerals and cemented in a 'cherty' siliceous matrix. In many cases, the contacts of mafic rocks of unit 2 with felsic rocks (unit 1) and quartz-megaphyric rocks (unit 4) are gradational and characterized by the presence of cummingtonite and magnetite porphyroblasts (*see* 6.1. Silicic-Feldspathic Alteration; Plate 6.1, a). In volcaniclastic rocks, felsic clasts are commonly associated with cummingtonite, whereas hornblende and chlorite and, in some cases, garnet, are abundant in the mafic matrix. On surface, one exposure of pillowed rocks shows evidence of silicification (2b/10s), with buff-coloured cummingtonite-bearing pillow interiors outlined by medium to dark green margins containing hornblende-cummingtonite-garnet-magnetite (*see* Plate 6.1, c–d).

Unit 11. Gabbro.

A small body of massive, medium green, coarse grained, hypidiomorphic gabbro intrudes volcanic rocks southeast of Anderson Bay. It consists mainly of coarse grained Ca-amphibole up to 1 cm in size, with minor interstitial aggregates of fine grained epidote. The amphibole probably replaced primary clinopyroxene.

3.2. Stratigraphic Facing.

Most of the alteration at the Linda deposit overlies the massive sulphide mineralization. This configuration requires that stratigraphic facing is down and to the southeast (Figure 3.1). Along-strike from the deposit to the northeast, heterolithic volcanic breccias (6a) in contact with quartz-megaphyric felsic rocks (4) contain clasts of the same lithology (4). These breccias (6a) were interpreted to have incorporated clasts of the underlying unit during transport and, therefore, they also indicate southeasterly facing of the lithological sequence in this area. The Berry Creek fault may form the contact between the metavolcanic rocks and Amisk metasedimentary rocks on islands in Wekusko Lake and, in one exposure on the shoreline.

Pillowed flows near Kormans Lake and east of the Rod minesite are strongly deformed. The pillow shapes indicate a general northeasterly facing direction but are equivocal with respect to the facing direction of the stratigraphic sequence (*i.e.* northwest or southeast?). Pillowed flows north of Anderson Bay were interpreted by Jeffery (1982, *unpubl.*) to face northwest, but the shapes are too ameboid for confident appraisal.

The Stall Lake deposit faces north (Walford and Franklin, 1982; Studer, 1982); the Rod deposit (Coats *et al.*, 1970) and the Linda I showing (Jeffery, 1982, *unpubl.*) do not yield facing directions. Near Anderson Creek, equidistant between Stall Lake and the surface projection of the Linda deposit, a one-metre thick bed of heterolithic breccia forms an intercalation between pillowed flows. Along the southeast contact of the breccia, the pillow selvedges show truncation against the breccia bed, interpreted to be the result of scouring (*see* Figure 4.1, a). On the northwest, pillow selvedges are continuous, indicating emplacement of the flow on top of a pre-existing breccia bed. On the basis of these observations, this outcrop was interpreted to face northwest and to constrain the locus of the change in facing direction to an area between Anderson Creek and the Linda deposit (*see* 4.1.2. The Anderson Bay Structure).

3.3. Stratigraphy.

The major lithological units can be interpreted in terms of a generalized stratigraphic sequence for the Linda area on the southeast limb of the Anderson Bay

anticline (Figure 3.4). In view of the deformation, the absolute thickness of units is unlikely to have stratigraphic significance. Lithological units and sequences are similar on both sides of the trace of the Anderson Bay structure, but the differences are significant. Mafic rocks (2d) to the northwest of the structural trace commonly contain plagioclase phenocrysts and hornblende pseudomorphs after clinopyroxene phenocrysts. To the southeast, mafic rocks of unit 2 are aphyric or plagioclase-phyric. Felsic rocks comprising unit 4 contain quartz megacrysts on both sides of the structural trace, but the unit is more heterogeneous and more mafic on the southeast, commonly containing metamorphic hornblende and epidote. The unit is markedly thicker on the northwest, but this may be due to structural repetition or thickening (*see* 4.5. Discussion).

Major units on the southeast of the Linda area show lateral continuity and, in the absence of alteration, a relatively uniform degree of strain. The presence of cryptic bedding-parallel faults cannot be ruled out, but the simplest interpretation is that of a stratigraphic succession. The lenticular nature of some of the subunits may be primary. In the northeast, the staurolite-bearing metasedimentary rocks (unit 9) between Kormans Lake and Wekusko Lake are very similar to Amisk Group metasediments (*e.g.* in the Snow Lake townsite) normally considered to overlie Amisk Group metavolcanic rocks (Froese and Moore, 1980). In view of the pinching out of units 4 and 7 in this area and the occurrence of the metasedimentary intercalation (Figure 3.1), it seems probable that this area contains structural complexities, the precise nature of which remains unknown. The metasediments of unit 9 in the Linda area are correlative with Amisk Group metasediments and are thus shown at the top of the generalized stratigraphic sequence (Figure 3.4), in accordance with the regional geology (Froese and Moore, 1980).

Chapter 4
Structural Geology of the Linda Area

The structural geology of the Linda area was mapped independently of deformational sequences proposed for the Snow Lake region (Froese and Moore, 1980; Jackson, 1983) to ensure the collection of an internally consistent structural database, which can subsequently be interpreted and correlated with the regional structure. Thus the structural designations in the following chapter apply specifically to the Linda area. 'S' refers to planar fabrics, 'L' to linear fabrics and 'F' to folds; subscripted numbers indicate the relative chronological sequence inferred from observed relationships. For example, S_0 denotes primary planar fabric elements such as bedding and lithological contacts, and S_1 fabric elements include modified primary features such as flattened clasts and quartz phenocrysts (Table 4.1). 'D' refers to the hypothetical event during which the planar and linear fabric elements of a particular generation were formed. For example, D_0 refers to the volcanic 'event' during which S_0 developed, and D_1 refers to the first (recognized) deformation to which the development of S_1 and L_1 is attributed. Similar schemes for the classification of structural data are in common usage (*e.g.* Hobbs *et al.*, 1976).

An L-S tectonic fabric dominates the structure of the Linda deposit and the entire Snow Lake region. Primary features, such as sulphide lenses, pillows and clasts, show a northeasterly trending elongation. For example, the main sulphide body of the Linda deposit exceeds 1500 metres in plunge-length; the maximum strike-width is less than 200 metres. Planar primary structures, such as lithological contacts and bedding, are structurally transposed into northeasterly strikes with dips to the northwest. In the Linda area, a general parallelism of S_0 and S_1 fabrics suggests that the rocks underwent pervasive high strain. Structural observations on outcrop and in drill core imply two main deformational events.

Table 4.1. Structures in the Linda Area.

	Planar Fabric Elements	Linear Fabric Elements	Folds
D_0	contacts and bedding		
unknown			Anderson Bay structure?
D_1	transposed S_0		
	flattened quartz phenocrysts	elongate quartz phenocrysts	F_1 minor folds?
	flattened clasts	elongate clasts	
	flattened pillows	elongate pillows	
	metamorphic segregations	mineral lineation	
	mineral schistosity		
	dimensional orientation of mimetic porphyroblasts		
D_2	crenulation cleavage	crenulation axes	
	mineral crystallographic orientation	intersection lineation	
	mineral dimensional and crystallographic orientation	mineral lineation?	
	discrete spaced cleavage		
	F_2 fold axial planes	F_2 fold axes	F_2 minor folds
late D_2?		fold axes	open flexural folds
	retrograde shears		
post-D_2	brittle fractures		

4.1. D_1 Deformation.

4.1.1. S_1 Planar Fabric Elements.

D_1 deformation is manifested in flattening and elongation of pillows, of clasts in fragmental units, and of quartz eyes in quartz-megaphyric rocks, by mineral foliation, and by transposition of primary structures. In heterolithic fragmental rocks, the degree of flattening of individual clasts typically shows some dependence on lithology. Mafic to intermediate clasts are more flattened than felsic or epidotized clasts and, in some cases, are crescent-shaped, conforming to the margins of more competent clasts. In matrix-supported breccias, the mineral schistosity in the matrix is similarly deflected around the more competent clasts. Lenticular clasts with multiple terminations on one end and re-entrant angles filled by matrix material were inferred to result from the flattening of originally angular to subangular clasts.

Pillowed rocks near Kormans Lake (Map, in pocket) contain some crescent-

shaped (molar-tooth) pillows resembling those attributed by Borradaile (1982) to heterogeneous strain. Bleached pillowed rocks east of the Rod minesite are prolate, although margins show an S_1 mineral schistosity (*see* Plate 6.1, c; Note that the view in this plate is down the plunge of the lineation.). Epidotized knots in mafic rocks (2a) are elongate and show a consistent obliquity to S_1 as defined by mineral foliation and layering (Figure 4.1, d; *see* 4.1.3. Relationships of S_0 and S_1 Fabrics).

In felsic rocks and altered felsic rocks, S_1 is defined by a fine compositional layering, consisting of concentrations of aligned micaceous minerals. The layering anastomoses around granoblastic quartzo-feldspathic domains. The definition of the fabric varies from very weak and diffuse or entirely absent in the most leucocratic and 'cherty' rocks, to strong in felsic rocks with greater abundances of biotite, muscovite or chlorite, to a pronounced gneissosity in some altered rocks. Minerals associated with the micaceous layers include muscovite, biotite, chlorite, epidote, staurolite and garnet. Muscovite and chlorite and, in some cases, epidote, typically show S_1 crystallographic orientation parallel to the layering. Staurolite and garnet appear mimetic, with a skeletal or poikiloblastic texture showing S_1 dimensional alignment, but with mainly random crystallographic orientations. Biotite is similarly mimetic after S_1 layering, but (001)-planes commonly define a foliation oblique to the layering (*see* 4.2.1. S_2 Planar Fabric Elements). The width and spacing of micaceous layers varies from very fine (.1 mm at .5–1 mm intervals), usually in leucocratic rocks, to coarse (up to 5–8 mm at 10–30 mm intervals). The widest layers occur in altered rocks, in many cases, imparting a mica-staurolite banded structure.

In felsic volcanic breccias, the matrix typically contains greater abundances of phyllosilicate minerals and is more schistose than the clasts. In altered breccias, the matrix seems more intensely affected by both alteration and subsequent deformation; the resulting fabric consists of felsic clasts with a granoblastic texture in a schistose matrix. There is a complete gradation from gneissic altered rocks to felsic volcaniclastic rocks with a schistose matrix. Transitional varieties resemble volcaniclastic rocks but show sharp contacts between clasts and matrix; a constant thickness of matrix shows an even distribution around monolithologic felsic domains with a very regular size distribution. This structure is observed even in altered rocks in which the leucocratic domains contain no feldspar, *i.e.* are apparently completely

Figure 4.1. (following page) Structural map of the Linda area, highlighting facing directions which constrain the change in stratigraphic facing to lie between the area south of Stall Lake (not shown) and the Linda deposit. The insets illustrate outcrops on which an angular deviation was observed between S_0 and S_1 fabrics. The base map and key to map symbols are the same as in Figure 4.2.

a. Intercalation of heterolithic volcanic breccia and plagioclase-hornblende (pyroxene)-phyric pillowed mafic flows. The breccia is matrix-supported, poorly sorted and not graded. The contact on the southeast side of the breccia bed shows slight irregularities and pillow selvedges are truncated against the breccia. The truncation of the selvedges was interpreted to be the result of syndepositional scouring. Along the contact on the northwest side, pillow selvedges are continuous, suggesting emplacement on top of the breccia bed. These relationships require northwesterly stratigraphic facing. S_1, defined by flattened pillows and clasts and by mineral foliation, is oblique to the S_0 contacts. Note that the S_0/S_1 vergence is not consistent with an F_1 anticlinal closure along the trace of the Anderson Bay structure.

b. Bedding in felsic volcanic breccia defined mainly by variations in the abundance of coarse quartz-megaphyric and aphyric felsic clasts. S_1, defined by flattened clasts, is oblique to the S_0 bedding.

c. Altered interbedded volcanic breccias and tuffaceous metasediments lie to the southeast of the contact (S_0). Bedding is defined mainly by variations in clast abundances and size, and by a single cherty bed (inset). The most northwesterly bed consists of lenticular leucocratic cummingtonite-magnetite-felsic domains resembling coarse clasts or flattened silicified pillows, in a garnet-amphibole-biotite matrix. The metasediments contain cummingtonite, hornblende, garnet, biotite and magnetite porphyroblasts which may obscure fine clasts. S_1, defined by flattened clasts and mineral schistosity, is oblique to S_0 bedding. S_1 may be parallel to the axial plane of $F_1(?)$ crenulated laminations within the cherty bed (inset, axial plane of crenulations indicated by S). Open flexures involving both the S_0 and the S_1 fabrics appear as gentle undulations.

d. Trails of epidotized knots in mafic volcanic rock, with semi-continuous alternating hornblende-rich and plagioclase phenocryst-rich layers (semi-continuous lines). The long axis of the epidotized knots is oblique to layering, which is asymmetrically deflected around the knots. S_1 mineral schistosity is parallel to the layers. The epidotized knots may be the boudinaged and rotated remnants of original epidotized layers. The plagioclase and hornblende-rich layers may also represent transposed S_0 layering or bedding, which accommodated more strain and deformed in a ductile manner around the more competent epidotized knots. The sense of rotation of the knots and the contortion of the matrix are consistent with noncoaxial sinistral shear.

---

silicified.

4.1.2. The Anderson Bay Structure.

Stratigraphic facing changes in the Linda area from the northwesterly facing homoclinal sequence which extends northward to Snow Lake (*see* 2.1. Lithology and Stratigraphy), to a southeasterly facing sequence near Wekusko Lake (Figure 4.1; *see* 3.2. Stratigraphic Facing). The presence of a nearly isoclinal F_1 fold, the Anderson

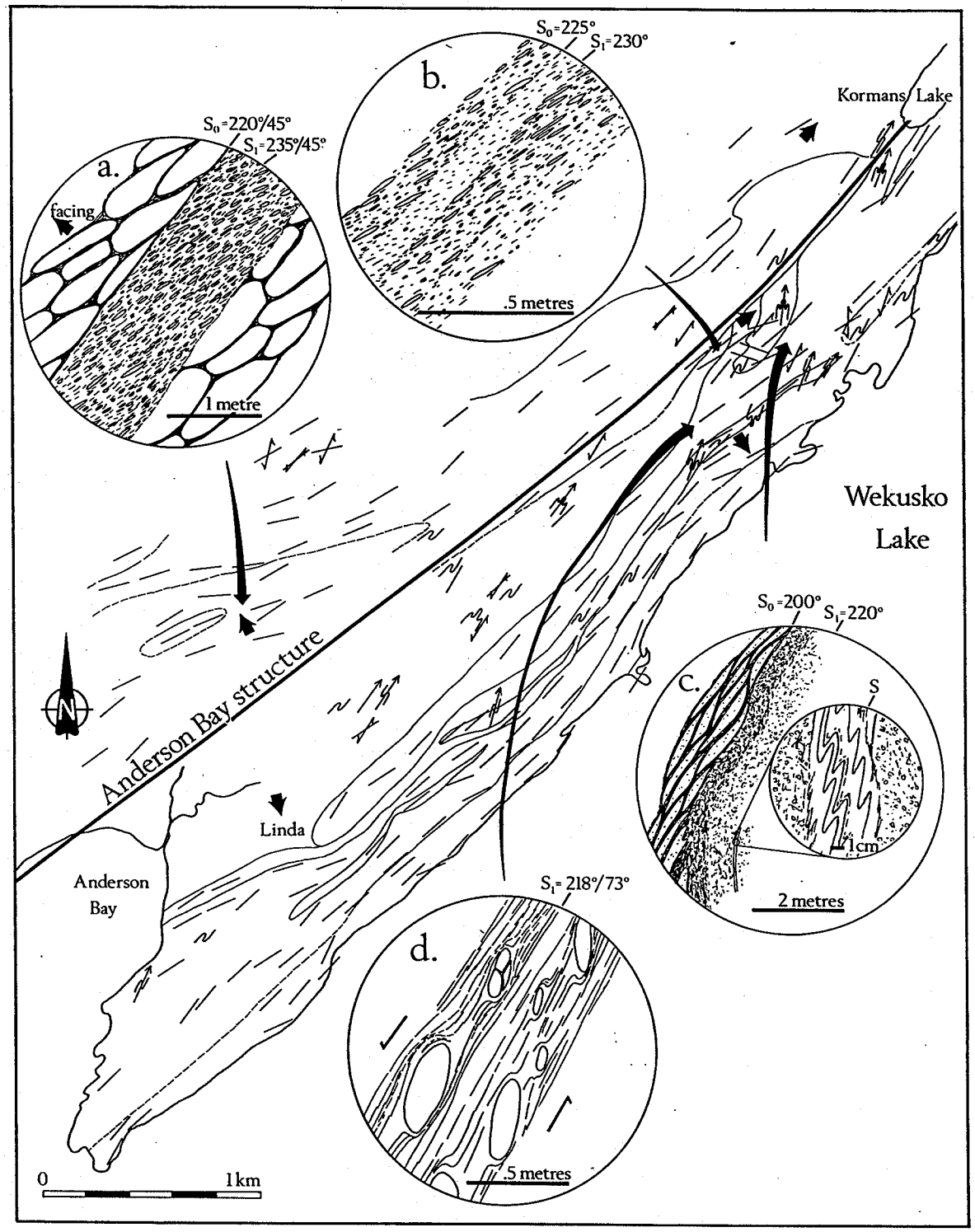
S_0=225°
S_1=230°
b.
.5 metres
Kormans Lake
S_0=220°/45°
S_1=235°/45°
a.
facing
1 metre
Wekusko
Lake
S_0=200°
S_1=220°
C.
S
1cm
2 metres
Anderson Bay structure
Linda
Anderson
Bay
S_1= 218°/73°
d.
.5 metres
0
1km

Bay anticline, with an axial trace lying between the Anderson Lake, Stall Lake and Rod deposits on the northwest limb, and the Linda deposit on the overturned southeast limb, was proposed by Falconbridge geologists (Jeffery, 1982, *unpubl.*). The felsic rocks hosting massive sulphide deposits were mapped as a continuous unit around the hinge of the anticline (Jeffery, 1982, *unpublished outcrop map*). Tight minor folds observed in drill core and on the surface were interpreted to be parasitic folds related to the major anticlinal structure. In subsurface cross-sections in which drilling extended further across strike to the northwest, intercalations of intermediate to mafic rocks (1d) within felsic rocks (unit 1) were interpreted to define the fold hinge (*ibid.*). On the basis of surface mapping, drill-hole data, and the lithological similarities of quartz-megaphyric felsic volcanic rocks in the area, Jeffery proposed a correlation between the units on each limb of the Anderson Bay anticline and interpreted the Anderson Lake, Stall Lake, Rod and Linda deposits to lie on the same stratigraphic horizon.

Outcrop mapping during this study showed that the lithological units are discontinuous and do not define a fold closure. With one exception (Figure 4.1, c), all minor folds on surface and in drill core reorient both S_0 and S_1 fabrics and were interpreted to be F_2 folds (*see* 4.2.2. F_2 Folds). Therefore, although a fold closure is suggested by the opposed facing directions, the correlation of stratigraphic units on each limb of the fold, the nature of the structure, and the precise location of the trace are problematic. The 'Anderson Bay structure' (Figures 3.1, 4.1 and 4.2) in this study, follows the trace of a lithological discontinuity, marked by the termination or lensing out of some units (Map, in pocket), and the change in facing direction.

4.1.3. Relationships of S_0 and S_1 Fabrics.

Primary contacts and bedding, and S_1 fabrics, are generally parallel in the Linda area, suggesting that this is a high strain zone. S_0 and S_1 fabrics strike mainly 220°–240° and dip 50°–70° (Figures 4.2 and 4.3). Poles to S_0 and S_1 define a strong maximum with a tendency to distribute along a great circle about a pole at 025°/35°. The partial girdle is best defined in the northeastern part of the area (Figure 4.2, b), which contains numerous F_2 minor folds (*see* 4.2.2. F_2 Folds). On the southeast side of the Anderson Bay structure, the poles define a more dispersed

girdle (Figure 4.2, c). The distribution maximum of S_0 and S_1 orientations changes slightly from 242°/55° northwest of the Anderson Bay structure, to 233°/55° in the northeast, to 225°/65° in the vicinity of the Linda deposit southeast of the Anderson Bay structure.

Three cases of slight angular deviations between S_0 contacts or bedding and S_1 flattening were observed and are illustrated and described in the insets to Figure 4.1. Northeast of Anderson Bay, heterolithic breccia has a scoured basal contact with pillowed flows and, thus, requires stratigraphic facing to the northwest (Figure 4.1, a; *see* 3.2. Stratigraphic Facing). The S_1 fabric as defined by flattened clasts and pillows shows a sinistral sense of cleavage vergence with S_0 (following Bell's (1981) definition of cleavage vergence). Note that the sinistral vergence indicates that S_1 is not axial planar to an anticline located to the southeast of this outcrop.

A sinistral sense of cleavage vergence between S_0 and S_1 was also observed in the southeasterly-facing stratigraphic sequence. Figure 4.1b illustrates felsic volcanic breccia in which flattened clasts, defining the S_1 fabric, show an oblique orientation to S_0 bedding. Similar relationships between the S_1 flattening plane and S_0 contacts are shown in Figure 4.2c. In this case, medium to coarse grained amphibole, biotite and garnet porphyroblasts obscure fine primary features, but clasts larger than about 2 cm were observed and the rock (to the southeast of the contact in Figure 4.2, c) was interpreted to be a tuffaceous metasediment. A partially covered bed (to the northwest of the contact), consists of lenticular (1–2 m × .2–.4 m), buff-coloured, cummingtonite-magnetite-bearing felsic enclaves in an anastomosing garnet-hornblende-biotite matrix. The primary derivation of the felsic enclaves is unknown; they resemble flattened silicified pillows, but could also be coarse clasts. The S_1 flattening plane is oblique to the contact. Within the tuffaceous metasediment, a thin (5 cm) cherty bed contains fine (1 mm), slightly mafic-enriched, recessive weathering laminations (Figure 4.1, c, inset). The laminations and the outer contacts of the cherty bed define asymmetrical crenulations, the axial plane of which could not be measured directly; within the broad limits, it was indistinguishable from S_1 flattening in the same outcrop. Both the S_0 contacts and the S_1 flattening plane are also involved in open flexural folds (*see* 4.2.2. F_2 Folds).

In the outcrop illustrated in Figure 4.1d, trails of epidotized knots occur in mafic volcanic rock with semi-continuous alternating hornblende-rich and plagioclase phenocryst(?)-rich layers. The long axis of the epidotized knots is oblique to layering which is asymmetrically disposed around the knots. The asymmetrical pressure shadows associated with the epidotized knots consist of contorted layered matrix material, *i.e.* to distinguish them from tails of epidotized material derived from the knots. S_1 mineral schistosity is parallel to the layers. The epidotized knots may have originated as semi-continuous layers which were subsequently boudinaged and rotated. The layering in the host rock may represent a transposed S_0 bedding or layering, which accommodated more strain and deformed in a ductile fashion around the more competent epidotized knots. The boudinage and the sense of obliquity between the long axes of the knots and the layering (S_1) indicate sinistral rotation and, thus, a sinistral sense of shear (compare Figure 4b in Driessche and Brun, 1987).

The sense of vergence of S_0/S_1 intersections remains unchanged throughout the Linda area despite the change in stratigraphic facing direction. Thus, the S_1 fabric as defined by the flattening plane and mineral schistosity does not appear to be axial planar to an anticlinal trace coincident with the Anderson Bay structure (Figure 4.1).

The orientations of the S_0/S_1 intersection lineations, as determined graphically, trend westerly and plunge 20–45°. Considerable uncertainties are associated with the trends, as the angles of intersection are small.

4.2. D_2 Deformation.

4.2.1. S_2 Planar Fabric Elements.

S_2 planar fabrics, associated with the D_2 deformational event, are defined by a crenulation cleavage which reorients the S_1 schistosity of phyllosilicate minerals, and by mineral foliation, most commonly of biotite. The crenulation cleavage is well developed in schistose altered rocks and within the schistose S_1 micaceous segregations in gneissose altered rocks and felsic volcanic rocks. Locally, a discrete S_2 cleavage overprints the S_1 fabric and, in these cases, the cleavage tends to be more continuous, penetrating into the granoblastic felsic domains. Biotite within S_1 micaceous segregations typically occurs as porphyroblasts or aggregates, elongate

Figure 4.2. (following page) Structural trend map of the Linda area, highlighting F_2 minor fold axes and fold asymmetry, and the strikes of S_0, S_1 and S_2 planes. The cleavage vergence of S_1/S_2 intersections is consistently dextral throughout the area. The insets are stereographic projections for the areas bounded by the dotted lines.

a. Northwest of the Anderson Bay structure; lineations (L) contoured at intervals of 1, 3, 6, and 10 points/1% area; poles contoured at intervals of 1, 5, 10, 15, and 20 points/1% area.

b. The area of complex structural relationships spanning the trace of the Anderson Bay structure; lineations (L) contoured at intervals of 1, 5, 10, and 15 points/1% area; poles contoured at intervals of 1, 5, 10, 15, and 20 points/1% area.

c. The vicinity of the Linda deposit southeast of the Anderson Bay structure; lineations (L) contoured at intervals of of 1, 5, 10, and 15 points/1% area; poles contoured at intervals of 1, 5, 10, 20, 30, and 40 points/1% area.

---

in the S_1 plane, but with the (001)-cleavage defining S_2. Less commonly, muscovite and chlorite occur as blades recrystallized parallel to S_2 along the hinges of the S_2 crenulation cleavage.

On the outcrop, S_2 is difficult to measure with confidence as it is developed only within the thin micaceous S_1 layers. In general, S_2 is present in felsic rocks throughout the Linda area. The strikes are generally similar to those of S_0 and S_1 fabrics (Figure 4.3) and the dips are nearly vertical or steeply inclined to the southeast. The vergence of S_1/S_2 intersections is consistently dextral throughout the area (Figure 4.2).

Some schists intersected in the subsurface have an *S–C* type of structure, and may represent zones of more intense D_2 or late D_2 shearing. In many cases, these are identifiable in the subsurface cross-sections (Sections A-A', C-C', in pocket) as zones of steeper dip (*i.e.* of lower foliation/core-axis angle). The mineralogy and textures are either non-definitive of metamorphic grade, or retrograde (*see* 5.2. Distal Alteration Zone *and* 6.4. Chlorite-Hornblende Mafic Schists).

4.2.2. F_2 Folds.

Tight to open, mesoscopic F_2 folds are relatively common in outcrops southeast of the Anderson Bay structure and in the subsurface. They reorient S_1 fabrics and S_0 lithological contacts, and range in amplitude from millimetre-scale crenulations to hectometre-scale folds (Figure 4.2; *see also* Figure 7.1 *and* Plate 7.1). On some outcrops east of the Rod minesite (Map, in pocket), S_0 contacts and parallel S_1 metamorphic fabrics have northwesterly strikes and may lie in the hinge

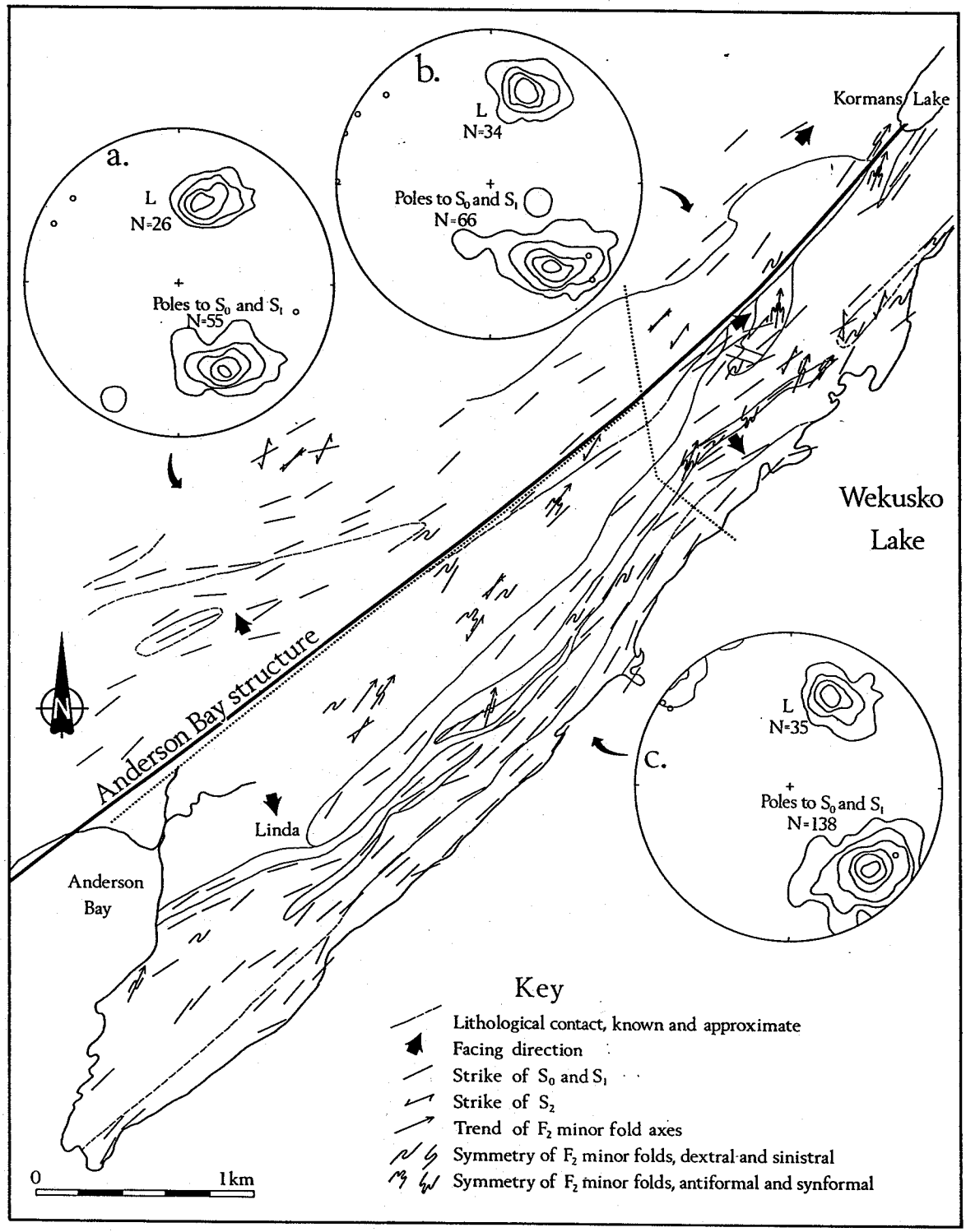
a.
L
N=26
Poles to S_0 and S_1
N=55
b.
L
N=34
Poles to S_0 and S_1
N=66
c.
L
N=35
Poles to S_0 and S_1
N=138
Kormans Lake
Wekusko Lake
Anderson Bay structure
Linda
Anderson Bay
N
0
1km
Key
Lithological contact, known and approximate
Facing direction
Strike of S_0 and S_1
Strike of S_2
Trend of F_2 minor fold axes
Symmetry of F_2 minor folds, dextral and sinistral
Symmetry of F_2 minor folds, antiformal and synformal

zones of larger scale F_2 folds. The minor folds show mainly dextral or Z-asymmetry throughout the area. Symmetrical and sinistral folds were also observed, but there was no clear pattern to their distribution. Quartz-megaphyric felsic rocks (unit 4) on the southeast of the Anderson Bay structure, contain many minor F_2 folds, both symmetrical and asymmetrical (Figure 4.2), defined by micaceous segregations or discontinuous hornblende-bearing layers (2–4 cm in width). Tight F_2 minor folds are typically 'similar' in style (Hobbs *et al.*, 1976) with a well defined S_2 axial planar mineral foliation or crenulation cleavage. The orientations of F_2 minor fold axes are essentially coaxial with the orientations of lineations (Figure 4.4). The consistently dextral vergence of S_1/S_2 intersections and the lack of systematic change in the F_2 fold asymmetry indicates that these are not likely to be related to a major F_2 fold along the Anderson Bay structure (*see also* 7.1.2. F_2 Microfolds).

Locally, S_0 and S_1 fabrics are reoriented by open flexures (*e.g.* Figure 4.1, c), typically with a wavelength of 1–5 metres and an amplitude of less than .5 metres. In some cases, they form asymmetrical kink folds with a dextral sense of vergence. These flexures are not associated with a distinct detectable penetrative fabric, and the fold axes were determined indirectly from the intersections of measured limb orientations. The flexural fold axes trend mainly north-northwest (Figure 4.4) and plunge 40°–70°, although one axis has an orientation which is indistinguishable from F_2 minor fold axes. The relationships of the flexural folds to D_2 structures is unknown and it may be that they post-date D_2 deformation (Table 4.1).

4.3. Linear Fabric Elements.

Lineations are defined by the elongation of clasts, pillows and sulphide lenses, by mineral lineations (quartz eyes, amphibole, kyanite, micas), by mineral aggregates (quartz eyes, garnet), and by intersections of planar fabric elements. The various linear fabric elements are apparently coaxial (except for S_0/S_1 intersections), but a small angular deviation would likely go undetected, especially as direct measurements were collected only on minerals and mineral aggregates. Mineral lineations were commonly measured on quartz eyes (relict megacrysts; *see* 5.3.1. Quartz Phenocrysts), the elongation of which involved a combination of strain and recrystallization. The principal flattening direction is defined by S_1 and the lineation was measured on S_1 surfaces. The lineation was therefore assigned to L_1,

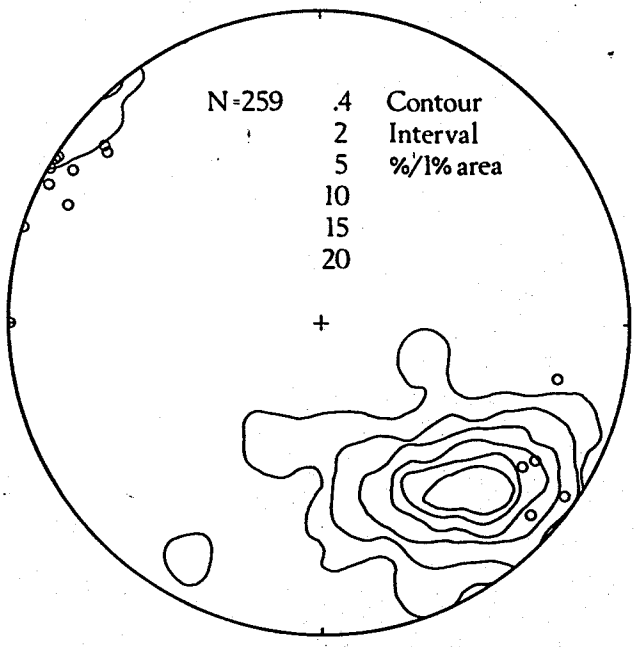

Figure 4.3. Stereographic projection of contoured poles to S_0 and S_1 in the mapped area. Fifteen poles to S_2 are indicated by circles.

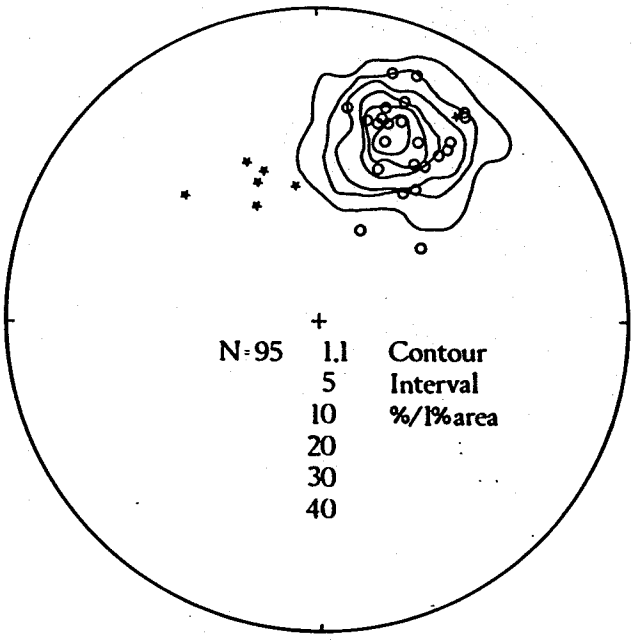

Figure 4.4. Stereographic projection of contoured lineations. Twenty-four fold axes of F_2 minor folds are indicated by circles. Seven fold axes of open flexural folds are indicated by stars.

with due note taken of the controversy regarding the origin of the lineation on a regional scale (*see* 2.2. Structure).

A slight variation in the orientation of the lineation is detectable in the Linda area. On the northwest of the Anderson Bay structure, lineations cluster about a trend of 015° with a plunge of 45° (Figure 4.2, a). To the southeast throughout most of the Linda area, the lineations define a strong distribution maximum centred on a trend of 020°–023° plunging at 35° (Figure 4.2, b and c). The main sulphide body of the deposit is elongate with an aspect ratio of at least 30:2:1, following a trend of approximately 030° plunging at 30°;this is indistinguishable from the lineations, given the accumulated uncertainties involved in subsurface projection and structural measurements. The lineations are also coaxial with F_2 minor fold axes and with a pole defined by the S_0 and S_1 partial girdle (Figure 4.4).

The S_0/S_1 intersection lineation, as determined graphically based on two locations, deviates from the general parallelism shown by other linear fabric elements. As previously noted, the occurrence of non-parallel S_0 and S_1 fabrics is uncommon in the Linda area, and possibly indicates enclaves of lower strain within the generally high strain zone.

4.4. Post-D_2 Deformation.

Locally in the drill core, very fine ($\leq$.5 mm), randomly oriented, brittle fractures cross-cut all other fabric elements. The fractures are filled with reddish-orange, hematized(?) carbonate, and a narrow zone (1–5 mm) of similar marginal alteration extends into the host rock. In some cases, the fractures form a network of sufficient density to allow the marginal alteration to coalesce, resulting in pervasively hematized carbonatized rock over .1–5 metres of drill-core intersection. There does not appear to be any rotation or displacement, other than dilation, associated with the fractures or fracture networks. They are relatively common in drill core (Sections A-A', C-C', in pocket), but with no systematic pattern apparent in their distribution.

4.5. Discussion.

Microstructural observations proved to be essential to some aspects of the interpretation of the structural geology (*see* 7. Relationships between Textures, Microstructures, Mineralogy and Deformation) and, hence, this discussion is of a

preliminary nature, based mainly on field and hand-sample observations.

The presence of a major structure between Anderson Creek and the Linda deposit is supported by several observations:

1. the change in stratigraphic facing;
2. the abrupt change in lithology in the northwestern part of the area; however, this break is subparallel to the general trend of lithological contacts;
3. the prevalence of S-C fabrics, quartz veins, and thin intercalations of felsic and mafic rocks observed in drill-core intersections at the northwestern part of the cross-sections (A-A' and C-C', in pocket);
4. the prevalence of F_2 minor folds.

Note also that the structural complexity of the Linda area apparently increases from southwest to northeast (Figure 4.2). The area in the vicinity of Kormans Lake, which was not mapped in detail (Map, in pocket), displays many F_2 minor folds and intercalations of various mafic, felsic and altered lithologies.

The only evidence in favour of a major fold closure within the Linda area is the change in stratigraphic facing direction between Anderson Creek and the Linda deposit. Unequivocal F_1 minor folds have not been observed in the Linda area and, F_2 minor folds do not show a systematic change in sense of asymmetry. The cleavage vergence between planar fabric elements (S_0/S_1, S_1/S_2) is constant throughout the area and, therefore, these fabrics are not simply axial planar to the proposed Anderson Bay anticline (Jeffery, 1982). However, microstructural observations indicate that the observed dextral cleavage vergence between S_1 and S_2 fabrics may be the result of reactivation and, thus, that changes in cleavage vergence cannot be relied on to reflect the position of the axial traces of major folds (*see* 7.5. Relationships to Megascopic Structures and Regional Isograds). In view of this ambivalence, and in recognition of the presence of a major structure of some description between Anderson Creek and the Linda deposit, the Anderson Bay structure has been introduced in this study. It follows the same trace as Jeffery's 'Anderson Bay anticline' and may represent a reactivated D_1 or pre-D_1 major fold.

The intercalation of Amisk metasediment (unit 9) with metavolcanic rocks, south of Kormans Lake, is spatially associated with the termination of quartz-megaphyric rocks (unit 4) which host the largest massive sulphide body of the Linda

deposit (*see* Figures 3.1–3.3). The overlying heterolithic breccias (unit 6a), which contain clasts of unit 4, extend further to the northeast and, in part, appear to overlie the metasedimentary intercalation. Although the stratigraphic facing direction of the metasediments in the Linda area is unknown, along strike to the northeast, immediately east of Kormans Lake, the same intercalation faces southeast (Figure 2 of Froese and Moore, 1980). Thus, a faulted relationship is implied in the Linda area, placing older Amisk metavolcanic rocks over younger Amisk pelitic metasediments. The structural relationships seem to be similar to those of the McLeod Road thrust fault, which passes about 1 km to the north of Kormans Lake (*see* Figure 2.2). However, cautionary notes are warranted; a change in stratigraphic facing is implied between the McLeod Road thrust fault and the similar fault interpreted in the Linda area and, the McLeod Road thrust fault and the possible extension of the late Berry Creek fault appear to converge in the vicinity of Kormans Lake. Structural and stratigraphic extrapolations through the area surrounding Kormans Lake are not justified.

There is no obvious evidence for the extension of a possible thrust fault to the southwest and the lithological sequence in the Linda area has been interpreted as a stratigraphic succession (*see* Figure 3.4). However, the presence of early cryptic bedding-parallel faults is a possibility.

D_1 deformation dominates the structural fabric of the Linda area and was apparently the most intense deformational event. S_1 is the principal flattening direction and, given the minor flattening associated with D_2 fabric development, it is unlikely that the pronounced L–S tectonite structure in the area is the result of an interference pattern produced by superimposed deformations. The elongation of primary structures (*e.g.* massive sulphide lenses, clasts, pillows and quartz megacrysts) is interpreted to be an L_1 stretching lineation. The L_1 and S_1 fabrics are interpreted to represent the principal elongation and flattening planes, respectively, of the D_1 strain ellipsoid.

Heterogeneous distribution of strain and strain partitioning can be partly inferred from variation in fabric development and aspect ratios. The influence of clast lithology in heterolithic breccias was previously described (*see* 4.1.1. S_1 Planar Fabric Elements) and, given the contrast in foliation development in clasts and matrix,

it can be inferred that the schistose matrix accommodated more strain, and that most of the shear-strain component was partitioned into the matrix (*e.g.* Ramsay and Huber, 1980). On a larger scale, similar relationships can be observed in the nearly massive 'cherty' felsic rocks (1a) and derived breccias (1c) intercalated with schistose rocks in the proximal alteration zone (10p).

4.6. Implications for the Snow Lake Area.

The relative temporal relationships of fabric elements in the Linda area allow the establishment of an internally consistent deformation sequence applicable to the Linda area (Table 4.1). The fabric elements can be correlated with similar elements which have a regional expression and, the observations and interpretations made in the Linda area provide constraints on the regional structure.

The most prominent features are an L-S tectonite structure of regional extent and the generally coaxial relationships of all linear fabric elements. Linear fabrics in the Snow Lake region lie in the S_1 plane, suggesting that these are, in part, L_1 structures and were transposed into mutual parallelism with L_2 linear fabric elements (e.g. F_2 fold axes). The elongation of primary features on a regional scale is proposed to be an L_1 stretching lineation, probably related to noncoaxial shearing.

Early tight to nearly isoclinal folds have been recognized locally on the basis of opposing facing directions (Bailes, 1988; Froese and Moore, 1980) and outcrop-scale F_1 minor folds have been observed in the Chisel Lake area (Galley, *pers. comm.*, 1988). However, the association of S_1 and L_1 fabric elements with early folding throughout the Snow Lake region is not well established. In zones of high strain, such as the Linda area, the relationships have been obscured by superimposed deformation and reactivation of earlier structures.

The Threehouse synform, Southeast Bay antiform and Whitefish Bay synform (*see* Figures 2.1 *and* 2.2) have been assigned to D_2 deformation and correlated with S_2 mineral foliation and F_2 minor folds (Froese and Moore, 1980). The axial planes of both the major and the minor structures strike northeasterly, parallel to the regional trends. The major fold structures, which are well defined in the vicinity of the gneiss domes, attenuate toward the south and have not been recognized in the Linda area. However, S_2 mineral foliation and, in particular, F_2 minor folds are well

developed in the Linda area. The F_2 minor folds are commonly tight and 'similar' in style, in contrast to the open flexures of the Threehouse synform and related major structures south of Snow Lake. D_2 minor structures in the Linda area seem unrelated to the Threehouse generation of major flexural folds. If this interpretation applies to the Snow Lake region, D_2 minor structures may pre-date the flexural folds of the Threehouse synform and related folds. The major fold structures may belong to D_3 deformation which may not have produced penetrative fabrics south of Snow Lake. In the Linda area, the relationship of minor open flexural folds to D_2 minor structures was not clear. Minor open folds were also reported by Jackson (1983), and it may be that these are D_3 minor structures related to the Threehouse synform. This sequence of deformational events also requires the reassignment of gneiss-dome emplacement to D_4.

Lineations of various generations and fabric elements all tend to be coaxial in the Snow Lake region, but show spatial variation. For example, lineations are oriented 065°/50° in the vicinity of the Snow Lake townsite (Galley *et al.*, 1988), 023°/35° in the Linda area, and 020°/14–23° in the Cook Lake area (Jackson, 1983). Near the Snow Lake townsite, the lineations parallel linear fabrics associated with retrograde alteration in gold-bearing shear zones (late-S_2, Galley *et al.*, 1988). This suggests the possibility that the early lineations were rotated during the late shearing.

Lineations in the vicinity of the gneiss domes show reorientation related to emplacement of the domes (Froese and Moore, 1980). The marked rotation in this area, and the apparent lack of rotation associated with the Threehouse synform and related major folds, except where the folds are also apparently influenced by the gneiss domes, has been used as evidence for the correlation of the lineations with the Threehouse structures, and for a coaxial relationship between the lineations and the Threehouse fold axis. The orientation of the Threehouse fold axis is not known independently of the lineations. An alternative interpretation of the relationships could be proposed in which the open folds of the Threehouse structures did not produce significant rotations of pre-existing lineations.

Chapter 5
Proximal and Distal Alteration Zones, and Mineralization

Two discrete alteration zones have been recognized in the subsurface, developed in dominantly felsic volcanic rocks (units 1 and 4). The altered rocks are characterized by assemblages of metamorphic minerals resulting from regional metamorphism of synvolcanic hydrothermal alteration. The extents of the distal and proximal zones were defined mainly on the basis of the occurrence of staurolite and/or kyanite, or the absence of feldspar. In addition to these alteration zones, minor alteration of lesser intensity or more limited extent includes calc-silicate rocks and silicified or 'cherty' rocks (*see* 6. Other Types of Alteration).

5.1. Location and Relationships to Stratigraphy.

The distal zone stratigraphically underlies both the sulphide mineralization and the proximal zone (*see* 3.2. Stratigraphic Facing), being separated from these by apparently unaltered, or weakly altered, felsic volcanic rocks. The mafic rocks of unit 2 end abruptly to the southwest and down-dip. The proximal alteration zone (10p), graphitic metasediment (3), and minor massive sulphide bodies (5) occur directly down-dip from unit 2 and there is no evidence for the continuation of the mafic rocks into, or beyond, the alteration zone (*see* Figures 3.1–3.3). In contrast, cherty felsic rocks (1a) extend into the proximal alteration zone (10p). The cherty felsic rocks, intercalated with intensely altered schistose rocks, occur as massive layers with little or no Fe-Mg alteration or penetrative fabric. They terminate within the alteration zone, but mineralized clast-supported breccias (1c) may represent a fragmented equivalent of the same rock. The proximal alteration zone is generally concordant to subconcordant in its down-dip extent, bifurcating around an intervening enclave of less intensely altered felsic rock. The spatial relationships between the proximal alteration zone and mafic rocks (2), cherty felsic rocks (1a), quartz-megaphyric felsic rocks (4), graphitic metasediment (3), and massive

sulphide bodies (5), persist throughout the plunge-length of the deposit, as interpreted from the cross-sections and logs of Jeffery (1982, *unpubl.*). Jeffery did not explicitly delineate a proximal alteration zone, nor propose a correlation between drill holes, although altered rocks were recorded in the drill-hole logs.

The concordancy or discordancy of the distal alteration zone, relative to stratigraphy, is difficult to assess on the basis of sections A-A' and C-C' (in pocket). The host rocks are mainly homogeneous felsic volcanic rocks without distinctive marker horizons and, therefore, clear evidence for the nature of the relationships is lacking. The minor intercalations of intermediate to mafic rocks (1d) may have lateral equivalents in the enclaves of chlorite±hornblende-bearing mafic schists (10m) within the distal zone (10d) (section A-A', in pocket). The possible correlation of these units between drill holes is poorly constrained. In cross-sections further down-plunge, Jeffery (1982, *unpubl.*) correlated these units (1d, 10m) and interpreted a marked discordancy between the mafic rocks and the distal alteration zone. He therefore concluded that the distal zone is discordant to stratigraphy. Comparison of cross-sections and logs throughout the plunge-length of the Linda deposit shows that, whereas the proximal alteration zone (10p) maintains a constant thickness and a constant relationship to the massive sulphide bodies (5), the separation of the distal and proximal zones increases from about 45 metres near the erosional surface to about 100 metres near the down-plunge limits of drilling. The separation of the distal zone (10d) and the massive sulphide bodies (5) necessarily increases in the same way. These observations imply that the distal zone (10d) is discordant to stratigraphy, cutting up-section in an up-plunge direction, *i.e.* from northeast to southwest in plan view.

5.2. Distal Alteration Zone.

The mineralogy of the distal alteration zone (10d) consists predominantly of quartz (53–80%), chlorite (2–22%) and muscovite (4–28%), the two latter minerals occurring in approximately equal modal proportions (Figure 5.1, a–b; Table 5.1, a). Most of the central volume of the zone is free of feldspar; the outer margin gradually increases in plagioclase content up to the proportions typical of the felsic volcanic host rocks ($\geq$ 30%). The altered rocks also contain 0–11% staurolite, 0–4% kyanite, 0–4% magnetite, and trace amounts to 5% Fe-sulphide minerals, mainly pyrite.

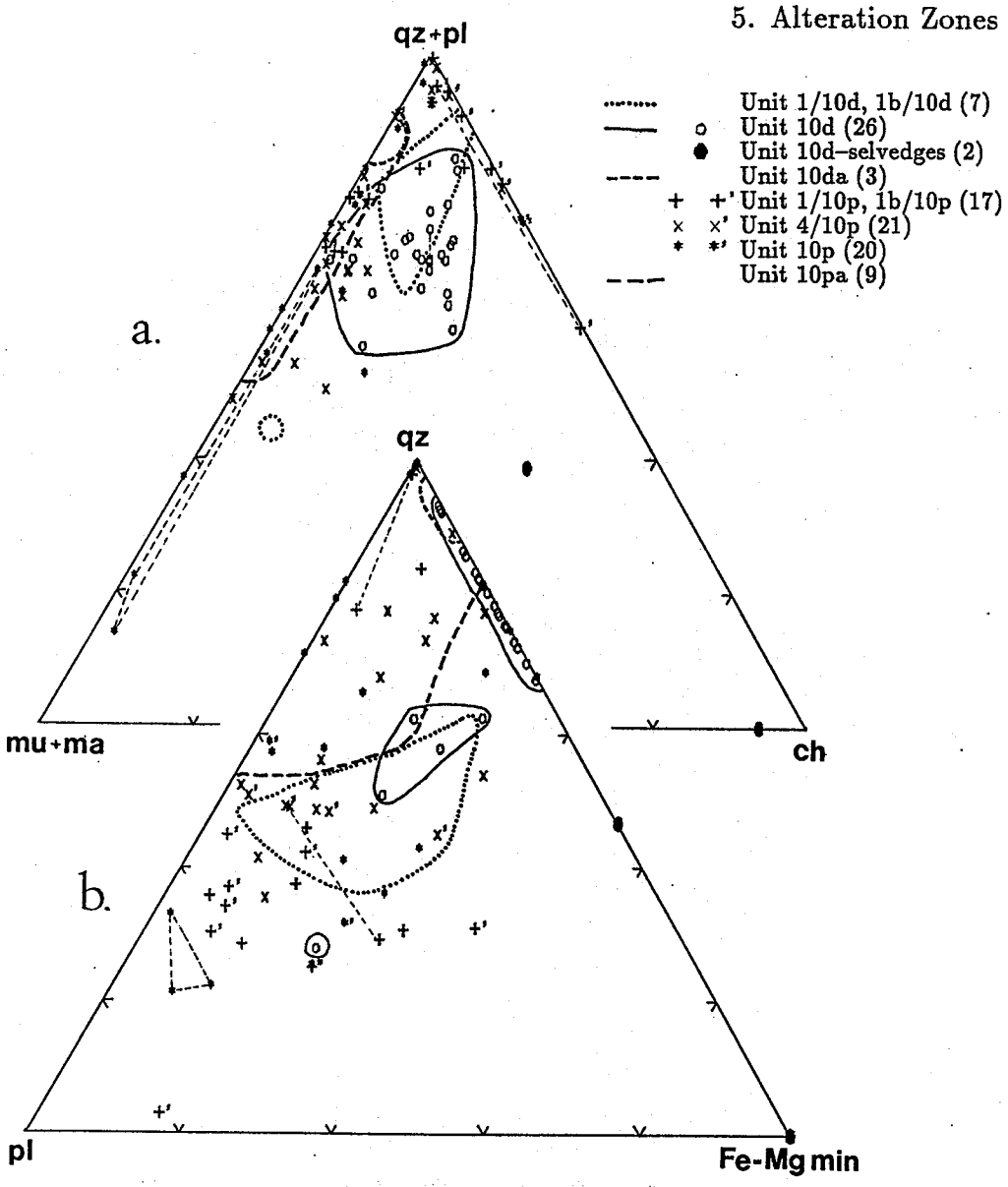

Figure 5.1. Summary of modal mineral proportions in the distal and proximal alteration zones. Field boundaries are not intended to have statistical significance. The number of points for each unit is indicated in the key in parentheses. Tie lines link enclaves which were separated from the same hand sample.

- **a.** Ternary proportions of quartz+plagioclase (qz+pl), muscovite+margarite (mu+ma) and chlorite (ch).
- **b.** Ternary proportions of plagioclase (pl), quartz (qz) and Fe-Mg silicate minerals (Fe-Mg min) consisting of garnet+biotite+chlorite+staurolite.

Margarite, biotite and garnet occur locally. Minerals present in trace amounts include tourmaline, apatite, epidote, allanite (used informally to designate metamict epidote associated with pleochroic halos), zircon, ilmenite, rutile, xenotime, monazite, sphalerite and sillimanite.

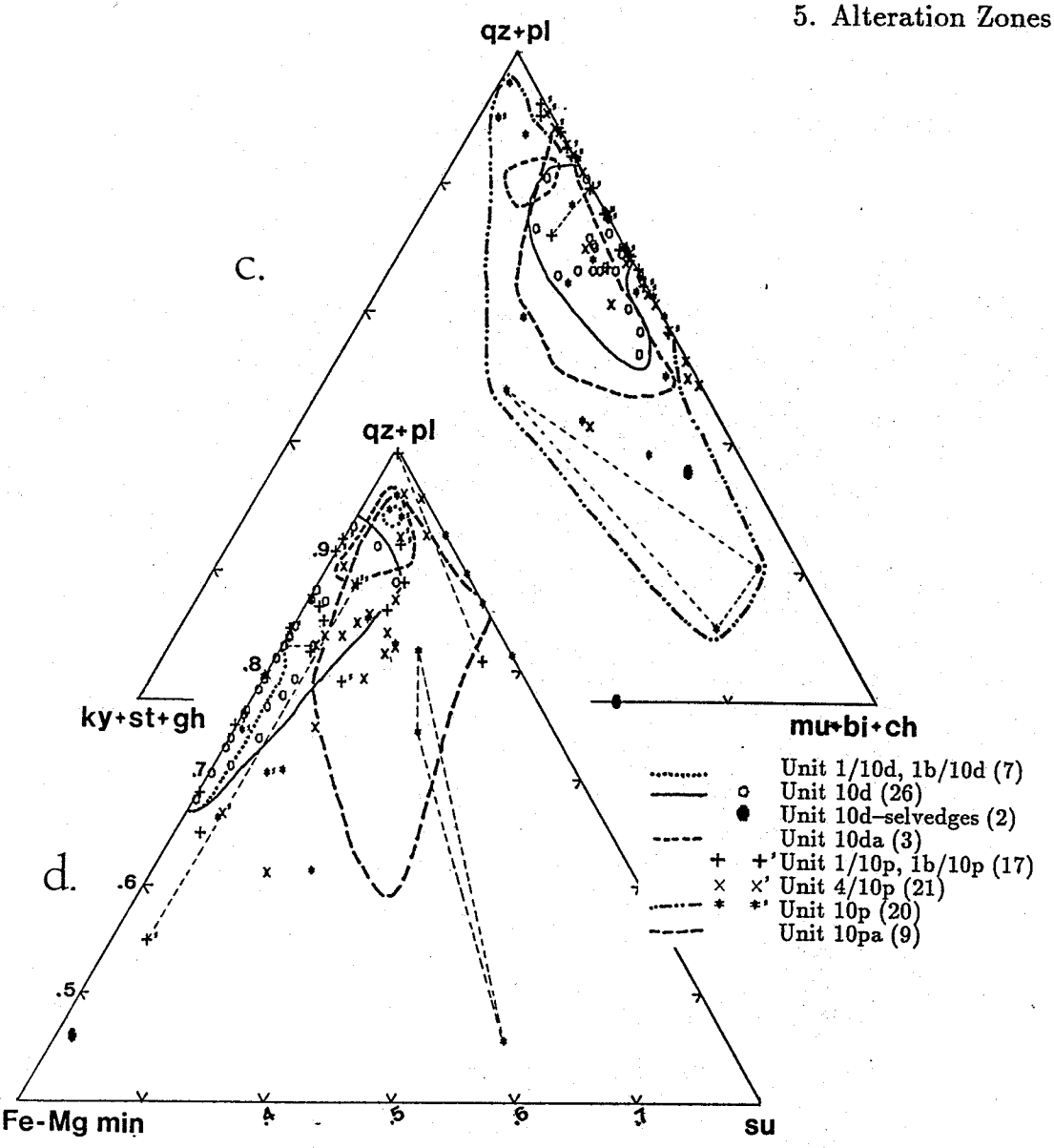

Figure 5.1. (continued).

c. Ternary proportions of kyanite+staurolite+gahnite (ky+st+gh), quartz+plagioclase (qz+pl) and muscovite+biotite+chlorite (mu+bi+ch).

d. Ternary proportions of Fe-Mg silicate minerals (Fe-Mg min) consisting of garnet+biotite+chlorite+staurolite, quartz+plagioclase (qz+pl) and sulphide minerals (su) consisting of pyrite+pyrrhotite+sphalerite+chalcopyrite.

Within the distal alteration zone, drill-core intersections of up to 5 metres in length contain an assemblage characterized by quartz, muscovite, gahnite, staurolite, and minor to trace amounts of sphalerite (unit 10da). In contrast to the common modal mineralogy of the surrounding distal alteration, muscovite is more abundant than chlorite, which occurs in amounts of less than 1% (Table 5.1). The

Table 5.1. Summary of Modal Mineral Percentages.
Ranges and averages (in parentheses) in altered rocks (Appendix A).
See 3.1. Description of Lithological Units for explanations of unit and code designations.
See Table A.2 for a key to the code and Table A.3 for mineral abbreviations.

a. Distal Alteration Zone.

Unit	Code	N	Qz	Pl	Ch	Mu	Ma	Bi	Ky	St	Gh	Gt	Py+Po	Mg
10d	o	20	53–80	0–t	2–22	4–28	0–5	0–5	0–4	0–11	0–t	0–2	t–5	0–4
			(67)	(0)	(12)	(16)	(0)	(0)	(t)	(3)	(0)	(0)	(t)	(1)
10d	vm	5	25–52	8–43	10–20	10–15	0	0–10	0–3	0–5	0	0–1	t–2	0
			(44)	(21)	(15)	(15)		(2)	(1)	(2)		(t)	(1)	
10da	o	3	74–80	0	t–1	9–14	0	t–1	0–1	2–9	t–8	0	1–5	0
			(78)		(t)	(11)		(t)	(0)	(4)	(3)		(3)	
1b/10d,	m	6	25–50	10–40	2–12	1–45	0	1–18	0	0–t	0	0–5	0–2	0–1
1/10d			(39)	(27)	(6)	(14)		(11)		(0)		(2)	(t)	(t)

b. Selvedges to Quartz Veins, Distal Alteration Zone.

Unit	Code	N	Qz	Pl	Ch	Mu	Ma	Bi	Ky	St	Gh	Gt	Py+Po	Mg
10d	womv	2	0–35	0	40–60	4–16	0	0	8–33	0–2	0	0	0–1	0

extent and boundaries of the muscovite-staurolite-gahnite assemblages are poorly delineated, in part because in some samples, gahnite and sphalerite were only recognized in thin section. However, by analogy with the proximal alteration zone in which this assemblage is common and occupies a discrete volume, a distinct alteration unit (10da) was defined to represent possible internal zoning.

Some quartz veins within the distal alteration zone are bounded by selvedges developed in the wall-rock schists and characterized by an increase in the abundance and grain size of porphyroblastic minerals, mainly kyanite and staurolite (*see* 5.5. Quartz Veins). The selvedges range in thickness up to 15 cm, grading abruptly into the host rock. Two chlorite-kyanite-muscovite schists in selvedges to quartz veins were sampled (24-277.5, 80-1571.5) and have a distinctive modal mineralogy (Figure 5.1, Table 5.1, b), with high proportions of chlorite (40 and 60%) and kyanite (8 and 33%), and low proportions of quartz (35 and 0%).

Most of the distal alteration zone has a rhythmic, banded or anastomosing, gneissic structure defined by orange-brown staurolite-rich layers (S_1), 2–8 mm in width, and buff to pale green silicic layers or lenses, 10–30 mm in width (Plate 5.1, a–b). Staurolite is elongate in the plane of the layering, typically with a single crystal occupying the full width of each layer. The layers are crenulated or

Table 5.1. (continued)

c. Proximal Alteration Zone.

Unit	Code	N	Qz	Pl	Ch	Mu	Ma	Bi	Ky	St	Gh	Gt	Py+Po	Mg
10p	mk,kr	10	5–50	0–60	t–6	t–71	0–40	0–5	2–25	0–12	0–t	0–t	t–8	0
			(27)	(20)	(1)	(28)	(5)	(2)	(9)	(2)	(0)	(0)	(5)	
10p	mys	4	37–60	0–35	1–14	8–29	0	1–10	0	4–10	0	1–6	0–5	0–t
			(50)	(10)	(4)	(17)		(7)		(6)		(4)	(3)	(0)
10p	mu	4	43–60	1–20	0–1	15–38	0	0–t	0	0–t	0–t	0	5–10	0
			(53)	(11)	(0)	(28)		(0)		(0)	(0)		(7)	
10pa		9	30–80	0–25	0–2	10–44	0–t	0–8	0–6	0–15	t–10	0–t	2–15	0
			(47)	(7)	(t)	(23)	(0)	(2)	(1)	(5)	(2)	(0)	(7)	
1b/10p	mu,mp	5	25–60	5–55	t–3	3–25	0	t–13	0–8	0	0	0–t	2–13	0
			(39)	(30)	(2)	(17)		(7)	(1)	(0)		(0)	(4)	(0)
4/10p	mkp	3	32–65	0–8	0–4	16–22	0	5–15	3–17	0–2	0	0	2–7	0
			(50)	(5)	(2)	(10)		(19)	(9)	(1)			(5)	
4/10p	mru	2	29–40	20–24	1–5	5–25	15–20	2–5	0–t	0	0	0	4–5	0
4/10p	m	12	34–60	0–47	0–11	3–50	0–t	0–12	0–1	0–1	0	0–t	t–6	0
			(44)	(19)	(4)	(24)	(0)	(3)	(t)	(0)		(0)	(3)	
4/10p	py	2	35–45	35–50	1–2	0–2	0	10	0	0	0	1	t–4	t

d. Plagioclase-layered Rocks.

Unit	Code	N	Qz	Pl	Ch	Mu	Ma	Bi	Ky	St	Gh	Gt	Py+Po	Mg
1,4,1/10p,	g	18	3–48	23–80	t–37	0–25	0–t	0–16	0–t	0–1	0	0–1	0–10	0
10p,4/10p			(31)	(43)	(9)	(4)	(0)	(6)	(0)	(0)		(0)	(2)	

corrugated (wavelength and amplitude of 1–2 cm), with recrystallization of the staurolite into moderately misoriented domains, imparting a 'wormy' appearance to the rock. Within the layers, muscovite and chlorite occur on interstices and gaps between staurolite crystals, and some sections of layers consist entirely of phyllosilicate minerals. The muscovite and chlorite form a very fine grained aggregate with a strong schistosity parallel to the layering and the staurolite elongation, and with a strong crenulation cleavage (S_2), in part wrapping around the ends of the staurolite crystals. Magnetite and biotite are commonly present, the former as subhedral porphryoblasts, up to 5 mm in size, showing flattening and tails extending parallel to the S_2 cleavage. Biotite occurs as poikiloblasts or aggregates, elongate parallel to S_1 layering and schistosity, but with (001)-cleavage planes parallel to the S_2 crenulation cleavage and crenulation axes. Biotite crystals also tend to be

Plate 5.1. (following page) Textures and microstructures of the distal alteration zone. The bar scale in each plate represents 1 mm.

a. 70-687.5 xpl (cross-polarized light) Staurolite-banded gneisses characterized by staurolite and phyllosilicate-bearing layers (A) intercalated with granular quartz-rich layers (B). A strong layer-parallel schistosity (S_1) is defined by muscovite and chlorite and, an obliquely oriented crenulation cleavage (S_2) is developed in the phyllosilicate minerals.

b. 70-687.5 xpl Detail of a, showing mimetic staurolite(st), strong crenulation cleavage (S_2) in muscovite(mu), and dark layer-parallel (S_1) trails of pleochroic haloes in biotite(bi).

c. 22-901 xpl Schist with kyanite porphyroblasts(ky) segmented and aligned parallel to the dominant schistosity (S_2) and engulfed by euhedral staurolite poikiloblasts(st) which contain quartz inclusion trails discordant to the external schistosity. Staurolite and kyanite show some coherent grain boundaries.

d. 80-1639.5 ppl (plane-polarized light) Quartz-chlorite-muscovite schist with dominant S_2 spaced cleavage and microlithons (A) which preserve a record of S_1 schistosity.

---

optically continuous across the full width of the layers. Minor amounts of quartz are present, as fine grained, lenticular inclusions in biotite, staurolite and the schistose phyllosilicate aggregate. In some cases, multiple trails of very fine grained trace minerals, mainly rutile, opaque minerals and zircon, occur parallel to the S_1 plane and, where overgrown by biotite porphyroblasts, are manifested by multiple trails of pleochroic haloes. In contrast to the staurolite-bearing layers, the intervening silicic domains are nearly massive, consisting of fine grained granular quartz with minor fine phyllosilicate blades.

Staurolite-banded gneisses grade to rocks which have a more diffuse, weakly layered structure cut by a spaced cleavage (S_2) formed by recrystallization of phyllosilicate aggregates into blades parallel to the crenulation cleavage. Rocks of this type occur both with and without kyanite and staurolite. Kyanite typically occurs as fine to coarse grained (up to 30 mm) subhedral porphyroblasts, with a preferred crystallographic orientation parallel to layering or schistosity, and defining a lineation. In some cases, the kyanite is brecciated and segmented, and the staurolite occurs as euhedral to anhedral poikiloblasts containing weakly sinusoidal trails of fine grained, lenticular quartz inclusions, with an oblique orientation relative to the external fabrics (Plate 5.1, c). Staurolite mantles kyanite and, in this case, grain boundaries between staurolite and kyanite are commonly coherent, presumably on (010)-planes in staurolite and the structurally similar (100)-planes in kyanite (Spry, 1969). Some chlorite and muscovite may be the result of retrogression, but the

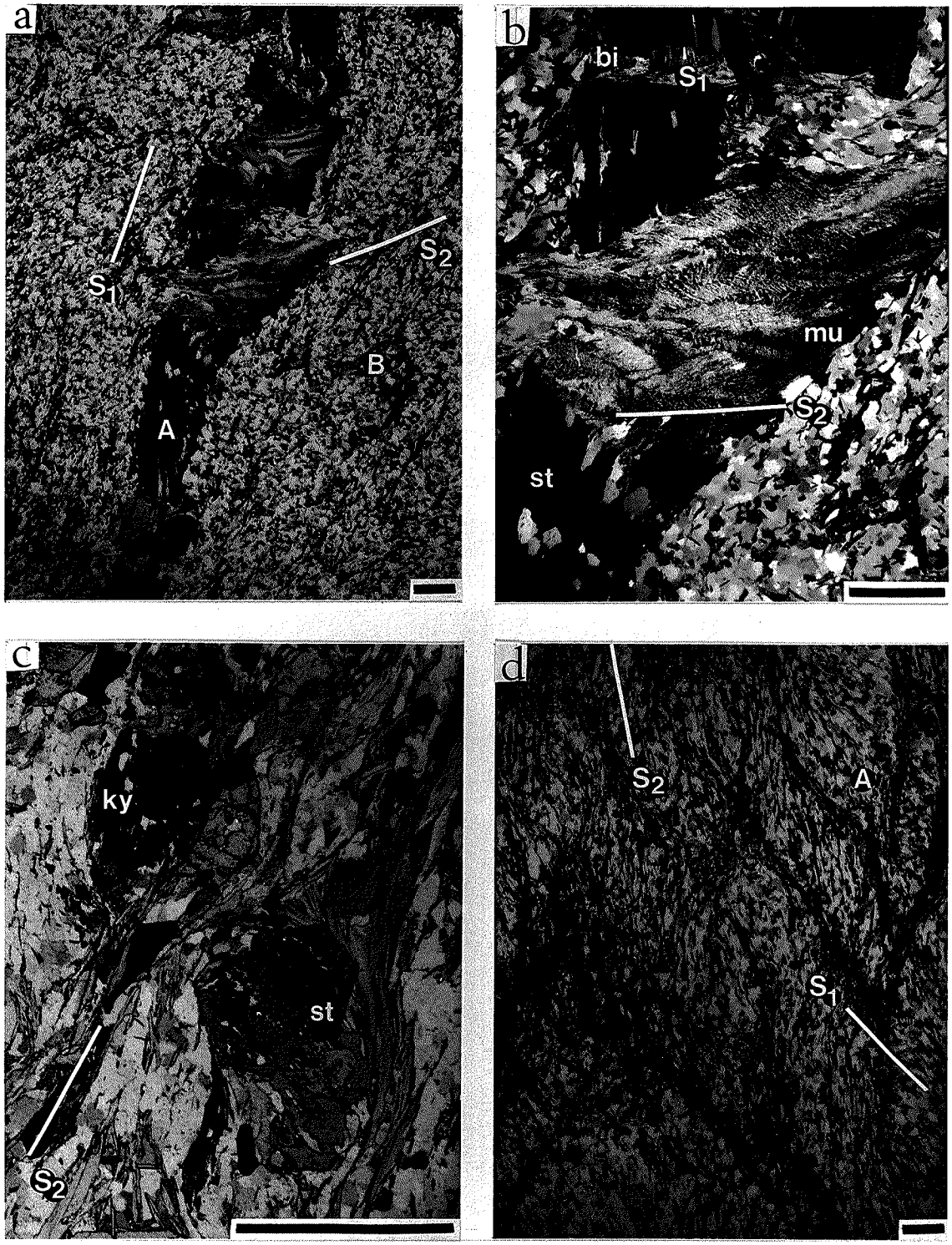
a
S1
S2
B
A
b
bi
S1
mu
S2
st
c
ky
st
S2
d
S2
A
S1

bladed habit and foliation render this difficult to distinguish from probable prograde phyllosilicate minerals.

Many quartz-chlorite-muscovite schists have a single planar fabric or show evidence of strong overprinting of an earlier schistosity and/or layering (Plate 5.1, d). For example, the rock structure may be dominated by a closely spaced (1–4 mm) cleavage (S_2) marked by concentrations of aligned phyllosilicate blades, whereas microlithons contain remnants of an oblique foliation (S_1) or intrafolial folds traced by a pre-existing schistosity. Locally, these schists have an S-C structure (Berthé *et al.*, 1979) with S and C planes defined by concentrations of aligned chlorite and muscovite.

5.3. Proximal Alteration Zone and Associated Rocks.

The proximal alteration zone (10p) envelops various lithological units and contains primary features which were relatively resistant during hydrothermal alteration, subsequent metamorphism and fabric development. These features include phenocrysts, especially quartz megacrysts (unit 4), lithic fragments in volcanic breccias (unit 1b), 'cherty' units (1a and 1c) and bedded graphitic metasediment (unit 3).

5.3.1. Quartz Phenocrysts.

The quartz megacrysts of unit 4 have been previously referred to by the non-genetic term 'quartz eyes' (Zaleski and Halden, 1988; Jeffery, 1982, *unpubl.*). Macroscopically, they have an intense blue colour and a flattened ellipsoidal shape, with tails extending in the plane of the S_1 fabric and long axes defining a lineation. The S_1 fabric, whether defined by metamorphic layering or by schistosity, is commonly deflected around the megacrysts. Microscopically, the megacrysts display a range of strain and recrystallization. This is evident from the following textural variations (Plate 5.2): monocrystalline grains exhibiting weak undulatory extinction (b–c); grains with a domainal substructure defined by slight misorientation of the crystal structure (j); grains with one or more undulatory domains showing serrate boundaries to fine grained strain-free recrystallized areas (i, k); and polycrystalline aggregates (l), in some cases, with a granoblastic-polygonal texture. Most samples show at least part of this range of megacrysts on the scale of a thin section (*e.g.* Plate 5.2, j–l), with a tendency for larger quartz grains to exhibit more strain and

Plate 5.2. (following page) Quartz phenocrysts exhibiting a progression of increasing strain and recrystallization. The bar scale in each plate represents 0.5 mm.

- **a.** 34-1500 ppl (plane-polarized light) Weakly strained embayed quartz-crystal clast in graphitic metasediment (unit 3). Embayments contain a very fine grained mixture of graphite, phyllosilicate minerals and quartz. Note that the embayment fillings are structureless, in contrast to the strong schistosity (S_1) of the matrix.
- **b.** and **c.** 22B-1974 xpl (cross-polarized light) Weakly strained embayed quartz phenocrysts (unit 4). Embayments contain a very fine grained, massive mixture of the same minerals as the matrix.
- **d.** 34-1666 ppl Quartz phenocryst (unit 4) with embayments marked by randomly oriented, very fine grained inclusions in a matrix of quartz optically continuous with the host crystal.
- **e.** 36A-1907 xpl Similar to d, but with recrystallization of the upper and lower parts of the phenocryst to polycrystalline strain-free aggregates. Mica schistosity (S_1) wraps around the phenocryst and defines asymmetrical tails at each end.
- **f.** 36A-1907 xpl Detail of an embayment in e.
- **g.** D4-15-1 xpl Quartz(qz) and plagioclase(pl) phenocrysts in unaltered or weakly altered unit 4.
- **h.** 35-1601 ppl Relict quartz phenocryst (unit 4/10p) showing domainal substructure and partial recrystallization. The phenocryst is partly engulfed by skeletal kyanite(ky) mimetic after a fine grained phyllosilicate aggregate defining S_1 schistosity, and after a bladed mineral defining S_2 foliation. The kyanite is an optically continuous single crystal.
- **i.** 35-1601 xpl Same view as h.
- **j.** 22B-2073.5 xpl Quartz phenocrysts (unit 4) with domainal substructure and slightly serrate contacts to fine grained quartz in pressure shadows.
- **k.** 22B-2073.5 xpl Relict quartz phenocryst (unit 4) dominated by two large undulatory domains with serrate contacts to fine grained, granoblastic recrystallized areas. The matrix contains phyllosilicate minerals and elongate plagioclase porphyroblasts which define an S_1 schistosity.
- **l.** 22B-2073.5 xpl Inequigranular quartz aggregate (unit 4) interpreted to be a relict phenocryst. The external contacts are discernible, although fine grained phyllosilicate minerals are also present on grain boundaries within the recrystallized area.

---

recrystallization. The external grain boundaries are usually well defined, smooth and rounded or, less commonly, subangular or with rectilinear outlines. In samples containing quartz aggregates which have irregular outlines and interlocking external contacts with adjacent grains, the aggregates may have a secondary origin, for example, hydrothermal or metamorphic.

Embayed monocrystalline and weakly substructured quartz grains were observed in several cases (Plate 5.2, a–f) in graphitic metasediment (3) and in megaphyric felsic rocks (4). The embayments contain a very fine grained, structureless

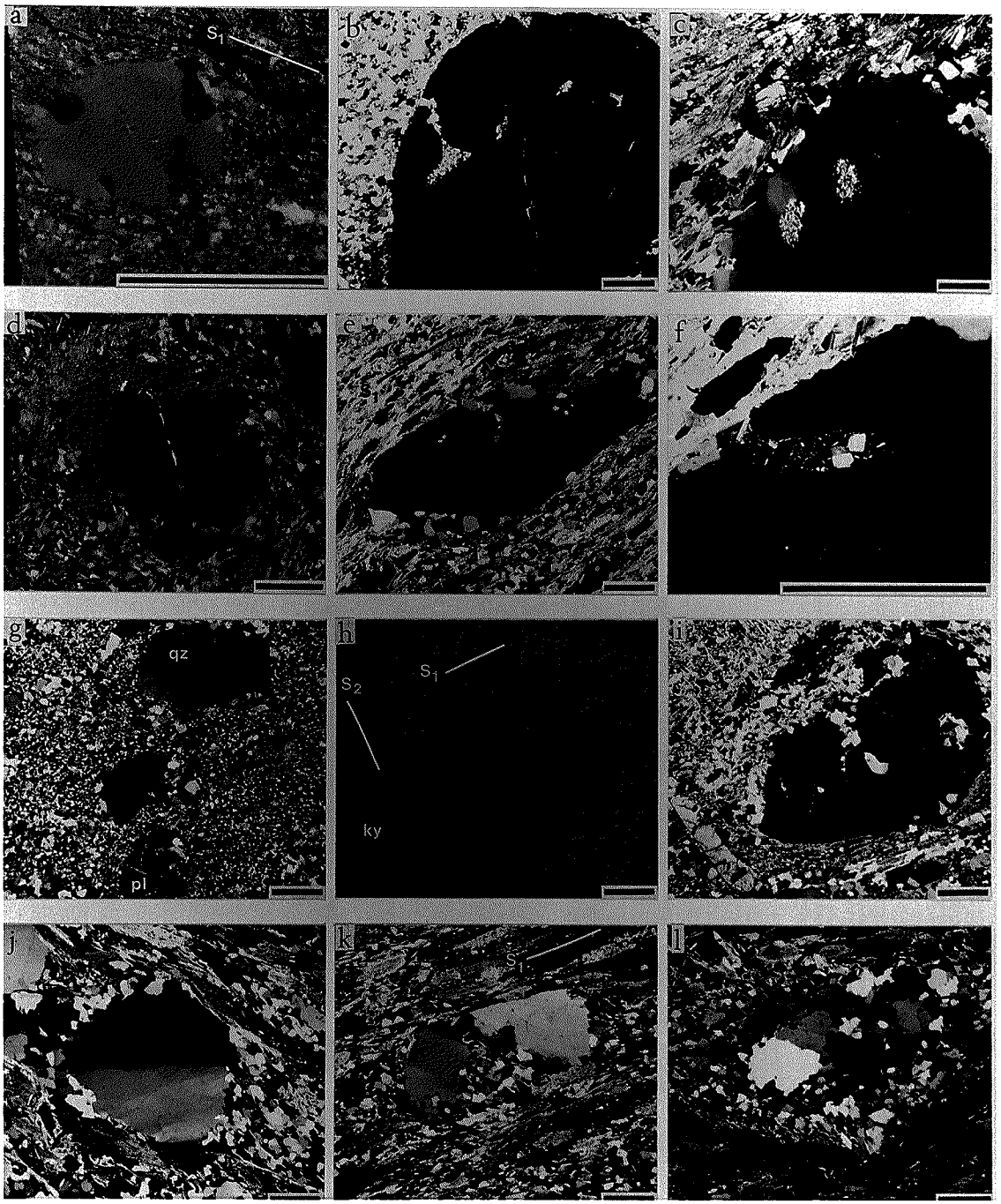
a
S_1
b
c
d
e
f
g
qz
pl
h
S_1
S_2
ky
i
j
k
S_1
l

mixture of the same minerals as the matrix of the host rock. The mineral schistosity of the host rock is absent within the embayment, which apparently acted as a pressure shadow during deformation.

Quartz megacrysts in unit 4 and its altered equivalents more commonly contain enclaves defined by a dusting of very fine grained, randomly oriented inclusions in a matrix of quartz, optically continuous with the quartz of the host grain (Plate 5.2, d–f). These enclaves have a concave form, necking toward the grain margin, and are identical in size and shape to the previously described embayments. They are interpreted to have originated as primary embayments which were subsequently filled by quartz during hydrothermal alteration, diagenesis or metamorphism. Recrystallized quartz grains and substructure domain boundaries commonly contain minor amounts of micas or other matrix minerals and may mimic embayments; therefore, the interpretation of a primary origin applies only to embayments in optically continuous areas of grains.

Monocrystalline quartz phenocrysts and undulatory domains of relict phenocrysts contain numerous extremely fine, nearly cryptocrystalline, inclusions of randomly oriented needles and hairs of rutile. These are generally absent, or of sparse occurrence, in recrystallized granoblastic quartz within pressure shadows or within the matrix. Rutile is a common trace mineral in some rocks (*see* 5.4. Plagioclase-layered Rocks), occurring as trails in plagioclase porphyroblasts.

The occurrence of embayed quartz grains, and the presence of very fine grained inclusions of rutile, is evidence for the crystallization of the quartz grains as primary phenocrysts (Vernon, 1987; 1986). Recrystallization obliterates these features, but where polycrystalline aggregates are associated with monocrystalline or weakly substructured crystals and preserve a vestige of their original shape, they can be interpreted as relict phenocrysts. Quartz megacrysts with identical habits occur in unaltered or weakly altered rocks of unit 4 (Plate 5.2, b–g) and in intensely altered mica schists of the proximal alteration zone (4/10p) (Plate 5.2, h–i). They were apparently resistant to hydrothermal alteration and, during dynamometamorphism, behaved as partially rigid inclusions in a more ductile matrix.

5.3.2. 'Cherty' Felsic Rocks and Brecciated Equivalents.

'Cherty' felsic rocks (1a) are present on three stratigraphic horizons which can

be traced into the proximal alteration zone as continuous layers, or correlated with breccias (1c) containing clasts of the same lithology. Megascopically, these rocks resemble massive plagioclase-phyric rhyolites. Chemically (*see* 11.1.1. Geochemistry of Felsic Rocks and Silicic-Feldspathic Altered Rocks), their high Na_2O and SiO_2 content indicates that they may have been albitized and silicified. Albitic plagioclase phenocrysts in the unit, and within clasts in the brecciated equivalent, occur as evenly distributed euhedral crystals, 0.2–1.5 mm in long axis, or in clusters of several grains resembling glomeroporphyritic aggregates (Plate 5.3, a). The phenocrysts have mainly simple Carlsbad twins and, in some cases, albite twins. The unit contains abundant quartz, as evenly distributed anhedral, weakly interlocking, equant grains, 0.04–0.2 mm in diameter, and rare isolated monocrystalline phenocrysts, up to 1 mm in diameter. The matrix consists of very fine grained (0.01–0.03 mm) interlocking quartz and albitic plagioclase with a weak fabric defined by preferred dimensional and crystallographic orientation. In some cases, quartz is also present on irregular semi-continuous veinlets, 0.25–1 mm in width, with contacts weakly interlocking with the matrix. Some veinlets cut plagioclase phenocrysts. Magnetite commonly occurs as finely disseminated grains and as euhedral porphyroblasts up to 2 mm in size, in one sample, with fine ($\leq$.25 mm) epitaxial quartz fibres in pressure fringes elongate parallel to the S_1 plane.

The breccias of unit 1c contain angular interlocking clasts, in general similar in texture and mineralogy to rocks of unit 1a (Plate 5.3, b). The width of the fractures is variable on a small scale, from a maximum width of 10 mm, to fractures which narrow and terminate. The matrix is dominated by subhedral Fe-sulphide minerals, mainly pyrite, by granoblastic-polygonal quartz, coarser in grain size (0.1–0.5 mm) than quartz within the clasts, and by fine ($\leq$.4 mm) muscovite blades and matted aggregates. Minor biotite, gahnite, chlorite and tourmaline are also present. The fractures and clasts define a very weak flattening (S_1) and lineation. Within the matrix, oblique to the flattening direction, sulphide minerals and aggregates show a strong dimensional fabric and muscovite blades define a schistosity (S_2). Small clasts ($\leq$5 mm) included within the matrix show flattening and elongate tails parallel to the S_2 mineral foliation. It appears that these breccias may have been mineralized mainly by the infilling of dilational structures.

Plate 5.3. (following page) 'Cherty' felsic rocks (unit 1a) and brecciated equivalents (unit 1c), matrix-supported breccias (unit 1b/10p), and bedding surfaces in metasedimentary rocks (units 3 and 10p). The bar scale in each plate represents 1 mm.

a. 34-1306.5 xpl (cross-polarized light) 'Cherty' felsic rocks (unit 1a) with plagioclase phenocrysts and glomeroporphyritic aggregates.

b. 34-1443.5 xpl Mineralized breccia (unit 1c) with plagioclase-phyric clasts of unit 1a and fractures filled by pyrite, muscovite and quartz. The trace of the fractures and flattening of the clasts defines a weak fabric (S_1). Pyrite and muscovite in the fractures define an oblique mineral foliation (S_2).

c. 22A-1752 partial xpl Matrix-supported breccia within the proximal alteration zone (1b/10p) with fine grained felsic clasts (A) in an intensely altered matrix (B) containing pyrite, kyanite and staurolite porphyroblasts, muscovite, quartz and plagioclase. Fabric development is weak and partly related to the local distribution of clasts.

d. 22A-1752 partial xpl Detail of c, showing mineralogical zoning around clast margins. The quartz-rich core (A) is mantled by an inner zone is enriched in muscovite (B); multiple semi-continuous trails of very fine grained tourmaline needles (C) trace slightly disharmonic microfolds around the clast margins. The orientation of the muscovite schistosity partly conforms to clast margins, and shows crenulation and some recrystallization which may be axial planar (S) to the microfolds. Kyanite(ky), pyrite(py), muscovite(mu) and quartz are visible in the matrix.

e. 34-1500 ppl (plane-polarized light) Bedding in graphitic metasediment (unit 3) defined by variations in the abundance of finely disseminated graphite (opaque laminae), Fe-sulphide minerals(su) and silicate minerals, including elongate and square quartz-crystal clasts(qz), margarite(ma) defining a strong bedding-parallel schistosity (S_1), and coarse grained kyanite poikiloblasts (ky) engulfing quartz and graphite trails.

f. 24-812 ppl Bedding surface (S_0) marked by a sharp change in mineral proportions, especially euhedral pyrite (black). The staurolite porphyroblast(st) overgrows bedding and S_1 muscovite(mu) schistosity.

5.3.3. Matrix-supported Volcaniclastic Breccias.

Matrix-supported volcaniclastic rocks (1b) dominate the upper part of the stratigraphic sequence of felsic volcanic rocks (1) and apparently represent the main protolith and host rock to the proximal alteration zone (10p). Similar rocks are also present locally on the periphery of the distal alteration zone (10d). Within the alteration zones, volcaniclastic rocks are generally recognizable only on the margins or in less altered enclaves. Identification is probably biased toward breccias containing lithic clasts of an intermediate size range, *i.e.* medium to coarse lapilli, with finer clasts obscured by overgrowths of phyllosilicate and poikiloblastic minerals, and recognition of coarser clasts limited by the diameter of the drill core (2.5 or 3.5 cm). Flattening of the clasts defines the S_1 fabric, in most cases, with a parallel

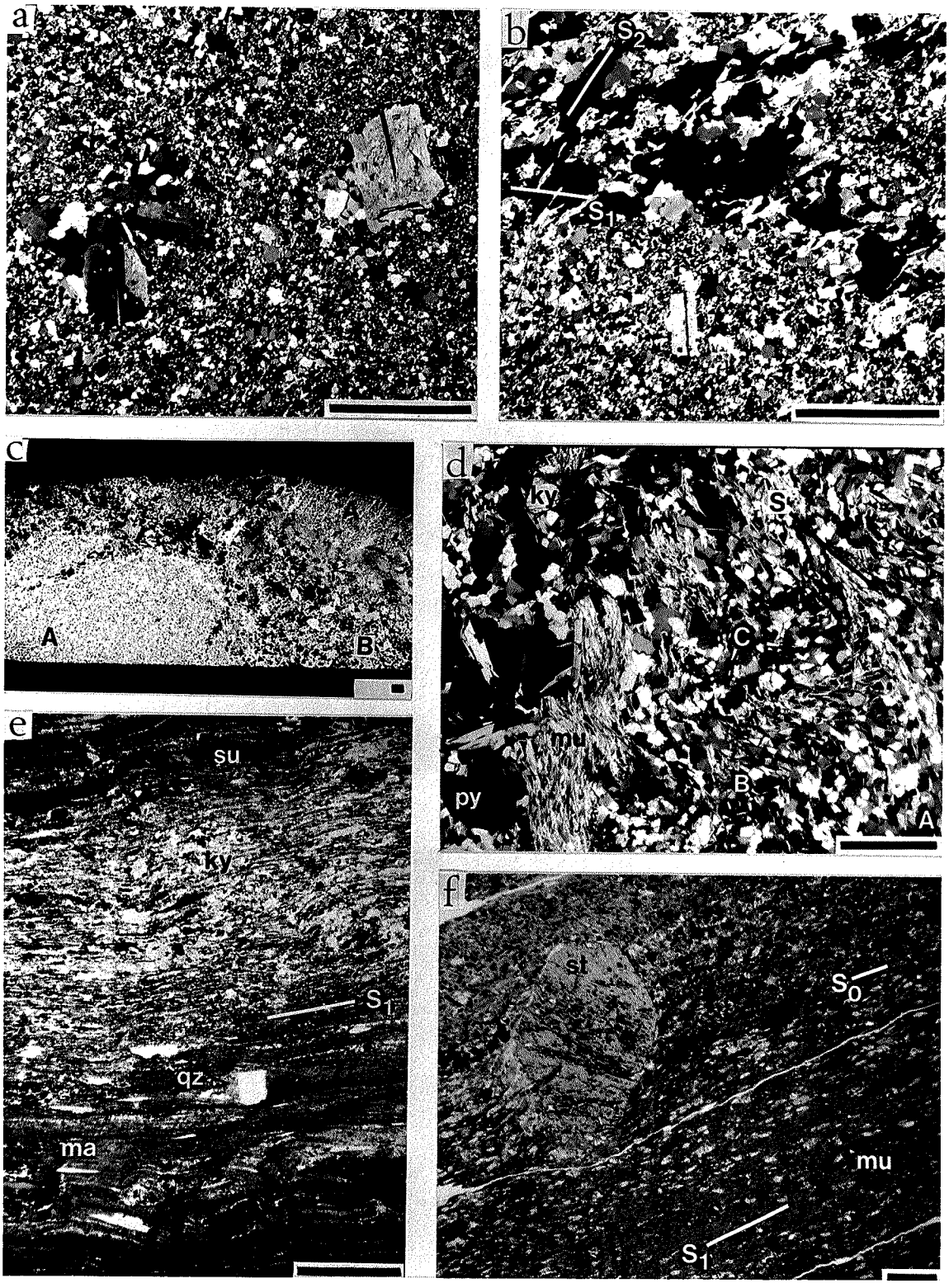
a
b
S_2
S_1
c
A
B
d
ky
S
C
mu
py
B
A
e
su
ky
S_1
qz
ma
f
st
S_0
mu
S_1

S_1 mineral foliation. The clasts consist of fine grained (0.05–0.2 mm) interlocking or granoblastic-polygonal quartz and plagioclase, with minor fine grained phyllosilicate minerals showing a weak foliation and, locally, with minor isolated quartz and plagioclase phenocrysts. Isolated quartz phenocrysts also occur in the matrix. The contacts between clasts and matrix are marked by: an abrupt change in grain size and texture of quartz and plagioclase to the coarser grained inequigranular and interlocking grains in the matrix; increased abundance of ferromagnesian minerals including micas, chlorite, and Fe-sulphide minerals; and more pronounced fabric development. The matrix generally shows a strong mineral schistosity parallel to flattening (S_1), and an oblique crenulation cleavage and schistosity (S_2). These fabrics, particularly the S_1 schistosity, conform to the lenticular outer margins of the clasts. Matrix plagioclase occurs in various habits, as fine untwinned grains intergrown with quartz, as strongly zoned porphyroblasts either equant or elongate parallel to flattening (S_1), and as poikiloblastic grains, mimetically overgrowing S_2 crenulations.

Matrix-supported breccias, with up to about 50% intensely altered matrix material were observed, in rare cases, within the proximal alteration zone (Plate 5.3, c–d). The clasts are composed of fine grained (0.05–0.1 mm) granoblastic-polygonal quartz-rich aggregates, with minor fine muscovite blades and poikiloblastic plagioclase of oligoclase composition. In this case, the clasts show zoning along contacts with the matrix, consisting of a muscovite-rich zone of about 1 mm width, and external to this, one or several concentric semi-continuous trails of fine grained tourmaline needles. The matrix contains subhedral pyrite and pyrite aggregates, kyanite, staurolite and plagioclase porphyroblasts (andesine), muscovite and chlorite blades, quartz, and trace amounts of biotite, tourmaline and rutile. The quartz occurs as granoblastic to weakly interlocking aggregates, texturally similar to those found in the clasts. Some clasts are surrounded by abundant plagioclase poikiloblasts and it is not clear whether the feldspar occurs in the clast margins or in the matrix. Muscovite schistosity partly conforms to the clast margins, and crenulation and minor recrystallization appears generally axial planar to slightly disharmonic microfolds traced by tourmaline trails along the clast margins (Plate 5.3, d). The folds and the trails defining them are best developed along clast margins oriented

perpendicular to the S_2 mineral foliation, being discontinuous or absent along margins parallel to the S_2 plane. Fabric intensities and orientations are locally variable, apparently conforming to local strain distribution as influenced by the distribution of matrix and clasts.

5.3.4. Metasedimentary Rocks.

Metasediments showing bedding surfaces can be recognized only within the proximal alteration zone, and graphitic metasediment (3) forms a discrete mappable unit. Bedding in this unit is defined by variation in the proportions of Fe-sulphide minerals, graphite and silicate minerals. Some beds consist of massive or semi-massive stratiform pyrrhotite and pyrite mineralization. Finely disseminated graphite forms thin (1 mm) laminar beds intercalated with phyllosilicate-rich beds, 1–10 mm in thickness. These beds contain many monocrystalline quartz-crystal clasts, in some cases, showing square euhedral habits and embayed margins, as previously described (Plates 5.2, a; 5.3, e). More commonly, the quartz-crystal clasts are lenticular. The matrix consists of fine grained quartz, abundant margarite and kyanite, minor muscovite, chlorite, phlogopite, and trace amounts of tourmaline, sphalerite, chalcopyrite and arsenopyrite. The margarite is strongly aligned parallel or subparallel to the bedding and quartz elongation. Kyanite occurs as coarse (0.25–20 mm) poikilitic or skeletal porphyroblasts, randomly oriented and overgrowing bedding. Inclusion trails and zones of finely disseminated graphite form asymmetrical microfolds within the kyanite porphyroblasts.

Locally within the proximal alteration zone, isolated bedding surfaces were intersected by drilling. These are marked by an abrupt asymmetrical change in mineral proportions, especially in the abundance of fine grained (0.05–1 mm) subhedral to euhedral disseminated pyrite (Plate 5.3, f). The best example occurs in sample 24-812, in which the bedding surface is also marked by an abrupt change in the abundances of quartz, plagioclase, muscovite, biotite, staurolite, tourmaline and rutile. Variations in the abundance and grain size of pyrite define very thin (0.25–1 mm) lenticular grading. Coarse (5–30 mm) kyanite porphyroblasts are present throughout, but are very abundant on some zones (5–10 mm in thickness) parallel to, but not obviously related to, the discrete bedding surface. Plagioclase and quartz occur as single grains (0.02–0.5 mm in length) or as aggregates with diffuse

margins intergrown with fine muscovite which is also present in interstices within the aggregates. The elongation of plagioclase grains and aggregates, and muscovite schistosity define a strong S_1 fabric which shows a slight but consistent obliquity to the bedding surface (S_0). Kyanite porphyroblasts define a lineation parallel to the S_1 fabric, and contain inclusion trails of pyrite, quartz and plagioclase, which show a consistent sense of obliquity to the external schistosity (S_1). Kyanite and staurolite porphyroblasts have discontinuous pressure fringes of epitaxial, weakly pleochroic, high-Mg chlorite. A crenulation cleavage (S_2) is present in the muscovite schist of the matrix. Where kyanite porphyroblasts are abundant, they show kinking with impingement and deformation of adjacent grains; the principal flattening plane is oblique to S_1 schistosity, and apparently parallel or subparallel to the S_2 crenulation cleavage.

5.3.5. Proximal Alteration Zone.

In the porphyroblastic schists of the proximal alteration zone (10p), the mineralogy is dominated by muscovite (mainly 5–40%) and, with infrequent exceptions, all assemblages contain muscovite, quartz and pyrite (Figure 5.1, Table 5.1, c). Minor to trace amounts of chlorite are common. Feldspar-absent rocks have a wide distribution in isolated occurrences without a discernible pattern. Pyrite, and Fe-sulphide minerals in general, are notably more abundant (0–10%) than in the distal alteration zone (Figure 5.1, d). The altered rocks also contain kyanite (0–25%), staurolite (0–12%), biotite (0–10%), and less commonly, garnet (0–6%). Margarite is locally abundant (up to 40%), particularly in altered metasediments. A bright green chromian muscovite, associated with titanite (up to 1%), occurs in thin zones ($\leq$ 5 cm of drill-core intersection) on both the hanging-wall and footwall peripheries of the largest massive sulphide body. Minerals commonly present in trace amounts include tourmaline (but up to 3% is present in some schists), apatite, epidote, allanite, zircon, sillimanite, rutile, xenotime, pyrrhotite, sphalerite, monazite, and chalcopyrite, and less commonly, ilmenite, arsenopyrite and galena (one occurrence).

Layering in the proximal zone is generally more diffuse and more variable in scale and definition than in the distal zone. Layering of medium thickness (0.5 cm–20 cm) is defined by differences in mineralogy or modal abundances of phyllosilicate,

Plate 5.4. (following page) Textures and microstructures of the proximal alteration zone. The bar scale in each plate represents 1 mm.

a. 22A-1638 partial xpl (cross-polarized light) Layering (S_1) defined by a quartz-rich zone (A) with disseminated muscovite, and by a porphyroblastic zone (B) containing skeletal kyanite and staurolite. The axial planes of corrugation in the layering and of a crenulation cleavage (S_2) are parallel to the elongation of pyrite aggregates (black).

b. 22A-1638 partial xpl Detail of a, showing a strained kyanite porphyroblast(ky) with crystallographic preferred orientation parallel to layering (S_1). Staurolite(st) mantles the kyanite with some coherent grain boundaries.

c. 22A-1638 partial xpl Detail of a; kyanite porphyroblasts(ky) show strain related to transposition into parallelism with the crenulation cleavage in muscovite(mu) and mimetic staurolite(st). The skeletal staurolite does not show undulatory extinction.

d. 34C-1377 partial xpl The core of a subhedral staurolite porphyroblast(st) is skeletal and appears to be mimetic after bladed or fibrous and porphyroblastic minerals. The outer margin contains few inclusions. Muscovite schistosity in the matrix partly conforms to the staurolite grain boundary.

e. 34-1539 ppl (plane-polarized light) Subhedral gahnite porphyroblasts with skeletal structure mimetic after layering (S_1). Muscovite defines an S_2 schistosity.

f. 19B-785 xpl Plagioclase porphyroblasts(pl) are dimensionally elongate parallel to layering (S_1) and contain numerous very fine, oriented inclusions of margarite (giving the mottled texture). Granoblastic aggregates of quartz(qz) are present between and within plagioclase grains.

---

porphyroblastic and sulphide minerals (Plate 5.4, a). Second order layering (0.1–5 mm) is commonly defined by the skeletal structure of mimetic porphyroblastic minerals, including kyanite, staurolite, gahnite, garnet and plagioclase (*e.g.* Plates 5.4, e; 7.2, b–e; 9.1, a). In many cases, the layering defined by poikiloblasts is rotated with respect to layering in the matrix.

Porphyroblastic minerals have a wide range of grain size up to about 1 cm, but more commonly less than 0.5 cm. Kyanite porphyroblasts showing a layer-parallel crystallographic foliation (S_1) commonly exhibit strain associated with transposition into the S_2 direction (Plate 5.4, a–c). As in the distal zone, in some cases, staurolite mantles kyanite with coherent grain boundaries between the two minerals (Plate 5.4, b). Kyanite, staurolite and gahnite occur in habits mimetic after S_1 layering and S_2 crenulation cleavage (Plate 5.4, c; *see also* Plate 7.2, c–e). In some cases, subhedral crystals of staurolite have an internal skeletal structure which appears mimetic after bladed and porphyroblastic minerals, and a thin outer zone (0.05–0.2 mm) which is nearly clear of inclusions (Plate 5.4, d).

The proximal zone has a Zn-rich core (10pa), characterized by assemblages in-

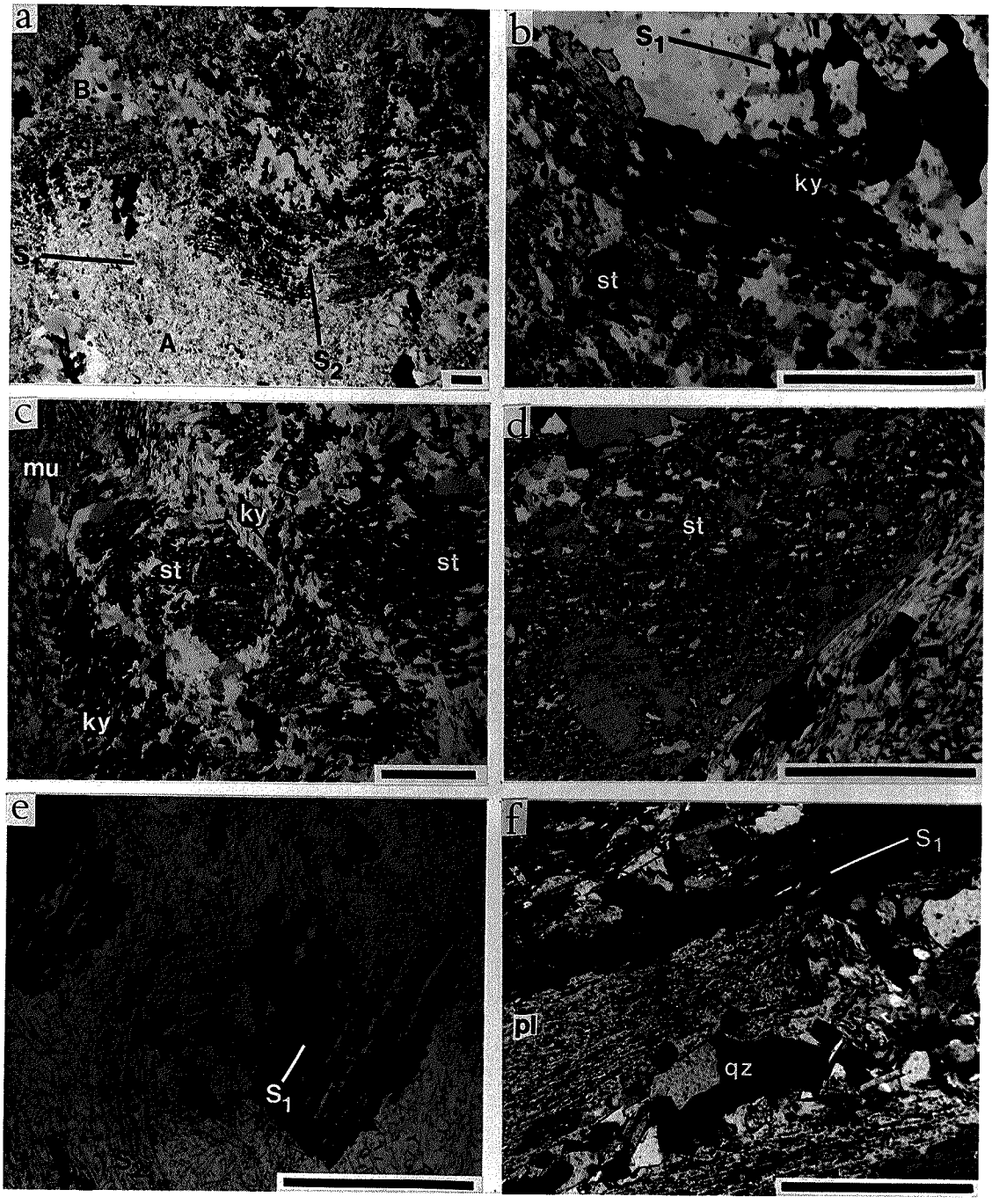
a
B
S1
A
S2
b
S1
ky
st
c
mu
ky
st
st
ky
d
st
e
S1
f
S1
pl
qz

cluding quartz (30–80%), muscovite (10–44%), gahnite (trace–10%) and Fe-sulphide minerals (2–15%), mainly pyrite (*e.g.* Plate 5.4, e). In most cases, staurolite is present (0–15%), as well as minor to trace amounts of sphalerite. The staurolite is pale orange-brown to yellow in hand sample and nearly non-pleochroic in thin section, apparently indicative of its low-Fe, Zn-rich composition (*see* 9.1.3. Staurolite and Gahnite). The unit has lower abundances of plagioclase (0–25%) and chlorite (0–2%) than the enveloping volume of the proximal zone. Biotite and kyanite are locally abundant in amounts of up to 8% and 6%, respectively.

The Zn-rich core zone (10pa) envelops graphitic metasediments (3) and associated non-graphitic silicate-rich metasediments, and massive and semi-massive sulphide mineralization (5). These rocks contain abundant pyrite and minor sphalerite, but usually, no gahnite. The volume enveloping the graphitic metasediments and associated sulphide lenses and extending approximately to the lower stratigraphic limits of unit 4/10p locally contains isolated bedding surfaces as previously described (*see* 5.3.4. Metasedimentary Rocks; *and* Plate 5.3, f). In many cases, rocks in this volume show diffuse layering, 5–50 mm in thickness, defined mainly by variations in the modal abundances of muscovite, margarite, plagioclase, quartz and kyanite. Phyllosilicate minerals define a layer-parallel crystallographic preferred orientation (S_1). Plagioclase occurs as poikilitic layer-parallel lenticular grains (0.1–5 mm in length) or aggregates containing numerous fine grained ($\leq$.05 mm) oriented (S_1) inclusions of margarite (Plate 5.4, f). Kyanite occurs as coarse grained (up to 1 cm) skeletal unoriented(?) porphyroblasts. Plagioclase in these rocks appears to have replaced margarite. The layering is possibly partly of sedimentary origin.

Plagioclase occurs as coarse grained (2–8 mm) porphyroblasts with zoning outlining a well defined annular ring structure of more calcic composition (labradorite-bytownite) (*see also* 5.4. Plagioclase-layered Rocks). In some cases, the plagioclase has undergone retrogression and is partially or completely pseudomorphed by a brownish-green, very fine grained, massive aggregate consisting of muscovite, calcite, chlorite, epidote(?) and, in some cases, margarite. The retrograde replacement is notably more intense in the calcic zones of porphyroblasts and tends to enhance the annular structure. Macroscopically this is manifested by the presence of brown ring structures, either in isolation or aggregated (depending on the distribution of

feldspar) and bearing a superficial resemblance to oolites. Retrogression of feldspar, and consequently the presence of brown 'oolites', is prevalent in altered metasediments, although other metamorphic minerals are not affected.

Calcite occurs locally in minor to trace amounts in metasediments, associated with retrogression as in the plagioclase, or associated with late cross-cutting structures. For example, calcite fills brittle dilational veinlets (up to 1 mm in width) in graphitic metasediment, occurring as fibres oriented perpendicular to the vein walls. The veinlets are oriented both parallel and perpendicular to bedding and mineral schistosity. Calcite and quartz are also present on veins up to 5 mm in width.

5.4. Plagioclase-layered Rocks.

A distinctive type of plagioclase-bearing rock, defined mainly on the basis of textural and microstructural criteria, contains abundant coarse grained (2–5 mm) plagioclase porphyroblasts. These rocks do not constitute a mappable unit, as their recognition partly depends on petrographic examination. They are most common in the uppermost part of the proximal alteration zone, stratigraphically above the small massive sulphide bodies and, especially, on the periphery of the largest massive sulphide body and its up-dip and down-dip extensions. Their occurrence is not limited to the alteration zone; they are also observed in quartz-megaphyric felsic rocks (4) and in felsic volcanic rocks (1) where these are intercalated with quartz-megaphyric rocks in the uppermost part of the sequence.

The modal mineralogy of plagioclase-layered rocks coincides with that of felsic volcanic rocks high in plagioclase and ferromagnesian minerals (Figure 5.1; Note that plagioclase-layered rocks have a 'prime' superscript affixed to the normal symbol for the unit in which they occur.). They generally contain high abundances of chlorite and biotite, and low abundances of muscovite and sulphide minerals, relative to the typical rocks of the proximal alteration zone.

The rocks are characterized by layers, 1–10 mm in thickness, of alternating plagioclase-rich and quartz-rich mineralogy. Phyllosilicate minerals are associated with plagioclase layers and, where abundant, form a schistose matrix to the plagioclase porphryoblasts. Plagioclase porphyroblasts and aggregates are elongate in the plane of the layering, but lack any preferred crystallographic orientation. The plagioclase layers are traversed by layer-parallel swarms of semi-continuous inclusion

Plate 5.5. (following page) Plagioclase-layered rocks with rutile trails. The bar scale in each plate represents 0.5 mm.

a. 29-1092 ppl (plane-polarized light) Multiple inclusion trails of fine grained rutile prisms occur in swarms (A) continuous across the section and are associated with coarse grained plagioclase porphyroblasts which are elongate parallel to the trails (S_1). Medium grained mica blades define an obliquely oriented schistosity (S_2). Some plagioclase porphyroblasts and their included trails show a slight rotation apparently due to a component of layer-parallel shortening. Note the colliform shape of plagioclase grain boundaries to phyllosilicate minerals (B).

b. 34C-1831 xpl (cross-polarized light) Quartz(qz) trails in plagioclase(pl) commonly consist of aggregates, with a width of one quartz grain.

c. 22A-1788 ppl Trails and clots of fine rutile prisms, defining S_1, outline a porphyroclastic relict quartz phenocryst and its recrystallized tails. The phenocryst contains numerous very fine, randomly oriented needles of rutile (not visible).

d. 22A-1788 ppl Detail of b. Rutile(ru) trails and clots outline the tail of the porphyroclast. Some fine mica blades(mc) are also present. Poikiloblastic calcic plagioclase forms an overgrowth (pl, high relief).

e. 19-1237b xpl Plagioclase aggregates with compositional zoning defining an annular structure. The rings are narrow zones of high An-content. Note that the zoning is commonly continuous across several plagioclase grain boundaries.

f. 19-1237b xpl Detail of f. Compositional zoning encompasses several plagioclase crystals, mainly extending parallel to the S_1 plane, and has a colliform shape. Rutile trails and quartz trails are present as in previous samples.

---

trails, consisting mainly of rutile (Plate 5.5, a–d). In many cases, the swarms are continuous over the width of a thin section (2.5 cm), although individual trails may anastomose or become diffuse. The continuity of swarms seems mainly governed by the degree of S_2 crenulation, as inclusion trails can also be observed in rotated porphyroblasts. In addition to rutile, trails may contain opaque minerals, zircon, apatite and tourmaline. Where the trails cross into biotite or chlorite, rutile is generally absent and the trail is traced mainly by pleochroic haloes. Within plagioclase, the trails are well defined by numerous, very fine rutile prisms (up to 0.05 mm in length and with aspect ratios of 2–10) which are strongly aligned in the plane of the layering (*i.e.* defining a lineation within the S_1 plane).

The trails of accessory minerals are most pronounced within plagioclase porphryoblasts and they are invariably associated with plagioclase-layered rocks. However, they are commonly continuous across areas of phyllosilicate minerals and, in some cases, were observed in areas of granoblastic quartz aggregates interstitial to porphyroblasts. In quartz-megaphyric rocks, the trails wrap around relict phenocrysts and outline elongate tails of recrystallized quartz (Plate 5.5, c–d). In

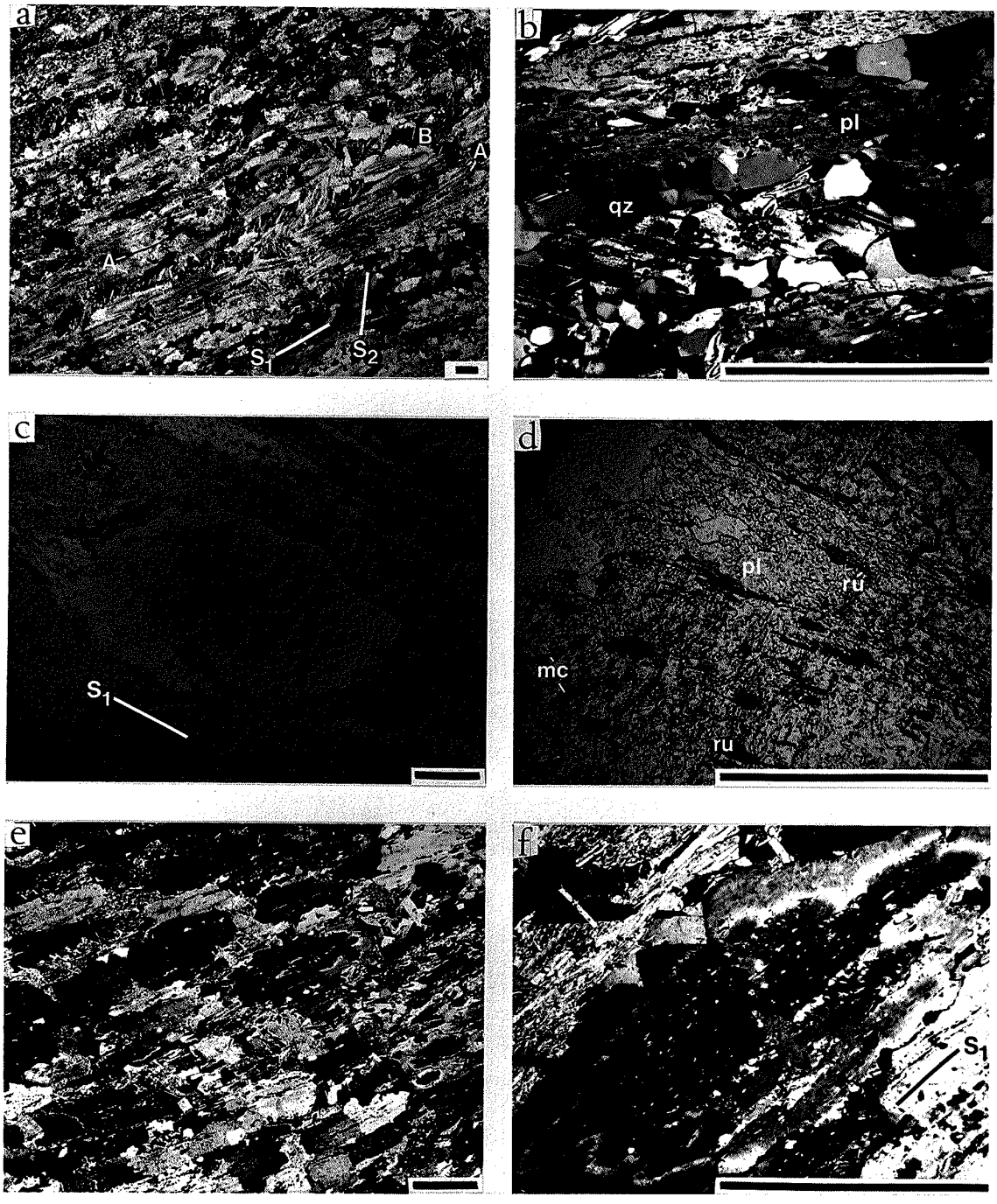
a
B
A
A
S_1
S_2
b
pl
qz
c
S_1
d
pl
rú
mc
ru
e
f
S_1

contrast, monocrystalline phenocrysts and undulatory enclaves contain rutile as numerous minute needles, forming randomly oriented hair-like inclusions (*see* 5.3.1. Quartz Phenocrysts).

The plagioclase porphyroblasts also contain inclusion trails of a more punctuated nature, consisting of quartz and quartz aggregates (Plate 5.5, b). The inclusions are elongate parallel to layering (widths of 0.01–0.1 mm and aspect ratios of 2–15). In some cases, fine monocrystalline quartz inclusions are notably more elongate (aspect ratios up to 10) than the nearly equant, granoblastic quartz grains in the matrix.

The plagioclase porphyroblasts show well developed zoning with an atoll structure (Plate 5.5, e–f). Typically, an andesine-labradorite core of uniform composition forms 50–75% of the grain area. This is mantled by a zone of labradorite-bytownite composition, in some cases, marked by a compositional discontinuity. The calcic zone forms an annular ring which shows normal zoning to an andesine-labradorite margin. The porphyroblasts are mainly untwinned (95%), and in twinned crystals, pericline twins are more common than albite twins. The An-contents were determined by optical methods on albite twins, supplemented by a few microprobe analyses and, therefore, are imprecise. However, contrasts in relief and changes in the optical orientation of albite twins from length-fast to length-slow in the calcic zone of some grains (a transition occurring at An_{75}; Deer *et al.*, 1966), provided additional information on relative compositional changes.

In many cases, a ribbon microperthitic to cryptoperthitic texture, resembling exsolution lamellae, is present (*e.g.* Plate 9.1, a). The compositional ranges suggest the possibility of Bøggild intergrowths of An_{46}–An_{60} and Huttenlocher intergrowths of An_{66}–An_{90} (Smith, 1983).

The nature of the outer grain boundaries of plagioclase porphyroblasts varies between samples. Most commonly, porphyroblasts have simple curved margins. In many cases, the compositional zoning encompasses several adjacent crystals, crossing grain boundaries which are oriented perpendicular to layering (S_1), thus enhancing the elongate appearance of the porphyroblasts (Plate 5.5, e–f). Grains which are poikiloblastic to skeletal in habit have irregular contacts and zoning is interrupted by inclusions. In some cases, grains occurring in a phyllosilicate matrix

have cuspate colloform margins convex toward the matrix, and with the compositional zoning following the shape of the outer contacts.

5.5. Quartz Veins.

Quartz veins are abundant in the alteration zones, particularly in the distal alteration zone. Most are barren, white, monomineralic veins, concordant to the schistosity of the host rock (S_1) and, in many cases, contain tectonic inclusions of wall-rock schists in tightly infolded re-entrants, also concordant to the external schistosity. In the Zn-rich core of the proximal zone (10pa), isolated euhedral inclusions of gahnite occur within some quartz veins. The veins are typically 15–30 cm in drill-core length, but vary from thin ($\leq$ 0.5 cm) veins, occurring singly or in swarms, to thick veins representing up to 1.5 metres of drill-core intersection.

In the alteration zones, contacts between concordant quartz veins and wall rocks are of two main types: contacts characterized by an increasing abundance and grain size of porphyroblastic staurolite, kyanite and biotite in the wall rock approaching the vein contact; and contacts, mainly involving chlorite-muscovite schists, characterized by a single very strong schistosity. In the first type, the S_2 crenulation cleavage is very intense in the selvedge and porphyroblasts are either dimensionally aligned parallel to the S_2 plane, or aligned in the S_1 plane and show intense kinking or crenulation in the S_2 plane. In some cases, possibly representing a transition between the two types of contacts, the crenulation cleavage (S_2) increases in intensity toward the contact until it is transposed into parallelism with the S_1 mineral schistosity. The second type of contact is commonly associated with quartz veins occurring in swarms in which veins may represent 10–60% of the total rock volume over a drill-core length of several metres. The host rock between the veins is a silky schist without gneissic layering. These quartz veins and selvedges are associated with local high strain zones which, in many cases, show steeper apparent dips (*i.e.* lower angles between the rock fabric and core axis), and transitional contacts with the host rock. In some cases, selvedges contain brown-green structureless mixtures of retrograde minerals, partly replacing plagioclase, or entirely pseudomorphing poikiloblastic augen which have a habit similar to plagioclase. In some cases, fine ($\leq$ 1 mm in width) calcite veinlets are present in the phyllosilicate schists, and although oriented subparallel to schistosity, in detail can be seen to

transect the fabric of the host rock.

Discordant quartz veins, and some concordant veins, typically contain calcite and have selvedges characterized by coarse grained, randomly oriented, calc-silicate minerals. These veins occur in all rock units, including the distal and proximal alteration zones. They are closely associated with statically crystallized, calc-silicate alteration (unit 10i) (*see* 6.2.2. Static Calc-silicate Alteration).

5.6. Massive and Semi-Massive Sulphide Mineralization.

5.6.1. Massive and Semi-massive Sulphide Bodies.

Four distinct massive sulphide bodies were intersected in the cross-sections represented by A-A' and C-C' (Figures 3.2–3.3), and these bodies have some distinctive mineralogical and textural features. The lowermost body in the stratigraphic sequence is associated with graphitic metasediments (3). The contacts are transitional over a few centimetres and involve an increase in medium to coarse grained pyrite and pyrrhotite porphyroblasts in weakly layered concentrations parallel to bedding. The massive sulphide mineralization is intercalated with mineralized kyanite-margarite schists in layers of about 20–60 cm in thickness. Contacts to the proximal alteration are transitional by a decrease in the proportion of sulphide minerals in sulphide-rich intercalations. The mineralogy of the silicate-rich layers shows a concomitant decrease in margarite abundance and an increase in muscovite and plagioclase abundance. The internal structure of the massive sulphide layers is nearly massive, but they commonly contain irregular seams (up to 5 mm in width) and blebs of pyrrhotite, chalcopyrite and sphalerite, interstitial to euhedral pyrite porphyroblasts. Calcite, although not common, is locally abundant in granular intergrowths with pyrite in zones of up to one metre of drill-core intersection. It also occurs on irregular seams or veins (up to 5 cm in width), commonly in association with sphalerite and pyrite.

Higher in the sequence, a massive sulphide body was intersected over 1 metre and 7 metres in cross-sections A-A' and C-C', respectively. This body consists of granular, medium to coarse grained pyrite and calcite, with minor pyrrhotite and quartz. In the case of the thicker intersection, the pyrite-calcite rocks are intercalated, in layers of 15–75 cm in thickness, with silicate-rich layers containing quartz, calcite, biotite, and muscovite, with minor pyrite, pyrrhotite and chalcopy-

rite. Down-dip from this massive sulphide body, in cross-section C-C', another body, 2 metres in thickness, consists of medium to coarse grained, granular pyrite, with minor pyrrhotite and quartz. Some of the quartz occurs as augen resembling relict phenocrysts.

The largest massive sulphide body occurs uppermost in the sequence within unit 4, and consists of structureless granular, medium to coarse grained, idioblastic pyrite (60–90%) and granoblastic calcite (10–40%). Locally, magnetite occurs as disseminated porphyroblasts, up to 3 mm in size, and pyrrhotite and minor sphalerite and chalcopyrite are present in the place of calcite, interstitial to euhedral pyrite on irregular seams or interconnected enclaves. Minor barren calcite enclaves and veins, up to 10 cm in thickness, cut the pyrite-calcite rock. The veins are commonly curved, forming structures resembling open folds, but lacking any penetrative fabric. The massive sulphide body is generally very homogeneous, but local enclaves of silicate minerals are present.

5.6.2. Silicate Enclaves in the Main Massive Sulphide Body.

The main massive sulphide body contains enclaves of silicate minerals, and associated semi-massive zones representing up to 2 metres of drill-core intersection. There are three types of enclaves: 1) leucocratic enclaves consisting of pyrite, quartz and schistose muscovite, with blue quartz augen resembling relict phenocrysts; 2) melanocratic enclaves consisting of symplectites containing calc-silicate minerals and, typically having a zonal structure; and 3) one occurrence of a melanocratic enclave containing anthophyllite, staurolite and gahnite. The first type of enclave is similar to rocks in the proximal alteration zone, but types 2 and 3 are unique.

Anthophyllite was observed in a single small enclave (6 cm of drill-core intersection, 24-1131a-1) in association with quartz, anorthite (An_{97}, microprobe analysis), staurolite and gahnite, with trace amounts of biotite and arsenopyrite. This assemblage is bounded immediately by a zone consisting of quartz and pyrite, and by an outer calc-silicate zone, consisting of blue-green hornblende, calcic plagioclase, quartz, pyrite, pyrrhotite, magnetite and minor sphalerite. The calc-silicate zone is transitional to the pyrite-calcite host rocks. Adjacent to the pyrite-calcite rocks, epidote is also present. Magnetite porphyroblasts (1–3 mm in size) are evenly distributed throughout the pyrite-calcite host rock and the calc-silicate zone.

Within the anthophyllite-bearing enclave, a layered structure (4 mm in thickness) is weakly defined by concentrations of felsic and ferromagnesian minerals, and by trails of equant, fine grained quartz. Fine grained biotite blades, which occur mainly as disseminated inclusions in anthophyllite, are aligned parallel to layering. Other silicate minerals, and gahnite, are unoriented, but the internal structure of coarse poikiloblasts is commonly mimetic after layering (Plate 5.6, a). Staurolite and gahnite poikiloblasts are medium to coarse grained, anhedral and, in part, interstitial to radiating sheaves of acicular, coarse grained (up to 10 mm long) prisms of anthophyllite (Plate 5.6, b). Staurolite and anthophyllite also occur as skeletal crystals which commonly form a network engulfing numerous fine quartz grains (0.02–0.05 mm) and, in some cases, appear to be mimetic after randomly oriented or radiating fibrous minerals. Poikiloblastic minerals show moderate degrees of strain, as indicated by undulatory extinction (Plate 5.6, c). Anorthite occurs as medium to coarse grained anhedral grains, interstitial to ferromagnesian minerals. Quartz varies in habit, forming fine grained, nearly granoblastic aggregates, with interlocking contacts, and medium grained, strained and elongate grains, with sutured contacts. Monocrystalline or substructured lenticular grains up to 3 mm long are engulfed by porphyroblastic and sulphide minerals (Plate 5.6, c). These grains contain numerous, randomly oriented rutile hairs and resemble relict quartz phenocrysts.

The mineralogy, textures and microstructures of the calc-silicate zone are similar to those of calc-silicate enclaves encountered locally throughout the largest massive sulphide body (Plate 5.6, d–j). They are characterized by quartz, pyrite, pyrrhotite, blue-green amphibole and calcic plagioclase. Minor amounts of gahnite and sphalerite are ubiquitous. Epidote is abundant near contacts with pyrite-calcite host rocks and adjacent to weakly mineralized calcite veins (up to 2 cm in width) present locally in the enclaves.

The mineral textures and microstructures contrast markedly with the proximal alteration zone in that there is little or no evidence of rhythmic layering or penetrative fabrics, except in local domains (*e.g.* quartz aggregates in the following paragraph). The enclaves are characterized by coarse symplectic intergrowths involving plagioclase and amphibole, amphibole and pyrrhotite, plagioclase and

Plate 5.6. (following two pages) Silicate enclaves in the main massive sulphide body, including rocks containing anthophyllite, staurolite and gahnite (a–c), and calc-silicate enclaves (d–p). The bar scale in each plate represents 0.25 mm.

a. 24-1131a xpl (cross-polarized light) A skeletal staurolite(st) porphyroblast with internal structure mimetic after layering (S_1), and with fibrous areas which contain many fine quartz inclusions.

b. 24-1131a partial xpl Sheaf of acicular radiating anthophyllite(at) with anhedral interstitial staurolite(st) between some of the prismatic crystals. The anthophyllite contains quartz inclusions and many oriented inclusions of fine grained biotite(bi).

c. 24-1131a xpl Relict quartz phenocryst engulfed by staurolite(st) and anthophyllite(at). The phenocryst and the anthophyllite show undulatory extinction.

d. 24-1129a xpl Coarse grained poikiloblasts of plagioclase(pl) and amphibole(am) in a symplectic intergrowth with sulphide minerals(su) and epidote(ep). The field of view is 13 mm wide.

e. 24-1129a ppl (plane-polarized light) Gahnite(gh) inclusions in plagioclase(pl) resembling symplectic intergrowths and corona structures.

f. 24-1129a ppl Detail of f. Very fine gahnite(gh) inclusions in plagioclase. Some inclusions appear to be oriented parallel to lattice planes in the plagioclase (very fine inclusions, lower centre).

g. 24-1160 ppl Relict quartz phenocrysts(qz) with irregular outlines. Calcic plagioclase(pl) occurs in symplectic intergrowths with pyrrhotite(po).

h. 24-1160 xpl Detail of plagioclase in g. Compositional zoning in plagioclase follows the outlines of pyrrhotite(po) inclusions.

i. 24-1129a ppl Quartz-rich aggregates(qz) with stringers of sulphide minerals(su) and skeletal amphibole(am).

j. 24-1129a xpl Same view as i. A weak directional fabric is defined by trails of fine grained recrystallized quartz, overgrown by the skeletal amphibole.

k. 24-1129a ppl Contact between a calc-silicate enclave and a calcite vein (A). A single plagioclase porphyroblast(pl) contains inclusions of sulphide minerals(su) and gahnite(gh). The plagioclase and sulphide minerals have a fine corona of epidote(ep).

l. 24-1129a xpl Same view as k. Gahnite and epidote(ep) are more easily distinguished. Epidote rims plagioclase (twinned) on both the external and the internal grain boundaries. Faint cleavage is visible in the calcite in the vein (A).

m. 24-1191 ppl Skeletal garnet(gt), with pyrrhotite(po), fine chlorite blades (ch) defining a schistosity, and medium grained, randomly oriented, biotite porphyroblasts(bi). The view represents zone 5 in Table 5.2.

n. 24-1191 ppl Detail of m. Garnet(gt) appears to be mimetically replacing chlorite(ch) and, in part, mantling pyrrhotite(po).

o. 24-1190.5 ppl Trails and swarms of fine rutile prisms(ru) in elongate plagioclase porphyroblasts(pl). The view is equivalent to zone 6 in Table 5.2. Compare the microstructures in this enclave, to those found in plagioclase-layered rocks (Plate 5.5).

p. 24-1190.5 xpl Same view as o. Inclusion trails and aggregates of quartz(qz) are also present. In the nearly extinct plagioclase grain(pl), rutile prisms(ru) are visible as very fine bright needles.

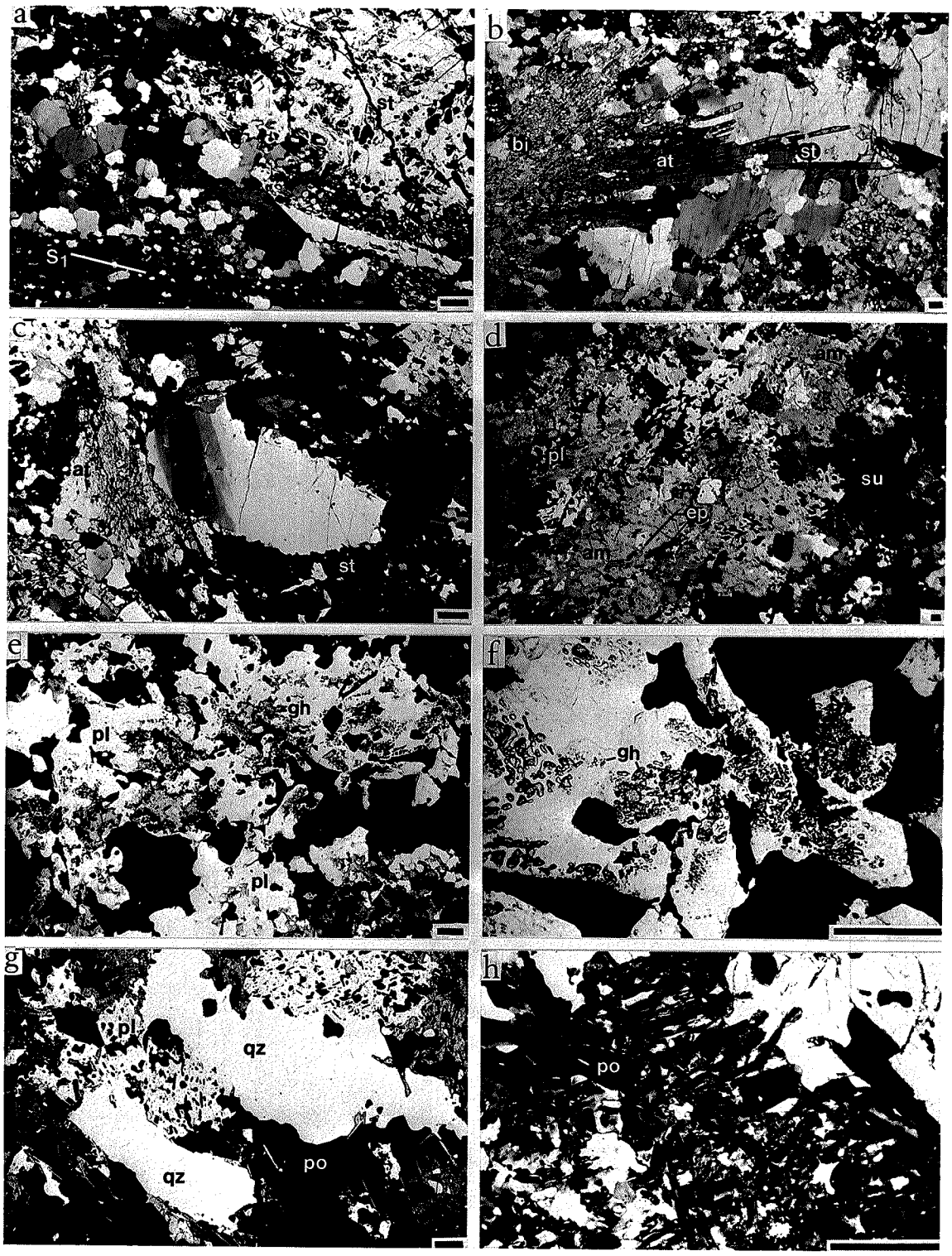
a
st
S1
b
bi
at
st
c
ar
st
d
am
pl
su
ep
am
e
gh
pl
pl
f
gh
g
pl
qz
qz
po
h
po

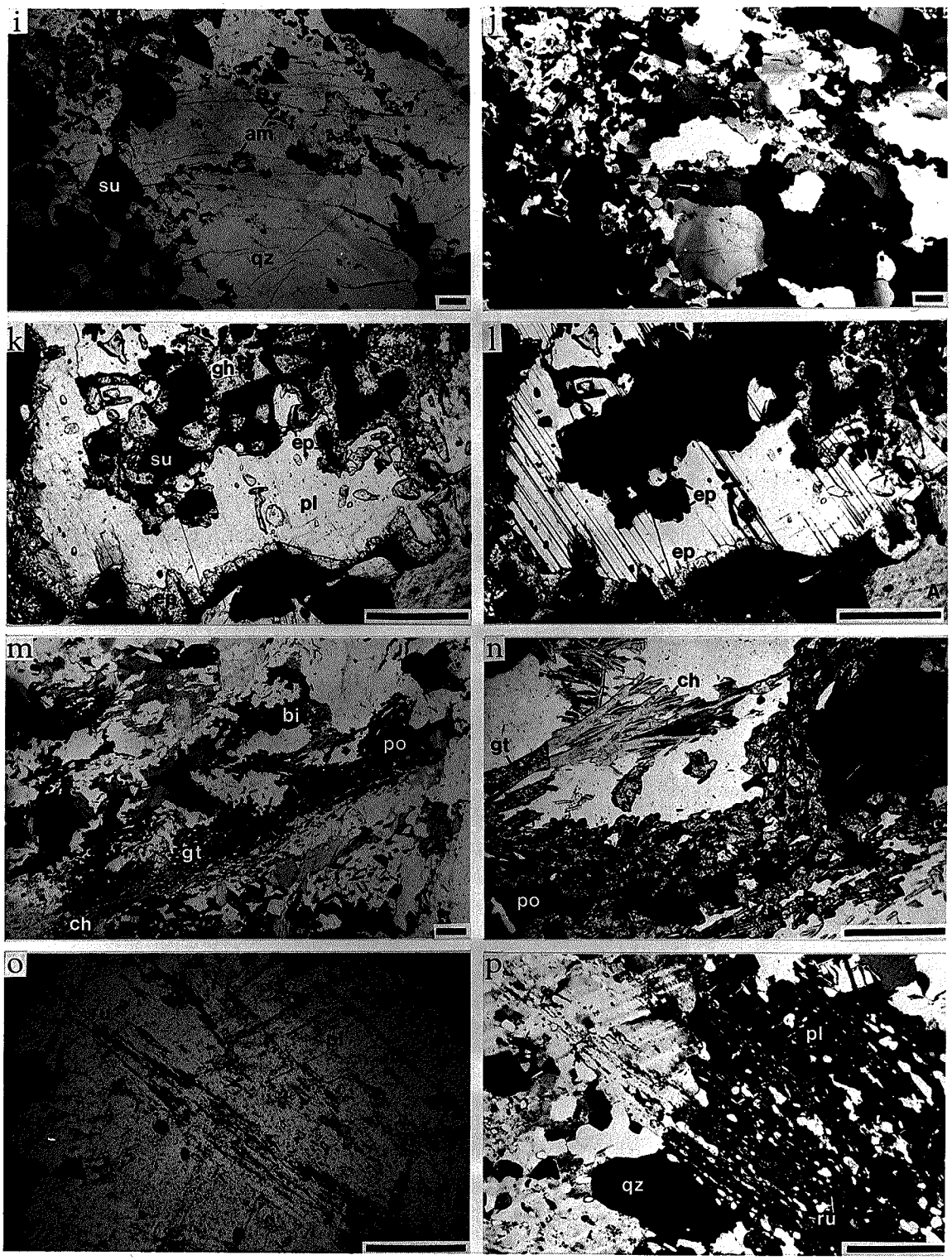
i
am
su
qz
j
k
gh
su
ep
pl
ep
l
ep
ep
m
bi
po
gt
ch
n
ch
gt
po
o
p
pl
qz
ru

pyrrhotite, gahnite and sulphide minerals, and plagioclase and gahnite. The minerals are generally coarse grained (0.5–5 mm), anhedral, and skeletal to poikiloblastic, with intergrowths typically occurring on a scale of 0.05–0.5 mm. Small (0.02–0.1 mm) equant inclusions of quartz occur in all minerals. Gahnite occurs mainly as skeletal inclusions within plagioclase, although local sulphide aggregates contain many small (0.02–0.5 mm) euhedral inclusions of gahnite, or are intergrown with anhedral gahnite. In plagioclase, the coarsest inclusions of gahnite have scalloped grain boundaries. In many cases, they occupy up to 50% of the grain area and tend to be concentrated within the central parts of the grain, giving the appearance of gahnite mantled by plagioclase (Plate 5.6, e–f, k–l). In addition to their involvement in symplectic intergrowths, sulphide minerals occur in fine grained (0.01–0.5 mm) subhedral crystals (mainly pyrite) and in irregular ganglion aggregates, up to 10 mm in size, with many apophyses commonly forming an interconnecting network (*e.g.* Plate 5.6, e).

Plagioclase occurs mainly as untwinned (95%) porphyroblasts, riddled with symplectic inclusions (10–40%). Fine oscillatory compositional zoning is commonly present around the margins of inclusions, particularly symplectic pyrrhotite, resulting in an intricate lacy internal texture (Plate 5.6, h). Zoning is also present around outer contacts, but the definition and width of zones is variable, and may be partly determined by the species of the adjacent mineral, although this is not well established. In general, the compositional change is from calcic plagioclase adjacent to inclusions and outer grain boundaries, to less calcic plagioclase in inclusion-free internal areas.

Quartz-rich aggregates (up to 15 mm in size) occur with both granoblastic and inequigranular textures, the latter comprised of medium grained (0.5–2 mm), strained, undulatory grains showing weakly sutured mutual contacts or mantled by fine grained (0.05–0.2 mm) recrystallized grains. In some cases, a weak directional fabric within the aggregates is defined by trails of fine grained recrystallized quartz associated with fine grained (0.1–0.25 mm) sulphide minerals and aggregates and stringers of interstitial skeletal amphibole (Plate 5.6, i–j). The outer margins of the quartz aggregates are irregular, commonly interlocking with sulphide minerals and penetrated by skeletal amphibole, optically continuous with amphibole in the

matrix. The aggregates resemble recrystallized quartz phenocrysts.

Calcite veins and aggregates which cut the enclaves, although typically very irregular in shape, have sharp contacts to the wall rock, in some cases, marked by a discontinuous seam (up to 1 mm in width) of sulphide minerals. The seams have scalloped margins and many finger-like projections into both the vein and the wall rock. The veins are nearly monomineralic, consisting of medium grained (0.5–2 mm), equant calcite, which varies from granoblastic with smooth grain boundaries to interlocking with serrate contacts. Calcite shows weak undulatory extinction and slight kinking or bending of lamellar twins in some grains. Minor amounts of quartz and pyrite are present in the veins.

Epidote is present in the wall-rock assemblage, in addition to all the other minerals of the enclaves. Calcite penetrates about 3 mm into the wall rock, either on grain boundaries, or forming coarse (0.1–0.5 mm) symplectic intergrowths with amphibole which resemble replacement textures. Corona structures are evident; epidote forms a very fine (0.01–0.02 mm) rim between plagioclase and calcite, and in some cases, between plagioclase and sulphide minerals, and quartz and calcite (Plate 5.6, k–l). The epidote coronas commonly consist of fibres oriented perpendicular to grain boundaries. Epidote also occurs as medium to coarse grained (1–3 mm) subhedral crystals dusted with numerous fine (0.01–0.1 mm) euhedral pyrite inclusions, and in symplectic intergrowths with hornblende, sulphide minerals and calcic plagioclase.

Garnet was observed in one location (24-1191), in an enclave with a strongly defined zonal structure. Six distinct mineralogical zones (Table 5.2) occur within the length of a thin section (about 4 cm). Detailed electron-microprobe traverses, characterizing the mineral chemistry of each zone, are reported in chapter 10 (10.4. Calc-silicate Enclave in the Main Massive Sulphide Body). The contacts between zones are marked by changes in mineral assemblage and in compositions of mineral species.

The textures of zones 1 to 4 are identical with those present in calc-silicate enclaves as previously described. Zone 5 is distinguished by the occurrence of chlorite and garnet. A pale green chlorite occurs mainly as fine grained ($\leq$ 0.5 mm) bladed aggregates defining a moderately strong schistosity parallel to zonal contacts. It

Table 5.2. Mineralogy of Zones in a Calc-Silicate Enclave. Sample 24-1191

Zone 1: calcite, pyrite—typical lithology of the massive sulphide body.

Zone 2: (1–4 mm); calcite, pyrite, epidote, actinolite, ±quartz.

Zone 3: (1–2 mm); quartz, pyrite, epidote, actinolite/hornblende (patchy zoning), bytownite (An_{86}–An_{91}, patchy zoning).

Zone 4: (6–8 mm); quartz (partly in aggregates up to 8 mm in size), pyrite, pyrrhotite (monoclinic), hornblende, bytownite (An_{72}–An_{86}, patchy zoning, symplectic intergrowths with pyrrhotite).

Zone 5: (1–6 mm); quartz, pyrrhotite (trace hexagonal cores in mainly monoclinic grains), pyrite, garnet (skeletal, rimming pyrrhotite and partly mimetic after chlorite), hornblende (no contacts to chlorite), chlorite (defines schistosity parallel to zone contacts), biotite, oligoclase/andesine (An_{29}–An_{34}, reverse zoned elongate porphyroblasts with rutile inclusion trails parallel to zone contacts), andesine/labradorite (An_{41}–An_{67}, patchy and normal zoning, symplectic intergrowths with pyrrhotite).

Zone 6: quartz (partly in aggregates and phenocrysts up to 4 mm in size), biotite, oligoclase/andesine (An_{27}–An_{34}, habit as in zone 5), andesine/labradorite (An_{41}–An_{54}, normal zoning, cores contain gahnite inclusions), pyrrhotite (minor hexagonal cores in mainly monoclinic grains), pyrite, chlorite, sphalerite (trace), gahnite (inclusions in plagioclase).

has a habit similar to that of chlorite in the proximal and distal alteration zones. Biotite is present as randomly oriented, anhedral, fine to medium grained (0.1–1 mm) porphyroblasts and aggregates, which show traces of retrogression to a dark green chlorite along grain boundaries and cleavage planes. Garnet occurs as skeletal grains and aggregates overgrowing fine (0.05–0.2 mm) quartz grains and forming a semi-continuous layer up to 6 mm thick (Plate 5.6, m–n). It contains many inclusions of pyrrhotite, mainly as irregular interconnected or isolated ganglions with scalloped margins. In some cases, pyrrhotite occupies most of the aggregate (up to 70–80%) and garnet seems to be rimming pyrrhotite. Garnet also occurs in a skeletal bladed habit identical to that of chlorite. In many cases, fine blades preserve

textural continuity across sharp high-angle grain boundaries between chlorite and garnet (Plate 5.6, n). Garnet appears to have mimetically replaced chlorite. The distribution of minerals in zone 5 is asymmetrical; most of the hornblende occurs between the garnet layer and zone 4, and most of the biotite and chlorite occurs between the garnet layer and zone 6.

Zone 6 contains gahnite, as inclusions in plagioclase, identical to those present in calc-silicate enclaves. Trace amounts of sphalerite are also present as anhedral grains, up to 1 mm in size, associated with either sulphide or silicate minerals. In some cases, fine grains of sphalerite (0.02–0.1 mm) occur with gahnite, as inclusions in plagioclase, or on the periphery of plagioclase grains which contain gahnite.

Plagioclase in zones 5 and 6 occurs in 2 distinct habits which show a correlation with An-content. Both zones contain medium to coarse grained (0.5–5 mm), poikiloblastic grains and aggregates, elongate parallel to the zonal contacts and containing well defined inclusion trails of rutile. The plagioclase and rutile trails are similar in habit and microstructural relations to those of plagioclase-layered rocks (Plate 5.6, o–p). The poikiloblasts show a weak reverse compositional zoning from an oligoclase core to an andesine rim. Within zone 5, plagioclase also occurs in symplectic intergrowths with pyrrhotite, similar to those in zone 4 and in many calc-silicate enclaves, but with slightly lower An-contents (labradorite to andesine). In zone 6, plagioclase with a similar habit and compositional range contains inclusions of gahnite and sphalerite. It should be noted that the An-contents (Table 5.2) represent the ranges encountered during microprobe analysis and that the outermost margins of plagioclase grains in both zones, regardless of habit, probably converge to an andesine composition.

Chapter 6
Other Types of Alteration

A variety of alteration types were observed at the Linda deposit, distinct either in location, or in mineralogy, from the porphyroblastic schists and gneisses of the proximal and distal alteration zones. These alteration types include silicic-feldspathic alteration (1a, 10s) and calc-silicate alteration (10c, 10e) of mafic to felsic precursor rocks; statically crystallized calc-silicate alteration (10i); chlorite-hornblende schists (10m); and retrograde alteration.

6.1. Silicic-Feldspathic Alteration.

Microcrystalline, nearly massive rocks with a bleached appearance are common at the Linda deposit and include the previously discussed 'cherty' felsic rocks (1a) (*see* 5.3.2. 'Cherty' Felsic Rocks and Brecciated Equivalents), as well as 'cherty' rocks which occur in close association with mafic rocks (10s). Silicic-feldspathic alteration is difficult to recognize and characterize, particularly in drill core; it mimics massive rhyolitic flows and the highly silicic and sodic whole-rock geochemistry is difficult to infer, even during petrographic examination. Although in general, these rocks were mapped as a distinct unit or subunit (1a, 2/10s) on a lithological basis, their identification as altered rocks, especially in the case of unit 1a, is based partly on geochemistry (*see* 11.1.1. Geochemistry of Felsic and Silicic-Feldspathic Altered Rocks). The modal mineralogy of silicic-feldspathic rocks is summarized in Table 6.1; unit 1a will not be discussed further here (*see* 5.3.2. 'Cherty' Felsic Rocks and Brecciated Equivalents).

In the subsurface, the mafic volcanic rocks of unit 2 have transitional contacts with felsic rocks over intervals of up to 10 metres. In the mafic volcanic rock of unit 2, fine (0.2–2 mm) laths and prisms of blue-green hornblende define a strong lineation in an otherwise nearly massive rock. In the transitional contact zone, amphibole shows an abrupt increase in grain size, decrease in abundance, and change in

Table 6.1. Summary of Modal Mineral Percentages.

Ranges and averages (in parentheses) in silicic-feldspathic altered rocks (Appendix A.)

See 3.1. Description of Lithological Units for explanations of unit and code designations.
See Table A.2 for a key to the code and Table A.3 for mineral abbreviations.

a. Cherty Felsic Rocks (1a), Clasts from Felsic Breccias (1b) and Cherty Breccias (1c).

Unit	Code	N	Qz	Pl	Hb	Cm	Ep	Cl	Gt	Bi	Ch	Op
1a		8	22–55	23–70	0–4	0–9	0–2	0–2	0–2	0–8	0–10	0–5
			(40)	(51)	(t)	(1)	(t)	(t)	(t)	(2)	(1)	(1)
1b	a	4	34–70	30–65	0	0	0	0	0–1	t–1	0–t	0–t
			(55)	(43)					(t)	(1)	(t)	(0)
1c	a	2	29–33	65–70	0	0	0	0	0	0–t	0	0

b. Silicified-Feldspathized Mafic Volcanic Rocks (2/10s, 2b/10s, 2e/10s).

Unit	Code	N	Qz	Pl	Hb	Cm	Ep	Cl	Gt	Bi	Ch	Op
2/10s,	n	5	5–45	38–60	t–15	1–12	0–t	0	0–4	0–4	0–11	t–3
2b/10s			(28)	(48)	(8)	(8)	(0)		(t)	(1)	(3)	(2)
2e/10s												

habit and composition (Plate 6.1, a–b); blue-green hornblende and clear cummingtonite occur as medium to coarse grained (1–8 mm), poikilitic to skeletal, acicular sheaves. They vary from 'bowtie' aggregates, which have sigmoidal asymmetry and define a weak foliation, to sheaves which define a moderately strong lineation and foliation within fine layers, about 0.5 mm in width. The skeletal habit is commonly mimetic after the layering. The transition zone is also characterized by fine to medium grained (0.5–3 mm) magnetite porphyroblasts and, locally, by fine to coarse grained, garnet porphyroblasts and minor amounts of disseminated fine grained chlorite and sulphide minerals. The proportion of mafic minerals fluctuates across the zone on a scale of 0.1–2 metres and ranges from 10–40%. Modal variation on a smaller scale defines diffuse layers, 0.5–10 mm in thickness.

Cummingtonite-rich and hornblende-rich domains are defined by the distribution of amphiboles, but the minerals also show minor mutual epitaxial overgrowths (Plate 6.1, b). Cummingtonite, garnet and magnetite all have nearly chlorite-free, leucocratic halos, but grain contacts with chlorite were also observed. The felsic matrix is a microcrystalline (0.02–0.1 mm) granoblastic to interlocking aggregate of quartz and sodic plagioclase. The plagioclase is mainly untwinned ($\leq$1%) and simi-

Plate 6.1. (following page) Silicified-feldspathized mafic rocks. The bar scale in the photomicrographs represents 1 mm.

a. Transitional contact zone of unit 2 as seen in drill core. Unit 2 lies to the left (not visible) and the contact zone in this direction contains a higher proportion of coarse grained, acicular, hornblende sheaves. The weakly coloured core to the right of the pen contains abundant cummingtonite. Disseminated magnetite porphyroblasts show leucocratic halos. The pen is 16 cm long.

b. 34A-1484 ppl (plane-polarized light) Hornblende(hb) and cummingtonite (cm) in the transitional contact zone, forming skeletal radiating sheaves and 'bowties'. The opaque phase is magnetite.

c. Outcrop of silicified-feldspathized pillowed flows, looking down the axis of the stretching lineation (YZ-section). Note the bleached appearance and the mafic rims. The hammer handle is 40 cm long.

d. Detail of the outcrop in c, showing bleached pillow interior (to the left of the pen) with weakly coloured cummingtonite, and a layered mafic rim containing hornblende, garnet, cummingtonite and felsic minerals. The lens cap is 5 cm in diameter.

e. 34A-1760.5 ppl Volcaniclastic rock with a felsic clast (central band) in a mafic matrix. The flattening of the clast and chlorite schistosity in the matrix define S_1. Randomly oriented amphibole porphyroblasts change from hornblende(hb) in the matrix to optically continuous skeletal cummingtonite(cm) in the clast.

f. 22-413 ppl Textures within an intermediate enclave (clast?) in unit 1d. Cummingtonite(cm) and minor hornblende(hb) define a strong schistosity (S_1) and lineation. The subhedral garnet porphyroblast(gt) engulfs cummingtonite. Euhedral magnetite and fine grained anhedral pyrrhotite are also present.

---

lar to quartz in relief, suggesting an oligoclase composition. Some plagioclase occurs in anhedral grains (up to 1 mm in size), with a corroded and substructured appearance, and resembles relict phenocrysts. Irregular discontinuous veinlets, less than 1 mm in width, contain fine grained (0.1–1 mm) quartz, or quartz and plagioclase.

Mafic volcanic rocks of unit 2 typically contain 3–25% quartz, 22–54% plagioclase and 40–74% hornblende. In their altered state (2/10s, 2b/10s, 2e/10s), they are notably more felsic, containing 5–45% quartz, 38–60% plagioclase, trace amounts to 15% hornblende, and 1–12% cummingtonite (Table 6.1, b). The transition to typical felsic rocks (1, 4) occurs with an increase in biotite content, stronger definition of a finely layered and schistose structure, and with the disappearance of amphibole.

The best documented example of silicic-feldspathic alteration occurs in a well exposed outcrop northeast of the Rod minesite (Map, in pocket; unit 2b/10s). Pillowed flows in the area have buff-coloured bleached pillow interiors which contain skeletal cummingtonite and garnet, and minor fine grained disseminated biotite and

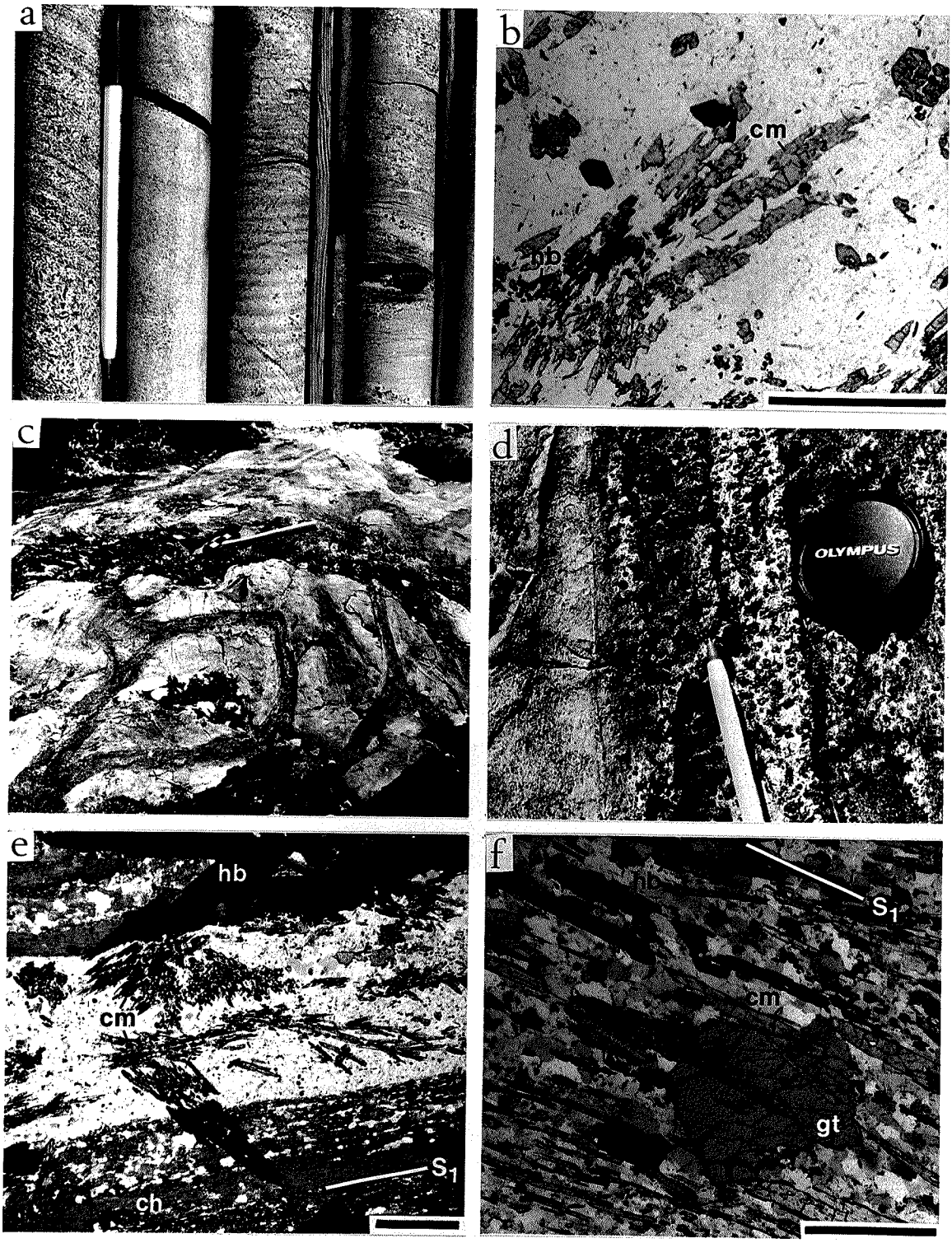
a
b
cm
hb
c
d
OLYMPUS
e
hb
cm
S1
cb
f
S1
cm
gt

magnetite, in a matrix of quartz and plagioclase (Plate 6.1, c–d). The pillows are outlined by mafic, more schistose zones, 2–20 cm in width, which contain abundant garnet porphyroblasts (1–10 mm in diameter), hornblende, cummingtonite and magnetite, as well as 10–50% interstitial leucocratic minerals. In some cases, the mafic zones have a layered structure, 0.5–3 cm in thickness, defined by concentrations of amphiboles intercalated with concentrations of garnet and cummingtonite in a leucocratic matrix (Plate 6.1, d). Contacts with pillow interiors are abrupt, but the exact relationship of the mafic zone to primary selvedges and interpillow material is not clear. Many quartz veins are present and commonly resemble tension gashes which have a maximum width in pillow interiors and narrow or pinch out near the margins or in the mafic zones. The texture and mineralogy of the pillow interiors are similar to those observed in subsurface transitional contact zones between mafic and felsic rocks.

The surface exposure of altered pillowed flows is part of an area of extensive alteration. The overlying unit of volcaniclastic rocks (2e) has garnet-hornblende-cummingtonite assemblages which resemble the mafic zones rimming altered pillows. The textures are coarsely porphyroblastic and, as a result, the minimum size of recognizable primary clasts is about 1 cm (*see* 3.1. Description of Lithological Units). The clasts are leucocratic and partly overgrown by porphyroblastic minerals, particularly cummingtonite. In some cases, single optically continuous amphibole crystals change from a hornblende in the matrix to cummingtonite in a relict clast (*e.g.* Plate 6.1, e).

In the subsurface, isolated intervals of volcaniclastic rocks, consisting of felsic clasts in a more mafic matrix, resemble the altered rocks described above. However, in the drill-core intersections, garnet is less abundant and the matrix (to the clasts) commonly consists of chlorite schist (S_1) with randomly to strongly oriented sheaves and poikiloblasts of coarse grained hornblende (Plate 6.1, f). Crystals of amphibole are commonly optically continuous into the leucocratic clasts, but change abruptly in habit and composition to a skeletal cummingtonite (Plate 6.1, e).

Figure 6.1a illustrates the proportions of modal quartz, plagioclase and amphibole in mafic and intermediate volcanic rocks (Units 2 and 6), in the transitional contact zone of unit 2 (2/10s), and in 'cherty' felsic rocks (1a). Tie lines link domains

separated from the same sample, for example, clasts and matrix in volcaniclastic rocks (6), and cummingtonite-rich and hornblende-rich domains in the transitional zone (2/10s). The ambiguity in distinguishing silicic-feldspathic alteration from primary mineralogy is apparent. The assemblages trend toward the quartz-plagioclase join, and apparently to more sodic plagioclase compositions; but only in the case of intense alteration, which exceeds the modal (and geochemical) ranges normally expected in igneous rocks (*see* 11.2.1. Silicic-Feldspathic Alteration and Metamorphic Segregation), is the presence of alteration clearly indicated. Note also that the compositional effects of sorting in volcaniclastic rocks are difficult to evaluate, particularly in the case of fine material, the record of which is obliterated during metamorphic recrystallization.

6.2. Calc-silicate Alteration of Felsic Rocks.

Two types of calc-silicate alteration of felsic rocks can be distinguished on the basis of structural and textural relationships, and mineralogy. 'Concordant calc-silicate alteration' is concordant to S_1 layering and schistosity, and characterized mainly by epidote and biotite. In contrast, 'static calc-silicate alteration' is generally massive, in some cases discordant to tectonic fabrics, and characterized by Ca-amphibole, epidote and calcite (Figure 6.1, b–d). The calc-silicate enclaves within the main massive sulphide body and margarite-bearing rocks were discussed in the context of proximal alteration (*see* 5.6.2. Silicate Enclaves in the Main Massive Sulphide Body *and* 5.3.5. Proximal Alteration Zone).

6.2.1. Concordant Calc-silicate Alteration.

Calc-silicate alteration occurs locally in felsic rocks (1/10c, 1b/10c, 4/10c) throughout the subsurface cross-sections (Sections A-A', C-C', in pocket) of the Linda deposit, but is most prevalent in a large volume which envelops the distal alteration zone. This volume has been designated as a calc-silicate alteration zone and the outer margin (*see* Figures 3.2 and 3.3) represents a poorly defined limit for semi-continuous alteration. Local enclaves lacking calc-silicate minerals occur within the zone and enclaves of calc-silicate minerals occur outside the zone. Calc-silicate alteration is characterized mainly by the presence of epidote and biotite and, less commonly, of muscovite and calcite (Table 6.2, a). The rocks generally have a leucocratic appearance and layered structure (S_1) defined by epidote, biotite,

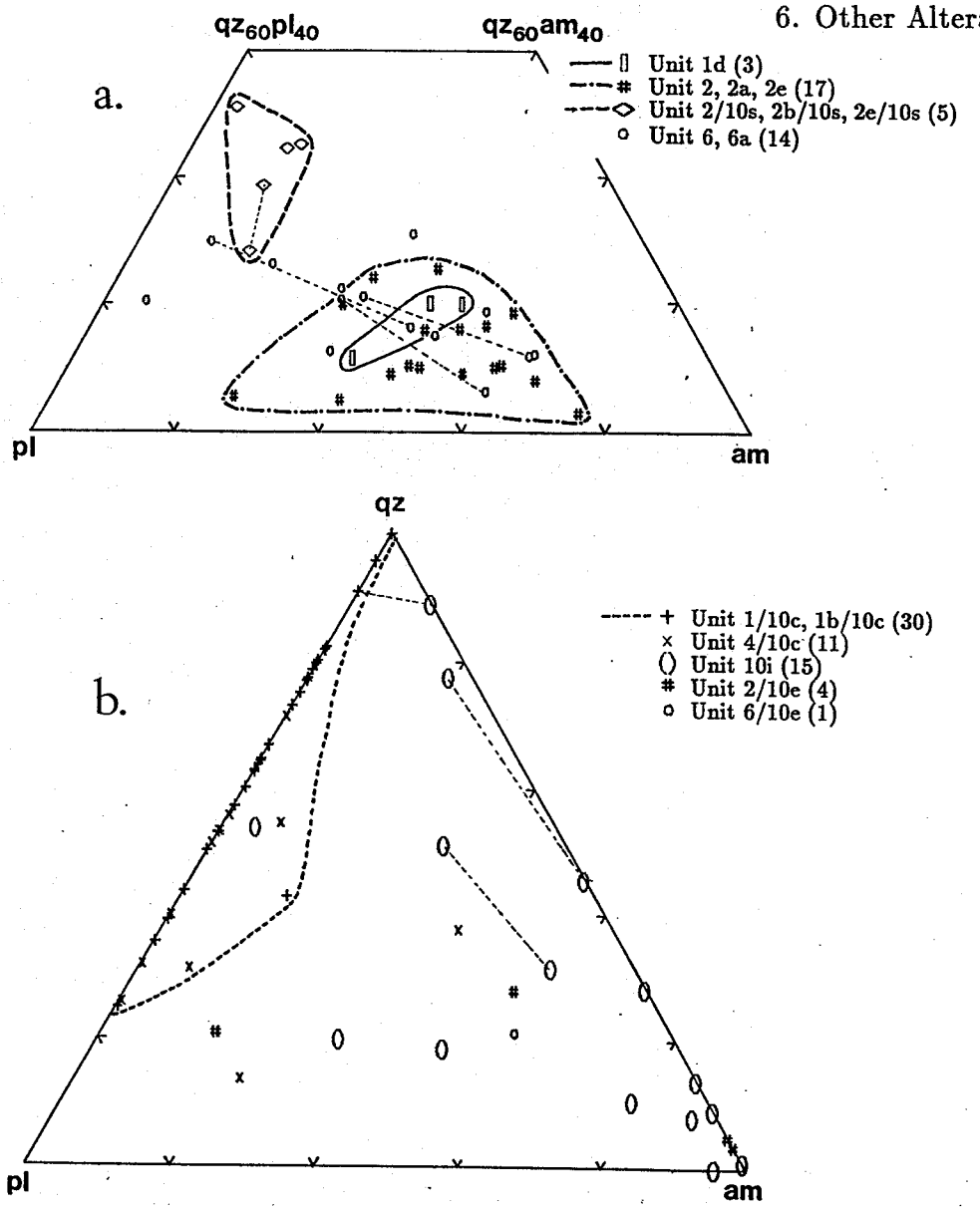

Figure 6.1. Summary of modal mineral proportions in silicic-feldspathic and calc-silicate altered rocks. Field boundaries have no statistical significance. Tie lines link domains extracted from the same sample.

a. Ternary proportions of quartz (qz), plagioclase (pl) and hornblende + cummingtonite (am) in silicic-feldspathic altered rocks.

b. Ternary proportions of quartz (qz), plagioclase (pl) and Ca-amphibole (am) in calc-silicate rocks.

muscovite and, in some cases, calcite. Contacts between felsic rocks and calc-silicate felsic rocks are transitional, consisting of a gradual increase in the epidote content of micaceous layers. In drill core, as the abundance of epidote increases, the layers acquire the appearance of punctuated trails of white laths. The epidote occurs as fine to medium grained, poikilitic, anhedral aggregates and subhedral

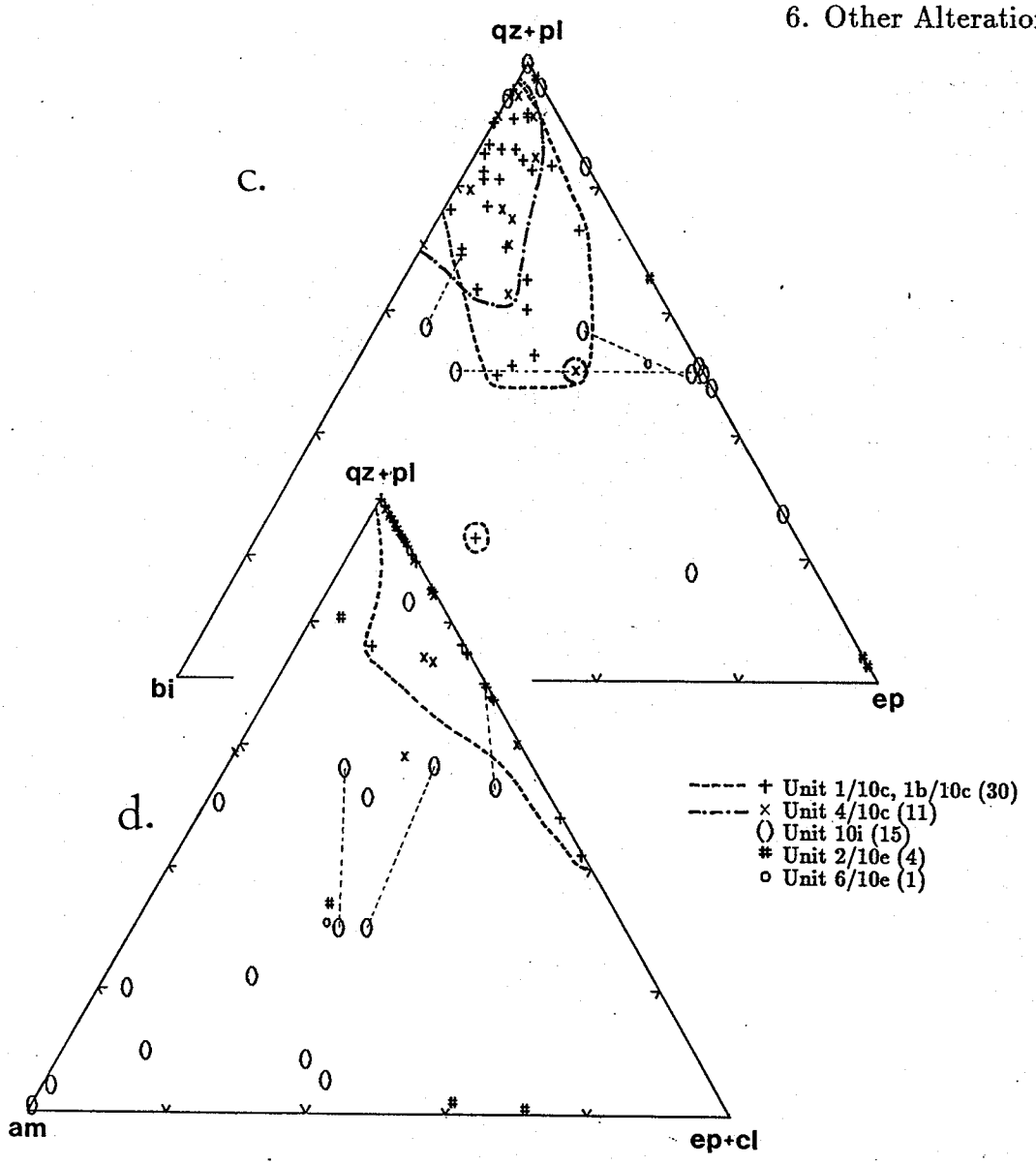

Figure 6.1. (continued).

c. Ternary proportions of quartz + plagioclase (qz+pl), biotite (bi) and epidote (ep) in calc-silicate rocks.

d. Ternary proportions of quartz + plagioclase (qz+pl), Ca-amphibole (am) and epidote + calcite (ep+cl) in calc-silicate rocks.

prisms, defining S_1 layering and dimensional mineral foliation. In some cases, it contains a dark, finely fractured core (1–15% area), inferred to be metamict allanite. (One semi-quantitative microprobe analysis detected Ce, La and Nd (*see* Appendix B).) Minor to trace amounts of calcite occur interstitially; more abundant calcite occurs in lenticular aggregates and pods, elongate in the S_1 plane. Chlorite is present in trace amounts and is probably of retrograde origin. Plagioclase has a

Table 6.2. Summary of Modal Mineral Percentages.

Ranges and averages (in parentheses) in calc-silicate altered rocks (Appendix A.)

See 3.1. Description of Lithological Units for explanations of unit and code designations.
See Table A.2 for a key to the code and Table A.3 for mineral abbreviations.

a. Concordant Calc-silicate Alteration of Felsic Rocks (1b/10c, 1/10c, 4/10c).

Unit	Code	N	Qz	Pl	Am	Ep	Cl	Gt	Bi	Ch	Mu	Op
1b/10c	pq,pl	5	35–60	20–45	0–12	1–10	0–5	0–3	4–12	0–t	0–15	0–2
			(44)	(35)	(2)	(5)	(1)	(1)	(7)	(0)	(4)	(1)
1/10c	pql,lm	6	27–55	2–18	0	0–22	2–48	0	2–26	0–t	0–55	0–1
			(44)	(10)		(10)	(10)		(12)	(0)	(10)	(0)
1/10c	mpq	10	15–51	0–47	0	3–23	0–t	0–t	5–25	0–t	2–20	0–3
			(32)	(24)		(8)	(t)	(0)	(15)	(0)	(11)	(1)
1/10c	p	9	17–54	5–60	0	t–30	0–1	0–2	5–44	0-18	0–12	0–3
			(41)	(25)		(8)	(t)	(t)	(16)	(3)	(6)	(1)
4/10c	pl,hp	5	10–37	24–65	0–16	t–15	0–20	0	2–20	0–2	0–t	t–2
			(26)	(43)	(4)	(7)	(8)		(10)	(1)	(t)	(1)
4/10c	p	6	23–50	13–53	0-25	t–27	0–1	0–1	3–18	0–24	0–16	t–3
			(32)	(31)	(4)	(9)	(t)	(t)	(11)	(4)	(7)	(1)

b. Static Calc-silicate Alteration.

Unit	Code	N	Qz	Pl	Am	Ep	Cl	Gt	Bi	Ch	Mu	Op
10i	hl	6	3–45	0–35	4–78	0–29	2–25	0	0–25	0–t	0	0–4
			(20)	(11)	(32)	(8)	(13)		(6)	(0)		(t)
10i	h	9	1–48	0–32	12–97	t–33	t–1	0	0–28	0–2	0–t	0–5
			(20)	(7)	(52)	(14)	(t)		(5)	(0)	(0)	(1)

c. Epidotized Mafic Volcanic Rocks.

Unit	Code	N	Qz	Pl	Am	Ep	Cl	Gt	Bi	Ch	Mu	Op
2/10e	ql	3	1–18	0–12	28–38	16–45	7–35	0–7	0	0	0	0–5
			(7)	(4)	(34)	(32)	(19)	(2)				(1)

d. Epidotized-Carbonatized Volcaniclastic Intermediate Rocks.

Unit	Code	N	Qz	Pl	Am	Ep	Cl	Gt	Bi	Ch	Mu	Op
6/10e	hqpl	1	15	15	40	24	2	0	4	0	0	t

calcic composition, inferred from its high relief, and typically occurs as poikilitic to skeletal, medium to coarse grained, aggregates and porphyroblasts, elongate in the S_1 plane. In some samples, it shows annular zoning and a schiller texture of fine lamellae. K-feldspar, with weak tartan twinning suggestive of an intermediate microcline, was observed in 4 samples. In one case, its distribution is restricted

to layers which have a high muscovite content. It also occurs as fine to medium grained, interstitial and poikiloblastic grains. In general, epidote and micas define penetrative D_1 and D_2 fabrics and, thus, the bulk-rock composition which allowed their metamorphic crystallization could have been a feature of the premetamorphic protolith.

6.2.2. Static Calc-silicate Alteration.

Zones of massive, coarse grained, calc-silicate mineralogy are volumetrically minor in comparison to concordant calc-silicate alteration. They form drill-core intersections up to 1.5 metres long, but mainly 5–30 cm, and occur in all lithological units. Contacts with the host rock are gradational and, in some cases, discordant to S_1 layering in the host rock. In general, the calc-silicate alteration in the gradational zones appears to be interleaved with the host rock on a fine scale (1–10 mm). With increasing intensity of alteration, the calc-silicate minerals increase in abundance and the layering in the host rock becomes obscured by randomly oriented felted Ca-amphibole. Static calc-silicate alteration is characterized by medium to coarse grained, pale green, acicular Ca-amphibole, and fine to coarse grained, equant epidote (Table 6.2, b). Near contacts to the host rock, biotite is present and the amphibole is darker. Plagioclase is either absent, or present in accessory amounts, and increases in abundance in the gradational zones. Titanite is a common trace or accessory mineral. The calc-silicate zones are commonly associated with quartz veins which contain minor calcite and, in some cases, form a central zone to the calc-silicate alteration.

The modal assemblages of the two types of calc-silicate alteration are quite distinct (Figure 6.1, b–d). Static calc-silicate alteration is interpreted to have crystallized post-tectonically. It seems to have filled narrow dilational structures and to have been accompanied by more extensive wall-rock alteration.

6.3. Epidotization and Carbonatization of Mafic Rocks.

Intensely epidotized and carbonatized rocks (2/10e, 6/10e) occur locally in mafic and intermediate volcanic rocks. In unit 2, epidotized-carbonatized rocks form discrete intersections, 2–15 cm in drill-core length. They consist of pale green zones, in contrast to the dark green host rock, and have numerous fractures, 1–10 mm in width, filled with white calcite. The altered zones commonly comprise up to 10% of

the rock, over 1–2 metres of drill core. They are typically asymmetrical, having an abrupt contact on one side and grading into the host rock on the other, but without any consistent direction to the asymmetry. The structure is mainly massive but heterogeneous, and consists of domains of fine grained (0.01–0.5 mm) aggregates of epidote, blue-green amphibole and calcite (Table 6.2, c), cut by numerous stringers, irregular pods and veinlets of calcite and minor quartz. The veinlets form up to 20% of the rock, ranging in width from seams of less than 0.2 mm (which commonly pinch out), up to 8 mm. They vary from irregular in shape and disposition, to fine conjugate fracture sets with slight apparent displacements of up to 4 mm. The fractures do not continue into the host rock, either pinching out or terminating at a fracture subparallel to the contact. The general appearance is of a thin breccia zone containing intensely altered fragments of host rock in a calcite matrix.

Epidote occurs as very fine ($\leq$.01 mm), mainly granoblastic aggregates, heavily dusted by submicroscopic to extremely fine inclusions which impart a brown colour approaching opacity. The inclusions tend to be concentrated in the grain centres, but also cross grain boundaries as though pseudomorphing a pre-existing structure, but without any identifiable shape. Amphibole occurs in anhedral to subhedral grains, interlocking with epidote and intergrown with calcite, in some cases, with a weakly symplectic texture. Calcite varies from very fine grained ($\leq$.01–0.2 mm) and interlocking with epidote and amphibole, to fine grained (up to 0.5 mm) in irregular interlocking monomineralic aggregates. Quartz occurs in trace to minor amounts, as inclusions, in calcite veinlets, and, in some cases, as single skeletal crystals (up to 0.25 mm) engulfing epidote and amphibole. Titanite is common in trace amounts forming anhedral grains and aggregates.

Amphibole occurs in similar amounts in the altered zones and in the adjacent host rock. The abrupt contacts occur by a change in the mineralogy interstitial to amphibole, from the epidote-calcite of the altered zone to the microcrystalline aggregate of plagioclase and quartz common to the matrix of unit 2. Amphibole habit changes slightly, becoming subhedral, acicular and defining a moderately strong directional fabric. In gradational contact zones, epidote persists, occurring with plagioclase and quartz and forming the matrix to amphibole.

The mafic to intermediate rocks of unit 6 typically contain epidote and calcite

in trace to minor amounts (Table 6.1, d) and concordant streaks, veinlets and veins of calcite are ubiquitous. Discrete calcite intervals (in drill core) commonly form up to 10% of the rock over several metres and this is not reflected in the modal proportions reported for the sample suite (*see* Table A.1). Epidotized-carbonatized rocks have a streaky layered structure (S_1), on a 0.5–1 mm scale, defined by domains variously rich in clear epidote, blue-green amphibole, felsic minerals and, less commonly, biotite. Amphibole and epidote occur in medium to coarse grained (0.5–5 mm), skeletal to poikilitic, elongate porphyroblasts, defining a strong layer-parallel, dimensional mineral foliation (S_1). Skeletal crystals are commonly mimetic after layering and contain layer-parallel trails of quartz inclusions and aggregates. Amphibole also defines a moderately strong, S_1 crystallographic foliation and, in some layers, a weak obliquely oriented, S_2 crystallographic foliation. Some layers contain biotite as fine to medium grained (0.1–1 mm) blades, typically aligned parallel to the S_1 plane. Calcic plagioclase (high relief) occurs in fine grained ($\leq$.25 mm) skeletal aggregates, interstitial to quartz. Titanite is present in trace amounts. Calcite occurs in discrete layer-parallel lenticular domains, which also contain amphibole, and minor quartz and epidote. Calcite is inequigranular (0.05–1.5 mm), with interlocking to sutured grain boundaries, and shows a weak layer-parallel dimensional orientation (S_1).

6.4. Chlorite-Hornblende Mafic Schists.

Mafic schists (10m) which occur locally in the alteration zones, particularly in the distal alteration zone, are distinctive in that they contain hornblende. Hornblende was not generally observed in altered rocks inferred to have had felsic precursors and, the possibility exists that chlorite-hornblende schists represent alteration of a mafic precursor. Their distribution is limited mainly to the lowermost (stratigraphically) parts of the distal alteration zone (Section A-A', in pocket). Jeffery (1982, *unpubl.*) correlated them with mafic to intermediate intercalations (1d) in the felsic volcanic rocks (1) hosting the distal alteration zone. The evidence in the cross-sections logged for this study (A-A', C-C'; in pocket) is equivocal as regards this proposed correlation.

Mafic schists in the distal alteration zone form 15–30 metres of drill-core intersection. Most of this is chlorite schist; amphibole increases in abundance toward a

central zone of about 2 metres in drill-core length, which contains up to 85% hornblende. The rocks generally have a well developed *S-C* structure, with *C*-planes defined by schistose chlorite and *S*-planes variously defined, by medium to coarse grained (up to 4 mm) augen of biotite, blue-green hornblende, felsic aggregates, and chlorite schistosity. Biotite and hornblende porphyroblasts and, in some cases, garnet, commonly contain inclusion trails of quartz oriented at a high oblique angle to the *S-C* fabrics. Biotite and hornblende have sigmoidal tails with a consistent sense of asymmetry resulting from transposition into the *C*-direction where they abut against the spaced *C*-cleavage (*see* 7.2.2. Sinistral Kinematic Indicators). One sample (73-834) contains subhedral prismatic epidote porphyroblasts (up to 1 mm long) in the chlorite schist, as well as minor amounts of fine grained anhedral calcic plagioclase (high relief) grains and aggregates. Some very fine grained retrogression affects most minerals, but is localized and apparently post-dates the *S-C* fabric development.

The amphibole-rich central zone contains blue-green amphibole as coarse grained (1–10 mm) anhedral, weakly or randomly oriented, interlocking poikiloblasts. These show abundant inclusion trails of quartz and, locally, the poikiloblasts are weakly mimetic after quartz-rich layering. Minor chlorite occurs both as layer-parallel schistose aggregates, interstitial to hornblende, and as medium grained (up to 1 mm) blades, weakly layer-parallel, and engulfed by hornblende.

In the chlorite-hornblende schist, it is not possible to distinguish unequivocally between the possible influence of premetamorphic alteration, as opposed to syntectonic alteration during fabric development. Although the mineral assemblage, amphibole-chlorite-epidote-plagioclase, is typical of greenschist facies (Winkler, 1979), in this case, the pale green pleochroism of the chlorite suggests a high Mg content, the clear non-pleochroic character of the epidote suggests a low-Fe variety, and the high relief of the plagioclase suggests a calcic plagioclase. The relative timing of the development of the *S-C* fabrics with respect to metamorphism is difficult to deduce.

6.5. Retrogression.

Two types of retrogression, with a mappable distribution in the subsurface (Sections A-A', C-C'; in pocket), can be distinguished at the Linda deposit. These

include cross-cutting fractures and fracture networks, closed or with a hairline-filling, associated with buff-orange weathering, hematite-carbonate wall-rock alteration which extends 1–10 mm into the host rock. The fractures occur in all lithological units and, where relatively dense and extensive (*i.e.* more than 30 cm of drill-core), are indicated on the cross-sections. They were avoided during sampling and will not be considered further. The other type of retrogression is not extensive and consists of the replacement of porphyroblastic minerals, especially staurolite, kyanite and plagioclase, by fine grained massive aggregates of muscovite, calcite, chlorite and possibly other unidentified retrograde minerals. In some cases, relicts of the original porphyroblast mineral can be identified. Where significant, this type of retrogression is also indicated on the cross-sections.

Chapter 7
Relationships between Textures, Microstructures, Mineralogy and Deformation

A sequence of progressively developed fabric elements, defined by textural and structural relationships indicative of relative age, can be observed at the Linda deposit. These have been described in the context of lithology, alteration and structural geology and will be summarized here (Table 7.1), highlighting the microstructural observations. The relationships between sequentially developed tectonic fabrics, mineral textures, and observed and inferred mineral assemblages, can be used to deduce a pressure-temperature-time path.

7.1. Microstructures.

7.1.1. Fabric Elements and Mineralogy.

At the Linda deposit, planar fabric elements, and the habit, orientation and degree of strain of the minerals defining them, proved to be the most useful criteria for deducing a paragenetic sequence (Table 7.1). Linear fabric elements have an intrinsic ambiguity resulting from the apparently coaxial relationship between L_1 and L_2 (*see* 4.3. Linear Fabric Elements). Primary features and relicts, such as embayed quartz phenocrysts and subhedral plagioclase phenocrysts, allow some inference of the primary mineralogy. The massive microcrystalline interlocking felsic matrix of some rocks, for example, 'cherty' felsic rocks, may have a primary (hydrothermal?) origin or, in any case, metamorphic recrystallization probably occurred without substantially changing the primary assemblage. Graphite and pyrite are both commonly reported as primary or early diagenetic minerals in sulphidic black shales and slates (Tracy and Robinson, 1988 and Ferry, 1981 for brief reviews; Pettijohn, 1975), and pyrite (as well as Cu and Zn sulphide minerals) is one of the precipitates in recent and active, seafloor sulphide mounds and in fluids emanating from black smoker vents (*e.g.* Franklin, 1986; Bäcker *et al.*, 1985). At the Linda deposit,

these minerals define bedding and, it is probable that they are, at least in part, pre-dynamometamorphic in origin (*see* Plate 5.3, e–f). Pyrite and tourmaline occur in the matrix of altered breccias, and tourmaline also occurs in mineralogical zoning around the outer margins of clasts (*see* Plate 5.3, c–d). Studies in metamorphosed Appalachian and Caledonian massive sulphide deposits have supported a diagenetic or hydrothermal origin for finely zoned tourmaline which was apparently armoured by a matrix of sulphide minerals (Taylor and Slack, 1985; 1984). At the Linda deposit, tourmaline commonly occurs as euhedral prismatic crystals defining an S_1 crystallographic and dimensional foliation and is interpreted to be synmetamorphic (*e.g. ibid.*; Davies, 1985). Although the distribution and occurrence of other minerals at the Linda deposit is partly a function of primary bulk-rock composition and a record of primary structures is preserved locally (*e.g. see* 5.3.4. Metasedimentary Rocks), the minerals have apparently crystallized during regional metamorphism.

Flattened and elongated quartz phenocrysts and lithic clasts define S_1 planar and L_1 linear fabrics. The spectrum of strain and recrystallization observed in the phenocrysts (*see* 5.3.1. Quartz Phenocrysts) supports their identification as primary relicts and, the identification of the stretching lineation as an L_1 fabric element. The S_1 compositional layering is associated with layer-parallel mineral schistosities which consist of crystallographic and dimensional preferred orientations, the latter generally defined by skeletal or poikiloblastic minerals with habits mimetic after the pre-existing layering. Phyllosilicate minerals, especially muscovite, chlorite and margarite; rutile inclusions in plagioclase (*see* 5.4. Plagioclase-layered Rocks); and kyanite, define crystallographic foliations. Note that this supports the interpretation of muscovite, chlorite and margarite as prograde metamorphic minerals in the sense that they crystallized at an early stage of fabric development. Layer-parallel dimensional preferred orientations are shown by virtually all porphyroblastic minerals. However, garnet is the only porphyroblastic mineral which does not also occur in habits mimetic after S_2 fabrics. (One possible exception is the garnet in a calc-silicate enclave in the pyrite-calcite body (*see* 5.6.2. Silicate Enclaves in the Main Massive Sulphide Body; Plate 5.6, m–n).)

Locally, particularly in the proximal alteration zone, kyanite occurs in porphyroblasts with c-axes and long dimensions aligned in the S_1 schistosity. These

Table 7.1. Summary of Fabric Elements and Mineralogy.

a. Distal (10d, 10da) and Proximal (10p, 10pa) Alteration Zones, 'Cherty' Felsic Rocks (1a) and Graphitic Metasediment (3).

	Structure or Texture	Defining Minerals
pre-D_1	embayed, monocrystalline phenocrysts	quartz
	subhedral to euhedral phenocrysts	plagioclase
	bedding (S_0)	graphite, pyrite
	stringer and disseminated mineralization	pyrite
D_1	flattened, strained or recrystallized phenocrysts (S_1)	quartz
	compositional layering, layer-parallel crystallographic foliation (S_1)	muscovite, chlorite, margarite, biotite, rutile (trails), kyanite, tourmaline
	compositional layering, mimetic porphyroblasts (S_1)	garnet, staurolite, kyanite, gahnite, biotite, plagioclase, tourmaline
D_2	crenulation cleavage (S_2)	muscovite, chlorite, margarite, kyanite, staurolite
	crystallographic foliation, dimensional foliation (S_2)	biotite, muscovite, chlorite
	mimetic porphyroblasts (S_2), with deflection of S_2 crenulation cleavage in matrix	gahnite, staurolite, kyanite, biotite, plagioclase
	rotated inclusion trails or sigmoidal tails	magnetite, gahnite, staurolite, kyanite, plagioclase, biotite
late D_2	random orientations, undulatory extinction	anthophyllite, gahnite, staurolite
post-D_2	random orientations, $\pm$symplectic and corona structures	fibrolitic sillimanite, calcite, pyrite, pyrrhotite, epidote, amphibole, sphalerite, plagioclase

crystals commonly show strain and substructure (*see* Plate 5.4, a–c) and, in some cases, kinking, associated with D_2 crenulation. Kyanite showing this habit commonly occurs in biotite-free rocks and, in some cases, is engulfed by staurolite and/or kyanite mimetic after S_1 and S_2 fabrics. These features were interpreted as evidence of syn-D_1 crystallization of kyanite, *i.e.* an early generation with respect to kyanite mimetic after S_1 and S_2 fabrics.

Table 7.1. (continued)

b. Concordant (10c) and Static (10i) Calc-silicate Rocks.

	Structure or Texture	Defining Minerals
D_1	flattened, strained or recrystallized phenocrysts (S_1)	quartz
	compositional layering, layer-parallel crystallographic foliation (S_1)	muscovite, epidote, biotite
	compositional layering, mimetic porphyroblasts (S_1)	epidote, biotite, plagioclase
D_2	crenulation cleavage (S_2)	muscovite, epidote
	crystallograpic foliation (S_2)	biotite
	rotated inclusion trails or sigmoidal tails	epidote, plagioclase, biotite
post-D_2	random orientations	Ca-amphibole, epidote, calcite

In the staurolite-banded gneisses of the distal alteration zone, staurolite is mimetic after S_1 layering and shows corrugation related to D_2 (*see* Plate 5.1, a–b). The staurolite crystals do not show detectible crystallographic orientation or undulatory extinction and, although they appear to have a substructure related to the corrugation, the grain boundaries show high to low angles of crystallographic misfit (judging from extinction angles, as cleavage is not visible) and are non-coherent (Spry, 1969). These grains were interpreted to have crystallized prior to D_2, mimetic after the S_1 layering, and to have recrystallized during D_2, clearing any D_2 strain. Staurolite with this habit has the strong pleochroism typical of Fe-rich staurolite (*e.g.* Deer *et al.*, 1966).

The S_2 fabric most commonly consists of a crenulation cleavage defined by the transposition of S_1 schistosity in phyllosilicate minerals (*see* Plates 5.1, b; 5.4, c; 7.1, a–b; 7.2, a), in some cases, accompanied by slight compositional segregation into phyllosilicate-rich hinges and more quartzo-feldspathic limbs. It resembles 'stage 3' cleavage (Bell and Rubenach, 1983), *i.e.* 'differentiated crenulation cleavage with continuity across the crenulation cleavage', or zonal crenulation cleavage (Gray, 1977). Less commonly, phyllosilicate minerals occur as blades, recrystallized parallel to S_2, mainly on the hinges of the crenulation cleavage (*see* Plate 7.2, c–e), as in 'stage 4' of Bell and Rubenach (1983). In some cases, the recrystallized hinge zone of the crenulation cleavage is discontinuous, but without recrystallization parallel

to S_2 (*see* Plate 7.1, d). In these cases, microlithons show a weakly sigmoidal structure or a straight herringbone structure and adjacent microlithons alternate between dextral and sinistral asymmetry. It resembles the discrete cleavage of Gray (1977) and Swager (1985).

In contrast to other phyllosilicate minerals, biotite occurs in porphyroblasts commonly mimetic after S_1 compositional layering or, have an S_1 dimensional orientation, but with the (001)-cleavage defining a strong S_2 orientation. Bladed or augen-shaped porphyroblasts with sigmoidal tails occur in the hinges of the S_2 crenulation cleavage defined by muscovite and chlorite. The sigmoidal tails occur where biotite abuts against the S_1 compositional layering defined by quartzofeldspathic domains; the asymmetry suggests some reactivation of S_1, post-dating the development of S_2 (*e.g.* Figure 13 of Bell, 1986).

Gahnite, staurolite, kyanite and biotite have all been observed as porphyroblasts mimetic after both S_1 and S_2 fabrics. The porphyroblasts are skeletal, typically with one or more spaced central spines defining S_2, and several lateral ribs, defining S_1 (*see* Plate 7.2, c–e). The orientation of the ribs is oblique to the spine, *i.e.* mimicking the S_1 and S_2 relationships. Staurolite with this habit is faintly to nearly non-pleochroic, suggesting a low-Fe composition. The porphyroblasts consistently display asymmetrical mimetic structures (*see* 7.2.3. Opposed Cleavage Vergence between Porphyroblasts and Matrix), rather than the symmetrical 'millipede' structures ascribed to progressive bulk inhomogeneous shortening (Bell, 1986; Bell *et al.*, 1986; Bell and Rubenach, 1980). The S_2 crenulation cleavage is deflected around the porphyroblasts. Porphyroblastic minerals with these features were interpreted to have grown during D_2. D_2 deformation apparently continued after the porphyroblasts ceased to grow, but further strain was accommodated in the matrix (*e.g. ibid.*, Bell, 1985; 1981; Olesen, 1982).

Poikiloblastic gahnite, staurolite, kyanite, biotite and plagioclase contain numerous aggregates and inclusion trails of quartz which define an internal S_1 layering, and which, in many cases, are obliquely oriented with respect to the S_1 layering in the matrix. The continuity of the layering between the matrix and the porphyroblast is commonly unbroken.

Skeletal kyanite, mimetic after both S_1 and S_2 fabrics, occurs in association

with biotite, the weak pleochroism of which is suggestive of a phlogopitic composition. The kyanite was interpreted to be a syn-D_2 generation, distinct from the previously described syn-D_1 kyanite. In some cases, kyanite of both generations occurs in the same sample (*e.g.* 22B-1638, 22-901).

Plagioclase porphyroblasts and aggregates define S_1 layering in felsic rocks and, in altered rocks, are associated with phyllosilicate layers. The long dimension of porphyroblasts defines a foliation parallel to the S_1 plane and the porphyroblasts contain layer-parallel inclusion trails of quartz, rutile and trace minerals (*see* 5.4. Plagioclase-layered Rocks; Plate 5.5), or margarite (*see* 5.3.5. Proximal Alteration Zone; Plate 5.4, f). Plagioclase is generally unstrained and, in some cases, contains inclusion trails which trace F_2 microfolds and has a habit mimetic after D_2 crenulations.

Acicular prismatic needles of fibrolitic sillimanite are present in trace amounts in altered rocks, occurring as radiating clusters on grain boundaries, particularly between plagioclase grains. Although the needles are unoriented, they tend to nucleate on grain boundaries which are parallel to the S_2 fabric and elongate parallel to the lineation. They were interpreted to be post-tectonic, but their nucleation sites are partly controlled by earlier structures.

Minerals in the staurolite-anthophyllite-gahnite silicate enclave in the pyrite-calcite body (*see* 5.6.2. Silicate Enclaves in the Main Massive Sulphide Body) were inferred to have crystallized during late-D_2. They are unoriented, but show weak substructure development and undulatory extinction, indicating some degree of strain (*see* Plate 5.6, a–c). Within calc-silicate enclaves, the only penetrative fabrics appear to be relicts of S_1 layering and mineral foliation within the domains least affected by calc-silicate alteration (*see* Plate 5.6, m). The pyrite-calcite host rocks have a massive structure. In the enclaves, the prevalence of crystallographically controlled symplectic textures (*see* Plate 5.6, d–h) and interface-controlled corona structures (*see* Plate 5.6, k–l), were interpreted to indicate post-tectonic crystallization. Note that in the enclaves, gahnite occurs as inclusions in plagioclase and, that in the least affected domains, elongate plagioclase grains contain layer-parallel trails of rutile inclusions (*see* Plate 5.6, o–p). The gahnite, the rutile trails, and the plagioclase containing them, were interpreted to be relicts of the

original dynamometamorphic assemblage.

Concordant calc-silicate rocks (Table 7.1, b) have S_1 layering defined mainly by dimensionally oriented mimetic epidote and epidote aggregates, in association with muscovite and biotite. In some cases, elongate epidote porphyroblasts contain inclusion trails of quartz and show an oblique orientation with respect to the layering. Epidote layers are locally crenulated, but the epidote appears unstrained and grain boundaries show high to low degrees of lattice misfit. Micas in these rocks generally define the same fabrics as the micas of the alteration zones, except that biotite is not mimetic after S_2 fabrics, although it does define an S_2 crystallographic foliation. Epidote was interpreted to have crystallized during D_1 and to have undergone recrystallization subsequent to D_2 crenulation. Static calc-silicate rocks (Table 7.1, b) are massive; layering is confined to transitional contact zones and appears to be mimetic after the structure of the host rock. Static calc-silicate rocks were interpreted to have crystallized post-tectonically.

7.1.2. F_2 Microfolds.

Tight asymmetrical F_2 folds, which reorient S_1 layering and schistosity, are locally common in the subsurface. With few exceptions, the S_2 crenulation cleavage and biotite schistosity appear to be axial planar to the minor folds. F_2 folds in thinly bedded graphitic metasediment reorient S_0 bedding and bedding-parallel S_1 schistosity defined by margarite and by flattened quartz phenocrysts (Figure 7.1, Plate 7.1). The graphitic metasediment provides a rare opportunity to examine, in detail, the relationships between several fabric elements; unfortunately the broken nature of the drill core precludes orientation of the samples in 3 dimensions (*see* 7.2. Kinematic Indicators).

The shape of the F_2 microfold is asymmetrical, having one thin limb with tight parasitic drag folds, and a thicker limb with open parasitic drag folds (Figure 7.1, a–b; Plate 7.1). Kyanite porphyroblasts, present at various positions around the fold, are mimetic after S_1 and S_2 fabrics (Plate 7.1, c). The S_2 cleavage recorded by the kyanite resembles spaced kink bands, and changes vergence across the nose of the fold. The cleavage is nearly perpendicular to bedding and to S_1 on the thicker limb, and forms a divergent fan around the fold. Some deflection of the S_2 crenulation cleavage occurs around the kyanite porphyroblasts. One porphyroblast on the thin

Figure 7.1. (following page) Microstructural relationships exhibited by an F_2 microfold in margarite-kyanite graphitic metasediment (34-1500). The outlined areas correspond to the photomicrographs in Plate 7.1. The fabric elements consist of the following: laminated, S_0 bedding defined by finely divided graphitic (stippled); bedding-parallel S_1 dimensional orientation of flattened quartz-crystal clasts (qz, smooth outline); bedding-parallel S_1 margarite schistosity (dashes); S_1 inclusion trails (short dashes) in kyanite (ky, rough semi-continuous outline) which is mimetic after S_1 and S_2; S_2, zonal and discrete herringbone, crenulation cleavage (dash-dot) in margarite schist; S_2 crenulation cleavage in mimetic kyanite (dash-dot); and weak S_3 crenulation cleavage (dash-double dot). Note the following relationships, discussed more thoroughly in the text: bedding and S_1 schistosity traces an F_2 microfold which has a thick limb showing open parasitic folds and a thin limb showing tight parasitic folds, S_2 crenulation cleavage apparently fans around the fold, but more so on the thick limb, and more so in kyanite relative to the margarite matrix; the S_1/S_2 vergence changes in mimetic kyanite, in parasitic folds traced by graphitic laminae, and in margarite, in accordance with position around the fold; the axial plane of the F_2 fold is curved and lies close to the thin limb; quartz-crystal clasts are flattened parallel to S_1 and change orientation around the nose of the fold; S_2 crenulation cleavage deflects around kyanite porphyroblasts (especially in area d). Sinistral rotation (as illustrated, without 3-dimensional significance) is indicated by these features. A single grain of arsenopyrite(as) with minor sphalerite, has quartz pressure fringes which appear to be face-controlled overgrowths.

limb of the fold (Plate 7.1, d), shows an apparent sinistral rotation, with the S_1 and S_2 cleavages of the matrix curving around and defining a complex δ-type pressure shadow (Passchier, 1987). On the side of the porphyroblast facing into the fold, the S_1 planes of the margarite schistosity pass continuously into the kyanite.

The S_2 crenulation cleavage, defined by the transposed S_1 schistosity of margarite, also changes vergence across the fold. Inside the graphitic marker, the cleavage has a herringbone structure, consisting of domains of opposingly oriented S_1 schistosity, separated by discrete discontinuities (Plate 7.1, d). The S_2 cleavage, defined by crenulated margarite, fans around the fold, but less so than the S_2 cleavage recorded by kyanite; *i.e.* it more closely approaches an axial planar relationship, especially on the tighter limb. The trace of the axial plane in the section, as defined by change in cleavage vergence, apparently lies very close to the thin limb of the graphitic marker. Most of the S_2 cleavage traces on the inside of the fold are continuous and emerge on the thicker limb. A single arsenopyrite grain has quartz pressure fringes, apparently of face-controlled syntaxial type (*e.g.* Gray and Durney, 1979).

The S_0, S_1 and S_2 fabric elements all show an open curvature, possibly related to a very weak S_3 crenulation cleavage which transects the section (Figure 7.1).

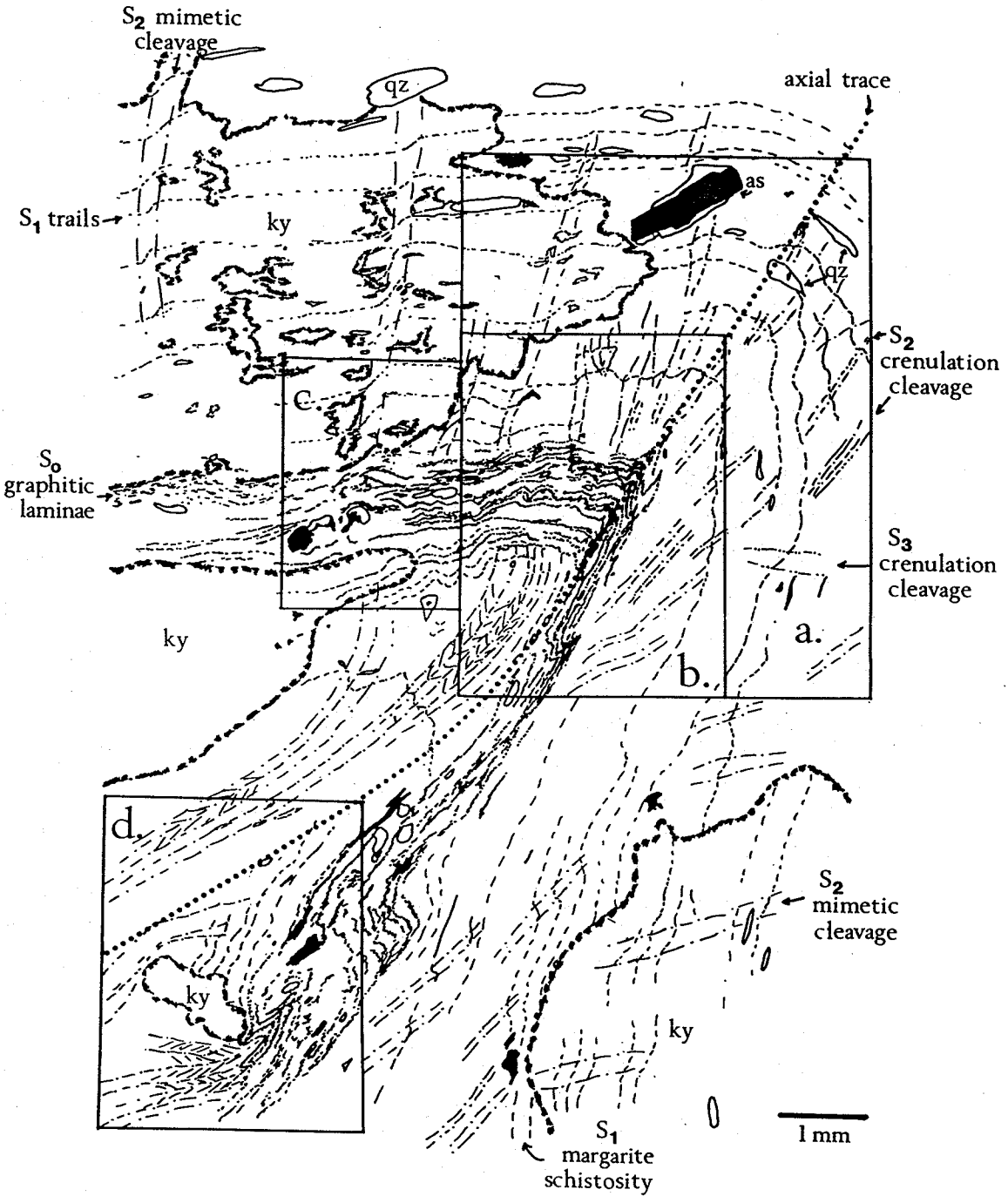
S2 mimetic cleavage
qz
axial trace
as
S1 trails
ky
qz
S2 crenulation cleavage
c.
So graphitic laminae
S3 crenulation cleavage
ky
a.
b.
d.
S2 mimetic cleavage
ky
ky
S1 margarite schistosity
1 mm

Plate 7.1. (following page) Details of microstructural relationships of the F_2 microfold in Figure 7.1. The bar scale in each plate represents 1 mm. (See figure for locations and further explanations.)

a. Hinge area showing the change in microstructural style and vergence between the thick limb and thin limb. Both S_0 and S_1 are continuous, except for local development of S_2 as a discrete crenulation cleavage (*e.g.* inside the graphitic marker, lower left). The large, tabular, opaque grain is arsenopyrite(as), with minor sphalerite, and quartz pressure fringes. Quartz-crystal clasts are flattened parallel to the S_1 margarite schistosity, and show some S_2 crenulation. Part of a kyanite porphryoblast(ky) is mimetic after S_1 and S_2 fabrics.

b. Detail of the hinge area in the graphitic marker. Thin graphitic laminae appear to be continuous. The style of the parasitic folds changes from open kinks to nearly isoclinal across the hinge.

c. Kyanite porphyroblast(ky) on the thick limb, showing mimetic structure after S_1 and S_2, resembling kink bands. Note the dextral cleavage vergence and its continuity across the graphitic marker(gr).

d. Kyanite porphyroblast(ky) inside the graphitic marker(gr) with asymmetrical distribution of zonal and discrete S_2 crenulation cleavage in the matrix. On the right, the cleavage is tight and the graphitic laminae describe tight microfolds with curved axial traces. On the upper left, S_1 margarite schistosity is weakly crenulated near the porphyroblast and S_1 trails pass continuously into the kyanite. Sinistral rotation is inferred to have tightened the crenulation cleavage on the right, and partly decrenulated the cleavage on the upper left.

The weak crenulation cleavage (stage 2; Bell and Rubenach, 1983) is also visible in sections cut parallel to S_2 and, in the drill-core sample, a weak L_3 crenulation cross-cuts the L_2 crenulation axes on S_1 surfaces. Some of the curvature of S_2 can be related to interference of kyanite porphyroblasts.

In this example (Figure 7.1, Plate 7.1), the S_2 cleavage is approximately axial planar to the microfold, and the cleavage vergence of S_2 and S_1-S_0 on each limb is correct for an F_2 fold. The main fanning of S_2 occurs on the thicker limb, and to a lesser extent in kyanite on the opposite limb. Note that the fanning is exaggerated by the general curvature and is much reduced when the curved axial plane is taken into account. On the thicker limb, the S_2 cleavage is relatively open and resembles kinking.

Some possibilities, not necessarily mutually exclusive, are suggested by the observations. Kyanite may record early stages of S_2, and by implication, of F_2 development. The fold and associated crenulation cleavage continued to tighten, rotating the kyanite porphyroblasts, which preserved incipient S_2 as kink bands recorded by the mimetic habit. This does not explain the asymmetry of the fold nor the asymmetry of S_2 development on each limb. One limb is tectonically thinned

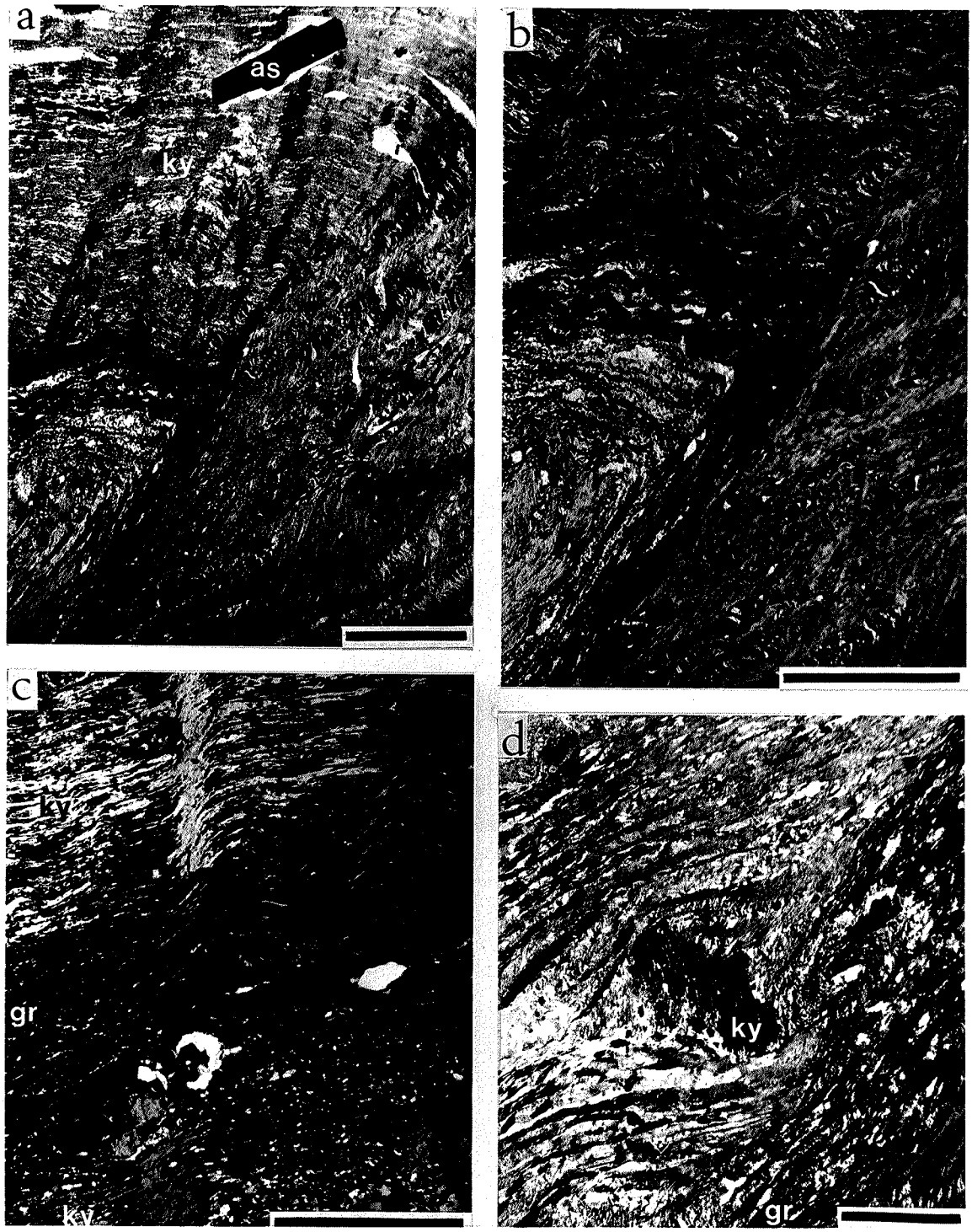
a
as
ky
b
c
ky
gr
ky
d
ky
gr

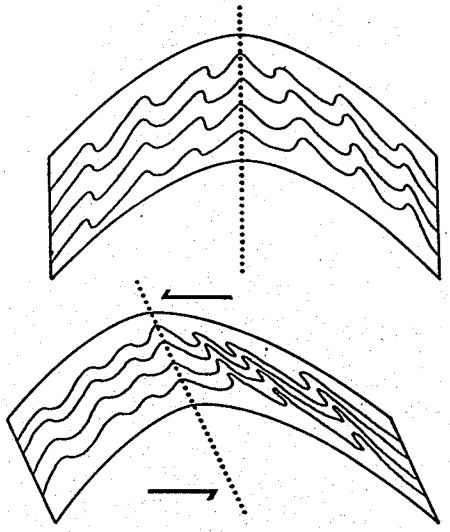

Figure 7.2. Schematic illustration of a possible configuration leading to the F_2 microfold of Figure 7.1. Sinistral shearing on shear planes with a nearly perpendicular orientation to the axial plane of an open fold leads to asymmetry defined by a thickened limb with decrenulated parasitic folds, and a thinned limb with tightened parasitic folds. The angle between the axial trace and the thinned limb is reduced.

and its microstructures are tightened with respect to the other limb. These features are interpreted to be the result of shearing, with transposition and deformation influenced by the original orientation of the markers relative to the shear plane (Figure 7.2). A sinistral sense of shear (in the section, without any larger scale significance) is required, with the tightened limb oriented in the extensional field of the strain ellipse, and the thicker limb oriented in the compressional field of the strain ellipse (Ramsay, 1980). This further implies that a pre-existing, uniformly developed, axial planar cleavage would undergo tightening on the thinned limb and decrenulation on the thickened limb (Figure 7.2; *e.g.* Figure 8 of Skjernaa, 1980; Figure 7 of Bak *et al.*, 1975). The curvature of S_1-S_0 and S_2 and, in part, the fanning of S_2 relative to a bisectrix, can also be accounted for by sinistral shearing. The relationship of S_3 is not clear, but it could be a new crenulation cleavage related to the shearing.

This interpretation implies that the S_2 cleavage may initially have been axial planar to the F_2 microfold and that subsequent transposition was responsible for many of the fabric relationships now observed. If this microstructure is a reasonable analogue for large scale structures, it implies that F_2 folds may have undergone later shearing resulting in one tectonically thinned limb, which would resemble a high

strain zone as a function of its original orientation in the strain ellipse. This suggests that the S_2 fabric, if it was initially axial planar to F_2 folds, has been reoriented.

7.1.3. S_1 Rutile Trails.

Rutile trails were described in some detail (*see* 5.4. Plagioclase-layered Rocks), including their relationships to quartz porphyroclasts in quartz-megaphyric felsic rocks. At the Linda deposit, rocks containing rutile trails nearly form a mappable subunit, and this would certainly be the case if the trails could be reliably identified on a hand-sample scale. Their occurrence is restricted to unit 4 and the uppermost parts of the proximal alteration zone and may reflect structural control, primary compositional control (*i.e.* requiring a protolith containing rutilated quartz), metamorphic control (*i.e.* requiring enclosing minerals which do not incorporate large amounts of Ti in their structure), or some combination of these factors. The trails are similar to 'Tuttle' deformation lamellae, named for Tuttle's (1949) investigation of the planar arrays of fluid inclusions commonly observed in strained quartz (Spry, 1969). 'Tuttle' lamellae are characterized by their continuity across grain boundaries and by orientations independent of crystallographic control by the host crystals (*ibid.*). Tuttle (1949) found their orientation to be similar over a large geographic area and suggested that the inclusions had been localized along shear planes. The rutile trails at the Linda deposit are interpreted to be 'Tuttle' deformation lamellae which originated by the recrystallization of rutilated quartz phenocrysts and to represent localized fine D_1 shear planes. Given the subsequent recrystallization of plagioclase and phyllosilicate minerals, evaluating the magnitude and the significance of the shear strain and its relationship to bulk strain is problematic.

Trembath (1986) reported similar trails of rutile, transgressing matrix and porphyroblastic staurolite, gahnite and kyanite, in altered quartz-phyric rocks at the Anderson Lake mine. However, he did not indicate their distribution or frequency of occurrence. He interpreted them as fine shear planes which pre-dated the crystallization of porphyroblastic minerals. In aluminous altered rocks in the Harare greenstone belt, Zimbabwe, Kerrich *et al.* (1987) described rutile 'disposed in linear stringer-like arrays', without proposing any mode of origin.

7.2. Kinematic Indicators.

Detailed sampling and petrography was done mainly on drill core. In some cases, it was possible to approximately orient the core samples in 3 dimensions by recording the direction to surface and the plunge of the drill hole at the sample location and by taking advantage of the general uniformity in the regional dip of S_1 fabrics and the lineations in the S_1 plane. The angle between the core axis and the S_1 plane is generally small enough to allow unambiguous discrimination between the 2 possible orientations of the lineation resulting from 180° rotation of the core along the core axis. (If S_1 and the core axis are perpendicular, the bilateral symmetry precludes the determination of a unique orientation for the sample.) The method has a large margin of error, but suffices to relate the sense of asymmetry of structures in subsurface samples to the structures mapped on the surface. The method is not trustworthy in core which was previously split, as the core may have been inadvertantly rotated, top to bottom, and its broken nature makes continuity difficult to establish. Kinematic indicators used to deduce the sense of shear were of 4 basic types: S-C fabrics, drawn-out sigmoidal tails on lithic clasts and porphyroclasts, rotated porphyroblasts, and drag folds in the wall rock adjacent to quartz veins.

7.2.1. Dextral S_1/S_2 Cleavage Vergence.

The cleavage vergence of S_1 and the S_2 fabrics defined by phyllosilicate minerals is dextral, as determined from surface mapping in the Linda area (*see* 4. Structural Geology of the Linda Area; Figure 4.2), and this generally applies to the subsurface as well. Some very localized high strain zones were observed, in some cases comprising 2 cm of drill core with contacts transitional over 1 cm. These are marked by tightened S_2 crenulation cleavage, subparallel to the S_1 schistosity, and by increased flattening and elongation of clasts in volcaniclastic rocks (Plate 7.2, a). In a few cases, a new crenulation on the S_1-S_2 surface cross-cuts the crenulation axes of the S_2 crenulation cleavage. It is steeper than the L_2 lineation, having a rake of about 90°. These high strain zones, and particularly the associated lineation, were observed only in isolated examples and their significance is difficult to evaluate. However, it may be important to note that they are apparently distinct from the single-fabric schists, described in the alteration zones (*see* 5.2. Distal Alteration

Plate 7.2. (following page) Cleavage and porphyroblast relationships. The bar scale in each plate represents 1 mm.

a. 19-543b partial xpl (cross-polarized light) Transition from 'normal' D_2 strain (bottom), to a high strain zone (top) in which the S_2 crenulation cleavage in muscovite is transposed into coincidence with S_1, defined by flattened clasts (A).

b. 24-812 ppl (plane-polarized light) Staurolite porphyroblast which overgrew S_0 bedding and S_1 schistosity. The sense of rotation was sinistral up-plunge, as interpreted from the discordance between S_0-S_1 in the porphyroblast and in the matrix, and from the asymmetry of the $S_1(S_0)$ planes in the vicinity of the porphyroblast. Chlorite pressure fringes (A) are mainly, but not entirely, consistent with this interpretation.

c. 22A-1625 partial xpl Skeletal staurolite porphyroblast(st), mimetic after S_1 and S_2 fabrics. The S_1/S_2 cleavage recorded by the porphyroblast has the opposite sense of vergence from that in the matrix (*see text for further discussion*). Garnet porphyroblasts(gt) are mimetic only after S_1 layering.

d. Detail of c. The skeletal staurolite is a nearly non-pleochroic, optically continuous, single crystal. Compare the S_1/S_2 cleavage vergence of the porphyroblast with that of the matrix in c.

e. 22A-1625 partial xpl Similar to c. Skeletal staurolite showing S_1/S_2 cleavage vergence opposed to that in the matrix. S_2 in the matrix is a discrete crenulation cleavage.

f. 28-137 ppl Part of a garnet porphyroblast with sigmoidal S_1 inclusion trails suggesting sinistral rotation. Biotite schistosity near the pressure shadows and the S_1/S_2 cleavage vergence in the matrix (not visible), suggest dextral rotation. This sample also contains clasts with σ-type tails (*see* 7.2.2. Sinistral Kinematic Indicators) consistent with a sinistral sense of motion.

Zone), in that the S_2 crenulation cleavage is rotated into parallelism with the S_1 plane, thus conforming to the S_1 orientation. These zones apparently represent a reactivation of S_1 layering and they may be a more extreme example of the previously described sigmoidal asymmetry of S_2 crenulation cleavage and biotite porphyroblasts near contacts with S_1 quartzo-feldspathic domains (*see* 7.1.1. Fabric Elements and Mineralogy).

7.2.2. Sinistral Kinematic Indicators.

Sigmoidal tails on lithic clasts were observed along bedding contacts between volcaniclastic breccias with a high proportion of felsic clasts and finer grained volcanogenic metasediments or tuffs. The coarser, more clast-rich beds apparently accommodated less strain relative to finer, or more matrix-rich beds. The drawn-out tails were interpreted to be elongated in the direction of shear, giving a sinistral, up-plunge sense of motion (Ramsay and Huber, 1980; Ramsay, 1980). The clasts resemble porphyroclasts with recrystallized material defining σ-type tails, i.e. in

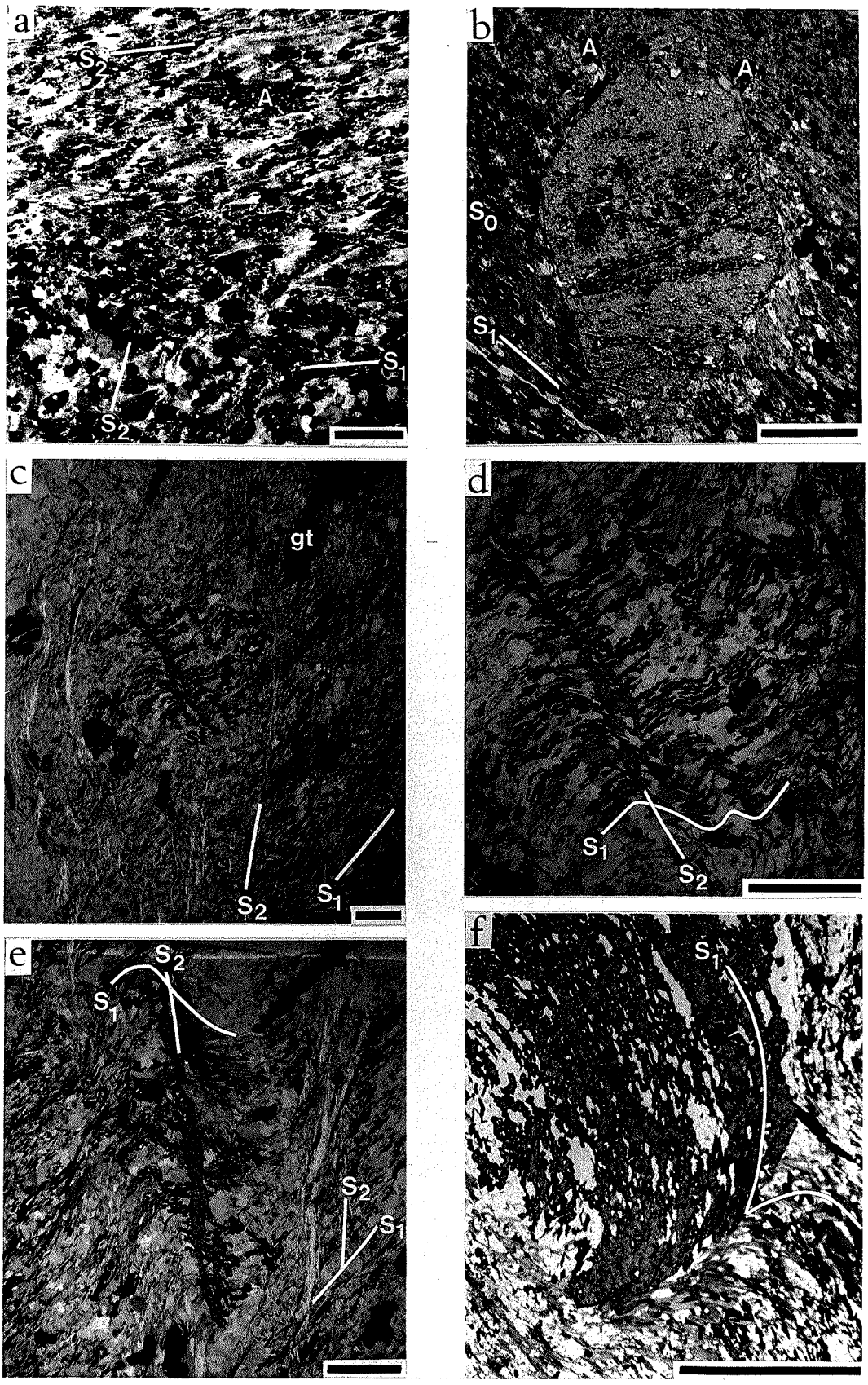
a
S_2
A
S_1
S_2
b
A
A
S_0
S_1
c
gt
S_2
S_1
d
S_1
S_2
e
S_2
S_1
S_2
S_1
f
S_1

which the long axis of the relatively rigid body lies close to the flow plane (Passchier, 1987; Simpson and Schmid, 1983) and the tails lie parallel to the S_1 (and S_0) plane. They do not appear to have rolled (*e.g.* Driessche and Brun, 1987) but, rather, appear to be the result of heterogeneous strain distribution in which the main body of each clast was pinned by impingement on its neighbours. In this case, the sense of movement could apply to D_1, as the asymmetry is defined only by S_0 and S_1 fabric elements.

The vergence asymmetry of S-C fabrics, particularly within hornblende-chlorite mafic schists (10m), was also used to determine sense of shear (Berthé *et al.*, 1979; Simpson and Schmid, 1983). Some of these schists contain augen-shaped hornblende and biotite porphyroclasts, with associated tails and pressure shadows of σ-type or early stages of δ-type, showing a slight rotation of the pressure shadow (Passchier, 1987; Takagi and Ito, 1988). The S-C fabric and the porphyroclasts consistently indicated a sinistral sense of shear.

Drag folds traced by S_1 layering adjacent to quartz veins are uncommon as most of the veins are concordant. However, where a sense of rotation was discernible, it also indicated sinistral up-plunge motion.

Porphyroblasts, in most cases, have nearly planar inclusion trails, obliquely oriented with respect to the matrix and showing little evidence of rotation during growth. The porphyroblastic schists of the alteration zones had commonly been fragmented during previous splitting of the core and porphyroblasts were seldom used as kinematic indicators. An exception to this is observed in a staurolite porphyroblast which overgrows an S_0 bedding surface and bedding-parallel S_1 schistosity (Plate 7.2, b). The surfaces within the porphyroblast are straight, suggesting that rotation occurred after the porphyroblast had ceased growing (*e.g.* Vernon, 1978; Spry, 1969). The sense of obliquity between S_0-S_1 in the porphyroblast and S_0-S_1 in the matrix, and the asymmetry of the surfaces at the grain contact, indicates sinistral up-plunge rotation. Chlorite pressure fringes occur around part of the grain boundary, as well as fringing kyanite porphyroblasts in the same sample. They are curved, indicating a component of noncoaxial strain during deformation (Ramsay and Huber, 1980; Gray and Durney, 1979), but their sense of curvature is not entirely consistent.

7.2.3. Opposed Cleavage Vergence between Porphyroblasts and Matrix.

Skeletal staurolite and kyanite porphyroblasts, mimetic after S_1 and S_2 fabrics have been previously described (*see* 7.1.1. Fabric Elements and Mineralogy) and examples are illustrated in Plate 7.2, c–e. In these examples, and in most other cases (excepting Plate 7.1), the vergence of S_1 and S_2 intersections in the mimetic porphyroblasts is opposite in sense to the vergence of S_1 and S_2 intersections in the matrix. The S_2 fabric in the porphyroblasts closely mimics the form of a zonal crenulation cleavage and, in many cases, it is continuous with the cleavage in the matrix. The degree of obliquity of the S_1/S_2 angle changes along the ribs and spine, both of which show curvature with the same sense of convexity. The porphyroblasts are typically unstrained, optically continuous, single crystals. They were interpreted to have grown during D_2 and to record incremental stages of fabric development (Figure 7.3) (*e.g.* Bell, 1985). At each stage of their growth, the porphyroblasts acted as a rigid inclusions with the result that further increments of strain were partitioned into the phyllosilicate-rich matrix (*ibid.*; Bell *et al.*, 1986; Bell, 1981). In addition to the observed sinistral vergence of S_1 and S_2 within the porphyroblasts, this implies a sinistral sense of rotation of the fabric in the matrix, with respect to the porphyroblast, while the porphyroblast was growing. The elongate inclusions along the spine of the porphyroblast record an earlier sense of asymmetry of the S_2 crenulation; the S_1 fabric along the ribs and in the matrix records progressive sinistral rotation with respect to earlier orientations. Similarly, the orientation of the spine of the porphyroblast records earlier orientations of the S_2 crenulation cleavage; however, the S_2 cleavage in the matrix shows dextral rotation with respect to this earlier orientation and, as noted previously, changes vergence with respect to S_1. The porphyroblast records an earlier sinistral sense of cleavage vergence which was present early during D_2 deformation. The dextral cleavage vergence is apparently a pervasive late D_2 overprint.

Another example of conflicting sense of asymmetry between porphyroblast and matrix, in this case involving garnet, is illustrated in Plate 7.2f. The garnet is mimetic after S_1 layering and contains inclusion trails of quartz which follow a sigmoidal trace. The sigmoidal trails and their sense of asymmetry are consistent with a sinistral up-plunge sense of rotation of the matrix while the porphyroblast was

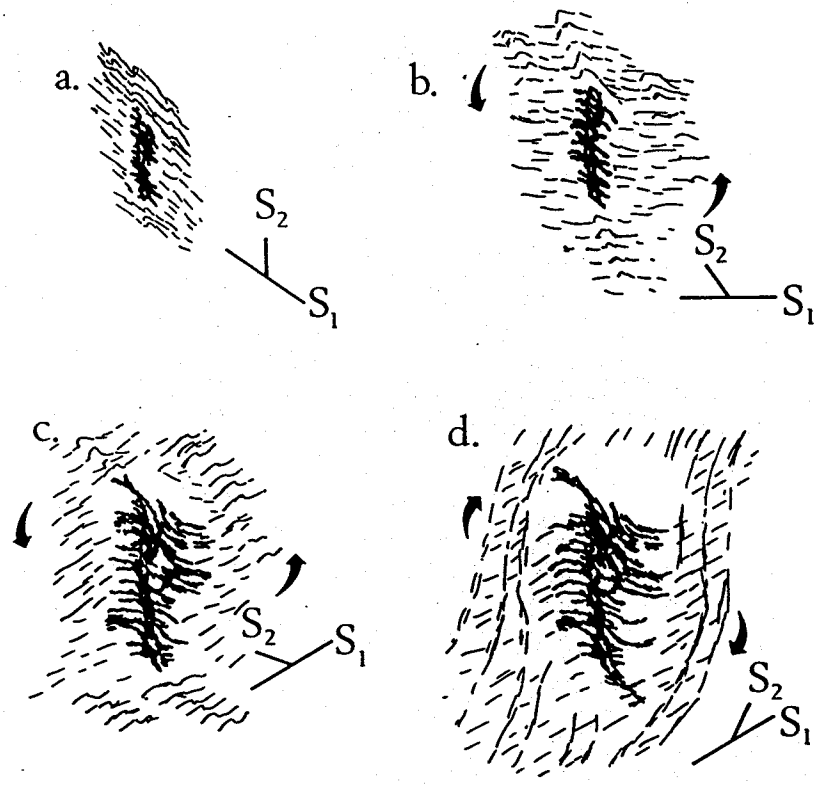

Figure 7.3. Sequential stages of porphyroblast growth and the evolution of S_1/S_2 cleavage vergence inferred from the relationships in Plate 7.2, c–e. S_1 and S_2 underwent sinistral rotation while the porphyroblast was growing (a–c). Late reactivation with the opposite sense of rotation, imposed dextral S_1/S_2 cleavage vergence on the matrix, while the porphyroblast preserved a record of the earlier sinistral vergence (d).

growing. (It was possible to orient this sample with respect to the surface geology; therefore, the sense of rotation has significance in a larger context.) However, the biotite schistosity in the matrix adjacent to the porphyroblast suggests the opposite sense of rotation, in agreement with dextral cleavage vergence of S_1/S_2 in the matrix.

Bell (1986) gave several examples of apparently opposed senses of rotation between porphyroblasts and matrix which he attributed to reactivation of pre-existing fabrics. The general tendency of mineral fabrics to reflect the last incremental strain imposed at the close of deformation has been remarked on (Williams, 1985), especially with reference to quartz c-axis fabrics (Bouchez and Nicolas, 1983; Brunel, 1980). In the Linda area, the kinematic indicators apparently apply to early D_2 and, in one case, possibly to D_1, and consistently indicate a sinistral sense of shear. In contrast, the cleavage vergence between S_1 and S_2 as defined by phyllosilicates,

either as a crenulation cleavage or a crystallographic preferred orientation of biotite, consistently has a dextral asymmetry. Note that these fabric elements defining S_2 are precisely those which are visible and can be measured in outcrop, both in the Linda area and in the Snow Lake region (Froese and Moore, 1980). The presence of mimetic porphyroblasts preserving an earlier sinistral cleavage vergence between S_1 and S_2 suggests that the main sense of motion was sinistral up-plunge and that the dextral cleavage vergence is a late D_2 phenomenon.

7.3. Fabric Formation.

7.3.1. S_1 Layering.

Mineral schistosity and crenulation cleavage is strongly developed in S_1 micaceous layers, in contrast to the nearly massive structure of quartzo-feldspathic domains. Following the ideas of Bell (1981) and Bell *et al.* (1986), the microstructure is the result of deformation partitioning; the quartzo-feldspathic domains were enclaves of low strain and were dominated by coaxial progressive shortening, whereas the micaceous layers were anastomosing zones of high strain and accommodated both noncoaxial shearing and shortening. Note that the model does not require noncoaxial strain, *i.e.* that the high strain zones could also be dominated by shortening, and that fabric relationships, whether symmetrical or asymmetrical, can be used to discriminate between these possibilities (*ibid.*). At the Linda deposit, layering and S_1 mineral foliations are parallel and therefore uninformative. A substantial component of D_1 shear strain is inferred mainly from the strong development of stretching lineations, which were interpreted to be mainly L_1 (*see* 4. Structural Geology of the Linda Area), and from isolated D_1 kinematic indicators (*see* 7.2.2. Sinistral Kinematic Indicators). Note also that the exact nature of the heterogeneities which initiated strain partitioning is not predicted by the model; these may depend on the type of protolith and may be obliterated or reconstituted during subsequent deformation.

The structure and inferred geochemical characteristics of the S_1 compositional layering bear some similarities to a pressure-solution cleavage, in the broad sense of Beach (1979) and Beach and King (1978), in which diagenetic and metamorphic reactions are an integral part of solute release and transport. It involved the segregation of quartzo-feldspathic domains and anastomosing micaceous layers (*e.g.*

Robin, 1979; Kerrich, 1977), and the development of pressure shadows, for example, those associated with quartz megacrysts (*e.g.* Rutter, 1983; Kerrich, 1977). The multiple trails of trace minerals, mainly zircon, but also rutile and apatite, which are common within micaceous layers, may represent insoluble residues such as those reported along styolites and residual seams (*ibid*; *also* Pettijohn, 1979). However, they also bear some resemblance to 'Tuttle' deformation lamellae (Spry, 1969) and similar seams in white mica, oriented parallel to (001), have been attributed to grain-boundary sliding (Swager, 1985; Gray, 1979a; 1979b). At the Linda deposit, unambiguous evidence of truncation of earlier structures, such as phenocrysts or clasts, against the micaceous layers, has not been observed, and the layers are commonly of sufficient width (up to 8 mm) to preclude any inter-penetration of primary structures, in constrast to the commonly sited evidence in favour of pressure solution (*e.g.* Rutter, 1983). Such evidence, if initially present, may not have survived subsequent metamorphism and deformation.

The micaceous layers are more strongly defined and wider within the alteration zones and, in many cases, the change is transitional from fine semi-continuous layers observed in felsic volcanic rocks. This may support the interpretation of the layers as pre-dynamometamorphic fractures related to the hydrothermal alteration (Bailes *et al.*, 1987; Trembath, 1986). The similar difficulty in distinguishing between matrix and clast relationships, and metamorphic-segregation layering, has been previously remarked on (*see* 3.1. Definition of Lithological Units). Alternative reasons for the differences in the definition of layering can be proposed; the mineralogy of the primary and low grade protoliths of metamorphosed altered rocks would include a high proportion of hydrous phyllosilicate minerals, which may have been more conducive to the processes of metamorphic segregation (Rutter, 1983; Beach and King, 1978; Robin, 1979; Kerrich, 1977). Bailes' *et al.* (1987) contention that the presence of Mg-Fe-Ca metamorphic minerals, *i.e.* 'diagnostic' of premetamorphic alteration, within the layers, is evidence that they are fractures which localized hydrothermal fluids, is not convincing. It assumes that the metamorphic minerals are mimetic after fracture-fillings or wall-rock alteration zones, but similar mimetic layering of porphyroblastic Mg-Fe(-Zn) minerals is also observed mimicking S_2 differentiated crenulation cleavage. In the latter case, the pre-existing structure is clearly of tec-

tonic origin and also involved the segregation of the same metamorphic minerals, 'diagnostic' of premetamorphic alteration. It is important to distinguish whether the dynamometamorphic mineralogy and structures preserve a memory of pre-existing chemical alteration, or pre-existing structures, or both.

The recrystallization and strain shown by quartz megacrysts illustrates the importance of intracrystalline plasticity (dislocation creep) as a mechanism of deformation at the Linda deposit. This is commonly cited as the dominant process at medium to high metamorphic grades (Kerrich, 1977). This is supported by deformation maps subdivided into dominance fields for various processes as a function of temperature, stress, and strain rate, which have been determined for monomineralic aggregates (Rutter, 1976). Presumably the aggregates were relatively homogeneous materials, much less capable of sustaining heterogeneous strain distributions than inhomogeneous, polymineralic, inequigranular rocks. The deformation mechanism is also strongly dependent on grain size, with fine grained materials, *i.e.* with large ratios of surface area to volume, favouring pressure solution (Rutter, 1983; Kerrich, 1977).

Ultimately, the ability of a rock to sustain local contrasts in deviatoric stress should determine the importance of solution transfer as a deformation mechanism. At the Linda deposit, evidence of competency contrast and strain partitioning, associated with D_1 and D_2 are observed, and this heterogeneity would have been conducive to stress-induced diffusion transfer. The distinction of diagenetic, or low grade, pressure solution as a separate process seems artificial (*see also discussions by* Beach, 1979; Robin, 1979; Beach and King, 1978). The main difference seems to be that in the first case, there may be a tendency to localize stress along a discrete contact between rigid bodies, and in the second case, a stress gradient is sustained across a transition zone. Presumably, there is a continuous transition between the two cases.

7.3.2. S_2 Cleavage.

The S_2 cleavage at the Linda deposit, as recorded by mimetic porphyroblasts, by crenulated phyllosilicates, and by recrystallized phyllosilicates on crenulation hinges, apparently formed as a crenulation cleavage. Similarly, corrugation of staurolite bands seems to be a manifestation of the same fabric, at a longer wavelength,

governed by the physical properties of the layering (*see* 5.2. Distal Alteration Zone). The differences in amplitude and wavelength between the crenulation cleavage and the corrugation of layering seem determined by the difference in competency between staurolite and phyllosilicate minerals and by the thickness of the feature being folded. Phyllosilicate minerals have a propensity to intracrystalline glide on (001)-planes (*e.g.* Spry, 1969), whereas staurolite crystals appear to have behaved more rigidly. The crenulation, particularly as preserved in earlier stages of development (*e.g.* Plates 7.1, c; 7.2, c–e), resembles kink bands. Cosgrove (1976) attributed this style of crenulation to high anisotropy of the medium, a property which might be expected in the phyllosilicate-rich schists of the Linda deposit. The differentiated zonal structure indicates that solution transfer was operative between limbs and hinges (Swager, 1985). Herringbone structure, with a discrete discontinuity separating the microlithons, could be the result of dissolution of hinges or kink-band boundary migration (*ibid.*). At the Linda deposit, the latter mechanism is more probable as there is no detectable residual seam or recrystallization of phyllosilicate minerals parallel to S_2 and, the herringbone structure is most common in the 'brittle' minerals, margarite and chlorite (*e.g.* Plate 7.1). Swager (1985) attributed recrystallization at hinges to the localization of stored strain energy in these zones, deformation on the limbs occurring mainly by grain-boundary sliding.

Gray and Durney (1979) examined several examples of crenulation cleavages and their relationships to independent strain indicators. They concluded that the crenulation cleavage formed parallel to the maximum flattening plane and, in cases of noncoaxial strain, passively tracked the orientation of the bulk progressive strain ellipse. They reported departures of up to 4° under conditions of high noncoaxial shear strain.

The crystallization of porphyroblastic minerals takes advantage of, or introduces, a competency contrast into the rock. Following the interpretation of Bell and Rubenach (1983), and Bell (1986, 1981), the volume of the porphyroblast and its immediate matrix is a domain of low strain, dominated by shortening and enveloped by an anastomosing crenulation cleavage which accommodated higher strain and any noncoaxial shearing component of deformation. This is exactly analogous to the previous interpretation of quartzo-feldspathic domains and S_1 micaceous

layering and implies strain partitioning associated with D_2. At the Linda deposit, strain partitioning during D_2 allowed the preservation of sinistral S_1/S_2 cleavage vergence in mimetic porphyroblasts, while the crenulation cleavage in the matrix was rotated into a new dextral sense of cleavage vergence.

7.4. Mineralogy and Reaction History.

7.4.1. Paragenetic Sequence.

The relationships between mineralogy, textures, and fabric elements can be used to construct the general paragenetic sequence summarized in Figure 7.4 for the distal and proximal alteration zones, graphitic metasediment, and massive sulphide bodies and their enclaves. Primary magmatic and hydrothermal minerals, and diagenetic minerals are encompassed by D_0 and include: quartz and plagioclase phenocrysts; quartz, plagioclase, pyrite and graphite of hydrothermal or diagenetic origin; and rutile inclusions in quartz phenocrysts. Syn-D_1 minerals include those which define S_1 layering and show layer-parallel crystallographic preferred orientation (*i.e.* muscovite, margarite, chlorite, kyanite, rutile and minor biotite). The range of quartz, plagioclase, pyrite and graphite has been extended into D_1 and beyond, to indicate probable recrystallization. Pyrrhotite shows some layer-parallel distribution and dimensional orientation. Garnet is mimetic only after S_1 layering, and was therefore inferred to be a syn-D_1 mineral. Fe-rich staurolite commenced crystallization prior to D_2, although it underwent subsequent recrystallization. Early D_2 refers to minerals which show an S_2 crystallographic preferred orientation (*i.e.* biotite, minor muscovite and chlorite) or, are mimetic after S_1 and S_2 but also deflect the S_2 crenulation cleavage (*i.e.* plagioclase, Fe-poor staurolite, kyanite and gahnite). Randomly oriented minerals showing weak strain related to late D_2 include staurolite, anthophyllite and gahnite in the staurolite-anthophyllite enclave in the largest massive sulphide body. Minerals showing a crystallographic preferred orientation parallel to the axial planes of the S_2 crenulation cleavage and showing either dextral vergence to S_1 or reactivation of S_1, were inferred to have undergone some late D_2 recrystallization. Post-D_2 includes randomly oriented minerals involved in symplectic and corona structures, *i.e.* garnet, plagioclase, calcite, pyrrhotite, pyrite, epidote and Ca-amphibole in calc-silicate enclaves in the largest massive sulphide body and, traces of fibrolitic sillimanite. The retrograde min-

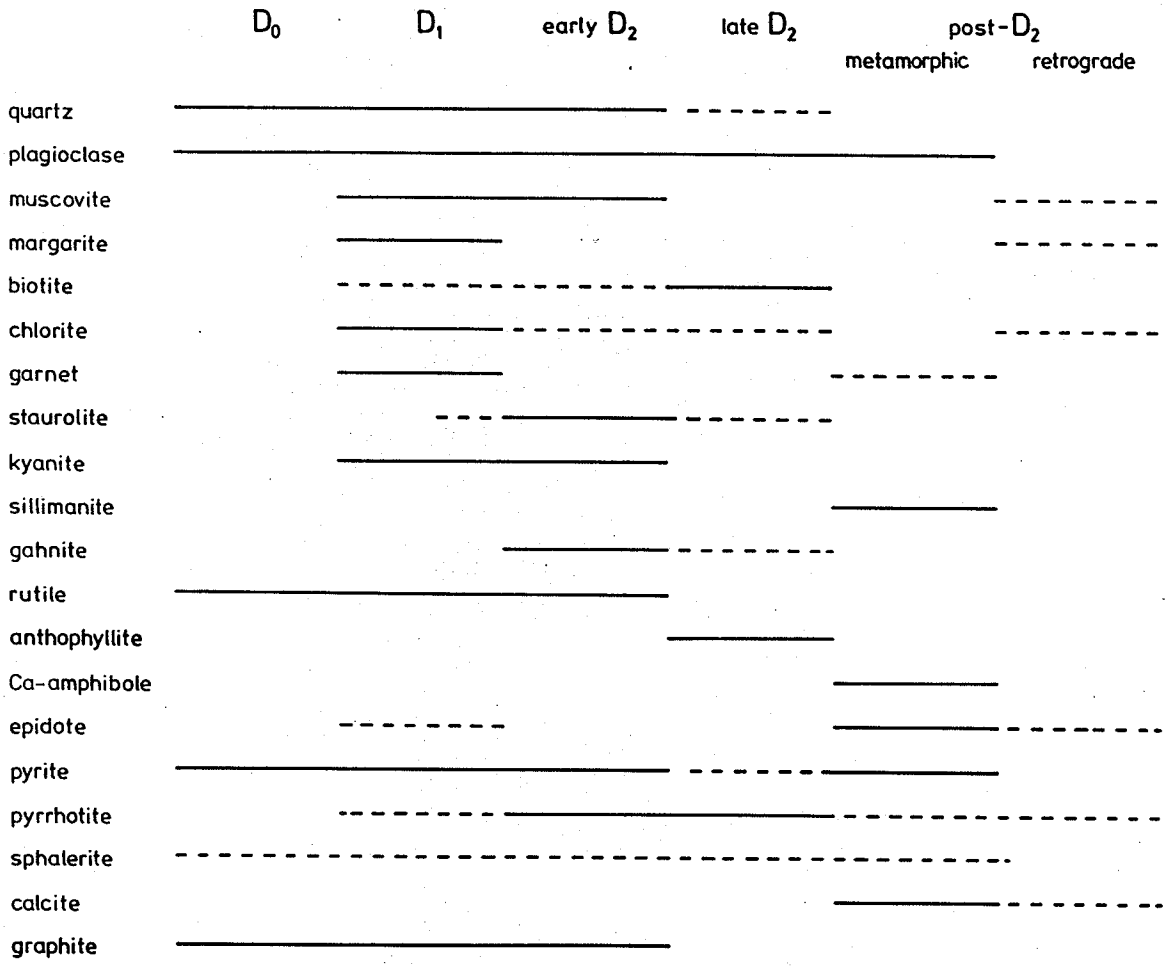

Figure 7.4. Paragenetic sequence for the minerals in the distal and proximal alteration zones, graphitic metasediment, and silicate enclaves in the largest massive sulphide body. The dashed lines indicate minor amounts of crystallization relative to the overall abundance of each mineral.

erals, *i.e.* muscovite, margarite, chlorite and calcite, were distinguished by their occurrence in fine grained massive aggregates or pseudomorphs.

7.4.2. Inferred Prograde Metamorphic Reactions.

The observed mineral assemblages and the paragenetic sequence allow some inference of the sequence of reactions which occurred in response to prograde metamorphism. In part, this relies on the inference of probable reactants which were entirely consumed by the overstepping of reactions (Tracy and McLellan, 1985) and, thus, is distinct from an approach relying on the identification of low-variance assemblages involved in reversible reactions (*see* 10.1.2. Mineral Equilibria). In some case studies, careful observations of inclusions armoured by porphyroblastic

minerals, and of zoning profiles, facilitated the identification of reactant minerals (Karabinos, 1985; Tracy, 1982; Thompson *et al.*, 1977; Tracy and Thompson, 1976). At the Linda deposit, with the exception of margarite-plagioclase rocks (*see* 5.3.5. Proximal Alteration Zone), the minerals which occur as inclusions also occur in the matrix and, in general, consist of ubiquitous trace minerals (*e.g.* zircon, rutile, apatite) and quartz.

Prograde reactions proposed by Froese and Moore (1980) for the Snow Lake region are listed in order of increasing grade in Table 7.2a. Reactions 1, 2 and 4 are the isograd reactions delineating the regional metamorphic zones. The Linda deposit is located in the biotite-staurolite zone (*see* 2.3. Metamorphism), however, the complete reaction assemblages for reactions 1 and 2, and the assemblage, anthophyllite-staurolite-quartz, have all been observed at the Linda deposit. In part, this apparent contradiction illustrates the necessity of considering the effect of Zn, Mn, F and S_2 on mineral stabilities (*see* 9.3. Halogen Contents of Phyllosilicate Minerals *and* 10. Models of Mineral Equilibria). For example, from petrography alone, it was possible to infer that D_1 staurolite is a high-Fe variety (*i.e.* 'normal' pleochroism), while D_2 staurolite is a low-Fe variety (*i.e.* nearly non-pleochroic). However, both types coexist with muscovite and chlorite. The role of mineral chemistry is dealt with at length in Part III; here, suffice it to point out that these reactions (Table 7.2, a) are represented by low-variance assemblages at the Linda deposit and, therefore, are divariant continuous reactions or acted as buffers of reversible equilibria. They are apparently inadequate to describe a prograde sequence of overstepped reactions in the altered rocks.

At the Linda deposit, the presence of syn-D_1 kyanite, without biotite, suggests the occurrence of a kyanite-producing reaction at lower grade than the kyanite-biotite producing reaction (Table 7.2, a) of Froese and Moore (1980). Pyrophyllite is suggested as a probable precursor for early kyanite (reaction 5; Table 7.2, b). Early D_2 kyanite is commonly associated with biotite, as well as with chlorite, staurolite and muscovite, and a reaction similar to reaction 2 may account for the assemblage. In any case, reaction 2 places a lower limit on the stability field of the assemblage. However, the stability of biotite may be enhanced by substitution of F in the hydroxyl site (*see* 9.3.2. Implications to the Stability of Metamorphic Assemblages).

Table 7.2. Metamorphic Reactions.

	a. Proposed for the Snow Lake area (Froese and Moore, 1980).
1.	$chlorite + almandine + muscovite \rightleftharpoons biotite + staurolite + quartz + H_2O$
2.	$chlorite + staurolite + muscovite \rightleftharpoons biotite + aluminosilicate + H_2O$
3.	$chlorite + almandine + quartz \rightleftharpoons anthophyllite + staurolite + H_2O$
4.	$staurolite + muscovite + quartz \rightleftharpoons biotite + aluminosilicate + garnet + H_2O$
	b. Proposed Prograde Reactions in Altered Rocks at the Linda Deposit.
5.	$pyrophyllite \rightleftharpoons kyanite + quartz + H_2O$
6.	$chloritoid + kyanite \rightleftharpoons staurolite + quartz + H_2O$
7.	$chloritoid + chlorite + muscovite + quartz \rightleftharpoons staurolite + biotite + H_2O$
8.	$chloritoid + O_2 \rightleftharpoons staurolite + magnetite + quartz + H_2O$
9.	$chloritoid + quartz \rightleftharpoons Fe\text{-}anthophyllite + staurolite + H_2O$
10.	$chloritoid \rightleftharpoons Fe\text{-}anthophyllite + staurolite + hercynite + H_2O$
11.	$garnet + sphalerite + S_2 \rightleftharpoons ZnFe\text{-}spinel + Fe\text{-}sulphide + quartz + O_2$
	c. Proposed Prograde Reactions in Margarite-bearing Altered Rocks at the Linda Deposit.
12.	$kyanite + calcite + H_2O \rightleftharpoons margarite + CO_2$
13.	$pyrophyllite + calcite \rightleftharpoons margarite + quartz + H_2O + CO_2$
14.	$margarite + quartz + calcite \rightleftharpoons anorthite + CO_2 + H_2O$
15.	$margarite + quartz + clinozoisite \rightleftharpoons anorthite + CO_2 + H_2O$
16.	$margarite + quartz \rightleftharpoons anorthite + kyanite + H_2O$
17.	$pyrophyllite + dolomite \rightleftharpoons margarite + chlorite + quartz + H_2O + CO_2$
18.	$chloritoid + calcite + quartz + H_2O \rightleftharpoons chlorite + margarite + CO_2$

After the closure of D_2 deformation, the rocks crossed the kyanite-sillimanite phase boundary, resulting in the crystallization of trace amounts of sillimanite. This is also supported by the occurrence of sillimanite in Amisk Group metasediments in the region (Froese and Moore, 1980); apparently kyanite persisted metastably in the altered rocks.

Garnet occurs as a syn-D_1 mineral, suggesting its formation by low grade reactions and its persistence by virtue of high Mn content (*see* 9.1.6. Garnet). Reaction 4 (Table 7.2, a) apparently did not occur at the Linda deposit. The presence of the

complete assemblage of reaction 1 indicates that garnet was involved in staurolite-producing reactions.

Many staurolite-bearing parageneses at the Linda deposit suggest the involvement of chloritoid in the reactant assemblage. Chloritoid was not observed, however, Trembath (1986) reported chloritoid at the Joannie alteration zone at the southwest end of Anderson Lake. The bulk-rock compositions of some samples from the Linda deposit lie within the field of chloritoid-bearing rocks as defined by Hoschek (1967) (*see* 11.2.4. Staurolite-bearing Rocks). The assemblages, kyanite-staurolite-quartz and chlorite-staurolite-biotite-quartz, suggest reactions 6 (Winkler, 1979; Hoschek, 1967) and 7 (Thorpe and Burt, 1980). The assemblage staurolite-magnetite-quartz suggests the oxidation of chloritoid (reaction 8; Winkler, 1979; Ganguly and Newton, 1968). These reactions (*i.e.* 6–8) have been commonly used to mark the transition to amphibolite-facies and medium grade metamorphism and generally occur at about 550°C, showing little pressure dependency in the range of 4–7 kbar (*ibid.*). They involve only Fe-Mg silicates and, therefore, Fe-rich staurolite compositions. At the Linda deposit, these reactions apparently commenced during D_1 but were mainly synkinematic with D_2.

Bulk-rock compositions at the Linda deposit were apparently too aluminous to allow the production of staurolite + garnet through chloritoid-consuming reactions. Although staurolite-garnet producing reactions cannot be entirely discounted, it seems that in most reactant assemblages, kyanite, chlorite, or muscovite, were present in excess. The aluminous bulk-rock compositions may contribute to the paucity of garnet in the altered rocks. Garnet may also have been consumed in subsequent reactions, for example, reaction 11 involving the sulphidation of sphalerite and garnet to produce spinel, Fe-sulphide and quartz (Spry, 1987).

The occurrence of anthophyllite-staurolite-gahnite-quartz at the Linda deposit represents the assemblage of highest apparent grade. Froese and Moore (1980) suggested reaction 3 for the assemblage, chlorite-anthophyllite-staurolite, reported at the Stall Lake mine (Hutcheon, 1977). Reaction 3 should occur at slightly higher grade than the isograd mapped by reaction 2 (Froese and Moore, 1980). At the Linda deposit, reactions which involve chloritoid may be more appropriate, given the indications of the probable presence of chloritoid at lower grades and the general

paucity of garnet.

Grieve and Fawcett (1974) investigated the stability of chloritoid and discussed their results in relation to previous work and natural occurrences. Reaction 10 was experimentally reversed and, reaction 9, at slightly lower temperatures, was derived by Schreinemakers analysis. The assemblage at the Linda deposit, with the additional components, Mn and Zn, implies the occurrence of a reaction similar to 10, but probably involving sphalerite as an additional reactant. The additional components apparently change the topology, shifting the reaction to lower temperatures and allowing the stable coexistence of quartz, Zn-spinel, anthophyllite and staurolite. At the Linda deposit, this assemblage was interpreted to have crystallized during late-D_2. The relative stabilities of reactions 8 and 10 are partly determined by f_{O_2}, with magnetite favoured over hercynite at higher f_{O_2} (*ibid.*).

The stability of the staurolite-bearing assemblages could be extended to lower temperatures by the incorporation of Zn in staurolite. For example, Thorpe and Burt (1980) attributed a localized occurrence of staurolite in a greenschist terrane to local Zn-rich bulk-rock compositions in which the staurolite-forming reaction proceeded at a lower temperature. This does not seem to be the general case at the Linda deposit; the earliest formed staurolite is generally the most Fe-rich. However, D_2 recrystallization is interpreted to have reequilibrated the mineral chemistries, and they are presumably a function of bulk-rock composition, f_{S_2} and f_{O_2} at constant metamorphic grade.

Prograde reactions in margarite-bearing rocks at the Linda deposit can be considered in a different chemical system (Table 7.2, c), although reaction 5, accounting for syn-D_1 kyanite, is still applicable. The observed assemblages are similar to those reported for amphibolite-facies or 'mesometamorphic' assemblages in the Alps (Guggenheim, 1984; Bucher-Nurminen *et al.*, 1983; Frey *et al.*, 1982; Frey, 1978; Frey and Orville, 1974) and many of the same prograde reactions may be pertinent to the Linda deposit. In the Alps, calcite is the main Ca-mineral at low grades or in diagenesis and X_{CO_2} is a significant factor in the equilibria. Figure 7.5 is based on reactions (Table 7.2, c) deduced by the cited authors (especially Bucher-Nurminen *et al.*, 1983) recalculated using the program, GE0CALC-PTX (Berman *et al.*, 1987). The syn-D_1 margarite-quartz(-kyanite) assemblages may suggest the

presence of pyrophyllite and calcite at lower grades; however, the abundant margarite and general lack of calcite implies either that calcite was not abundant in the protolith, or that X_{CO_2} was relatively low. The upper stability of quartz and margarite is limited by reaction 16 producing anorthite and kyanite. Plagioclase-kyanite-quartz and plagioclase-kyanite-quartz-margarite assemblages, in which the plagioclase and kyanite were interpreted to be syn-D_2, occur at the Linda deposit. The limiting reaction becomes divariant and is suppressed to lower temperatures with the incorporation of Na into plagioclase (Guggenheim, 1984; Frey and Orville, 1974). The effect is illustrated in Figure 7.5 by isopleths of anorthite activity projected from the divariant surface. Na is much less soluble in margarite (*ibid.*) and, therefore, has little effect. The upper limit of margarite-quartz stability is insensitive to X_{CO_2} and has a temperature maximum of about 600°C at 8 kbar (*e.g.* Guggenheim, 1984).

With the addition of Mg to the system, Frey (1978) suggested reaction 17 as the dolomitic analogue to reaction 13, producing chlorite in addition to margarite and quartz. Similarly, reaction 18 (*ibid.*) consumes chloritoid and produces margarite and chlorite. Both of these reactions could account for syn-D_1 intergrowths of chlorite and margarite and, reaction 18, in bulk-rock compositions in which chloritoid was not entirely consumed, could account for the occasional occurrence of syn-D_2 staurolite in these rocks. Fox (1975) and Frey (1978) pointed out that the indifferent crossing of reactions 16 and 6, which provide maximum stability limits for margarite + quartz and minimum limits for staurolite + quartz, respectively, occurs at a minimum pressure of about 5.5 kbar (a_{H_2O}=1). The stability of the staurolite-margarite-quartz assemblage is limited to a temperature interval between about 540–575° at 6 kbar (*ibid*). These observations also apply to the Linda deposit. The stability interval may be considerably broadened at lower temperatures with the incorporation of Zn into staurolite; however, at least some of the staurolite at the Linda deposit has a high-Fe composition.

Post-D_2 mineral assemblages were not isochemical during metamorphism and apparently required, at least, carbonatization. They will not be considered further here (*see* 10.4. Calc-silicate Enclave in the Main Massive Sulphide Body), except to point out that, some carbonate may have been derived from decarbonation of

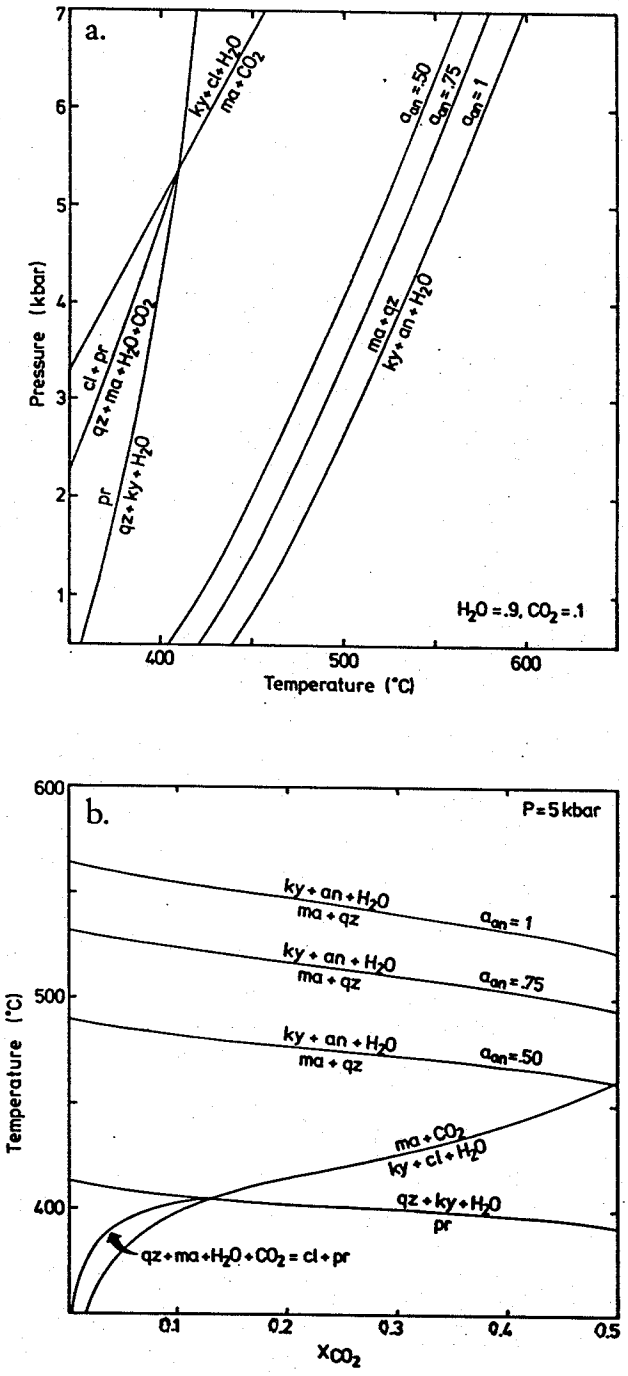

Figure 7.5. Reactions in the SiO_2-Al_2O_3-CaO-H_2O-CO_2 system applicable to margarite-bearing rocks, calculated using GE0CALC-PTX (Berman *et al.*, 1987). Abbreviations: an–anorthite, cl–calcite, ky–kyanite, ma–margarite, pr–pyrophyllite, qz–quartz.

a. Pressure-temperature grid at $X_{H_2O}/(X_{H_2O} + X_{CO_2}) = 0.9$. The enlarged stability field of plagioclase + kyanite with increasing Na content is indicated by isopleths of anorthite activity (a_{an}).

b. Temperature-CO_2 grid at 5 kbar. Isopleths of anorthite activity as in a.

the protolith of margarite-bearing rocks.

7.4.3. Pressure-Temperature-Deformation Path.

The observations at the Linda deposit and the inferred sequence of reactions can be combined into a schematic P-T-deformation path (Figure 7.6). The reactions which provide the most reliable estimates of temperature and pressure are those which involve nearly stoichiometric phases and are least susceptible to changes in fluid composition, including f_{S_2} and f_{O_2}. The schematic path followed by the volume of rock containing the Linda deposit tracks through the kyanite field at low grade, as recorded by syn-D_1 kyanite. The path presumably crossed numerous phyllosilicate-forming, discontinuous and continuous, reactions. The occurrences of D_1 to early D_2 Fe-rich staurolite suggest that the first staurolite-forming reactions, represented by the reaction of chloritoid and kyanite, may have commenced at grades typical of amphibolite facies. The continuous staurolite-forming reaction (*i.e.* reaction 4, Figure 7.6), involving the consumption of chlorite and muscovite, applies to a bulk-rock, Mg/(Mg+Fe) ratio of 0.4 (Hoschek, 1967). Margarite-quartz stability was not exceeded. This implies that all the syn-D_2 staurolite-gahnite, staurolite-anthophyllite-gahnite and biotite-kyanite assemblages crystallized in the narrow temperature interval bracketed by the two stippled reactions. The 'isograd' assemblages at the Linda deposit were not a function of temperature (or pressure) but of compositional variables, f_{S_2} and f_{O_2}, which shifted and expanded the pertinent equilibria to a zone of mutual overlap within the narrow temperature range effective during D_2. Many of the reactions were continuous and divariant in P and T and, therefore, P-T changes partly determine the mineral compositions, but not the observed variety of assemblages. The projections of the divariant surfaces on to the P-T plane all intersect the trajectory followed by the Linda deposit during D_2 on a relative time scale. After the closure of D_2 deformation, the path crossed into the stability field of sillimanite and metamorphic conditions started to decline.

7.5. Relationships to Megascopic Structures and Regional Isograds.

The microstructural relationships at the Linda deposit reveal complexities which are not apparent, or can only be guessed at, from mesoscopic features and map patterns. Detailed microscopic observations have the potential to resolve apparent contradictions and ambiguities in regional interpretation. However, by their

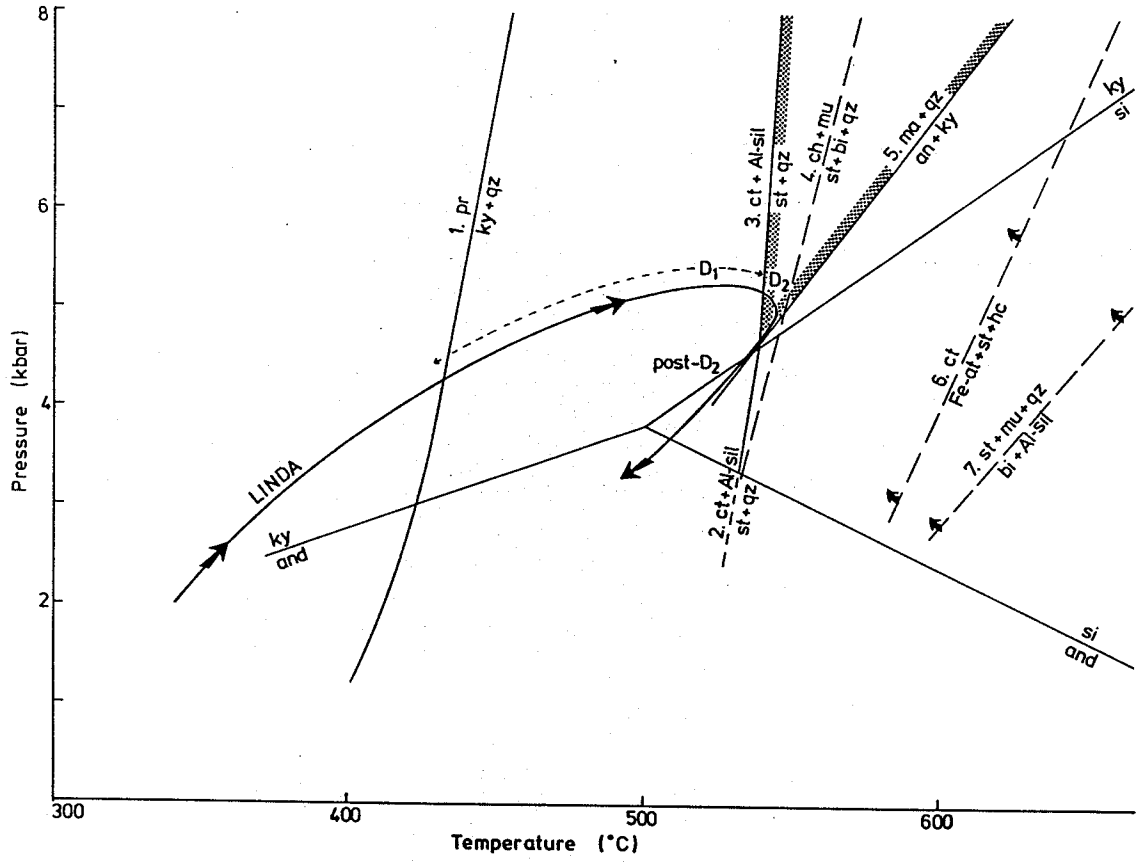

Figure 7.6. Pressure-temperature-deformation path followed by the Linda deposit. Syn-D_2 minerals crystallized in the interval bounded by the stability limits of staurolite + quartz and margarite + quartz. Reactions normally occurring at higher grade (dashed) occurred at lower temperatures at the Linda deposit (as indicated by the small arrows) as a function of bulk-rock composition, f_{S_2} and f_{O_2}. Abbreviations: Al-sil–aluminosilicate, an–anorthite, and–andalusite, bi–biotite, ch–chlorite, ct–chloritoid, Fe-at–ferro-anthophyllite, hc–hercynite, ky–kyanite, ma–margarite, mu–muscovite, pr–pyrophyllite, qz–quartz, si–sillimanite, st–staurolite. Sources of reaction data: 1–Kerrick (1968); 2–Richardson (1968); 3–Hoschek (1967); 4–Hoschek (1969); 5–Storre and Nitsche (1974); 6–Grieve and Fawcett (1974); 7–Hoschek (1969); aluminosilicate stability fields–Holdaway (1971).

nature, the observations tend to be isolated and difficult to correlate or extrapolate to a larger scale. This difficulty is illustrated by the rutile trails and swarms which were interpreted to be 'Tuttle' deformation lamellae related to shear strain during D_1. Their distribution is limited to quartz-megaphyric felsic rocks (4) and the upper parts of the proximal alteration zone. In its lateral extension to the northeast, unit 4 wedges out against an intercalation of Amisk metasedimentary rocks (9) in what may be a thrusted relationship (*see* 4.5. Discussion). Unit 4 could hide structural complexities, the nature of which cannot be evaluated on the basis of the available

observations.

Kinematic indicators associated with early D_2 and, possibly with D_1, consistently recorded a sinistral up-plunge sense of movement. Late D_2 cleavage vergence recorded a dextral sense of movement and is apparently associated with reactivation of S_1. The late D_2 fabric elements, *i.e.* S_2 crenulation cleavage and biotite schistosity, are the prominent D_2 features on outcrops in the Linda area and the Snow Lake region. The general uniformity of S_2 orientations (Froese and Moore, 1980) is interpreted here as a reflection of their origin as a late overprint. This has important implications in that, the axial traces of F_2 major folds cannot be mapped on the basis of changes in cleavage vergence and the presence of cleavage-transected folds is to be expected (*e.g.* Borradaile, 1978). Similarly, late D_2 shear strain can modify or impose structural styles onto pre-existing F_2 folds (or other structures), as in the example of the illustrated F_2 microfold (Figure 7.1, Plate 7.1). The new structural style may be markedly asymmetrical on opposing limbs of the earlier fold, as a function of the orientation of each limb in the new finite strain ellipsoid.

Late D_2 is interpreted to have reoriented early S_2 crenulation cleavages, apparently in a stress regime significantly different from that operative during early D_2. This raises the question of redefining late D_2 as a D_3 deformation. Given the similarity in early D_2 and late D_2 fabrics, *i.e.* mainly crenulation cleavages, the local continuity of cleavages despite reorientation, and absence of correlated megascopic structures (as to the present time), a conservative approach is warranted.

Fabric formation during D_1 and D_2 required solution transfer and devolatization reactions. The scale of element mobility and associated volume changes is critical to the interpretation of bulk-rock geochemistry. Insofar as fabric formation was dominantly accomplished by redistribution on a hand-sample scale, *i.e.* metamorphism occurred in a closed system, the modifications imposed by metamorphism are relatively predictable. Decarbonation, dehydration, and possibly, desulphidation reactions imply some degree of volatile mobility. If the precursor minerals can be identified, volume and density changes associated with the metamorphic reactions can be inferred. However, quartz in pretectonic and syntectonic veins may have been derived from silica released during desilicification reactions (*e.g.* Beach and Jack, 1982; Beach, 1979). Similarly, calcite in the largest massive sulphide body

and in veins could have originated in decarbonation reactions; the large amounts of Ca suggest synmetamorphic mobility of Ca.

Occurrences of margarite have not been reported in the Snow Lake region, including metamorphosed synvolcanic alteration zones. Margarite, especially in fine grained intergrowths with other phyllosilicate minerals, is not easily identified and the lack of reported occurrences may simply reflect lack of recognition. However, most of the massive sulphide deposits in the area lie at higher metamorphic grades than the Linda deposit and it may be that the stability of margarite + quartz was exceeded.

The Linda deposit lies in the staurolite-biotite zone of regional metamorphism, as based on assemblages in pelitic metasediments (Froese and Moore, 1980). As illustrated in Figure 7.6, this grade of metamorphism is consistent with the assemblages observed at the Linda deposit. The consideration of compositional parameters is critical. It is interesting to note that, in general, there is very little difference between mineral assemblages reported at the Anderson Lake and Stall Lake mines (Trembath, 1986; Walford and Franklin, 1982; Froese and Moore, 1980; Hutcheon, 1977) and those at the Linda deposit, despite the higher grade location of the former with respect to regional isograds. The corollary of this observation is that the trace of the metamorphic isograds cannot be constrained by parageneses observed in altered rocks. Presumably, metamorphic grade could be determined by considering mineral chemistries in the context of f_{O_2} and f_{S_2}.

It has commonly been observed in the Snow Lake area (*ibid.*), that metamorphosed alteration zones contain kyanite (± biotite), whereas pelitic metasediments contain sillimanite (+ biotite). The shift to lower temperatures, of the kyanite-biotite forming reaction at the Linda deposit suggests an explanation. In altered rocks, bulk-rock compositional factors caused this reaction to proceed at lower temperatures within the stability field of kyanite. The kyanite persisted metastably, even if the rocks were subjected to higher grades of metamorphism (*e.g.* Anderson Lake and Stall Lake mines). In metasediments, the reaction proceeded at 'normal' temperatures within the stability field of sillimanite, and was likely the first volumetrically significant aluminosilicate-forming reaction.

Chapter 8
Reconstruction of the Synvolcanic Alteration System

The preceeding chapters demonstrate that the Linda deposit has been extensively tectonized and metamorphosed and that the basic reconstruction of its synvolcanic features and setting present a challenge. In this regard, the Linda deposit is typical of many hydrothermal deposits in the ancient record, both in the Snow Lake region (Trembath, 1986; Walford and Franklin, 1982; Studer, 1982; Hutcheon, 1977; Coats *et al.*, 1970; Martin, 1966 Williams, 1966; 1961) and elsewhere (*e.g.* Ducktown, Tennessee, Nesbitt and Kelly, 1980; Addy and Ypma, 1977).

8.1. Synvolcanic Setting.

Sulphide mineralization and alteration at the Linda deposit occurred in association with volcanism and volcanogenic sedimentation in a subaqueous environment, as indicated by the presence of pillowed flows and thinly bedded, graphitic and sulphidic metasediments. Felsic rocks change in character upward in the stratigraphic sequence from mainly homogeneous and aphyric (unit 1), to intercalated matrix-supported breccias (1b) and 'cherty' felsic rocks (1a), the latter interpreted to be altered felsic rocks (*see* 11.2.1. Silicic-Feldspathic Alteration and Metamorphic Segregation). This sequence is overlain by quartz-megaphyric felsic rocks (4). Near the proximal alteration zone, cherty felsic rocks are represented by mineralized, clast-supported breccias (1c). The differences in the two types of breccias, *i.e.* matrix-supported (1b) and clast-supported (1c), have genetic significance. Matrix-supported breccias appear to be volcaniclastic breccias which were transported to their site of deposition; they do not have an obvious direct relationship to hydrothermal activity and their mineralization and alteration in the proximal zone post-dated their emplacement. Clast-supported breccias (1c) occur only near the proximal zone and are brecciated lateral equivalents of silicified and spilitized felsic rocks (1a). The clasts are angular, interlocking and monolithologic; the matrix is

clearly not composed of clastic material but seems to be void-filling mineralization. Clast-supported breccias are genetically related to the hydrothermal alteration and are interpreted to be the result of *in situ* hydrothermal fragmentation and mineralization. Cherty felsic rocks may have periodically acted as impermeable cap-rocks during the development of the hydrothermal system, causing an accumulation of pressure followed by hydrothermal fracturing.

Quartz-megaphyric felsic rocks, similar to unit 4, were interpreted by Walford and Franklin (1982) as subaqueous pyroclastic flow deposits. Although primary textures and structures are mainly obliterated, the poorly sorted, poorly graded nature of unit 4, with respect to quartz phenocrysts, is consistent with this hypothesis. The thickness of the unit has no absolute stratigraphic significance (*see* 4. Structural Geology of the Linda Area). However, its lateral continuity and homogeneity, the planar upper surface and undulating lower surface (*i.e.* as if related to the topography of a depositional surface) are characteristic of pyroclastic flow deposits (Fisher and Schminke, 1984). A pyroclastic origin for unit 4 implies that explosive felsic volcanism was the culmination of most of the felsic volcanic and hydrothermal activity in the Linda area. The source and location of the vent area(s) of the felsic volcanism is unknown. However, pyroclastic flows are generally considered to require a subaerial source, although once generated, the flow can transport (possibly in a modified cold form) and deposit its load subaqueously (*ibid.*, and references therein).

Bailes (1988; 1987; 1986) identified alteration, of possible synvolcanic origin, in the Sneath Lake pluton. On the basis of petrographic and geochemical data, Walford and Franklin (1982) proposed that this body was the intrusive equivalent of the quartz-megaphyric felsic rocks. Its position, intruding the base of the volcanic sequence, suggested that it may have provided the thermal energy to drive the hydrothermal systems in the area.

8.2. The Linda Hydrothermal System.

The proximal alteration zone and graphitic metasediment lie down-dip of the termination of the mafic volcanic rocks of unit 2; 'cherty' felsic rocks continue, as mineralized clast-supported breccias, into the alteration zone and terminate within it. By analogy with the Noranda area, in which all massive sulphide deposits

are associated with synvolcanic faults (Dimroth *et al.*, 1985), the termination of these units, and the position of the graphitic metasediment and the altered rocks, could be explained by the presence of a synvolcanic growth fault (Figure 8.1). The growth fault acted as a conduit which focussed hydrothermal fluids and the resulting alteration and mineralization were localized mainly on the down-thrown side (*e.g. ibid.*; Franklin, 1986). The thinly bedded laminated metasediments contain only minor clastic material and, thus, suggest that a euxinic environment of restricted circulation formed in an enclosed basin on the down-thrown side of the growth fault. Hydrothermal discharges, localized on the fault, produced chemical precipitates, including Fe and Zn sulphide minerals. The exact trace of the proposed fault cannot be identified and is probably obscured by alteration and deformation. Cherty felsic rocks (1a) and their hydrothermally brecciated equivalents (1c), partly underlie mafic volcanic rocks (2) on the up-thrown side of the proposed fault. This implies that the cherty felsic rocks were continuous across the fault and that each, in turn, acted as a cap-rock which was subsequently ruptured by hydrothermal activity and displaced by growth faulting. Thus, an episodic sequence of hydrothermal, volcanic and faulting events is implied, as illustrated in Figure 8.1. The emplacement of quartz-megaphyric felsic rocks (4) is associated with the decline of the system; the unit exhibits alteration and mineralization but was not truncated by the fault. The slight thickening of the unit and undulation of the lower surface above the inferred trace of the fault may suggest a topographic low associated with the fault.

Within this scenario, two possible models can be proposed for the alteration system, differing in their interpretation of the significance of the proximal and distal alteration zones in the primary synvolcanic system.

8.2.1. Model 1—Distal Zone as Reservoir; Proximal Zone as Conduit.

The occurrence and general relationships of two alteration zones at the Linda deposit are similar to those described at the Anderson Lake and Stall Lake mines by Walford and Franklin (1982). Model 1 conforms to the interpretation of these authors. Beneath the orebodies at the mines, an upper alteration zone cuts the stratigraphy at an oblique angle (30°), and extends down to intersect a lower semi-conformable alteration zone. The discordant zones were interpreted to be alteration pipes which channelled hydrothermal fluids from a lower semiconformable reservoir.

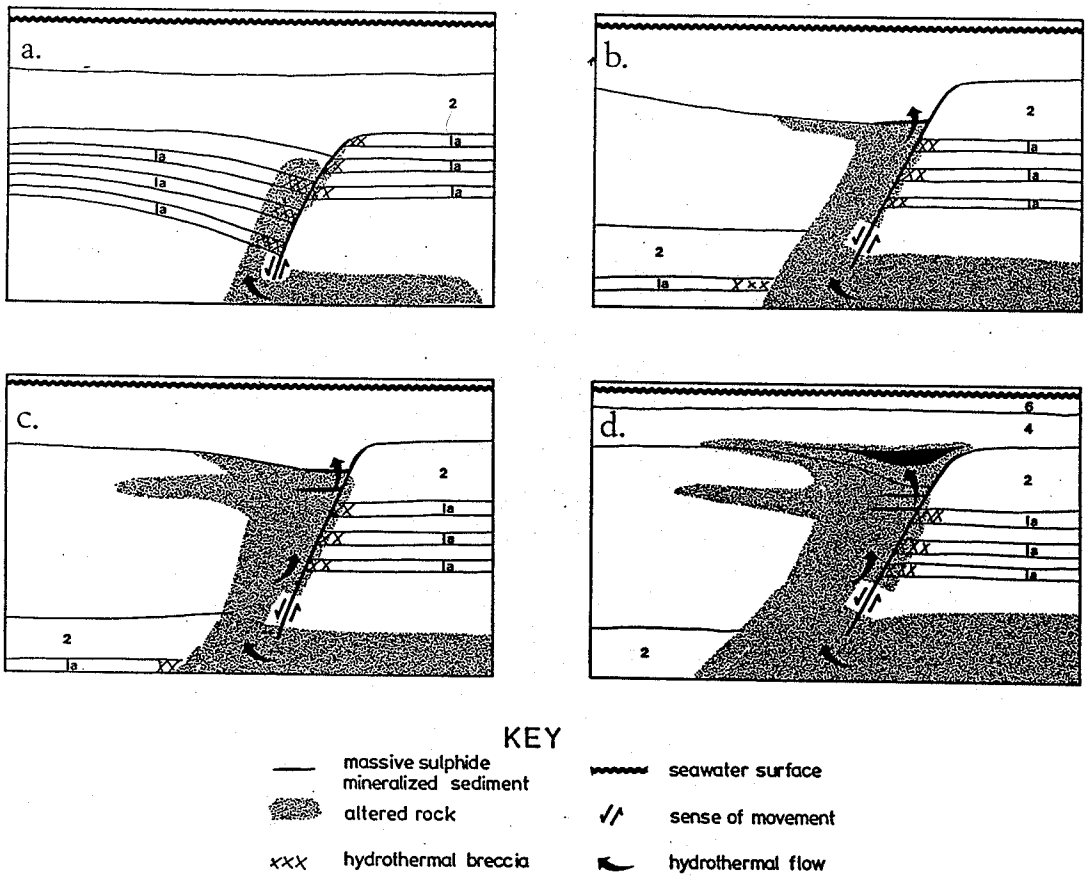

Figure 8.1. Generalized schematic representation of a possible sequence of volcanic, hydrothermal and faulting events leading to an interpretative reconstruction of the Linda deposit prior to regional deformation. The correlation of the physical features of this representation with the Linda alteration zones, as presently observed, is partly dependent on the choice of model for the hydrothermal system, *i.e.* Model 1 or Model 2.

- **a.** An early stage in the development of the hydrothermal system. Synvolcanic faulting has displaced altered felsic rocks (1a) which may earlier have acted as impermeable cap-rocks. Mafic volcanic rocks (2) are continuous across the fault and across the top of a conduit which channels hydrothermal fluids along the fault. A semiconformable reservoir supplies hydrothermal fluid to the conduit.
- **b.** Mafic volcanic rocks (2) have been displaced along the fault and the conduit discharges hydrothermal fluids at the seafloor surface in a fault-controlled depression. The distribution of alteration and hydrothermal precipitates is skewed away from the fault scarp.
- **c.** The system evolves while fault-related subsidence continues. New volcanic breccias were emplaced and the extent and intensity of stratabound alteration is a combined function of deposition rates, sediment permeability, and rates of hydrothermal discharge. The trace of the fault is obscured by alteration.
- **d.** Quartz-megaphyric felsic rocks (4) were emplaced and maintained their continuity across the fault. The felsic deposit filled the fault-controlled depression and hydrothermal activity continued, altering and mineralizing the unit. The mechanism of emplacement of the massive sulphide body within unit 4, *i.e.* subsurface replacement or deposition between flow units, is unknown.

The reservoir horizon was interpreted to have a regional extent and to have been intersected by several fluid conduits, *i.e.* at the Anderson Lake and Stall Lake mines, and the Ram zone (*ibid.*). Applying this model to the Linda deposit, the proximal alteration zone would represent a discordant conduit which channelled hydrothermal fluids from a reservoir, represented by the distal alteration zone. Zaleski (1986) and Jeffery (1982, *unpubl.*) proposed a correlation of the distal alteration zone, across the Anderson Bay structure, with the regional reservoir horizon of Walford and Franklin (1982).

An intersection between the distal and proximal zones has not been documented at the Linda deposit; it would presumably lie up-plunge beyond the present-day erosional surface, or down-plunge beyond the limits of drilling. The proximal alteration zone is discordant to stratigraphy in the sense that mafic volcanic rocks (2) and felsic flows (1a) terminate against, or within, the altered rocks. However, the proximal alteration is partly stratiform and largely stratabound. Assuming the proximal zone to represent a conduit, the present structural down-dip bifurcation of the zone (*see* Figures 3.2–3.3) could be interpreted in two ways. The lowermost (with respect to stratigraphic facing) bifurcation could represent part of the alteration conduit (*i.e.* the cross-stratal alteration in Figure 8.1). The uppermost bifurcation is then a broad funnel-shaped top to the conduit, where hydrothermal discharge occurred on to the seafloor, or by subsurface perculation partly spreading laterally on a permeable unit (*i.e.* conformable alteration in Figure 8.1). The conduit (lower bifurcation) and the upper stratabound and stratiform alteration (upper bifurcation) were transposed into near-parallelism by subsequent regional deformation (*see* Figure 3.2–3.3). In the second alternative, the bifurcations could represent stacked funnel-shaped tops, the lower bifurcation associated with mineralized metasediments and small massive sulphide bodies, and the upper bifurcation associated with the main massive sulphide body (*i.e.* the two areas of conformable alteration in Figure 8.1). The proximal alteration zone would consist of stratiform and stratabound alteration at the successive tops of the evolving conduit.

Several observations favour the second alternative. The cross-sectional projections (A-A', C-C', in pocket) of the Linda deposit are only moderately oblique (*i.e.* 30°) to the YZ-section of a generalized strain ellipsoid (*see* 3. Local Geology of

the Linda Area), and thus approach a 'least-deformed' representation. This is also indicated by the relative disposition of the massive sulphide lenses, which appear to be stacked, rather than displaced by shearing. Secondly, much of the disseminated mineralization associated with the lower (and upper) bifurcation, especially in the vicinity of the small massive sulphide lenses, appears to be stratiform. Lastly, the Zn-rich core (10pa) of the proximal alteration zone extends along the lower bifurcation (*see* Figures 3.2–3.3). Zn enrichment is expected to occur in the lower-temperature, peripheral or outer areas of a mineralizing hydrothermal system and would be unusual in the core of an alteration pipe (Lydon, 1988; 1984; Franklin, 1986; Hutchinson, 1982; Knuckey *et al.*, 1982; Franklin *et al.*, 1981). Trembath (1986) reported a similar Zn-rich horizon, extending westward from the massive sulphide body at the Anderson Lake mine; he interpreted the horizon as a paleodepositional surface.

The proximal alteration zone has a high proportion of muscovite, similar to the upper parts of the discordant pipe at the Anderson Lake mine. At the Anderson Lake mine, the pipe is zoned with a chlorite-biotite-kyanite core enveloped by staurolitic rhyolite and, an upper 'halo' of muscovite schist (Walford and Franklin, 1982). The staurolitic rhyolite has some textural and mineralogical similarities to the staurolite-banded gneisses of the distal alteration zone at the Linda deposit; however, the staurolitic rhyolite is apparently a weakly altered rock which preserves some primary features and contains plagioclase (*ibid.*; Trembath, 1986). At the Anderson Lake mine, The most intensely altered parts of the lower semiconformable reservoir are dominated by chlorite, biotite and minor muscovite and garnet (Walford and Franklin, 1982). Albite was reported to be abundant at the intersection of the pipe zone with the semiconformable reservoir (*ibid.*).

Model 1 interprets the distal alteration zone as a reservoir rock. This zone is hosted by felsic volcanic rocks (1), and is enriched in Mg-Fe silicate minerals and, to some extent, in Fe-sulphide minerals, relative to the host rock. As intersected by drilling, this zone cannot constitute an adequate source of metals or S for the massive sulphide bodies higher in the section and a distinction must be made between source rocks and reservoir rocks. Morton and Franklin (1987) and Franklin (1986) considered numerous examples of volcanogenic massive sulphide deposits.

They concluded that, in general, lower semiconformable alteration zones should consist of silicic alteration, about 1 km below the deposit, developed in rocks which include some mafic lithologies. Skirrow (1987) investigated extensive silicification in the Edwards Lake area, 1–2 km stratigraphically below the Chisel Lake mine. He found that the silicic alteration was slightly discordant and migrated laterally and up-section toward the Chisel Lake mine and, concomitantly, graded to an Fe-Mg type of alteration. He proposed a model whereby the Fe-Mg alteration observed in his study area correlated laterally with semiconformable Fe-Mg alteration about 500 metres below the massive sulphide deposit.

At the Linda deposit, extensive zones of silicic alteration, particularly in mafic volcanic rocks, have not been identified. The relationship of the relatively small area of silicified pillows northeast of the Rod mine is not known.

8.2.2. Model 2—Distal Zone as Conduit; Proximal Zone as Stratabound and Stratiform, Near-surface Alteration.

Model 2 differs from Model 1 in the primary significance attributed to the proximal and distal alteration zones; *i.e.* in their identification as parts of the alteration system. The basic reconstruction is different, although many of the details of Model 1 apply to both cases. The proximal alteration zone and its present structural bifurcation (*see* Figures 3.2–3.3) are interpreted as near-surface stratabound and stratiform alteration at the top of a conduit, as in the previous model. However, the discordancy of this zone is attributed entirely to the localization of alteration and sedimentation on the down-thrown side of an active growth fault; the control is mainly of a topographic nature. The thickness of the proximal alteration and the semiconformable nature of the Zn-rich core zone (10pa) would result from the accumulation of alteration products at, or near, successive depositional surfaces. In this model, the intersection between alteration associated with near-surface discharges and the main cross-stratal conduit is not represented in the volume sampled by drilling; the proximal alteration and associated mineralization are random sections through deposits peripheral to the main hydrothermal vent.

The distal alteration zone, as intersected by drilling, may represent part of the conduit which channelled the hydrothermal fluids. However, its position is not easily reconciled with the approximate trace of the inferred synvolcanic fault which con-

trolled surface discharges. Either the conduit followed some unidentified structure, or subsequent deformation was sufficiently heterogeneous to obscure the relationships. The concordancy or discordancy of the distal zone cannot be evaluated on the basis of the cross-sections logged for this study. However, Jeffery (1982, *unpubl.*) interpreted the zone to be discordant, cutting across mafic volcanic intercalations (1d) in felsic volcanic rocks (1). Also, as previously discussed (*see* 5.1. Location and Relationships to Stratigraphy), the distal zone apparently cuts upward through the stratigraphy in an up-plunge direction, approaching to within 45 metres of the proximal zone at the point when they are truncated by the present-day erosional surface and, implying that their intersection lies beyond this surface. Unfortunately, these drill-hole interpretations must be treated with caution, as the existence of a discrete proximal alteration zone was first recognized during this study (Zaleski, 1986).

Model 2 is more successful at explaining the mineralogical characteristics of the alteration zones in the context of other case studies and genetic models. Noranda-type deposits typically have an Mg-chlorite rich pipe with an upper halo of sericitic alteration (*e.g.* Morton and Franklin, 1987; Franklin, 1986; Knuckey *et al.*, 1982; Riverin and Hodgson, 1980). At the Linda deposit, the Mg-Fe silicate mineralogy of the distal alteration zone is more typical of a conduit. As previously noted (*see previous section*), the muscovite-rich proximal alteration and its Zn-rich core are more consistent with lower-temperature near-surface regimes, peripheral to a conduit. In Model 2, neither the source rock nor possible reservoir horizons have been identified.

8.2.3. Comparison of Models 1 and 2.

Some fundamental differences are implicit between the two proposed models, particularly with regard to the scale of the hydrothermal alteration system. Model 1 requires that near-surface stratiform and stratabound alteration, the hydrothermal conduit, and part of a lower reservoir zone, are all contained within the volume sampled by drilling. Model 2, requires that only near-surface alteration and part of the hydrothermal conduit lie within the same volume and the source rocks, reservoir rocks and part of the conduit lie outside this volume. Model 2 thus implies a much larger magnitude for the hydrothermal alteration system.

In terms of geochemical modelling of fluid-rock interactions, Model 1 implies, thermochemical evolution of fluid contained in the distal alteration zone (reservoir), and its expulsion into the proximal zone (conduit), with further evolution in a pressure and temperature gradient associated with upwelling and, possible mixing with seawater. In Model 2, an evolved fluid arrives at the distal zone (conduit) and continues to evolve during upwelling, with near-surface mixing and precipitation as the dominant processes in the proximal alteration zone. The nature of any thermochemical model is thus highly dependent on the selection of a physical model. It is also possible that the feasibility of the various thermochemical models might be used to test the physical models. However, the former tend to have myriad non-unique path-dependent solutions (*e.g.* Janecky and Shanks, 1988; Bowers and Taylor, 1985; Janecky and Seyfried, 1984; Reed, 1982).

Models 1 and 2 have distinct pre-deformational geometries. Model 1 requires a semiconcordant distal alteration zone, disposed at a high angle to an overlying discordant cross-stratal proximal alteration zone. Model 2 requires a discordant cross-stratal distal alteration zone, disposed at a high angle to an overlying semi-concordant proximal alteration zone. These initial configurations can be subjected to hypothetical simple shear to give the observed geometry of the Linda deposit. Figure 8.2 illustrates that the direction of intersection, *i.e.* whether up-plunge or down-plunge, is dependent on the initial configuration and on the sense of shear. If the correct physical model could be ascertained by independent means, the direction of the intersection could be used as a kinematic indicator. For a sinistral up-plunge sense of shear, Model 1 predicts an up-plunge intersection of the proximal and distal alteration zones (Figure 8.2, a), whereas for the same shear sense, Model 2 predicts a down-plunge intersection of the two zones (Figure 8.2, b). Drilling has sampled only a fraction of the volume depicted in the figure and, the ambiguities involved in distinguishing discordant and concordant primary relationships in their transposed states are accurately represented.

8.3. Implications.

Massive sulphide deposits in the Snow Lake region are a quandary in terms of the nature of the lower semiconformable alteration zones. In contrast to the zones of intense, deep or medial, subsurface silicification observed in other vol-

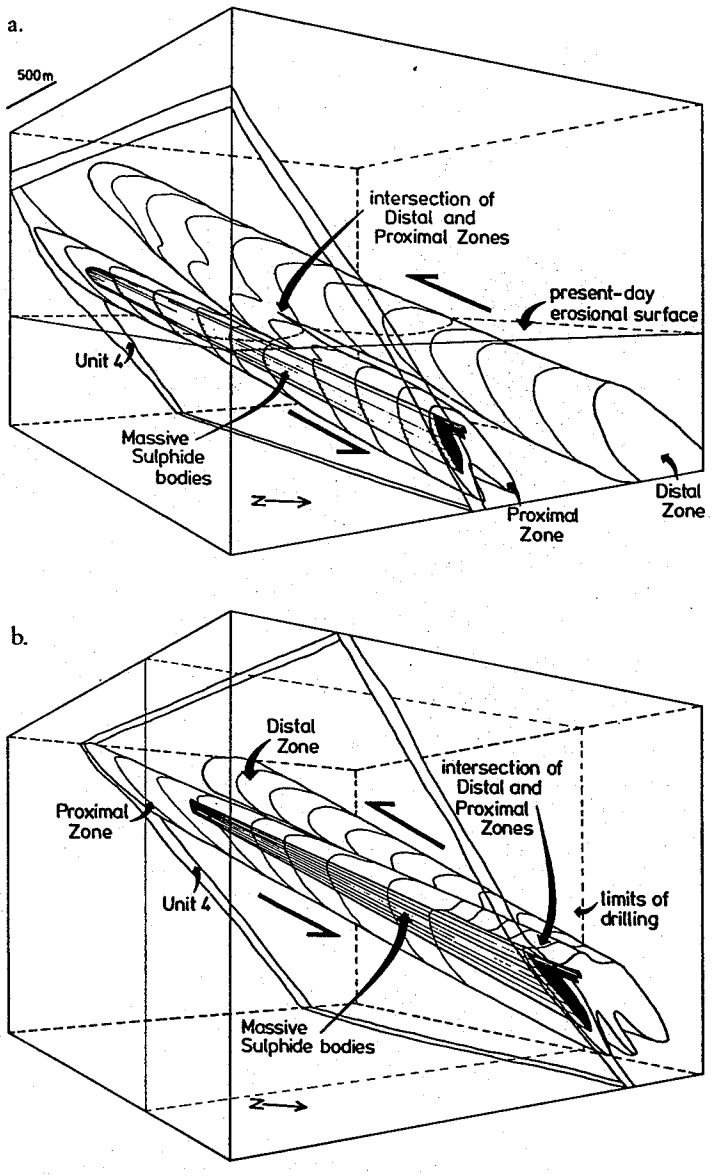

Figure 8.2. Schematic perspective views comparing the implications of Model 1 and Model 2, with respect to the present-day configuration of the Linda deposit. The views assume simple shear, parallel to the regional stretching lineation, with a sinistral up-plunge sense of movement. The diagram is drawn approximately to scale and gives an accurate representation of the ambiguity of the primary relationships after transposition.

a. Model 1. An up-plunge intersection of the distal zone (reservoir) and proximal zone (conduit) occurs beyond the present-day erosional surface. The proximal zone is discordant to stratigraphy, as represented by unit 4, cutting up-plunge to intersect the semiconformable distal zone.

b. Model 2. A down-plunge intersection of the proximal zone (stratabound, near-surface alteration) and distal zone (conduit) occurs beyond the limits of drilling. The distal zone is discordant to stratigraphy (unit 4 as datum), cutting down-plunge to intersect the stratabound proximal zone.

canogenic Cu-Zn massive sulphide deposits (Morton and Franklin, 1987; Gibson *et al.*, 1983; MacGeehan, 1977), in the Snow Lake region, they apparently developed at relatively shallow subsurface levels with respect to the massive sulphide bodies and contain Fe-Mg(-Mn-Zn) silicate minerals. For example, at the Anderson Lake mine, lower semiconformable alteration lies 150 metres below the orebody (Walford and Franklin, 1982) and, at the Linda deposit, the distal alteration zone approaches to about 100 metres of the largest massive sulphide body (within 45 metres of the proximal alteration zone). Although these thicknesses have no absolute stratigraphic significance, relative to the thickness of massive sulphide bodies and volcanic units, it is possible to infer that the semiconformable zones lay at unusually shallow depths below the depositional surfaces. A possible solution to the quandary is Skirrow's (1987) model which links the lower semiconformable alteration beneath the Chisel Lake mine, laterally and down-section to deeper level silicic alteration. Skirrow's model could be combined with Model 1 of the Linda deposit to provide a more regionally extensive source area for metalliferous fluids. Model 2 is an alternative solution to the same problems and likewise implies a more regionally disposed source area.

PART III

MINERAL AND WHOLE-ROCK CHEMISTRY

Chapter 9
Mineral Chemistry

A suite of 21 samples was selected for determination of mineral compositions by electron-probe microanalysis (*see* Appendix B). The suite represents the variety of mineral assemblages occurring in altered rocks of the Linda deposit (Figure 9.1, Table 9.1) and includes the following alteration types: proximal alteration (10p, 1b/10p, 4/10p); distal alteration (10d) and the muscovite-staurolite-gahnite cores to these zones (10pa, 10da); graphitic metasediment (3); calc-silicate and anthophyllite-staurolite-gahnite enclaves (10p) in the main massive sulphide body; concordant calc-silicate felsic rocks (1/10c); static calc-silicate rocks (10i); and cummingtonite-bearing silicic-feldspathic altered rocks (1d, 2/10s). The main focus of the sampling was on the proximal and distal alteration zones, in order to adequately represent the parageneses and to obtain maximum-phase assemblages.

9.1. Mineral Chemistry and Definition of Assemblages.

The porphyroblastic schists in the Linda deposit require careful petrographic evaluation in terms of textural criteria of equilibrium. Garnet, staurolite, gahnite, kyanite and, in many cases, biotite are typically coarse grained (1–10 mm) and vary from sieved to skeletal, with abundant inclusions of quartz. They occur as isolated porphyroblasts with few mutual contacts. Minor to trace amounts of sphalerite, rutile and tourmaline occur as fine disseminated grains. Mineral grains in mutual contact were analysed where possible. Alternatively, grains within an area of approximately 5–10 mm in diameter were assumed to have equilibrated, the diameter being determined by the grain sizes and the spacing of porphyroblastic minerals. The thin sections were therefore subdivided into smaller areas containing porphyroblastic, schistose and fine disseminated minerals. Table B.3 presents a compilation of individual spot analyses by sample and area. Table 9.2 is a compilation of means and standard deviations (1σ) derived for each sample; the number of analyses is

 (text continues on page 167)

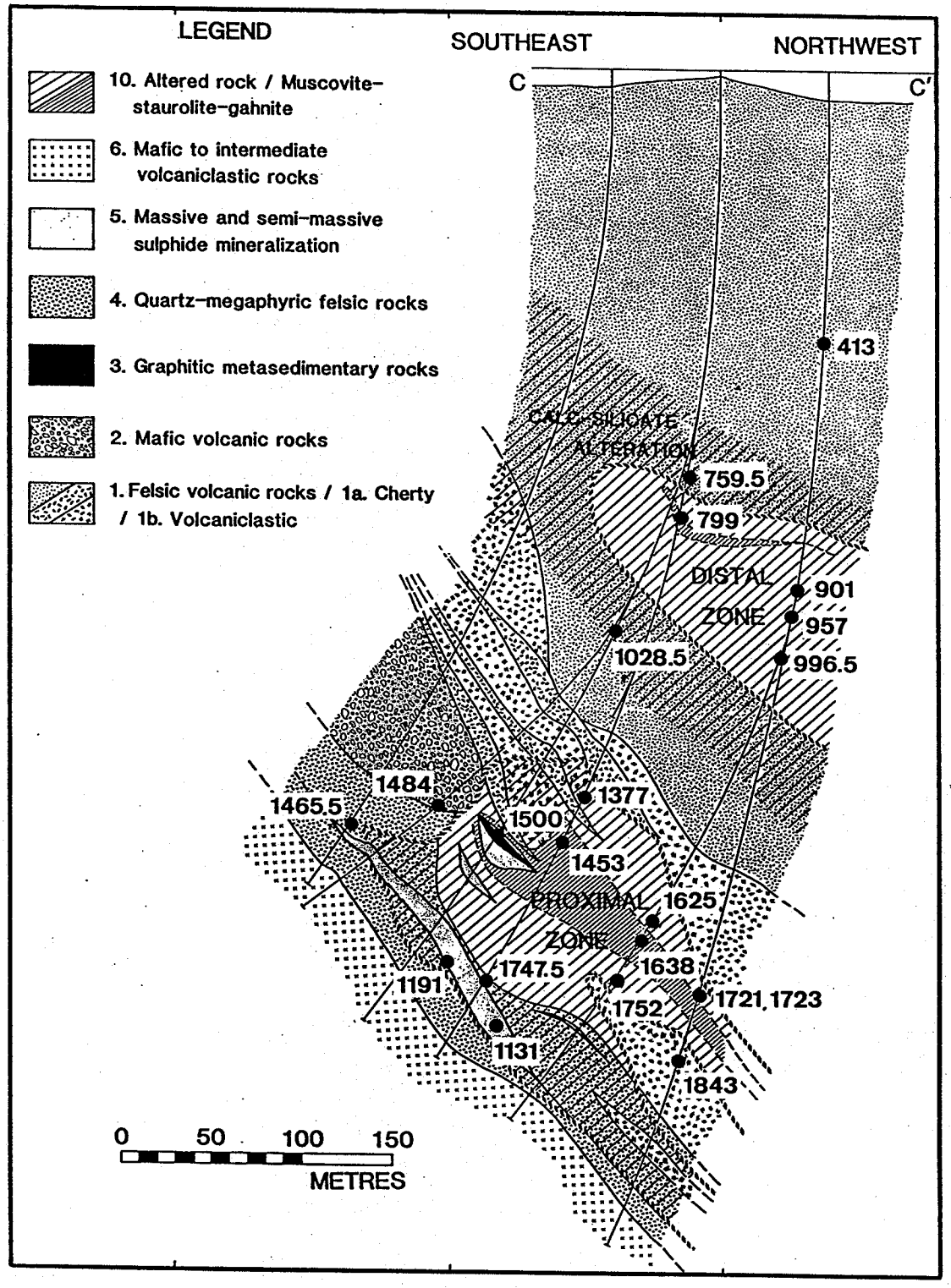

Figure 9.1. Location of samples of the electron-probe microanalysis suite. Samples have all been projected into Section C-C' (identical to Figure 3.3).

Table 9.1. Electron-Probe Microanalysis Sample Suite. Summary of Mineral Assemblages. (Analysed minerals in boldface.)

a. Distal Alteration Zone.

Sample	Unit	Assemblages	Trace Minerals
22-901	10d	quartz, **muscovite**, **chlorite**, **kyanite**, **staurolite**, pyrite.	plagioclase,[2] apatite, allanite, tourmaline, sphalerite, zircon, rutile, ilmenite.[1]
22-957	10d	quartz, **muscovite**, **staurolite**, **chlorite**, **margarite**, pyrite.	garnet, tourmaline, sphalerite, apatite, allanite, magnetite, ilmenite, rutile, monazite, xenotime.
22-996.5	10d	quartz, **chlorite**, **muscovite**, **staurolite**, magnetite.	ilmenite, pyrite, apatite, allanite.
34-799a	10da	quartz, **muscovite**, **gahnite**, **staurolite**, pyrite.	**sphalerite**, tourmaline, **chlorite**, apatite, chalcopyrite, sillimanite,[3] rutile.
34-799b	10da	quartz, muscovite, **gahnite**, pyrite, **sphalerite**.	tourmaline, chalcopyrite, rutile, chlorite.

b. Proximal Alteration Zone.

Sample	Unit	Assemblages	Trace Minerals
22A-1625	10p	quartz, **muscovite**, **chlorite**, **staurolite**, **garnet**, **biotite**, pyrite, monoclinic pyrrhotite.[1]	tourmaline, **sphalerite**, allanite, apatite, zircon, chalcopyrite, rutile.
22A-1638	10pa	quartz, **muscovite**, **staurolite**, **kyanite**, pyrite, **gahnite**, **sphalerite**.	**tourmaline**, apatite, zircon, pyrrhotite, chalcopyrite, rutile.
22A-1752	1b/10p	quartz, **muscovite**, pyrite, **plagioclase**, **kyanite**, **chlorite**, **staurolite**.	tourmaline, rutile, apatite, **biotite**, chalcopyrite.
22B-1721	10p	quartz, **muscovite**, **biotite**, **plagioclase**, **garnet**, **staurolite**, pyrite, **chlorite**, hexagonal pyrrhotite, monoclinic pyrrhotite.[1]	**epidote**, apatite, zircon, allanite, ilmenite, chalcopyrite, sillimanite,[3] calcite.[1]
22B-1723	10pa	quartz, **muscovite**, **staurolite**, pyrite, **gahnite**, **chlorite**,[3] **biotite**.	**sphalerite**, margarite, apatite, tourmaline, zircon, galena, rutile, garnet, calcite.[1]
34C-1377	10p	quartz, **muscovite**, **plagioclase**, **staurolite**, pyrite, **kyanite**, **biotite**, **tourmaline**, **chlorite**	**sphalerite**, apatite, zircon, rutile, xenotime, sillimanite.[3]
34C-1453	10pa	quartz, **muscovite**, **staurolite**, **gahnite**, pyrite, monoclinic pyrrhotite.[1]	**biotite**, **chlorite**, apatite, zircon, allanite, rutile, ilmenite, xenotime, monazite.
34C-1747.5	4/10p	quartz, **muscovite**, **kyanite**, **staurolite**, **biotite**, **chlorite**,[3] pyrite.	apatite, monoclinic pyrrhotite,[1] hexagonal pyrrhotite, chalcopyrite, rutile.

Table 9.1 (continued).

c. Graphitic Metasediment.

Sample	Unit	Assemblages	Trace Minerals
34-1500	3	quartz, graphite, **margarite, kyanite,** pyrite, monoclinic pyrrhotite,[1] hexagonal pyrrhotite, **biotite, chlorite,**[3] **muscovite,** sphalerite.	arsenopyrite, chalcopyrite, tourmaline.

d. Silicate Enclaves in the Main Massive Sulphide Body.

Sample	Unit	Assemblages	Trace Minerals
24-1131	10p	quartz, **plagioclase, staurolite, anthophyllite,** pyrite, **gahnite,** monoclinic pyrrhotite,[1] magnetite, chalcopyrite.	**biotite,**[3] arsenopyrite, hexagonal pyrrhotite, sillimanite.[3]
24-1191	10p	*see* Table 5.2.	

e. Proximal Alteration Zone, Cr-mica-Plagioclase Schist.

Sample	Unit	Assemblages	Trace Minerals
32-1465.5	10p	quartz, **Cr-muscovite,** pyrite, plagioclase, titanite.	apatite, chalcopyrite, pyrrhotite.

f. Silicic-Feldspathic Altered Mafic Rocks.

Sample	Unit	Assemblages	Trace Minerals
22-413	1d	**plagioclase,** quartz, **cummingtonite, hornblende, garnet,** magnetite.	monoclinic pyrrhotite,[1] **chlorite,** biotite, chalcopyrite, ilmenite, apatite, allanite.
34A-1484	2/10s	plagioclase, quartz, **cummingtonite, hornblende, chlorite,** magnetite.	ilmenite, apatite, chalcopyrite, pyrite, calcite.[1]

g. Concordant Calc-silicate Felsic Rocks.

Sample	Unit	Assemblages	Trace Minerals
22B-1843	1/10c	quartz, plagioclase, **biotite, muscovite, epidote,** pyrite.	**allanite,** calcite, titanite, apatite, zircon, pyrrhotite.
34-1028.5	1/10c	quartz, plagioclase, **epidote, biotite, muscovite,** K-feldspar, calcite, pyrite.	titanite, hexagonal pyrrhotite, monoclinic pyrrhotite,[1] chalcopyrite, apatite.

h. Static Calc-silicate Rocks.

Sample	Unit	Assemblages	Trace Minerals
34B-759.5	10i	**actinolite, epidote, biotite,** quartz, calcite, plagioclase, K-feldspar.	allanite, titanite.

[1] Retrograde.

[2] Inferred from altered pseudomorphs.

[3] Not part of the equilibrium assemblage.

Table 9.2, a. MUSCOVITE and MARGARITE MINERAL CHEMISTRY

Sample(N)	22-901	(6) stan	22-957	(4) stan	22-996.5	(5) stan	22A-1625 S1-mat	(2) stan	22A-1625 S2-blade	(2) stan	22A-1638	(2) stan	22A-1752	(2) stan	22B-1721	(5) stan	22B-1723	(10) stan
	mean	dev	mean	dev	mean	dev	mean	dev	mean	dev	mean	dev	mean	dev	mean	dev	mean	dev
SiO2	45.73	0.36	46.01	0.33	46.17	0.09	43.58	0.21	45.81	0.26	44.68	0.26	46.73	1.02	45.53	0.83	45.17	0.75
TiO2	0.40	0.05	0.28	0.05	0.29	0.04	0.31	0.02	0.47	0.04	0.32	0.02	0.29	0.06	0.30	0.01	0.41	0.04
Al2O3	36.12	0.35	35.65	0.80	36.17	0.26	35.87	0.08	36.53	0.05	36.28	0.23	35.46	1.08	36.21	0.55	36.30	0.61
Cr2O3	0.00	0.00	0.00	0.00	0.00	0.00	0.00	0.00	0.00	0.00	0.00	0.00	0.00	0.00	0.00	0.00	0.00	0.00
FeO	2.09	0.18	2.46	0.31	2.62	0.18	2.41	0.10	1.32	0.03	0.80	0.08	1.17	0.10	1.94	0.21	1.56	0.08
MnO	0.00	0.00	0.00	0.00	0.00	0.00	0.00	0.00	0.00	0.00	0.00	0.00	0.00	0.00	0.00	0.00	0.00	0.00
MgO	0.65	0.05	0.67	0.07	0.69	0.04	2.49	0.03	0.76	0.02	0.59	0.03	0.61	0.17	0.74	0.02	0.80	0.06
BaO	0.17	0.02	0.27	0.04	0.28	0.07	0.15	0.00	0.17	0.01	0.12	0.01	0.02	0.05	0.14	0.02	0.10	0.05
CaO	0.00	0.00	0.00	0.00	0.02	0.03	0.00	0.00	0.00	0.00	0.00	0.00	0.00	0.00	0.36	0.42	0.75	0.41
Na2O	1.54	0.08	1.17	0.05	1.23	0.02	1.42	0.04	1.59	0.06	2.07	0.03	2.30	0.24	0.92	0.07	0.98	0.05
K2O	9.13	0.19	8.81	0.43	8.37	0.37	7.96	0.07	8.65	0.15	7.53	0.25	8.16	0.49	9.22	0.48	8.68	0.33
F	0.00	0.00	0.00	0.00	0.00	0.00	0.00	0.00	0.00	0.00	0.00	0.00	0.00	0.00	0.00	0.00	0.00	0.00
H2O(c)	4.53	0.03	4.51	0.04	4.54	0.01	4.45	0.01	4.53	0.02	4.43	0.01	4.52	0.05	4.51	0.02	4.50	0.04
Total	100.35	0.61	99.81	0.72	100.37	0.53	98.62	0.22	99.82	0.42	96.80	0.31	99.26	1.01	99.87	0.41	99.24	0.81
Si	6.059	0.019	6.120	0.016	6.097	0.017	5.871	0.012	6.061	0.011	6.053	0.008	9.196	0.117	6.125	0.087	6.020	0.080
Aliv	1.941	0.019	1.880	0.016	1.903	0.017	2.129	0.012	1.939	0.011	1.947	0.008	1.804	0.117	1.875	0.087	1.980	0.080
Alvi	3.702	0.034	3.710	0.063	3.727	0.034	3.569	0.008	3.759	0.003	3.847	0.005	3.739	0.049	3.740	0.024	3.730	0.020
Ti	0.040	0.005	0.028	0.006	0.029	0.004	0.031	0.001	0.047	0.004	0.033	0.005	0.028	0.006	0.030	0.001	0.040	0.000
Cr	0.000	0.000	0.000	0.000	0.000	0.000	0.000	0.000	0.000	0.000	0.000	0.000	0.000	0.000	0.000	0.000	0.000	0.000
Fe	0.232	0.020	0.274	0.036	0.290	0.020	0.272	0.012	0.146	0.003	0.090	0.001	0.129	0.011	0.216	0.023	0.170	0.010
Mn	0.000	0.000	0.000	0.000	0.000	0.000	0.000	0.000	0.000	0.000	0.000	0.000	0.000	0.000	0.000	0.000	0.000	0.000
Mg	0.128	0.009	0.133	0.014	0.136	0.008	0.500	0.007	0.149	0.002	0.119	0.004	0.120	0.035	0.147	0.004	0.160	0.010
site	4.102	0.010	4.145	0.030	4.181	0.014	4.372	0.010	4.101	0.002	4.089	0.006	4.017	0.029	4.130	0.019	4.100	0.020
Ba	0.009	0.001	0.014	0.002	0.014	0.004	0.008	0.000	0.009	0.001	0.006	0.000	0.001	0.002	0.007	0.001	0.010	0.000
Ca	0.000	0.000	0.000	0.000	0.002	0.005	0.000	0.000	0.000	0.000	0.000	0.000	0.000	0.000	0.052	0.060	0.110	0.060
Na	0.396	0.021	0.301	0.013	0.314	0.006	0.370	0.013	0.407	0.016	0.544	0.009	0.591	0.060	0.236	0.018	0.250	0.010
K	1.543	0.026	1.495	0.080	1.409	0.059	1.368	0.008	1.460	0.020	1.301	0.041	1.380	0.087	1.564	0.080	1.480	0.060
site	1.947	0.027	1.810	0.090	1.740	0.057	1.746	0.004	1.876	0.004	1.851	0.033	1.973	0.058	1.859	0.047	1.840	0.040
F	0.000		0.000		0.000		0.000		0.000		0.000		0.000		0.000		0.000	
H(c)	4.000		4.000		4.000		4.000		4.000		4.000		4.000		4.000		4.000	
O	24.000		24.000		24.000		24.000		24.000		24.000		24.000		24.000		24.000	

Table 9.2, a. MUSCOVITE and MARGARITE MINERAL CHEMISTRY (continued)

Sample(N)	22B-1843	(5)	32-1465.5	(8)	34-799	(6)	34-1028.5	(2)	34-1500	34-1500	(4)	34C-1377	(3)	34C-1453	(9)	34C-1747.5	(6)
	mean	stan dev	mean	stan dev	mean	stan dev	mean	stan dev	mu(1)	ma mean	stan dev	mean	stan dev	mean	stan dev	mean	stan dev
SiO2	46.61	0.11	46.52	0.34	45.25	0.44	47.53	0.73	46.73	31.08	0.22	46.82	0.28	46.68	0.39	45.82	0.15
TiO2	0.65	0.12	0.50	0.17	0.35	0.05	0.78	0.23	0.00	0.08	0.01	0.36	0.02	0.37	0.03	0.31	0.03
Al2O3	32.43	0.27	33.62	0.21	36.77	0.42	32.04	0.44	36.80	50.96	0.10	37.03	0.31	36.31	0.33	36.70	0.21
Cr2O3	0.00	0.00	0.34	0.16	0.00	0.00	0.00	0.00	0.00	0.00	0.00	0.00	0.00	0.00	0.00	0.00	0.00
FeO	2.29	0.18	1.13	0.11	1.20	0.07	2.30	0.01	0.00	0.07	0.07	1.20	0.07	1.60	0.13	1.65	0.08
MnO	0.00	0.00	0.00	0.00	0.00	0.00	0.00	0.00	0.00	0.00	0.00	0.00	0.00	0.00	0.00	0.00	0.00
MgO	2.04	0.10	1.36	0.02	0.58	0.08	2.10	0.01	1.22	0.27	0.04	0.81	0.08	0.66	0.06	0.64	0.03
BaO	0.34	0.14	0.34	0.04	0.13	0.02	0.20	0.02	0.48	0.00	0.00	0.08	0.05	0.04	0.06	0.07	0.07
CaO	0.01	0.03	0.00	0.00	0.02	0.02	0.03	0.03	0.04	11.09	0.23	0.00	0.00	0.00	0.00	0.00	0.00
Na2O	0.24	0.01	0.62	0.02	1.68	0.09	0.21	0.01	0.78	0.64	0.04	1.47	0.06	1.89	0.15	1.65	0.07
K2O	10.41	0.32	9.92	0.26	8.36	0.17	10.73	0.19	9.41	0.23	0.06	8.05	0.19	7.92	0.27	9.07	0.22
F	0.00	0.00	0.44	0.27	0.00	0.00	0.00	0.00	0.00	0.00	0.00	0.00	0.00	0.00	0.00	0.00	0.00
H2O(c)	4.46	0.02	4.25	0.14	4.50	0.03	4.50	0.05	4.56	4.51	0.02	4.59	0.03	4.56	0.02	4.55	0.01
Total	99.49	0.58	98.86	0.59	98.82	0.53	100.20	1.15	100.02	98.92	0.41	100.40	0.68	100.03	0.42	100.45	0.34
Si	6.271	0.024	6.253	0.018	6.035	0.041	6.339	0.021	6.143	4.132	0.015	6.115	0.004	6.137	0.027	6.045	0.016
Aliv	1.729	0.024	1.747	0.018	1.965	0.041	1.661	0.021	1.857	3.868	0.015	1.885	0.004	1.863	0.027	1.955	0.016
Alvi	3.414	0.022	3.579	0.016	3.818	0.019	3.376	0.030	3.847	4.118	0.011	3.815	0.008	3.765	0.028	3.753	0.008
Ti	0.066	0.012	0.051	0.018	0.035	0.005	0.078	0.240	0.000	0.007	0.002	0.035	0.002	0.036	0.003	0.031	0.003
Cr	0.000	0.000	0.036	0.017	0.000	0.000	0.000	0.000	0.000	0.000	0.000	0.000	0.000	0.000	0.000	0.000	0.000
Fe	0.258	0.020	0.127	0.011	0.134	0.008	0.257	0.005	0.000	0.008	0.008	0.131	0.008	0.176	0.014	0.182	0.009
Mn	0.000	0.000	0.000	0.000	0.000	0.000	0.000	0.000	0.000	0.000	0.000	0.000	0.000	0.000	0.000	0.000	0.000
Mg	0.409	0.020	0.272	0.006	0.115	0.015	0.417	0.003	0.239	0.054	0.007	0.158	0.016	0.128	0.012	0.126	0.005
site	4.147	0.011	4.066	0.014	4.102	0.015	4.128	0.002	4.086	4.186	0.024	4.139	0.012	4.106	0.021	4.092	0.015
Ba	0.018	0.007	0.018	0.002	0.007	0.001	0.010	0.001	0.025	0.000	0.000	0.004	0.003	0.002	0.003	0.004	0.004
Ca	0.002	0.004	0.000	0.000	0.002	0.003	0.004	0.004	0.006	1.580	0.028	0.000	0.000	0.000	0.000	0.000	0.000
Na	0.064	0.002	0.163	0.006	0.434	0.021	0.053	0.001	0.199	0.165	0.010	0.371	0.015	0.481	0.039	0.421	0.017
K	1.786	0.050	1.701	0.040	1.422	0.031	1.793	0.011	1.578	0.038	0.009	1.342	0.024	1.328	0.049	1.527	0.035
site	1.870	0.046	1.881	0.038	1.864	0.029	1.860	0.007	1.807	1.783	0.028	1.717	0.019	1.811	0.069	1.951	0.040
F	0.000		0.187	0.115	0.000		0.000		0.000	0.000		0.000		0.000		0.000	
H(c)	4.000		3.813	0.115	4.000		4.000		4.000	4.000		4.000		4.000		4.000	
O	24.000		23.813		24.000		24.000		24.000	24.000		24.000		24.000		24.000	

Table 9.2, b. BIOTITE MINERAL CHEMISTRY

Sample(N)	22A-1625	(5) stan	22A-1752	(2) stan	22B-1843	(5) stan	22B-1721	(4) stan	22B-1723	(5) stan	24-1131	(7) stan	24-1191 zone 6	(2) stan
	mean	dev	mean	dev	mean	dev	mean	dev	mean	dev	mean	dev	mean	dev
SiO2	37.87	0.35	38.40	0.11	37.65	0.60	36.87	0.14	37.15	0.61	38.88	0.28	38.51	0.23
TiO2	1.02	0.05	1.00	0.01	1.42	0.25	1.20	0.05	1.27	0.08	0.90	0.18	0.99	0.04
Al2O3	19.19	0.15	18.92	0.07	18.69	0.14	19.46	0.03	18.79	0.12	17.13	0.26	17.61	0.11
FeO	10.75	0.15	9.73	0.14	11.60	0.38	15.98	0.15	14.32	0.15	12.48	0.26	14.98	0.26
MnO	0.24	0.01	0.20	0.01	0.45	0.03	0.14	0.01	0.17	0.03	0.05	0.05	0.33	0.04
MgO	17.52	0.15	19.34	0.14	16.58	0.12	13.71	0.18	15.61	0.25	18.29	0.16	16.13	0.09
ZnO	0.00	0.00	0.00	0.00	0.00	0.00	0.00	0.00	0.00	0.00	0.03	0.08	0.00	0.00
BaO	0.00	0.00	0.00	0.00	0.00	0.00	0.00	0.00	0.00	0.00	0.29	0.03	0.00	0.00
CaO	0.00	0.00	0.02	0.02	0.05	0.03	0.03	0.03	0.03	0.02	0.04	0.05	0.00	0.00
Na2O	0.41	0.02	0.38	0.02	0.10	0.02	0.32	0.05	0.28	0.07	0.18	0.02	0.25	0.02
K2O	9.24	0.43	8.57	0.38	9.30	0.12	9.18	0.13	8.72	0.22	8.19	0.33	8.49	0.11
F	1.67	0.15	2.83	0.08	0.38	0.19	0.92	0.05	1.51	0.09	1.57	0.14	0.90	0.20
H2O(c)	3.37	0.08	2.88	0.05	3.95	0.10	3.66	0.03	3.39	0.05	3.42	0.06	3.72	0.00
Total	100.57	0.72	101.06	0.07	100.00	0.55	101.07	0.27	100.62	0.52	100.79	0.30	101.51	0.18
Si	5.452	0.022	5.460	0.006	5.472	0.048	5.405	0.012	5.423	0.060	5.600	0.031	5.569	0.033
Aliv	2.548	0.022	2.540	0.005	2.528	0.048	2.595	0.012	2.577	0.060	2.400	0.031	2.431	0.016
Alvi	0.709	0.011	0.631	0.003	0.675	0.032	0.769	0.013	0.658	0.033	0.510	0.027	0.570	0.004
Ti	0.111	0.004	0.106	0.001	0.155	0.027	0.132	0.005	0.139	0.009	0.098	0.019	0.107	0.004
Fe	1.294	0.022	1.157	0.014	1.411	0.051	1.959	0.020	1.749	0.024	1.503	0.036	1.812	0.031
Mn	0.029	0.001	0.023	0.001	0.055	0.003	0.018	0.002	0.021	0.003	0.006	0.007	0.040	0.004
Mg	3.760	0.042	4.098	0.025	3.591	0.042	2.995	0.033	3.396	0.070	3.927	0.026	3.475	0.020
Zn	0.000	0.000	0.000	0.000	0.000	0.000	0.000	0.000	0.000	0.000	0.004	0.009	0.000	0.000
site	5.903	0.044	6.016	0.042	5.888	0.046	5.873	0.011	5.963	0.060	6.047	0.022	6.005	0.063
Ba	0.000	0.000	0.000	0.000	0.000	0.000	0.000	0.000	0.000	0.000	0.016	0.002	0.000	0.000
Ca	0.000	0.000	0.003	0.003	0.007	0.004	0.004	0.004	0.005	0.003	0.006	0.008	0.000	0.000
Na	0.114	0.006	0.105	0.005	0.028	0.005	0.091	0.014	0.079	0.019	0.051	0.005	0.070	0.005
K	1.697	0.071	1.555	0.070	1.725	0.020	1.716	0.025	1.624	0.035	1.505	0.059	1.566	0.020
site	1.811	0.075	1.662	0.080	1.761	0.017	1.811	0.023	1.709	0.050	1.579	0.052	1.636	0.025
F	0.759	0.069	1.273	0.037	0.173	0.087	0.424	0.024	0.695	0.043	0.717	0.063	0.412	0.089
H(c)	3.241	0.069	2.727	0.037	3.827	0.087	3.576	0.024	3.305	0.043	3.283	0.063	3.588	0.089
O	23.241		22.727		23.827		23.576		23.305		23.283		23.588	

Table 9.2, b. BIOTITE MINERAL CHEMISTRY (continued)

Sample(N)	24-1191	(4)	34-1028.5	(5)	34-1500	(6)	34B-759.5	(6)	34C-1377	(5)	34C-1453	34C-1747.5	(6)
	zone 5	stan		stan		stan		stan		stan	(1)		stan
	mean	dev	mean	dev	mean	dev	mean	dev	mean	dev		mean	dev
SiO2	38.19	0.28	37.33	0.41	41.68	0.15	38.34	0.27	39.82	0.06	37.61	37.34	0.24
TiO2	0.98	0.15	1.15	0.22	0.34	0.02	0.74	0.46	0.72	0.01	0.92	1.18	0.06
Al2O3	17.04	0.20	18.67	0.45	17.21	0.23	17.72	0.37	18.50	0.08	16.94	18.69	0.21
FeO	14.36	0.45	13.33	0.95	1.30	0.08	11.45	0.82	9.04	0.03	16.89	13.79	0.23
MnO	0.36	0.03	0.41	0.04	0.05	0.04	0.18	0.02	0.28	0.02	0.00	0.11	0.02
MgO	17.01	0.27	15.42	0.49	25.25	0.15	17.72	0.61	19.75	0.08	16.32	15.72	0.15
ZnO	0.00	0.00	0.00	0.00	0.00	0.00	0.00	0.00	0.00	0.00	0.00	0.00	0.00
BaO	0.00	0.00	0.00	0.00	0.16	0.01	0.02	0.04	0.00	0.00	0.00	0.00	0.00
CaO	0.00	0.00	0.07	0.04	0.01	0.02	0.03	0.04	0.00	0.00	0.00	0.00	0.00
Na2O	0.26	0.02	0.09	0.02	0.33	0.02	0.04	0.04	0.41	0.01	0.24	0.40	0.05
K2O	8.48	0.10	9.45	0.40	8.73	0.47	10.12	0.31	78.18	0.21	8.05	8.97	0.27
F	0.67	0.42	0.00	0.00	- 3.53	0.13	0.09	0.19	2.18	0.15	3.45	1.64	0.13
H2O(c)	3.81	0.21	4.09	0.05	2.66	0.05	4.10	0.09	3.23	0.08	2.46	3.33	0.07
Total	100.86	0.18	100.01	0.86	99.76	0.69	100.50	0.54	101.17	0.26	101.43	100.48	0.63
Si	5.553	0.023	5.472	0.012	5.766	0.016	5.556	0.030	5.606	0.005	5.502	5.453	0.028
Aliv	2.447	0.023	2.528	0.012	2.234	0.016	2.444	0.030	2.394	0.005	2.498	2.547	0.028
Alvi	0.473	0.023	0.699	0.054	0.573	0.037	0.583	0.061	0.676	0.005	0.424	0.670	0.028
Ti	0.107	0.016	0.127	0.023	0.035	0.002	0.081	0.050	0.076	0.001	0.101	0.130	0.006
Fe	1.746	0.059	1.636	0.134	0.151	0.010	1.388	0.101	1.064	0.003	2.067	1.684	0.025
Mn	0.045	0.004	0.051	0.004	0.006	0.005	0.022	0.002	0.033	0.002	0.000	0.013	0.002
Mg	3.687	0.048	3.367	0.076	5.207	0.022	3.828	0.128	4.143	0.020	3.558	3.420	0.041
Zn	0.000	0.000	0.000	0.000	0.000	0.000	0.000	0.000	0.000	0.000	0.000	0.000	0.000
site	6.058	0.016	5.880	0.043	5.971	0.018	5.903	0.039	5.992	0.018	6.150	5.917	0.025
Ba	0.000	0.000	0.000	0.000	0.009	0.001	0.001	0.003	0.000	0.000	0.000	0.000	0.000
Ca	0.000	0.000	0.011	0.007	0.001	0.002	0.004	0.006	0.000	0.000	0.000	0.000	0.000
Na	0.073	0.007	0.026	0.006	0.087	0.005	0.012	0.012	0.112	0.004	0.068	0.113	0.014
K	1.573	0.019	1.768	0.063	1.541	0.078	1.871	0.056	1.469	0.035	1.503	1.671	0.043
site	1.645	0.022	1.804	0.059	1.639	0.082	1.888	0.054	1.581	0.037	1.571	1.784	0.038
F	0.306	0.193	0.000		1.545	0.054	0.039	0.087	0.971	0.070	1.596	0.757	0.062
H(c)	3.694	0.193	4.000		2.455	0.054	3.961	0.087	3.029	0.070	2.404	3.243	0.062
O	23.694		24.000		22.455		23.961		23.029		22.404	23.243	

Table 9.2, c. CHLORITE MINERAL CHEMISTRY

Sample(N)	22-413	(4)	22-901	(6)	22-957	(5)	22-996.5	(6)	22A-1625	(4)	22A-1752	(6)	22B-1721	(5)	22B-1723	(2)
	mean	stan dev	mean	stan dev	mean	stan dev	mean	stan dev	mean	stan dev	mean	stan dev	mean	stan dev	mean	stan dev
SiO2	24.90	0.20	25.30	0.40	24.81	0.27	24.79	0.19	26.30	0.53	26.29	0.22	25.10	0.17	25.99	0.57
TiO2	0.07	0.01	0.04	0.03	0.05	0.03	0.06	0.03	0.07	0.01	0.05	0.03	0.06	0.03	0.05	0.05
Al2O3	22.91	0.05	24.44	0.28	23.62	0.10	24.18	0.27	24.52	0.60	24.34	0.28	24.00	0.14	23.64	0.23
FeO	25.22	0.18	20.59	0.16	22.62	0.35	23.53	0.13	14.73	0.18	15.23	0.46	20.45	0.26	18.35	0.28
MnO	0.07	0.04	0.30	0.02	0.35	0.02	0.31	0.03	0.43	0.01	0.38	0.02	0.29	0.03	0.35	0.00
MgO	16.63	0.12	19.32	0.21	17.42	0.20	17.45	0.10	22.72	0.43	23.20	0.29	19.51	0.21	20.69	0.63
ZnO	0.00	0.00	0.00	0.00	0.00	0.00	0.00	0.00	0.11	0.11	0.00	0.00	0.00	0.00	0.12	0.12
BaO	0.00	0.00	0.00	0.00	0.00	0.00	0.00	0.00	0.00	0.00	0.00	0.00	0.00	0.00	0.00	0.00
CaO	0.01	0.02	0.00	0.00	0.02	0.04	0.00	0.00	0.00	0.00	0.00	0.00	0.00	0.00	0.00	0.00
Na2O	0.00	0.00	0.00	0.00	0.00	0.00	0.00	0.00	0.02	0.03	0.00	0.00	0.00	0.00	0.03	0.03
K2O	0.00	0.00	0.01	0.00	0.01	0.02	0.00	0.00	0.16	0.18	0.02	0.04	0.00	0.00	0.00	0.00
F	0.00	0.00	0.00	0.00	0.09	0.18	0.07	0.15	0.00	0.00	0.36	0.27	0.00	0.00	0.00	0.00
H2O(c)	11.68	0.06	12.00	0.04	11.67	0.08	11.82	0.08	12.23	0.12	12.11	0.10	11.92	0.06	12.03	0.01
Total	101.48	0.51	102.00	0.30	100.62	0.71	102.18	0.42	101.26	0.90	101.82	0.50	101.33	0.34	101.23	0.20
Si	5.113	0.018	5.055	0.075	5.083	0.030	5.016	0.028	5.156	0.060	5.135	0.033	5.050	0.014	5.182	0.119
Aliv	2.887	0.018	2.945	0.075	2.917	0.030	2.984	0.028	2.844	0.060	2.865	0.033	2.950	0.014	2.818	0.119
Alvi	2.660	0.017	2.810	0.022	2.787	0.022	2.785	0.031	2.823	0.116	2.741	0.039	2.745	0.014	2.739	0.071
Ti	0.010	0.002	0.006	0.004	0.008	0.004	0.009	0.004	0.010	0.001	0.007	0.005	0.009	0.005	0.007	0.007
Fe	4.331	0.010	3.441	0.035	3.876	0.040	3.981	0.021	2.415	0.044	2.488	0.074	3.442	0.058	3.059	0.051
Mn	0.011	0.007	0.051	0.004	0.060	0.003	0.053	0.005	0.072	0.001	0.063	0.003	0.050	0.004	0.059	0.000
Mg	5.089	0.013	5.752	0.058	5.319	0.048	5.262	0.026	6.642	0.187	6.753	0.087	5.849	0.039	6.148	0.181
Zn	0.000	0.000	0.000	0.000	0.000	0.000	0.000	0.000	0.015	0.016	0.000	0.000	0.000	0.000	0.017	0.017
Ca	0.002	0.004	0.000	0.000	0.005	0.010	0.000	0.000	0.000	0.000	0.000	0.000	0.000	0.000	0.000	0.000
Na	0.000	0.000	0.000	0.000	0.000	0.000	0.000	0.000	0.007	0.011	0.000	0.000	0.000	0.000	0.010	0.010
K	0.000	0.000	0.002	0.000	0.003	0.005	0.000	0.000	0.038	0.045	0.004	0.009	0.000	0.000	0.000	0.000
site	12.103	0.006	12.062	0.044	12.058	0.017	12.090	0.012	12.023	0.054	12.057	0.019	12.094	0.015	12.038	0.093
F	0.000		0.000		0.057	0.113	0.044	0.098	0.000		0.223	0.164	0.000		0.000	
H(c)	16.000		16.000		15.943	0.113	15.956	0.098	16.000		15.777	0.164	16.000		16.000	
O	28.000		28.000		27.943		27.956		28.000		27.777		28.000		28.000	

Table 9.2, c. CHLORITE MINERAL CHEMISTRY (continued)

Sample(N)	24-1191 zone 5 mean	(3) stan dev	24-1191 zone 6 mean	(3) stan dev	34-799 mean	(4) stan dev	34-1500 mean	(2) stan dev	34A-1484 mean	(6) stan dev	34C-1377 mean	(5) stan dev	34C-1453 mean	(3) stan dev	34C-1747.5 (1)
SiO2	26.30	0.64	26.03	0.64	25.04	0.17	30.44	0.44	24.68	0.08	26.59	0.31	25.12	0.18	24.94
TiO2	0.02	0.03	0.02	0.03	0.04	0.02	0.08	0.00	0.05	0.03	0.05	0.03	0.00	0.00	0.07
Al2O3	22.43	0.14	22.49	0.55	24.34	0.20	21.73	0.24	22.78	0.15	24.46	0.21	24.33	0.22	24.00
FeO	18.32	0.21	19.19	0.19	17.03	1.06	15.23	0.46	26.85	0.40	13.01	0.18	21.24	0.32	19.70
MnO	0.57	0.03	0.58	0.03	0.14	0.03	0.38	0.02	0.09	0.02	0.50	0.01	0.14	0.01	0.17
MgO	21.59	0.15	20.58	0.19	21.77	0.80	23.20	0.29	15.65	0.23	24.51	0.34	19.16	0.07	19.60
ZnO	0.06	0.08	0.06	0.08	0.12	0.12	0.00	0.00	0.00	0.00	0.00	0.00	0.00	0.00	0.00
BaO	0.00	0.00	0.00	0.00	0.00	0.00	0.00	0.00	0.00	0.00	0.00	0.00	0.00	0.00	0.00
CaO	0.00	0.00	0.00	0.00	0.00	0.00	0.00	0.00	0.01	0.02	0.00	0.00	0.00	0.00	0.00
Na2O	0.00	0.00	0.00	0.00	0.00	0.00	0.00	0.00	0.00	0.00	0.00	0.00	0.00	0.00	0.00
K2O	0.05	0.07	0.05	0.08	0.00	0.00	0.78	0.22	0.00	0.00	0.03	0.05	0.00	0.00	0.00
F	0.00	0.00	0.00	0.00	0.22	0.22	1.49	0.06	0.00	0.00	0.30	0.25	0.46	0.33	0.00
H2O(c)	12.02	0.04	11.92	0.05	11.90	0.10	12.16	0.04	11.61	0.05	12.22	0.10	11.75	0.21	11.84
Total	101.36	0.28	100.92	0.28	100.50	0.24	102.18	0.82	101.72	0.53	101.54	0.74	101.99	0.50	100.32
Si	5.246	0.030	5.237	0.110	5.006	0.038	5.675	0.052	5.098	0.018	5.157	0.028	5.035	0.036	5.051
Aliv	2.754	0.030	2.763	0.110	2.994	0.038	2.325	0.052	2.902	0.018	2.843	0.028	2.965	0.036	2.949
Alvi	2.522	0.020	2.573	0.037	2.741	0.030	2.452	0.027	2.643	0.020	2.751	0.029	2.784	0.009	2.781
Ti	0.003	0.004	0.003	0.004	0.006	0.004	0.011	0.001	0.007	0.005	0.008	0.004	0.000	0.000	0.011
Fe	3.057	0.044	3.230	0.044	2.847	0.188	0.814	0.057	4.637	0.066	2.110	0.035	3.561	0.040	3.337
Mn	0.096	0.005	0.098	0.005	0.023	0.006	0.046	0.002	0.016	0.004	0.082	0.002	0.024	0.002	0.029
Mg	6.420	0.032	6.172	0.032	6.484	0.215	8.511	0.068	4.816	0.061	7.084	0.041	5.723	0.031	5.916
Zn	0.009	0.012	0.008	0.012	0.018	0.018	0.000	0.000	0.000	0.000	0.000	0.000	0.000	0.000	0.000
Ca	0.000	0.000	0.000	0.000	0.000	0.000	0.000	0.000	0.003	0.004	0.000	0.000	0.000	0.000	0.000
Na	0.000	0.000	0.000	0.000	0.000	0.000	0.000	0.000	0.000	0.000	0.000	0.000	0.000	0.000	0.000
K	0.012	0.017	0.014	0.010	0.000	0.000	0.185	0.051	0.000	0.000	0.006	0.013	0.000	0.000	0.000
site	12.119	0.004	12.099	0.036	12.120	0.033	12.019	0.013	12.122	0.017	12.042	0.006	12.091	0.015	12.073
F	0.000		0.000		0.137	0.137	0.879	0.031	0.000		0.185	0.151	0.293	0.211	0.000
H(c)	16.000		16.000		15.863	0.137	15.121	0.031	16.000		15.815	0.151	15.707	0.211	16.000
O	28.000		28.000		27.863		27.121		28.000		27.815		27.707		28.000

Table 9.2, d. STAUROLITE MINERAL CHEMISTRY

Sample(N)	22-901	(4)	22-901	(4)	22-957	(3)	22-957	(3)	22-996.5	(6)	22A-1625	(6)	22A-1638	(6)	22A-1752	(6)
	core mean	stan dev	rim mean	stan dev	core mean	stan dev	rim mean	stan dev	mean	stan dev	mean	stan dev	mean	stan dev	mean	stan dev
SiO2	27.10	0.11	27.38	0.14	26.80	0.06	26.50	0.50	27.18	0.28	26.66	0.29	26.76	0.62	27.08	0.23
TiO2	0.45	0.03	0.48	0.04	0.49	0.03	0.45	0.02	0.41	0.11	0.46	0.09	0.40	0.05	0.45	0.05
Al2O3	53.86	0.53	53.41	0.31	52.62	0.41	52.02	0.75	53.71	0.27	54.02	0.35	54.44	0.51	53.67	0.47
ZnO	1.21	0.06	1.12	0.03	1.75	0.04	1.82	0.07	0.02	0.05	4.83	0.28	6.91	0.13	3.94	0.33
FeO	11.65	0.29	11.27	0.18	11.77	0.13	11.24	0.29	13.90	0.15	8.04	0.23	6.40	0.12	8.01	0.37
MnO	0.65	0.04	0.61	0.03	0.68	0.01	0.60	0.06	0.61	0.03	0.86	0.03	0.54	0.02	0.74	0.03
MgO	1.97	0.05	1.90	0.05	1.86	0.05	1.68	0.05	2.01	0.09	2.27	0.08	2.19	0.06	2.07	0.17
H2O(c)	1.63		1.62		1.59		1.58		1.63		1.62		1.63		1.62	
Total	98.52		97.79		97.56		95.89		99.47		98.76		99.27		97.58	
Si	7.637	0.073	7.737	0.056	7.684	0.033	7.703	0.039	7.668	0.065	7.533	0.086	7.513	0.160	7.651	0.060
Aliv	0.363	0.073	0.263	0.056	0.316	0.033	0.297	0.039	0.332	0.065	0.467	0.086	0.487	0.160	0.349	0.060
Alvi	17.530		17.530		17.530		17.530		17.530		17.530		17.530		17.530	
Ti	0.096	0.008	0.102	0.009	0.106	0.007	0.098	0.005	0.087	0.023	0.098	0.019	0.085	0.012	0.096	0.009
site	17.626		17.632		17.636		17.628		17.617		16.628		17.615		17.626	
Zn	0.251	0.013	0.233	0.007	0.371	0.006	0.391	0.019	0.005	0.011	1.007	0.061	1.433	0.034	0.822	0.067
Fe	2.745	0.081	2.663	0.039	2.831	0.047	2.734	0.106	3.280	0.044	1.899	0.053	1.503	0.032	1.893	0.088
Mn	0.155	0.009	0.146	0.008	0.166	0.003	0.148	0.012	0.145	0.006	0.207	0.008	0.129	0.004	0.178	0.008
Mg	0.825	0.026	0.799	0.022	0.797	0.006	0.729	0.013	0.845	0.040	0.954	0.033	0.917	0.028	0.870	0.072
site	3.976	0.108	3.841	0.053	4.165	0.050	4.002	0.105	4.275	0.066	4.067	0.057	3.982	0.072	3.762	0.091
H	3.060		3.060		3.060		3.060		3.060		3.060		3.060		3.060	
O	47.812		47.739		48.044		47.875		48.108		47.855		47.734		47.605	

Sample(N)	228-1721	(8)	228-1723	(6)	24-1131	(7)	34-799	(6)	34C-1377	(3)	34C-1377	(3)	34C-1453	(12)	34C-1747.5	(6)
	mean	stan dev	mean	stan dev	mean	stan dev	mean	stan dev	core mean	stan dev	rim mean	stan dev	mean	stan dev	mean	stan dev
SiO2	27.07	0.23	26.73	0.16	26.60	0.19	26.84	0.29	26.71	0.18	26.67	0.27	26.45	0.22	26.87	0.18
TiO2	0.46	0.04	0.42	0.03	0.29	0.06	0.38	0.03	0.39	0.05	0.37	0.02	0.42	0.04	0.48	0.07
Al2O3	53.14	0.47	53.27	0.42	52.57	0.57	54.27	0.58	53.68	0.28	53.29	0.50	53.66	0.49	53.78	0.39
ZnO	2.29	0.08	6.15	0.09	5.05	0.16	7.16	0.17	5.21	0.03	5.23	0.10	5.28	0.31	1.58	0.02
FeO	11.10	0.26	8.14	0.10	10.01	0.13	6.53	0.35	7.18	0.07	7.23	0.06	9.29	0.27	11.02	0.22
MnO	0.55	0.02	0.58	0.03	0.22	0.02	0.23	0.02	1.00	0.02	1.03	0.04	0.21	0.03	0.40	0.04
MgO	1.89	0.12	2.05	0.06	2.50	0.12	1.90	0.24	2.52	0.09	2.23	0.07	1.70	0.11	2.08	0.13
H2O(c)	1.61		1.61		1.59		1.63		1.62		1.61		1.61		1.62	
Total	98.11		98.95		98.83		98.94		98.31		97.66		98.62		97.83	
Si	7.703	0.073	7.622	0.066	7.667	0.087	7.545	0.065	7.578	0.053	7.609	0.044	7.528	0.088	7.598	0.033
Aliv	0.297	0.073	0.378	0.066	0.333	0.087	0.455	0.065	0.422	0.053	0.391	0.044	0.472	0.088	0.402	0.033
Alvi	17.530		17.530		17.530		17.530		17.530		17.530		17.530		17.530	
Ti	0.098	0.010	0.090	0.006	0.062	0.012	0.081	0.007	0.084	0.011	0.080	0.006	0.089	0.010	0.103	0.015
site	17.628		17.620		17.592		17.611		17.610		17.610		17.619		17.633	
Zn	0.481	0.017	1.296	0.014	1.076	0.058	1.485	0.041	1.091	0.007	1.102	0.019	1.108	0.060	0.330	0.003
Fe	2.641	0.141	1.941	0.024	2.412	0.021	1.535	0.074	1.703	0.021	1.724	0.020	2.211	0.071	2.606	0.064
Mn	0.133	0.005	0.141	0.006	0.054	0.006	0.056	0.004	0.240	0.006	0.249	0.012	0.050	0.008	0.096	0.010
Mg	0.801	0.051	0.873	0.025	1.076	0.058	0.795	0.096	1.065	0.033	0.947	0.031	0.721	0.048	0.877	0.060
site	4.057	0.115	4.250	0.041	4.618	0.049	3.871	0.131	4.099	0.004	4.021	0.037	4.090	0.075	3.910	0.114
H	3.060		3.060		3.060		3.060		3.060		3.060		3.060		3.060	
O	47.930		48.066		48.401		47.631		47.881		47.811		47.857		47.740	

Table 9.2, e. SPHALERITE MINERAL CHEMISTRY

Sample(N)	22A-1625	(2) stan dev	22A-1638	(7) stan dev	22B-1723	(2) stan dev	24-1191	(2) stan dev	34-799b	(2) stan dev	34-799a (1)	34C-1377 (1)
	mean		mean		mean		mean		mean			
Fe	7.76	0.09	6.36	0.29	8.36	0.10	7.67	0.10	7.26	0.09	5.27	2.44
Mn	0.41	0.03	0.03	0.05	0.15	0.03	0.21	0.03	0.00	0.00	0.00	0.00
Zn	57.88	0.34	60.59	0.44	57.58	0.37	58.48	0.34	58.54	0.34	60.56	65.85
Cd	0.24	0.12	0.00	0.00	0.47	0.15	0.00	0.00	1.10	0.08	0.00	0.00
Cu	0.07	0.04	0.02	0.04	0.20	0.04	0.00	0.00	0.21	0.04	0.00	0.00
S	33.15	0.29	33.27	0.17	32.87	0.38	33.30	0.13	33.53	0.34	34.23	31.75
Total	99.51	0.45	100.27	0.45	99.63	0.79	99.66	0.16	100.64	0.09	100.06	100.04
Fe	0.139	0.002	0.114	0.005	0.150	0.002	0.137	0.002	0.130	0.002	0.094	0.044
Mn	0.007	0.001	0.001	0.001	0.003	0.001	0.004	0.001	0.000	0.000	0.000	0.000
Zn	0.885	0.005	0.927	0.007	0.881	0.006	0.895	0.005	0.896	0.005	0.926	1.007
Cd	0.002	0.001	0.000	0.000	0.004	0.001	0.000	0.000	0.010	0.001	0.000	0.000
Cu	0.001	0.001	0.000	0.001	0.003	0.001	0.000	0.000	0.003	0.001	0.000	0.000
site	1.035	0.009	1.042	0.007	1.040	0.010	1.036	0.007	1.038	0.008	1.021	1.051
S	1.034	0.009	1.038	0.005	1.025	0.012	1.039	0.009	1.046	0.011	1.067	0.990

Table 9.2, f. GAHNITE MINERAL CHEMISTRY

Sample(N)	22A-1638	(5) stan dev	22B-1723	(7) stan dev	24-1131	(5) stan dev	24-1191 zone 6	(6) stan dev	34-799 core	(3) stan dev	34-799 rim	(3) stan dev	34C-1453	(6) stan dev
	mean		mean		mean		mean		mean		mean		mean	
SiO2	0.02	0.03	0.03	0.04	0.10	0.09	0.27	0.50	1.08	1.53	0.25	0.35	0.02	0.05
TiO2	0.00	0.00	0.00	0.00	0.00	0.00	0.00	0.00	0.00	0.00	0.00	0.00	0.00	0.00
Al2O3	59.02	0.70	58.62	0.38	58.22	0.35	58.20	0.50	58.63	1.26	58.71	0.51	58.68	0.23
FeO	5.01	0.14	7.27	0.30	9.38	0.49	5.82	0.25	5.61	0.18	5.38	0.13	8.75	0.38
MnO	0.15	0.01	0.23	0.02	0.08	0.01	0.21	0.02	0.03	0.04	0.03	0.04	0.00	0.00
MgO	2.39	0.09	2.44	0.20	3.03	0.16	1.72	0.06	2.27	0.19	2.04	0.10	1.81	0.11
ZnO	32.67	0.28	31.13	0.63	29.32	0.47	33.69	0.22	32.06	0.30	32.88	0.13	30.53	0.58
Total	66.59	0.72	68.59	0.28	70.81	0.40	99.90	0.54	67.62	0.54	66.41	0.26	69.26	0.37
Si	0.000	0.001	0.001	0.001	0.003	0.003	0.008	0.015	0.031	0.044	0.007	0.010	0.001	0.002
Aliv	2.040	0.005	2.023	0.005	2.001	0.006	2.019	0.013	2.009	0.045	2.033	0.012	2.029	0.002
site	2.040	0.005	2.024	0.005	2.004	0.004	2.027	0.004	2.040	0.002	2.040	0.005	2.030	0.002
Fe	0.123	0.003	0.178	0.007	0.229	0.012	0.143	0.007	0.136	0.005	0.132	0.004	0.215	0.010
Mn	0.004	0.000	0.006	0.001	0.002	0.000	0.005	0.001	0.001	0.001	0.001	0.001	0.000	0.000
Mg	0.105	0.004	0.106	0.009	0.131	0.006	0.075	0.003	0.098	0.008	0.089	0.005	0.079	0.005
Zn	0.707	0.010	0.673	0.016	0.631	0.011	0.732	0.007	0.688	0.007	0.713	0.003	0.661	0.011
site	0.939	0.008	0.963	0.007	0.993	0.005	0.956	0.012	0.924	0.021	0.935	0.009	0.955	0.004
O	4.000		4.000		4.000		4.000		4.000		4.000		4.000	

Table 9.2, g. GARNET MINERAL CHEMISTRY

Sample(N)	22-413 core (1)	22-413 rim (1)	22A-1625 rim mean	(3) stan dev	22A-1625 core (1)	22B-1721 rim mean	(7) stan dev	22B-1721 core (1)	24-1191 zone 5 rim-mean	(3) stan dev	24-1191 zone 5 core(1)
SiO2	37.21	37.28	36.57	0.09	35.95	36.90	0.25	37.00	37.27	0.11	37.18
TiO2	0.00	0.00	0.00	0.00	0.17	0.02	0.03	0.10	0.02	0.04	0.12
Al2O3	21.20	21.46	21.29	0.12	20.76	21.41	0.17	20.93	20.83	0.08	20.86
Cr2O3	0.00	0.00	0.00	0.00	0.00	0.00	0.00	0.00	0.00	0.00	0.00
FeO	32.76	33.23	19.67	0.17	14.46	25.75	0.40	21.79	19.10	0.14	18.10
MnO	3.42	2.87	15.90	0.08	22.80	9.64	0.17	13.04	15.15	0.68	16.19
MgO	2.94	2.96	3.16	0.05	1.71	2.85	0.06	2.11	1.98	0.08	1.92
CaO	2.76	3.05	2.15	0.10	2.42	3.01	0.40	4.53	5.51	0.41	5.36
Na2O	0.00	0.00	0.00	0.00	0.07	0.00	0.00	0.00	0.00	0.00	0.00
Total	100.32	100.85	98.80	0.22	98.40	99.56	0.31	99.50	99.87	0.32	99.73
Si	5.972	5.948	5.941	0.010	5.931	5.950	0.025	5.983	6.000	0.007	5.993
Aliv	0.028	0.052	0.059	0.010	0.069	0.050	0.025	0.017	0.003	0.005	0.007
Alvi	3.983	3.985	4.019	0.010	3.968	4.008	0.049	3.972	3.951	0.011	3.958
Ti	0.000	0.000	0.000	0.000	0.021	0.002	0.004	0.012	0.003	0.005	0.015
site	3.983	3.985	4.019	0.010	3.989	4.010	0.049	3.984	3.954	0.011	3.973
Fe	4.397	4.434	2.672	0.015	1.995	3.473	0.066	2.947	2.572	0.024	2.440
Mn	0.465	0.388	2.187	0.013	3.186	1.317	0.026	1.786	2.065	0.088	2.211
Mg	0.703	0.704	0.766	0.009	0.420	0.685	0.015	0.508	0.476	0.019	0.461
Ca	0.475	0.521	0.375	0.015	0.428	0.515	0.071	0.785	0.951	0.072	0.926
Na	0.000	0.000	0.000	0.000	0.022	0.000	0.000	0.000	0.000	0.000	0.000
site	6.040	6.048	6.000	0.017	6.052	5.990	0.025	6.026	6.063	0.014	6.038
O	18.000	18.000	18.000		18.000	18.000		18.000	18.000		18.000

Table 9.2, h. CALCIC AMPHIBOLE MINERAL CHEMISTRY

Sample(N)	22-413	(3)	24-1191	(4)	24-1191	(3)	24-1191	24-1191	(5)	24-1191	(7)	34A-1484	(5)	34B-759.5	(8)
		stan	zone 2	stan	zone 3	stan	zone 3	zone 4	stan	zone 5	stan		stan		stan
	mean	dev	mean	dev	core-mean	dev	rim (1)	mean	dev	mean	dev	mean	dev	mean	dev
SiO2	40.24	0.59	52.75	0.47	43.29	1.08	52.12	44.01	0.47	43.51	1.06	42.22	0.56	53.10	1.27
TiO2	0.32	0.02	0.12	0.05	0.41	0.11	0.00	0.37	0.05	0.28	0.07	0.25	0.02	0.09	0.06
Al2O3	15.92	0.32	4.27	0.65	14.28	1.34	3.40	13.64	0.65	14.27	0.76	14.40	0.52	3.88	0.97
FeO(c)	10.42	1.35	6.83	0.87	7.45	0.98	5.23	6.31	0.87	5.77	1.08	8.68	1.22	8.01	0.68
Fe2O3(c)	10.76	1.56	3.69	1.23	6.98	0.79	5.97	7.89	1.23	8.24	0.85	13.32	1.56	0.75	0.5
MnO	0.27	0.02	0.70	0.08	0.69	0.02	0.57	0.88	0.08	1.01	0.06	0.28	0.05	0.25	0.04
MgO	6.63	0.15	16.49	0.53	11.03	0.73	16.69	11.44	0.53	11.16	0.99	7.29	0.31	17.70	0.79
ZnO	0.00	0.00	0.00	0.00	0.00	0.00	0.00	0.00	0.00	0.05	0.08	0.00	0.00	0.00	0.00
CaO	9.79	0.40	12.23	0.31	11.38	0.05	11.54	11.11	0.31	10.94	0.14	8.87	0.67	13.38	0.14
Na2O	1.74	0.04	0.40	0.04	1.43	0.17	0.30	1.42	0.04	1.47	0.03	1.27	0.08	0.27	0.08
K2O	0.26	0.01	0.06	0.04	0.29	0.04	0.00	0.26	0.04	0.25	0.04	0.16	0.03	0.21	0.12
F	0.00	0.00	0.00	0.00	0.00	0.00	0.00	0.00	0.00	0.00	0.00	0.00	0.00	0.00	0.00
H2O(c)	1.99	0.03	2.11	0.01	2.05	0.01	2.08	2.06	0.01	2.05	0.02	2.02	0.01	2.11	0.02
Total	98.34	1.00	99.64	0.45	99.29	0.11	97.91	99.39	0.45	99.00	0.23	98.76	0.48	99.75	0.53
Si	6.070	0.011	7.491	0.071	6.327	0.135	7.499	6.402	0.071	6.348	0.108	6.253	0.049	7.535	0.113
Aliv	1.930	0.011	0.509	0.071	1.673	0.135	0.501	1.598	0.071	1.652	0.108	1.747	0.049	0.465	0.113
Alvi	0.901	0.025	0.207	0.044	0.789	0.109	0.075	0.741	0.094	0.804	0.057	0.769	0.072	0.186	0.059
Ti	0.036	0.002	0.012	0.005	0.045	0.012	0.000	0.040	0.005	0.031	0.007	0.027	0.002	0.010	0.006
Fe+3(c)	1.219	0.161	0.395	0.134	0.768	0.085	0.647	0.864	0.134	0.905	0.097	1.484	0.164	0.080	0.054
Fe+2(c)	1.317	0.188	0.811	0.105	0.911	0.122	0.630	0.767	0.105	0.705	0.136	1.077	0.156	0.951	0.087
Mn	0.035	0.002	0.085	0.010	0.085	0.002	0.069	0.108	0.010	0.125	0.007	0.035	0.006	0.031	0.005
Mg	1.491	0.014	3.490	0.115	2.402	0.149	3.579	2.480	0.115	2.425	0.199	1.609	0.058	3.743	0.134
Zn	0.000	0.000	0.000	0.000	0.000	0.000	0.000	0.000	0.000	0.000	0.000	0.000	0.000	0.000	0.000
Ca	1.584	0.085	1.861	0.048	1.783	0.003	1.779	1.732	0.048	1.710	0.023	1.409	0.114	2.034	0.017
Na	0.416	0.085	0.139	0.048	0.217	0.003	0.221	0.268	0.048	0.290	0.023	0.591	0.114	0.000	0.001
B-site	2.000		2.000		2.000		2.000	2.000		2.000		2.000		2.034	0.017
Na	0.104	0.088	0.010	0.040	0.189	0.050	0.000	0.133	0.040	0.126	0.022	0.000	0.000	0.073	0.022
K	0.049	0.002	0.011	0.007	0.055	0.009	0.000	0.047	0.007	0.046	0.008	0.031	0.006	0.038	0.022
A-site	0.153	0.089	0.021	0.042	0.244	0.057	0.000	0.181	0.042	0.172	0.025	0.031	0.006	0.111	0.043
F	0.000		0.000		0.000		0.000	0.000		0.000		0.000		0.000	
H(c)	2.000		2.000		2.000		2.000	2.000		2.000		2.000		2.000	
O	23.000		23.000		23.000		23.000	23.000		23.000		23.000		23.000	

Table 9.2, i. FE-MG AMPHIBOLE MINERAL CHEMISTRY

Sample(N)	22-413	(5)	24-1131	(10)	34A-1484	(7)
		stan		stan		stan
	mean	dev	mean	dev	mean	dev
SiO2	52.60	0.18	53.25	0.93	52.50	0.15
TiO2	0.00	0.00	0.00	0.00	0.01	0.02
Al2O3	1.13	0.13	3.59	1.05	1.06	0.16
FeOt	27.23	0.32	19.96	0.27	27.46	0.32
MnO	0.62	0.05	0.94	0.13	0.54	0.03
MgO	14.65	0.38	19.40	0.49	14.29	0.13
ZnO	0.00	0.00	0.00	0.00	0.00	0.00
CaO	0.40	0.06	0.35	0.04	0.35	0.11
Na2O	0.06	0.04	0.20	0.14	0.10	0.02
K2O	0.00	0.00	0.00	0.00	0.00	0.00
F	0.00	0.00	0.26	0.04	0.00	0.00
H2O(c)	1.99	0.02	1.96	0.02	1.98	0.00
Total	98.67	0.31	99.77	0.46	98.28	0.26
Si	7.917	0.019	7.664	0.113	7.940	0.013
Aliv	0.083	0.019	0.336	0.113	0.060	0.013
Alvi	0.117	0.016	0.273	0.067	0.130	0.020
Ti	0.000	0.000	0.000	0.000	0.001	0.002
Fet	3.428	0.047	2.402	0.037	3.474	0.041
Mn	0.079	0.007	0.114	0.015	0.069	0.003
Mg	3.286	0.075	4.161	0.096	3.220	0.032
Zn	0.000	0.000	0.000	0.000	0.000	0.000
Ca	0.065	0.009	0.053	0.006	0.056	0.017
C-site	6.974	0.014	7.004	0.016	6.950	0.010
Na	0.019	0.011	0.055	0.039	0.028	0.005
K	0.000	0.000	0.000	0.000	0.000	0.000
A-site	0.019	0.011	0.055	0.039	0.028	0.005
F	0.000		0.120	0.018	0.000	
H(c)	2.000		1.880	0.018	2.000	
O	23.000		22.880		23.000	

Table 9.2, j. EPIDOTE MINERAL CHEMISTRY

Sample(N)	22B-1721 (1)	22B-1843 mean	(5) stan dev	24-1191 zone 3 mean	(6) stan dev	24-1191 zone 2 mean	(2) stan dev	34-1028.5 mean	(5) stan dev	34B-759.5 mean	(6) stan dev
SiO2	38.02	37.90	0.84	38.26	0.21	38.21	0.00	38.10	0.28	37.68	0.36
TiO2	0.00	0.39	0.61	0.07	0.03	0.04	0.04	0.09	0.01	0.05	0.05
Al2O3	25.76	26.56	0.97	25.24	0.46	25.03	0.24	26.76	0.29	26.59	0.64
Fe2O3t	9.55	8.04	0.15	10.38	0.52	10.69	0.23	8.54	0.36	8.35	0.62
MnO	0.74	0.29	0.13	0.38	0.04	0.36	0.04	0.32	0.04	0.07	0.07
MgO	0.04	0.05	0.05	0.03	0.04	0.07	0.07	0.05	0.01	0.02	0.04
ZnO	0.00	0.00	0.00	0.00	0.00	0.00	0.00	0.00	0.00	na	
CaO	20.62	22.27	0.42	22.94	0.21	22.37	0.04	21.80	0.73	24.43	0.21
Na2O	0.00	0.00	0.00	0.00	0.00	0.00	0.00	0.00	0.00	0.00	0.00
K2O	0.00	0.01	0.02	0.00	0.00	0.00	0.00	0.00	0.00	0.00	0.00
F	0.00	0.00	0.00	0.00	0.00	0.00	0.00	0.00	0.00	0.00	0.00
H2O(c)	1.86	1.88	0.03	1.89	0.01	1.89	0.01	1.88	0.01	1.90	0.02
Total	96.59	97.39	1.52	99.17	0.33	98.65	0.04	97.54	0.62	99.21	0.89
Si	3.063	3.025	0.031	3.029	0.014	3.039	0.002	3.034	0.018	2.978	0.014
Aliv	0.000	0.007	0.031	0.000	0.000	0.000	0.000	0.000	0.000	0.011	0.014
Alvi	2.447	2.492	0.054	2.355	0.035	2.347	0.021	2.512	0.028	2.456	0.039
Fe+3	0.579	0.483	0.018	0.618	0.032	0.640	0.015	0.512	0.023	0.497	0.038
site	3.026	2.975	0.037	2.974	0.013	2.986	0.007	3.023	0.020	2.952	0.006
Ti	0.000	0.024	0.037	0.004	0.002	0.002	0.003	0.005	0.001	0.003	0.003
Mn	0.051	0.020	0.009	0.025	0.003	0.024	0.002	0.021	0.002	0.005	0.005
Mg	0.005	0.006	0.006	0.003	0.004	0.008	0.009	0.006	0.002	0.002	0.005
Zn	0.000	0.000	0.000	0.000	0.000	0.000	0.000	0.000	0.000	na	
Ca	1.780	1.904	0.034	1.946	0.017	1.906	0.005	1.860	0.057	2.069	0.012
Na	0.000	0.000	0.000	0.000	0.000	0.000	0.000	0.000	0.000	0.000	0.000
K	0.000	0.001	0.002	0.000	0.000	0.000	0.000	0.000	0.000	0.000	0.000
site	1.835	1.955	0.056	1.978	0.016	1.941	0.008	1.893	0.054	2.079	0.007
F	0.000	0.000		0.000		0.000		0.000		0.000	
H(c)	1.000	1.000		1.000		1.000		1.000		1.000	
O	12.500	12.500		12.500		12.500		12.500		12.500	

indicated in parentheses.

Different textural generations of minerals can be distinguished and, in part, define the S_1 and S_2 fabric elements (*see* 7.1.1. Fabric Elements and Mineralogy; Table 7.1). However, in most cases, systematic compositional trends, relating to textural generation, were not detected.

9.1.1. Phyllosilicate Minerals.

Phyllosilicate minerals, particularly muscovite and chlorite, define S_1 and S_2 schistosities. S_2 is mainly a crenulation of minerals defining S_1, but in some cases, a second generation of phyllosilicate minerals recrystallized parallel to S_2. With the exception of two specimens (*i.e.* muscovite in 22A-1625 and chlorite in 24-1191), no significant compositional differences were detected between the different mineral generations. Chlorite mainly occurs in intergrowths with muscovite defining the S_1 schistosity, and also as blades parallel to the S_2 plane and random or weakly oriented aggregates in the pressure shadows of porphyroblastic minerals. Compositional differences correlating with chlorite habit were not detected (excepting 24-1191) and chlorite was considered to be part of the equilibrium assemblage if it exhibited mutual contacts with other minerals in the section. Margarite occurs in minor amounts in fine intergrowths with muscovite and chlorite defining the S_1 schistosity. With the exception of graphitic metasediment (34-1500), in which margarite is the most abundant phyllosilicate mineral, the intergrowths were too fine ($\leq 20\mu$) to allow quantitative analysis of margarite and only mixtures were recorded (Table B.3, a; *see* Figure 9.4). Biotite typically occurs as blades defining an S_2 schistosity.

Biotite compositions are Mg-rich (Figure 9.2), ranging in Mg/(Fe+Mg) from 0.55–0.98 and, in most cases, the mica is a phlogopite *sensu stricto*. The most Mg-rich composition occurs in graphitic metasediment (34-1500) and closely approaches end-member phlogopite. The mica is nearly colourless and would be difficult to identify optically in a cursory examination.

Muscovite contains minor amounts of the celadonite end member (Table 9.2, a). In the single sample (22A-1625) in which compositional differences may correlate with habit, fine grained muscovite in schistose aggregates defining the S_1 fabric is significantly more celadonitic than the coarser blades which define an S_2 cleavage in the hinge zones of the crenulation. The S_1 muscovite was assumed to

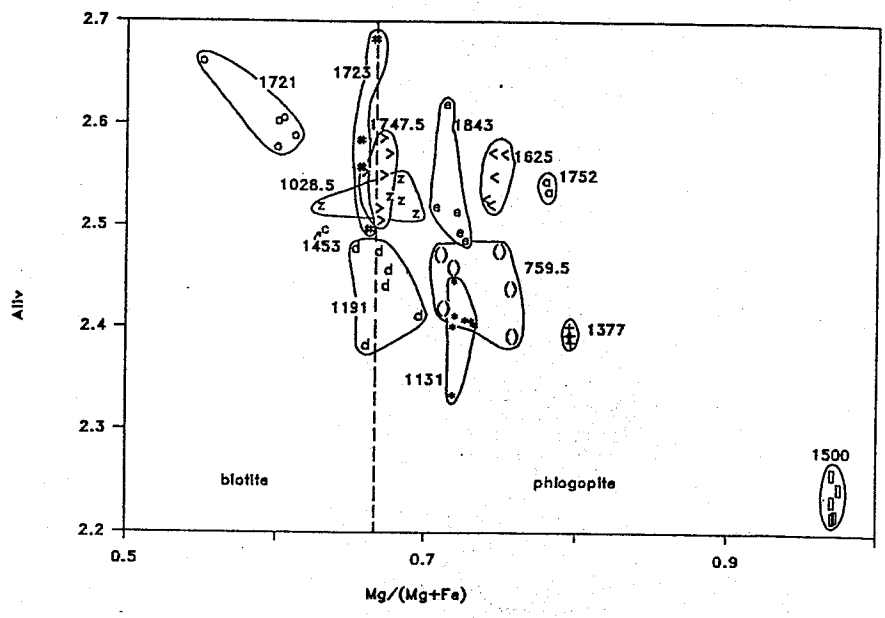

Figure 9.2. Biotite compositions in terms of Mg/(Mg+Fe_t) and tetrahedral Al (pfu). Diagram adapted from Deer *et al.* (1966) and Guidotti (1984). Sample numbers are indicated without drill-hole prefixes.

be in equilibrium with the assemblage, as it is more abundant and more commonly in contact with porphyroblastic minerals. One sample (32-1465.5) in the suite contains Cr-bearing muscovite, which has an intense green colour in hand sample and contains up to .59 weight% Cr_2O_3. This was the only detectible occurrence of Cr in the microanalysis sample suite.

Chlorite compositions are also Mg-rich, generally ranging in Mg/(Fe+Mg) from 0.56–0.93. The exception to this is retrograde chlorite which occurs on grain boundaries between calcite and epidote in a sample representative of calc-silicate enclaves (24-1191); semi-quantitative analyses showed it to be Fe-rich with Mg/(Fe+Mg) of 0.11–0.46 (2 analyses, Table B.3, c). The same sample also contains Mg-chlorite (Mg/(Fe+Mg)=0.65–0.68) which was interpreted to be part of the prograde assemblage. The classification of Foster (1962) shows most of the chlorites to be high-Mg ripidolites, with some overlap into sheridanite compositions (Figure 9.3). The most magnesian chlorite, clinochlore–sheridanite, occurs in minor amounts in pressure shadows in graphitic metasediment (34-1500) and is not part of the equilibrium assemblage. Chlorite in altered mafic rocks (22-413, 34A-1484) is the most Fe-rich; chlorite in the distal alteration zone is generally more Fe-rich than chlorite in the proximal alteration zone. In most cases, chlorite analyses are lower in Mg/(Fe+Mg)

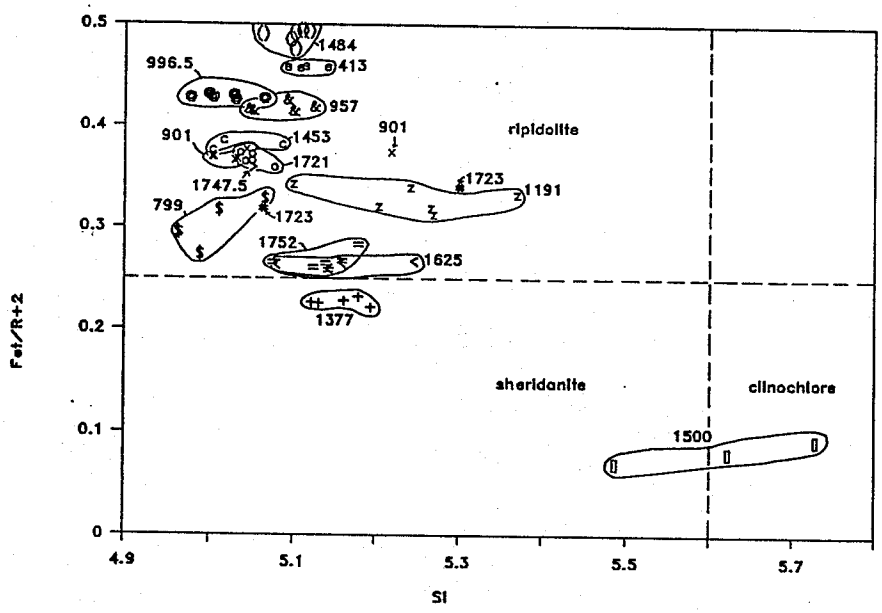

Figure 9.3. Chlorite mineral chemistry in terms of tetrahedral Si (pfu) and Fe_t/R^{+2}. Diagram adapted from Foster (1962). Sample numbers are indicated without drill-hole prefixes.

than analyses of coexisting biotite, contrary to the usual Fe-Mg distribution between equilibrated grains (Thompson, 1976a; 1976b). Analytical problems associated with an appropriate choice of standards (Appendix B), resulting in a loss of accuracy, and the uncertainties inherent in the assumption that the iron is entirely ferric, contribute to the uncertainty associated with the observed distribution. However, analyses of coexisting chlorite and biotite grains show a systematic positive correlation of Fe/Mg consistent with chemical equilibrium.

ZnO was analysed in all phyllosilicate minerals and was detected in minor amounts ($\leq$.26 weight%, Table B.3, b, c) in chlorite (in 5 samples) and biotite (1 sample). The detection limit for ZnO is relatively high (0.16 weight%, Table B.2) and, given the difficulty in discriminating between Zn-bearing inclusions and structural Zn in the analysed mineral, Zn in phyllosilicate minerals was not considered to be significant. There is no evidence for the presence of Zn-rich chlorite, such as that described from Franklin, New Jersey (up to 9.60 weight% ZnO; Frondel and Ito, 1975), or of zincian biotite, as reported from gahnite-bearing gneisses from Kemiö, Finland (up to 0.24 weight%; Dietvorst, 1980).

Muscovite and biotite contain substantial Na and, in some cases, trace amounts of Ba, substituting for K at the interlayer A-site (Table B.3, a, b). Paragonite

was not identified. Figure 9.4 illustrates the proportions of K-Na-Ca in muscovite and margarite analyses. Muscovite Na/(Na+K) ranges from 0.08–0.26. Note that the high proportion of Ca in some muscovite analyses is actually due to the presence of fine mixtures of muscovite and margarite. Many muscovite analyses in margarite-bearing rocks showed no CaO, suggesting that the level of Ca-saturation in muscovite is below the detection limit (0.04 weight%, Table B.2). One exception to this is sample 22B-1721; margarite was not identified, although white mica has Ca/(Ca+Na+K) of up to 0.09. This sample also contains garnet, plagioclase and trace amounts of epidote. Guidotti (1984) reported several analyses from one-mica rocks in which muscovite showed higher Ca contents than muscovite which coexisted with margarite. He made the observation that data from mica pairs may not give the saturation limits of Ca in muscovite. Frey *et al.* (1982) reported very low CaO ($\leq$ 0.10 weight%) in muscovite associated with margarite. They also noted that the most important substitution in margarite is the coupled exchange: $Na^{+}Si^{+4} \rightleftharpoons Ca^{+2}Al^{+3}$, and their compilation of Alpine margarite analyses shows a considerable spread to more sodic compositions. The margarite at the Linda deposit is very aluminous compared to analyses reported by Frey *et al.* (1982), with nearly equal amounts of Si and Al at the tetrahedral site, thus approaching an end-member margarite.

Biotite and, to a lesser extent, muscovite, have a high proportion of vacancies at the A-site, as inferred from low cation totals. Low site-occupancy is commonly reported for biotite associated with sulphide minerals (e.g. Mohr and Newton, 1983).

Biotite commonly contains F at the (OH)-site, with up to 0.40 of the site occupied by F in the phlogopite of 34-1500. Minor amounts of F (close to the detection limit of 0.39 weight%, Table B.2) were detected in some chlorite analyses. F was not detected in muscovite. Chlorine was analysed in most hydrous minerals, but was detected only in retrograde Fe-rich chlorite in the calc-silicate enclave sample (24-1191) (*see also* 9.3. Halogen Contents of Phyllosilicate Minerals).

9.1.2. Aluminosilicate Minerals.

Kyanite occurs both as syn-D_1 and syn-D_2 porphyroblasts. The analyses show very slight deviation from ideal end-member compositions, involving minor substi-

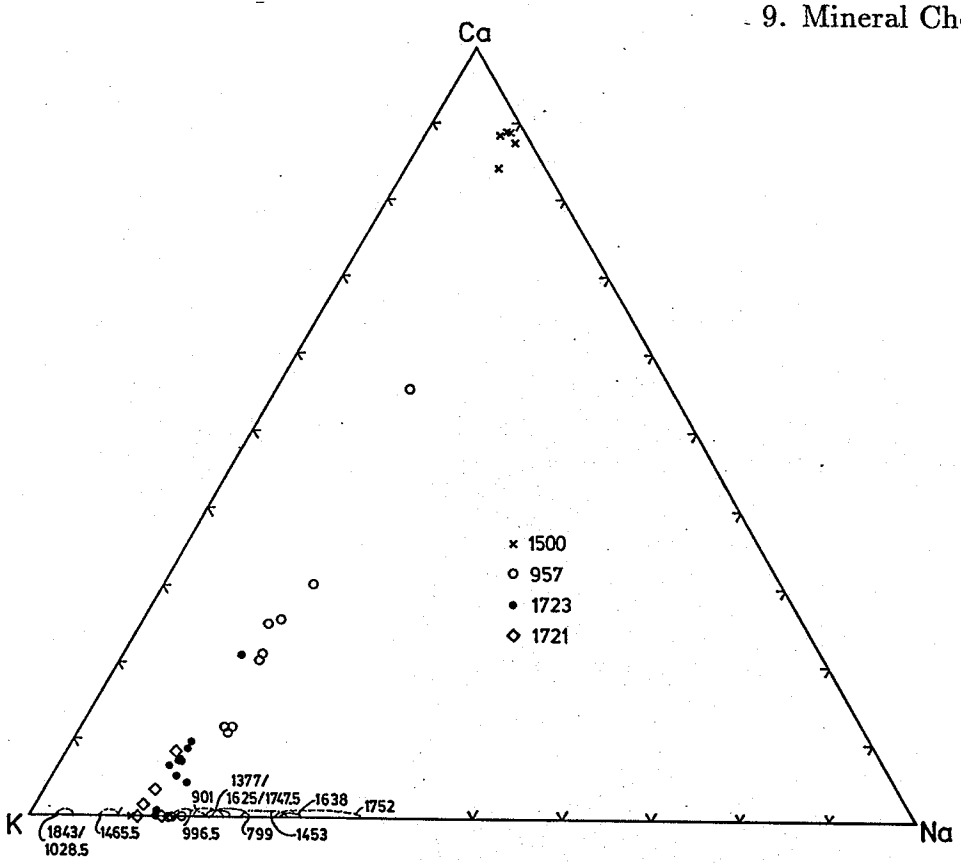

Figure 9.4. White mica mineral chemistry in terms of K-Ca-Na (atomic proportions). The extension of the muscovite compositions toward the Ca-Na tie line is mainly due to the presence of muscovite-margarite intergrowths on a scale finer than the resolution of the electron beam (*i.e.* $\leq 20\,\mu$).

tution of Fe^{+3} for Al^{+3} to a maximum of 1.2% of the site (Table B.3, k). Sillimanite is present in some samples as randomly oriented fibrolite on grain boundaries; it was interpreted to be post-tectonic and not part of the equilibrium assemblage (Table 9.1).

9.1.3. Staurolite and Gahnite.

Staurolite occurs in a wide variety of parageneses and representing this feature was a primary consideration in the selection of the sample suite. Staurolite compositions span a broad range of Zn/(Fe+Zn), from 0–0.57, at the tetrahedral Fe-bearing site (Table 9.2, d). Gahnite was observed only in staurolite-bearing rocks, with two exceptions, *i.e.* 34-799b, a narrow (5 mm) gahnite-sphalerite zone in a staurolite-bearing host rock (34-799a), and 24-1911, which contains gahnite as symplectic inclusions in plagioclase (*see* 10.4. Calc-silicate Enclave in the Main Massive Sulphide Body). In the case of staurolite and gahnite porphyroblasts which

are mimetic after both S_1 and S_2 fabrics (*see* Plates 5.4, c; 7.2, c–e), no systematic compositional differences were detected between areas of grains pseudomorphing S_1 layering and those pseudomorphing S_2 cleavage. Core and rim zoning was also investigated. In many samples, porphyroblasts are anhedral and highly skeletal and, consequently, the rims are weakly defined. Although there is some compositional variation within and between porphyroblasts, it did not show a systematic correlation with the optically identified core and rim. In these cases, the analyses were generally averaged, and the standard deviation of the compositional range was treated as a measure of within-sample or within-area (*i.e.* 5–10 mm diameter as previously defined) variation, that is, essentially as a measure of uncertainty associated with the identification of the equilibrium composition.

In samples containing subhedral porphyroblasts, in some cases the definition of the rim is enhanced by a narrow zone containing fewer inclusions than the core (*see* Plates 5.1, c; 5.4, d), and core and rim compositions were slightly but systematically different. Spry (1987) attributed similar trends, but of larger magnitude, in Zn-Fe spinels to retrograde cation diffusion and exchange in the rims. At the Linda deposit, the slight differences between core and rim compositions in staurolite and gahnite could be produced by changes in $\log f_{S_2}$ and $\log f_{O_2}$ (*see* 10.1.3. Petrogenetic Grid) and, the compositional trends were not the same in each sample. In view of these considerations, rim compositions were assumed to have equilibrated with the assemblage. Figure 9.5a shows the proportions of Fe_t, Zn and Mg in staurolite, gahnite and sphalerite. The compositional spectrum is mainly due to Fe-Zn substitution, with relatively minor variation in Mg content. The control exerted on staurolite compositions by bulk-rock composition, f_{S_2} and f_{O_2} are illustrated by the tie lines and field boundaries distinguishing the sulphide and oxide assemblage associated with each sample. Staurolite coexisting with sphalerite + gahnite is notably enriched in both Zn and Mg. Most of these samples also contain pyrite and rutile, indicating relatively high f_{S_2}. The most Fe-rich, Mg-poor staurolite occurs without sphalerite or gahnite and coexists with pyrite + magnetite (22-996.5, 24-1131) or pyrite + ilmenite ± pyrrhotite (22-901, 22-957, 22B-1721, 34C-1453). There is a general correspondence between gahnite and staurolite compositions in each sample, supporting the assumption of equilibrium. The compositional spread in Fe/Zn

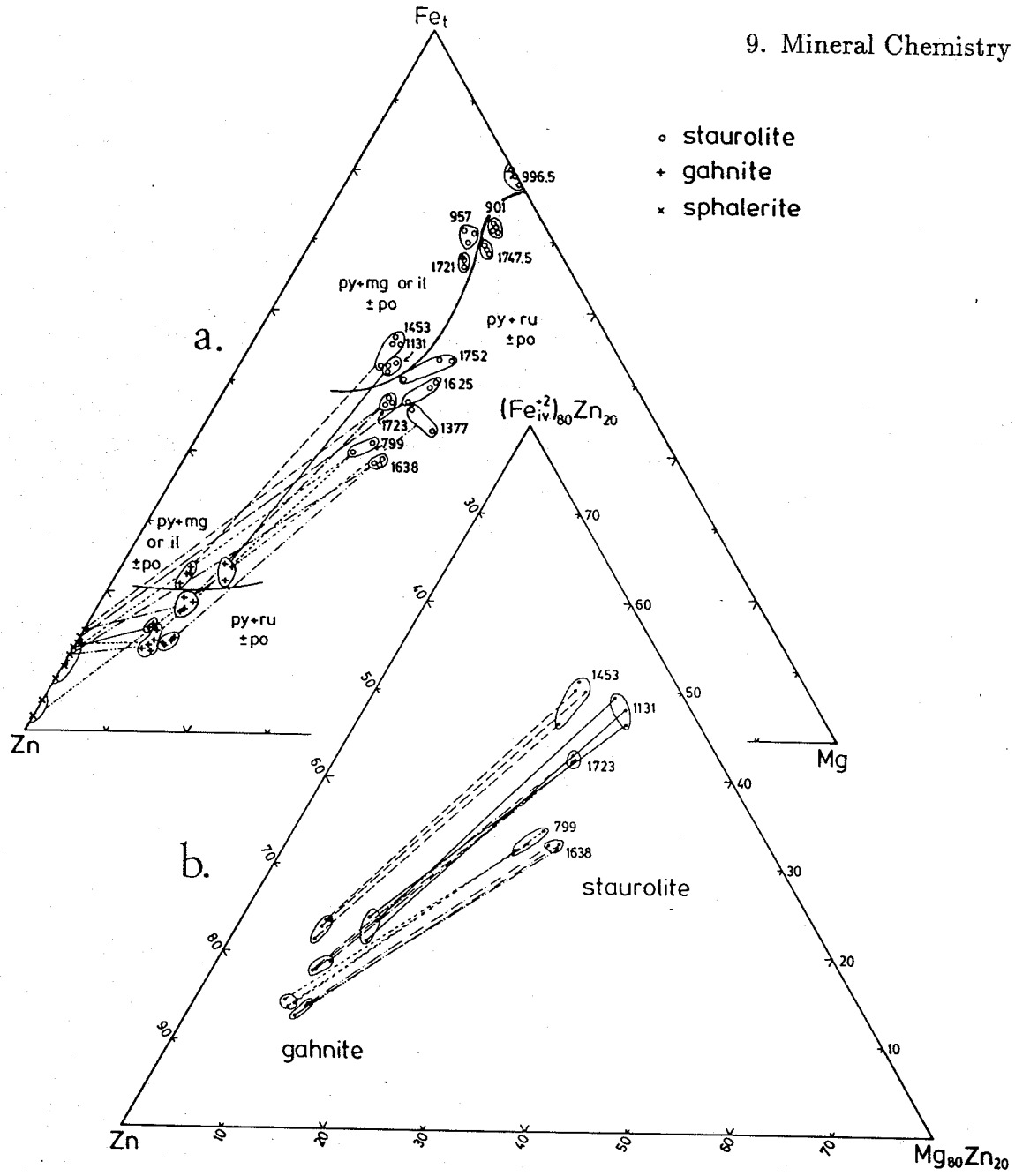

Figure 9.5. Mineral chemistry of staurolite, gahnite and sphalerite.

a. Zn-Fe$_t$-Mg (atomic proportions) in areas of 5–10 mm in diameter for all staurolite-bearing samples (numbered without drill-hole prefixes). Each point represents 1–3 analyses and ornamented tie lines link the mineral assemblages in each sample. The solid dividing line separates assemblages coexisting with pyrite and either magnetite or ilmenite, from assemblages coexisting with pyrite and rutile. Pyrrhotite occurs in some samples on both sides of the line. Note that total Fe is represented as Fe^{+2}.

b. Zn-Fe^{+2}(iv-site)-Mg (atomic proportions) in coexisting staurolite and gahnite, with ornamented tie lines linking analyses from within the same area. Only Fe^{+2} at the tetrahedral Fe-bearing site was included, omitting Fe^{+3} (calculated) and Fe^{+2} at the Mn-bearing U(1)-site. Samples 22A-1638, 22B-1723 and 34-799 contain sphalerite.

of staurolite is apparently mainly a function of the bulk-rock Zn content; the compositional gap (Figure 9.5, a; *i.e.* between 34C-1453 and 22B-1721) is probably due to a gap in the bulk-rock compositions of the sample suite. The spread in Mg content is apparently mainly a function of high f_{S_2} and f_{O_2}, with samples containing rutile + pyrite being enriched in Mg relative to samples containing pyrite with magnetite or ilmenite.

Figure 9.5b focusses on staurolite-gahnite bearing samples, showing the compositions of coexisting grains, *i.e.* within areas of 5–10 mm in diameter. In contrast to Figure 9.5a, only Fe^{+2} at the tetrahedrally co-ordinated Fe-site (Holdaway *et al.*, 1988; Holdaway *et al.*, 1986; Appendix B) is included in the proportions (Table B.3, d). The diagram should more closely approximate the partitioning of Zn, Fe^{+2} and Mg at tetrahedral sites in staurolite and gahnite. Sample 24-1131 is anomalous with respect to the assemblages in the alteration zones in that it is a muscovite-free staurolite-anthophyllite-gahnite rock and contains pyrite, pyrrhotite and magnetite. It was interpreted to have crystallized during late D_2 (*see* 5.6.2. Silicate Enclaves in the Main Massive Sulphide Body). Samples 22A-1638 and 34-799 contain relatively abundant sphalerite and 22B-1723 contains trace amounts; all three samples contain pyrite. Sample 34C-1453 contains pyrite and pyrrhotite. Bulk composition, f_{S_2} and f_{O_2} influence the slopes of the tie lines, indicating that $\log K$ of the exchange reactions is partly a function of composition and that the tetrahedral-site mixing is at least partly non-ideal (*e.g.* Ganguly and Saxena, 1987).

There is very limited scatter among tie lines within each sample, suggesting that equilibrium was attained on the scale of a thin section. Only sample 34C-1453 has some tendency to show distinct tie lines for grains from different areas. In the derivation of balanced reactions, within-sample average compositions and standard deviations were used (*see* 10.1.2. Mineral Equilibria).

9.1.4. Sulphide Minerals.

Sulphide minerals generally occur in layers parallel to S_1, as fine disseminated grains, as anhedral grains and aggregates, and as subhedral grains. In some samples, the distribution is controlled by primary structures, *i.e.* bedding in graphitic metasediment (34-1500; *see* Plate 5.3, e) and matrix/clast relationships in breccias (22A-1752; *see* Plate 5.3, c–d). In many cases, grains and aggregates are elongate

parallel to the S_2 plane, although the distributions define an S_1 (or S_0) layering. Pyrite is the dominant sulphide mineral. Pyrrhotite occurs both in low temperature, monoclinic and in high temperature, hexagonal polymorphs (Appendix B); monoclinic pyrrhotite commonly mantles grain boundaries and fractures in hexagonal pyrrhotite. These features were interpreted to indicate the presence of hexagonal pyrrhotite during high temperature metamorphism and its subsequent partial inversion to the retrograde monoclinic polymorph. Three samples (22A-1638, 34-799, 24-1191) contain abundant relatively coarse grained sphalerite intergrown with silicate, sulphide and oxide minerals. More commonly, sphalerite occurs in trace amounts as fine grained disseminations and inclusions associated with silicate and oxide minerals. Sphalerite is susceptible to retrograde cation exchange which tends to increase its Zn content (Jamieson and Craw, 1987; Bristol, 1974) and, therefore, the most Fe-rich analyses in each sample were assumed to most closely preserve a high temperature equilibrium composition (Table 9.2, e; *see* 9.2. Sphalerite Geobarometry). Sphalerite in contact with monoclinic pyrrhotite has probably undergone retrograde exchange (*i.e.* 24-1191).

9.1.5. Plagioclase.

Plagioclase occurs in 5 of 14 samples from the distal and proximal alteration zones (Table 9.1, a,b,e). In one case (22-901), its presence in trace amounts was inferred from the presence of fine grained retrograde polymineralic aggregates in pseudomorphs with a poikiloblastic habit typical of plagioclase. Plagioclase is also present in silicic-feldspathic altered mafic rocks (Table 9.1, f) and in calc-silicate rocks (Table 9.1, g, h), but only plagioclase in 22-413, representing the former, was analysed. The composition of plagioclase ranges from oligoclase, associated with paragonitic muscovite or with cummingtonite, to anorthite (An_{97}) coexisting with staurolite and anthophyllite (Figure 9.6; Table B.3, m). The maximum Or-content in the analyses was $Or_{1.1}$; the feldspars are nearly binary solid solutions.

Plagioclase compositions, in some cases, correlate with textural habit. In sample 34C-1377, plagioclase occurs as weakly zoned anhedral syn-D_2 poikiloblasts, and in pressure shadows in association with chlorite; the compositions are $An_{34}Or_{1.1}$–$An_{35}Or_{0.3}$ and $An_{22}Or_{1.1}$–$An_{28}Or_{0.4}$, respectively. The matrix-supported breccia of 22A-1752 (*see* Plate 5.3, c) contains oligoclase of $An_{22}Or_{0.4}$–$An_{27}Or_{0.2}$ within

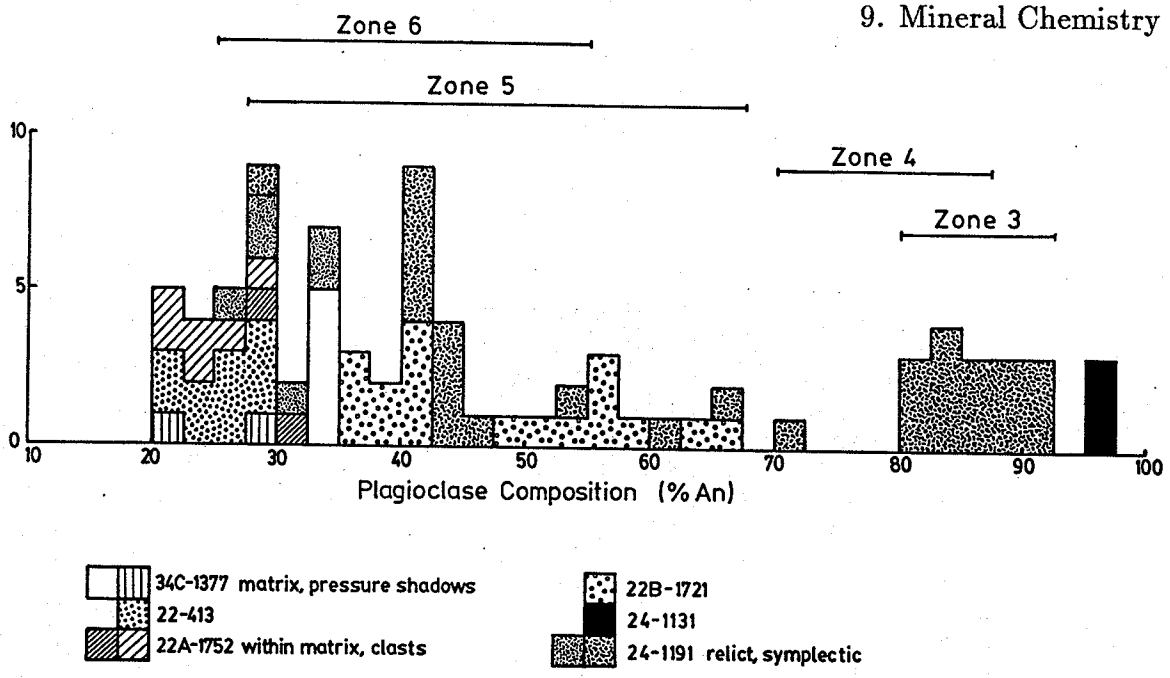

Figure 9.6. Histogram summarizing the An-content of plagioclase analyses (Table B.3, m). Or-contents do not exceed 1.1%. Plagioclase compositions in 34C-1377 and 24-1191 show a dependence on habit; in 34C-1377, plagioclase in the pressure shadows of porphyroblasts is more sodic than plagioclase poikiloblasts in the matrix; in 24-1191, relict syn-D_2 porphyroblasts are more sodic than post-kinematic symplectic grains. In 22A-1752 (a breccia), plagioclase within quartzo-feldspathic clasts is more sodic than plagioclase in the mineralized matrix. Grains in 22B-1721 and 24-1191 are zoned (*see text for further discussion*). Zones 3–6 refers to the compositional range of plagioclase within the mineralogical zones of 24-1191 (*see* Table 5.2).

the clasts, in association with quartz and muscovite, and andesine of $An_{29}Or_{0.1}$–$An_{31}Or_{0.3}$ in the matrix, in association with the general mineral assemblage (Table 9.1, b).

Plagioclase in sample 22B-1721, displays annular zoning similar to that commonly observed in the Linda deposit (*see* 5.3.5. Proximal Alteration Zone *and* 5.4. Plagioclase-layered Rocks). The zoning was imaged using BSE (back-scattered electron) (Plate 9.1, a) and was analysed (Table B.3, m). The zoning consists of the following: a large core (30–50%area) of relatively homogeneous andesine ($An_{37}Or_{0.3}$–$An_{41}Or_{0.3}$); an irregular, semi-continuous mantle (0–25 μ wide) of bytownite (approximately An_{80}, semi-quantitative analysis with a focussed beam); a wide zone (40–60%area) of labradorite with a 'schiller' texture of extremely fine lamellae and a bulk composition of $An_{65}Or_{0.2}$–$An_{48}Or_{0.3}$; and an outer mantle (10–25 μ wide) of andesine ($An_{48}Or_{0.3}$–$An_{42}Or_{0.3}$). The internal contact between the

Plate 9.1. (following page) Zoning in porphyroblastic minerals.

a. Back-scattered electron image (15 kV) of zoned plagioclase in sample 22B-1721. The bar scale on the right represents 100 μ. The zoning consists of (A) a homogeneous andesine core with a sharp internal contact to; (B) a semi-continuous mantle of bytownite with wispy extensions and an abrupt contact to; (C) a heterogeneous zone, with fine calcic lamellae and a labradorite bulk composition showing semi-continuous oscillations to; (D) an outermost mantle of andesine. The porphyroblast is elongate in the S_1 plane and contains inclusions of zircon (small bright spots) and quartz (black inclusions, qz), the latter also elongate in the S_1 plane. Bytownite mantles some inclusions.

b. 22A-1625 (partial cross-polarized light) Garnet porphyroblast(gt), elongate in the S_1 plane and mimetic after S_1 layering, contains elongate inclusions of quartz, sphalerite and rutile. Fractures are filled by monoclinic pyrrhotite. Note the contrast in habit to staurolite porphyroblasts(st) which are mimetic after S_1 and S_2 fabrics. Garnet zoning profiles were collected in traverses parallel and perpendicular to S_1 (Figure 9.7). The bar scale represents 1 mm.

---

andesine core and bytownite mantle is sharp and commonly marked by microcracks with slight retrogression, suggesting some degree of lattice misfit. Other internal contacts are abrupt but apparently gradational; the outermost internal contact is commonly transitional with semi-continuous fine ($\leq$10 μ) oscillations. The bytownite has some wispy extensions, particularly into the labradorite zone, in part associated with inclusions. Within the andesine core, judging from the imaging, bytownite partly mantles some inclusions.

The schiller texture of the labradorite zone is interpreted to be the result of exsolution in a compositional range nearly coincident with that of Bøggild intergrowths, *i.e.* about An_{45}–An_{62} (Smith, 1983; Ribbe, 1983). The distribution of bytownite does not appear to be a growth feature; it nucleated on inclusions and possibly on the andesine core. However, Grove *et al.* (1983) interpreted the presence of bytownite (An_{88}) overgrowths on andesine (An_{39}) cores at Thetford, Vermont, as an equilibrium growth feature resulting from prograde reactions producing Ca-plagioclase and its heterogeneous nucleation on andesine cores. In the Thetford example, plagioclase occurs in mafic metavolcanic rocks which contain Ca-amphibole. Grove's TEM investigation of the Thetford bytownite showed that it contains Huttenlocher intergrowths (*i.e.* about An_{68}–An_{88}; Ribbe, 1983), which he interpreted to be due to metastable spinodal decomposition.

The plagioclase in 22B-1721 was not investigated in sufficient detail to allow detailed interpretation. However, the grains are entirely porphyroblastic and mainly

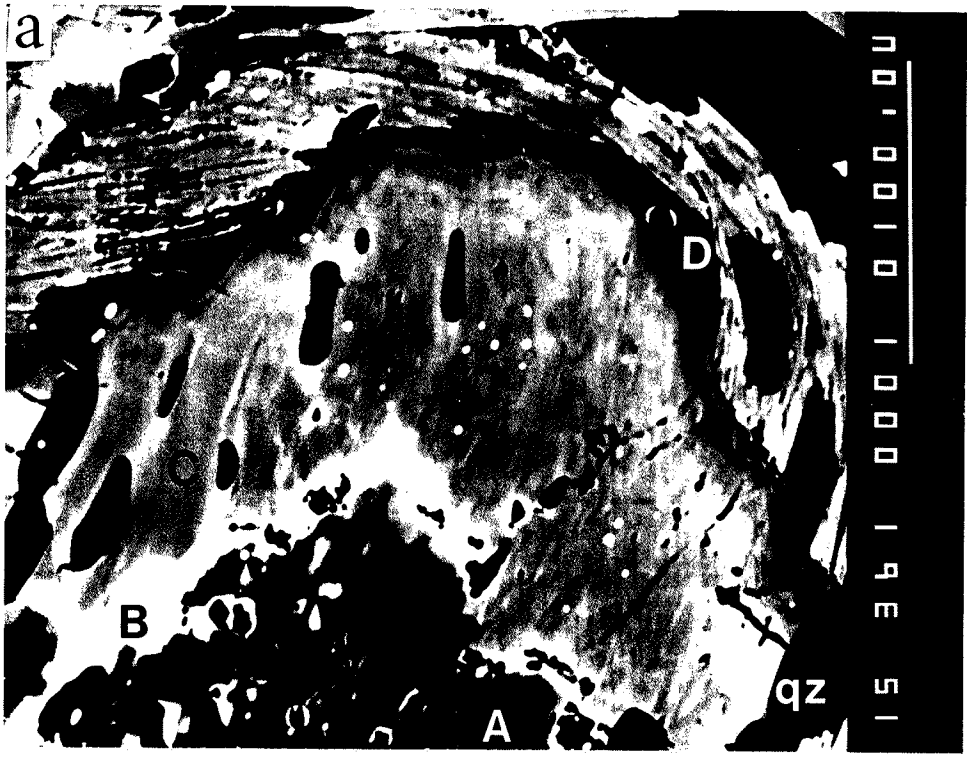
a
D
B
A
qz
0.1000 mm

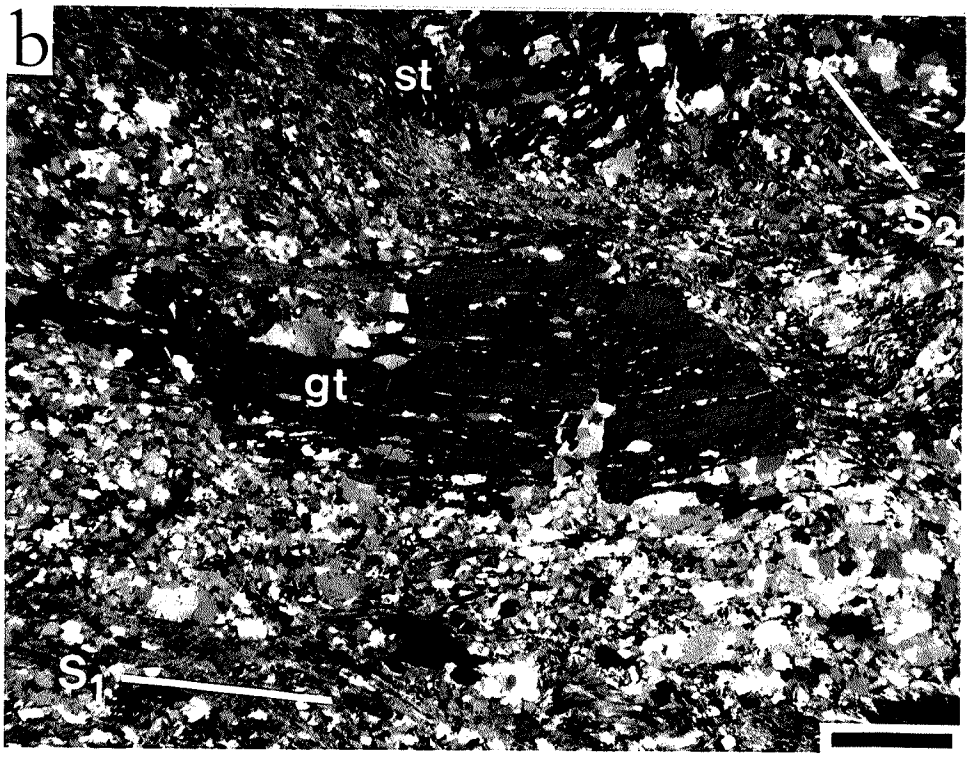
b
st
gt
S_1
S_2

syn-D_2 and, the gross changes from andesine core to a labradorite zone may reflect a sequence of prograde reactions. The outermost rim may also be due to prograde reactions or to retrogression.

In the calc-silicate enclave (24-1191), plagioclase composition varies from oligoclase to anorthite, concomitantly with mineralogical zoning across the section (*see* Table 5.2, Figure 9.6). Zones 5 and 6 are closest to the interior of the enclave and contain plagioclase in two distinct habits, which again correlate with An-content. In both zones, poikiloblastic grains which are elongate parallel to mineralogical zone boundaries, show reverse compositional zoning from oligoclase cores (An_{27}–An_{29}) to andesine rims (An_{34}). These grains contain inclusion trails of rutile (*see* 5.6.2. Silicate Enclaves in the Main Massive Sulphide Body; Plate 5.6, o–p) and seem to be relicts of the syn-D_2 porphyroblasts typical of plagioclase-layered rocks. Randomly oriented plagioclase involved in symplectic intergrowths occurs in both zones. In zone 6, plagioclase intergrown with and mantling gahnite shows normal and patchy zoning from cores of An_{54} to rims of An_{41}. In zone 5, plagioclase in a similar relationship to pyrrhotite shows normal and patchy oscillatory zoning, from An_{67} adjacent pyrrhotite inclusions to An_{41} at the outer grain boundary (*e.g. see* Plate 5.6, h). Zones 4 and 3 contain plagioclase that is considerably more calcic, *i.e.* An_{72}–An_{86} and An_{86}–An_{91} respectively, and the mineral assemblages in these zones likewise indicate more calcic bulk-rock compositions (*see* 10.4. Calc-silicate Enclave in the Main Massive Sulphide Body *for further discussion*). It is not clear whether the paucity of compositions in the range of about An_{50}–An_{80} is real (Figure 9.6), *i.e.* possibly a function of solvus relationships in intermediate to calcic plagioclase or of disequilibrium between calcic and less calcic bulk-rock compositions. Alternatively, it may simply represent incomplete sampling of plagioclase compositions during microanalysis. However, schiller textures suggestive of lamellar intergrowths were discernable in symplectic plagioclase mantling pyrrhotite. The sample combines bulk-rock compositional zoning with complex reverse, normal and oscillatory zoning in plagioclase of various habits, and it is possible that the full compositional spectrum of plagioclase is not represented by the analyses.

9.1.6. Garnet.

Garnet porphyroblasts contain inclusion trails of quartz parallel to S_1 fabrics

and are strongly elongate in the S_1 plane (Plate 9.1, b). Garnet grain boundaries with phyllosilicate minerals and staurolite within the S_1 compositional layering have euhedral faces; grain boundaries with quartz-rich layers are anhedral and marked by an abrupt increase in the abundance of quartz inclusions. Zoning profiles parallel and perpendicular to S_1 fabrics were investigated in the two garnet-bearing samples of the proximal alteration zone (22A-1625, 22B-1721) to determine if the garnet grains are the corroded relicts of originally more equant grains or whether they are mimetic after a pre-existing compositional layering.

The zoning is defined primarily by Mn-Fe substitution. For example, in a coarse porphyroblast in sample 22A-1625, the proportion of spessartine end member ranges from 52.9 mol% in the core to 36.3 mol% in the rim; the proportion of almandine end member ranges from 32.3 mol% in the core to 44.9 mol% in the rim (Table B.3, g). The zoning is regular and concentric, irrespective of inclusions, skeletal habit, or the orientation of grain boundaries (Figure 9.7); it defines the same S_1 flattening as the porphyroblast. The zoning profiles indicate the growth of garnet as tabular grains on compositional layers enriched in Mn. The grains may have been involved in subsequent prograde reactions, but their shape is primarily a syn-D_1 growth feature. For the purpose of balancing reactions (*see* 10.1.2. Mineral Equilibria), garnet rims were assumed to be in equilibrium with the rock assemblage.

In both garnet-bearing samples from the proximal alteration zone, Fe/Mg increases with decreasing Mn from core to rim (Figure 9.8). Ca proportions generally decrease toward the rims, but there is some suggestion of depletion in the cores with respect to the zone intermediate between cores and rims (Figure 9.8, b). Syn-D_2 garnet in cummingtonite-bearing rocks (22-413) shows less pronounced zoning and apparently has a weakly defined reversal in Fe/Mg with decreasing Mn. Garnet in the calc-silicate enclave (24-1191) has a skeletal mimetic habit (*see* Plate 5.6, m–n). Although it is zoned in terms of Mn (Figure 9.8, a), no relationship to physical features was apparent.

9.1.7. Tourmaline.

Tourmaline is a common trace constituent of the altered rocks, occurring in prismatic acicular crystals 0.01–0.5 mm in diameter. The tourmaline prisms commonly define a lineation in the S_1 plane and contain very fine inclusions of quartz,

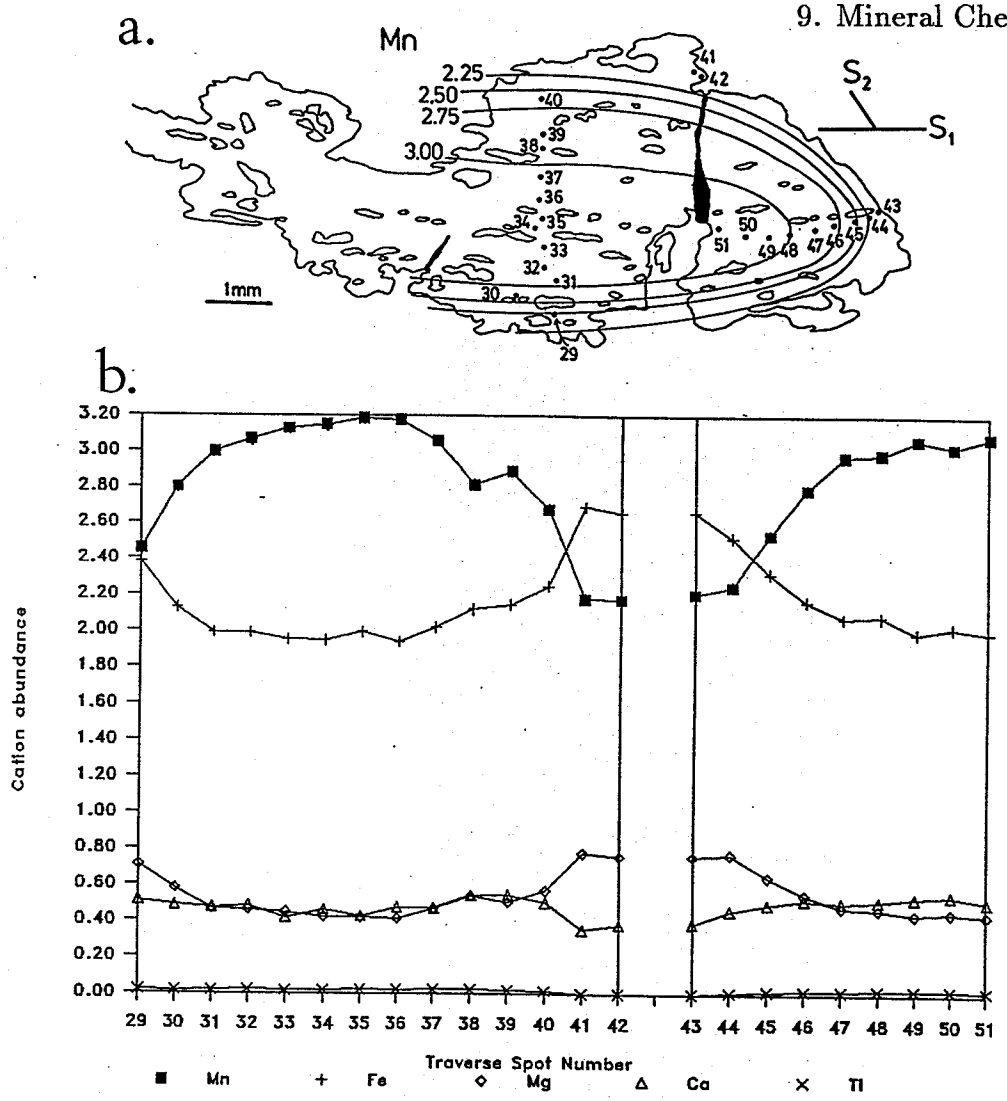

Figure 9.7. Compositional zoning in the garnet porphyroblast (22A-1625) illustrated in Plate 9.1b.

a. Contours of Mn (pfu) decrease from core to rim and define concentric zoning. The contours have the same overall shape as the porphyroblast, suggesting that the garnet grew as a tabular crystal. The numbered points are the locations of the spot analyses in b.

b. Compositional profiles of Fe, Mn, Mg, Ca and Ti (pfu) along the traverses shown in a.

also aligned parallel to the S_1 plane. Relatively coarse tourmaline in two samples was analysed (22A-1638, 34C-1377; Table B.3, l). The crystals are weakly zoned, containing a medium blue-green (transmitted light) core, typically forming 50–60% of the grain area, and showing an abrupt contact with a pale green rim. They are dravites within the field of 'Ca-poor metapelites and metapsammites coexisting with an Al-saturating phase', according to the classification of Henry and Guidotti

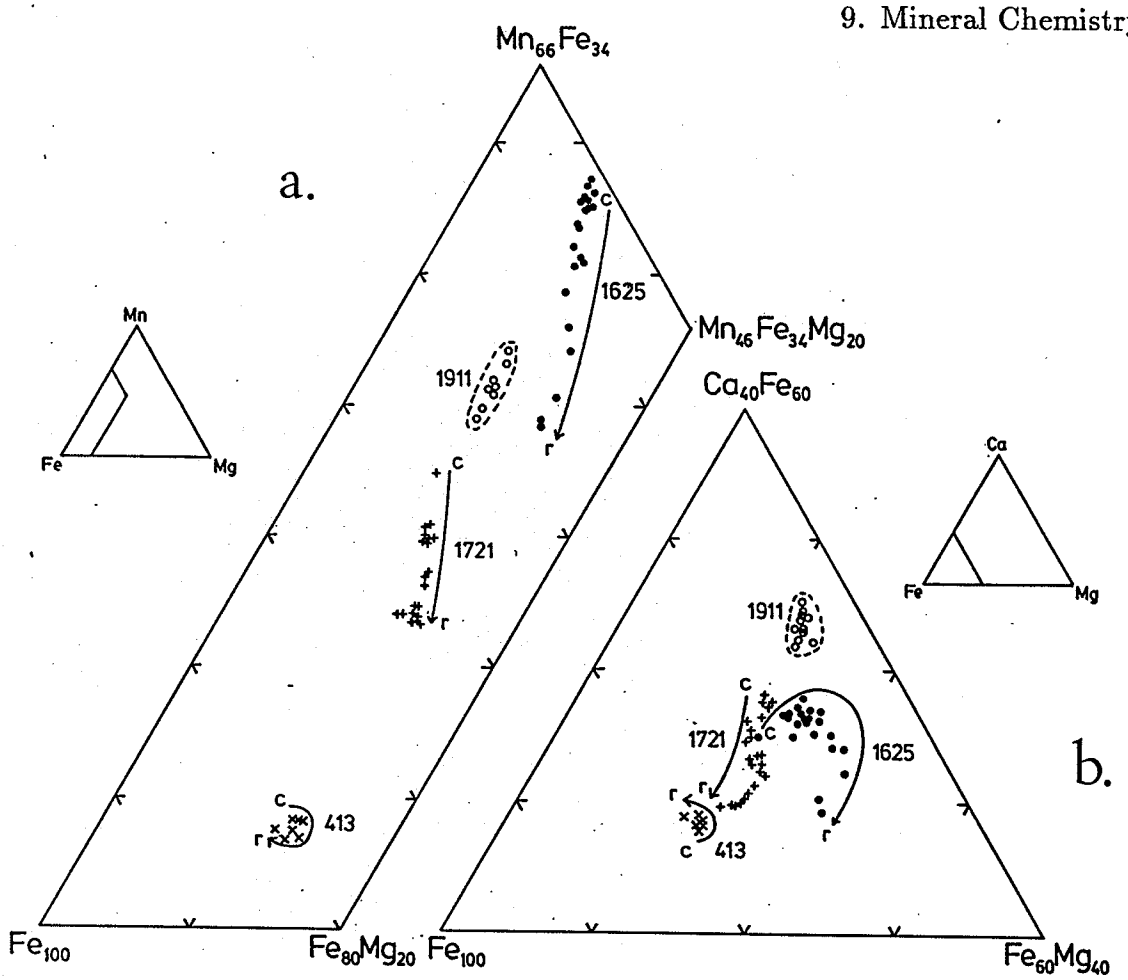

Figure 9.8. Garnet mineral chemistry.
a. in terms of Fe-Mn-Ca (atomic proportions). Core(c) to rim(r) zoning in 22A-1625 and 22B-1721 increases in Fe/Mg with decreasing Mn.
b. in terms of Fe-Ca-Mg (atomic proportions). Core(c) to rim(r) zoning in 22A-1625 and 22B-1721 decreases in Ca.

(1985). The zoning patterns do not define systematic trends, but there may be a tendency for rim compositions to converge. These characteristics, *i.e.* zoning marked by compositional discontinuities and a lack of systematic core-rim trends, are common in the compilation of tourmaline analyses (*ibid.*) and were interpreted by Henry and Guidotti to indicate a detrital origin for the cores. This conclusion does not apply to the Linda deposit, as there is continuity of inclusion types and shapes across tourmaline cores and rims, the cores are idiomorphic, and there is no evidence for abundant detrital influx in general. The tourmaline occurs in altered volcanic and volcanogenic rocks.

Taylor and Slack (1984) analysed the chemical and stable-isotopic compositions of tourmalines from several Appalachian and Caledonian stratabound massive sul-

Figure 9.9. (following page) Classification of amphiboles on the basis of structure and mineral chemistry.
a. Calcic amphiboles. Diagram and terminology after Hawthorne (1982). Tie lines link core(c) and rim(r) compositions.
b. Fe-Mg amphiboles. Orthorhombic and monoclinic amphiboles are projected on to one diagram. The inserts show the classification scheme of Leake (1978) and the areas detailed in the figure.

---

phide deposits, and found that nearly all the tourmalines were dravites, independent of paragenesis or metamorphic grade. They likewise observed a lack of systematic trends in zoning patterns. They suggested a pre-metamorphic, hydrothermal or diagenetic origin for some tourmaline; in particular, tourmaline associated with massive sulphide was apparently protected from dynamometamorphic recrystallization (*see also* Davies, 1985; Taylor and Slack, 1985). They suggested that boron derived from seawater may have been incorporated into pore waters, or into a hydrothermal fluid. At the Linda deposit, tourmaline prisms and their quartz inclusions define tectonic fabrics and, hence, they crystallized during metamorphism of a B-bearing protolith.

9.1.8. Amphiboles.

Four amphibole species are represented in the sample suite (Table 9.1, d, f, g, h), *i.e.* anthophyllite, cummingtonite, hornblende and actinolite. The calcic amphiboles generally range from tschermakite to actinolite, have low alkali contents and A-site occupancies, and moderately high $Mg/(Mg+Fe^{+2})$ (Figure 9.9, a). Total iron was recast as Fe^{+3} and Fe^{+2} in calcic amphibole analyses after the method of Robinson *et al.* (1982) (*see* Appendix B). Synkinematic to late kinematic amphiboles (22-413, 34A-1484) have ferro-tschermakite to tschermakitic hornblende compositions and coexist with cummingtonite (Figure 9.9, b). These samples probably underwent premetamorphic sililic-feldspathic alteration (*see* 11.2.1. Silicic-Feldspathic Alteration and Metamorphic Segregation) and the amphibole compositions analysed do not represent the full spectrum of synkinematic amphibole in mafic volcanic rocks at the Linda deposit.

Post-kinematic amphiboles occur in static calc-silicate rocks (34B-759.5) and in zoned calc-silicate enclaves (24-1191) in the main massive sulphide body. In the former case, radiating acicular sprays of actinolitic hornblende and actinolite coexist with epidote and calcite. Amphibole compositions in the calc-silicate enclave correlate with the mineralogical zoning across the sample (*see* Table 5.2). Am-

a. Calcic Amphibole Mineral Chemistry

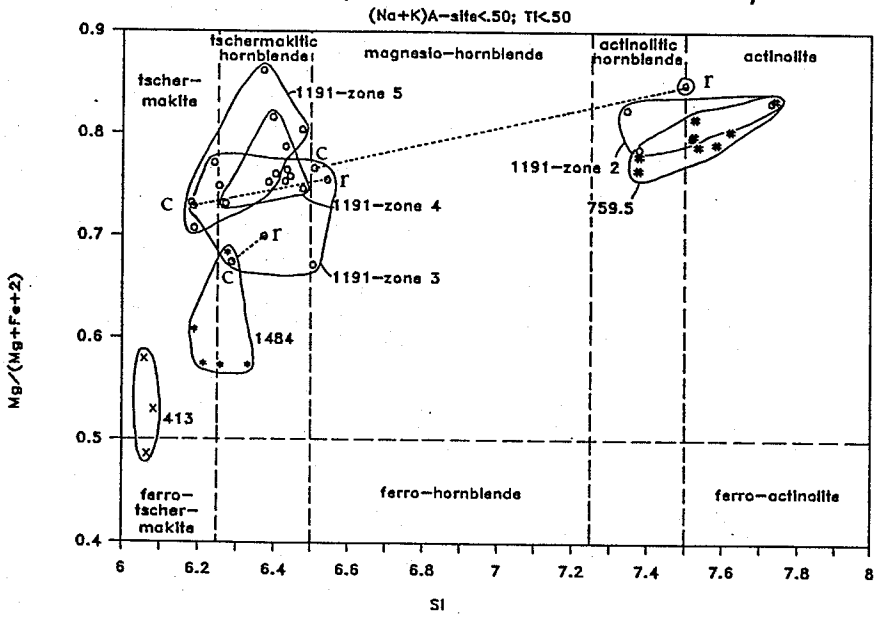

b. Fe-Mg Amphibole Mineral Chemistry

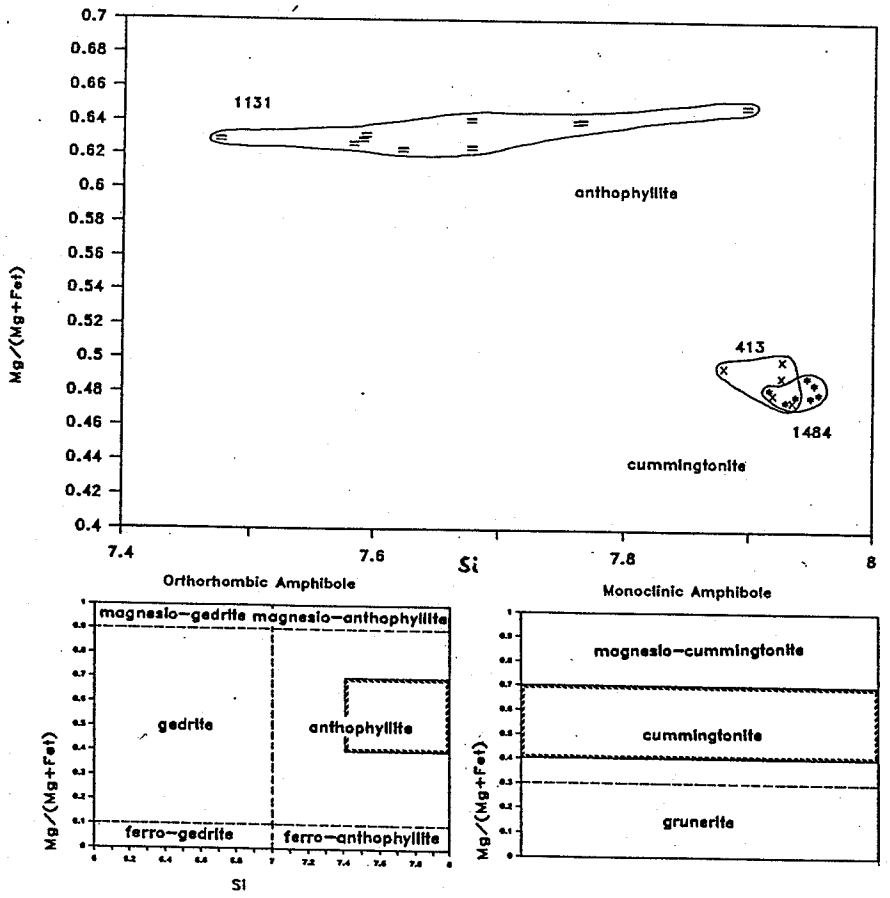

phiboles in zones 5–3 have similar Si contents; they range from tschermakite to magnesio-hornblende and decrease systematically in $Mg/(Mg+Fe^{+2})$. The decrease in $Mg/(Mg+Fe^{+2})$ may be due to an increase in Fe^{+2}/Fe^{+3} (Table 9.2, h). (The values of Fe^{+2}/Fe^{+3} are not reliable, in view of the assumptions involved in their calculation (F. Hawthorne, *pers. comm.*, 1989).) Amphibole compositions in zone 3 extend to slightly higher Si contents than amphiboles in zones 4 and 5. This trend is also shown by core and rim compositions in zone 3, with rims tending to be more siliceous, in one case with actinolitic hornblende rimming magnesio-hornblende (Figure 9.9, a). Zone 2 contains actinolitic hornblende and actinolite defining patchy compositional zoning. There is a wide compositional gap, comprising most of the magnesio-hornblende field, in the analyses representing 24-1191. Robinson *et al.* (1982) compiled analyses of associated hornblende and actinolite and concluded that the compositions of the mineral pairs could be explained by the existence of a solvus. In the case of sample 24-1191 at the Linda deposit, the evidence of textural and chemical disequilibrium suggests that the amphibole compositions could also reflect disequilibrium relationships.

Fe-Mg amphiboles at the Linda deposit are most commonly monoclinic; anthophyllite was observed in a single silicate enclave in the main massive sulphide body. Figure 9.9b classifies the Fe-Mg amphiboles at the Linda deposit. Calculation of Fe^{+3}/Fe^{+2} showed Fe^{+3} to be negligible (Appendix B) and therefore all iron is assumed to be ferrous. Anthophyllite was the only amphibole in which F was detected (Table 9.2, i; *see* 9.3.1. F/OH Relationships and Metamorphic Fluids).

9.1.9. Epidote.

Epidote in concordant and static calc-silicate rocks shows the lowest proportion of epidote end member at the Linda deposit, varying from $Ep_{44.5}$–$Ep_{56.2}$ (Table 9.2, j; Table B.3, j). Epidote in the calc-silicate enclave (24-1191) occurs in zones 2 and 3, but an insufficient number of analyses was collected to establish the presence of any within-sample compositional correlations. In general, the compositions show a higher proportion of epidote component than that in other calc-silicate rocks, *i.e.* ranging from $Ep_{56.5}$–$Ep_{65.9}$. A single analysis of fine grained epidote occurring in trace amounts in a schist of the proximal alteration zone (22B-1721) has a composition of $Ep_{57.4}$. The Mn content is low in all samples and Mn was assigned to the

Ca-site (Deer *et al.*, 1966), rather than considered as piedmontite solid solution. The Mn content of epidote in the static calc-silicate rock (34B-759.5) is notably lower than that of other samples in the suite.

9.2. Sphalerite Geobarometry.

Quantitative analyses of sphalerite were obtained from 6 samples (Table 9.2, e). Most samples showed wide within-sample compositional variation, especially in Fe/Zn (Table B.3, e); as previously discussed (*see* 9.1.4. Sulphide Minerals), this probably reflects the susceptibility of sphalerite to retrograde exchange. Some very fine grains approach end-member ZnS. In general, the most Fe-rich compositions are listed in Table 9.2e and these were assumed to most closely approximate the equilibrium compositions during metamorphism.

The sphalerite geobarometer has been calibrated (Hutchison and Scott, 1981) for sphalerite coexisting with pyrite and hexagonal pyrrhotite and is independent of temperature in the ranges typical of amphibolite-facies metamorphism. Increasing pressure, increasing f_{S_2} in the pyrite-field (*i.e.* in the absence of pyrrhotite), and down-temperature exchange, all have the effect of increasing the Zn content of sphalerite (*ibid.*; Jameison and Craw, 1987; Bristol, 1974). Minor amounts of Mn and Cd, and trace amounts of Cu have no detectible influence on the pressure dependency of the composition (*ibid.*; Craig and Scott, 1974).

The most Fe-rich sphalerite analysed at the Linda deposit (22B-1723) contains 14.5 mol% FeS and occurs as a relatively coarse inclusion in a syn-D_2 staurolite porphyroblast. The assemblage equilibrated with pyrite and, hence, sphalerite geobarometry yields a limiting maximum pressure. Using the calibration function of Hutchison and Scott (1981):

$$\mathrm{P(kb)} = 42.30 - 32.10 \log \mathrm{mol\%FeS}$$

(standard error of ± 0.30 kb), the maximum equilibrium pressure of the sphalerite is 5.0 kb.

The sphalerite analyses in 22A-1625 (Table 9.2, e) were collected from relatively coarse inclusions in a syn-D_1 garnet porphyroblast (*i.e.* in the garnet of Plate 9.1, b). The sample contains pyrite and monoclinic pyrrhotite and, it is probable that sphalerite equilibrated with pyrite and hexagonal pyrrhotite under metamorphic

conditions. The sphalerite geobarometer for the average composition of 13.6 mol% FeS (range: 13.3–13.8, 2 analyses, Table B.3, e), yields a pressure of 6.0 kb (range: 5.7–6.2). This pressure exceeds the maximum value derived from 22B-1723, and could be interpreted as the effective pressure during D_1, or alternatively, as indicative of minor retrogression of the sphalerite composition, possibly associated with the inversion of hexagonal pyrrhotite to the monoclinic polymorph.

In the calc-silicate enclave sample (24-1191), sphalerite occurs as coarse grains in contact with pyrite and monoclinic pyrrhotite containing remnants of hexagonal cores; they probably have been retrogressed. For the remaining samples in which sphalerite analyses were collected (34-799, 34C-1377, 22A-1638), the compositions are generally more Zn-rich and define a bimodal compositional distribution. These samples contain pyrite; the compositional range of sphalerite reflects metamorphic equilibration under $\log f_{S_2}$ conditions in the pyrite-field for the Fe-rich end of the range, and retrograde exchange in the Zn-rich end of the range.

9.3. Halogen Contents of Phyllosilicate Minerals.

9.3.1. F/OH Relationships and Metamorphic Fluids.

Biotite analyses from the Linda deposit commonly contain substantial amounts of F and, all biotite in the proximal alteration zone contains F in the range of 0.86–3.77 weight% (Table B.3, b). None of the analysed samples from the distal alteration zone contained biotite. F was not detected in muscovite which coexists with F-bearing biotite; evidently F/OH partitioning between biotite and muscovite favoured biotite sufficiently to result in muscovite F contents below the detection limit (0.46 weight%, Table B.2). Distribution coefficients of about 5 have been determined in high grade pelitic schists (Evans, 1969) and, values of about 8–16 apply to hydrothermal sericite and biotite from the Santa Rita porphyry copper deposit (Parry *et al.*, 1984). The latter range of values would be consistent with muscovite F contents below the detection limit for the F content of coexisting biotite at the Linda deposit. F was detected only in Cr-muscovite (32-1465.5), which is not associated with biotite, at levels of 0.46–0.77 weight%.

Chlorite associated with F-bearing biotite at the Linda deposit, in some cases, contained detectible levels of F, ranging from 0.39–1.55 weight% (Table B.3, c). In three cases it was possible to derive distribution coefficients, $K_D^{bi-ch} =$

Table 9.3. Distribution of F/OH between Biotite and Co-existing Minerals.

a. Biotite-Chlorite

$K_D^{bi-ch} = (X_F/X_{OH})_{bi}/(X_F/X_{OH})_{ch}$

Sample	area	K_D^{bi-ch}
22A-1752	B	23.7
34C-1377	B	18.9
34-1500	H	11.8

b. Biotite-Anthophyllite

$K_D^{bi-at} = (X_F/X_{OH})_{bi}/(X_F/X_{OH})_{at}$

Sample	area	K_D^{bi-at}
24-1131	C	3.69
24-1131	D	3.49

$(X_F/X_{OH})_{bi}/(X_F/X_{OH})_{ch}$, for coexisting grains. These range from 12–24 (Table 9.3, a) and are systematically lower for more Mg-rich mineral chemistries. In the staurolite-anthophyllite-gahnite assemblage (24-1131), biotite occurs as inclusions in anthophyllite. The distribution coefficient, $K_D^{bi-at} = (X_F/X_{OH})_{bi}/(X_F/X_{OH})_{at}$, is about 3.5 (Table 9.3, b), assuming hydroxyl sites fully occupied by (OH+F+Cl). Cl was not detected and OH was calculated from stoichiometry (Appendix B).

In general, the F content of hydrous minerals shows a strong positive correlation with Mg/(Mg+Fe) (*e.g.* Guidotti, 1984; Munoz, 1984; Gunow *et al.*, 1980), termed the 'Fe-F avoidance' principle and explained as an electronic bonding phenomenon in transition metals (Valley *et al.*, 1982). Gunow *et al.* (1980) suggested the derivation of F-intercept values to compensate for the compositional dependency and express the degree of F enrichment as an independent parameter. The F-intercept value for biotite was formulated as,

$$iv(F)_{bi} = 1.52X_{Mg} + .42X_{ann} + .20X_{sid} - \log X_F/X_{OH}$$

in which X_{Mg} refers to the mole fraction of Mg at the octahedral site, and X_{ann} and X_{sid}, the mole fractions of annite and siderophyllite respectively, were formulated as follows:

$$X_{ann} = 1 - (X_{Mg} + X_{sid})$$

$$X_{sid} = ((3 - Si/Al)/1.75)(1 - X_{Mg}).$$

At fixed temperature, $iv(F)_{bi}$ is proportional to $\log f_{H_2O}/f_{HF}$ in the fluid which equilibrated with the mica (Munoz, 1984), and hence, smaller values of $iv(F)_{bi}$ correlate with larger degrees of F enrichment.

Figure 9.10 illustrates the relationships for the Linda deposit. F contents of biotite from the proximal alteration zone show a positive correlation with Mg/(Mg+Fe). Biotite analyses from concordant and static calc-silicate rocks (22B-1843, 34-1028.5, 34B-759.5) have lower F contents, below or near the detection limit, for values of Mg/(Mg+Fe) equivalent to those in proximal zone samples, suggesting that calc-silicate rocks equilibrated in a higher f_{H_2O}/f_{HF} regime. F-intercept values, $iv(F)_{bi}$, corrected for compositional effects by the method of Gunow *et al.* (1980), show a relatively narrow range in the proximal alteration zone (Figure 9.10, b), with within-sample averages from 1.5–2.0. A single biotite analysis (34C-1453) has an anomalously high F content with respect to its relatively Fe-rich composition. This particular sample contains trace amounts of biotite in association with minor quantities of apatite. The range of $iv(F)_{bi}$ for kyanite-bearing rocks is still more narrowly defined and represents the F-richest range of the suite, *i.e.* averages from 1.5–1.7.

The relatively narrow ranges of $iv(F)_{bi}$ for samples of various bulk-rock compositions suggests that the biotites within each group equilibrated with a metamorphic fluid of similar f_{H_2O}/f_{HF} at a constant temperature. It implies that biotite was involved in mineral equilibria which buffered f_{H_2O}/f_{HF}. The most probable equilibria are F-OH exchange reactions with muscovite and chlorite. However, note that 24-1131 does not contain these minerals and F-OH exchange between biotite and anthophyllite presumably buffered the fluid composition.

The equilibrium constants for F-OH exchange between phlogopite, annite, siderophyllite, muscovite and fluids of various f_{H_2O}/f_{HF}, have been determined experimentally (Munoz and Ludington, 1977; 1974). Munoz (1984) presented the following relationship, linking fluid composition to $iv(F)_{bi}$:

$$\log f_{H_2O}/f_{HF} = 2100/T + iv(F)_{bi}.$$

Fluid compositions derived from this relationship at an assumed temperature of 550°C are indicated on the right-hand scale in Figure 9.10b. Kyanite-biotite as-

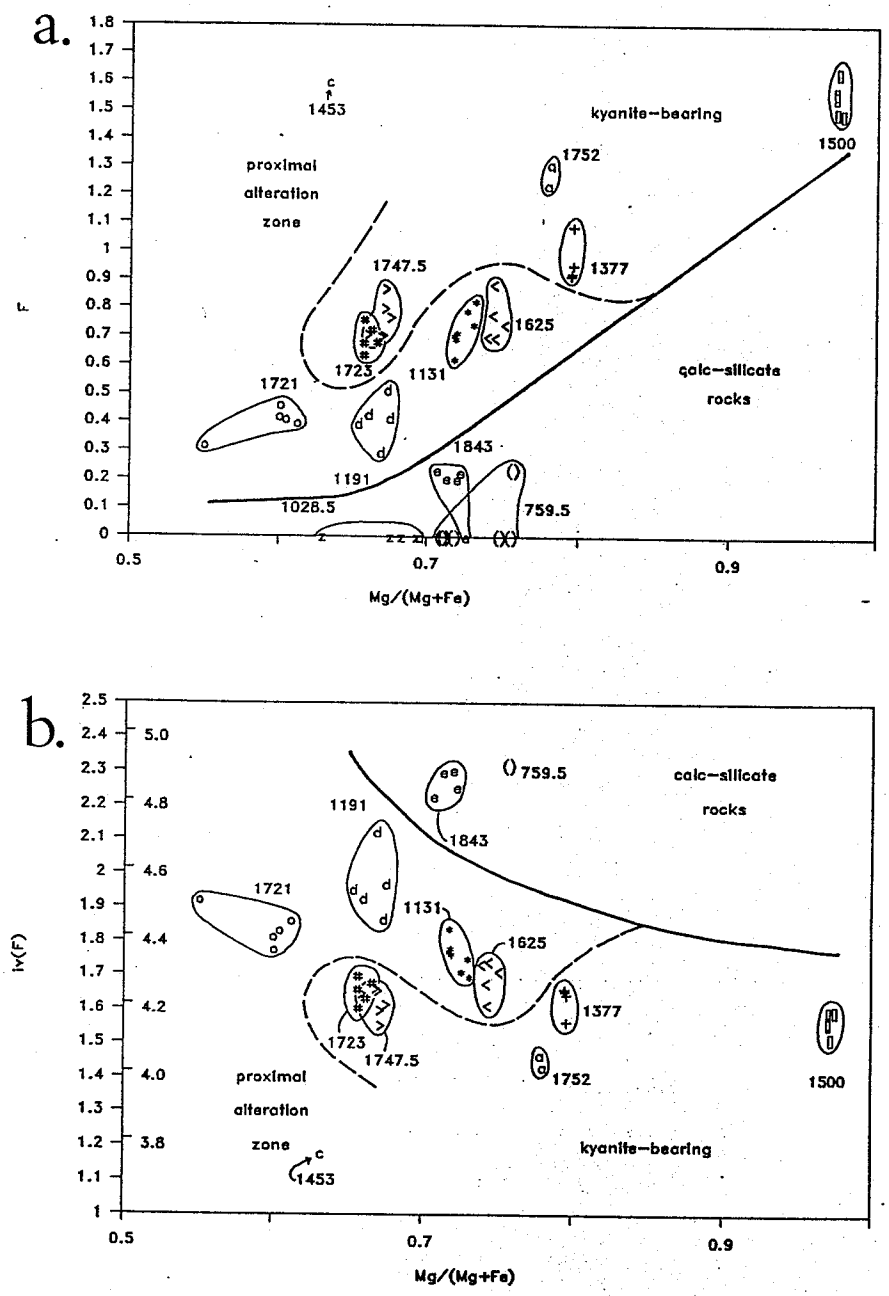

Figure 9.10. Biotite compositions showing relationships between Mg/(Mg+Fe) and F. In both figures, the wide solid line separates samples of the proximal alteration zone from calc-silicate rocks and, the dashed line separates proximal-zone samples containing kyanite from those without kyanite.

a. F (pfu) as a function of Mg/(Mg+Fe). Note the positive correlation, particularly for samples from the proximal alteration zone.

b. F-intercept value, $iv(F)_{bi}$, determined by the method of Gunow *et al.* (1980), as a function of Mg/(Mg+Fe). Values of $\log f_{H_2O}/f_{HF}$ in coexisting fluids, at an assumed temperature of 550°C, are shown on the right-hand scale of the y-axis.

semblages apparently equilibrated with relatively F-rich fluids, having a maximum $\log f_{H_2O}/f_{HF}$ of 4.3 at 550°C. Excepting the calc-silicate enclave (24-1191), assemblages in the proximal alteration zone equilibrated with fluids of $\log f_{H_2O}/f_{HF}$ of less than 4.5. In contrast, concordant and static calc-silicate rocks (22B-1843, 34B-759.5) equilibrated with fluids of the lowest F content, *i.e.* $\log f_{H_2O}/f_{HF}$ above about 4.8. The uncertainty inherent in the assumption of a temperature imposes an uncertainty on the absolute values of $\log f_{H_2O}/f_{HF}$. However, the relative changes in fluid composition implied by the mineral chemistries and assemblages are independent of temperature.

9.3.2. Implications for the Stability of Metamorphic Assemblages.

The biotite hydroxyl site strongly partitions F/OH relative to the hydroxyl sites of the coexisting minerals at the Linda deposit. Biotite which coexists with kyanite, *i.e.* an assemblage of higher 'apparent' metamorphic grade than the staurolite-biotite regional zone encompassing the Linda deposit (*see* 7.5. Relationships to Megascopic Structures and Regional Isograds), generally has lower $iv(F)_{bi}$ than biotite not associated with kyanite. The incorporation of F at the hydroxyl site presumably allowed the biotite-kyanite producing reaction to proceed at lower temperatures and extended the stability field of the assemblage to lower metamorphic grades.

Experimental work has shown enhanced thermal stability for F-bearing phlogopite and reduced stability for F-bearing annite, further supporting the Fe-F avoidance principle (as discussed by Munoz, 1984). In natural assemblages, F-bearing biotite and amphibole have been observed in granulite-facies rocks (Petersen *et al.*, 1982; Valley *et al.*, 1982) and, divariant behaviour of reactions involving the consumption of biotite has been attributed to F-OH exchange equilibria (Evans, 1969). Guidotti (1984) discussed examples and principles of enhanced thermal stability of F-bearing biotite. In view of the observations at the Linda deposit, it appears that divariant behaviour of F-OH micas must also be considered for biotite-forming reactions. In the case of the Linda deposit, the equilibria were displaced to lower temperatures and, thus, allowed the stable coexistence of kyanite and F-bearing biotite within the staurolite-biotite zone of regional metamorphism.

9.3.3. Implications for Hydrothermal Alteration.

It has been suggested that the F content of metamorphic minerals can be inherited from the protolith (Guidotti, 1984; Valley *et al.*, 1982). The evidence for internally buffered $\log f_{H_2O}/f_{HF}$ at the Linda deposit suggests that fluid mobility during metamorphism was limited. F and Cl-bearing micas have commonly been reported from hydrothermal mineral deposits, *i.e.* porphyry copper deposits (Parry *et al.*, 1984; Gunow *et al.*, 1980), stratabound Pb-Zn deposits (*e.g.* Munoz, 1984) and U, Sn, W and Mo mineralization associated with granitic intrusions (*e.g. ibid.*). Schmidt (1988) reported F-rich phyllosilicate minerals from alteration at the Arctic volcanogenic, Cu-Zn-Pb, massive sulphide deposit in Alaska. Routine microanalysis of F and Cl in minerals has been facilitated by the recent advances in automated WDS electron-probes (Guidotti, 1984; Munoz, 1984). Previous to this, few mineral analyses of suites from volcanogenic massive sulphide deposits reported F and Cl, and it may be that the significance of the halogens has not been recognized. At the Linda deposit, f_{HF} was a significant factor in metamorphic equilibria in altered rocks and it seems probable that the F was inherited from the hydrothermal protolith. However, note that due to Fe-F avoidance and the analogous Mg-Cl avoidance (Munoz, 1984) that, considering the generally Mg-rich mineral chemistries, it is not possible to draw conclusions regarding the relative importance of F and Cl in the protolith. Presumably, most Cl present in the protolith would have been partitioned into fluid inclusions during metamorphism.

Chapter 10
Models of Mineral Equilibria

The Linda deposit occupies a small volume with respect to the scale of regional metamorphism and, thus, it can be assumed that syn-D_2 assemblages equilibrated at essentially the same temperature and pressure in all samples and that the variety of parageneses is a function only of bulk-rock and fluid compositions. The pronounced changes in bulk-rock composition were inherited from the hydrothermally altered protolith and are not the result of synmetamorphic element mobility, although this does not preclude migration during fabric development.

Post-kinematic assemblages, *i.e.* static calc-silicate rocks, pyrite-calcite massive sulphide bodies and zoned enclaves, present a different problem in that they may have crystallized at some other point along the post-tectonic part of the P-T-deformation path (*see* Figure 7.6). The petrographic and structural relationships in post-kinematic assemblages imply some degree of open-system behaviour and, in some cases (*e.g.* sample 24-1191), it appears that equilibrium was not achieved even on a fine scale. Chemical contributions from outside the volume represented by a hand sample were apparently an integral part of the reaction history.

10.1. Mineral Assemblages Modelled in the SiO_2-Al_2O_3-FeO-MgO-ZnO-K_2O-H_2O-S_2-O_2 System.

The silicate-sulphide-oxide mineral assemblages in the proximal and distal alteration zones equilibrated during D_2 at the maximum metamorphic grade achieved by the Linda deposit (*see* 7.4.3. Pressure-Temperature-Deformation Path). Most mineral assemblages from the proximal and distal alteration zones and the graphitic metasediment contain quartz, pyrite and muscovite, and no feldspar (*see* Table 9.1). The mineral compositions (*see* Table 9.2, a–f) can be modelled in the SiO_2-Al_2O_3-FeO-MgO-ZnO-K_2O-H_2O-S_2-O_2 system (*see* Table 10.1, a). Log f_{H_2O}/f_{HF} had a limited range of values in the alteration zones (*see* 9.3. Halogen Contents of Phyllosil-

Figure 10.1. (following page) Summary of mineral compositions in the proximal and distal alteration zones in a schematic reaction grid in the system SiO_2-Al_2O_3-FeO-K_2O-H_2O, in terms of $\log a_{FeO}$ and $\log a_{Al_2SiO_5}$. The grid assumes fixed pressure and temperature, the presence of quartz and $f_{H_2O} = 1$, and was constructed after the method of Nesbitt (1986a; 1986b). Assemblages from the Linda deposit are plotted to give a consistent sequence of $X_{\text{Fe end member}}$. Positions of samples are indicated at the intersections of the lines for the constituent minerals. The drill-hole prefix has been omitted from sample numbers.

---

icate Minerals) and, therefore, f_{H_2O} was assumed to have been constant (although apparently somewhat less than one). Na_2O in muscovite and biotite, and CaO in margarite, were omitted from the model. Garnet contains substantial spessartine end member and, therefore, two garnet-bearing samples were modelled separately in an expanded system containing the additional component, MnO (*see* Table 10.1, b).

10.1.1. Mineral Compositions.

The compositions of silicate and oxide minerals range widely in Fe/Mg and, in the case of staurolite and gahnite, also in Fe/Zn. Figure 10.1, constructed after the method of Nesbitt (1986a, 1986b), schematically illustrates the mole fraction (X) of the Fe end member for the coexisting minerals in each sample and the relative position of the assemblage in terms of $\log a_{Al_2SiO_5}$ and $\log a_{FeO}$. The mole-fraction lines represent the reaction of an idealized Fe end member (for each mineral species) to FeO, Al_2O_3, SiO_2 and H_2O. The slopes are determined by the reaction stoichiometry and the relative position of intercepts is inferred from the respective values of the mole fraction of Fe end member. Assemblages are plotted at the point of intersection of their constituent minerals; assemblages containing kyanite are saturated in Al_2SiO_5 and lie on the x-axis at $\log a_{Al_2SiO_5}$=0. Reactions which form magnetite or Fe-sulphide minerals reduce a_{FeO} with increasing f_{O_2} and f_{S_2}, respectively. The x-axis is equivalent to a composite measure of any equilibria with a capacity to buffer a_{FeO}.

Silicate and oxide minerals compete for Fe with sulphide minerals and magnetite; silicate and oxide minerals which equilibrated at low a_{FeO} generally have high Mg contents, and in the case of garnet, high Mn and Ca contents (Nesbitt, 1986a; 1986b). The samples from the Linda deposit contain substantial Zn in staurolite and gahnite, the behaviour of which may not be adequately represented in

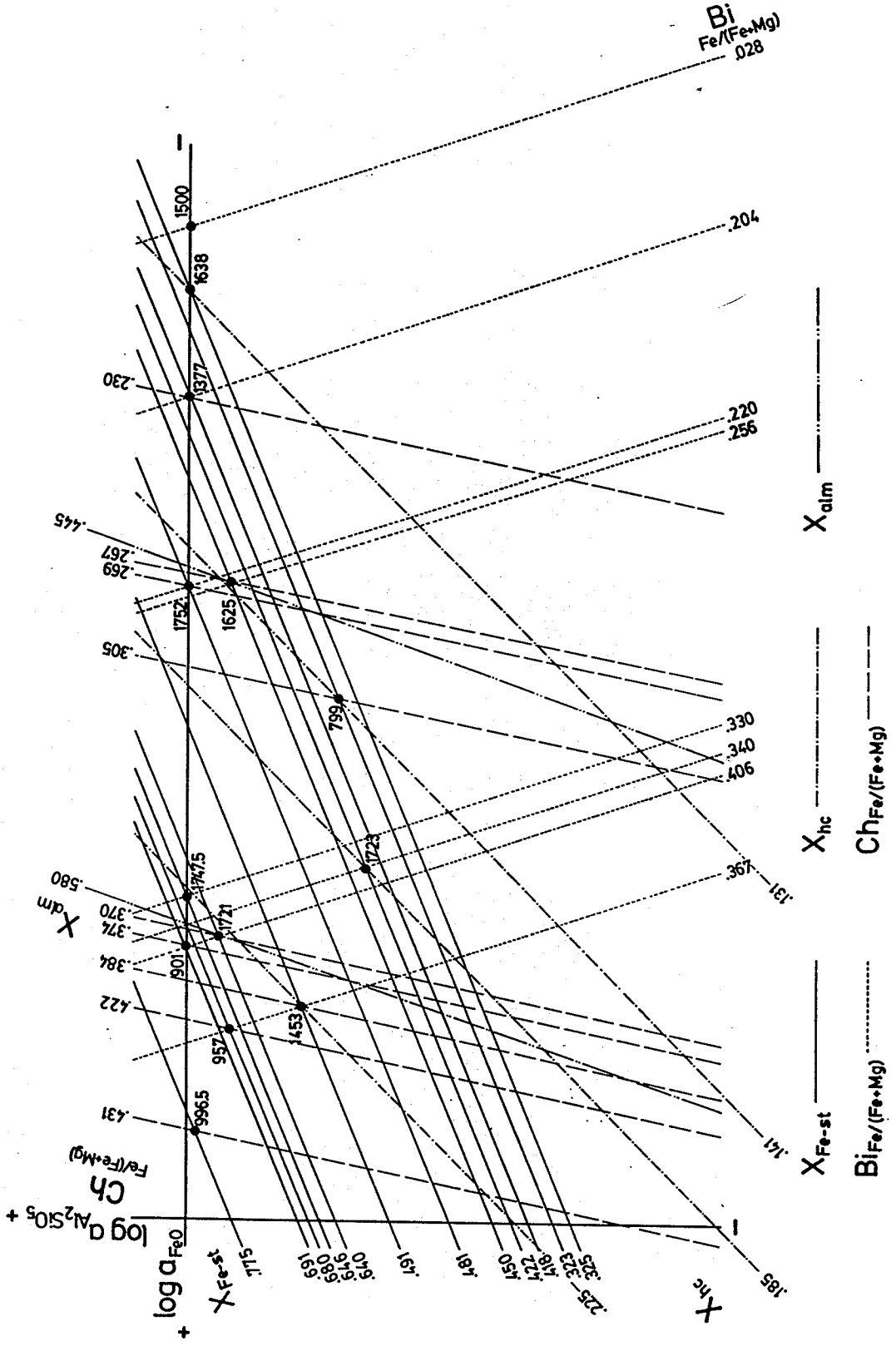
Bi
Fe/(Fe+Mg)
.028
.204
.220
.256
.330
.340
.406
.367
.131
.141
.185
.225
.323
.325
.450
.472
.478
.481
.670
.680
.690
.691
.715
.161
1500
1638
1377
1752
1625
1799
1723
1475
1721
1901
1453
957
996.5
.230
.445
.267
.269
.305
.580
.370
.374
.384
.422
.431
X_{alm}
X_{hc}
$X_{Fe\text{-}st}$
$Ch_{Fe/(Fe+Mg)}$
$Bi_{Fe/(Fe+Mg)}$
X_{hc}
$X_{Fe\text{-}st}$
X_{alm}
log a_{FeO} + log $a_{Al_2SiO_5}$ + Ch
Fe/(Fe+Mg)

Figure 10.1, as Zn is a chalcophile element (Goldschmidt, 1958).

As used here, Figure 10.1 primarily summarizes the Fe content of mineral compositions of the sample suite. For example, staurolite ranges in $X_{Fe-staurolite}$ from 0.78 in sample 22-996.5, which contains magnetite, pyrite and ilmenite, to 0.33 in sample 22A-1638, which contains pyrite, sphalerite and rutile (*see* 10.1.3. Petrogenetic Grid). Biotite ranges in Fe/(Fe+Mg) from 0.37 in 34C-1453, which contains pyrite and pyrrhotite, to 0.03 in 34-1500, which contains pyrite, pyrrhotite, graphite and sphalerite. The two garnet-bearing samples have relatively low $X_{almandine}$ of 0.59 and 0.46. A single discrepancy occurs in the biotite of 22B-1721 which is higher in Fe/(Fe+Mg) than would be predicted from the compositions of the associated minerals. Insomuch as it is possible to construct an internally consistent grid, using the $X_{Fe\ end\ member}$ values to determine the relative positions of assemblages, the basic assumptions, that each assemblage represents equilibrium and the mineral compositions are functions of bulk-rock composition, f_{S_2} and f_{O_2}, and not of temperature, pressure or f_{H_2O}, are permitted.

10.1.2. Mineral Equilibria.

In the model system, 6 samples contained assemblages which define a univariant reaction, and 1 sample (34C-1377) contained an assemblage which was used to define the bundle of univariant reactions at an invariant point (Table 10.1, a). The occurrence of assemblages which apparently defy the petrological phase rule can be explained by the coexistence of silicate, sulphide and oxide minerals which had the capacity to buffer the fugacities of O_2 and S_2. (Spear *et al.* (1982) give an analogous explanation for assemblages involving equilibria among hydrous minerals.) The reactions were balanced using the recalculated mineral formulae (*see* Table 9.2, a–g), with the exception of quartz, pyrite and kyanite, which were assumed to be ideal stoichiometric minerals. Staurolite formulae were recalculated from analyses according to the suggestions of Holdaway *et al.* (1988) and Holdaway (1986) (*see* Appendix B), which involves recasting an ideal amount (0.250 ions) of Fe as Fe^{+3}. Ferric iron is not part of the model system, and the relative values of reaction coefficients do not depend significantly on the uncertainties attached to the choice of an appropriate structural model for staurolite. Ferric iron was ignored in balancing the reactions. The activity of Fe in the model is determined by the coexistence of

Table 10.1. Model Mineral Reactions.

a. The SiO_2-Al_2O_3-FeO-MgO-ZnO-K_2O-H_2O-O_2-S_2 System.

	Sample	Reaction	m[1]
1.	22-901	$8.47ky + 0.14ch + 1.89py + 0.27sp + 0.55H_2O + 1.08O_2 \rightleftharpoons st + 1.46qz + 2.03S_2$	1.87
2.	22A-1638	$st + 5.10sp + 2.29O_2 \rightleftharpoons 8.70gh + 7.38qz + 0.72py + 1.70H_2O + 1.93S_2[+0.10ky]^2$	0.84
3.	22A-1752	$qz + 2.33ky + 0.73bi + 0.32py + 4.02H_2O + 0.16O_2 \rightleftharpoons 0.43ch + 0.82mu + 0.32S_2$	2.00
4.	22B-1723	$st + 5.28sp + 2.18O_2[+0.02bi]^2 \rightleftharpoons 8.85gh + 7.63qz + 0.95py + 1.34H_2O + 1.70S_2[+0.02mu]^2$	0.78
5.	34-799a	$st + 5.39sp + 2.42O_2 \rightleftharpoons 8.85gh + 7.51qz + 0.81py + 1.76H_2O + 2.01S_2[+0.001ch]^2$	0.83
6.	34C-1377	$qz + 3.70ky + 1.17bi + 1.17py + 5.97H_2O + 0.15O_2 \rightleftharpoons 0.65ch + 1.29mu + 0.30S_2$	2.00
7.	34C-1377	$1.65ch + 2.99mu + 1.28sp + 0.30py + 0.79O_2 \rightleftharpoons st + 3.99qz + 2.71bi + 13.33H_2O + 0.94S_2$	1.19
8.	34C-1377	$8.59ky + 0.13ch + 1.01py + 1.28sp + 0.54H_2O + 1.15O_2 \rightleftharpoons st + 1.67qz + 1.65S_2$	1.44
9.	34C-1377	$9.34ky + 0.24bi + 1.08py + 1.28sp + 1.76H_2O + 1.18O_2 \rightleftharpoons st + 1.46qz + 0.26mu + 1.72S_2$	1.45
10.	34C-1453	$1.68gh + 1.32ch + 2.31mu + 0.72py + 0.36O_2 \rightleftharpoons st + 2.05qz + 2.04bi + 10.96H_2O + 0.72S_2$	2.00

b. The SiO_2-Al_2O_3-FeO-MgO-MnO-ZnO-K_2O-H_2O-O_2-S_2 System.

	Sample	Reaction	m[1]
11.	22A-1625	$0.13gt + 3.20mu + 1.36ch + 0.32py + 1.14sp + 0.73O_2 \rightleftharpoons st + 2.60bi + 4.91qz + 11.52H_2O + 0.89S_2$	1.22
12.	22B-1721	$0.08gt + 3.27mu + 1.57ch + 2.12py + 1.06O_2 \rightleftharpoons st + 3.00bi + 4.35qz + 12.29H_2O + 2.12S_2$	2.00

[1] $m = \log f_{S_2} / \log f_{O_2}$. [2] Coefficient not significant within 2σ error.

pyrite and S_2 and the critical variables, a_{Mg}, a_{Zn} and a_{Al_2} (*see* 10.1.3. Petrogenetic Grid), are determined by the proportions of Mg, Zn and Al_2 in the system.

The computer programs, FINGER (Gordon, 1987, *unpubl.*; based on the program, REACTION (Finger and Burt, 1972)) and LU (*ibid.*; adapted from a PC-MATLAB subroutine (Moler *et al.*, 1987)), facilitated the derivation of balanced reactions. The slopes (m) of the univariant reactions in $\log f_{O_2} / \log f_{S_2}$ were de-

rived from the reaction stoichiometry (Table 10.1). The significance of the reaction coefficients with respect to the within-sample standard deviations of mineral analyses at the 2σ level was tested by linear regression on subsets of the minerals, fitting the regression to the composition of one mineral chosen as a dependent variable (Gordon, *pers. comm.*, 1988; Greenwood, 1968). The procedure was iterated, taking each analysed mineral in turn as the dependent variable. Residual values in excess of the sum of weighted 2σ standard deviations associated with the analyses, were interpreted to indicate that the coefficients of the reaction, as balanced, are significant. Errors on the independent and dependent variables were taken into account by summing the 2σ standard deviations for each element from each mineral analysis, employing the regression coefficient of the mineral as a weighting factor.

The evaluation of 2σ errors was critical in the case of reactions involving the decomposition of gahnite (22B-1723, 34-799, 22A-1638). The balanced reactions tended to involve kyanite, chlorite, or biotite and muscovite, with relatively small stoichiometric coefficients; gahnite decomposition apparently occurred within a 3-phase triangle to staurolite, sphalerite, and either kyanite, or an Fe-Mg phyllosilicate mineral. However, the coefficients of kyanite or the phyllosilicate minerals were not significant within the 2σ errors and, therefore, the reactions cannot be discriminated from the degenerate decomposition of gahnite to staurolite and sphalerite. The reactions, as balanced exactly, are shown in Table 10.1; minerals whose coefficients are less than the 2σ confidence limits are in square brackets. Gahnite compositions in these samples lie on the staurolite-sphalerite tie line when the within-sample errors are considered. Note also that the same procedure showed that the coefficient of chlorite in reactions 1 and 8, and the coefficients of biotite and muscovite in reaction 9, are significant in balancing the MgO component, and, that the coefficient of garnet in reactions 11 and 12 is significant in balancing the MnO component.

For comparative purposes, some of the equilibria were reformulated as over-determined systems by including additional components, and were balanced by linear regression (Table 10.2). This formulation is over-determined in an algebraic sense in that the number of equations (*i.e.* equations of mass balance for each component) exceeds the number of variables (*i.e.* the stoichiometric coefficients of each mineral). In a thermodynamic sense, this essentially defines an assemblage

Table 10.2. Over-determined Model Reactions solved by Linear Regression.

Regression standard errors (1σ) in parentheses.

	Sample	Reaction	d.f.[1]	m[2]
13.	22A-1638 Mn[3]	$1(0.10)st + 5.14(0.73)sp + 2.22(0.40)O_2 \rightleftharpoons 8.76(0.94)gh + 7.44(0.97)qz + 0.07(0.97)ky + 0.72(0.11)py + 1.71(0.10)H_2O + 1.86(0.42)S_2$	1	0.84
14.	22A-1638 Mn	$1(0.07)st + 5.19(0.09)sp + 2.25(0.09)O_2 \rightleftharpoons 8.83(0.07)gh + 7.51(0.07)qz + 0.72(0.07)py + 1.71(0.07)H_2O + 1.89(0.11)S_2$	2	0.76
15.	34-799 Mn,Ti	$1(0.03)st + 5.38(0.05)sp + 2.41(0.04)O_2 \rightleftharpoons 8.84(0.03)gh + 7.55(0.03)qz + 0.82(0.03)py + 0.08(0.03)ru + 1.73(0.03)H_2O + 2.00(0.05)S_2$	2	0.83
16.	22A-1625 Mn,Ti,Na	$0.08(0.22)gt + 3.05(0.23)mu + 1.59(0.35)ch + 1.11(0.54)sp + 0.24(0.48)ru + 0.81(0.64)O_2 \rightleftharpoons 1(0.48)st + 2.69(0.61)bi + 4.96(1.77)qz + 12.90(2.08)H_2O + 1.04(0.88)S_2$	1	1.29
17.	22A-1625 Mn,Ti,Na	$0.09(0.17)gt + 3.04(0.18)mu + 1.57(0.27)ch + 1.11(0.43)sp + 0.81(0.51)O_2 \rightleftharpoons 1(0.38)st + 2.65(0.48)bi + 5.05(1.39)qz + 12.79(1.63)H_2O + 1.04(0.70)S_2$	2	1.28
18.	22A-1625 Mn,Ti,Na,Ca	$0.08(0.14)gt + 3.04(0.15)mu + 1.57(0.22)ch + 1.11(0.35)sp + 0.81(0.41)O_2 \rightleftharpoons 1(0.31)st + 2.65(0.39)bi + 5.04(1.13)qz + 12.80(1.33)H_2O + 1.04(0.57)S_2$	3	1.29

[1] Statistical degrees of freedom.

[2] $m = \log f_{S_2} / \log f_{O_2}$.

[3] Additional components with respect to Table 10.1.

with some degree of variance and, thus, this approach may be particularly useful in the modelling of continuous reactions. The general method followed that of Lang and Rice (1985); however, these authors used a non-linear regression which allowed the evaluation of residuals in the independent and dependent variables.

The over-determined formulations were done by adding the minor components, TiO_2, MnO, CaO and Na_2O, to the models of those samples in which they occur in more than one analysed or observed mineral. The additional phase, rutile, was incorporated into the models for samples in which it occurs. This alternative method of deriving the reactions results in comparable stoichiometric coefficients for the major phases, *i.e.* those selected to define the reactions of Table 10.1. The

slopes (m) are generally indistinguishable. The method allows the derivation of a standard error for each coefficient (Table 10.2, in parentheses); however, this error is related to the fit of the regression and not to analytical uncertainties. It is possible to reduce the magnitude of the regression standard deviations by increasing the number of statistical degrees of freedom (*i.e.* number of components less the number of phases), *e.g.* by increasing the number of minor components in the model. This can artificially reduce the standard deviations, even though the additional component may not be significant in the reaction. For example, including CaO in garnet in reaction 18 (Table 10.2) increases the degrees of freedom to 3 and reduces the magnitude of the standard deviations of the coefficients, although there is no other Ca-bearing phase and the value of this component is relegated entirely to the residuals. Similarly, reaction 17 shows lower standard deviations than reaction 16, through the omission of rutile, increasing the degrees of freedom by one. Note also that the involvement of garnet in these reactions is significant within the 2σ confidence limits of the within-sample standard deviation, despite the relatively high regression standard deviation associated with the coefficient of garnet. The method of solving an exactly determined system of equations (Table 10.1) is essentially equivalent to weighting the major components to the exclusion of minor components and, thus, seems preferable in low-variance assemblages. Similarly, the evaluation of the significance of reaction coefficients with respect to analytical uncertainties seems a more rigorous approach than reliance on the potentially misleading standard deviations generated by fitting a regression line.

10.1.3. Petrogenetic Grid.

A petrogenetic grid (Figure 10.2) in the SiO_2-Al_2O_3-FeO-MgO-ZnO-K_2O-H_2O-S_2-O_2 system was derived by a Schreinemakers analysis (Nordstrom and Munoz, 1986; Zen, 1966) of the observed assemblages and the balanced reactions (Table 10.1, a). The grid is projected from quartz, pyrite, muscovite of the composition analysed in each sample, and H_2O. The slopes of the univariant lines, as determined from the balanced reactions, apply only to the particular mineral compositions involved in the reaction. The slopes are constrained to be positive by the reaction topologies (*i.e.* with O_2 and S_2 on opposite sides), but the equilibrium mineral compositions will vary along the univariant lines, introducing curvature for reactions involving Fe-

Mg-Zn minerals. The slopes of sphalerite-absent reactions are constant at m=2 in the stability field of pyrite. The reaction involving the decomposition of chlorite to kyanite and biotite occurs in a lower-order compositional subsystem, without ZnO, and is likewise constrained to a slope of m=2 in the pyrite field. Other slopes are shown schematically, to illustrate the topology, while maintaining thermodynamic consistency. All the assemblages contain pyrite and, in some cases, rutile, and, with few exceptions, do not contain pyrrhotite, magnetite or ilmenite; therefore, the equilibria are shown almost entirely within the stability field of pyrite.

The grid was determined for a 9-component system with 12 phases; each invariant point has one phase absent and each non-degenerate univariant line has two phases absent. Two chemical potentials are shown as axes (S_2, O_2) and four chemical potentials are constant, thus, each non-degenerate univariant reaction involves four phases in the Zn-Al_2-Mg subsystem. The triangular insets (Figure 10.2) are projections on to the Zn-Al_2-Mg plane illustrating the phase relationships between silicate, oxide and sulphide minerals. The activity of Fe is determined by the presence of pyrite and S_2 in all assemblages and need not be shown explicitly. The relative positions of mineral compositions have been exaggerated to enhance the topological relationships. The samples vary widely in bulk-rock composition, but the presence of quartz, muscovite and pyrite in all samples, and the assumption of constant a_{H_2O}, fixes 4 compositional parameters, allowing the depiction of the assemblages in 5 compositional variables, *i.e.* Al_2, Mg and Zn defining the projection plane, and S_2 and O_2 as axes. All the equilibria are dehydration reactions and variation in a_{H_2O} will shift their positions; however, it is unlikely that a_{H_2O} variations were sufficiently extreme to alter the topology of the reaction grid. Similarly, the activity of end-member muscovite in the muscovite analyses varies slightly. Although the activity is not strictly constant, the magnitude of the variation is not significant. However, the celadonite component (*i.e.* $K_2(Fe^{+2},Mg)_2Al_2(Si_8O_{20})(OH)_4$; Guidotti and Sassi, 1976) of muscovite is significant, as projection from an ideal end-member muscovite would result in an incorrect topology for some reactions involving biotite.

Samples from the Linda deposit are located on the grid in the correct relative positions; the slopes at the sample points are schematic. Assemblages containing either chlorite, or kyanite + biotite, can be modelled in a ZnO-absent subsystem with

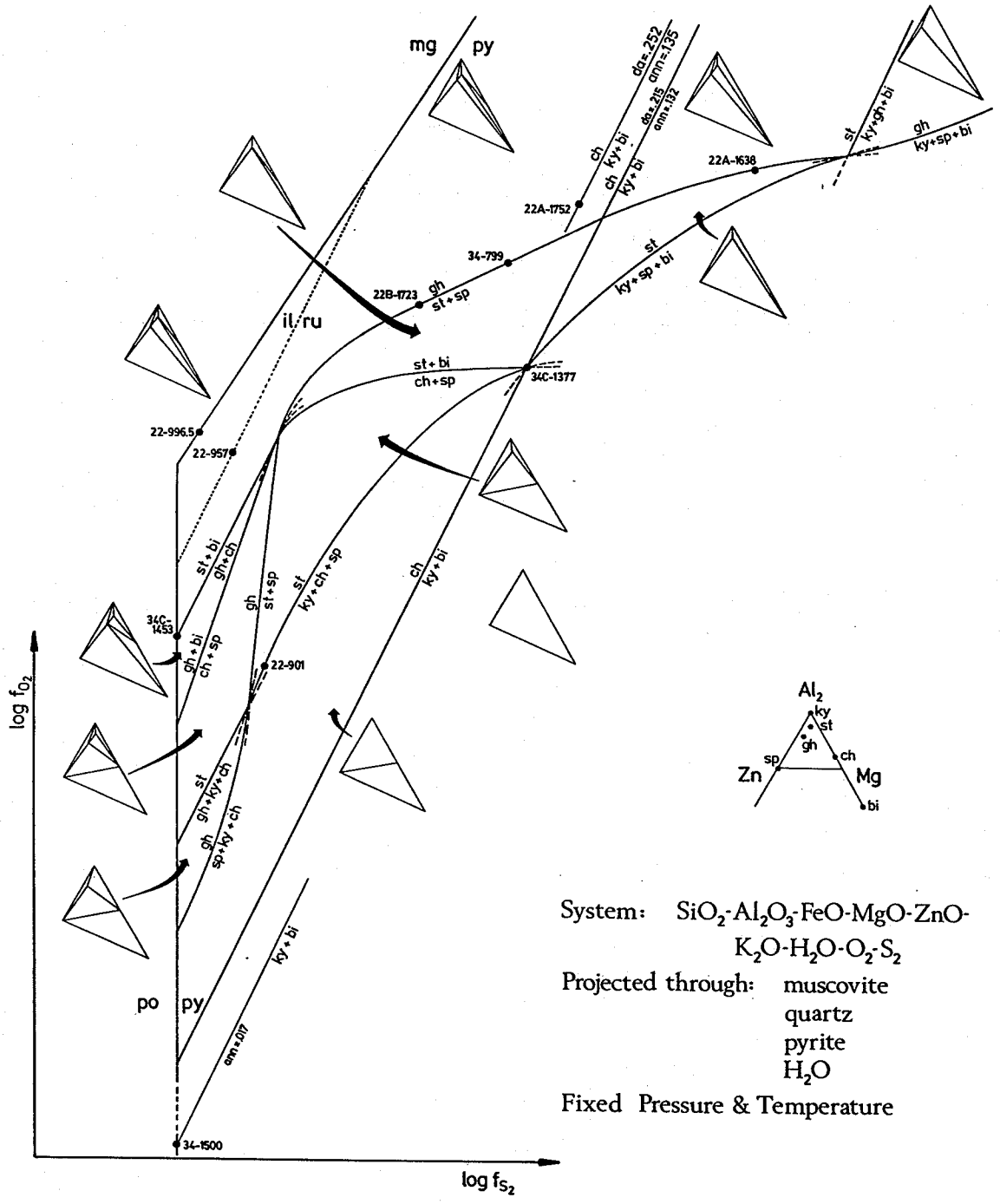

Figure 10.2. Petrogenetic grid in the system SiO_2-Al_2O_3-FeO-MgO-ZnO-K_2O-H_2O-O_2-S_2, derived by a Schreinemakers analysis of the reactions in Table 10.1a. The grid is projected through quartz, muscovite (of the analysed composition), pyrite and H_2O, at fixed pressure and temperature. The insets are projections on to the Zn-Al_2-Mg plane. The locations of sample assemblages in the grid are indicated.

isopleths of Fe end member activity in continuous sulphidation-oxidation reactions. Some isopleths are labelled with the mole fractions of daphnite and annite in chlorite and biotite, respectively. The relative position of the samples was selected to give isopleths of increasing Mg/Fe with increasing $\log f_{S_2}$, as expected for Mg-Fe silicate minerals in the pyrite field (*e.g.* Nesbitt, 1986a; 1986b). The grid and the locations of observed assemblages are internally consistent (excepting 34C-1747.5, discussed below); note the general correspondence between Figure 10.1, which shows samples arranged in terms of decreasing a_{FeO}, and the grid of Figure 10.2, with samples plotted in terms of relative $\log f_{O_2}$ and $\log f_{S_2}$.

10.1.4. Discussion.

The sulphidation of chlorite to biotite + kyanite in the ZnO-absent subsystem involves one less component and one less phase and, thus, defines a univariant line passing through the invariant point defined by the assemblage of 34C-1377 (Figure 10.2). Both ends of the reaction are stable, limiting the stability of chlorite and of biotite + kyanite to values of $\log f_{S_2}$ below and above the line, respectively. The slope of this reaction, and the slopes of isopleths of the activity of Fe end member component in Fe-Mg silicate minerals, are fixed at m=2 in the pyrite field by the stoichiometry of FeS_2/FeO. Biotite and chlorite of a particular $a_{\text{Fe end member}}$ (*i.e.* that of 34C-1377) coexist with kyanite only along the univariant line. For the pressure and temperature conditions in effect during D_2 at the Linda deposit, the most Mg-rich chlorite and the most Fe-rich biotite (in the presence of kyanite) should be limited by this reaction. In general, the isopleths defined by chlorite-bearing samples (22-901, 22-957, 22-996.5, 22A-1752, 34-799, 34C-1453) and biotite-kyanite bearing samples (22A-1752, 34-1500) are consistent with this requirement. Some divariant behaviour is shown by 22A-1752 which contains the 3-phase assemblage with slightly more Fe-rich compositions than those on the limiting reaction line. The biotite in 22A-1752 is more F-rich ($iv(F)_{bi}$=1.45; *see* Figure 9.10, b) relative to that of 34C-1377, and this may have stabilized biotite + kyanite to lower f_{S_2}. An unexplained discrepancy occurs in 34C-1747.5, which contains biotite with a_{annite}=0.33, coexisting with kyanite, pyrite, pyrrhotite and staurolite. This assemblage cannot be located on the grid of Figure 10.2 and there is no obvious explanation for the divariant behaviour.

In order to reduce the variance of Fe-Mg silicate equilibria, sulphide-oxide assemblages are commonly identified or invoked for their buffering capacity; for example, Nesbitt's (1986a; 1986b) treatment of equilibria relies on f_{O_2}/f_{S_2} fixed by the coexistence of magnetite and pyrrhotite and, at higher f_{O_2} and f_{S_2}, by magnetite and pyrite. Isopleths of Fe-Mg silicate compositions provide points of intersection with the sulphide-oxide reaction lines. Bryndzia and Scott (1987b) identified assemblages in which chlorite, quartz and an aluminosilicate mineral occur with pyrite, pyrrhotite and magnetite, in order to apply their experimental calibration (1987a) of daphnite activity at the magnetite-pyrite-pyrrhotite triple-point to mineral analyses from the Anderson Lake and Stall Lake mines.

The equilibria involving Fe-Mg-Zn silicate, oxide and sulphide minerals are sliding-scale buffers of f_{O_2} and f_{S_2}; mineral compositions vary with f_{O_2} and f_{S_2} along the univariant reaction lines (Figure 10.2). This contrasts with the usual treatment of Fe-Mg isopleths and reactions defined by the compositions of silicate minerals (*e.g.* Bryndzia and Scott, 1987a, 1987b; Nesbitt, 1982; Froese, 1971), for example, as in the equilibria involving kyanite, biotite and chlorite in the ZnO-absent subsystem. Note that although Spry and Scott (1986a) achieved experimental reversals of the reaction of Fe-Zn spinel to Fe-Zn sphalerite and corundum in the presence of a magnetite-pyrite-pyrrhotite buffer, the reaction they investigated is itself a univariant sliding-scale buffer. Thus, the experiments at the triple-point relied on either a fortuitous intersection of the equilibria in f_{O_2}/f_{S_2} space, or the interpretation of a metastable assemblage.

Isopleths of the activity of the Fe end member component in Fe-Mg in silicate minerals intersect the univariant reactions involving Fe-Mg-Zn minerals, as shown in the petrogenetic grid (Figure 10.2; 34-1500). The activity of the Zn end member component in reactions involving Fe-Mg-Zn staurolite or spinel increases along the univariant lines with increasing $\log f_{O_2}$ and $\log f_{S_2}$. This can be seen in the compositions of silicate and oxide minerals from the Linda deposit, in which more Mg-rich compositions occur in samples generally lying at higher relative values of $\log f_{S_2}$; more Zn-rich compositions lie at higher relative values of both $\log f_{O_2}$ and $\log f_{S_2}$. At very low values of $\log f_{O_2}$ and $\log f_{S_2}$ (as represented by the graphite-pyrite-pyrrhotite bearing sample, 34-1500) sphalerite, kyanite, and

phlogopite, which approaches an end-member composition, are stable in preference to staurolite or gahnite.

The decomposition of gahnite to staurolite and sphalerite occurs in a K_2O-absent subsystem and is a degenerate reaction due to the compositional colinearity of these 3 minerals. The reaction involves 2 fewer phases, *i.e.* muscovite, biotite, chlorite and kyanite are absent; however, the compositional colinearity means that Al_2/Mg is constant and effectively acts as one component. Thus, the assemblage is univariant and the mineral compositions vary along the line, rather than defining isopleths. The reaction cuts across the grid, limiting gahnite to relatively high $\log f_{O_2}$ and low $\log f_{S_2}$ conditions. Spry and Scott's (1986a) theoretical and experimental investigation of Fe-Zn spinel generally limited its stability to values of $\log f_{O_2} / \log f_{S_2}$ near or above the magnetite-pyrite-pyrrhotite triple-point. From observations at the Linda deposit, it seems that the presence of Mg in gahnite expands the range of its stability well into the pyrite field and into the field of rutile + pyrite. Support for this is also found in the spinel analyses and the compilation of zincian spinel-bearing assemblages from the Appalachians and the Scandinavian Caledonides (Spry and Scott, 1986b). Many assemblages contain pyrite, in some cases with rutile, and the compositions of the associated spinels tend to be higher in Mg end member (*i.e.* 0.074–0.089) than those not associated with pyrite (*i.e.* 0–0.078).

In an assemblage from the Osborne Lake mine (15 km northeast of the Linda deposit; *see* Figure 2.1), located in the biotite-sillimanite-garnet zone of regional metamorphism (Froese and Moore, 1980), Froese (*pers. comm.*, 1988) derived the following non-degenerate reaction for the decomposition of gahnite:

$$gahnite + pyrrhotite + S_2 + H_2O \rightleftharpoons sphalerite + staurolite + cordierite + O_2.$$

Strictly speakly, this reaction is consistent with the degenerate reaction when the 2σ within-sample errors are considered. However, the decomposition within a 3-phase triangle to a product assemblage which includes an Fe-Mg mineral may also be the result of a change in topology at higher grade. These possibilities could be tested by acquiring more mineral analyses in an enlarged sample suite.

Garnet-bearing samples required the inclusion of an MnO component in the model system. The evaluation of the significance of the coefficient of garnet in

assemblage is multivariant and equilibrated at the magnetite-pyrite-pyrrhotite invariant point. The staurolite and gahnite contain 0.26 and 0.64 mole fraction of the Zn end member, respectively, suggesting that sphalerite was present at lower grade, and possibly at the grade represented by the assemblage under different f_{S_2} and f_{O_2} conditions. This is consistent with the degenerate decomposition of gahnite to staurolite + sphalerite (Figure 10.2), which precludes the coexistence of sphalerite and staurolite at the magnetite-pyrite-pyrrhotite triple-point. The incorporation of Zn into staurolite and spinel is interpreted to have enabled the stable coexistence of the anthophyllite-staurolite-gahnite-quartz assemblage within the staurolite-biotite zone of regional metamorphism.

10.3. Cummingtonite-Hornblende Assemblages.

Silicic-feldspathic altered mafic rocks contain the assemblage cummingtonite-hornblende-chlorite-plagioclase-magnetite-quartz and, in the case of 22-413, garnet (*see* Plate 6.1, f). Froese and Moore (1980) proposed the reaction:

$$chlorite + almandine + hornblende + quartz \rightleftharpoons plagioclase + cummingtonite + H_2O,$$

occurring at metamorphic grades slightly in excess of the biotite-staurolite isograd reaction. At the Linda deposit, the garnet contains 0.04–0.09 mole-fraction spessartine, 0.07–0.09 mole-fraction grossular and 0.10–0.13 mole-fraction pyrope. The reaction was apparently divariant, allowing the stable coexistence of the assemblage through a temperature interval. However, this reaction is predicted to occur within the staurolite-biotite zone (*ibid.*) and, therefore, the assemblage is consistent with the grade of the Linda deposit.

10.4. Calc-Silicate Enclave in the Main Massive Sulphide Body.

10.4.1. Mineralogical Zoning and Mineral Chemistry.

The textures of minerals defining the zones in the calc-silicate enclave, particularly symplectic intergrowths and corona overgrowths, indicate post-kinematic crystallization and, by implication, post-kinematic reaction between the calcite-pyrite host rock and the enclave (*see* Plate 5.6, d–p). Synkinematic minerals (*i.e.* chlorite, rutile, biotite, plagioclase and quartz) increase in abundance toward the interior of the enclave and are relict. Zone 6, which consists mainly of relict minerals in the innermost part of the enclave (Table 10.3) as intersected by drilling, does not

Table 10.3. Summary of Assemblages and Mineral Chemistry in Calc-silicate Enclave, 24-1191

	Zone 1	Zone 2	Zone 3	Zone 4	Zone 5	Zone 6
zone width (mm)	host rock	1–4	1–2	6–8	1–6	enclave
$Mg/(Mg+Fe^{+2})$:						
Hornblende			0.725	0.764	0.774	
Actinolite		0.811	0.850			
$Mg/(Mg+Fe_t)$:						
Biotite					0.679	0.657
Chlorite					0.677	0.656
Fe^{+2}/Fe^{+3}:						
Hornblende			1.19	0.887	0.779	
Actinolite		2.05	0.973			
Epidote		Ep_{63-66}	Ep_{56-66}			
Garnet					Alm_{38-43} Pyr_{7-9} Sps_{32-41} Grs_{14-17}	
Plagioclase:						
symplectic			An_{86-91}	An_{72-86}	An_{41-67}	An_{41-54}
relict					An_{29-34}	An_{27-34}
oxide inclusions					ru	ru, gh
Sulphide minerals	py	py	py	py, po	py, po	py, po, sp
structural state (po)				monoclinic	monoclinic, hexagonal	monoclinic, hexagonal
Other minerals	calcite	calcite, ± quartz	quartz	quartz	quartz	quartz

contain muscovite, and in this respect, it contrasts with the mineralogy typical of the proximal alteration zone. The textures, microstructures and mineralogy resemble plagioclase-layered rocks (*see* 5.4. Plagioclase-layered Rocks). The petrographic observations suggest that the enclave is a lithic inclusion or relict of synkinematic minerals, engulfed by the pyrite-calcite host rock.

Assuming that the assemblage within each zone approached equilibrium, the mineral chemistries and parageneses are consistent with amphibolite-facies metamorphism (*e.g.* Bird and Helgeson, 1981). For example, plagioclase rims are at

least as calcic as andesine and, the plagioclase associated with epidote in zone 3 is a bytownite or an anorthite (Table 10.3). Monoclinic pyrrhotite and traces of Fe-rich Cl-bearing chlorite were interpreted to be due to minor late retrogression; the absence of hexagonal pyrrhotite in zone 4 probably reflects the lower abundance and smaller grain size of pyrrhotite in this zone. Across the zoning, from enclave to host rock, hornblende and actinolite decrease in $Mg/(Mg+Fe^{+2})$, mainly as a result of increased Fe^{+2}/Fe^{+3}. This change in amphibole compositions is approximately paralleled by a change in sulphide mineral assemblage from pyrite-pyrrhotite to pyrite and by the appearance of epidote. The general trend to more calcic assemblages and mineral compositions toward the calcite-pyrite host suggests that the zonal sequence cannot be accounted for simply by carbonatization and sulphidation of the enclave, but requires cation exchange.

Calc-silicate enclaves occur locally in the main massive sulphide body, but zone 5 in 24-1191 is the only occurrence of garnet within an enclave. The garnet contains 0.32–0.41 mole-fraction spessartine and .38–0.43 mole-fraction almandine, and in this respect, is similar to garnet analyses from the proximal alteration zone (Table 9.2, g). It is higher in grossular (0.14–0.17 mole-fraction) and slightly lower in pyrope (0.07–0.09 mole-fraction) component. Amphibole increases in Mn content through zones 3 to 5, from 0.085, to 0.108, to 0.125 pfu. Garnet crystallized along a narrow zone with a higher bulk-rock Mn content which was apparently unique to 24-1191 among calc-silicate enclaves. This interpretation is analogous to that for the isolated occurrences of syn-D_1 garnet in the alteration zones (*e.g. see* Plate 9.1, b); however, in the case of the enclave, the garnet appears to occur as post-kinematic pseudomorphs after bladed chlorite and as mantles on pyrrhotite (*see* Plate 5.6, m–n). The garnet and garnet aggregates define a narrow (1–6 mm) band parallel to rutile trails (S_1) in relict plagioclase and to mineral schistosity (S_1); thus, it seems to have crystallized along an S_1 zone of Mn enrichment.

Zone 6 contains zincian minerals, *i.e.* symplectic gahnite with traces of sphalerite as inclusions in plagioclase, and sphalerite as part of the zonal assemblage. The relationships suggest that the sulphidation of gahnite in zone 6 produced the sphalerite associated with pyrite and pyrrhotite in the matrix. In zones 4 to 6, $\log f_{S_2}$ was apparently buffered by pyrite + pyrrhotite, whereas zones 1 to 3 contain only pyrite,

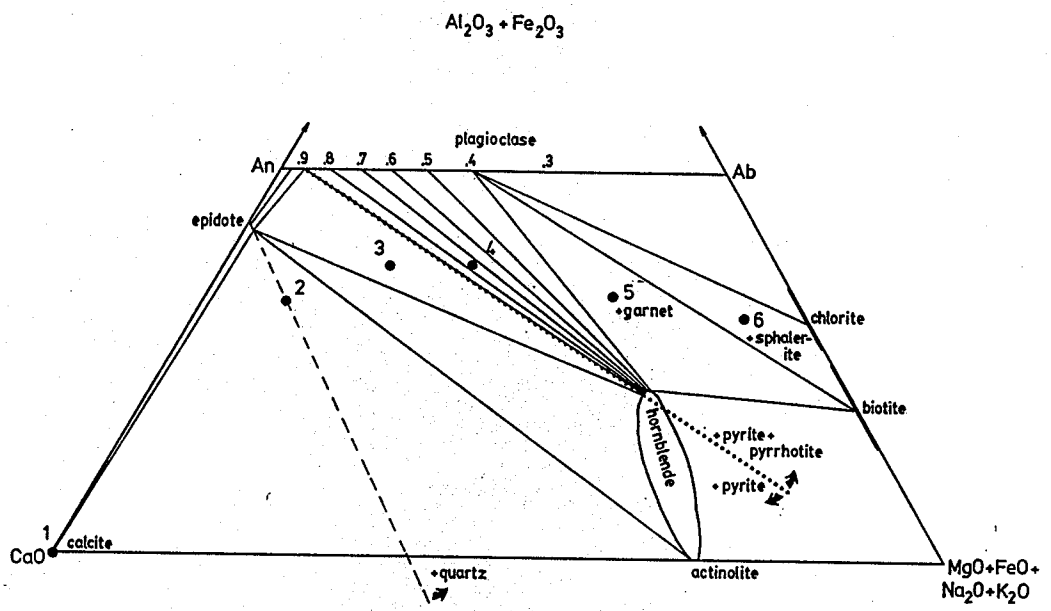

Figure 10.3. Schematic ternary phase diagram for the assemblages in zones 1–6 (numbered dots) of 24-1191. The projection changes across the diagram as indicated by the additional phases. Gradients in $\log f_{S_2}$ are implied by the sulphide mineral assemblages and, in $\log f_{CO_2}$ by the presence of calcite at one apex.

thus recording an increase in $\log f_{S_2}$. The increase in Fe^{+2}/Fe^{+3} in amphibole and the appearance of epidote in the assemblage suggests that the former effect may be partly due to a coupled substitution of the type: $(Mg^{+2},Fe^{+2})Si^{+4} \rightleftharpoons Fe^{+3},Al^{+3}$. The presence of epidote suggests an increase in Fe^{+3} and in $\log f_{O_2}$. The changes in sulphide-oxide-silicate assemblage apparently record gradients of increasing $\log f_{S_2}$, $\log f_{O_2}$ and $\log f_{CO_2}$, and decreasing $\log f_{H_2O}$ toward the host rock. Note however, that only zone 6 contains zincian minerals, and that this may mark a pre-existing zone of high Zn bulk-rock composition, similar to the occurrence of garnet in Mn-rich zones as previously proposed. In other calc-silicate enclaves, inclusions of gahnite in plagioclase and matrix sphalerite occur in association with epidote and amphibole (Plate 5.6, e–f), *i.e.* equivalent to zones 3–4 in 24-1191. Locally, sphalerite occurs with pyrite and calcite, *i.e.* zone 1 or possibly implying a transition zone between 1 and 2 in zincian bulk-rock compositions. In the context of zoning in 24-1191, these observations indicate that the absence of zincian minerals in zones 2–5 is a feature inherited from the protolith of the enclave.

Figure 10.3 is a schematic summary of the changes in mineral assemblages and compositions across the zones of 24-1191. The compositional variations involve more

components and phases than can be accommodated in a thermodynamically valid projection (Greenwood, 1975). The assemblages are illustrated in a modified ACF diagram, with a varying projection indicated by the additional phases. In addition to the changes in fluid composition, Ca becomes proportionately more abundant with respect to other cationic components and, Ca and Fe are the only cations present in major amounts in zone 1. In terms of modelling mineral equilibria, 24-1191 represents a problem in metasomatic mass transfer rather than of isochemical metamorphism of a protolith.

10.4.2. Discussion.

Synmetamorphic mass transfer was an important process during the development of mineralogical zoning along the contacts of silicate enclaves in the pyrite-calcite massive sulphide body. The presence of corona structures and symplectic intergrowths showing fine compositional zoning around inclusions (*i.e.* zoning in plagioclase intergrown with pyrrhotite; Plate 5.6, g–h) suggests that mineral reactions were interface-controlled and thus subject to kinetic factors (Tracy and McLellan, 1983). The fine mineralogical zones apparently attained only partial equilibrium (*ibid.*), in contrast to the rocks of the proximal and distal alteration zones, in which homogeneous equilibrium was generally established on a hand-sample scale. The textures characteristic of calc-silicate enclaves would be difficult to reconcile with the occurrence of mineral reactions along the contact of premetamorphic protoliths of different bulk-rock composition; the fine disequilibrium features would have had to survive the entire P-T-deformation path. Even in the case of post-tectonic recrystallization of calc-silicate minerals and calcite, some memory of the earlier history might be expected, as is observed in relict grains in the interior of enclaves. The observations imply that calcite was introduced synmetamorphically, and that infiltration metasomatism of the protolith was the major mechanism in producing pyrite-calcite rocks.

Some of the enclaves contain relicts resembling plagioclase-layered rocks with rutile trails (*e.g.* 24-1191; *see* Plate 5.6, o–p), the origin and significance of which were previously discussed (*see* 7.1.3. S_1 Rutile Trails *and* 7.5. Relationships to Megascopic Structures and Regional Isograds) with reference to their interpretation as 'Tuttle' deformation lamellae and their unknown relationship to megascopic

tectonic structures. The distribution of plagioclase-layered rocks in unit 4 and in enclaves in the pyrite-calcite body, as well as the relative time relationships inferred from the textures of the zoned contacts, suggests that synmetamorphic infiltration of carbonatizing fluids may have taken advantage of the presence of a pre-existing structure.

In terms of reconstructing synvolcanic alteration, it is critical to discriminate synmetamorphic metasomatism from metamorphism of an altered protolith. At the Linda deposit, the calcite in the largest massive sulphide body is interpreted to have been introduced during metamorphism. However, the disposition of synvolcanic alteration around the body and in the stratigraphic footwall suggests that the sulphide minerals could have been derived from a pre-existing volcanogenic massive sulphide body.

Chapter 11
Whole-Rock Geochemistry

Major and trace elements (of particular importance: Zn, Zr and V), and specific gravity were determined in a suite of 303 samples representing the lithologies and types of alteration observed at the Linda deposit (Appendix C, *see* Table C.5 for a compilation of analyses). In order to facilitate graphical presentation of the data, the units have been grouped on the basis of geochemical characteristics into four broad categories:

1. felsic rocks and silicic-feldspathic altered rocks (units 1, 1a, 1b, 1c, 2/10s, 2b/10s, 2e/10s and 4);
2. the distal and proximal alteration zones (units 1/10d, 1b/10d, 1/10p, 1b/10p, 4/10p, 10d, 10da, 10p, and 10pa);
3. calc-silicate rocks (units 1/10c, 1b/10c, 4/10c, 10i, 2/10e, and 6/10e);
4. mafic to intermediate rocks (units 1d, 2, 2a, 2e, 6, and 6a).

In some cases, the geochemical fields defined by units and subdivisions are outlined on the figures in the following chapter; the field boundaries have no statistical significance and are intended as a visual aid to the presentation. The number of analyses representing each unit or subdivision is indicated in parentheses in the keys to the figures. In some hand samples, lithologically or mineralogically distinct domains were separated for geochemical analysis (*see* Appendix C). These consist of clasts or matrix extracted from breccias, small-scale mineralogical variations which may represent differences in intensity or type of alteration, and bedding in metasediments. Geochemically distinct separates from the same hand sample are linked by dashed tie lines.

Plagioclase-layered rocks characterized by 'Tuttle' deformation lamellae, consisting of rutile trails (*see* 5.4. Plagioclase-layered Rocks), occur in units 1, 4, 1/10p, 4/10p and 10p. These rocks constitute a sub-category, based on microstructural fea-

tures, which transgresses lithological units and alteration types. As in chapters 5 and 6, plagioclase-layered rocks are grouped with the unit in which they occur, but in order to determine whether they have a unique geochemical signature, they have been distinguished by a 'prime' attached to the usual symbol for the unit (*e.g.* o and o').

Many samples, particularly of altered rocks, contain more than 1% S, precluding accurate analysis of FeO and Fe_2O_3/FeO (and H_2O; Appendix C). Samples in which ferrous iron was analysed (with 7 exceptions) contain Fe mainly in the ferrous state. In view of these observations, and to facilitate comparisons, iron is presented either as FeO_t, or as $iv(FeO_t)$; the latter represents total iron after the subtraction of an amount of normative pyrite equivalent to the analysed S content (*see* 11.1.2. Geochemistry of the Proximal and Distal Alteration Zones).

11.1. Summary of Results.

11.1.1. Geochemistry of Felsic Rocks and Silicic-Feldspathic Altered Rocks.

Felsic volcanic rocks of units 1 and 4 envelop the distal and proximal alteration zones and represent the main host rock and precursor to alteration (*see* 5.1. Location and Relationships to Stratigraphy). These rocks were defined as 'least altered', based mainly on the absence of kyanite, staurolite and gahnite, and the presence of only minor amounts of sulphide and calc-silicate minerals. Excluding intermediate to mafic intercalations (1d), the rocks of unit 1 range in SiO_2 from 60.6–86.9%, with 'cherty' felsic rocks (1a and 1c) constituting the high end of the range, *i.e.* from 72.4–83.6% with one analysis at 65.9% SiO_2 (Figure 11.1, a). Four felsic clasts extracted from matrix-supported breccias (1b) are similar or higher in SiO_2 to units 1a and 1c, *i.e.* 81.3–86.9%. There is no well defined correlation between SiO_2 and total alkali content. Cherty felsic rocks have a bimodal distribution; the samples with the highest SiO_2 content (*i.e.* 78.7–83.6%) also have the highest alkali content (5.0–7.1%). Alkalis in other cherty felsic rocks range from 2.2–5.5%. In general, the alkali content is mainly Na_2O (Figure 11.1, b). Among cherty felsic rocks (1a and 1c), only one sample contains K_2O in excess of 1.3% (I3-42-5), and in the high silica-high alkali subgroup, K_2O is always less than 0.3%. All samples of unit 1c (clast-supported 'cherty' breccias) fall in the high silica-high alkali subgroup, with

the exception of one strongly mineralized sample (34-1443.5-2; *see* Plate 5.3, a–b). A clast extracted from the same breccia sample (34-1443.5-1) falls into the high silica-high alkali subgroup. (Figure 11.1, a; note the tie line linking '×' symbols.) Despite their high silica contents, felsic clasts extracted from unit 1b have total alkali, K_2O and CaO contents comparable to the lower silica subgroup (Figure 11.1, a–b). Na_2O was not detected in two samples of unit 1; these occur on the periphery of the distal alteration zone, but texturally and mineralogically resemble biotite-layered rocks with relatively low modal abundances of calcic plagioclase (*i.e.* 10 and 30%). Geochemically, they have the features of the distal alteration zone (*see* 11.1.2. Geochemistry of the Proximal and Distal Alteration Zones).

Unit 4 ranges in SiO_2 from 51.2–78.2%; however, excepting 3 analyses, the other 19 samples have more than 66% SiO_2 (Figure 11.1, a). The lowest SiO_2 occurs in a sample extracted from the weakly mineralized matrix of a breccia (34A-1644.5-2); a clast extracted from the same sample contains 78.2% SiO_2 (34A-1644.5-1). (Figure 11.1, a; note the tie line linking $*$' symbols.) Both clast and matrix are characterized by rutile trails. Total alkali levels in unit 4 vary from 1.8–6.8%, encompassing almost the entire range of the felsic rocks of unit 1. Unit 4 generally has higher K_2O/Na_2O than unit 1 and CaO/Na_2O similar to hornblende-bearing rocks of unit 1 (Figure 11.1, b). Plagioclase-layered rocks tend to show some of the most potassic and calcic compositions.

Rocks which were identified on outcrop or in drill core as bleached mafic rocks contain 63.9–71.2% SiO_2, the most siliceous being a sample (H9-52-1) from the core of a bleached pillow (Figure 11.1, a; *see* Plate 6.1, c). Bleached mafic rocks have total alkali contents similar to those of felsic rocks (*i.e.* 3.2–5.4%), likewise consisting predominantly of Na_2O (*i.e.* 3.1–5.0%; Figure 11.1, b). They are more calcic than most felsic rocks of similar silica content, and slightly higher in CaO/Na_2O than felsic rocks of similar soda content.

Both the high silica-high alkali subgroup of 'cherty' felsic rocks and the clasts extracted from unit 1b have MgO contents near or below the detection limit (Figures 11.2 and 11.3). Cherty felsic rocks range in FeO_t from 0.18–8.73%, and the values show some correlation with S content (Table C.5) in samples which contain sulphide minerals. Figures 11.2 and 11.3 illustrate FeO_t 'corrected' by the subtraction of

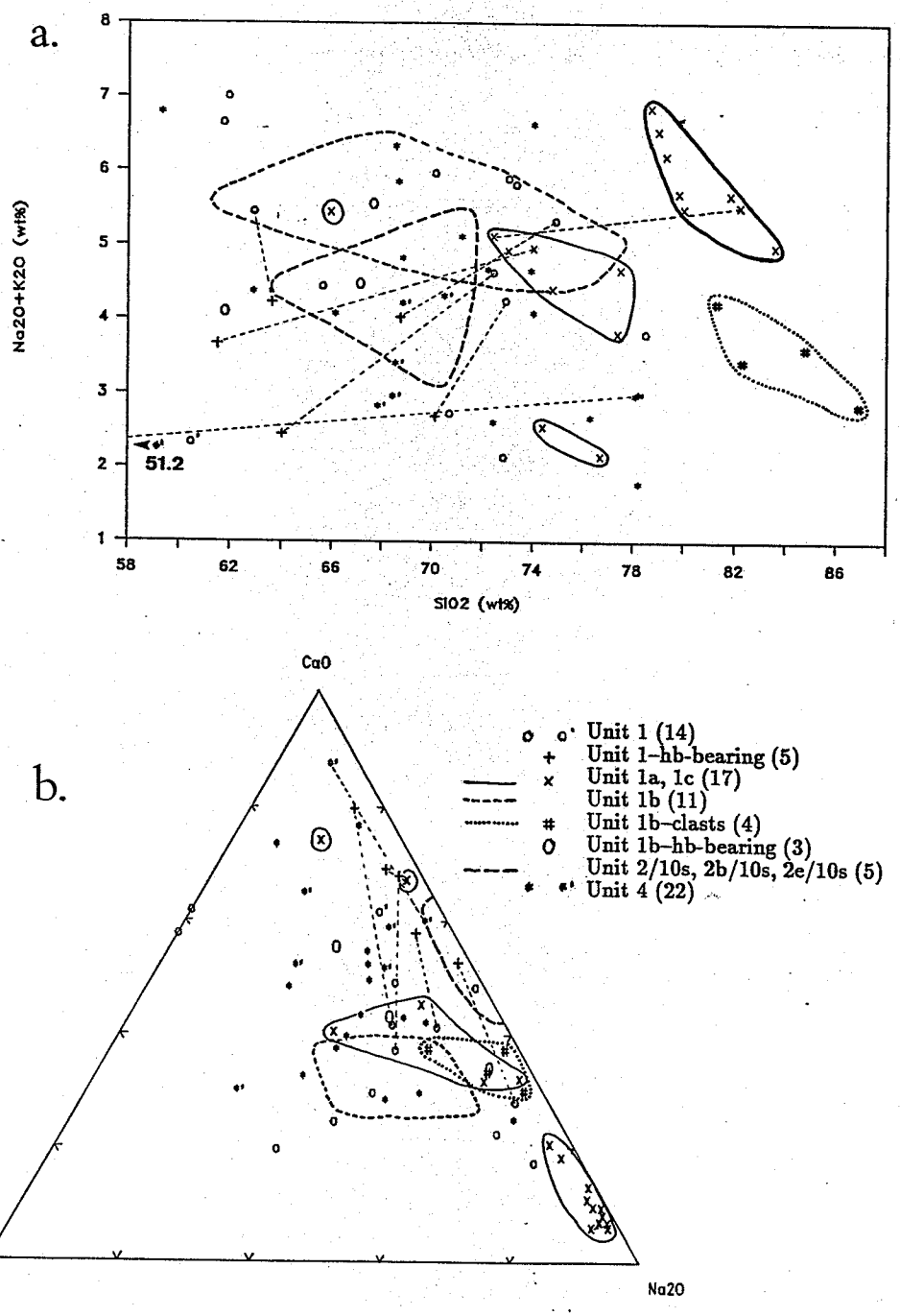

Figure 11.1. Alkalis, SiO_2 and CaO in felsic rocks and silicic-feldspathic altered rocks.

a. Total alkalis (Na_2O+K_2O weight%) as a function of SiO_2 (weight%). The high silica-high alkali subgroup of units 1a and 1c is highlighted by a thick field boundary.

b. K_2O-CaO-Na_2O (molar) ternary proportions.

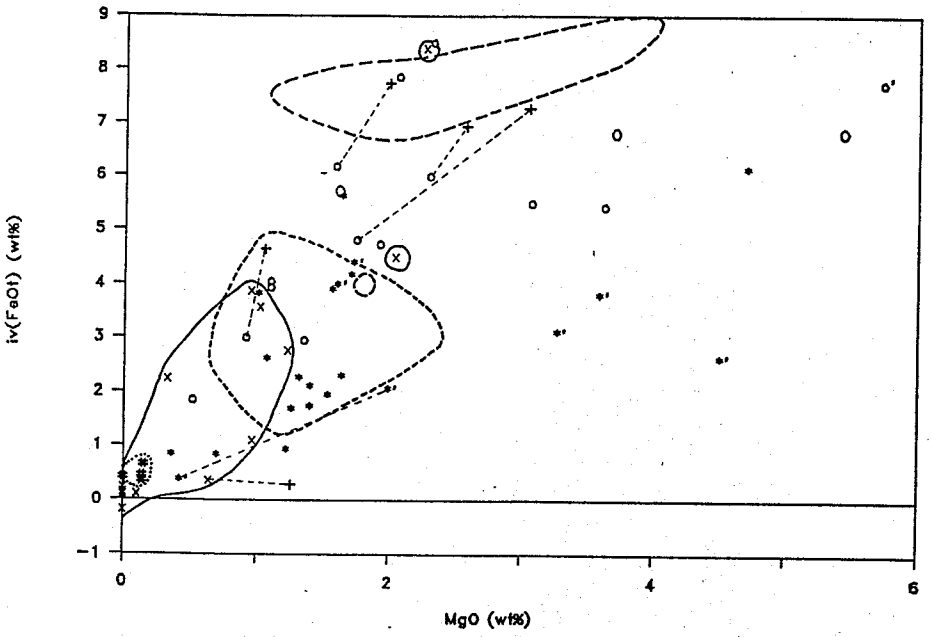

Figure 11.2. $iv(FeO_t)$ (weight%) as a function of MgO (weight%) in felsic and silicic-feldspathic altered rocks. $iv(FeO_t)$ is the iron content after the subtraction of normative FeS_2 from the analysis. The key is same as in Figure 11.1.

normative FeS_2 (*see* 11.1.2. Geochemistry of the Proximal and Distal Alteration Zones). The remaining iron, $iv(FeO_t)$, is presumably fixed mainly in magnetite and silicate minerals. Clasts extracted from unit 1b have FeO_t contents of less than 1%.

In terms of both MgO and $iv(FeO_t)$, felsic volcaniclastic rocks of unit 1b define a more restricted range than units 1 or 4 (Figure 11.2). In general, units 1 and 4 are compositionally dispersed. The S contents are mainly low and, hence, the subtraction of normative FeS_2 has little influence on iron content. However, some plagioclase-layered rocks with 'Tuttle' lamellae contain minor amounts of sulphide minerals and, with the subtraction of normative pyrite, they tend to form a more coherent trend of $iv(FeO_t)$/MgO ratios below those of the rest of the suite. (Note the symbols with 'prime' superscripts.) Bleached mafic rocks (2/10s, 2b/10s, 2e/10s) contain S near or below the detection limit (0.04%, Table C.1) and lie at high $iv(FeO_t)$/MgO values, but still overlap the fields of felsic rocks.

Hornblende-bearing zones were extracted from the typical biotite-layered felsic rocks of unit 1 and from cherty rocks (1a). In most cases, the hornblende-bearing separates show lower silica than the host rock and, in all cases, have higher MgO and $iv(FeO_t)$ (Figures 11.1 and 11.2). Hornblende-bearing samples of unit 1b overlap

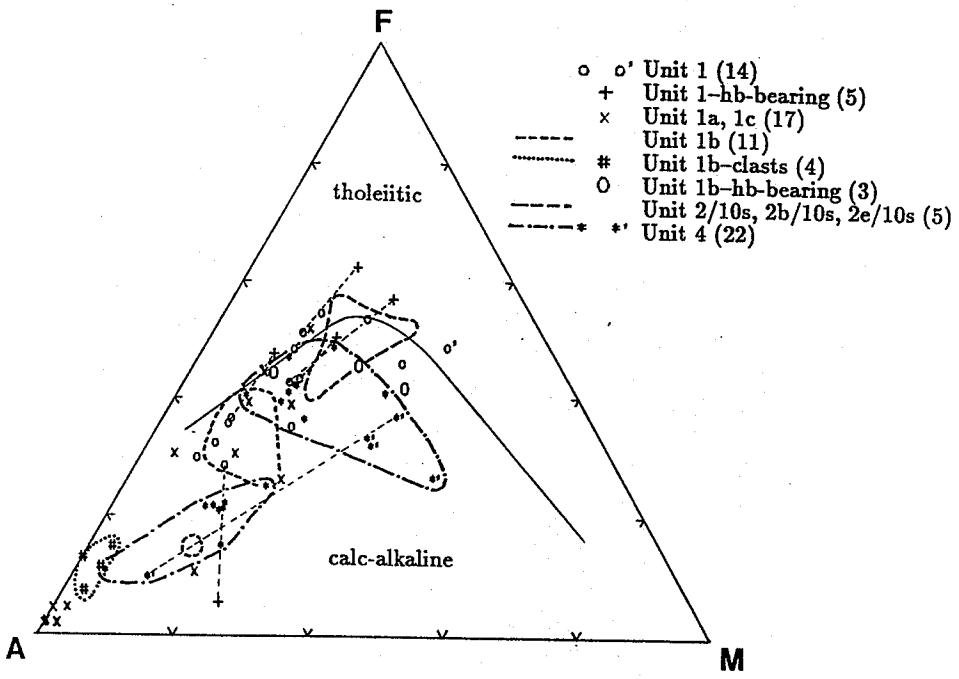

Figure 11.3. AFM diagram (weight proportions) for felsic and silicic-feldspathic altered rocks. A=Na_2O+K_2O, F=$iv(FeO_t)$, M=MgO. Calc-alkaline and tholeiitic boundary from Irvine and Barager (1971).

the low silica end of the field defined by the unit and are generally higher in MgO and FeO_t. Hornblende-bearing separates from unit 1 show a weak tendency to higher CO_2 (0.1–3.2%) than other hornblende-bearing samples (0.1–0.2%) and, higher CO_2 than unit 1 (0–1.1%). A textural correlation is apparent in that the hornblende in the high-CO_2 rocks consists of statically crystallized acicular prisms and shows leucocratic halos to the biotite layering (*see* 3.1. Description of Lithological Units). Two hornblende-bearing samples of unit 4 consistently plotted within the fields defined by other samples of the same unit and were not distinguished from the rest of the unit.

The AFM diagram (Figure 11.3) summarizes some of the geochemical features discussed above. The felsic rock units lie mainly within the calc-alkaline field (Irvine and Barager, 1971), with overlap into the tholeiitic field mainly confined to hornblende-bearing felsic rocks and altered mafic rocks. The high silica-high alkali subgroup of cherty felsic rocks, as well as clasts from unit 1b, lie near the alkali apex of the triangle. The low $iv(FeO_t)$/MgO ratio of plagioclase-layered rocks places them well into the calc-alkaline field. (Note 'prime' superscripts.)

Figure 11.4 illustrates the overall positive correlation between TiO_2 and Al_2O_3.

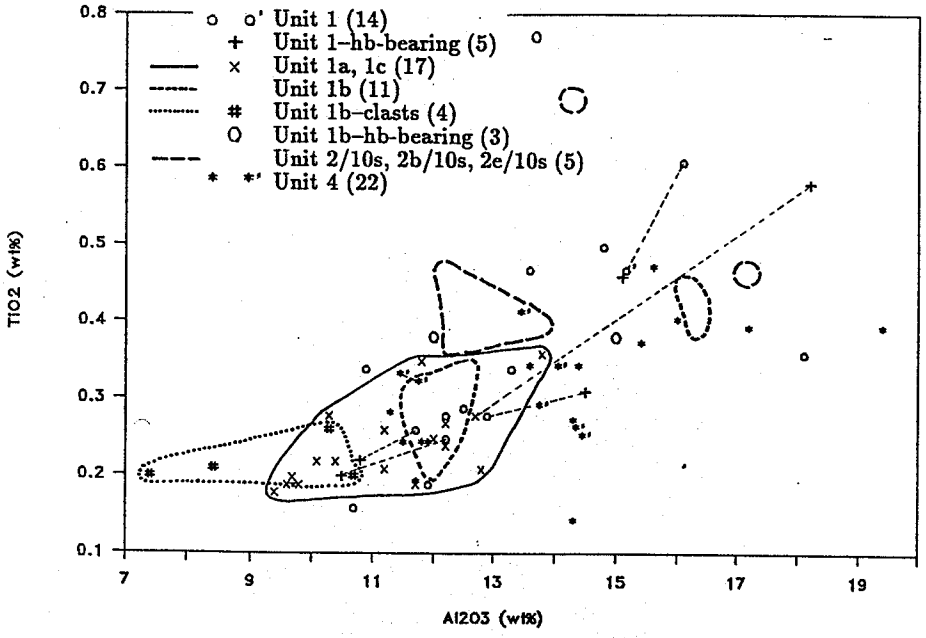

Figure 11.4. TiO_2 (weight%) as a function of Al_2O_3 (weight%) in felsic and silicic-feldspathic altered rocks.

Despite the occurrence of abundant rutile trails, plagioclase-layered rocks cannot be distinguished from other felsic rocks on the basis of whole-rock TiO_2 values. Bleached mafic rocks (2/10s, 2b/10s, 2e/10s) tend to have slightly elevated TiO_2; however, a large degree of overlap with felsic rocks is apparent.

Felsic rocks at the Linda deposit have low values of log Zr/TiO_2 (Figure 11.5, a). For example, units 1a and 1c, which fall in the rhyolite field of Floyd and Winchester (1977) in terms of SiO_2, have only slightly higher log Zr/TiO_2 than units 1 and 4, which lie mainly in the field of dacites and rhyodacites. Altered mafic rocks have significantly lower log Zr/TiO_2 than the felsic rocks; they have SiO_2 levels of dacites and rhyodacites, but log Zr/TiO_2 indistinguishable from the mafic rocks of unit 2 with which they are associated (*see* Figure 11.19, a).

Most samples of unit 4 contain vanadium in excess of 20 ppm, regardless of their major-element composition (Figure 11.5, b). Vanadium is similarly high in samples of unit 1 from the same stratigraphic position as unit 4, *i.e.* high in the stratigraphy either as intercalations or immediately below unit 4. The 3 samples of unit 4 which contain less than 10 ppm V occur as isolated enclaves of quartz-megaphyric felsic rocks at other stratigraphic levels. One sample (80-1138-1) originates from below the distal alteration zone, and 2 samples (34-1834.5-1, 31-989.5-1) represent

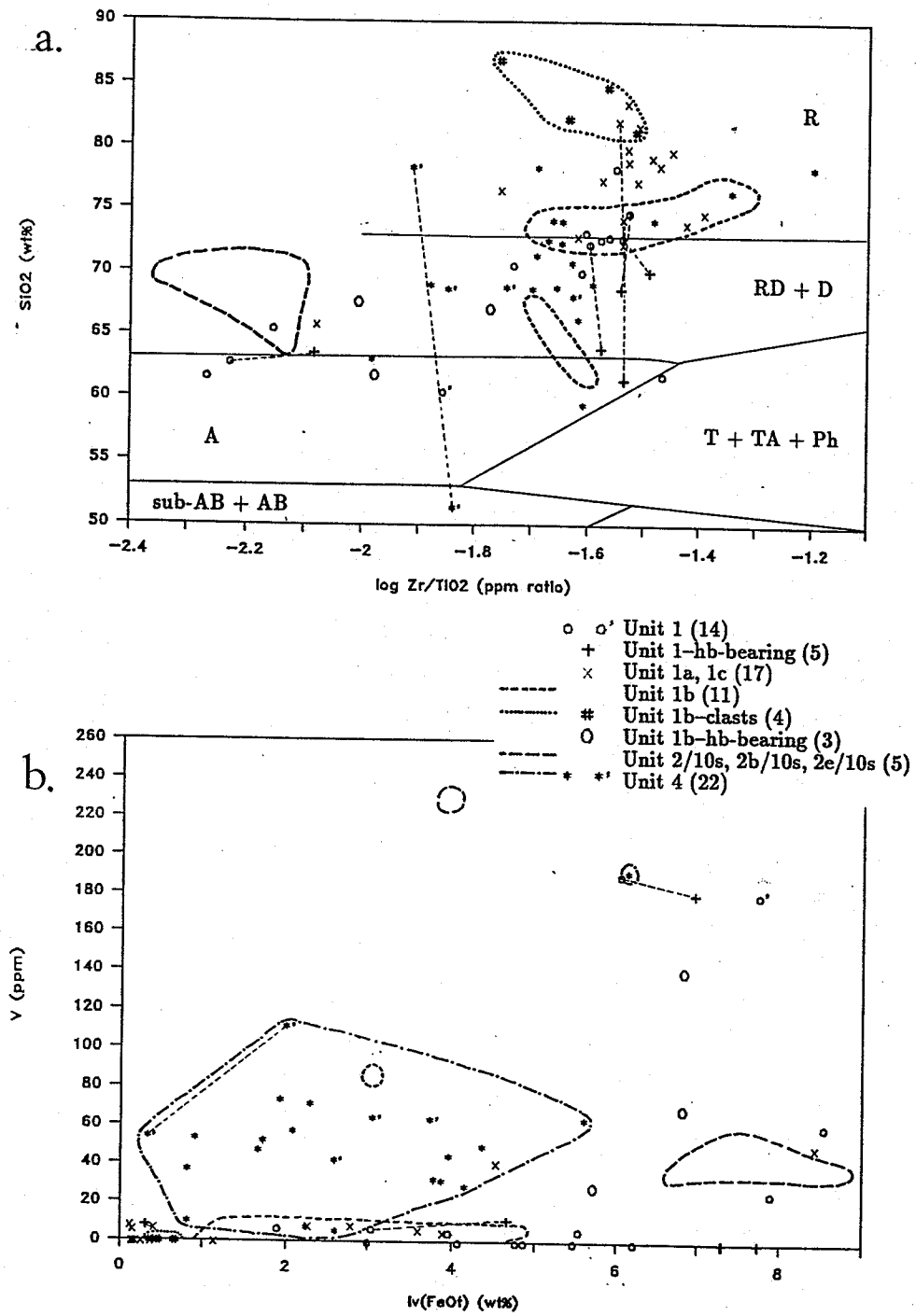

Figure 11.5. Trace-element signature of felsic and silicic-feldspathic altered rocks.

a. SiO_2 (weight%) as a function of log Zr/TiO_2 (ppm ratio). Field boundaries from Floyd and Winchester (1977). Abbreviations: R=rhyolite, D=dacite, RD=rhyodacite, A=andesite, AB=alkali basalt, T=trachyte, TA=trachy-andesite, Ph=phonolite.

b. V (ppm) as a function of $iv(FeO_t)$ (weight%).

intercalations of unit 4 in the overlying intermediate to mafic rocks of unit 6. The V-rich felsic rocks overlie the mafic rocks of unit 2 and, laterally and down-dip, an abrupt contact with underlying felsic rocks of low ($\leq$15 ppm) V apparently passes through the upper part of the proximal alteration zone (*see* Figure 11.20 *and* 11.2.2. Vanadium and Zr/TiO_2 in Quartz-megaphyric Felsic Rocks). Note that the high V levels also occur in all surface samples of unit 4, along-strike to the northeast and on the northwest side of the Anderson Bay structure, as well as in the single sample of the quartz-megaphyric rocks of unit 7 (J8-23-1; Table C.5). Silicified mafic rocks typically contain V at levels similar to those of unit 4.

11.1.2. Geochemistry of the Proximal and Distal Alteration Zones.

Geochemical samples from the proximal and distal alteration zones include the following units: incipiently altered felsic rocks (1/10d, 1b/10d, 1/10p, 1b/10p); altered quartz-megaphyric rocks (4/10p); muscovite-staurolite-gahnite schists (10pa, 10da); and the predominant schists of the alteration zones (10d, 10p). Note that unit 4/10p includes intensely altered rocks and that the precursor lithology is recognizable by virtue of the resistance of quartz megacrysts to alteration and deformation. The samples range in silica content from 31.9–83.0% (Figure 11.6, a). Two samples of selvedges to quartz veins (24-277.5-1, 80-1571.5-1; Table C.5) in the distal alteration zone have silica contents which are significantly lower than the rest of the zone, *i.e.* 31.9 and 52.4% as compared to a minimum of 67.8% in other samples of the distal zone. The selvedge samples are chemically anomalous in most major elements and were treated as a subgroup. The proximal alteration zone generally shows a wider compositional range than the distal zone, and this broad spectrum can, in part, be related to the greater variety of primary lithological types. Most of the samples defining the low silica end of the range (*i.e.* $\leq$55%) are mineralized metasediments in the proximity of the graphitic metasediment (unit 3) and are associated with massive sulphide bodies. For example, three separates extracted from 24-812 (note linking tie lines) represent different beds defined by changes in the abundance of pyrite, kyanite, tourmaline and phyllosilicate minerals (*see* Plate 5.3, f). If these metasediments formed as primary sulphidic chemical sediments, they did not require a precursor to act as a substrate for alteration. If they formed by hydrothermal alteration of a pre-existing sediment or tuff, then their precursor

lithology has not been identified.

Altered rocks in the distal alteration zone have lower Na_2O+K_2O than the proximal zone and are characterized by low contents of Na_2O and CaO (Figure 11.6, a and b). Most samples from the distal zone have Na_2O below the detection limit (0.5%, Table C.1). In most cases, samples with slightly elevated contents of CaO (*i.e.* $\geq$.50%) contain either margarite or garnet. The single sample from the distal zone which has 2.9% Na_2O and 1.80% CaO (80-1176-1) has undergone retrogression and contains sericitic pseudomorphs of porphyroblastic minerals. Samples from the periphery of the zone (unit 1/10d) have higher levels of Na_2O and K_2O.

Both the distal and proximal zones contain similar levels of K_2O; however, the proximal zone extends to higher values of up to 3.49%. The proximal zone is significantly more sodic and more calcic, showing little compositional overlap with the distal zone; this might be expected from the modal abundance of paragonitic muscovite and plagioclase in the former, as opposed to chlorite in the latter (Table A.1). Within the proximal zone, 3 separates from metasediment sample 24-812 are notably high in Na_2O. Other low silica samples (those with less than 68% SiO_2), including some metasediments, contain more than 2.5% K_2O and have Na_2O and CaO generally comparable to that of most other samples from the zone. Rocks of units 4/10p, 1/10p and 1b/10p tend to have higher proportions of CaO than unit 10p (Figure 11.2, b). Plagioclase-layered rocks with rutile trails ('prime' superscript) tend to have the highest levels of CaO and comprise most of the samples plotting above a molar ratio of $CaO/K_2O=2$.

Units 10da and 10pa define a combined trend from 62.4–82.1% SiO_2 at low CaO and moderately low Na_2O (Figure 11.6). K_2O occurs mainly in the range of 0.5–3.5%. These core units in each alteration zone appear to form a chemically coherent group apparent in most of the variation diagrams. In the distal zone, unit 10da is enriched in Na_2O with respect to most of the enveloping altered rocks.

The distal alteration zone contains significantly higher levels of MgO than the proximal zone, with very little overlap at equivalent levels of SiO_2 (Figure 11.7). The core zones (10da, 10pa) are distinguished by relatively low MgO independent of SiO_2, and by a narrow range of FeO_t negatively correlated with SiO_2. As might be predicted from the occurrence of gahnite, the core zones show high values of Zn

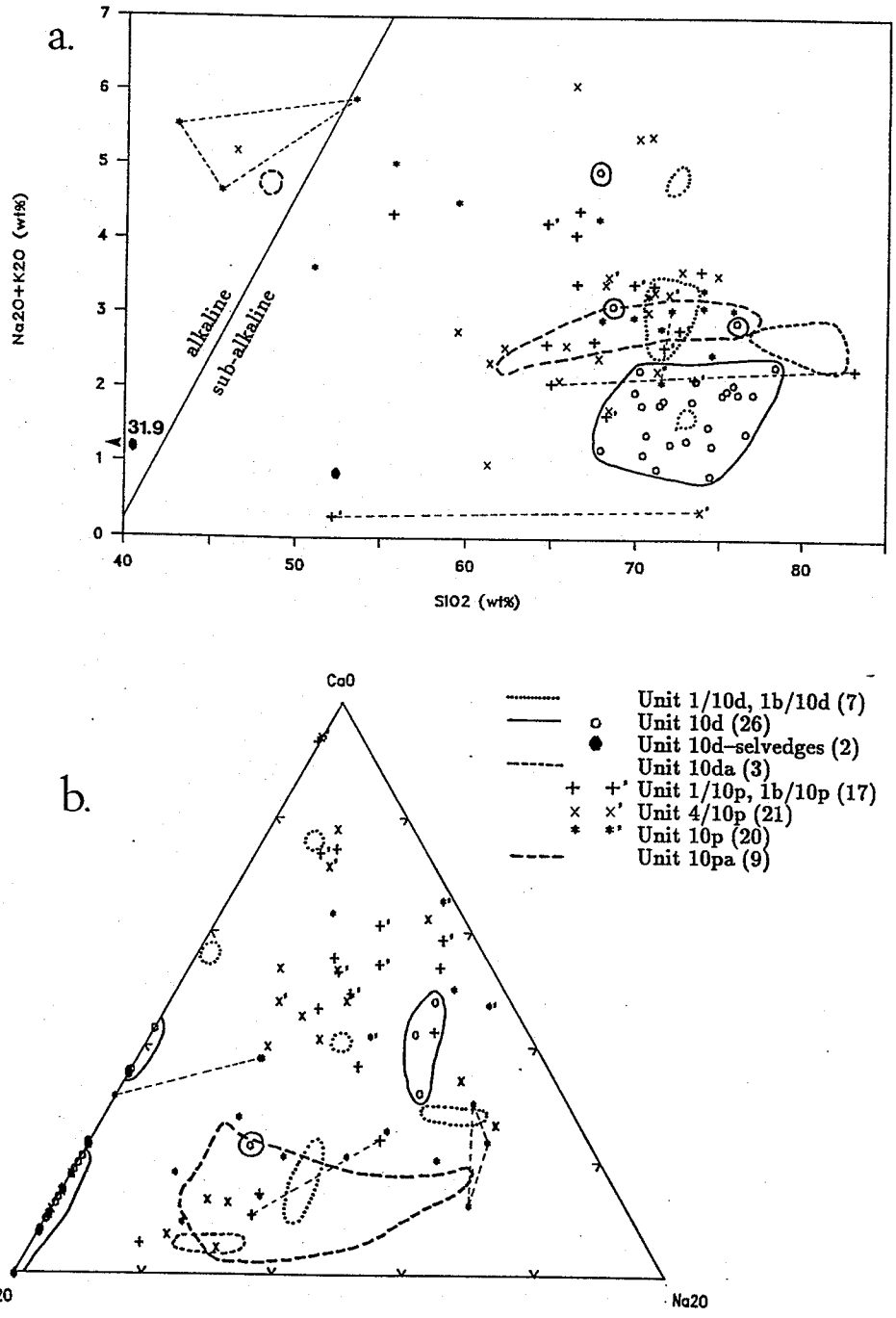

Figure 11.6. Alkalis, SiO_2 and CaO in the distal and proximal alteration zones.

a. Total alkalis (Na_2O+K_2O weight%) as a function of SiO_2 (weight%). Alkaline and sub-alkaline boundary from Irvine and Barager (1971).

b. K_2O-CaO-Na_2O (molar) ternary proportions.

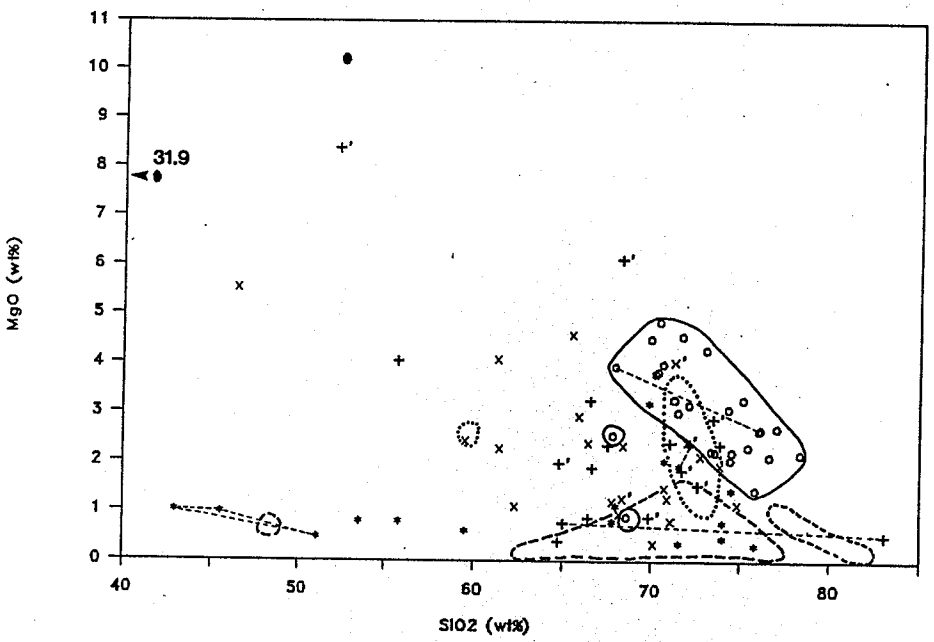

Figure 11.7. MgO (weight%) as a function of SiO_2 (weight%) in the distal and proximal zones. The key is the same as in Figure 11.6.

(Figure 11.8, a), from 1500 to more than 10000 ppm in 10pa, and at least 900 ppm in 10da. Two samples of unit 10p plotting within the field of 10pa are enveloped (physically) by 10pa, but contain either sphalerite or zincian staurolite, rather than gahnite. As determined by microprobe mineral analyses (*see* 9.1.3. Staurolite and Gahnite), many altered rocks contain zincian staurolite, and this is reflected in slightly higher Zn contents of the whole-rock samples.

Much of the FeO_t in altered rocks, particularly in the proximal alteration zone, occurs in sulphide minerals (Table A.1). Geochemically, this is reflected in a general positive correlation between FeO_t and S shown by the units (Figure 11.8, b). Units 10d and 1/10d do not show a trend, consistent with the petrographic observation that most of their Fe occurs in silicate minerals or (less commonly) in magnetite. Superimposed on Figure 11.8b are lines for FeS_2 and FeS, representing the compositions of stoichiometric pyrite and triolite. Samples lying on the pyrite line could have their entire Fe and S contents accounted for by pyrite, especially as sulphide minerals containing base metals other than Fe are not abundant. For example, this suggests that the difference in Fe and S between the clast (22A-1752-2) and the mineralized breccia (22A-1752-1) from which it was extracted (*see* Plate 5.3, c), could be due mainly to different abundances of pyrite. (Figure 11.8, b; note the tie

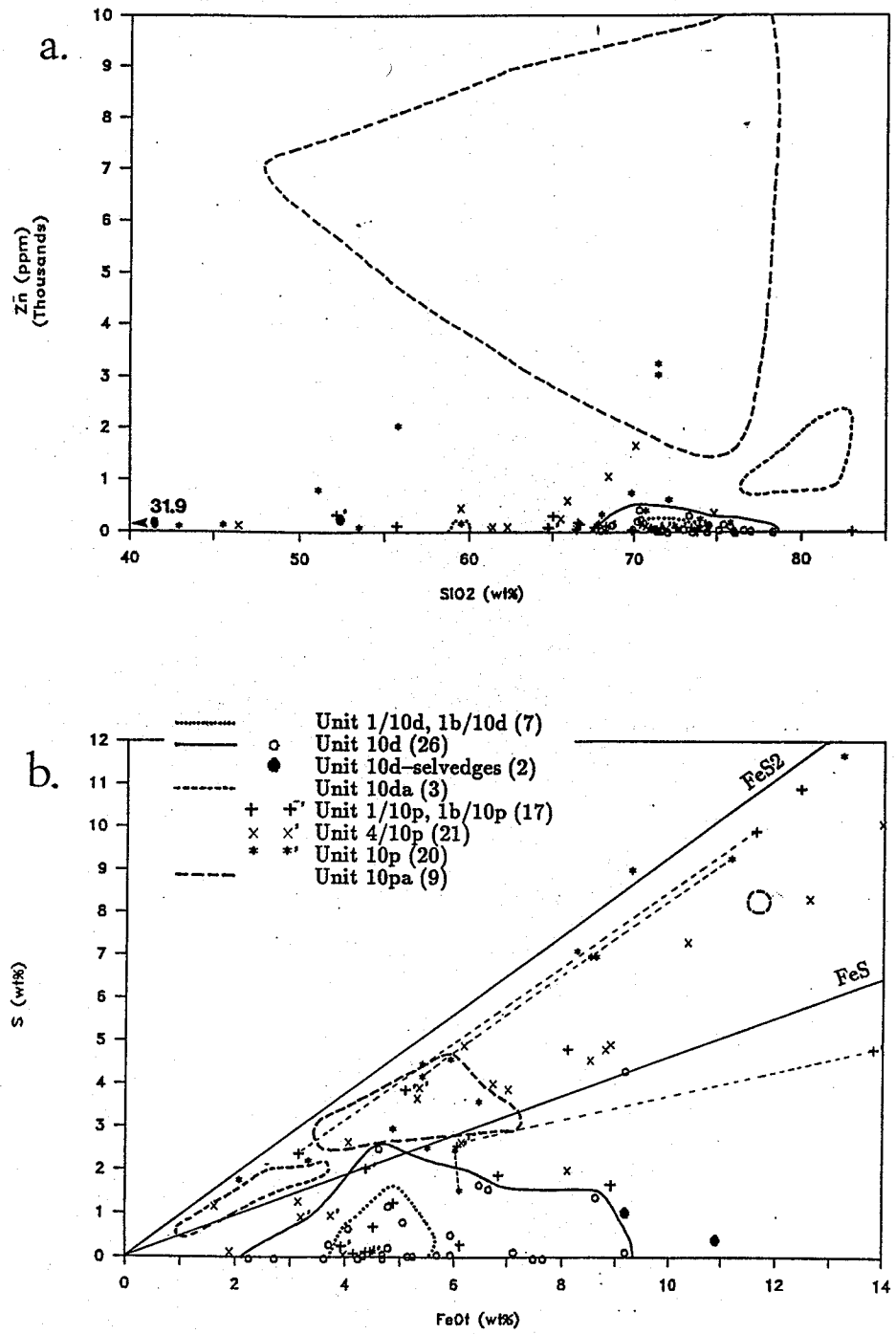

Figure 11.8. FeO_t, Zn and S in the distal and proximal zones.

a. Zn (1000 ppm) as a function of SiO_2 (weight%). The muscovite-gahnite-staurolite bearing core zones of the proximal (10pa, long dashes) and distal (10da, short dashes) alteration zones contain high levels of Zn.

b. S (weight%) as a function of FeO_t (weight%). Lines equivalent to FeS_2 and FeS are indicated.

line linking '+' symbols.) Samples lying above the pyrite line contain S in excess of that which could be combined with Fe in a 2:1 molar ratio, probably due to analytical error. (The calibration limit for S was 3% (Table C.1); therefore the high values may be inaccurate.) Samples below the pyrite line could have their FeO_t contents fixed in a combination of sulphide, silicate, and oxide minerals. Samples which can be linked by a tie line with the same slope as the pyrite line could have the difference in their Fe and S contents accounted for by different normative abundances of pyrite. This suggests that it may be useful to project to an intercept value on the x-axis by subtracting S and Fe equivalent to normative pyrite from the analyses. This effectively compensates for the compositional dependency between Fe and S, especially in view of the observed dominance of modal pyrite over other sulphide minerals in the suite. The Fe-intercept value, $iv(FeO_t)$, thus derived shows little or no correlation with SiO_2, in contrast to the negative correlation shown by FeO_t. The zincian core zones have $iv(FeO_t)$ mainly between 0 and 2 (FeO_t ranges from 1–12.5), suggesting that the difference in FeO_t between and within 10pa and 10da can be attributed to variations in the abundance of pyrite. The distal zone (10d) has higher values of $iv(FeO_t)$ than the proximal zone (10p) at equivalent SiO_2 and, the values of $iv(FeO_t)$ in the distal zone are generally only slightly lower than the values of FeO_t. This reflects the generally low S and sulphide mineral contents typical of the distal zone. In contrast, the proximal zone has notably lower $iv(FeO_t)$ than FeO_t, and some samples, particularly metasediments and other low silica samples, tend to cluster near zero.

Figure 11.9 compares the relationship between FeO_t and MgO with that between $iv(FeO_t)$ and MgO in the altered rocks. FeO_t shows essentially no correlation with MgO; in contrast, the intercept value, $iv(FeO_t)$, shows a positive correlation with MgO. The $iv(FeO_t)$ intercept value is effectively an estimate of the amount of Fe in the bulk rock available to silicate and oxide minerals. The distal and proximal zones are similar in $iv(FeO_t)$/MgO, but the distal zone is enriched in both $iv(FeO_t)$ and MgO with respect to the proximal zone. Note also that the field of the distal zone is similar in absolute value and shape in both figures (Figure 11.9, a and b), and the positive correlation (Figure 11.9, b) is entirely due to the shift of the proximal zone (especially of high FeO_t samples) toward zero. The zincian core

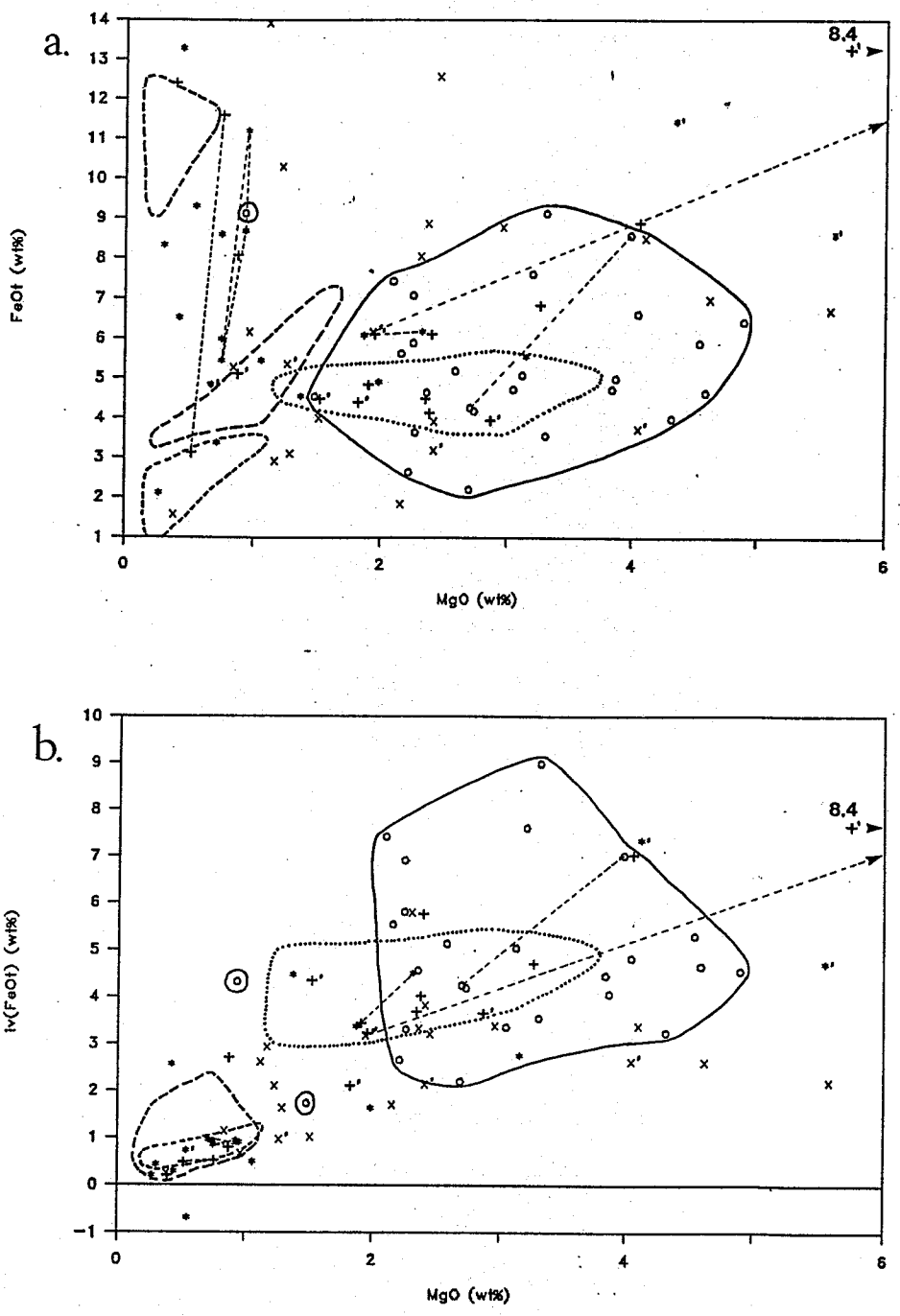

Figure 11.9. FeO_t, $iv(FeO_t)$ and MgO in the distal and proximal zones. The key is the same as in Figures 11.8 and 11.10. The selvedge samples lie at values beyond the range of the figures.

a. FeO_t (weight%) as a function of MgO (weight%).

b. $iv(FeO_t)$ (weight%) as a function of MgO (weight%). $iv(FeO_t)$ is the iron content after the subtraction of normative FeS_2 from the analysis.

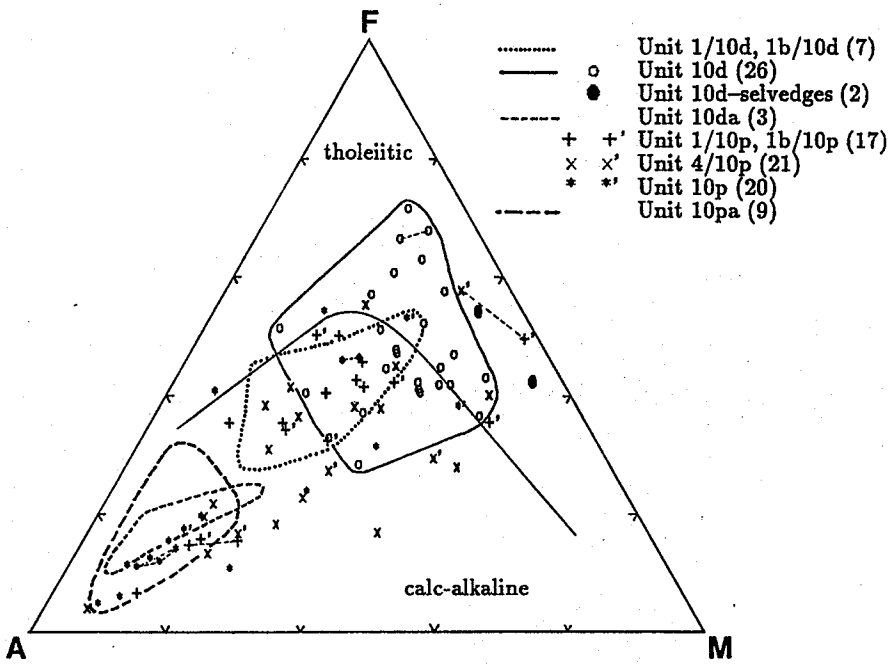

Figure 11.10. AFM diagram (weight proportions) in the distal and proximal zones. A=Na_2O+K_2O, F=$iv(FeO_t)$, M=MgO. Calc-alkaline and tholeiitic boundary from Irvine and Barager (1971).

zones (10da, 10pa) are chemically indistinguishable when 'corrected' for normative pyrite. Note that they shift from FeO_t-rich compositions (Figure 11.9, a) to compositions clustering near or below a molar ratio of $iv(FeO_t)$/MgO=1 (Figure 11.9, b).

Figure 11.10 illustrates the relationships of altered rocks in terms of AFM components, with the F-apex represented by $iv(FeO_t)$. The subtraction of normative pyrite from the analyses shifts most of the altered rocks, especially those of the proximal zone, into the calc-alkaline field. Many analyses of the distal zone, including the 2 selvedge samples, lie within the tholeiitic field. The distal zone straddles the field boundary between tholeiitic and calc-alkaline and does not show systematic variations. In contrast, the proximal zone approximates a 'calc-alkaline' trend and the zincian core zones (10pa, 10da) show high proportions of alkalis.

TiO_2 and Al_2O_3 in altered rocks generally define a positive correlation with considerable scatter, particularly at high levels of TiO_2 and Al_2O_3 (Figure 11.11). The single analysis from the distal alteration zone with 0.57% TiO_2 was derived from the sample which had undergone retrogression (80-1176-1). Plagioclase-layered rocks with rutile trails show both high and low values of TiO_2 and TiO_2/Al_2O_3.

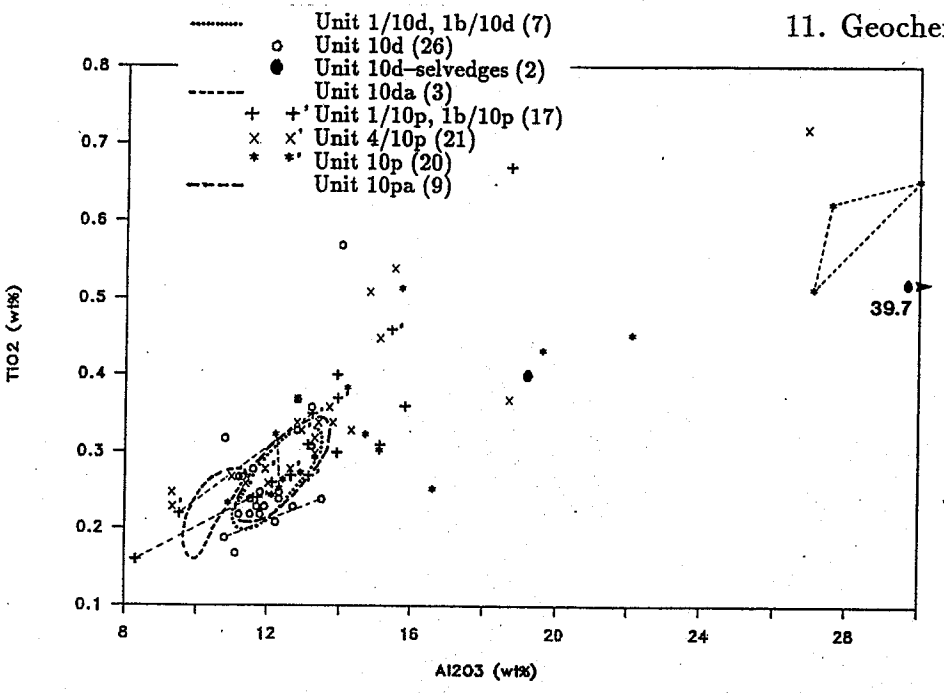

Figure 11.11. TiO_2 (weight%) as a function of Al_2O_3 (weight%) in the distal and proximal zones.

Low silica metasediments have high values of Al_2O_3 and define a trend of positively correlated TiO_2 and Al_2O_3.

Log Zr/TiO_2 ranges from about -1.8 to -1.4 in the distal alteration zone (Figure 11.12, a), approximately coincident with the range of felsic rocks of units 1, 1a, 1b and 1c (*compare* Figure 11.5, a). Selvedge samples lie within the same range of log Zr/TiO_2, albeit at much lower values of SiO_2. Units 10p and 1/10p of the proximal zone have log Zr/TiO_2 mainly from -1.65 to -1.4, with some samples showing higher or lower ratios. The zincian core zones define the narrowest range of log Zr/TiO_2, from -1.6 to -1.45. Significantly lower ratios of log Zr/TiO_2 (mainly from -2.1 to -1.6) are found in quartz-megaphyric rocks of unit 4/10p, showing little overlap with the rocks of the proximal zone. The samples of units 1/10p and 10p having log Zr/TiO_2 similar to that of unit 4/10p (less than -1.6) are all closely associated with 4/10p, originating from the same stratigraphic level.

Vanadium in altered rocks shows the same correlation with stratigraphy as noted for felsic rocks. Relatively high levels of V (in excess of 20 ppm, Figure 11.12, b) occur throughout unit 4/10p and in samples of units 10p and 1/10p from the same stratigraphic position. V enrichment shows a correlation with low values of log Zr/TiO_2, *i.e.* all samples with more than 20 ppm V have log Zr/TiO_2 of less

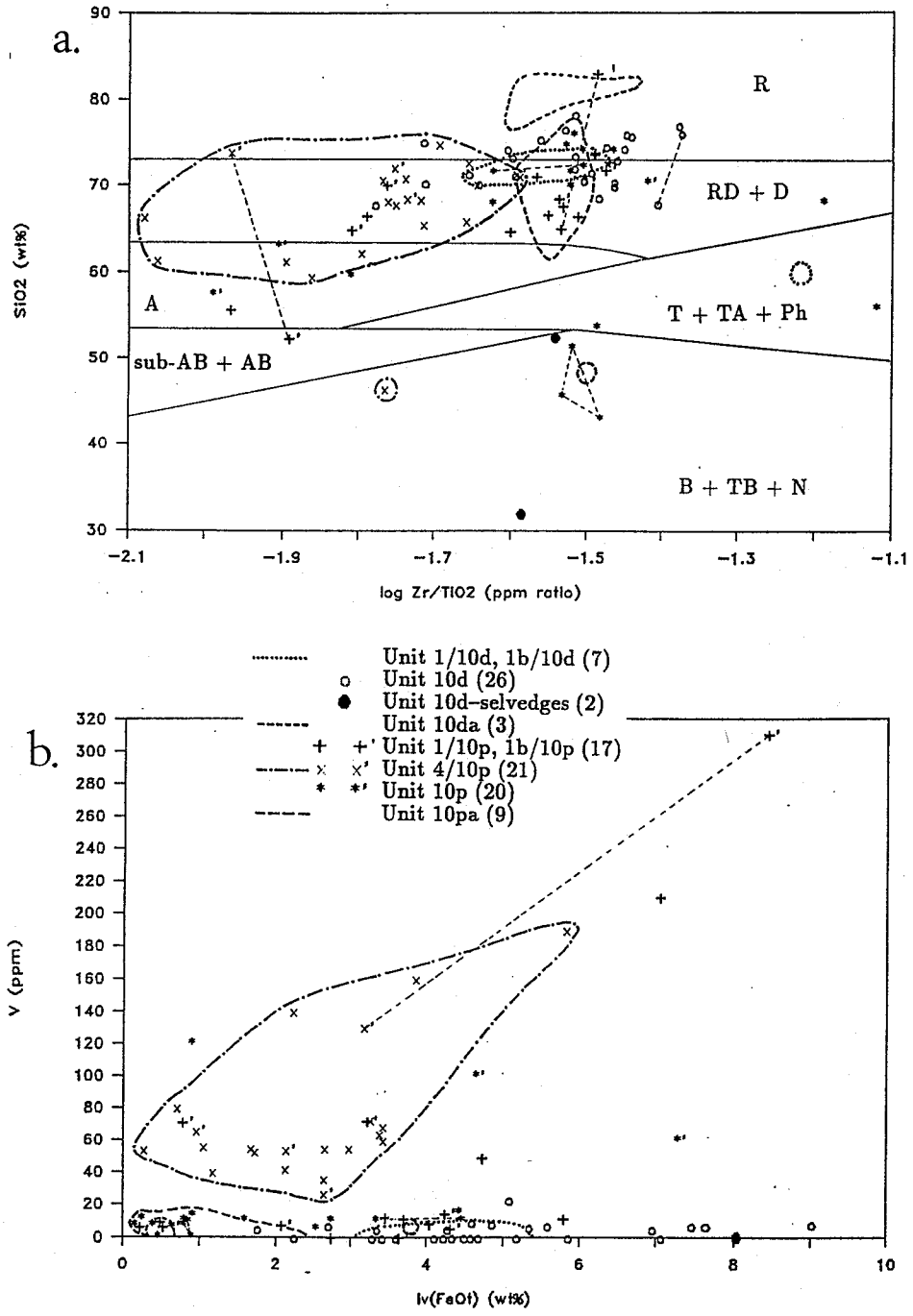

Figure 11.12. Trace-element signature of the distal and proximal zones.

a. SiO_2 (weight%) as a function of log Zr/TiO_2 (ppm ratio). Field boundaries from Floyd and Winchester (1977). Abbreviations: R=rhyolite, D=dacite, RD=rhyodacite, A=andesite, AB=alkali basalt, T=trachyte, TA=trachyandesite, Ph=phonolite, B=basanite, TB=trachybasanite, N=nephelinite.

b. V (ppm) as a function of $iv(FeO_t)$ (weight%).

than -1.6 (Figure 11.12, a). Vanadium occurs in concentrations of 46–280 ppm in samples of graphitic metasediment (34-1498.5-1), associated semi-massive sulphide (34-1525.5-1) and schistose intercalations in graphitic metasediment (19-848-1). This appears to be a localized enrichment, as the enveloping schists, including some metasediments, have low levels of V (*see* Figure 11.20).

11.1.3. Geochemistry of Calc-silicate Rocks.

Concordant calc-silicate rocks closely associated with the proximal and distal alteration zones (*i.e.* units 1/10c, 1b/10c, 4/10c) range in SiO_2 mainly from 55.9-73.7% (Figure 11.13, a). One sample with 77.0% SiO_2 is from a clast (24-624.5-1) extracted from a calc-silicate bearing breccia (24-624.5-2) (Note tie line linking '+' symbols.). Drill-core samples of calc-silicate rocks generally contain 1.46–6.56% K_2O. Static calc-silicate rocks (unit 10i) and calc-silicate altered mafic rocks (units 2/10e and 6/10e) tend to be less siliceous and potassic, and significantly more calcic and magnesian than concordant calc-silicate rocks (Figures 11.13 and 11.14). Two samples of unit 10i containing more than 3% K_2O have abundant biotite. High values of CaO in unit 10i correlate with high values of CO_2 ($\geq$1.0%) and with the presence of calcite as an accessory mineral (Table A.1). This also applies to calc-silicate altered mafic rocks, particularly unit 2/10e, which ranges in CaO from 8.60–23.85%. The distinctive whole-rock compositions of various types of calc-silicate rocks are apparent in an AFM projection (Figure 11.15); units 2/10e, 6/10e and 10i lie almost entirely in the tholeiitic field, and unit 10i is characterized by high proportions of MgO. Units 4/10c and 1/10c lie mainly in the calc-alkaline field.

The values of log Zr/TiO_2 (Figure 11.16, a) and V (Figure 11.16, b) in calc-silicate rocks follow the same stratigraphic pattern as observed in felsic rocks and rocks of the proximal zone, thus, low log Zr/TiO_2 and high V are associated with unit 4/10c and with other lithological units from the same stratigraphic level. This correlation applies equally to unit 10i, despite the petrographic observations which suggest post-kinematic metasomatism (*see* 6.2.2. Static Calc-silicate Alteration). Note also that unit 4/10c defines a trend of positively correlated SiO_2 and log Zr/TiO_2 (Figure 11.16, a). In contrast, units 4 (*see* Figure 11.5, a) and 4/10p (*see* Figure 11.12, a) do not show any obvious correlation, although they have similar ranges of log Zr/TiO_2 and SiO_2 to 4/10c.

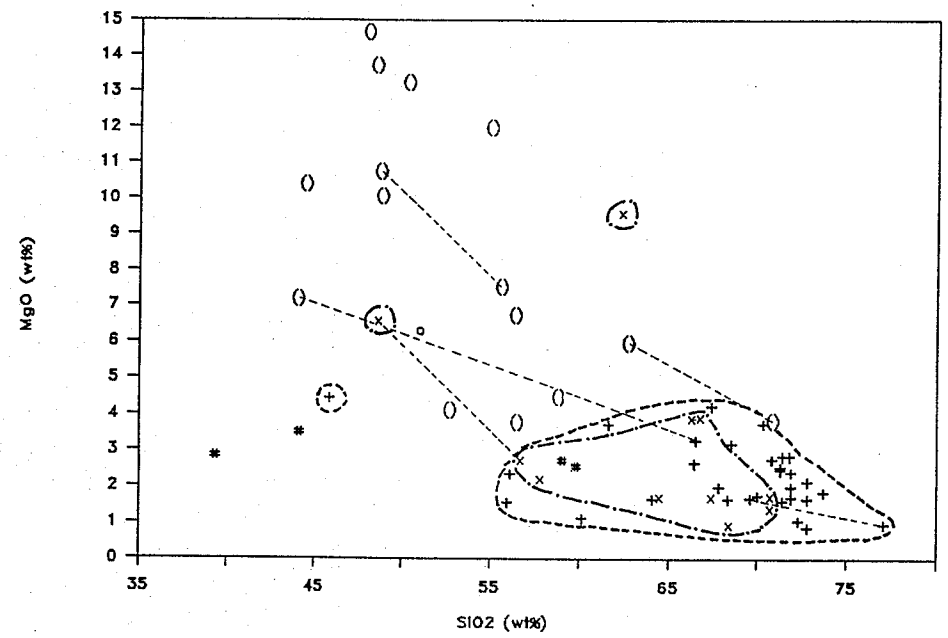

Figure 11.13. MgO (weight%) as a function of SiO_2 (weight%) in calc-silicate rocks. The key is the same as in Figure 11.14.

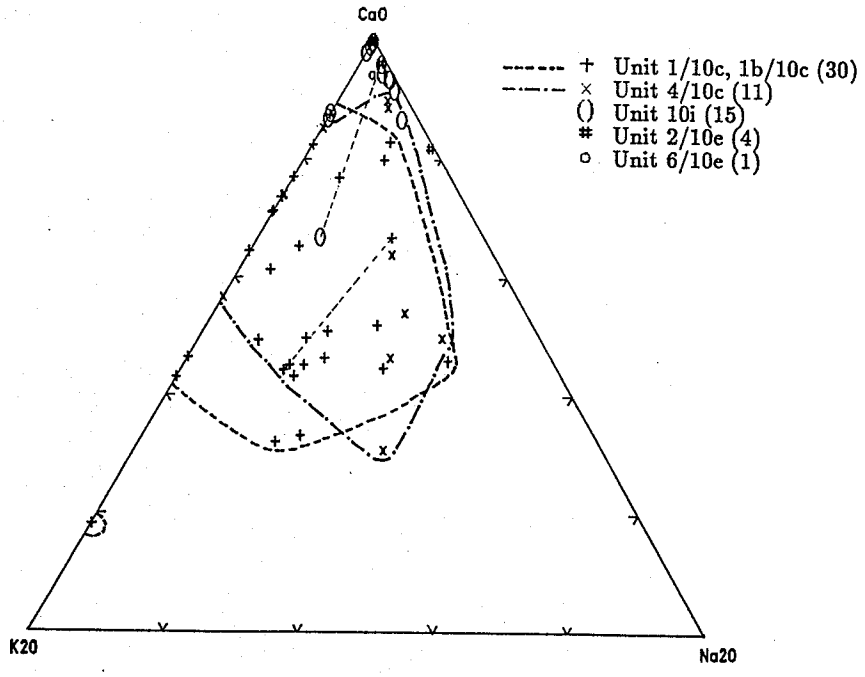

Figure 11.14. K_2O-CaO-Na_2O (molar) ternary proportions in calc-silicate rocks.

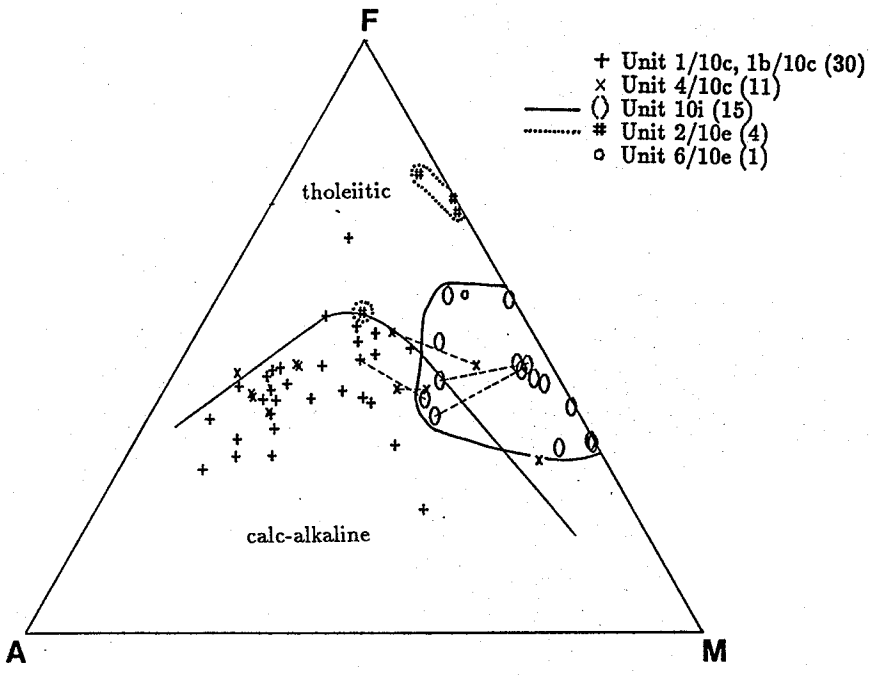

Figure 11.15. AFM diagram (weight proportions) for calc-silicate rocks. A=Na_2O+K_2O, F=$iv(FeO_t)$, M=MgO. Calc-alkaline and tholeiitic boundary from Irvine and Barager (1971).

11.1.4. Geochemistry of Mafic Volcanic Rocks.

Mafic volcanic rocks of units 2, 2a, 6, 6a and 1d fall mainly in the field of sub-alkaline basalts and andesites (Figure 11.17), as defined by Irvine and Barager (1971), and on both sides of the boundary between high-alumina and tholeiitic basalts proposed by Kuno (1968). The mafic rocks of unit 2 which plot above Kuno's boundary contain 16.6–19.5% Al_2O_3; those below the boundary contain 16.2–16.8% Al_2O_3. For comparison, note that Skirrow (1987) defined basalts which exceeded 17% Al_2O_3 as 'high-alumina'.

Unit 1d has SiO_2 and total alkali contents typical of andesites and basaltic andesites (Cox *et al.*, 1979). Unit 6 consists mainly of basalt and basaltic andesite, but 3 clasts extracted from volcaniclastic rocks have basaltic andesite and andesitic compositions. (Figure 11.17; Note tie lines linking 'o' symbols.) A single sample with 60.1% SiO_2 represents a local more felsic variety of unit 6. On average, unit 2 is slightly lower in SiO_2 than unit 6, particularly as some of the low SiO_2 samples of the latter represent separates of the matrix of volcaniclastic rocks.

In an AFM projection (Figure 11.18), units 2 and 6 lie mainly in the tholeiitic field, in common with the Hangingwall Andesite at the Anderson Lake mine, the

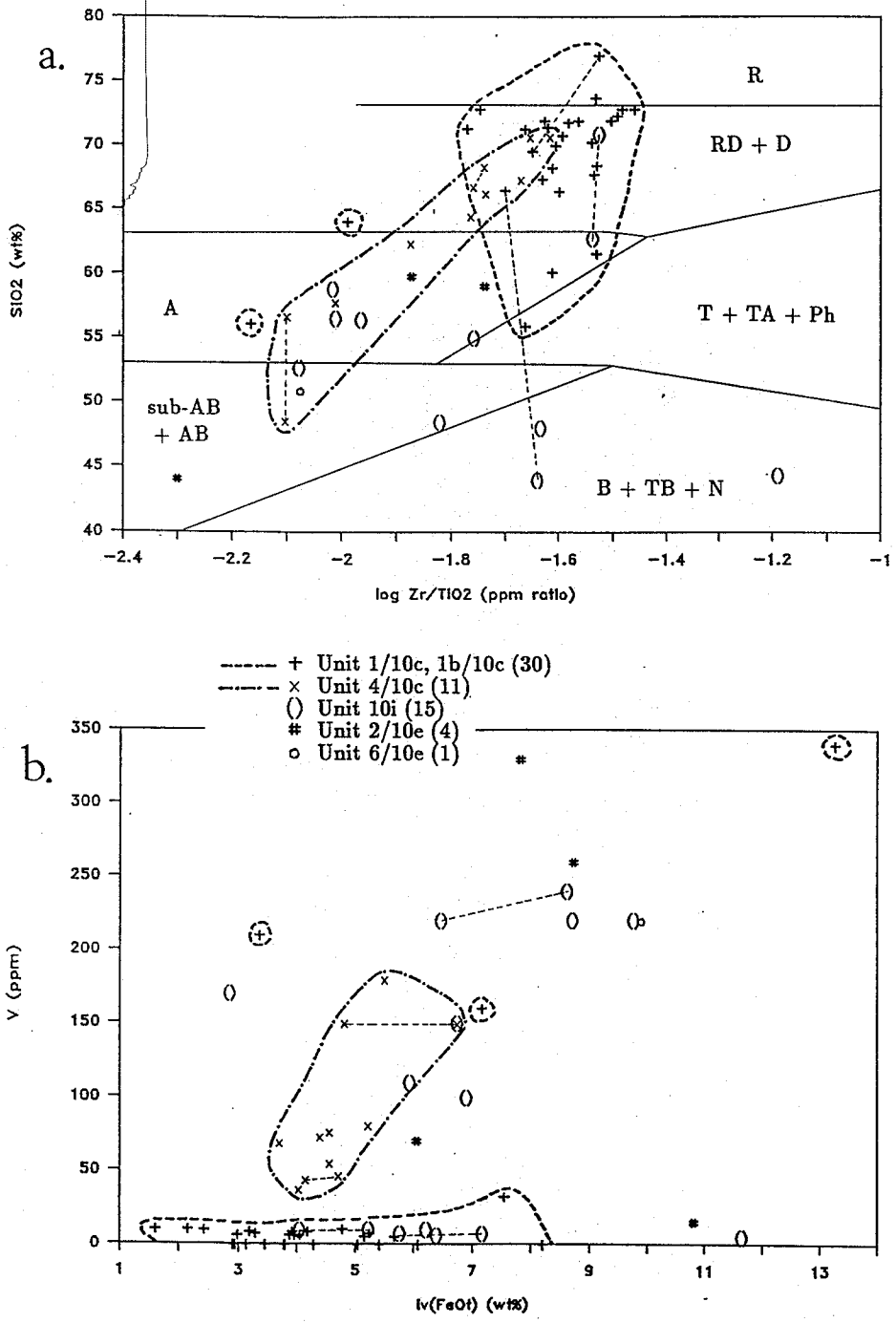

Figure 11.16. Trace-element signature of calc-silicate rocks.

a. SiO_2 (weight%) as a function of log Zr/TiO_2 (ppm ratio). Field boundaries from Irvine and Barager (1971). Abbreviations: R=rhyolite, D=dacite, RD=rhyodacite, A=andesite, T=trachyite, TA=trachyandesite, Ph=phonolite, AB=alkali basalt, B=basanite, TB=trachybasanite, N=nephelinite.

b. V (ppm) as a function of $iv(FeO_t)$ (weight%).

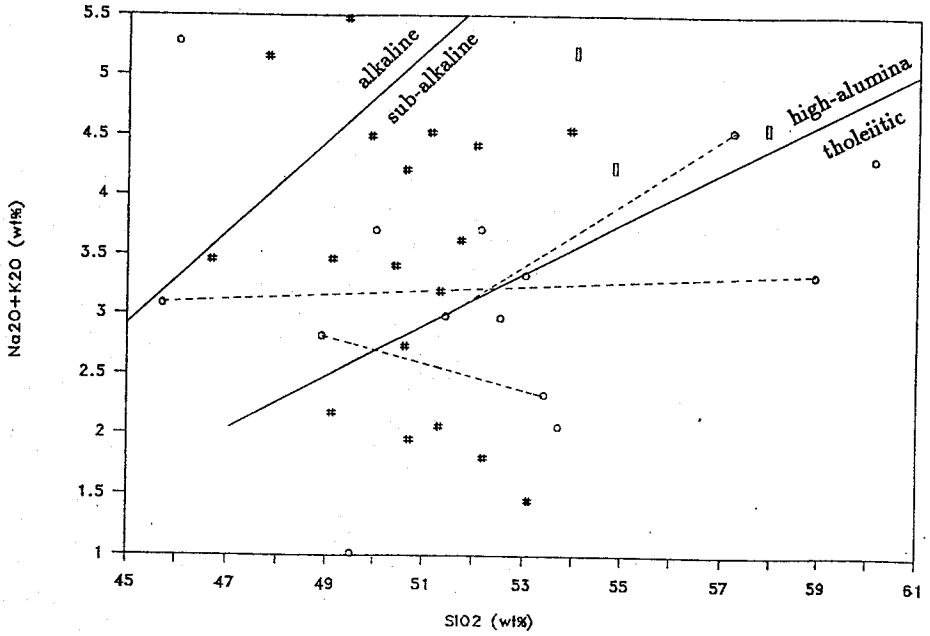

Figure 11.17. Total alkalis (Na_2O+K_2O weight%) as a function of SiO_2 (weight%) in mafic and intermediate rocks. Alkaline and sub-alkaline boundary from Irvine and Barager (1971); high-alumina and tholeiitic boundary from Kuno (1968). The key is the same as in Figure 11.18, but the fields of 10s and 10e have been omitted.

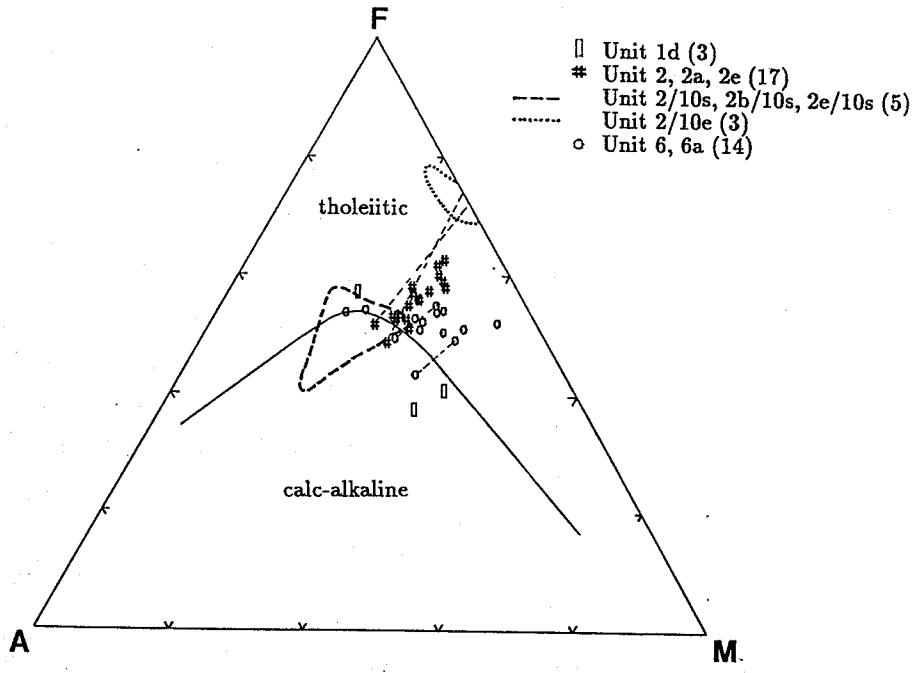

Figure 11.18. AFM diagram (weight proportions) for mafic and intermediate rocks. $A=Na_2O+K_2O$, $F=iv(FeO_t)$, M=MgO. Calc-alkaline and tholeiitic boundary from Irvine and Barager (1971). Fields of silicic (10s) and calc-silicate (10e) altered mafic rocks are shown for comparison.

Threehouse Basalt (Walford and Franklin, 1982) and mafic flows in the Edwards Lake area (Skirrow, 1987). Unit 1d and clasts and felsic intercalations in unit 6 lie mainly in the calc-alkaline field. The fields of silicic (10s) and calc-silicate (10e) altered mafic rocks are shown for comparison. Silicic alteration shifted the compositions toward the alkali apex. Calc-silicate altered rocks have been shifted away from the alkali apex; however, note that the compositions of 'less altered' mafic rocks, extracted from the same sample, are the only analyses of unit 2 which lie in the calc-alkaline field. (Note the tie lines linking '#' symbols with the dotted calc-silicate field.)

Log Zr/TiO_2 in units 2 and 6 varies from -2.4 to -1.9 (Figure 11.19, a). Separates of both clasts and matrix lie within the same range; however, several samples in which Zr was not detected are not plotted (Table C.5). The values are similar to those of silicified mafic rocks and lower than those of most other felsic (*see* Figure 11.5, a) and altered rocks (*see* Figure 11.16, a). The lowest values of log Zr/TiO_2 occur in unit 1d, one sample having a value of -2.42 and 2 other samples having Zr below the detection limit (20 ppm; Table C.1). Vanadium in mafic rocks ranges mainly from 180–330 ppm and shows a positive correlation with $iv(FeO_t)$. Unit 2 contains somewhat higher levels of V than units 1d and 6, *i.e.* mainly 280–330 ppm. These levels are significantly higher than those of V-rich felsic and altered rocks which rarely contain more than 200 ppm V (*see* Figures 11.5, b and 11.16, b). Silicified mafic rocks contain 36–55 ppm V, with one exception having 230 ppm.

11.2. Discussion.

11.2.1. Silicic-Feldspathic Alteration and Metamorphic Segregation.

The high silica contents of units 1a and 1c, and of clasts extracted from unit 1b, exceed the range typically accessible to differentiation by magmatic processes (*e.g.* Cox *et al.*, 1979) and, thus, suggest that the rocks were subject to some other mechanism of silicic enrichment. Units 1a and 1c are nearly massive and show little or no evidence of metamorphic segregation or fabric development. The sulphide mineralization and Fe-Mg-Zn hydrothermal alteration in brecciated cherty rocks (1c) is fracture-controlled and apparently cross-cuts silicic-sodic alteration (*see* 5.3.2. 'Cherty' Felsic Rocks and Brecciated Equivalents *and* 8.1. Synvolcanic Setting). The stratigraphic, structural and petrographic relationships suggest that the

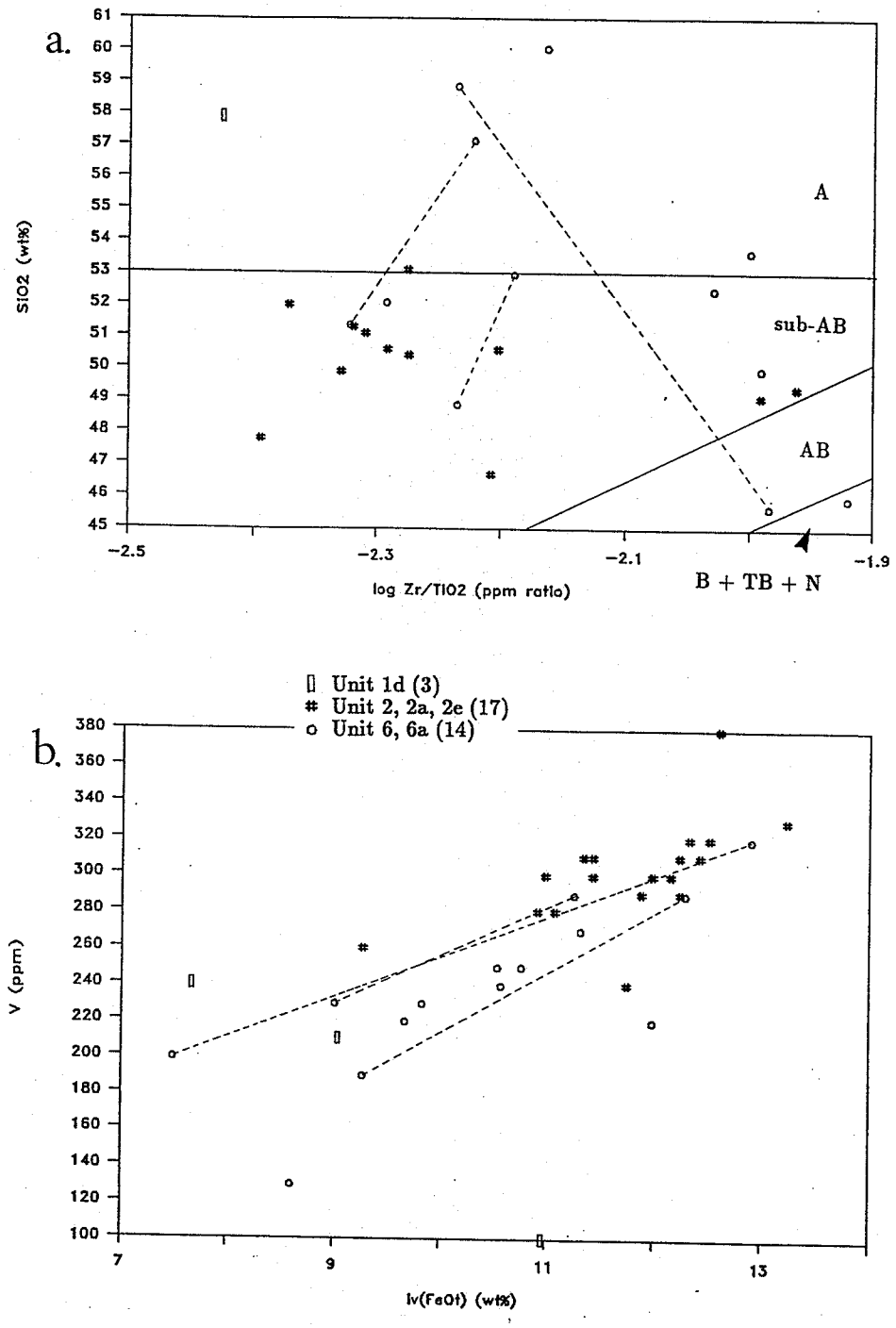

Figure 11.19. Trace-element signature of mafic and intermediate rocks.

a. SiO_2 (weight%) as a function of log Zr/TiO_2 (ppm ratio). Field boundaries from Floyd and Winchester (1977). Abbreviations: A=andesite, AB=alkali basalt, B=basanite, TB=trachybasanite, N=nephelinite.

b. V (ppm) as a function of $iv(FeO_t)$ (weight%).

silicic-sodic alteration preceeded the main sulphide mineralization and hydrothermal alteration, although cyclicity is not precluded. The highly sodic composition of the cherty felsic rocks with the highest silica contents could be the result of near-seafloor synvolcanic silicification and spilitization (*e.g.* Múnha *et al.*, 1980).

Bleached mafic rocks also have compositions consistent with silicic and sodic enrichment and their alteration is interpreted to have been synvolcanic. Lithologically and chemically, they are similar to silicified mafic rocks south of the Chisel Lake mine (Skirrow, 1987). Skirrow (1987) attributed silicification of mafic flows to a near-seafloor process occurring soon after their emplacement. This may also apply to silicified flows observed northeast of the Rod minesite (H9-52-1; *see* Plate 6.1, c). At the Linda deposit, silicification of mafic rocks of unit 2, as intersected in drill core (*see* Plate 6.1, a), is related to the contact of the unit with felsic rocks. In the Matagami area, Quebec, MacGeehan (1977) reported silicification of basalt adjacent to the upper and lower intrusive contacts of gabbroic sills. Skirrow (1987) related silicification of volcaniclastic breccias to synvolcanic felsic intrusions emplaced 0.3–2 km below the seafloor surface. At the Linda deposit, intrusive rocks have not been recognized and the alteration may be more directly related to the synvolcanic hydrothermal system.

Geochemically, it would be extremely difficult to distinguish the silicified mafic rocks from felsic rocks on the basis of major-element composition. It is interesting that alteration of cherty felsic rocks (in which the precursor was interpreted to have had a felsic composition similar to that of the host rocks) achieved distinctly higher levels of SiO_2 and Na_2O than in altered mafic rocks. Skirrow (1987) likewise reported a maximum of 83.22% SiO_2 in a silicified felsic rock, and a maximum of 73.06% in a silicified mafic rock. It may be that some natural limit exists, governed by the initial proportion of immobile major elements, the available void space, and allowable volume changes.

At the Linda deposit, the Zr/TiO_2 ratio of silicified mafic rocks was apparently preserved during the alteration process. The higher log Zr/TiO_2 of felsic rocks interpreted to have undergone silicic enrichment supports the conclusion that these rocks had felsic precursors and are not likely to be the silicified equivalents of any of the observed mafic rocks. In some cases, Zr and TiO_2 have been interpreted as

relatively immobile during hydrothermal silicification (e.g. Skirrow, 1987; Vivallo, 1987). However, Skirrow (1987) concluded that the distribution of silicic alteration showed a correlation with primary geochemical composition. He attributed values of log Zr/TiO_2 of -1.7 to -1.4 in silicified mafic rocks and of -2 to -1.7 in 'least-altered' mafic precursors to magmatic differentiation and subsequent selective alteration.

The compositions of breccias of unit 1b may partly reflect segregation of clastic material by fragmentation, transportation or depositional processes; however, the compositions of extracted felsic clasts also indicate silicic enrichment. The matrix of these breccias is not obviously altered and it may be that the clasts were altered prior to incorporation in the breccias. However, despite their high silica content, the clasts are significantly lower in Na_2O and higher in CaO than spilitized-silicified cherty felsic rocks and, thus, apparently underwent some different mechanism of silica enrichment. The breccias of unit 1b typically show well developed metamorphic fabrics, defined by a schistose phyllosilicate-rich matrix and granoblastic quartzo-feldspathic clasts (*see* 5.3.3. Matrix-supported Volcaniclastic Breccias). Metamorphic differentiation commonly involves silica migration (*see* 7.3. Fabric Formation), and in the case of the breccias, silica may have migrated from the matrix to create or enhance the quartzo-feldspathic domains in pre-existing clasts. According to this interpretation, as regards dynamometamorphism, the crucial differences between cherty felsic rocks (1a and 1c) and felsic breccias (1b) would be in the availability of hydrous phyllosilicate minerals, the presence of initial heterogeneity in their distribution, and the relative competency of rock domains. The creation and enhancement of siliceous domains by metamorphic processes has been previously documented (Beach and Jack, 1982; Beach, 1979; Robin, 1979; Beach and King, 1978; Kerrich, 1977). However, my interpretation implies that silica enrichment and migration effected a chemical modification that was parasitic on pre-existing primary structures. It also implies that, in some cases, it may be possible to discriminate metamorphic silica-gain from synvolcanic alteration on the basis of Na_2O content.

The general compositional ranges and the compositional scatter of units 1 and 4 indicate that most of the samples are unlikely to represent igneous compositions and, hence, unaltered precursor rocks are probably not represented. For example,

igneous differentiation typically produces positively correlated trends between SiO_2 and alkalis (McBirney, 1984), trends not observed in the Linda suite. Felsic volcanic rocks, particularly felsic glasses, are notably susceptible to alkali exchange which apparently occurs through mechanisms of hydration and diffusion which need not involve hydrothermal fluids (Fisher and Schminke, 1984; Scott, 1971). The compositional scatter at the Linda deposit, particularly the overlap with cherty felsic rocks, illustrates the difficulties inherent in the identification of silicic-feldspathic alteration on the basis of hand-sample examination and petrography in metamorphic rocks. Note also that the silica content of unit 4 is partly determined by the proportion of quartz megacrysts and, that with partial or complete recrystallization and the development of quartz pressure shadows, the proportion of primary phenocrysts cannot be accurately estimated.

11.2.2. Vanadium and Zr/TiO_2 in Quartz-megaphyric Felsic Rocks.

The correlation between high V and low Zr/TiO_2 in unit 4 (and other units stratigraphically associated with unit 4) occurs consistently throughout the 'least-altered' rocks and their altered equivalents, including both Fe-Mg and calc-silicate alteration (Figure 11.20). The distinctive geochemical signature correlates predominantly with a particular stratigraphic interval, rather than strictly with a lithological unit, or type or intensity of alteration. Down-dip of the mafic rocks of unit 2, the lower contact of the interval can be traced as a change from felsic or altered rocks with less than 15 ppm V to those with 20-320 ppm V. (The detection limit was 5 ppm (Table C.1).) The resolution of the contact is dependent on the spacing between samples. The contact passes through altered rocks approximately 30 metres above the graphitic metasediment, and continues down-dip through the enclave of less intensely altered rocks around which the proximal zone bifurcates. These observations are interpreted as evidence for the origin of high V and low Zr/TiO_2 as a primary magmatic feature which was preserved throughout the subsequent hydrothermal and metamorphic history.

The chemical concordance of post-kinematic calc-silicate rocks of unit 10i with their host rocks in terms of V and log Zr/TiO_2 suggests either that unit 10i was emplaced by metasomatic replacement of the host rock without extensive void-filling, or that V, Zr and TiO_2 were sufficiently mobile to impart the same signature to the

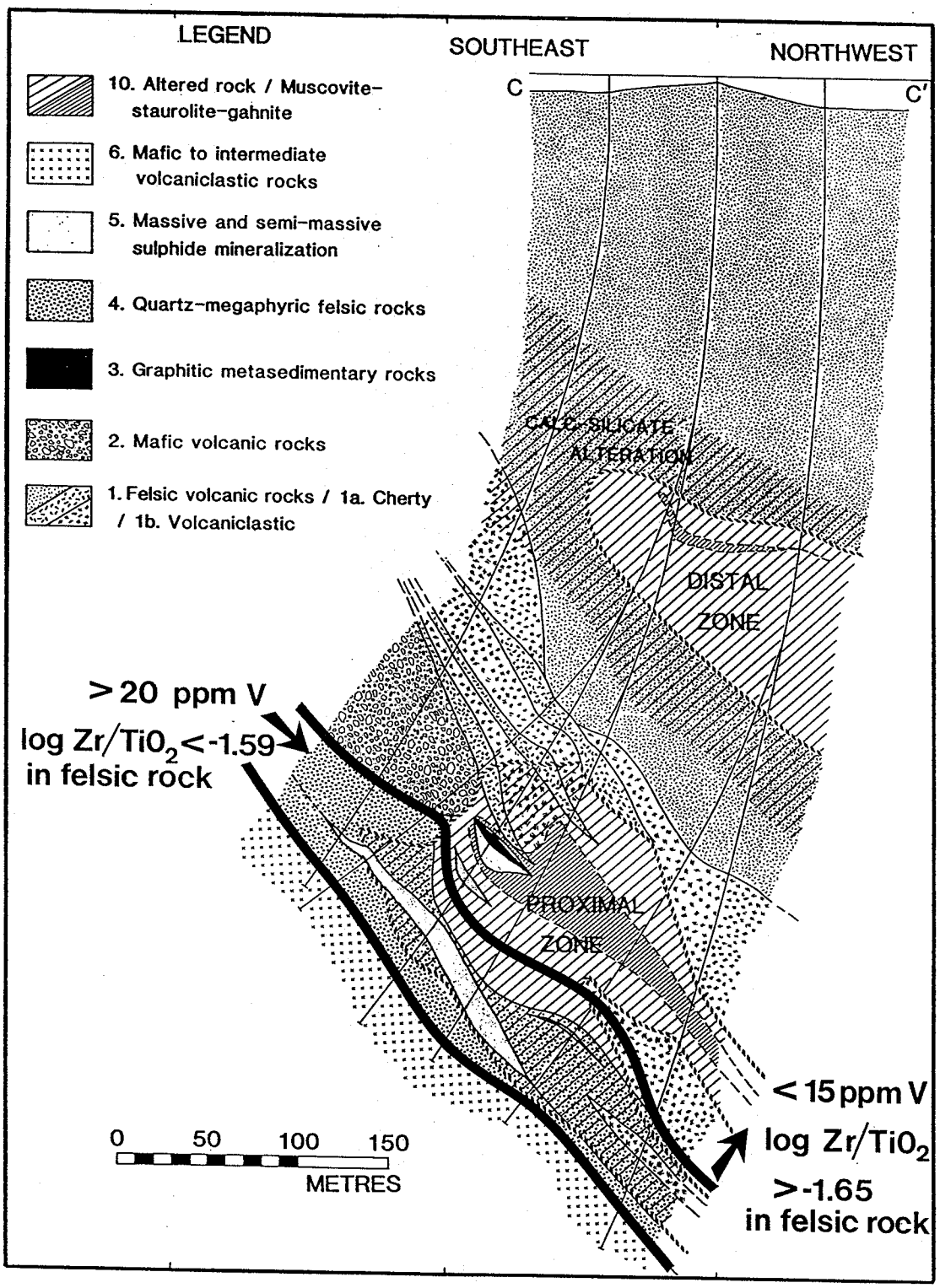

Figure 11.20. The distribution of correlated high V and low log Zr/TiO_2 in felsic rocks associated with unit 4 in section C-C'. A similar distribution is defined in section A-A' and in the surface geology. The distinctive trace-element signature occurs regardless of lithology, type or intensity of alteration.

metasomatic fluid. Petrography indicates that most samples of unit 10i represent various intensities of wall-rock alteration adjacent to a thin zone ($\leq$1cm) resembling a vein (*see* 6.2.2. Static Calc-silicate Alteration). Unit 10i is volumetrically minor in comparison to the host rock and, presumably, the parent metasomatic fluid could have acquired some trace and minor element characteristics of the host rock without causing a perceptible host-rock depletion. Skirrow (1987) reported possible mobility of Zr and TiO_2 in the case of high p_{CO_2} gradients. Experimental studies and case studies of seafloor alteration of basalts have concluded that V is immobile during hydrothermal alteration, even at high water/rock ratios (Seyfried and Mottl, 1982; Mottl *et al*, 1979; Humphris and Thompson, 1978). In altered metarhyolites and metabasalts in the Boliden-Långdal area, Sweden, Vivallo (1987) reported only minor mobility of V with respect to TiO_2, which was assumed to have been immobile.

The whole-rock compositions of unit 4 apparently represent a less differentiated magma than that represented by felsic rocks lower in the section. The low Zr/TiO_2 ratios at the Linda deposit are due to a combination of relatively low Zr with moderate levels of TiO_2. For example, TiO_2 concentrations are generally lower than in felsic intrusions in the Edwards Lake area characterized by Skirrow (1987) as 'high-TiO_2' (0.39–0.71%), and Zr concentrations are lower than in his suites of felsic intrusions (85–140 ppm).

The same geochemical signature of high V and low log Zr/TiO_2 is found in unit 4 on the northwest side of the Anderson Bay structure and, thus, stratigraphic correlation of quartz-megaphyric rocks on each side of the structure is not precluded on geochemical grounds (*see* Figures 2.2 and 3.1). The occurrence of the same geochemical features in unit 7, interpreted to be higher in the stratigraphy on the southeast of the Anderson Bay structure, suggests that V-rich felsic rocks may occur on more than one stratigraphic horizon. The average V content and log Zr/TiO_2 values of 32 samples of the Sneath Lake intrusion are 47 ppm and -1.78, respectively (Walford and Franklin, 1982; Note that they refer to the Sneath Lake intrusion as 'tonalite intrusion'.). These values are within the range recorded here for unit 4. Walford and Franklin (1982) proposed this body as the intrusive equivalent of quartz-megaphyric volcanic rocks in the area. The average values of V and

log Zr/TiO_2 for the Footwall Felsic and Hangingwall Felsic units at the Anderson Lake mine are 50 ppm, -1.65, and 24 ppm, -1.62, respectively; for the Footwall Felsic unit at the Stall Lake and Rod mines, the corresponding values are 5 ppm, -1.52 (*ibid.*). As these are averaged values and may represent a relatively wide stratigraphic interval, detailed comparison with the Linda deposit is difficult. However, Walford and Franklin (1982) attributed a correlated increase in TiO_2 and V concentrations toward the orebody at the Anderson Lake mine to enrichment during hydrothermal alteration. If the alternative interpretation proposed here is correct (*i.e.* that the high V and low Zr/TiO_2 preserve a memory of primary magmatic composition), V concentration and Zr/TiO_2 ratio in felsic and altered rocks could provide a geochemical tracer for primary stratigraphy in altered rocks.

11.2.3. Distal and Proximal Alteration Zones.

The calc-alkaline AFM trend followed by hydrothermally altered rocks is common to the footwall alteration of many volcanogenic massive sulphide deposits (Walford and Franklin, 1982; Riverin and Hodgson, 1980; MacGeehan, 1977). The erratic fluctuations of alkalis in most felsic rocks at the Linda deposit suggest alkali mobility and it may be that the calc-alkaline trend of these rocks is partly the result of alteration. This is certainly so for the silicified felsic and mafic rocks. Walford and Franklin (1982) reported calc-alkaline compositions for altered and less altered felsic rocks in the Snow Lake region, including the Sneath Lake tonalite which they considered likely to be representative of primary magmatic compositions. The calc-alkaline trend of the distal and proximal alteration zones can be explained by the low alkali-high $MgO+iv(FeO_t)$ composition of the former, and relatively high alkali-low $MgO+iv(FeO_t)$ of the latter. The two zones are similar in $iv(FeO_t)/MgO$, but the distal zone has some $iv(FeO_t)$-rich parts. With respect to chalcophile elements, the most important difference between the zones is the high S content of the proximal zone relative to the distal zone.

The proximal alteration zone is hosted by a variety of lithological precursors (1, 1a, 1b, 4) and includes rock types with various petrogenetic backgrounds, *e.g.* sulphidic and graphitic metasediments, void-filling mineralization in breccias, and hydrothermally altered rocks (*see* 5.3. Proximal Alteration Zone and Associated Rocks). The alteration was at least partly multi-episodic and presumably involved

various types of hydrothermal, and possibly, low temperature fluids. For example, silicic and albitic alteration of felsic rocks preceded sulphide mineralization and Fe-Mg alteration. This complex history is reflected in the broad compositional range of the zone, which contrasts with the relatively tight definition of compositional fields by the samples representing the distal zone. Chemically and lithologically, the distal zone forms a much more coherent and homogeneous suite, possibly reflecting a simpler evolution involving only Fe-Mg alteration of felsic precursors.

The higher abundance of micas in the proximal zone relative to the distal zone is mainly a function of higher Na_2O, as both zones contain similar levels of K_2O. The high Na_2O of muscovite and biotite is not detectable optically, and petrographic examination alone could lead to the erroneous interpretation of the proximal zone as K_2O enriched (Zaleski and Halden, 1988). The distal zone is strongly depleted in Na_2O and CaO, and enriched in FeO_t and MgO; hence, it resembles footwall alteration associated with other volcanogenic massive sulphide deposits (Riverin and Hodgson, 1977; Franklin *et al.*, 1981). As intersected by drilling, it is notably low in S and high in $iv(FeO_t)$. If this zone represents a conduit (Model 2; *see* 3.2. The Linda Hydrothermal System), the stringer mineralization typical of such zones (Lydon, 1988) has not been intersected. The lower semiconformable zone at the Anderson Lake mine is compositionally zoned from a Na_2O-depleted lower interval to an upper interval with sporadic Na_2O enrichment, locally in excess of 3% (Walford and Franklin, 1982). Staurolitic rocks, on the periphery of the semi-conformable zone have erratic Na_2O distribution from less than 1% to more than 2% (*ibid.*). In contrast, the distal zone at the Linda deposit is uniformly depleted in Na_2O and has a narrow transitional zone (1/10d) of increasing Na_2O toward the enveloping calc-silicate bearing felsic rocks (1/10c, 1b/10c). The proximal alteration zone is more sodic and calcic than the distal zone, and this may be related to interaction with seawater at or near the depositional surface. At least some of the metasediments formed in a euxinic basin, suggesting that the hydrothermal fluid may have been sufficiently dense to form a bottom layer or a brine pool (Costa *et al.*, 1981; Sato, 1972). Alternatively, by analogy with active hydrothermal vents observed on the seafloor (Lydon, 1988; Bäcker *et al.*, 1985; Ballard *et al.*, 1984), mixing between exiting hydrothermal fluid and seawater may have induced the pre-

cipitation of minerals. Calcite has already been proposed as a possible source of Ca now bound in metamorphic margarite and plagioclase. Anhydrite and epidote may be less likely in the protolith in view of the association, at least in some cases, with graphitic metasediment. However, anhydrite occurs in seafloor hydrothermal vents and chemical disequilibrium is common among hydrothermal products in active systems (Lydon, 1988).

In both alteration zones, the geochemical similarity of the zincian-rich core zones (10da, 10pa) suggests that some critical similarities are relevant to their mode of origin. In view of the geochemical and petrogenetic contrasts between the distal and proximal zones, and as the core zones were defined on the basis of metamorphic parageneses, their similarities may be partly due to the metamorphic processes which allowed the formation of gahnite and zincian staurolite. The zincian bulk-rock compositions are probably a primary synvolcanic feature. The occurrence of sphalerite in the proximal core zone, in some cases in enclaves without gahnite and in graphite-bearing rocks, suggests that the gahnite and zincian staurolite bearing rocks represent a Zn-rich volume in which high $\log f_{O_2}$ and $\log f_{S_2}$ (*see* 10.1.3. Petrogenetic Grid) were generated during metamorphism. The Zn-rich bulk-rock compositions have a wider extent than gahnite-bearing rocks and include the metasediments and massive sulphide lenses in this volume. Sphalerite may have been a primary precipitate which oxidized to gahnite and staurolite during metamorphism. For example, Wall and England (1979) concluded that some gahnite in metamorphic rocks originated by the interaction of metamorphic fluids with a sphalerite-bearing aluminous protolith. The isolated occurrence of zincian bulk-rock compositions in the distal zone is harder to explain, and the possibility of hydrothermal, diagenetic or synmetamorphic migration of Zn cannot be discounted. The slightly higher SiO_2 and Na_2O in the core zone (compared to the main part of the distal zone) are of unknown origin. But the similarity of the two core zones, despite the contrasting geochemical characteristics of the enveloping altered rocks, suggests that the whole-rock composition of the core zones may be partly of epigenetic origin. Nevertheless, it does appear possible to conclude that the Linda deposit is a Zn-rich deposit and, that prior to metamorphism, it contained abundant sphalerite.

The subtraction of normative FeS_2 from whole-rock geochemical analyses assumes that Fe and S were immobile during metamorphism and that Fe which is bonded to S was not available for metamorphic reactions (Tracy and Robinson, 1988). Pyrrhotite is commonly interpreted to be the result of metamorphic desulphidation of pyrite under conditions either closed (Mohr and Newton, 1983) or open (Ferry, 1981) to the migration of S. At the Linda deposit, for the most part, f_{S_2} was apparently maintained in the pyrite field although significant variations in f_{O_2}/f_{S_2} have been documented (*see* 10.1.3. Petrogenetic Grid). Local variations in sulphide-oxide assemblages, related to primary features such as bedding, suggests that f_{O_2} and f_{S_2} were internally buffered during metamorphism and, hence, that fluid mobility was limited.

The two samples of selvedges to quartz veins from the distal alteration zone have anomalous major-element compositions which can be attributed to their low silica content. During mesoscopic examination of drill core, these veins were considered as possibly syngenetic, as the selvedges contain an increased abundance of Al-Mg-Fe metamorphic minerals characteristic of altered rocks (*see* 5.5. Quartz Veins). The selvedges resembled wall-rock zoning such as might be expected to form a halo around a hydrothermal conduit. The geochemical evidence suggests the enriched Al-Mg-Fe composition of the selvedges is best explained by synmetamorphic silica depletion. This requires that the quartz veins developed as dynamometamorphic segregations resulting from the migration of silica from their immediate wall rock. Silica depletion may have a general application to the extremely schistose wall rocks adjacent to many concordant quartz veins. The scale of silica mobility has not been established, and it may be that some or all veins also contain quartz introduced from beyond the immediate wall rock.

11.2.4. Staurolite-bearing Rocks.

Some of the altered rocks from the Linda deposit fall within the geochemical fields defined by Hoschek (1967), encompassing 90% of the bulk-rock analyses in his compilation of chloritoid-bearing rocks (Figure 11.21, a–c). There is a tendency for samples from the proximal zone to have higher proportions of alkalis (Figure 11.21, b) and samples from the distal zone to have higher proportions of MgO (Figure 11.21, a). However, the analyses are bulk compositions of samples acquired by

homogenization of quartzo-feldspathic domains and porphyroblastic phyllosilicate-rich domains. The latter domains are likely to have whole-rock compositions in the fields of chloritoid-bearing rocks. Each of the fields as defined by Hoschek (1967) involves an FeO_t component, and in Figures 11.21, a–c, the Fe-intercept value, $iv(FeO_t)$, was used in its place. This reduces the Fe content of the remaining 'whole-rock', shifting the compositions away from the chloritoid field. Even accounting for a possible shift in 'effective' bulk-rock composition due to the presence of Fe-sulphide minerals, some samples lie within the bulk-rock compositional field of chloritoid.

Trembath (1986) reported chloritoid in the Joannie alteration zone, located in an area of lower regional metamorphic grade than the Linda deposit. A chloritoid-consuming reaction may be more feasible in some altered rocks than the garnet-chlorite-muscovite consuming reaction which defines the staurolite-biotite regional isograd in the Snow Lake area (Froese and Moore, 1980). As might be expected, the isograd is defined by different reactions in rocks of different bulk-rock composition (*see* 7.4.2. Inferred Prograde Metamorphic Reactions).

11.2.5. Calc-silicate Rocks.

The two main types of calc-silicate felsic rocks, *i.e.* concordant and static, clearly have different whole-rock compositions. In most cases, concordant calc-silicate rocks have compositions similar to felsic rocks, but with a tendency towards higher CaO. The textural relationships of epidote, calcic plagioclase and micas indicate that the rocks acquired their present whole-rock compositions prior to D_1 (*see* 6.2.1. Concordant Calc-silicate Alteration). Their distribution around the distal alteration zone, although locally erratic, suggests that the two units (10d and 1/10c) may be genetically related; thus, the calc-silicate envelop may be part of the synvolcanic alteration system. At the Millenbach mine, Noranda, Quebec, the outer periphery of the footwall alteration pipe and the outermost margins of wall-rock alteration adjacent to hydrothermal veins are characterized by slight increases in CaO and Na_2O and by the presence of epidote (Riverin and Hodgson, 1980).

Static calc-silicate rocks are not directly related to the synvolcanic alteration, but represent late metamorphic mobility of Ca-bearing carbonatizing fluids. These rocks may be related to the carbonate metasomatism which was previously proposed for the calcite-pyrite rocks of the main massive sulphide body (*see* 10.4. Calc-silicate

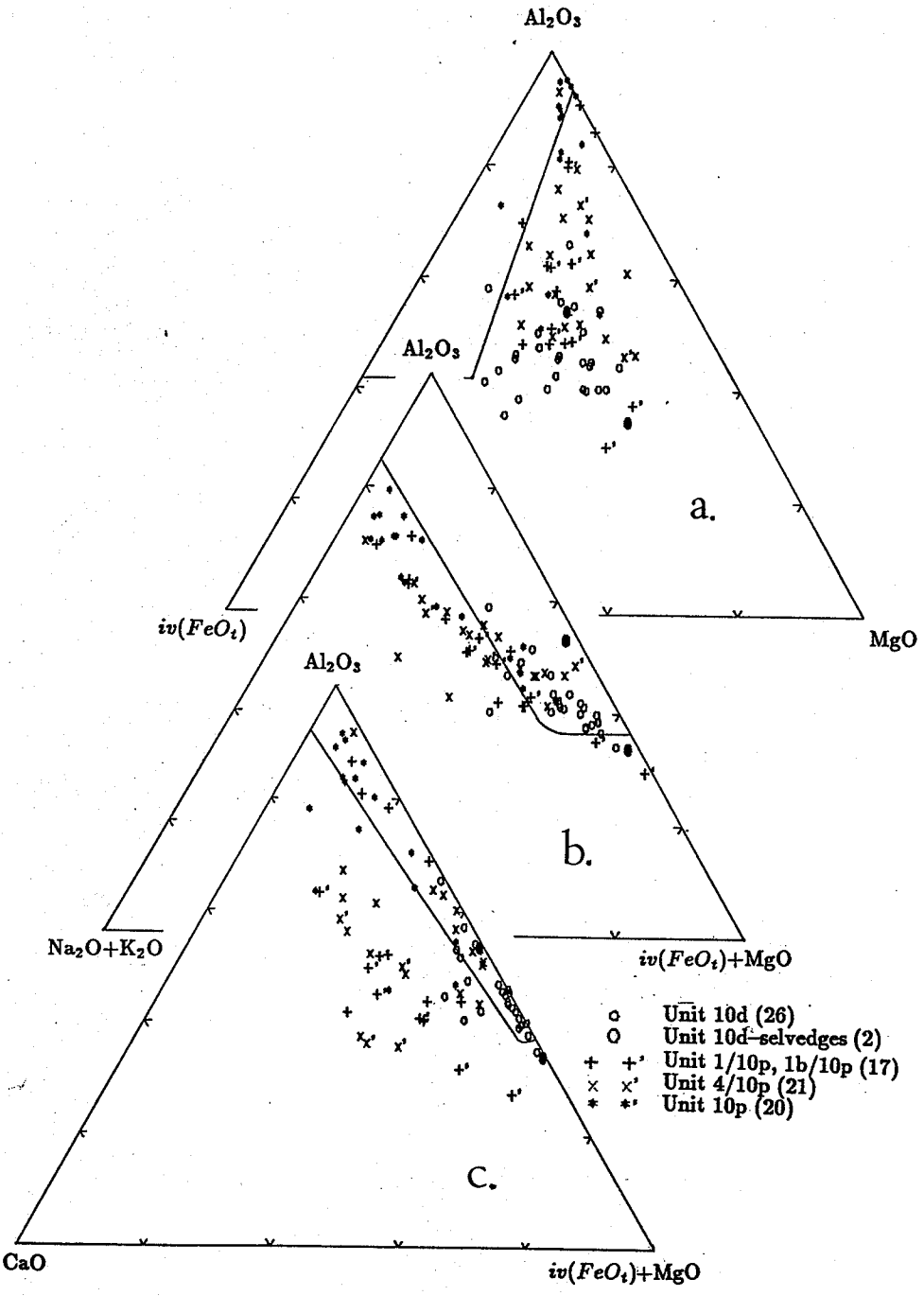

Figure 11.21. Rocks of the proximal and distal alteration zones in terms of Hoschek's (1967) fields encompassing 90% of chloritoid-bearing rocks.

a. $iv(FeO_t)$-Al_2O_3-MgO ternary (molar proportions).

b. (Na_2O+K_2O)-Al_2O_3-($iv(FeO_t)$+MgO) ternary (molar proportions).

c. CaO-Al_2O_3-($iv(FeO_t)$+MgO) ternary (molar proportions).

Enclave in the Main Massive Sulphide Body). In some cases, it seems that CaO and carbonate were highly mobile during metamorphism, but that the carbonatizing metamorphic fluids were channelled, resulting in intensive metasomatism along restricted pathways.

11.2.6. Plagioclase-layered Rocks.

Samples characterized by the presence of 'Tuttle' deformation lamellae are indistinguishable in TiO_2 content from other felsic rocks. This is consistent with the origin of the trails as previously proposed (*see* 7.1.3. S_1 Rutile Trails), by recrystallization of rutilated quartz phenocrysts. However, these rocks do tend to have low total alkalis, Na_2O/K_2O and $iv(FeO_t)/MgO$. In altered rocks, plagioclase-layered rocks, except for their high CaO content, do not define any coherent geochemical trends, although they have some tendency to be 'rogues' with respect to the geochemical field of their parent unit. The high CaO content may reflect the abundance of calcic plagioclase porphyroblasts. However, these rocks are commonly closely associated with the largest massive sulphide body, which consists of pyrite and calcite. The evidence for a substantial synmetamorphic influx of calcite into this massive sulphide body was previously presented (*see* 10.4. Calc-silicate Enclaves in the Main Massive Sulphide Body), and it may be that the influence of this metasomatic event extends beyond the immediate vicinity of pyrite-calcite rocks.

11.3. Implications for Geochemical Modelling.

A qualitative model can be proposed for the evolution of the synvolcanic hydrothermal system at the Linda deposit, accounting for the sequential development of primary features and the general geochemical characteristics of the alteration. In the proximal zone, silicification and albitization of felsic rocks preceded the Fe-Mg-Zn hydrothermal alteration and sulphide mineralization. The latter developed through a period of time during which sulphidic and graphitic sediments accumulated at a depositional surface and volcanic units underwent alteration. With the emplacement of unit 4, alteration and mineralization eventually declined. Most of the features of the proximal alteration zone indicate stratiform and stratabound mineralization and alteration; a cross-stratal conduit has not been identified. It may be that the proximal zone represents a 'distal' accumulation of sulphide minerals in the lithofacial sense of the term. The relationships of the massive sulphide

mineralization within unit 4 have been obscured by synmetamorphic introduction of calcite. For example, the occurrence of the anthophyllite-staurolite-gahnite enclave within the pyrite-calcite rocks of the massive sulphide body suggests that this unique low alkali-low CaO alteration in the proximal zone may have had a more extensive distribution. Similarly, the occurrence of relict gahnite in many of the enclaves suggests the prograde desulphidation of early sphalerite. It appears that only part of the synvolcanic hydrothermal system was preserved in a recognizable state.

The primary significance of the distal zone is equivocal, although it does appear to have developed as subsurface hydrothermal alteration related to the stratiform and stratabound alteration of the proximal zone. This would be consistent with the genetic models presented in chapter 8, either Model 1 which identified the distal zone as a reservoir, or Model 2 which identified the distal zone as a conduit. Only a part of the distal zone was intersected by drilling, and it may well be that its overall lithological and geochemical homogeneity is partly the result of bias toward the volume most accessible to drilling. It may not be representative of the zone as a whole. The alteration zones associated with the Anderson Lake mine (projected to surface) have a lateral extent in excess of 2 km (*see* Figure 3 of Walford and Franklin, 1982).

Fabric development at the Linda deposit involved centimetre and millimetre-scale metamorphic segregation. In the selvedges of quartz veins, silica was mobile on a scale approaching metres. The scale of open-system behaviour during diagenesis and prograde dynamometamorphism is not clear. The intensity of fabric development is heterogeneous on a large scale, *e.g.* the schistose alteration zones as compared to nearly massive cherty rocks, as well as on a small scale, *e.g.* the schistose matrix of breccias as compared to granulose quartzo-feldspathic clasts. Strain distribution was partly governed by the properties of the rock or rock domain and, therefore, the superimposed modifications are not likely to be equivalent for precursors and hydrothermally altered rocks. The silicic enrichment of clasts in breccias during the development of phyllosilicate schistosity (*see* 11.2.1. Silicic-Feldspathic Alteration and Metamorphic Segregation) provides evidence of element redistribution on a small scale. Similar processes could be envisaged on a larger scale and

may account for a large proportion of the quartz veins.

The difference in intensity of fabric development between 'less altered' rocks and their altered equivalents introduces additional complications into any mass-transfer calculation attempting to describe synvolcanic processes. It is necessary to consider element mobility, volume changes, and density changes during metamorphism, and to discover a means of discriminating these from the modifications incurred during hydrothermal alteration. Many case studies of synvolcanic alteration have assumed mass transfer at constant volume (Skirrow, 1987; Gibson *et al.*, 1983; Riverin and Hodgson, 1980; Roberts and Reardon, 1978) and have obtained plausible solutions in relatively undeformed metamorphic terranes. Schistose alteration zones imply volume reduction, but it may be that this was accommodated by prograde phase changes and increased whole-rock density. The first step in semi-quantitative modelling of synvolcanic processes in dynamometamorphic terranes requires mass-balance calculation of the processes of fabric development.

PART IV

CONCLUSION

Chapter 12. Synthesis, Summary of Conclusions, and Implications. References.

Chapter 12
Synthesis, Summary of Conclusions, and Implications

12.1. Reconstruction of the Primary Features of the Linda Deposit.

The present configuration of the Linda deposit is the result of polyphase deformation superimposed on the primary stratigraphy and structure. The deposit is dominated by an L-S tectonic fabric in which the largest massive sulphide body has a minimum aspect ratio of 30:2:1, and primary structures have been transposed into subparallel orientations, blurring the distinction between discordant and concordant primary relationships. Despite its tectonized nature, it is possible to reconstruct a substantial part of the primary physical features by attention to local preservation of primary structures and by comparison with massive sulphide deposits in less deformed terranes.

The Linda deposit has two discrete zones of Fe-Mg alteration, the distal alteration zone and the proximal alteration zone; the latter was recognized and delineated during the course of this study. The presence of Fe-Mg alteration zones in felsic rocks comprising the stratigraphic footwall to massive sulphide mineralization is a characteristic feature of many massive sulphide deposits in the Snow Lake region (Walford and Franklin, 1982; Skirrow, 1987; Trembath, 1986). At the Linda deposit, the distal alteration zone is a relatively homogeneous zone of Na_2O and CaO depletion, the most common lithology being a quartz-rich staurolite-banded gneiss. In contrast, the proximal alteration zone is markedly heterogeneous, encompassing sulphidic and graphitic chemical sediments, massive sulphide bodies, and altered felsic rocks. Several observations, and the significance attributed to them, suggest that the proximal zone may have been the site of a synvolcanic fault:

1. Mafic volcanic rocks of unit 2 and cherty felsic rocks (1a) terminate at, or within, the proximal zone. Cherty felsic rocks are represented in the proximal

zone by mineralized clast-supported breccias (1c), which may have originated as hydrothermal or fault breccias.

2. Metasedimentary rocks and, in particular, graphitic and sulphidic metasediments occur down-dip of the termination of unit 2 and suggest the local development of a euxinic basin.
3. The distribution of alteration is skewed toward a volume of rock lying down-dip of the terminated units. In seafloor deposits (Franklin, 1986) and in the massive sulphide deposits of the Noranda camp (Dimroth *et al.*, 1985), hydrothermal alteration is typically focussed on the down-thrown side of synvolcanic growth faults.
4. Commencing with unit 4, the upper units in the stratigraphic sequence are continuous. Unit 4 appears to be associated with the decline of hydrothermal activity and, concomitantly, with the cessation of movement on the proposed growth fault.

In the Noranda camp, Dimroth *et al.* (1985) reported that, without exception, the massive sulphide deposits are associated with synvolcanic faults. At the Linda deposit, the association of the listed features with the proximal alteration zone is strong evidence for the presence of a synvolcanic fault, although the precise trace has not been located and displacement has not been documented. This interpretation also raises the possibility that the location of other deposits in the Snow Lake region may have been similarly controlled.

Dimroth *et al.* (1985) suggested a periodicity to massive sulphide deposition in the Noranda area. They interpreted extensive occurrences of silicified rocks as evidence of prolonged diffuse hydrothermal activity which was focussed during episodes of active faulting and subsidence. The faulting was directly related to magmatic activity, and the sulphide mineralization thus triggered was subsequently terminated by the 'next paroxysmic effusive phase' (*ibid.*). The general setting in the Snow Lake region may have been similar, in that the massive sulphide deposits are associated with abundant quartz-megaphyric felsic rocks for which a pyroclastic origin has been proposed (Walford and Franklin, 1982).

Despite the case that can be made for a growth fault at the Linda deposit, the location of a hydrothermal conduit remains uncertain. Most of the proximal alter-

ation seems to be stratabound, and in many cases, stratiform; this may represent successive depositional surfaces in a topographic low on the down-thrown side of the proposed fault. The clast-supported breccias which mainly underlie the metasediments may be related to cross-stratal permeability; however, they occur over a stratigraphic interval of less than 100 metres (after deformation). At this point, it may be well to take note of Figure 8.2, as a graphic reminder of the present structural configuration of the deposit and the subtleties involved in identifying 'cross-stratal' relationships.

An intersection between the distal and proximal alteration zones has not been documented and the significance of the distal zone to the hydrothermal system is obscure. In terms of geochemistry and mineralogy, it resembles the staurolitic lateral extension of the semiconformable alteration zone at the Anderson Lake mine (Walford and Franklin, 1982). At the Linda deposit, it is not clear whether the distal zone was 'semiconformable'; *i.e.* whether Model 1 or Model 2 in Chapter 8 is more appropriate.

A comprehensive physical model of the hydrothermal system is a prerequisite for detailed geochemical modelling of synvolcanic fluid-rock interactions. Parts of a physical model can be proposed for the Linda hydrothermal system and several conclusions of importance to a geochemical model can be summarized:

1. Sulphidic metasediments and local graphitic metasediments were an important hydrothermal product. Their deposition could have involved mixing of hydrothermal fluid and seawater (Janecky and Seyfried, 1984), or a density-stratified fluid (Zierenberg and Shanks, 1988; Costa *et al.*, 1983).
2. Silicic and albitic alteration near the seafloor surface preceded the main Fe-Mg-Zn alteration and may have been cyclical.
3. High V concentrations and low Zr/TiO_2 appear to be a primary magmatic signature of quartz-megaphyric felsic rocks and intercalated rocks. The distinctive geochemical signature was preserved regardless of type or intensity of hydrothermal alteration and, thus, may provide a stratigraphic tracer in altered rocks. High V and low Zr/TiO_2 is common to quartz-megaphyric rocks of unit 4 on both sides of the Anderson Bay structure, to unit 7 higher in the stratigraphy in the Linda area, and to the Sneath Lake tonalite (Table 2 of

Walford and Franklin, 1982). The significance of these observations requires further investigation; however, the potential exists for evaluating the primary magmatic relationships between these units.

4. Calcite in the main massive sulphide body at the Linda deposit is of epigenetic origin and not directly related to the synvolcanic alteration. This has potential implications for the occurrence of calcite and statically crystallized calc-silicate minerals in other deposits in the Snow Lake region (*e.g.* Chisel Lake mine; Williams, 1961).
5. The common occurrence of gahnite and zincian staurolite in altered rocks reflects the metamorphic desulphidation of sphalerite. By inference, the original hydrothermal deposit had a higher proportion of sphalerite. Most assay techniques used by exploration geologists do not detect Zn in silicate and oxide minerals, as this does not represent 'extractable' base metal from an economic perspective. Metamorphosed Zn-rich deposits could commonly have their proportion of Zn underestimated, if assay results have been used; this may be important in the classification of massive sulphide deposits in terms of proportions of Zn, Cu and Pb (Franklin, 1986; Franklin *et al.*, 1981).
6. Chlorine and bisulphide ions have commonly been assumed to be the most important ligands involved in the transportation of metal complexes (Lydon, 1988; Franklin *et al.*, 1981). The high F content of metamorphic biotite and anthophyllite at the Linda deposit suggests high F content in the protolith and, thus, F^- ion may have been significant in the hydrothermal fluid, as is the case in porphyry Cu and Mo deposits (Munoz, 1984; Parry *et al.*, 1984; Gunow *et al.*, 1980). Similarly, the common occurrence of apatite and tourmaline suggest high F and B contents in the protolith.
7. Metamorphic devolatization reactions may have resulted in the redistribution of volatile constituents on a large scale, as has been suggested for margarite-bearing rocks (*see* 7.4.2. Inferred Prograde Metamorphic Reactions).

12.2. Structure and Stratigraphy.

The Anderson Bay structure has been introduced in this study to replace the proposed F_1 Anderson Bay anticline (Jeffery, 1982), in acknowledgment that there is a major structural feature between Anderson Creek and the Linda deposit, the

nature and relationships of which are enigmatic. The generic term 'structure' emphasizes the ambiguity and allows indication of the feature on geological maps without any interpretative or genetic connotation. It may be that more work focussing on the Anderson Bay structure will solve the problem. This study has identified several pertinent points:

1. The Linda deposit and the stratigraphic sequence on the southeast side of the Anderson Bay structure are overturned, in agreement with the conclusions of (Jeffery, 1982). The stratigraphic facing direction changes in the area between Anderson Creek and the Linda deposit.

2. Lithological units are not continuous across the trace of the Anderson Bay structure and direct stratigraphic correlation is not warranted. Correlation is not precluded and, in particular, the geochemical signature of high V and low Zr/TiO_2 is common to quartz-megaphyric felsic rocks on both sides of the structure. The generalized stratigraphic sequence for the Anderson Lake and Stall Lake mines (Walford and Franklin, 1982) is similar to that for the Linda deposit (*see* Figure 3.4). The association of massive sulphide mineralization and alteration with the lateral termination of mafic volcanic (or subvolcanic?) units and with lenses of graphitic metasediments is common to several deposits in the region (*ibid.*; Studer, 1982; Coats *et al.*, 1970).

3. Cleavage vergence of S_0/S_1 and S_1/S_2 does not change across the Anderson Bay structure; however, cleavages were reactivated and probably do not preserve their original vergence relationships. The presence of cleavage-transected folds can be expected in the area. The Anderson Bay structure may have been reactivated after its initial formation.

4. The sequence of lithological units on the southeast side of the Anderson Bay structure has been interpreted as a stratigraphic succession. However, the structural complexity increases towards Kormans Lake (*see* Figures 3.1, 4.1, 4.2) and towards an area northeast of Kormans Lake, where the McLeod Road thrust fault may converge with a possible extension of the Berry Creek fault (Figures 2.1, 2.2). Within the area mapped for this study, Amisk Group pelitic metasediments (unit 9) may be in a thrusted relationship with the overlying unit of mafic to intermediate volcanic rocks (unit 6). The continuation of

the proposed thrust fault to the southwest has not been identified, but the possibility of a cryptic suture in the Linda area cannot be ignored.

5. Microstructural features which consist of abundant S_1 'Tuttle' deformation lamellae, defined by rutile trails in quartz-megaphyric felsic rocks (unit 4), are inherently difficult to relate to a major structure. The difference in scale makes physical correlation tenuous; the amount of strain required to produce the 'Tuttle' lamellae and the amount of bulk strain which they may represent are unknown. They have been emphasized somewhat in this study for the following reasons: their prevalence in unit 4, which hosts the largest pyrite-calcite body and terminates in the northeast in the vicinity of unit 9 (*see above*); the 'Tuttle' lamellae appear to record microstructural evidence of D_1 deformation despite the recrystallization of the host minerals; their description, documentation and interpretation in this study may contribute to their recognition elsewhere.

The Linda deposit lies in a high strain zone with respect to the area to the northwest of the Anderson Bay structure. Some analogies can be drawn between the F_2 microfold examined in detail in Chapter 7 (*see* 7.1.2. F_2 Microfolds; Figure 7.1) and the structure of the area mapped for this study (Figure 3.1). The lithological units on the southeast side of the Anderson Bay structure are generally thinner than similar units to the northwest, a general observation without an implied stratigraphic correlation. Numerous tight F_2 minor folds occur mainly on the southeast. The structural styles on the southeast and northwest sides of the Anderson Bay structure resemble the thinned tightened limb, and the thickened decrenulated limb, respectively, of the F_2 microfold. As in the case of the microfold, this suggests that the high strain in the Linda area may be an artifact of the orientation of the units in a later superimposed stress regime. The units on the northwest of the Anderson Bay structure may have been oriented in the compressional field of the strain ellipsoid and undergone tectonic thickening, whereas the units on the southeast were oriented in the extensional field and underwent thinning and tightening of pre-existing structures. Note that this interpretation would require a dextral sense of late shear and transposition on shear planes subparallel to the Anderson Bay structure and S_1, in order to achieve the presently observed configuration. The interpretation implies that the change in the degree of strain

recorded by the rocks on either side of the Anderson Bay structure is not simply a function of heterogeneous strain distribution, but also of orientation in the strain ellipsoid.

All early D_2 and $D_1(?)$ kinematic indicators observed at the Linda deposit show a sinistral sense of movement. Mimetic skeletal porphyroblasts at the Linda deposit preserve an S_1/S_2 cleavage vergence which is opposed to the cleavage vergence of the phyllosilicate matrix (*see* 7.2.3. Opposed Cleavage Vergence between Porphyroblasts and Matrix). In the Linda area and much of the Snow Lake region, phyllosilicate minerals record a dextral cleavage vergence which is apparently the result of late D_2, or possibly D_3, reactivation. This reactivation occurred on the S_1 cleavage and rotated S_2 without substantially reorienting S_1. Note that this interpretation of the microstructural relationships is analogous to the dextral shear parallel to S_1 proposed for the Linda area in the previous paragraph. The same reactivation could thus account for microstructural, outcrop, and map-scale observations. The late reactivation has not been correlated with any major structure; the Berry Creek fault may be related, but at present, little information is available regarding its history. However, it appears that dextral S_1/S_2 cleavage vergence is widespread in the Snow Lake region (Figure 2 of Froese and Moore, 1980; Galley *et al.*, 1988); if the causal relationship inferred at the Linda deposit is generally applicable, reactivation on a regional scale is indicated. Examination of porphyroblast/matrix relationships elsewhere in the Snow Lake region may provide more evidence in this regard.

12.3. Metamorphism.

The mineral parageneses at the Linda deposit are consistent with the biotite-staurolite zone of amphibolite-facies regional metamorphism, in accordance with the location of the deposit with respect to the isograds mapped in the Snow Lake region (Froese and Moore, 1980; Froese and Gasparrini, 1975). Regional metamorphism at the Linda deposit did not exceed the stability field of margarite + quartz. The occurrence of assemblages of higher (and lower) apparent grade is the result of unusual bulk-rock compositions. For example, manganiferous garnet coexists with chlorite and muscovite, zincian staurolite coexists with anthophyllite, and F-rich biotite coexists with kyanite, all at the regional metamorphic grade achieved by the relatively small volume containing the Linda deposit. The parageneses represent a

metamorphic facies at the same grade as the country rock. The similarity of the parageneses observed at the Linda deposit to a prograde metamorphic series is due to the presence of additional components which are normally negligible in pelitic metasediments. Many metamorphic reactions which are discontinuous in typical pelitic metasediments (and thus, produce index assemblages indicative of metamorphic grade) are continuous reactions in altered bulk-rock compositions and produce assemblages stable over a range of temperature and pressure. In the continuous reactions, the mineral compositions are indicative of grade.

The influence of bulk-rock composition on metamorphic reactions provides an explanation for the commonly observed dichotomy between kyanite-biotite assemblages in alteration zones and sillimanite-biotite assemblages in pelitic metasediments. The reaction

$$chlorite + staurolite + muscovite \rightleftharpoons biotite + aluminosilicate + H_2O$$

was able to proceed at lower temperatures, within the stability field of kyanite, in F-bearing altered rocks. The kyanite persisted metastably through prograde metamorphism within the sillimanite field, while the same aluminosilicate-biotite producing reaction was initiated in F-poor pelitic metasediments.

Metamorphic reactions at the Linda deposit involved silicate, oxide and sulphide minerals and were modelled in the SiO_2-Al_2O_3-FeO-MgO-ZnO-K_2O-H_2O-S_2-O_2 system. Despite the range of bulk-rock compositions, the presence of quartz, muscovite and pyrite in most assemblages and the assumptions of fixed pressure, temperature and f_{H_2O} allowed chemographic derivation of a petrogenetic grid in $\log f_{S_2}$-$\log f_{O_2}$ (*see* Figure 10.2). Decreasing $\log f_{O_2}$ and increasing $\log f_{S_2}$ results in a sequence of assemblages which progressively contain gahnite, zincian staurolite or sphalerite. At low $\log f_{O_2}$-$\log f_{S_2}$ and at high $\log f_{O_2}$-$\log f_{S_2}$, chemographic analysis indicates that the sequence is modified, with gahnite being more stable than staurolite with increasing $\log f_{S_2}$. Calibration of the petrogenetic grid derived here could be attempted using thermodynamic data, for example, for composition of Fe-Mg silicate minerals involved in continuous sulphidation reactions (Bryndzia and Scott, 1987a; Tso *et al.*, 1979; Popp *et al.*, 1977; Hammarbäck and Lindqvist, 1972). Sphalerite geobarometry yielded metamorphic pressures of about 5 kb and

the maximum temperature is limited to about 550°C by the coexistence of margarite + quartz (*see* Figure 7.6).

Metamorphism involved element migration, in some cases on scales exceeding the size of a hand sample. The textural and structural relationships of the pyrite-calcite rocks were interpreted as evidence for post-tectonic synmetamorphic carbonate metasomatism. The critical evidence includes:

1. The pyrite-calcite rocks contain a silicate enclave of metamorphic assemblages characteristic of low alkali and low calcic bulk-rock compositions, *i.e.* anthophyllite-staurolite-gahnite.
2. Zoning along contacts between pyrite-calcite rocks and silicate enclaves shows features of textural and mineralogical disequilibrium or partial equilibrium, *e.g.* symplectic and corona structures (*see* Plate 5.6), and progressive change in plagioclase composition over 4 cm from oligoclase-andesine to bytownite (*see* Table 5.2).
3. In 'least-altered' cores, some enclaves contain microstructures identical to those of felsic rocks of unit 4, *e.g.* 'Tuttle' deformation lamellae consisting of rutile trails (*see* Plate 5.6, o–p).
4. The pyrite-calcite rocks and zoning along contacts to enclaves shows textures typical of static crystallization, in contrast to the strong directional fabrics of the altered felsic host rocks.

The enclaves are thus wall-rock inclusions which were engulfed by the pyrite-calcite body during synmetamorphic infiltration of carbonate. The origin of the anthophyllite-staurolite-gahnite enclave remains enigmatic, as this assemblage was observed only in the single occurrence as an isolated enclave. Its low alkali mineralogy is atypical of the proximal alteration zone.

Dynamometamorphic fabric formation also involved element migration, but in this case, the scale of mobility seems to have been more limited. Metamorphic-segregation layering possibly evolved in a closed system on a hand-sample scale, but mass-balance calculations directed at the geochemistry of the fabrics are needed to establish this. At least in some cases, silica was mobile on a larger scale; concordant quartz veins acquired silica from desilification of wall rocks. Discordant quartz veins represent late or post-tectonic migration of silica and, thus, it appears that the

major proportion of quartz veins at the Linda deposit are of epigenetic origin and not related to synvolcanic hydrothermal alteration.

12.4. Conclusion.

This thesis commenced with a tribute of Eskola and his followers, among whom I now number myself. There is a certain irony in the realization that a good part of the research has been devoted to rediscovering the concept of metamorphic facies at the Linda deposit, and finding that the seminal work of Eskola on the 'pneumatolytic formations' of the Orijärvi region does indeed still apply. In part, this illustrates the fascinating variety of mineral assemblages and textures displayed by metamorphosed altered rocks, such that it requires some convincing that the rocks were subject to the laws of nature and thermodynamics, and are thus, amenable to a logical scientific examination and exposition. This thesis therefore also concludes with a homage to Eskola.

References

Addy, S.K. and Ypma, P.J.M. (1977): Origin of massive sulfide deposits at Ducktown, Tennessee: an oxygen, carbon, and hydrogen isotope study. *Econ. Geol.* **72**, 1245–1268.

Armstrong, J.E. (1941): Wekusko (Herb) Lake, Manitoba. *Geological Survey of Canada Map* **665A**, *with descriptive notes.*

Bäcker, H., Lange, J. and Marchig, V. (1985): Hydrothermal activity and sulphide formation in axial valleys of the East Pacific Rise crest between 18 and 22 degrees S. *Earth Planet. Sci. Lett.* **72**, 9–22.

Bailes, A.H. (1988): GS–8 Chisel–Morgan Lakes project. *Manitoba Energy and Mines, Minerals Division, Report of Field Activities* **1988**, 53–61.

Bailes, A.H. (1987): GS–12 Chisel–Morgan Lakes project. *Manitoba Energy and Mines, Minerals Division, Report of Field Activities* **1987**, 70–79.

Bailes, A.H. (1986): Chisel–Morgan Lakes project. *Manitoba Energy and Mines, Minerals Division, Report of Field Activites* **1986**, 71–76.

Bailes, A.H. (1971): Preliminary compilation of the geology of the Snow Lake–Flin Flon–Sherridon area, Manitoba. *Manitoba Mines Branch, Geological Paper* **1/71**, 27 pages.

Bailes, A.H., Gordon, T.M. and Hunt, P.A. (1988): GS–10 zircon geochronology of the Richard Lake tonalite, a possible synvolcanic pluton in the Snow Lake area. *Manitoba Energy and Mines, Minerals Division, Report of Field Activities* **1988**, 63–65.

Bailes, A.H., Syme, E.C., Galley, A., Price, D.P., Skirrow, R. and Ziehlke, D.J. (1987): Early Proterozoic volcanism, hydrothermal activity, and associated ore deposits at Flin Flon and Snow Lake, Manitoba. *Field Trip Guidebook, GAC–MAC Joint Annual Meeting, Saskatoon, Saskatchewan*, 95 pages.

Bak, J., Korstgård, J. and Sørensen, K. (1975): A major shear zone within the Nagssugtoquidian of West Greenland. *Tectonophys.* **27**, 191–209.

Ballard, R.D., Hekinian, R. and Francheteau, J. (1984): Geological setting of hydrothermal activity at 12 degrees 50' N on the East Pacific Rise: a submersible study. *Earth Planet. Sci. Lett.* **69**, 176–186.

Beach, A. (1979): Pressure solution as a metamorphic process in deformed terrigenous sedimentary rocks. *Lithos* **12**, 51–58.

Beach, A. and King, M. (1978): Discussion on pressure solution. *J. Geol. Soc. Lond.* **135**, 649–651.

Beach, A. and Jack, S. (1982): Syntectonic vein development in a thrust sheet from the external French Alps. *Tectonophys.* **81**, 67–84.

Bell, A.M. (1981): Vergence: an evaluation. *J. Struct. Geol.* **3**, 197–202.

Bell, T.H. (1986): Foliation development and refraction in metamorphic rocks: reactivation of earlier foliations and decrenulation due to shifting patterns of deformation partitioning. *J. Metamorphic Geol.* **4**, 421–444.

Bell, T.H. (1985): Deformation partitioning and porphyroblast rotation in metamorphic rocks: a radical reinterpretation. *J. Metamorphic Geol.* **3**, 109–118.

Bell, T.H. (1981): Foliation development: the contribution, geometry and significance of progressive bulk inhomogeneous shortening. *Tectonophys.* **75**, 273–296.

Bell, T.H., Rubenach, M.J. and Fleming, P.D. (1986): Porphyroblast nucleation, growth and dissolution in regional metamorphic rocks as a function of deformation partitioning during foliation development. *J. Metamorphic Geol.* **4**, 37–67.

Bell, T.H. and Rubenach, M.J. (1983): Sequential porphyroblast growth and crenulation cleavage development during progressive deformation. *Tectonophys.* **92**, 171–194.

Bell, T.H. and Rubenach, M.J. (1980): Crenulation cleavage development—evidence for progressive bulk inhomogeneous shortening from 'millipede' microstructures in the Robertson River Metamorphics. *Tectonophys.* **68**, T9–T15.

Berman, R.G., Brown, T.H. and Perkins, E.H. (1987): GE0-CALC. Software for calculation and display of pressure-temperature-composition phase diagrams. *copywrite (c) The University of British Columbia.*

Berthé, D., Choukroune, P. and Jegouzo, P. (1979): Orthogneiss, mylonites and non coaxial deformation of granites: the example of the South Amorican shear zone. *J. Struct. Geol.* **1**, 31–42.

Bird, D.K. and Helgeson, H.C. (1981): Chemical interaction of aqueous solutions with epidote-feldspar mineral assemblages in geologic systems II. Equilibrium constraints in metamorphic/geothermal processes. *Am. J. Sci.* **281**, 576–614.

Borradaile, G.J. (1982): Tectonically deformed pillow lava as an indicator of bedding and way-up. *J. Struct. Geol.* **4**, 469–479.

Borradaile, G.J. (1978): Transected folds: a study illustrated with examples from Canada and Scotland. *Geol. Soc. Am. Bull.* **89**, 481–493.

Bouchez, J.L. and Nicolas, A. (1983): Fabric asymmetry and shear sense in movement zones. *Geologische Rundschau* **72**, 401–419.

Bowers, T.S. and Taylor, H.P.Jr. (1985): An integrated chemical and stable-isotope model of the origin of mid-ocean ridge hot spring systems. *J. Geophys. Res.* **90**, 12583–12606.

Bristol, C.C. (1974): Sphalerite geobarometry of some metamorphosed orebodies in the Flin Flon and Snow Lake districts, Manitoba. *Can. Mineral.* **12**, 308–315.

Brunel, M. (1980): Quartz fabrics in shear-zone mylonites: evidence for a major imprint due to late strain increments. *Tectonophys.* **64**, T33–T44.

Bryndzia, L.T. and Scott, S.D. (1987a): The composition of chlorite as a function of sulfur and oxygen fugacity: an experimental study. *Am. J. Sci.* **287**, 50–76.

Bryndzia, L.T. and Scott, S.D. (1987b): Application of chlorite-sulfide-oxide equilibria to metamorphosed massive sulfide ores, Snow Lake, Manitoba. *Econ. Geol.* **82**, 963–970.

Bucher-Nurminen, K., Frank, E. and Frey, M. (1983): A model for the progressive regional metamorphism of margarite-bearing rocks in the central Alps. *Am. J. Sci.* **283-A**, 370–395.

Byers, A.R. (1969): The Coronation Mine Project. In *Geological Survey of Canada, Paper* **68–5**, 1–5.

Coats, C.J.A., Clarke, L.A., Buchan, R. and Brummer, J.J. (1970): Geology of the copper-zinc deposits of Stall Lake Mines Ltd., Snow Lake area, N. Manitoba. *Econ. Geol.* **65**, 970–984.

Cosgrove, J.W. (1976): The formation of crenulation cleavage. *J. Geol. Soc. Lond.* **132**, 155–178.

Costa, U.R., Barnett, R.L. and Kerrich, R. (1983): The Mattagami Lake Mine Archean Zn-Cu sulfide deposit, Quebec: Hydrothermal coprecipitation of talc and sulfides in sea-floor brine pool—evidence from geochemistry, $^{18}O/^{16}O$ and mineral chemistry. *Econ. Geol.* **78**, 1144–1203.

Cox, K.G., Bell, J.D. and Pankhurst, R.J. (1979): The Interpretation of Igneous Rocks. George Allen and Unwin Ltd., London, 450 pages.

Craig, J.R. and Scott, S.D. (1974): Sulfide phase equilibria. In Ribbe, P.H. (*ed.*): Sulfide Mineralogy, *MSA Short Course Notes* **1**, CS1–CS104.

Davies, M.D. (1985): Tourmalines from Appalachian–Caledonian massive sulfide deposits: textural, chemical, and isotopic relationships—a discussion. *Econ. Geol.* **80**, 2038–40.

Deer, W.A., Howie, R.A. and Zussman, J. (1966): An Introduction to the Rock-Forming Minerals. Longman Group Ltd., London, 528 pages.

Dietvorst, E.J.L. (1980): Biotite breakdown and the formation of gahnite in metapelitic rocks from Kemiö, southwest Finland. *Contrib. Mineral. Petrol.* **75**, 327–337.

Dimroth, E., Imreh, L., Cousineau, P., Leduc, M. and Sanschagrin, Y. (1985): Paleogeographic analysis of mafic submarine flows and its use in the exploration for massive sulphide deposits. In Ayres, L.D., Thurston, P.C., Card, K.D. and Weber, W. (*eds.*): Evolution of Archean Supracrustal Sequences, *Geol. Assoc. Can. Spec. Paper* **28**, 203–222.

Driessche, J. and Brun, J.-P. (1987): Rolling structures at large shear strain. *J. Struct. Geol.* **9**, 691–704.

Dutrow, B.L., Holdaway, M.J. and Hinton, R.W. (1986): Lithium in staurolite and its petrologic significance. *Contrib. Mineral. Petrol.* **94**, 496–506.

Eskola, P. (1915): On the relations between the chemical and mineralogical composition in the metamorphic rocks of the Orijärvi region. *Bulletin de la Commission Géologique de Finlande* **18**, 108–145.

Evans, B.W. (1969): Chlorine and fluorine in micas of pelitic schists from the sillimanite-orthoclase isograd, Maine. *Am. Mineral.* **54**, 1209–1211.

Ferry, J.M. (1981): Petrology of graphitic sulfide-rich schists from south-central Maine: an example of desulfidation during prograde regional metamorphism. *Am. Mineral.* **66**, 908–930.

Finger, L.W. and Burt, D.M. (1972): Reaction. A Fortran IV computer program to balance chemical reactions. *Geophysical Laboratory, Washington, D.C.*

Fisher, R.V. and Schmincke, H.-U. (1984): Pyroclastic Rocks. Springer-Verlag, New York, 472 pages.

Fleming, T. (*unpubl.*): Anderson Lake mine tour. *Hudsons Bay Mining and Smelting tour guide.*

Floyd, P.A. and Winchester, J.A. (1977): Identification and discrimination of altered and metamorphosed volcanic rocks using immobile elements. *Chem. Geol.* **21**, 291–306.

Foster, M.D. (1962): Interpretation of the composition and a classification of the chlorites. *U.S.G.S. Prof. Paper* **414-A**, 29 pages.

Fox, J.S. (1975): Three-dimensional isograds from the Lukmanier Pass, Switzerland, and their tectonic significance. *Geol. Mag.* **112**, 547–564.

Franklin, J.M. (1986): Volcanic-associated massive sulphide deposits—an update. In Andrew, C.J., Crowe, R.W.A., Finlay, S., Pennell, W.M. and Pyne, J.F. (*eds.*):

Geology and Genesis of Mineral Deposits in Ireland. *Irish Association for Economic Geology, Dublin*, 49–69.

Franklin, J.M., Lydon, J.W. and Sangster, D.F. (1981): Volcanic-associated massive sulfide deposits. In Skinner, B.J. (*ed*): Economic Geology, 75th Anniversary Volume, 485–627.

Frey, M. (1978): Progressive low-grade metamorphism of a black shale formation, central Swiss Alps, with special reference to pyrophyllite and margarite bearing assemblages. *J. Petrol.* **19**, 95–135.

Frey, M., Bucher, K., Frank, E. and Schwander, H. (1982): Margarite in the Central Alps. *Schweiz. Mineral. Petrog. Mitt.* **62**, 21–45.

Frey, M. and Orville, P.M. (1974): Plagioclase in margarite-bearing rocks. *Am. J. Sci.* **274**, 31–47.

Froese, E. (1981): Applications of Thermodynamics in the Study of Mineral Deposits. *Geological Survey of Canada, Paper* **80–28**, 38 pages.

Froese, E. (1977): Oxidation and sulphidation reactions. In Greenwood, H.J. (*ed*): Short Course in Application of Thermodynamics to Petrology and Ore Deposits. *MAC Short Course Handbook, vol* **2**, 84–98.

Froese, E. (1971): The graphical representation of sulfide-silicate phase equilibria. *Econ. Geol.* **66**, 335–341.

Froese, E. (1969): Metamorphic rocks from the Coronation mine and surrounding area. *Geological Survey of Canada, Paper* **68-5**, 55–77.

Froese, E. and Moore, J.M. (1980): Metamorphism in the Snow Lake area, Manitoba. *Geological Survey of Canada, Paper* **78-27**, 16 pages.

Froese, E. and Gasparrini, E. (1975): Metamorphic zones in the Snow Lake area. *Can. Mineral.* **13**, 162–167.

Frondel, C. and Ito, J. (1975): Zinc-rich chlorites from Franklin, New Jersey. *Nueus Jb. Mineral. Abh.* **123(2)**, 111–115.

Gale, G.H. and Koo, J. (1977): Evaluation of massive sulphide environments. *Canada-Manitoba Non-renewable Resource Evaluation Program, 2nd Annual Report* **1976–1977**, *Man. Dept. of Mines, Resources and Environmental Management*, 43–62.

Galley, A., Ames, D.E. and Franklin, J.M. (1988): Geological setting of gold mineralization, Snow Lake, Manitoba. *Geological Survey of Canada, Open File* **1700**.

Ganguly, J. and Saxena, S.K. (1987): Mixtures and Mineral Reactions. Springer-Verlag, New York, 291 pages.

Ganguly, J. and Newton, R.C. (1968): Thermal stability of chloritoid at high pressure and relatively high oxygen fugacity. *J. Petrol.* **9**, 444–446.

Gibson, H.L., Watkinson, D.H. and Comba, C.D.A. (1983): Silicification: hydrothermal alteration in an Archean geothermal system within the Amulet Rhyolite Formation, Noranda, Quebec. *Econ. Geol.* **78**, 954–971.

Goldschmidt, V.M. and Muir, M. (*ed.*) (1958): Geochemistry. Claredon Press, Oxford, 730 pages.

Gordon, T.M. (1981): Metamorphism in the Crowduck Bay area, Manitoba. *Geological Survey of Canada, Paper* **81-1A**, 315–316.

Gordon, T.M. and Gall, Q. (1982): Metamorphism in the Crowduck Bay area, Manitoba. *Geological Survey of Canada, Paper* **82–1A**, 197–201.

Govindaraju, K. (1984): 1984 compilation of working values and sample description for 170 international reference standards of mainly silicate rocks and minerals. *Geostandards Newsletter Spec. Issue* **8**, 3–16 plus appendices.

Gray, D.R. (1979a): Microstructure of crenulation cleavage differentiation: implications of solution-deposition processes. *J. Struct Geol.* **1**, 73–80.

Gray, D.R. (1979b): Microstructure of crenulation cleavages: an indicator of cleavage origin. *Am. J. Sci.* **279**, 97–128.

Gray, D.R. (1977): Morphologic classification of crenulation cleavage. *J. Geol.* **85**, 229–235.

Gray, D.R. and Durney, D.W. (1979): Investigations on the mechanical significance of crenulation cleavage. *Tectonophys.* **58**, 35–79.

Greenwood, H.J. (1975): Thermodynamically valid projections of extensive phase relations. *Am. Mineral.* **60**, 1–8.

Greenwood, H.J. (1968): Matrix methods and the phase rule in petrology. *XXIII International Geological Congress* **6**, 267–279.

Grieve, R.A.F. and Fawcett, J.J. (1974): The stability of chloritoid below 10 kb P(H2O): *J. Petrol.* **15**, 113–139.

Grove, T.L., Ferry, J.M. and Spear, F.S. (1983): Phase transitions and decomposition relations in calcic plagioclase. *Am. Mineral.* **68**, 41–59.

Guggenheim, S. (1984): The brittle micas. In Bailey, S.W. (*ed.*): Micas. *Reviews in Mineralogy* **13**, Mineral. Soc. Am., 61–104.

Guidotti, C.V. (1984): Micas in metamorphic rocks. In Bailey, S.W. (*ed.*): Micas. *Reviews in Mineralogy* **13**, Mineral. Soc. Am., 357–468.

Guidotti, C.V. and Sassi, F.P. (1976): Muscovite as a petrogenetic indicator mineral in pelitic schists. *N. Jahrb. Mineral. Monatsh.* **127**, 97–142.

Gunning, H.G. (1959): Origin of massive sulphide deposits. *Can. Inst. Mining Metall. Trans.* **62**, 318–321.

Gunow, A.J., Ludington, S. and Munoz, J.L. (1980): Fluorine in micas from the Henderson molybdenite deposit, Colorado. *Econ. Geol.* **75**, 1127–1137.

Hammarbäck, S. and Lindqvist, B. (1972): The hydrothermal stability of annite in the presence of sulfur. *Geol. Föreningens i Stockholm Förhandlingar* **94**, 549–564.

Harrison, J.M. (1949): Geology and mineral deposits of File–Tramping Lakes area, Manitoba. *Geological Survey of Canada, Memoir* **250**, 92 pages.

Hawthorne, F.C. (1982): Crystal chemistry of the amphiboles. In Veblen, D.R. (*ed.*): Amphiboles and Other Hydrous Pyriboles—Mineralogy, *Reviews in Mineralogy* **9A**, Mineral. Soc. Am., 1–102.

Henry, D.J. and Guidotti, C.V. (1985): Tourmaline as a petrogenetic indicator mineral: an example from the staurolite-grade metapelites of NW Maine. *Am. Mineral.* **70**, 1–15.

Hobbs, B.E., Means, W.D. and Williams, P.F. (1976): John Wiley and Sons, Inc., New York, 571 pages.

Hoffman, P.F. (1988): United plates of America, the birth of a craton: Early Proterozoic assembly and growth of Laurentia. *Ann. Rev. Earth Planet. Sci.* **16**, 543–603.

Holdaway, M.J., Dutrow, B.L. and Hinton, R.W. (1988): Devonian and Carboniferous metamorphism in west-central Maine: The muscovite-almandine geobarometer and the staurolite problem revisited. *Am. Mineral.* **73**, 20–47.

Holdaway, M.J., Dutrow, B.L. and Shore, P. (1986): A model for the crystal chemistry of staurolite. *Am. Mineral.* **71**, 1142–1159.

Holdaway, M.S. (1971): Stability of andalusite and the aluminum silicate phase diagram. *Am. J. Sci.* **271**, 97–131.

Hoschek, G. (1969): The stability of staurolite and chloritoid and their significance in metamorphism of pelitic rocks. *Contrib. Mineral. Petrol.* **22**, 208–232.

Hoschek, G. (1967): Untersuchungen zum stabilitätsbereich von chloritoid und staurolith. *Contrib. Mineral. Petrol.* **14**, 123–162.

Humphris, S.E. and Thompson, G. (1978): Trace element mobility during hydrothermal alteration of oceanic basalts. *Geochim. Cosmochim. Acta* **42**, 127–136.

Hutcheon, I. (1979): Sulfide-oxide-silicate equilibria, Snow Lake, Manitoba. *Am. J. Sci.* **279**, 643–665.

Hutcheon, I. (1977): The metamorphism of sulfide-bearing pelitic rocks from Snow Lake, Manitoba. *Ph.D. Thesis (unpublished), Carlton University, Ottawa*, 205 pages.

Hutchinson, R.W. (1982): Syn-depositional hydrothermal processes and Precambrian sulphide deposits. In Hutchinson, R.W., Spence, C.D. and Franklin, J.M. (*eds.*): Precambrian Sulphide Deposits, *Geol. Assoc. Can. Spec. Paper* **25**, 762–791.

Hutchinson, R.W. (1965): Genesis of Canadian massive sulphides reconsidered by comparison to Cyprus deposits. *Can. Inst. Mining Metall. Trans.* **68**, 286–300.

Hutchison, M.N. and Scott, S.D. (1981): Sphalerite geobarometry in the Cu-Fe-Zn-S system. *Econ. Geol.* **76**, 143–153.

Irvine, T.N. and Baragar, W.R.A. (1971): A guide to the chemical classification of the common volcanic rocks. *Can. J. Earth Sci.* **8**, 521–548.

Jackson, A.R.N. (1983): Volcanism and genesis of Cu-Zn mineralization at Cook Lake, Snow Lake greenstone belt, Manitoba. *M.Sc. Thesis (unpublished), University of Western Ontario, London*, 155 pages.

Jamieson, R.A. and Craw, D. (1987): Sphalerite geobarometry in metamorphic terranes: an appraisal with implications for metamorphic pressure in the Otago Schist. *J. Metamorphic Geol.* **5**, 87–99.

Janecky, D.R. and Shanks III, W.C. (1988): Computational models of chemical and sulfur isotopic reaction processes in seafloor hydrothermal systems: chimneys, massive sulfides, and subjacent alteration zones. *Can. Mineral.* **26**, 805–825.

Janecky, D.R. and Seyfried, W.E.Jr. (1984): Formation of massive sulfide deposits on oceanic ridge crests: Incremental reaction models for mixing between hydrothermal solutions and seawater. *Geochim. Cosmochim. Acta* **48**, 2723–2738.

Jeffery, B.D. (1982): Evaluation Report. Corporation Falconbridge Copper. Linda-McKayseff properties, Snow Lake, Manitoba. *unpublished*, 41 pages.

Karabinos, P. (1985): Garnet and staurolite producing reactions in a chlorite-chloritoid schist. *Contrib. Mineral. Petrol.* **90**, 262–275.

Kerrich, R. (1977): An historical review and synthesis of research on pressure solution. *Zbl. Geol. Paläont.* **1**, 512–550.

Kerrich, R., Fyfe, W.S., Barnett, R.L., Blair, B.B. and Willmore, L.M. (1987): Corundum, Cr-muscovite rocks at O'Briens, Zimbabwe: the conjunction of hydrothermal desilicification and LIL-element enrichment—geochemical and isotopic evidence. *Contrib. Mineral. Petrol.* **95**, 481–498.

Kerrick, D.M. (1968): Experiments on the upper stability limit of pyrophyllite at 1.8 kilobars and 3.9 kilobars water pressure. *Am. J. Sci.* **266**, 204–214.

Knuckey, M.J., Comba, C.D.A. and Riverin, G. (1982): Structure, metal zoning and alteration at the Millenbach deposit, Noranda, Quebec. In Hutchinson, R.W., Spence, C.D. and Franklin, J.M. (*eds.*): Precambrian Sulphide Deposits. *Geol. Assoc. Can. Spec. Paper* **25**, 255–295.

Kuno, H. (1968): Differentiation of basaltic magmas. In Hess, H.H. and Poldervaart, A. (*eds.*): Basalts, Volume 2. Interscience, John Wiley and Sons, New York, 623-688.

Lang, H.M. and Rice, J.M. (1985): Regression modelling of metamorphic reactions in metapelites, Snow Peak, Northern Idaho. *J. Petrol.* **26**, 857–887.

Leake, B.E. (1978): Nomenclature of amphiboles. *Can. Mineral.* **16**, 501–520.

Lenton, P.G. (1981): Geology of the McKnight–McCallum Lakes area. *Manitoba Dept. of Energy and Mines, Min. Res. Div., Geol. Report* **GR 79-1**, 39 pages.

Lister, C.R.B. (1980): Heat flow and hydrothermal circulation. *Ann. Rev. Earth Planet Sci.* **8**, 95–117.

Lydon, J.W. (1988): Ore deposit models #14. Volcanogenic massive sulphide deposits Part 2: Genetic models. *Geoscience Canada* **15**, 43–65.

Lydon, J.W. (1984): Volcanogenic massive sulphide deposits Part 1: a descriptive model. *Geoscience Canada* **11**, 195–202.

MacGeehan, P.J. (1977): The geochemistry of altered volcanic rocks at Matagami, Quebec: A geothermal model for massive sulphide genesis. *Can. J. Earth Sci.* **15**, 551–570.

McBirney, A.R. (1984): Igneous Petrology. Freeman, Cooper and Company, San Fransisco, 508 pages.

Martin, P.L. (1966): Structural analysis of the Chisel orebody. *Can. Inst. Mining Metall. Trans.* **69**, 208–214.

Mohr, D.W. and Newton, R.C. (1983): Kyanite-staurolite metamorphism in sulfidic schists of the Anakeesta Formation, Great Smoky Mountains, North Carolina. *Am. J. Sci.* **283**, 97–134.

Moler, C., Little, J., Bangerts, S. and Kleiman, S. (1987): PC-MATLAB for MS-DOS personal computers. The MathWorks, Inc., Sherborn, Massachusetts.

Moorhouse, W.W. (1965): Stratigraphic position of sulphides in the Archean. *Can. Inst. Mining Metall. Trans.* **68**, 261–264.

Morton, R.L. and Franklin, J.M. (1987): Two-fold classification of Archean volcanic-associated massive sulfide deposits. *Econ. Geol.* **82**, 1057–1063.

Mottl, M.J., Holland, H.D. and Carr, R.F. (1979): Chemical exchange during hydrothermal alteration of basalt by seawater—II. Experimental results for Fe, Mn and sulfur species. *Geochim. Cosmochim. Acta* **43**, 869–884.

Múnha, J., Fyfe, W.S. and Kerrich, R. (1980): Adularia, the characteristic mineral of felsic spilites. *Contrib. Mineral. Petrol.* **75**, 15–20.

Munoz, J.L. (1984): F-OH and Cl-OH exchange in micas with applications to hydrothermal ore deposits. In Bailey, S.W. (*ed.*): Micas, *Reviews in Mineralogy* **13**, Mineral. Soc. Am., 469–493.

Munoz, J.L. and Ludington, S. (1977): Fluorine-hydroxyl exchange in synthetic muscovite and its application to muscovite-biotite assemblages. *Am. Mineral.* **62**, 304–308.

Munoz, J.L. and Ludington, S. (1974): Fluoride-hydroxyl exchange in biotite. *Am. J. Sci.* **274**, 396–413.

Nesbitt, B.E. (1986a): Oxide-sulfide-silicate equilibria associated with metamorphosed ore deposits. Part I: theoretical considerations. *Econ. Geol.* **81**, 831–840.

Nesbitt, B.E. (1986b): Oxide-sulfide-silicate equilibria associated with metamorphosed ore deposits. Part II: pelitic and felsic volcanic terrains. *Econ. Geol.* **81**, 841–856.

Nesbitt, B.E. (1982): Metamorphic sulfide-silicate equilibria in the massive sulfide deposits at Ducktown, Tennessee. *Econ. Geol.* **77**, 364–378.

Nesbitt, B.E. and Kelly, W.C. (1980): Metamorphic zonation of sulfides, oxides, and graphite in and around the orebodies at Ducktown, Tennessee. *Econ. Geol.* **75**,

1010–1021.

Nordstrom, D.K. and Munoz, J.L. (1986): Geochemical Thermodynamics. Blackwell Scientific Publications, Palo Alto, California, 477 pages.

Olesen, N.Ø. (1982): Heterogeneous strain of a phyllite as revealed by porphyroblast-matrix relationships. *J. Struct. Geol.* **4**, 481–490.

Parry, W.T., Ballantyne, J.M. and Jacobs, D.C. (1984): Geochemistry of hydrothermal sericite from Roosevelt Hot Springs and the Tintic and Santa Rita porphyry copper systems. *Econ. Geol.* **79**, 72–86.

Passchier, C.W. (1987): Stable positions of rigid objects in non-coaxial flow—a study in vorticity analysis. *J. Struct. Geol.* **9**, 679–690.

Petersen, E.U., Essene, E.J. and Peacor, D.R. (1982): Fluorine end-member micas and amphiboles. *Am. Mineral.* **67**, 538–544.

Pettijohn, F.J. (1975): Sedimentary Rocks. Harper and Row, Publishers, New York, 628 pages.

Popp, R.K., Gilbert, M.C. and Craig, J.R. (1977): Stability of Fe-Mg amphiboles with respect to sulfur fugacity. *Am. Mineral.* **62**, 13–30.

Ramsay, J.G. (1980): Shear zone geometry: A review. *J. Struct. Geol.* **2**, 83–99.

Ramsay, J.G. and Huber, M.I. (1980): The Techniques of Modern Structural Geology, Volume 1: Strain Analysis. Academic Press Inc., London, 307 pages.

Reed, M.H. (1982): Calculation of multicomponent chemical equilibria and reaction processes in systems involving minerals, gases, and aqueous phase. *Geochim. Cosmochim. Acta* **46**, 513–528.

Ribbe, P.H. (1983): Exsolution textures in ternary and plagioclase feldspars; interference colors. In Ribbe, P.H. (*ed.*): Feldspar Mineralogy. *Reviews in Mineralogy* **2**, *second edition*, Mineral. Soc. Am., 241–270.

Richardson, S.W. (1968): Staurolite stability in a part of the system Fe-Al-Si-O-H. *J. Petrol.* **9**, 467–488.

Riverin, G. and Hodgson, C.J. (1980): Wall-rock alteration at the Millenbach Cu-Zn Mine, Noranda, Quebec. *Econ. Geol.* **75**, 424–444.

Roberts, R.G. and Reardon, E.J. (1978): Alteration and ore-forming processes at Mattagami Lake Mine, Quebec. *Can. J. Earth Sci.* **15**, 1–21.

Robin, P.-Y.F. (1979): Theory of metamorphic segregation and related processes. *Geochim. Cosmochim. Acta* **43**, 1587–1600.

Robinson, P., Spear, F.S., Schumacher, J.C., Laird, J., Klein, C., Evans, B.W., and Doolan, B.L. (1982): Phase relations of metamorphic amphiboles: natural occurrence and theory. In Veblen, D.R. and Ribbe, P.H. (*eds.*): Amphiboles: Petrology and Experimental Phase Relations, *Reviews in Mineralogy* **9B**, Mineral. Soc. Am., 1–227.

Rona, P.A. (1988): Hydrothermal mineralization at oceanic ridges. *Can. Mineral.* **26**, 431–465.

Rona, P.A. (1984): Hydrothermal mineralization at seafloor spreading centers. *Earth-Science Reviews* **20**, 1–104.

Roscoe, S.M. (1965): Geochemical and isotopic studies, Noranda and Matagami areas. *Can. Inst. Mining Metall. Trans.* **68**, 279–285.

Russell, G.A. (1957): Structural studies of the Snow Lake–Herb Lake area, Herb Lake mining division, Manitoba. *Manitoba Mines Branch Publ.* **55–3**, 33 pages.

Rutter, E.H. (1983): Pressure solution in nature, theory and experiment. *J. Geol. Soc. Lond.* **140**, 725–740.

Rutter, E.H. (1976): The kinetics of rock deformation by pressure solution. *Philos. Trans. R. Soc. Lond.* **A283**, 203–219.

Sato, T. (1972): Behaviours of ore-forming solutions in seawater. *Mining Geology* **22**, 31–42.

Schmidt, J.M. (1988): Mineral and whole-rock compositions of seawater-dominated hydrothermal alteration at the Arctic volcanogenic massive sulfide prospect, Alaska. *Econ. Geol.* **83**, 822–842.

Scott, R.B. (1971): Alkali exchange during devitrification and hydration of glasses in ignimbrite cooling units. *J. Geol.* **79**, 100–110.

Scott, S.D. (1974): In Sulfide Mineralogy **1**, *Reviews in Mineralogy.*, Mineral. Soc. Am., S1–S38.

Seyfried, W.E.Jr. and Mottl, M.J. (1982): Hydrothermal alteration of basalt by seawater under seawater-dominated conditions. *Geochim. Cosmochim. Acta* **46**, 985–1002.

Sharpe, J.I. (1965): Field relations of Matagami sulphide masses bearing on their disposition in time and space. *Can. Inst. Mining Metall. Trans.* **68**, 265–278.

Simmons, B.D. and Stoeterau (1978): Regional compilation map, *unpublished.*

Simpson, C. and Schmid, S.M. (1983): An evaluation of criteria to deduce the sense of movement in sheared rocks. *Geol. Soc. Am. Bull.* **94**, 1281–1288.

Skirrow, R.G. (1987): Silicification in a semiconformable alteration zone below the Chisel Lake massive sulphide deposit, Manitoba. *M.Sc. Thesis (unpublished), Carlton University, Ottawa*, 171 pages.

Skjernaa, L. (1980): Rotation and deformation of randomly oriented planar and linear structures in progressive simple shear. *J. Struct. Geol.* **2**, 101–109.

Smith, J.V. (1983): Phase equilibria of plagioclase. In Ribbe, P.H. (*ed.*): Feldspar Mineralogy. *Reviews in Mineralogy* **2**, *second edition*, Mineral. Soc. Am., 223–240.

Spear, F.S., Rumble III, D. and Ferry, J.M. (1982): Linear algebraic manipulation of N-dimensional composition space. In Ferry, J.M. (*ed.*): Characterization of Metamorphism through Mineral Equilibria, *Reviews in Mineralogy* **10**, Mineral. Soc. Am., 53–104.

Spry, A. (1969): Metamorphic Textures. Pergamon Press, Oxford, 352 pages.

Spry, P.G. (1987): Compositional zoning in zincian spinel. *Can. Mineral.* **25**, 97–104.

Spry, P.G. and Scott, S.D. (1986a): The stability of zincian spinels in sulfide systems and their potential as exploration guides for metamorphosed massive sulfide deposits. *Econ. Geol.* **81**, 1446–1463.

Spry, P.G. and Scott, S.D. (1986b): Zincian spinel and staurolite as guides to ore in the Appalachians and Scandinavian Caledonides. *Can. Mineral.* **24**, 147–163.

Storre, B. and Nitsche, K.-H. (1974): Zur stabilität von margarit im system CaO-Al_2O_3-SiO_2-H_2O. *Contrib. Mineral. Petrol.* **43**, 1–24.

Studer, R.D. (1982): Geology of the Stall Lake copper deposit, Snow Lake, Manitoba. *Can. Inst. Mining Metall. Bull.* **75**, **#837**, 66–72.

Suffel, G.G. (1965): Remarks on some sulphide deposits in volcanic extrusives. *Can. Inst. Mining Metall. Trans.* **68**, 301–307.

Swager, N. (1985): Solution transfer, mechanical rotation and kink-band boundary migration during crenulation-cleavage development. *J. Struct. Geol.* **7**, 421–429.

Syme, E.C., Bailes, A.H., Gordon, T.M. and Hunt, P.A. (1987): U-Pb zircon geochronology in the Flin Flon belt: age of Amisk volcanism. *Manitoba Energy*

and Mines, Report of Field Activities **1987**, 105–107.

Takagi, H. and Ito, M. (1988): The use of asymmetric pressure shadows in mylonites to determine the sense of shear. *J. Struct. Geol.* **10**, 347–360.

Taylor, B.E. and Slack, J.F. (1985): Tourmalines from Appalachian–Caledonian massive sulfide deposits: textural, chemical, and isotopic relationships—a reply. *Econ. Geol.* **80**, 2040–2046.

Taylor, B.E. and Slack, J.F. (1984): Tourmalines from Appalachian–Caledonian massive sulfide deposits: textural, chemical, and isotopic relationships. *Econ. Geol.* **79**, 1703–1726.

Thompson, A.B. (1976a): Mineral reactions in pelitic rocks: I. Prediction of P-T-X(Fe-Mg) phase relations. *Am J. Sci.* **276**, 401–424.

Thompson, A.B. (1976b): Mineral reactions in pelitic rocks: II. Calculation of some P-T-X(Fe-Mg) phase relations. *Am J. Sci.* **276**, 425–454.

Thompson, A.B., Tracy, R.J., Lyttle, P.T. and Thompson, J.B.Jr. (1977): Prograde reaction histories deduced from compositional zonation and mineral inclusions in garnet from the Gassetts schist, Vermont. *Am. J. Sci.* **277**, 1152–1167.

Thorpe, D.G. and Burt, D.M. (1980): A unique chloritoid-staurolite schist from near Squaw Peak, Phoenix, Arizona. *Arizona Geol. Soc. Digest* **12**, 193–200.

Tracy, R.J. (1982): Compositional zoning and inclusions in metamorphic minerals. In Ferry, J.M. (*ed.*): Characterization of Metamorphism through Mineral Equilibria, *Reviews in Mineralogy* **10**, Mineral. Soc. Am., 355–397.

Tracy, R.J. and Robinson, P. (1988): Silicate-sulfide-oxide-fluid reactions in granulite-grade pelitic rocks, central Massachusetts. *Am. J. Sci* **288-A**, 45–74.

Tracy, R.J. and McLellan, E.L. (1985): A natural example of the kinetic controls of compositional and textural equilibration. In Thompson, A.B. and Rubie, D.C. (*eds.*): Metamorphic Reactions. Kinetics, Textures, and Deformation. Springer-Verlag, New York. 118–137.

Tracy, R.J. and Thompson, A.B. (1976): Garnet composition and zoning in the determination of temperature and pressure of metamorphism, central Massachusetts. *Am. Mineral.* **61**, 762–775.

Trembath, G.D. (1986): The compositional variation of staurolite in the area of Anderson Lake mine, Snow Lake, Manitoba, Canada. *M.Sc. Thesis (unpublished), University of Manitoba, Winnipeg.* 187 pages.

Tso, J.L., Gilbert, M.C. and Craig, J.R. (1979): Sulfidation of synthetic biotites. *Am. Mineral.* **64**, 304–316.

Tuttle, O.F. (1949): Structural petrology of planes of liquid inclusions. *J. Geol.* **57**, 331–356.

Valley, J.W., Petersen, E.U., Essene, E.J. and Bowman, J.R. (1982): Fluorphlogopite and fluortremolite in Adirondack marbles and calculated C-O-H-F fluid compositions. *Am. Mineral.* **67**, 545–557.

Vernon, R.H. (1987): Evaluation of the 'quartz-eye' hypothesis—a reply. *Econ. Geol.* **82**, 1083–1084.

Vernon, R.H. (1986): Evaluation of the 'quartz-eye' hypothesis. *Econ. Geol.* **81**, 1520–1527.

Vernon, R.H. (1978): Porphyroblast-matrix microstructural relationships in deformed metamorphic rocks. *Geologische Rundschau* **67**, 288–305.

Vivallo, W. (1987): Early Proterozoic bimodal volcanism, hydrothermal activity, and massive sulfide deposition in the Boliden-Långdal area, Skellefte district, Sweden. *Econ. Geol.* **82**, 440–456.

Walford, P.C. and Franklin, J.M. (1982): The Anderson Lake Mine, Snow Lake, Manitoba. In Hutchinson, R.W., Spence, C.D. and Franklin, J.M. (*eds.*): Precambrian Sulphide Deposits. *Geol. Assoc. Can. Spec. Paper* **25**, 481–523.

Wall, V.J. and England, R.N. (1979): Zn-Fe spinel-silicate-sulphide reactions as sensors of metamorphic intensive variables and processes. *Geol. Soc. Am. Abstr. Programs* **11**, 534.

Whitmore, D.R.E. (1969): Geology of the Coronation copper deposit. *Geological Survey of Canada, Paper* **68–5**, 37–53.

Williams, H. (1966): Geology and mineral deposits of the Chisel Lake map-area, Manitoba. *Geological Survey of Canada, Memoir* **342**, 38 pages.

Williams, H. (1961): A petrographic study of the metamorphic rocks of the Chisel Lake area, northern Manitoba. *Ph.D. Thesis, (unpublished), University of Toronto, Toronto*, 211 pages.

Williams, P.F. (1985): Multiply deformed terrains—problems of correlation. *J. Struct. Geol.* **7**, 269–280.

Winkler, H.G. (1979): Petrogenesis of Metamorphic Rocks. Springer-Verlag, New York, 348 pages.

Zaleski, E. (1986): Geology of the Linda volcanogenic massive sulphide deposit, Snow Lake, Manitoba. *Geological Survey of Canada, Paper* **86–1A**, 15–20.

Zaleski, E. and Halden, N.M. (1988): Reconstruction of the synvolcanic alteration associated with the Linda massive sulphide deposit, Snow Lake, Manitoba. *Geological Survey of Canada, Paper* **88-1C**, 73–81.

Zen, E.-A. (1966): Construction of pressure-temperature diagrams for multicomponent systems after the method of Schreinemakers—a geometric approach. *U.S.G.S. Bull.* **1225**, 56 pages.

Zierenberg, R.A. and Shanks III, W.C. (1988): Isotopic studies of epigenetic features in metalliferous sediment, Atlantis II Deep, Red Sea. *Can. Mineral.* **26**, 737–753.

PART V

APPENDICES

Appendix A. Petrography.

Appendix B. Mineral Determinations.

Appendix C. Whole-rock Geochemical Analysis.

Appendix A

Petrography

Petrography was done on a sample suite of approximately 700 thin sections from surface outcrops and from drill core from 3 subsurface cross-sections (A-A', B-B', C-C'; *see* Figure 3.1) of the Linda deposit. Subsequent work was confined to the 2 cross-sections (A-A' and B-B'; in pocket) which were best constrained by drill holes. Section B-B' is available on request. Drill-hole samples were numbered according to the corresponding drill-hole footage (resolution of .5 feet or 15 cm), with an alphanumeric prefix referring to the drill-hole number as referenced on the logs provided by Falconbridge Ltd., and a single-digit suffix distinguishing lithological or mineralogical domains extracted for geochemical analysis (*see* Appendix C) from the same hand sample. The domains consist of clasts and matrix extracted from breccias, beds in metasediments, and centimetre-scale mineralogical variations which may be related to heterogeneous synvolcanic alteration, metamorphic fluids or metamorphic segregation.

The modal mineralogy of 303 samples selected for whole-rock geochemical analysis (Table C.5) is listed in Table A.1. The modal proportions were estimated visually on thin sections or areas of thin sections corresponding to the volume of rock separated for geochemical analysis. In the case of quartz-megaphyric rocks, the proportion of phenocrysts was generally estimated in a hand sample; the modal proportions of matrix minerals were estimated from thin sections and adjusted for quartz present as phenocrysts. Approximately half of the thin sections were etched and stained for K-feldspar. In some cases, plagioclase compositions were determined from the maximum extinction angles of albite twins (Deer *et al.*, 1966); however, plagioclase is commonly untwinned. In other cases, contrasts in relief with respect to quartz, and changes in the optic orientation of albite twins from length-fast to length-slow, allowed qualitative estimates of composition. The identity of opaque phases in covered thin sections was checked by shining a high intensity light on to the thin section at an oblique angle. In general, this enabled discrimination between oxide and sulphide phases, and between pyrite and pyrrhotite in samples in which they occur together. Chalcopyrite was also recognizable in reflected light, and sphalerite had a distinctive deep red colour in transmitted light. More com-

plete reflectance optical examination was done on polished thin sections prepared for electron-probe microanalysis (*see* Appendix B), including determination of the structural state of pyrrhotite.

A petrographic code was devised to supplement the lithological classification of samples and to account for variations on a scale smaller than that of mappable units (Tables A.1, A.2). The code is based mainly on mineralogical criteria, and also on characteristic textures or fabrics. In some cases, it also served to classify sample separates; for example, clasts (code=a) are distinguished from matrix (code=b). The code is essentially a short-hand notation for characteristic mineralogy and textures and was used to facilitate sorting and grouping of samples (*e.g.* in LOTUS 1-2-3 spreadsheets), and comparisons between physical and mineralogical features and geochemical analyses.

The abbreviations for mineral names in Table A.3 were used in Table A.1 and consistently throughout the text and tables of this study.

Explanatory Notes for Table A.1 (following page)

1. See Table A.2 for the key for the code (column 4).
2. Abbreviations: amph–amphibolite, brcc–breccia, calc-sil–calc-silicate, fs–felsic, gnss–gneiss, hetlith–heterolithic, inter–intermediate, min–mineralized, msdm–metasediment, ps–pseudomorph, scst–schist, s-mass–semi-massive, t–trace, volc–volcanic, y–opaque mineral present but proportion not differentiated from other opaque minerals.
3. See Table A.3 for mineral abbreviations.
4. See 3.1. Description of Lithological Units for an explanation of unit designations.
5. Subsurface samples are numbered according down-hole footage prefixed by a drill-hole number, and with a suffix distinguishing separates from the same sample (*e.g.* 24(drill hole)-097(footage=97.0)-1(first separate)). See Appendix C for further explanation.
6. Surface-sample numbers have a letter-number prefix coded to airphoto enlargements, an outcrop number, and a suffix distinguishing samples from the same outcrop.

Table A.1. Petrography and Modal Estimates.

Sample	Lithology	Unit	Code	qz	pl	am	cm	ep	cl	gt	bi	ch	mu	ma	ky	st	gh	to	py	po	sp	mg	traces etc.
24-097-1	bi-layered fs	1	epy	38	50	t		t	t	2	8	2	t										ap,al,op
24-657-1	bi-layered fs	1	epm	30	59					<1	5		5						1				al,ap
27-830-1	mu-ch-bi-layered fs	1	mvpy	50	16			t	t	3	5	10	15					t	1	t		y	ap,al,il
29-1146-1	bi-ch-layered fs	1	cepvx	25	55	2			t	2	8	5							y	y?		3	al?,il?
29-336b-1	qz-phyric fs	1	cpmi	15	54						15	1	15										ap,zi,op
29-711.5-1	bi-ch-layered fs	1	pxv	20	60			t?			9	5							t?	t		6	ap
31-705-1	qz-pl-phyric fs	1	cdhnx	35	43	8	8		t		1	1							<1			4	<1%ap
32-426-1	bi-layered fs	1	epx	40	40	1		t	t		17	t	t									2	ap
34C-1315-1	bi-layered fs	1	pxi	30	64	<1					4	t						t	t	t		2	ap
34-1130-1	bi-layered fs	1	epyxi	35	50				t	2	11	<1							t	t		2	ap
34-757.5-1	bi-layered fs	1	ep	45	30	t		<1			24									1			ap,al
H9-63-1	bi fs	1	pl	36	56				2	t	5		1										ap
H9-64-1	bi fs	1	ply	50	42				2	1	4	t	1										ap
34-1753.5-1	ch-pl-layered fs	1	gvpqu	25	43			4			5	20							3	y			ap,zi,il,ru,cp?
24-097-2	hb-zone in fs	1	fhlpv	55	10	20			5	t	5	5											ap,op
29-1146-2	hb-zone in fs	1	chfp	28	57	10			<1		3	2											<1op,al?
32-426-2	hb-zone in fs	1	fphx	40	40	14			t	<1	5	1										<1	ap
34C-1315-2	hb fs	1	fhyxi	35	45	10	1	1		3	1	1							t	t		3	ap
34C-1385-1	hb fs	1	fh	37	55	7		t		t									1	t		t	zi,al,ap
29-336a-1	qz-phyric fs	1a	c	28	70						t	t	1										1%op,ap,zi
29-501-1	pl-phyric fs	1a	dn	45	45	t	9				1	<1							t?			<1	ap,zi,il
31-259.5-1	qz-pl-phyric fs	1a	cd	35	63				t		1	<1	t							t?			1%ox,ap,su
32-1374.5-1	cherty fs	1a	vpxi	40	40						5	10										5	ap
34A-1292.5-1	cherty fs	1a	dx	55	44				t				t									1	ap
34C-1385-2	cherty fs	1a	ph	22	70	4		t		2	t								2			?	ru,ap
H8-14-1	cherty fs	1a	my	55	33			2	t	2	2		4										2%op,ap
I8-42-5	cherty fs	1a	pml	36	50				2		8		4										
19-688-1	cherty fs	1a/10p	cd	38	60						1								1	?			ap,ox
34-1397.5-1	cherty fs	1a/10p	dyvmx	40	48					3	t	3	3	1								2	ap
I8-13-1	calc-sil fs	1a/10c	pqlx	40	32			8	3		16	t	<1									1	al,ap
19-744.5-1	fs clast	1c	acd	30	70								t										op
27-1228-1	fs brcc?	1c	p	30	62				t	t	8	t	t						t	t		t	ap
34A-1360-1	cherty fs brcc	1c	du	47	48						<1		<1		<1				5				ap
34-1306.5-1	cherty brcc	1c	d	59	39						t	t	t		t				2				ap,zi?
34-1443.5-1	fs clast	1c	acd	33	65						<1		1										1%op,ap,zi
34-1443.5-2	min fs brcc	1c	cdum	34	53						1		6		<1	t			6	t?			ap,zi
19-440-1	fs volc brcc	1b	cp	32	55				t	2	10	t	1						t			?	ap
19-543-1	fs volc brcc	1b	p	20	72			t			4		2						2				ap,al?,zi,ru?
19-629-1	fs clast	1b	a	55	43					t	t		2										op
22A-1479-1	fs volc brcc?	1b	p	30	55			1	<1		14		t										ap,al,op
22B-1509.5-1	fs volc brcc	1b	cpi	30	58				t	t	12	<1											op,ap,zi
27-1165-1	bi-mu-layered fs	1b	cpmi	45	39			t	<1		10	t	6					t				t	ap,al
28-288-1	fs volc brcc?	1b	cphv	30	45	6		t			15	4								t?		t	ap,al,cp?
28-329.5-1	fs volc brcc?	1b	cmp	25	45						13	t	15					t		2			ap,zi
29-301.5-1	fs clast	1b	a	34	65						1												ap,zi,ox
29-362-1	fs volc brcc	1b	cdemp	40	48				<1	t	5	<1	7							<1			ap,zi,ox
32-1093.5-1	cherty clast	1b	a	70	30						t	t							t?				ap
32-1118.5-1	fs volc brcc	1b	cpy	40	45					1	12	t	2						t	t			su
32-828.5-1	bi-layered fs	1b	epui	37	45				t	<1	t	15	<1	t					3				ap,al,ox
32-950-1	fs volc brcc	1b	cep	60	32					1	t	5		<1									2%op
34A-1268-1	cherty clast	1b	ay	62	35						1	1	t	t					1?				
34C-1185-1	fs volc brcc	1b	pm	37	37			1	t	<1	22		3						t	t			ap,al
73-617-1	fs volc brcc	1b	cph	40	35	6	<1				15	2							2	y		y	ap,al,cp
80-1084.5-1	fs volc brcc	1b	cpnx	24	55	t	8				8	1							t			4	ap,al,il
22-413-1	volc brcc?	1d	nhx	10	46	18	18			3	t	t								t		5	ap,al,si
22-550-1	hetlith brcc	1d	h	20	30	50			t											t		t	ap,al
70-397-1	inter volc	1d	h	20	34	45			t		t								1				ox,cp
29-1197-1	qz-phyric mu-scst	4	mu	35	45				t	<1	1	1	15					t	3		t		ap,zi,al
29-464.5-1	qz-pl-phyric fs	4	dmpu	30	35				t		6	t	24						5		t		ap,zi
29-774-1	qz-pl-phyric fs	4	dpm	35	50						7	t	6							2			ap,zi
29-804-1	qz-phyric fs	4		50	47			t	t		1	<1	2							<1			ox,ap,ru
31-767-1	qz-pl-phyric fs	4	dmv	31	60			t?	t		2	3	4							t	t?		<1%ox,ap,zi
31-989.5-1	qz-phyric fs	4	mp	45	45			t			3	2	5					<1		t			<1%ox,ap,al
32-1169.5-1	qz-pl-phyric fs	4	dmp	30	55			1	t		6		8						t				al,ap,zi
32-1388-1	qz-pl-phyric fs	4	dpx	35	45						15	t	1						t	4		y	ap,zi,cp

Table A.1. Petrography and Modal Estimates. (continued)

Sample	Lithology	Unit	Code	qz	pl	am	cm	ep	cl	gt	bi	ch	mu	ma	ky	st	gh	to	py	po	sp	mg	traces etc.
32-1434.5-1	qz-pl-phyric fs	4	dmp	32	50			t	1		5		10										2%op,ap,al
32-1565-1	qz-phyric fs	4	vp	23	47						9	20							1	t			ap,ox,zi
34-1834.5-1	qz-phyric fs	4	pmi	50	35			2		<1	5	2	5					t		1			ox,ap
80-1138-1	qz-pl-phyric fs	4	p	46	50			t	t		3	<1	1										
H8-1-1	qz-phyric fs	4	pmlx	50	31			<1	3		10	t	5									1	al,ap
I7-29-1	qz-phyric fs	4	pmli	58	25			1	2		10	<1	4									<1	al,ap
I7-32-1	qz-phyric fs	4	pm	55	23			2	1		14		5										al,ap,zi
19-1233-1	qz-phyric bi-hb fs	4	gp	30	55	3		1	t		10	<1							<1	1			ap,al,zi,ru
24-1200-1	qz-phyric bi-ch fs	4	gp	35	50			<1			6	2	3							1			ap,al,zi
34A-1644.5-1	qz-phyric clast	4	gaui	48	48				t		1	t	t						3				ap,zi,sn?,ru
34A-1644.5-2	qz-phyric volc brcc	4	bgpui	30	50				t		10	t	t						10				ap,zi,al,sn?,ru
34C-1878-1	qz-phyric fs	4	gmvu	50	32				t			3	12						3				ap,zi,ru
I8-27-1	qz-phyric bi-gt fs	4	pyhti	40	40	4			t	4	10	1						1	t	<1			ap,zi,il?
I8-6-1	qz-phyric hb-bi fs	4	ph	30	50	8			<1		10	2											ap,zi,il?
22A-1191-1	bi-ch-gt-mu fs	1/10d	pvym	42	23			t	t	5	18	8	4										ap,al,il?
24-463.5-1	mu-pl scst	1/10d	m	40	40			<1			1	2	15					t	t?	2			al
70-1037.5-1	pl-bi-ch-gt-layered	1/10d	gvpy	45	35			<1		5	7	7	1					t					al,il
70-1153-1	bi-mu-gt-ch gnss	1/10d	pmvyi	35	30					5	16	5	8		t?				t?			1	ap,zi
80-1416-1	bi-mu-layered fs	1/10d	pmv	35	35				t		16	4	10						t				ox,ap,zi
31-312.5-1	fs volc brcc	1b/10d	cdmpv	25	15			t	t		9	6	45										ap,zi
80-1680.5-1	mu-bi-ch-layered fs	1b/10d	mvp	50	10				t		10	12	18						t	t?			ox,ap,al?,zi,il
19-1041.5b-1	pl-ch-bi-layered fs	1/10p	pv	3	80			t			8	8											1%il,ap,zi,al,r
22B-1783.5-1	bi-pl-layered fs	1/10p	py	45	40	t		1		1	12	t							1				
19-986-1	pl-bi-ch-st-layered	1/10p	gpv	30	60			t		t	5	3	1		1				t	t			ap,zi,il?,ru
24-1044-1	pl-ch-layered fs	1/10p	gvpu	30	25						5	37	t						t	3			ap,zi,ru,ox?
24-981a-1	pl-layered fs	1/10p	gv	37	55						3	5	t	t						t			ap,zi,il,ru
27-1324.5-1	pl-mu-ch-ma-layered	1/10p	gmvur	30	50			t		1		7	7	2				t	3	y			ap,al,zi,ru
27-1343-1	pl-ch-bi-layered fs	1/10p	gvp	25	50			<1	t		10	15							t				ap,zi,al,ru
29-1092-1	pl-mu-bi-layered fs	1/10p	cgmpu	30	30			1	t	t	10	1	23						5	y			ap,al,zi?,ru,il
34A-1679-1	pl-mu-layered fs	1/10p	gmuy	35	40					1	1	1	18					t	4				ap,zi,ru
19B-872-1	fs volc brcc	1b/10p	mupvi	60	5?						3	3	24						t	5			zi
19-1237-1	fs volc brcc	1b/10p	cpmv	27	55			t		t	10	3	3						t	2			ap,al,zi,ru?
19-662-1	fs volc brcc	1b/10p	mui	25	41						1	2	25		t	1		t	5				ap
22A-1515-1	fs volc brcc	1b/10p	cpvsi	28	37			t	t	<1	16	10	3			4		t	t?	t?		2	ap,ru?
22A-1551.5-1	qz-phyric volc brcc?	1b/10p	cpvi	30	35				t		18	15						t	2	y		y?	ap,zi
22A-1752-1	min cherty brcc	1b/10p	muk	50	12						t	2	15		8	t		<1	13		t		ap,si
22A-1752-2	cherty clast	1b/10p	am	78	1							t	21								t		ap
34-1275-1	fs volc brcc?	1b/10p	mp	30	37					t	13	<1	18						2	y			ap
19-1100-1	qz-phyric mu-scst	4/10p	mvupi	45	5						3	5	37			t			5	y	t		ap,zi
19-1250-1	qz-phyric mu fs	4/10p	mi	60	20					t	<1	1	t	17					2	t			ap,zi
22A-1885-1	qz-phyric ky-mu-bi	4/10p	mkpui	32	8						15	4	18		17				6		t		ap,zi,si?
22A-1975.5-1	qz-phyric bi-ep-gt	4/10p	puqy	46	36			2		1	10	1							4	y		y?	al
22A-1979-1	qz-phyric mu-ch scst	4/10p	mvusi	50	14							8	22			1		1		4	t		
22A-2004-1	qz-phyric mu-st scst	4/10p	omvus	47	1?				t		t	11	36	t?		1		t	4	y			ap,zi
22B-2036-1	qz-phyric mu-ch fs	4/10p	mvupi	36	30				t	<1	3	4	21			t		t	6				ap,zi,si
24-1082-1	qz-phyric ma-mu scst	4/10p	rmvu	40	24						2	5	5	20	t				4	y	y		ap
24-1228-1	qz-phyric bi-mu fs	4/10p	pvm	40	47						6	3	3					t	1	?		t?	ap,zi,il
28-343-1	qz-phyric mu scst	4/10p	om	48									50						1		1		ap,zi
29-1057-1	qz-phyric mu-ma scst	4/10p	cmrpu	29	20						5	1	25	15					5	y			zi,ru
29-1099-1	qz-phyric mu scst	4/10p	mu	38	32					t	t	1	24	t?				t	5		t		ap,zi
29-876-1	qz-phyric mu scst	4/10p	mvui	55	10							5	25		t?			t	y	5	t		ap,zi,cp
31-869.5-1	qz-phyric bi-ch-gt	4/10p	py	35	50				t	1	10	2	2						t?				<1%ox,ap,zi
34A-1565-1	qz-phyric mu-bi fs	4/10p	dmp	36	22						12	2	28					t	t	t			ap,zi
34C-1747.5-1	qz-phyric mu-bi-ky	4/10p	omukp	65							5	2	16		3	2			7	t			ap
34-1666-1	qz-phyric mu-bi-ky	4/10p	mpki	52	8				t		10		22		6				2	t			ap,zi
22A-1788-1	qz-phyric ch-bi fs	4/10p	gvpu	44	23			t			14	16							3				ap,al,zi,ru
24-1044-2	qz-phyric fs	4/10p	cgvp	48	40						4	5								3?			ru,al,ap,zi
34C-1831-1	qz-phyric mu-bi fs	4/10p	gmup	45	40					t	<1	3	<1	8					4				ap,zi,ru
34-1728-1	qz-phyric mu-bi fs	4/10p	gmpv	35	26						10	2	25						2	y			ap,zi,ru
22B-1044-1	qz-ch-mu-st-gt scst	10d	ovmsi	65						1		15	10			8				t?		1	il
22-901-1	qz-mu-ch-ky-st scst	10d	omvks	53	t?							12	28		3	3		t	1				al,ap,zi
22-957-1	qz-ch-mu-st-gt gnss	10d	ovmsr	65						2	t	15	12	y		6		t	<1			t	ap,al
22-996.5-1	qz-ch-mu-st-mg guss	10d	ovmsx	55								22	16			4			t?			3	al,ap
24-444.5-1	qz-mu-gt gnss	10d	omuvi	75	?				t	2		3	15				t	<1	5	y		y	ap
27-593.5-1	qz-ch-st-mu gnss	10d	ovsmx	80				t?				10	4			5			t			1	ap

Table A.1. Petrography and Modal Estimates. (continued)

Sample	Lithology	Unit	Code	qz	pl	am	cm	ep	cl	gt	bi	ch	mu	ma	ky	st	gh	to	py	po	sp	mg	traces etc.
27-733-1	qz-mu-ch-ma scst	10d	omvr	70					t			10	14	5				<1	1				ap,zi
34B-930-1	ch-mu-st fs scst	10d	vmski	52	8				t			20	15		1	3			1				ap,sn?
34B-967-1	ch-mu-st fs scst	10d	vmsi	50	15							16	12			5			2				ap,zi,al
34-863.5-1	ch-mu-ky fs scst	10d	vmki	50	15							15	15		3			t	2	t			ap
34-937-1	mu-ch-gt fs scst	10d	vmysi	45	25					1		16	10			1		t	2				ox,ap,zi
70-664-1	qz-st-ch gnss	10d	ovsmx	70							2	10	4			10			t			4	ap,al,zi
70-687-1	qz-st-ch-mu-bi gnss	10d	ovsmp	64				t?			5	11	7			11						2	ap,al,zi,su,il?
70-822.5-1	qz-mu-ch-st gnss	10d	omvsx	65				t?				12	15			6			y			2	ap,al,il?
70-876.5-1	qz-mu-ch-ky gnss	10d	omvki	70								10	16		4			<1	t				ox,ap,zi
70-934-1	qz-mu-ch-gt scst	10d	omvy	65					t	1		16	18						<1				ap
73-1107.5-1	qz-mu-ch-st scst	10d	omvs	69								15	15			1							ox,ap,zi
73-1170.5-1	qz-mu-ch-ky-st scst	10d	omvks	70					t			12	12		3	1		t	2	y			zi,al?,ox
73-1170.5-2	qz-mu-ch scst	10d	omvi	70								15	15					t					zi,al?,op
73-1224-1	qz-mu-ch-st gnss	10d	omvsx	69								10	15			4			<1	<1		2	ap,zi,il?
73-1257-1	qz-mu-ch scst	10d	omv	70					t			14	16					<1					ap,zi
73-1316-1	qz-mu-ky-st gnss	10d	omkst	65								2	26	<1	2	2		1	2				ap,zi
73-949-1	qz-mu-ch scst	10d	omv	70								5	25					t					ap,zi,op
80-1176-1	bi-ch-mu-st-gt gnss	10d	pvmi	25	43					1	10	10	10			t			t?				1%ox,ap,zi
80-1382-1	qz-mu-ch scst	10d	omv	65				<1				10	25										ap
80-1639.5-1	qz-ch-mu gnss	10d	ovm	65								20	15					t					ap,zi?
24-277.5-1	qz-ky-mu-ch scst	10d	wovmk	35								40	16	?	8				1				ap,zi
80-1571.5-1	ch-ky-mu-st scst	10d	wovkm									60	4		33	2			t	1			ap,zi,il
27-484-1	qz-mu-st-gh scst	10da	ot	80								t	14			2	1	2	1		t		ap
27-504-1	qz-mu-st-ky scst	10da	oki	80					t			t	9		1	9	t	t	1		t		ap
34-799-1	qz-mu-gh-st scst	10da	ou	74								1	10			2	8	t	5		t		ap,ru,si,cp
19B-785-1	ky-ma fs msdm	10p	ckru	30	60						1	1	t	3?	3			t	<1	2			ap,ru?
19-801-1	mu-ma-ky scst	10p	omrku	30								t?	41	12	10			t?	7	y	<1		ap,zi
19-950-1	ky-mu-bi scst	10p	ckmup	35	20			t?			5	1	15		18			t	6	t	t		ap,zi
22A-1625-1	qz-mu-ch-st-gt scst	10p	omvsy	47						3	1	14	29	y?		4		t	2	y	t		ap,zi
22B-1703-1	bi-mu-st-gt fs	10p	pmysx	37	35					4	10	1	8			4						1	ap,zi,su
22B-1721-1	qz-mu-bi-gt-st gnss	10p	mpysu	55	5				t	6?	8	1	15			5			5	y			al,ap,zi,si?
22B-1721-2	qz-mu-st-bi gnss	10p	omspy	60					t	1	8	1	15			10			5	y			al,ap,zi,si?
24-812-1	ky-mu-bi msdm	10p	kmup	10	35						3	1	20		25	t		<1	6				ap
24-812-2	mu-ky-to msdm	10p	mkut	5	15						1	1	66		5	1		2	4				ap
24-812-3	mu-ky-bi-ch msdm	10p	muk	5	5						2	2	63		15			<1	8				ap
24-991-1	mu fs gnss	10p	cmsk	50	35				t				8		2	3		<1	2				ap,zi
32-1465.5-1	mu-fu-sn scst	10p	dmu	43	11								38						7				1%sn,ap
34A-1614-1	mu-py scst	10p	mui	50	20								24						6	t	t		ap,zi
34C-1377-1	mu-st-ky scst	10p	mskut	23	15						3	1	30		5	12		3	8				ap,zi,si
34-1347-1	mu-ch-ky scst	10p	mvuk	44	16				t	t	1	6	27		2			t	4				ap,zi
34-1477-1	mu-py scst	10p	muj	60	13								15				t?		10	t	2		ap,apy?,zi
34-1551-1	qz-mu scst	10p	cmui	58	1				t		t	1	36			t		t	5	y			ap
34-1607.5-1	mu-ky scst	10p	gmk	45	30						2	2	14	t?	6			t	3				ru,si,ap,zi
34C-1626-1	pl-layered ch scst	10p	gvup	30	40						2	23			t	t			5	y			ap,zi,si,ru
34C-1710-1	pl-layered ch scst	10p	gv	25	49			t	t		t	25	y	y					1				zi
19B-663.5-1	qz-mu-gh-st scst	10pa		80	5?						2	<1	10			<1	1		2		t?		ap,zi
22A-1638-1	qz-mu-st-ky-gh scst	10pa	ouk	58									19		6	10	<1	t	6	t	1		ap,zi,cp
22A-1650-1	mu-st-gh scst	10pa	ui	50	15				t			t	22			8	1		4		<1		ap,zi
22A-1650-2	qz-mu-bi-st scst	10pa	opui	65					t		8	2	17			4	t?		4	y	t		ap,zi
22B-1723-1	qz-mu-st-gh scst	10pa	outi	47	t?				t	t	<1	<1	44	t		3	2	1	3		t		zi,ap
27-1295.5-1	mu-bi-st-gh scst	10pa	cpu	45	15						8	1	16			5	2		8	y			ap,zi,ox
34C-1435-1	mu-gh-ky scst	10pa	uk	30	25						<1	t	20		5	t	10	t	10		<1		zi,si
34C-1453-1	qz-mu-st scst	10pa	ou	45							<1	t	25			15	t		15	t	t		ap,zi
34-1539-1	mu-gh scst	10pa	ui	50	5						1	t	30				6	t	8	y	t		zi,ru
19-848-1	ma-qz-mu-ky scst	10p/5	orumk	35							?	t	8	40	5				5	7	?		ap,ru?
24-1131a-1	st-at-gh	10p/5	zsu	35	20						t					16	3		10	y		y	16%at,apy,cp
34-1525.5-1	s-mass su	10p/5	mupj	25	30				1		3		21							18	2		zi,cp
24-1190.5-1	qz-phyric py-bi-ch	4/10p	upv	33	40						8	3					1		15	y	<1		<1%cp,ap,zi
29-1019-1	qz-phyric? cl-py	4/5a	clu	25	19				47				1						8	y	<1		si,sn
34-1498.5-1	gr msdm	3	ourpi	10							2	1	t	2									85%op mainly gr
H8-10-1	qz-phyric bi-ky fs	4/10	kpu	45	35							8	t		8			<1	3				1%si,ox?,ap,zi
H9-13-1	qz-phyric bi-st-ky	4/10	pusk	48	30					t	12	t			2	2		t	5	t			1%si,ap,zi
H9-30-1	qz-phyric volc brcc?	4a/10	pm	45	40				1		10	t	4						t?				ox,ap,zi
H9-30-2	qz-phyric volc brcc?	4a/10	psmy	40	33					2	15	2	3			5		t	t			t?	ap,si,zi,il?
H9-30-3	qz-phyric volc brcc?	4a/10	hv	50	30	15					2	3										t?	ap,il?

Table A.1. Petrography and Modal Estimates. (continued)

Sample	Lithology	Unit	Code	qz	pl	am	cm	ep	cl	gt	bi	ch	mu	ma	ky	st	gh	to	py	po	sp	mg	traces etc.
H9-54-5	bi-st-ky fs	1/10	psk	50	26					20					1	3		t					ap,si,zi
H9-60-2	qz-phyric mu-st fs	4/10	ms	15	50					t	2	<1	23		<1	8		t					1%il?,1%si,ap,z
H9-6-2	qz-phyric st-ky-bi	4/10	skpm	24	50				t		6	t	3		4	12		t	t				1%ox,<1%si,ap
31-814-1	pl-ch-bi-gt fs	10m	vpy	25	50			<1		3	8	10	t							y		4	al,ap,il
73-834-1	ch-hb-bi mafic scst	10m	vhpqi	25	5	16		3			14	35							t	2			al,zi,cp
80-1265-1	ch-hb-gt mafic scst	10m	ovhyi	25		20		t	t	2		52								1		y	zi?,il
80-1286.5-1	amph	10m	ohv	10		85						3								2		y	zi?
80-1316-1	bi-ch-pl scst	10m	pv	10	60			t			17	12	1							t			si?,zi,il
19-157-1	pl-layered calc-sil	1/10c	vpy	40	30			2		1	5	18	2			?	t		2	t			ox,al,ap
19-274.5-1	calc-sil fs	1/10c	lm	27	18			<1	48		2	t	4						1	t			ap,al
22A-1350.5-1	calc-sil fs	1/10c	qpm	39	10			23	<1		21		7							t			al,ap
22B-1347-1	calc-sil fs	1/10c	pmq	40	20			5			21	t	13							1?			al
22B-1843-1	calc-sil fs	1/10c	pmqu	42	24			5	t		15		11						3	y			ap,al,zi,sn
22-685.5-1	calc-sil	1/10c	cpm	42	25			1	1	t	20		11						t				ap,al
22-789-1	calc-sil fs	1/10c	pqm	40				17			24		3						1				15%kf,al,ap
24-668-1	mu-bi-cl scst	1/10c	mpq	40	2				3		5		50							t			ap,al,zi
27-328-1	calc-sil fs	1/10c	pmq	50	30			5	t		8		7						t				ap,al
27-763-1	mu-bi-layered fs	1/10c	mpvui	60	24			<1	t		8	3	12						3	y			ap,al,il?
29-183.5-1	bi-cl-mu-layered fs	1/10c	p	33	60			t	1		5		1						t				ap
29-716-1	calc-sil fs	1/10c	mpq	27	35			3			3		20						2	t			ap,al
31-716-1	calc-sil fs	1/10c	cmpq	15	45			4		<1	10	t	25					t	t	1		t	ap,al,cp
32-657-1	calc-sil fs	1/10c	qp	40	20			20	t		20												ap
34A-1252-1	calc-sil fs	1/10c	qpl	55	15			20	3		6		1						t				<1%cp,ap,al
34A-992-1	calc-sil fs	1/10c	pqm	56	11			11			25		2						1				ap
34B-1032.5-1	bi-ch-mu fs	1/10c	pvmy	50	25			1		2	12	6	4					t	t	t			ap,al
34-1028.5-1	calc-sil fs	1/10c	pql	45	10			15	2		15		2						1				10%kf,ap
34-697.5-1	calc-sil fs	1/10c	pql	50	5			5	19		20	t	1										op,ap
70-462-1	calc-sil fs	1/10c	pq	45	25			12			18		t						t				ap,al
70-560-1	calc-sil	1/10c	pq	17	5			30	t		44								1			y	3%kf,ap,al
70-566.5-1	calc-sil gnss	1/10c	cmqp	40	22			7	t		6		15						t	t?			ap,al
73-1380.5-1	calc-sil fs	1/10c	pmyu	51	18			2	t	2	12		12					<1	3	y			ap,al
80-1738-1	calc-sil fs	1/10c	pmq	30	47			3	t		15		5										al,ap
80-1795-1	calc-sil fs	1/10c	pql	45	15			22	2		26								t	t?			al
22B-1911-1	pl-bi-layered fs	1b/10c	plu	43	38			1	5		12								2				sn
24-624.5-1	fs clast	1b/10c	apq	45	45			4	1	1	4												ox,ap,al
24-624.5-2	fs volc brcc	1b/10c	mpq	35	35			6	1	1	7		15							t			ox,ap,al
27-963.5-1	bi-mu-ep-layered fs	1b/10c	pmqy	60	20			3	t	2	10		5						t	t?			ap,al
D4-37-1	fs volc brcc?	1b/10c	hqpy	35	35	12		10			3	4	t	t									1%op,ap
22B-1950-1	qz-phyric hb-ch-bi	4/10c	hvp	23	13	25		t	t		15	24						<1					ap,ru?
24-1252.5-1	qz-phyric bi-ep fs	4/10c	pq	30	45			8	t	1	15	t	t					t	t?	1		y	ap,al,il?
27-1486-1	qz-phyric bi-ep-mu	4/10c	p	25	53			2			18	t	2						t?				ap,zi
27-1486-2	calc-sil	4/10c	pqh	35	24	5	15	y			20	1											2%op,sn
28-393.5-1	qz-phyric bi-cl fs	4/10c	pl	23	65			t	4		8	t	t							t			ap,al
29-739-1	qz-phyric mu-bi fs	4/10c	mpu	41	36			1			3		16						t	3			ap,al
32-1426-1	qz-pl-phyric ep-bi	4/10c	dqpm	24	19			27	1		15	t	12						2		t		
73-602-1	qz-phyric bi-ep fs	4/10c	pq	50	20			12	t		18	t							t?				ap,al
D4-9-1	qz-phyric cl brcc	4/10c	lhq	10	45	16		3	20		2	2	t										2%ox,ap,al
D4-9-2	qz-phyric cl-ep-hb	4/10c	lyhp	23	45	5		7	12		5	1								y			2%op,al,ap,il?
H9-10-1	qz-phyric bi-ep-cl	4/10c	pqlx	37	35			10	3		14								t			1	ap,al
19-1023.5-1	calc-sil	10i	cl	15	35	25		t	22		3	<1								t			al,ap,il?,sn
22A-1262-1	calc-sil	10i	qhp	48	2	12		26	t		12		<1										op,al,sn
22A-1262-2	calc-sil	10i	ohp	30	t?	36		33	<1														1%sn,al
24-1053-1	calc-sil	10i	h	18	32	47		2	<1		t	t								1			<1%sn,al,ap,zi,
24-471-1	calc-sil	10i	ohlq	3		75		8	14		t												<1%sn,op
27-1557-1	calc-sil	10i	hq	10	10	75		4	t			t								1			ap,sn
27-703.5-1	calc-sil	10i	h	1	t	97		t	t			2							t				ap,al
29-858-1	calc-sil fs	10i	lhq	45	35	4			12			t								3	1		ap
31-790-1	calc-sil	10i	hu	<1?	4	90		<1	1		t								5	y	t		zi,al,cp?
34B-759.5-1	calc-sil	10i	ohqpl	8		50		29	3		8												2%sn,al
34C-1841.5-1	calc-sil	10i	ohql	22		55		21	t										2	y			al,sn
34-697.5-2	calc-sil	10i	oplhq	40		5		5	25		25	t											op,ap
34-876.5-1	calc-sil	10i	hql	7	3	78		10	2										t				op,sn
73-677.5-1	hb-ep mafic	10i	hq	22	8	40		29	t		1												
73-677.5-2	hb-ep mafic	10i	phq	30	10	19		12	t		28								1				
28-199-1	mafic volc	2	hnvx	5	59	11	11	t?			t	11							t			3	

Table A.1. Petrography and Modal Estimates. (continued)

Sample	Lithology	Unit	Code	qz	pl	am	cm	ep	cl	gt	bi	ch	mu	ma	ky	st	gh	to	py	po	sp	mg	traces etc.
29-669-1	mafic volc	2	hv	15	30	48		t				5							t				
29-757.5-1	bi-gt amph	2	hpvy	15	35	25	t			5	10	8								2			2%ox,ap,cp?
31-272.5-1	pl-phyric mafic volc	2	dhx	3	22	74		t				t							t			1	ox,ap,zi
31-361-1	bi-hb-ch mafic	2	phv	15	25	22		t		<1	24	14											ap
31-399.5-1	mafic volc	2	h	15	22	60		2	t			t							t				ox,su,ap,al,zi
31-473-1	mafic volc	2	h	16	27	53		2											t				1%ox
31-521.5-1	mafic volc	2	h	10	30	59			<1										t				2%ox,al,ru,ap
31-558-1	mafic volc	2	hq	10	28	58		3											t	t?			1%ox
32-1323.5-1	mafic volc	2	h	9	45	45																	1%ox,ap,zi?
34A-1459b-1	pl-phyric? mafic	2	h	25	30	43		1															1%op,ap
34A-1463.5-1	mafic volc	2	h	10	40	48						1											1%op
29-478.5-1	inter volc	2a	hv	15	35	44		1				5							t				1%op,ap
29-580.5-1	mafic volc	2a	h	5	54	40		t											t	<1			ap,al
29-633.5b-1	pl-phyric mafic	2a	h	9	35	55			t			t											1%ox,ap
D4-38-1	inter volc	2a	hv	10	40	45			t			4										1?	1%ox
J8-2-1	mafic volc	2a	hx	8	25	65		<1			t								t			2	ap
28-272.5-1	altered volc brcc	2c	hvnx	10	40	29	5	t	<1			15										1	ap
29-685.5-2	hb-cm fs	2/10s	hn	45	40	10	5					t											ap,zi?
34A-1484-1	silicified mafic	2/10s	hnx	28	55	15	1					t										1	<1%ox,ap
34A-1484-2	silicified mafic	2/10s	nvx	36	45	t	12	t				4										3	ap
H9-52-1	silicified pillow	2b/10s	nypx	40	38	t	12			4	4											2	
H9-61-5	silicified clast	2e/10s	ahy	50	45	3	t			1	1												ap
29-633.5a-1	ep-cl mafic	2/10e	oqhl	2		38		45	15														op
29-685.5-1	ep-cl mafic	2/10e	hl	20	60	15		2	2										t				ox,sn
29-820a-1	ep-gt-cl amph	2/10e	hqylu	18	12	35		16	7	7									t				1%ox,al
34A-1459b-2	ep-cl mafic	2/10e	oqlh	1		28		35	35											5			<1%sn,al,zi?
I8-20-1	gt-bi amph	2/10	hyp	8	2	45		1	t	29	15	t											1%sn,op
24-1294-1	hb-ch matrix	6a	bhv	15	32	38		t	t		1	14								<1		t?	op
24-1294-2	hb-cm fs clast	6a	ah	30	60	10	t		t														ap,al,il?
27-1611.5-1	hb-ch matrix	6a	bhv	5	25	54		t				15											ap
27-1611.5-2	hb-cl fs clast	6a	ahl	20	44	31		t	4														1%il?,ap,al
29-1223.5-1	inter volc brcc	6a	chv	25	25	30			t		2	17											1%il?,ap,al,sn
32-1610-1	inter volc brcc	6a	hlv	17	24	48	<1		7		1	3							y	1			ap,zi,il?
34A-1760.5-1	inter volc brcc	6a	dhvn	20	40	25	4	t	1			10								t			ap,op
34D-2010-1	hb-ch matrix	6a	bhvn	8	15	40	1					35											ap,il?,cp
34D-2010-2	cm-hb fs clast	6a	anhv	20	40	15	20				<1	5											1%ox,al
22A-2075.5-1	mafic volc	6	hl	15	35	47	<1		2			1											1%ox
24-1285-1	inter volc	6	hp	25	50	19		t	<1		5	1								t			ox,ap,al
28-453.4-1	inter volc	6	ph	15	53	4		1	t	1	22	2								2			ox,ap,al
31-970.5-1	mafic volc	6	hpv	10	40	27		t	t		20	3								t			ap,al,il
34-1851-1	mafic volc	6	hp	10	20	52		t	t		18												<1%ox,al,ap,cp?
34C-1888-1	layered inter volc	6/10e	hqpl	15	15	40		24	2		4												op,ap,al
J8-23-1	qz-phyric fs	7	dp	37	55				t		8	t							t?	t?			ap,al,ox

Table A.2. Key to Petrographic Code.

a–clast extracted from fragmental rock
b–matrix from fragmental rock
c–quartz phenocrysts
d–plagioclase phenocrysts
e–biotite in metamorphic-segregation layering (S_1)
f–D_2 to post-kinematic hornblende zone with leucocratic halo, unit 1 only
g–plagioclase-rich layers (S_1) with 'Tuttle' deformation lamellae consisting of rutile trails (S_1)
h–Ca-amphibole$\geq$2%
i–slight retrogression
j–more than slight retrogression
k–kyanite$\geq$1%
l–calcite$\geq$1%
m–muscovite>2%
n–cummingtonite$\geq$1%
o–no plagioclase
p–biotite>2%
q–epidote>2%
r–margarite>1%
s–staurolite$\geq$1%
t–tourmaline$\geq$1%
u–sulphide minerals>2%
v–chlorite>2%
w–selvedge to quartz vein
x–magnetite$\geq$1%
y–garnet$\geq$1%
z–anthophyllite+gahnite

Notes:

1. Maximum of 5 designators per sample.
2. Units 10pa and 10da are defined by the assemblage muscovite-staurolite-gahnite and this is not repeated in the code designation.
3. Unit 4 is defined by quartz megacrysts and this is not repeated in the code designation.
4. Features a–g are given first.
5. h and k–z are given next, generally in order of abundance, except for o (no plagioclase) which comes first.
6. i and j are given last.

Table A.3. Mineral Abbreviations.

ac–actinolite
al–allanite
am–amphibole
ap–apatite
apy–arsenopyrite
at–anthophyllite
bi–biotite
ch–chorite
cl–calcite
cm–cummingtonite
cp–chalcopyrite
ep–epidote
fu–Cr-muscovite
gh–gahnite
gr–graphite
gt–garnet
hb–hornblende
il–ilmenite
kf–K-feldspar
ky–kyanite
ma–margarite
mg–magnetite
mn–monazite
mu–muscovite
op–opaque mineral
ox–oxide mineral
pl–plagioclase
po–pyrrhotite
py–pyrite
qz–quartz
ru–rutile
si–sillimanite
sn–titanite
sp–sphalerite
st–staurolite
su–sulphide mineral
to–tourmaline
xe–xenotime
zi–zircon

Appendix B

Mineral Determinations

Electron-microprobe mineral analyses were collected on a suite of 21 samples representing the various alteration types and mineral assemblages observed at the Linda deposit. The minerals for which analyses were obtained are: amphiboles: calcic amphibole, anthophyllite and cummingtonite; micas: biotite, margarite and muscovite; chlorite, epidote, garnet, gahnite, kyanite, plagioclase, sphalerite, staurolite, and tourmaline. The samples were prepared as polished thin sections by Vancouver Petrographics Limited. Preliminary work included microscopy in both transmitted and reflected light, and the preparation of 8″×10″prints of photomicrographs of each section. The occurrence and distribution of monoclinic (magnetic) and hexagonal (nonmagnetic) pyrrhotite was determined by applying a magnetic colloidal suspension to the polished thin sections, and examining them with a petrographic microscope. The suspension was prepared following the method of Scott (1974, *pages S-17–S-18*).

Electron-microprobe analytical work was done initially on a JEOL 8600, under the supervision of R.L.Barnett at the Department of Geology, University of Western Ontario, London. Subsequent analyses were done on a JEOL Superprobe 733 at the National Museum of Natural Sciences, Mineral Sciences Division, Ottawa under the supervision of Dr.T.S.Ercit. Most of the analyses collected at University of Western Ontario were repeated at the Museum of Natural Sciences; with the exception of feldspars in 6 specimens, epidote and muscovite, each in a single specimen, and amphibole in 2 specimens; only those analyses collected at the latter institution are reported (Table B.3). Instrument operating conditions, standards and methods reported here, refer to the Museum, with University of Western Ontario in square brackets where pertinent.

Mineral compositions were determined by wavelength dispersive spectrometry (WDS) using an accelerating potential of 15 keV, a beam current of 20–25 nA [10 nA] and a beam diameter of 10–16 μ. A focussed beam was used for some very fine disseminated grains of sphalerite. Mineral standards were used (Table B.1), excepting Ba for which the standard was Ba-bearing glass, and Zn for which, in some silicate analyses, the standard was a synthetic compound. The willemite

Table B.1. Standards used in Electron Microprobe Analyses.

	Minerals Analysed						
	sphalerite	chlorite plagioclase micas	epidote tourmaline amphibole	kyanite gahnite staurolite garnet	muscovite [UWO][2]	plagioclase [UWO][2]	epidote amphibole [UWO][2]
Element	Standards						
Si	na[1]	chlorite	diopside	almandine	orthopyroxene	albite	orthopyroxene
Ti	na[1]	biotite	titanite	titanite	kaersutite	na[1]	kaersutite
Al	na[1]	chlorite	gehlenite	gehlenite	anorthite 90	albite	kaersutite
Cr	na[1]	chromite	nichromite	nichromite	chromite	na[1]	chromite
Mg	na[1]	chlorite	diopside	diopside	orthopyroxene	na[1]	orthopyroxene
Mn	tephroite	willemite	tephroite	tephroite	rhodonite	na[1]	rhodonite
Fe	arsenopyrite	biotite	almandine	almandine	orthopyroxene	orthopyroxene	orthopyroxene
Cu	cuprite	na[1]	na[1]	na[1]	na[1]	na[1]	na[1]
Zn	sphalerite	$BaZnGeO_4$	$BaZnGeO_4$	willemite	na[1]	na[1]	na[1]
Cd	Cd-apatite	na[1]	na[1]	na[1]	na[1]	na[1]	na[1]
Ca	na[1]	diopside	diopside	diopside	diopside	anorthite 90	diopside
Ba	na[1]	sanbornite	sanbornite	na[1]	Ba-glass	Ba-glass	Ba-glass
Na	na[1]	albite	albite	albite	albite	albite	albite
K	na[1]	biotite	sanidine	na[1]	orthoclase	orthoclase	orthoclase
F	na[1]	fluoriebekite	fluoriebekite	na[1]	Li-fluoride	na[1]	Li-fluoride
Cl	na[1]	tugtupite	tugtupite	na[1]	tugtupite	na[1]	na[1]
S	sphalerite	na[1]	na[1]	na[1]	na[1]	na[1]	na[1]

[1] Not analysed. [2] Analyses done at the University of Western Ontario.

standard is zoned, and this problem was alleviated by consistently calibrating on the same grain. Data was processed with a conventional ZAF correction. During calibration, counts for major elements in standards were collected to a minimum 1σ precision of 0.5% [1%]. Counts on samples were collected to a 1σ precision of 0.5% [1%], or for maximum counting times of 25–40 seconds [20 seconds]. Each elemental analysis was recorded with the cumulative 1σ standard deviation for both standard and sample. Sample standard deviations exceeding 25.5% are considered to indicate that the element was not detected (*see* Table B.2 for detection limits of trace and minor elements). Within-sample averages and standard deviations were determined, and these represent a measure of real compositional scatter within the section.

Chlorite analyses tend to have slightly high weight% oxide totals, averaging

Table B.2. Detection Limits of Minor and Trace Elements.

Element	Minerals Analysed											
	ky	sp	fs	gt	to	am	ep	ch	bi	st	mu	gh
Al	m[1]	na[2]	m	m	m	m	m	m	m	m	m	m
Ba	na	na	nd[3]	na	nd	nd	nd	nd	0.12	na	0.10	na
Ca	na	na	m	m	m	m	m	0.04	0.04	na	0.04	na
Cd	na	0.28	na	na	na	na	na	na	na	na	na	na
Cl	na	na	na	na	nd	nd	nd	nd[4]	nd	na	nd	na
Cr	nd	na	na	nd	nd	nd	nd	nd	nd	nd	0.09	na
Cu	na	0.12	na	na	na	na	na	na	na	na	na	na
F	na	na	na	na	$\leq$0.57	0.47	nd	0.39	0.44	na	0.46	na
Fe	$\leq$0.24	m	0.11	m	m	m	m	m	m	m	0.10	m
K	na	na	0.04	na	nd	0.05	0.04	0.04	m	na	m	na
Mg	nd	na	na	m	m	m	0.04	m	m	m	m	m
Mn	nd	0.08	na	m	0.08	m	m	$\leq$0.13	0.08	0.10	0.04	0.07
Na	na	na	m	0.06	m	0.06	$\leq$0.11	0.05	0.06	na	m	na
S	na	m	na	na	na	na	na	na	na	na	na	na
Si	m	na	m	m	m	m	m	m	m	m	m	0.07
Ti	nd	na	na	0.06	m	0.06	0.05	0.05	m	m	0.06	nd
Zn	nd	m	na	nd	nd	0.16	nd	0.16	$\leq$0.24	m	nd	m

[1] Major element. [2] Not analysed. [3] Not detected.

[4] One exception with $\leq$0.60 weight%.

100.50–102.18%, after the addition of calculated H_2O. To a lesser degree, high totals also occur in biotite analyses, which were done using the same set of standards as chlorite. This is probably due to a systematic error introduced during calibration on the standards, and may be related to either the choice of standards or to inaccuracy in the reported standard compositions. Chlorite and biotite standards were used for major elements and, therefore, differences in matrix between the standard and the analysed mineral were minimized. However, phyllosilicates are inherently difficult to analyse accurately, as they tend to disintegrate under the electron beam. The element(s) in which the error occurs cannot be definitely identified, and this will contribute some uncertainty to the analyses. Similarly, the Mn-richest garnets (22A-1625) tend to have low oxide totals (98.15–99.17%), probably as the result of systematic error introduced through the use of tephroite, rather than spessartine, as an Mn standard. The possible contribution of hydrogarnet component was tested

by back-calculation assuming substitution of $Si^{+4} \rightleftharpoons 4H^{+}$ to bring the tetrahedral site to full occupancy. The proportion of hydrogarnet component was negligible.

Recalculation of weight% oxide (or weight% element analyses for sphalerite) analyses to mineral structural formulae was done by setting up the equations in LOTUS 1-2-3 spreadsheets. For silicate and oxide minerals (except staurolite and calcic amphibole), the method followed that of Deer *et al.* (1966), based on charge balance and normalization to a chosen number of anionic charges, and assignment to appropriate structural sites. Sphalerite analyses included determinations for both cations and sulphur, and these were recalculated to formulae without normalization. Weight% H_2O was back-calculated from stoichiometry, after adjustment for measured F and Cl contents. Similarly, weight% B_2O_3 in tourmaline was back-calculated from stoichoimetry.

Staurolite analyses were normalized to (Si+Al)=25.53 ions, after the proposed scheme of Holdaway *et al.* (1988) and Holdaway *et al.* (1986) for staurolite which formed under reducing conditions. Following Holdaway *et al.* (1988), anionic charges were assumed to total 96, and this was assumed to be balanced by H^{+}. Li_2O was not determined (Dutrow *et al.*, 1986) and weight% H_2O was back-calculated from the charge balance. The assignment of cations to structural sites, based on Holdaway (1986), includes .250 Fe^{+3} ions at the octahedral Al(3A) sites, a total of .250 ($Mn+Fe^{+2}$) ions at the U(1) site and Mg, Zn, Ti and remaining Fe at the tetrahedral(Fe) site. Weight% Fe_2O_3 and adjusted FeO were back-calculated. This method results in oxide totals averaging 98.46–100.33%, except for sample 22-957 which has anomalously low totals for unknown reasons. The low tetrahedral-site occupancies in most samples suggest that Li may be present in addition to vacancies (*ibid.*), and this may also be reflected in slightly low oxide totals.

Amphibole analyses were recast into structural formulae, after the method of Robinson *et al.* (1982), incorporating a calculation of Fe^{+3}/Fe^{+2} ratio and OH, based on stoichiometry. The method uses normalization to a fixed cationic site occupancy and 46 anionic charges, with charge balance accommodated by the proportions of Fe^{+3}/Fe^{+2}. Analyses of calcic amphiboles were normalized to Si+Al+Ti+Fe+Mn+Mg+Zn=13, thus assuming full occupancy of the tetrahedral sites (T=8), and of the octahedral sites (M1+M2+M3=5). A single analy-

sis was rejected on the grounds that it violated a chemical limit, requiring negative amounts of Fe^{+3} to achieve charge balance (*see ibid.*). Analyses of Fe-Mg amphiboles, *ie.* cummingtonite and anthophyllite, were normalized to 46 anionic charges, and with the assumption that Fe_t=Fe^{+2} (Table B.3, i). Fe^{+3} contents, calculated in analogous fashion to those of calcic amphiboles, but with normalization to Si+Al+Ti+Fe+Mn+Mg+Zn+Ca=15 (following Robinson *et al.*, 1982) tended to have low positive and negative values generally close to zero.

Iron is reported as FeO, except in staurolite as discussed, and epidote, kyanite and feldspar, in which all Fe was assumed to be Fe_2O_3. The occupancies of the octahedral sites in chlorite and biotite generally approach within 1% and 2%, respectively, of the ideal stoichiometry. Considering the high Mg compositions of these minerals, and the probability of some systematic error in the analyses, calculation of Fe^{+3} content did not seem justifiable. In the context of this study, the main effect of unrecognized Fe_2O_3 would be to give Mg/(Mg+Fe) values that are artificially low.

Epidote analyses (Table B.3, j) tend to have low oxide totals, averaging 97.39–99.21 weight%. This may be partly due to systematic error; Ce, La and Nd were commonly observed in EDS spectra, but were not analysed quantitatively. Fractured allanite cores in 22B-1843 showed up to .89% Ce_2O_3, .41% La_2O_3 and .64% Nd_2O_3. U, Th, Sm and Pr were not detected. These should be regarded as semi-quantitative analyses as the cores appear metamict and the oxide totals were 85–94 weight%. Petrographic examination showed that epidote commonly produced pleochroic halos in adjacent biotite grains, suggesting that the epidote may also be partly metamict. The low oxide totals are probably the combined result of incomplete elemental analysis and systematic errors introduced either during calibration (as discussed for chlorite and biotite), or through the matrix contrast between crystalline standards and partly metamict sample grains.

The energy dispersive spectrometer (EDS) on the electron probe was used to identify unknown minerals and to confirm optical identifications, particularly of fine grained phases occurring in trace amounts. Rutile, ilmenite, xenotime, allanite, monazite, apatite, zircon, sillimanite, and in one case, galena, were identified in this way, although quantitative analyses were not obtained. The EDS system was used

in tandem with back-scattered electron (BSE) imaging, which is sensitive to bulk differences in atomic number, to identify or define mineral zoning or fine grained intergrowths. This allowed the confirmation of mica-chlorite and muscovite-margarite intergrowths and exsolution lamellae in intermediate plagioclase. Paragonite was not identified as a discrete phase, despite the common occurrence of paragonitic muscovite and Na-biotite. Zoning and exsolution in plagioclase was imaged using BSE, and photographed (Plate 9.1). Zoning in garnet is mainly defined by coupled Fe-Mn substitution. These elements are adjacent in the periodic table, and the zoning was not visible in BSE images.

Table B.3.
Compilation of Electron Probe Mineral Analyses.

a. Muscovite and Margarite Mineral Chemistry.
b. Biotite Mineral Chemistry.
c. Chlorite Mineral Chemistry.
d. Staurolite Mineral Chemistry.
e. Sphalerite Mineral Chemistry.
f. Gahnite Mineral Chemistry.
g. Garnet Mineral Chemistry.
h. Calcic Amphibole Mineral Chemistry.
i. Fe-Mg Amphibole Mineral Chemistry.
j. Epidote Mineral Chemistry.
k. Kyanite Mineral Chemistry.
l. Tourmaline Mineral Chemistry.
m. Plagioclase Mineral Chemistry.

Explanatory Notes.

1. Area (column 2) refers to a subdivision of the probe section encompassing an area of 5–10 mm in diameter. Spot (column 3) refers to the area of the electron beam from which each individual mineral analysis was collected.
2. Abbreviations:

   Qualifying spot number: c—core, r—rim, m—matrix, an—anthophyllite, cm—cummingtonite.

   ave—average, stdev—1σ standard deviation.
3. Oxide totals: The first total assumes FeO_t, weight% oxides uncorrected for F, no H_2O or B_2O_3. Second total assumes FeO and Fe_2O_3 as calculated from stoichiometry (Tables B.3, d, h, j, k, m), corrected for F, H_2O calculated from stoichiometry (Tables B.3, a, b, c, d, h, i, j, l), and B_2O_3 calculated from stoichiometry (Table B.3, l).
4. The averages and standard deviations are compiled in Table 9.2 and were used in deriving the balanced reactions in Tables 10.1 and 10.2.

Table B.3. a. Muscovite and Margarite Mineral Chemistry.

			weight percent oxide or element (ZnO not detected)														
Sample	area	spot	SiO_2	TiO_2	$Al_2O_3Cr_2O_3$		FeO	MnO	MgO	BaO	CaO	Na_2O	K_2O	F	Total	H_2O	Total
22-901	A'	54	45.72	0.43	35.60	0.00	2.40	0.00	0.74	0.16	0.00	1.61	9.25	0.00	95.91	4.52	100.43
22-901	A'	57	45.31	0.41	35.93	0.00	2.21	0.00	0.64	0.19	0.00	1.64	8.77	0.00	95.10	4.49	99.59
22-901	A'	59	45.31	0.41	36.13	0.00	1.90	0.00	0.62	0.19	0.00	1.45	8.96	0.00	94.97	4.49	99.46
22-901	B	60	46.30	0.45	35.97	0.00	2.07	0.00	0.67	0.14	0.00	1.58	9.26	0.00	96.44	4.55	100.99
22-901	B	62	45.70	0.43	36.40	0.00	2.09	0.00	0.61	0.13	0.00	1.53	9.26	0.00	96.15	4.54	100.69
22-901	B	64	46.02	0.29	36.69	0.00	1.87	0.00	0.61	0.18	0.00	1.43	9.26	0.00	96.35	4.56	100.91
ave(6)			45.73	0.40	36.12	0.00	2.09	0.00	0.65	0.17	0.00	1.54	9.13	0.00	95.82	4.53	100.35
stdev			0.36	0.05	0.35	0.00	0.18	0.00	0.05	0.02	0.00	0.08	0.19	0.00	0.58	0.03	0.61
22-957	C	67	41.74	0.20	39.78	0.00	1.72	0.00	0.56	0.22	3.40	1.14	6.58	0.00	95.34	4.51	99.85
22-957	C	68	41.55	0.25	38.99	0.00	1.69	0.00	0.52	0.20	3.33	1.14	6.84	0.00	94.51	4.46	98.97
22-957	B	71	45.46	0.36	34.61	0.00	2.74	0.00	0.72	0.32	0.00	1.13	8.82	0.00	94.16	4.44	98.60
22-957	B	72	42.21	0.29	38.64	0.00	1.97	0.00	0.66	0.12	2.80	1.15	6.99	0.00	94.83	4.48	99.31
22-957	B	73	36.76	0.20	43.31	0.00	1.62	0.00	0.57	0.15	7.04	1.06	3.13	0.00	93.84	4.45	98.29
22-957	B	75	42.26	0.28	36.21	0.00	3.26	0.00	1.69	0.20	1.43	1.11	7.29	0.00	93.73	4.40	98.13
22-957	B	76	38.18	0.20	38.80	0.00	1.96	0.00	1.05	0.15	3.50	1.07	5.13	0.00	90.04	4.27	94.31
22-957	D	78	41.61	0.26	35.69	0.00	4.69	0.04	2.28	0.21	1.41	1.05	7.13	0.00	94.37	4.39	98.76
22-957	D	79	43.88	0.33	36.90	0.00	2.61	0.00	0.85	0.27	1.50	1.20	7.59	0.00	95.13	4.49	99.62
22-957	D	80	46.12	0.28	35.60	0.00	2.14	0.00	0.66	0.27	0.00	1.17	9.29	0.00	95.53	4.51	100.04
22-957	B	27	46.33	0.23	36.85	0.00	2.17	0.00	0.57	0.20	0.00	1.12	8.11	0.00	95.58	4.56	100.14
22-957	A	28	46.11	0.23	35.54	0.00	2.80	0.00	0.74	0.28	0.00	1.25	9.00	0.00	95.95	4.52	100.47
22-957	E	29	43.41	0.31	38.81	0.00	1.89	0.00	0.60	0.29	2.68	1.12	6.92	0.00	96.03	4.55	100.58
ave(4)			46.01	0.28	35.65	0.00	2.46	0.00	0.67	0.27	0.00	1.17	8.81	0.00	95.31	4.51	99.81
stdev			0.33	0.05	0.80	0.00	0.31	0.00	0.07	0.04	0.00	0.05	0.43	0.00	0.68	0.04	0.72
22-996.5	B	47	46.09	0.24	36.42	0.00	2.52	0.00	0.68	0.27	0.00	1.22	8.73	0.00	96.17	4.55	100.72
22-996.5	B	50	46.27	0.30	36.22	0.00	2.57	0.00	0.72	0.17	0.00	1.23	7.90	0.00	95.38	4.54	99.92
22-996.5	B	52	46.04	0.24	36.43	0.00	2.38	0.00	0.63	0.23	0.08	1.24	8.03	0.00	95.30	4.53	99.83
22-996.5	B	54	46.21	0.34	35.72	0.00	2.74	0.00	0.68	0.36	0.00	1.25	8.34	0.00	95.64	4.53	100.17
22-996.5	B	55	46.26	0.32	36.07	0.00	2.90	0.00	0.75	0.35	0.00	1.19	8.83	0.00	96.67	4.56	101.23
ave(5)			46.17	0.29	36.17	0.00	2.62	0.00	0.69	0.28	0.02	1.23	8.37	0.00	95.83	4.54	100.37
stdev			0.09	0.04	0.26	0.00	0.18	0.00	0.04	0.07	0.03	0.02	0.37	0.00	0.52	0.01	0.53
22A-1625	C	28	42.02	0.17	35.35	0.00	4.30	0.09	4.48	0.00	0.00	1.31	6.84	0.00	94.56	4.44	99.00
22A-1625	A	31	43.79	0.32	35.95	0.00	2.31	0.00	2.46	0.15	0.00	1.37	8.03	0.00	94.38	4.46	98.84
22A-1625	A	35	43.36	0.29	35.79	0.00	2.51	0.00	2.52	0.14	0.00	1.46	7.89	0.00	93.96	4.44	98.40
22A-1625	A	39	45.55	0.51	36.48	0.00	1.29	0.00	0.74	0.18	0.00	1.64	8.50	0.00	94.89	4.51	99.40
22A-1625	A	40	46.07	0.43	36.58	0.00	1.35	0.00	0.77	0.16	0.00	1.53	8.80	0.00	95.69	4.55	100.24
S1, ave(2)			43.58	0.31	35.87	0.00	2.41	0.00	2.49	0.15	0.00	1.42	7.96	0.00	94.17	4.45	98.62
S2, ave(2)			45.81	0.47	36.53	0.00	1.32	0.00	0.76	0.17	0.00	1.59	8.65	0.00	95.29	4.53	99.82
ave(4)			44.69	0.39	36.20	0.00	1.87	0.00	1.62	0.16	0.00	1.50	8.31	0.00	94.73	4.49	99.22
stdev			1.14	0.09	0.34	0.00	0.55	0.00	0.87	0.01	0.00	0.10	0.36	0.00	0.64	0.04	0.69
22A-1638	A	57	44.65	0.36	36.19	0.00	0.80	0.00	0.57	0.11	0.00	2.10	7.28	0.00	92.06	4.42	96.48
22A-1638	A	58	44.70	0.28	36.36	0.00	0.79	0.00	0.61	0.12	0.00	2.04	7.78	0.00	92.68	4.43	97.11
ave(2)			44.68	0.32	36.28	0.00	0.80	0.00	0.59	0.12	0.00	2.07	7.53	0.00	92.37	4.43	96.80
22A-1752	A	1r	46.08	0.20	36.16	0.00	1.11	0.00	0.42	0.00	0.00	2.19	8.56	0.00	94.72	4.51	99.23
22A-1752	A	2r	48.87	0.29	33.88	0.00	1.10	0.00	0.53	0.00	0.00	2.31	7.67	0.00	94.65	4.55	99.20
22A-1752	A	3c	46.78	0.30	36.13	0.00	1.15	0.00	0.58	0.13	0.00	2.10	8.76	0.00	95.93	4.56	100.49
22A-1752	A	4c	45.66	0.28	34.62	0.00	1.13	0.00	0.63	0.00	0.00	2.12	8.15	0.00	92.59	4.42	97.01
22A-1752	B'	5m	46.10	0.34	35.81	0.00	1.23	0.00	0.56	0.00	0.00	2.31	8.65	0.00	95.00	4.52	99.52
22A-1752	B'	6m	46.21	0.22	37.16	0.00	1.07	0.00	0.53	0.00	0.00	2.87	7.36	0.00	95.42	4.57	99.99
22A-1752	B'	7c	47.40	0.37	34.48	0.00	1.38	0.00	1.01	0.00	0.00	2.21	7.96	0.00	94.81	4.53	99.34
ave(7)			46.73	0.29	35.46	0.00	1.17	0.00	0.61	0.02	0.00	2.30	8.16	0.00	94.73	4.52	99.26
stdev			1.02	0.06	1.08	0.00	0.10	0.00	0.17	0.05	0.00	0.24	0.49	0.00	0.97	0.05	1.01
22B-1721	A	61	46.34	0.28	36.03	0.00	1.79	0.00	0.76	0.10	0.20	0.87	9.24	0.00	95.61	4.54	100.15
22B-1721	A	65	44.15	0.29	37.16	0.00	1.80	0.00	0.74	0.15	1.13	0.88	8.59	0.00	94.89	4.49	99.38
22B-1721	A	66	46.01	0.30	35.62	0.00	1.89	0.00	0.77	0.15	0.00	0.89	10.08	0.00	95.71	4.51	100.22
22B-1721	A	67	46.15	0.32	35.80	0.00	2.36	0.00	0.75	0.13	0.00	1.06	9.15	0.00	95.72	4.53	100.25
22B-1721	A	69	45.01	0.29	36.44	0.00	1.87	0.00	0.70	0.15	0.48	0.88	9.06	0.00	94.88	4.49	99.37
ave(5)			45.53	0.30	36.21	0.00	1.94	0.00	0.74	0.14	0.36	0.92	9.22	0.00	95.36	4.51	99.87
stdev			0.83	0.01	0.55	0.00	0.21	0.00	0.02	0.02	0.42	0.07	0.48	0.00	0.39	0.02	0.41
22B-1723	A	59	45.55	0.47	36.12	0.00	1.61	0.00	0.74	0.12	0.56	1.07	8.38	0.00	94.62	4.50	99.12
22B-1723	A	60	44.81	0.37	36.30	0.00	1.45	0.00	0.79	0.13	0.95	0.96	8.87	0.00	94.63	4.48	99.11
22B-1723	B'	64	46.52	0.49	35.01	0.00	1.62	0.00	0.79	0.14	0.05	1.04	9.35	0.00	95.01	4.51	99.52
22B-1723	B'	65	44.83	0.43	36.01	0.00	1.69	0.00	0.85	0.13	0.67	0.98	8.60	0.00	94.19	4.47	98.66
22B-1723	C	67	44.46	0.38	36.93	0.00	1.45	0.00	0.76	0.16	1.16	0.98	8.66	0.00	94.94	4.50	99.44
22B-1723	C	68	45.89	0.43	35.78	0.00	1.56	0.00	0.71	0.00	0.00	1.01	9.11	0.00	94.49	4.49	98.98
22B-1723	D	72	44.34	0.36	36.45	0.00	1.61	0.00	0.92	0.10	1.24	0.94	8.24	0.00	94.20	4.47	98.67
22B-1723	B	1	42.61	0.33	38.87	0.00	1.40	0.00	0.71	0.13	2.80	0.98	7.29	0.00	95.12	4.51	99.63

Table B.3. a. Muscovite and Margarite Mineral Chemistry. (continued)

			weight percent oxide or element (ZnO not detected)														
Sample	area	spot	SiO_2	TiO_2	Al_2O_3	Cr_2O_3	FeO	MnO	MgO	BaO	CaO	Na_2O	K_2O	F	Total	H_2O	Total
22B-1723	C	30	44.37	0.37	36.28	0.00	1.43	0.00	0.78	0.00	1.00	0.94	8.52	0.00	93.69	4.45	98.14
22B-1723	C	31	46.14	0.44	37.25	0.00	1.63	0.00	0.85	0.11	0.97	0.95	8.41	0.00	96.75	4.60	101.35
22B-1723	A	32	44.83	0.38	36.84	0.00	1.54	0.00	0.78	0.11	0.85	0.89	8.65	0.00	94.87	4.50	99.37
ave(10)			45.17	0.41	36.30	0.00	1.56	0.00	0.80	0.10	0.75	0.98	8.68	0.00	94.74	4.50	99.24
stdev			0.75	0.04	0.61	0.00	0.08	0.00	0.06	0.05	0.41	0.05	0.33	0.00	0.77	0.04	0.81
22B-1843	B	58	46.53	0.82	32.69	0.00	2.28	0.00	2.04	0.22	0.00	0.24	10.71	0.00	95.53	4.48	100.01
22B-1843	B	59	46.52	0.46	32.27	0.00	2.12	0.00	2.13	0.53	0.00	0.24	9.86	0.00	94.13	4.43	98.56
22B-1843	B	60	46.68	0.60	32.66	0.00	2.07	0.00	2.15	0.48	0.00	0.25	10.73	0.00	95.62	4.48	100.10
22B-1843	C	64	46.55	0.70	31.98	0.00	2.49	0.00	2.01	0.23	0.00	0.23	10.49	0.00	94.68	4.44	99.12
22B-1843	C	65	46.79	0.66	32.55	0.00	2.50	0.00	1.88	0.23	0.07	0.26	10.25	0.00	95.19	4.47	99.66
ave(5)			46.61	0.65	32.43	0.00	2.29	0.00	2.04	0.34	0.01	0.24	10.41	0.00	95.03	4.46	99.49
stdev			0.11	0.12	0.27	0.00	0.18	0.00	0.10	0.14	0.03	0.01	0.32	0.00	0.56	0.02	0.58
32-1465.5	C	38	46.96	0.32	33.72	0.29	1.29	0.00	1.37	0.30	0.00	0.64	10.00	0.51	95.40	4.24	99.43
32-1465.5	C	39	46.42	0.75	33.63	0.21	1.11	0.00	1.39	0.34	0.00	0.60	9.59	0.56	94.60	4.19	98.56
32-1465.5	C	40	46.40	0.81	33.59	0.09	1.15	0.00	1.38	0.29	0.00	0.62	10.20	0.00	94.53	4.46	98.99
32-1465.5	B'	41	46.92	0.53	33.66	0.43	1.18	0.00	1.33	0.33	0.00	0.67	9.80	0.46	95.31	4.27	99.39
32-1465.5	B	42	46.73	0.46	33.42	0.34	1.15	0.00	1.35	0.30	0.00	0.60	10.29	0.55	95.19	4.21	99.16
32-1465.5	B	43	46.12	0.46	33.78	0.52	0.89	0.00	1.33	0.39	0.00	0.60	9.85	0.77	94.71	4.08	98.46
32-1465.5	A	44	46.66	0.35	33.95	0.24	1.16	0.00	1.34	0.39	0.00	0.63	10.10	0.00	94.82	4.48	99.30
32-1465.5	A	45	45.96	0.34	33.20	0.59	1.11	0.00	1.39	0.36	0.00	0.63	9.53	0.66	93.77	4.09	97.59
ave(8)			46.52	0.50	33.62	0.34	1.13	0.00	1.36	0.34	0.00	0.62	9.92	0.44	94.79	4.25	98.86
stdev			0.34	0.17	0.21	0.16	0.11	0.00	0.02	0.04	0.00	0.02	0.26	0.27	0.49	0.14	0.59
34-799	A	48	44.73	0.35	36.74	0.00	1.20	0.00	0.57	0.16	0.05	1.72	8.36	0.00	93.88	4.47	98.35
34-799	A	49	45.08	0.42	36.94	0.00	1.22	0.00	0.63	0.11	0.00	1.68	8.18	0.00	94.26	4.50	98.76
34-799	A	52	44.67	0.29	36.93	0.00	1.22	0.00	0.59	0.13	0.00	1.51	8.64	0.00	93.98	4.47	98.45
34-799	B	53	45.66	0.40	36.09	0.00	1.30	0.00	0.56	0.10	0.00	1.65	8.34	0.00	94.10	4.49	98.59
34-799	B	54	45.68	0.29	37.46	0.00	1.08	0.00	0.44	0.14	0.04	1.81	8.46	0.00	95.40	4.55	99.95
34-799	B	55	45.69	0.35	36.48	0.00	1.18	0.00	0.69	0.11	0.00	1.69	8.15	0.00	94.34	4.51	98.85
ave(6)			45.25	0.35	36.77	0.00	1.20	0.00	0.58	0.13	0.02	1.68	8.36	0.00	94.33	4.50	98.82
stdev			0.44	0.05	0.42	0.00	0.07	0.00	0.08	0.02	0.02	0.09	0.17	0.00	0.50	0.03	0.53
34-1028.5	A	37	46.79	1.01	31.59	0.00	2.31	0.00	2.09	0.21	0.05	0.20	10.35	0.00	94.60	4.44	99.04
34-1028.5	A	40	48.26	0.54	32.48	0.00	2.29	0.00	2.11	0.18	0.00	0.21	10.73	0.00	96.80	4.55	101.35
ave(2)			47.53	0.78	32.04	0.00	2.30	0.00	2.10	0.20	0.03	0.21	10.54	0.00	95.70	4.50	100.20
34-1500	C	33	46.73	0.00	36.80	0.00	0.00	0.00	1.22	0.48	0.04	0.78	9.41	0.00	95.46	4.56	100.02
34-1500	F	37	31.11	0.07	50.91	0.00	0.00	0.00	0.25	0.00	11.30	0.60	0.32	0.00	94.56	4.51	99.07
34-1500	F	38	31.70	0.08	49.84	0.00	0.37	0.00	0.58	0.00	10.15	0.68	0.54	0.00	93.94	4.49	98.43
34-1500	F	39	31.30	0.06	51.13	0.00	0.00	0.00	0.26	0.00	11.34	0.65	0.18	0.00	94.92	4.54	99.46
34-1500	F	40	31.20	0.10	50.91	0.00	0.10	0.00	0.24	0.00	10.85	0.70	0.20	0.00	94.30	4.51	98.81
34-1500	G	42	30.72	0.07	50.87	0.00	0.17	0.00	0.33	0.00	10.88	0.61	0.20	0.00	93.85	4.48	98.33
ma. ave(4)			31.08	0.08	50.96	0.00	0.07	0.00	0.27	0.00	11.09	0.64	0.23	0.00	94.41	4.51	98.92
stdev			0.22	0.01	0.10	0.00	0.07	0.00	0.04	0.00	0.23	0.04	0.06	0.00	0.39	0.02	0.41
34C-1377	A	59	47.20	0.39	37.45	0.00	1.13	0.00	0.70	0.00	0.00	1.52	8.24	0.00	96.63	4.63	101.26
34C-1377	A	66	46.52	0.36	36.70	0.00	1.18	0.00	0.88	0.12	0.00	1.50	7.79	0.00	95.05	4.56	99.61
34C-1377	A	67	46.74	0.33	36.93	0.00	1.29	0.00	0.85	0.11	0.00	1.38	8.13	0.00	95.76	4.58	100.34
ave(3)			46.82	0.36	37.03	0.00	1.20	0.00	0.81	0.08	0.00	1.47	8.05	0.00	95.81	4.59	100.40
stdev			0.28	0.02	0.31	0.00	0.07	0.00	0.08	0.05	0.00	0.06	0.19	0.00	0.65	0.03	0.68
34C-1453	C	7	46.99	0.35	35.49	0.00	1.88	0.00	0.77	0.00	0.00	1.73	8.34	0.00	95.55	4.55	100.10
34C-1453	F	9	46.87	0.41	36.71	0.00	1.62	0.00	0.64	0.00	0.00	1.88	7.56	0.00	95.69	4.59	100.28
34C-1453	F	10	46.78	0.37	36.34	0.00	1.60	0.00	0.62	0.15	0.00	1.99	8.16	0.00	96.01	4.57	100.58
34C-1453	F	11	46.19	0.39	36.24	0.00	1.55	0.00	0.62	0.11	0.00	2.02	7.83	0.00	94.95	4.53	99.48
34C-1453	F	12	46.29	0.34	36.29	0.00	1.43	0.00	0.61	0.00	0.00	1.84	8.21	0.00	95.01	4.54	99.55
34C-1453	F	13	47.51	0.38	36.60	0.00	1.66	0.00	0.73	0.00	0.00	1.58	7.56	0.00	96.02	4.61	100.63
34C-1453	F	14	46.57	0.38	36.36	0.00	1.67	0.00	0.66	0.00	0.00	2.02	8.07	0.00	95.73	4.57	100.30
34C-1453	I	15	46.58	0.38	36.25	0.00	1.59	0.00	0.69	0.11	0.00	1.86	7.78	0.00	95.24	4.55	99.79
34C-1453	I	16	46.38	0.29	36.55	0.00	1.41	0.00	0.56	0.00	0.00	2.06	7.76	0.00	95.01	4.55	99.56
ave(9)			46.68	0.37	36.31	0.00	1.60	0.00	0.66	0.04	0.00	1.89	7.92	0.00	95.47	4.56	100.03
stdev			0.39	0.03	0.33	0.00	0.13	0.00	0.06	0.06	0.00	0.15	0.27	0.00	0.40	0.02	0.42
34C-1747.5	D	42	45.96	0.29	36.47	0.00	1.69	0.00	0.60	0.00	0.00	1.75	9.17	0.00	95.93	4.54	100.47
34C-1747.5	C	46	45.84	0.27	36.63	0.00	1.64	0.00	0.66	0.00	0.00	1.54	9.22	0.00	95.80	4.54	100.34
34C-1747.5	C	48	45.75	0.29	36.49	0.00	1.62	0.00	0.66	0.14	0.00	1.65	9.13	0.00	95.73	4.53	100.26
34C-1747.5	A	51	45.56	0.37	36.64	0.00	1.78	0.00	0.66	0.15	0.00	1.59	8.65	0.00	95.40	4.53	99.93
34C-1747.5	A	52	45.79	0.32	37.06	0.00	1.66	0.00	0.61	0.00	0.00	1.69	9.31	0.00	96.44	4.56	101.00
34C-1747.5	A	53	46.03	0.34	36.88	0.00	1.52	0.00	0.66	0.12	0.00	1.65	8.95	0.00	96.15	4.56	100.71
ave(6)			45.82	0.31	36.70	0.00	1.65	0.00	0.64	0.07	0.00	1.65	9.07	0.00	95.91	4.55	100.45
stdev			0.15	0.03	0.21	0.00	0.08	0.00	0.03	0.07	0.00	0.07	0.22	0.00	0.33	0.01	0.34

Table B.3. a. Muscovite and Margarite Mineral Chemistry. (continued)

			Structural formula normalized to 44 anionic charges														F+OH=4	
Sample	area	spot	Si	Al_{iv}	Al_{vi}	Ti	Cr	Fe	Mn	Mg	site	Ba	Ca	Na	K	site	F	OH
22-901	A'	54	6.071	1.929	3.644	.043	.000	.267	.000	.146	4.100	.008	.000	.415	1.567	1.990	.000	4.000
22-901	A'	57	6.047	1.953	3.701	.041	.000	.247	.000	.127	4.116	.010	.000	.424	1.493	1.928	.000	4.000
22-901	A'	59	6.047	1.953	3.732	.041	.000	.212	.000	.123	4.109	.010	.000	.375	1.526	1.911	.000	4.000
22-901	B	60	6.095	1.905	3.678	.045	.000	.228	.000	.131	4.082	.007	.000	.403	1.555	1.966	.000	4.000
22-901	B	62	6.038	1.962	3.708	.043	.000	.231	.000	.120	4.101	.007	.000	.392	1.561	1.960	.000	4.000
22-901	B	64	6.055	1.945	3.747	.029	.000	.206	.000	.120	4.101	.009	.000	.365	1.554	1.929	.000	4.000
ave(6)			6.059	1.941	3.702	.040	.000	.232	.000	.128	4.102	.009	.000	.396	1.543	1.947	.000	4.000
stdev			.019	.019	.034	.005	.000	.020	.000	.009	.010	.001	.000	.021	.026	.027	.000	.000
22-957	C	67	5.551	2.449	3.787	.020	.000	.191	.000	.111	4.110	.011	.484	.294	1.116	1.906	.000	4.000
22-957	C	68	5.583	2.417	3.759	.025	.000	.190	.000	.104	4.079	.011	.479	.297	1.173	1.960	.000	4.000
22-957	B	71	6.140	1.860	3.652	.037	.000	.310	.000	.145	4.143	.017	.000	.296	1.520	1.833	.000	4.000
22-957	B	72	5.647	2.353	3.742	.029	.000	.220	.000	.132	4.123	.006	.401	.298	1.193	1.899	.000	4.000
22-957	B	73	4.954	3.046	3.835	.020	.000	.183	.000	.114	4.153	.008	1.017	.277	.538	1.840	.000	4.000
22-957	B	75	5.755	2.245	3.568	.029	.000	.371	.000	.343	4.311	.011	.209	.293	1.267	1.779	.000	4.000
22-957	B	76	5.364	2.636	3.790	.021	.000	.230	.000	.220	4.261	.008	.527	.291	.919	1.746	.000	4.000
22-957	D	78	5.677	2.323	3.418	.027	.000	.535	.005	.464	4.449	.011	.206	.278	1.241	1.736	.000	4.000
22-957	D	79	5.862	2.138	3.674	.033	.000	.292	.000	.169	4.168	.014	.215	.311	1.294	1.833	.000	4.000
22-957	D	80	6.129	1.871	3.706	.028	.000	.238	.000	.131	4.102	.014	.000	.301	1.575	1.891	.000	4.000
22-957	B	27	6.097	1.903	3.814	.023	.000	.239	.000	.112	4.188	.010	.000	.286	1.362	1.658	.000	4.000
22-957	A	28	6.114	1.886	3.669	.023	.000	.310	.000	.146	4.149	.015	.000	.321	1.522	1.858	.000	4.000
22-957	E	29	5.723	2.277	3.755	.031	.000	.208	.000	.118	4.112	.015	.379	.286	1.164	1.844	.000	4.000
ave(4)			6.120	1.880	3.710	.028	.000	.274	.000	.133	4.145	.014	.000	.301	1.495	1.810	.000	4.000
stdev			.016	.016	.063	.006	.000	.036	.000	.014	.030	.002	.000	.013	.080	.090	.000	.000
22-996.5	B	47	6.074	1.926	3.733	.024	.000	.278	.000	.134	4.168	.014	.000	.312	1.468	1.794	.000	4.000
22-996.5	B	50	6.111	1.889	3.751	.030	.000	.284	.000	.142	4.207	.009	.000	.315	1.331	1.655	.000	4.000
22-996.5	B	52	6.091	1.909	3.773	.024	.000	.263	.000	.124	4.184	.012	.011	.318	1.355	1.697	.000	4.000
22-996.5	B	54	6.121	1.879	3.700	.034	.000	.304	.000	.134	4.172	.019	.000	.321	1.409	1.749	.000	4.000
22-996.5	B	55	6.085	1.915	3.678	.032	.000	.319	.000	.147	4.176	.018	.000	.304	1.482	1.803	.000	4.000
ave(5)			6.097	1.903	3.727	.029	.000	.290	.000	.136	4.181	.014	.002	.314	1.409	1.740	.000	4.000
stdev			.017	.017	.034	.004	.000	.020	.000	.008	.014	.004	.005	.006	.059	.057	.000	.000
22A-1625	C	28	5.679	2.321	3.311	.017	.000	.486	.010	.902	4.727	.000	.000	.343	1.179	1.523	.000	4.000
22A-1625	A	31	5.884	2.116	3.578	.032	.000	.260	.000	.493	4.362	.008	.000	.357	1.376	1.741	.000	4.000
22A-1625	A	35	5.859	2.141	3.561	.029	.000	.284	.000	.508	4.382	.007	.000	.383	1.360	1.750	.000	4.000
22A-1625	A	39	6.050	1.950	3.762	.051	.000	.143	.000	.146	4.103	.009	.000	.422	1.440	1.872	.000	4.000
22A-1625	A	40	6.072	1.928	3.757	.043	.000	.149	.000	.151	4.099	.008	.000	.391	1.480	1.879	.000	4.000
S1, ave(2)			5.871	2.129	3.569	.031	.000	.272	.000	.500	4.372	.008	.000	.370	1.368	1.746	.000	4.000
S2, ave(2)			6.061	1.939	3.759	.047	.000	.146	.000	.149	4.101	.009	.000	.407	1.460	1.876	.000	4.000
ave(4)			5.966	2.034	3.664	.039	.000	.209	.000	.324	4.236	.008	.000	.388	1.414	1.811	.000	4.000
stdev			.096	.096	.095	.009	.000	.063	.000	.176	.136	.001	.000	.023	.048	.065	.000	.000
22A-1638	A	57	6.061	1.939	3.852	.037	.000	.091	.000	.115	4.095	.006	.000	.553	1.261	1.819	.000	4.000
22A-1638	A	58	6.045	1.955	3.842	.028	.000	.089	.000	.123	4.083	.006	.000	.535	1.342	1.884	.000	4.000
ave(2)			6.053	1.947	3.847	.033	.000	.090	.000	.119	4.089	.006	.000	.544	1.301	1.851	.000	4.000
22A-1752	A	1r	6.124	1.876	3.789	.020	.000	.123	.000	.083	4.016	.000	.000	.564	1.451	2.016	.000	4.000
22A-1752	A	2r	6.441	1.559	3.705	.029	.000	.121	.000	.104	3.959	.000	.000	.590	1.290	1.880	.000	4.000
22A-1752	A	3c	6.148	1.852	3.745	.030	.000	.126	.000	.114	4.015	.007	.000	.535	1.469	2.011	.000	4.000
22A-1752	A	4c	6.197	1.803	3.736	.029	.000	.128	.000	.127	4.020	.000	.000	.558	1.411	1.969	.000	4.000
22A-1752	B'	5m	6.122	1.878	3.729	.034	.000	.137	.000	.111	4.010	.000	.000	.595	1.466	2.060	.000	4.000
22A-1752	B'	6m	6.065	1.935	3.814	.022	.000	.117	.000	.104	4.057	.000	.000	.730	1.232	1.963	.000	4.000
22A-1752	B'	7c	6.274	1.726	3.654	.037	.000	.153	.000	.199	4.043	.000	.000	.567	1.344	1.911	.000	4.000
ave(7)			6.196	1.804	3.739	.028	.000	.129	.000	.120	4.017	.001	.000	.591	1.380	1.973	.000	4.000
stdev			.117	.117	.049	.006	.000	.011	.000	.035	.029	.002	.000	.060	.087	.058	.000	.000
22B-1721	A	61	6.125	1.875	3.740	.028	.000	.198	.000	.150	4.115	.005	.028	.223	1.558	1.815	.000	4.000
22B-1721	A	65	5.899	2.101	3.752	.029	.000	.201	.000	.147	4.130	.008	.162	.228	1.464	1.862	.000	4.000
22B-1721	A	66	6.115	1.885	3.695	.030	.000	.210	.000	.153	4.088	.008	.000	.229	1.709	1.946	.000	4.000
22B-1721	A	67	6.113	1.887	3.703	.032	.000	.261	.000	.148	4.144	.007	.000	.272	1.546	1.825	.000	4.000
22B-1721	A	69	6.012	1.988	3.750	.029	.000	.209	.000	.139	4.127	.008	.069	.228	1.544	1.848	.000	4.000
ave(5)			6.053	1.947	3.728	.030	.000	.216	.000	.147	4.121	.007	.052	.236	1.564	1.859	.000	4.000
stdev			.087	.087	.024	.001	.000	.023	.000	.004	.019	.001	.060	.018	.080	.047	.000	.000
22B-1723	A	59	6.067	1.933	3.740	.047	.000	.179	.000	.147	4.113	.006	.080	.276	1.424	1.787	.000	4.000
22B-1723	A	60	5.996	2.004	3.722	.037	.000	.162	.000	.158	4.079	.007	.136	.249	1.514	1.906	.000	4.000
22B-1723	B'	64	6.191	1.809	3.685	.049	.000	.180	.000	.157	4.071	.007	.007	.268	1.588	1.870	.000	4.000
22B-1723	B'	65	6.018	1.982	3.718	.043	.000	.190	.000	.170	4.121	.007	.096	.255	1.473	1.831	.000	4.000
22B-1723	C	67	5.931	2.069	3.738	.038	.000	.162	.000	.151	4.089	.008	.166	.253	1.474	1.901	.000	4.000
22B-1723	C	68	6.124	1.876	3.753	.043	.000	.174	.000	.141	4.112	.000	.000	.261	1.551	1.812	.000	4.000
22B-1723	D	72	5.951	2.049	3.717	.036	.000	.181	.000	.184	4.118	.005	.178	.245	1.411	1.839	.000	4.000
22B-1723	B	1	5.670	2.330	3.767	.033	.000	.156	.000	.141	4.097	.007	.399	.253	1.238	1.896	.000	4.000

Table B.3. a. Muscovite and Margarite Mineral Chemistry. (continued)

			Structural formula normalized to 44 anionic charges														F+OH=4	
Sample	area	spot	Si	Al_{iv}	Al_{vi}	Ti	Cr	Fe	Mn	Mg	site	Ba	Ca	Na	K	site	F	OH
22B-1723	C	30	5.980	2.020	3.745	.038	.000	.161	.000	.157	4.100	.000	.144	.246	1.465	1.855	.000	4.000
22B-1723	C	31	6.013	1.987	3.736	.043	.000	.178	.000	.165	4.122	.006	.135	.240	1.398	1.779	.000	4.000
22B-1723	A	32	5.971	2.029	3.757	.038	.000	.172	.000	.155	4.121	.006	.121	.230	1.470	1.827	.000	4.000
ave(10)			6.024	1.976	3.731	.041	.000	.174	.000	.158	4.105	.005	.106	.252	1.477	1.841	.000	4.000
stdev			.077	.077	.020	.004	.000	.009	.000	.012	.018	.003	.058	.013	.057	.041	.000	.000
22B-1843	B	58	6.234	1.766	3.398	.083	.000	.255	.000	.407	4.143	.012	.000	.062	1.831	1.905	.000	4.000
22B-1843	B	59	6.299	1.701	3.450	.047	.000	.240	.000	.430	4.167	.028	.000	.063	1.703	1.794	.000	4.000
22B-1843	B	60	6.253	1.747	3.411	.060	.000	.232	.000	.429	4.133	.025	.000	.065	1.834	1.924	.000	4.000
22B-1843	C	64	6.291	1.709	3.386	.071	.000	.281	.000	.405	4.144	.012	.000	.060	1.809	1.881	.000	4.000
22B-1843	C	65	6.277	1.723	3.426	.067	.000	.281	.000	.376	4.149	.012	.010	.068	1.754	1.844	.000	4.000
ave(5)			6.271	1.729	3.414	.066	.000	.258	.000	.409	4.147	.018	.002	.064	1.786	1.870	.000	4.000
stdev			.024	.024	.022	.012	.000	.020	.000	.020	.011	.007	.004	.002	.050	.046	.000	.000
32-1465.5	C	38	6.276	1.724	3.589	.032	.031	.144	.000	.273	4.069	.016	.000	.166	1.705	1.887	.216	3.784
32-1465.5	C	39	6.245	1.755	3.579	.076	.022	.125	.000	.279	4.081	.018	.000	.157	1.646	1.821	.238	3.762
32-1465.5	C	40	6.233	1.767	3.553	.082	.010	.129	.000	.276	4.050	.015	.000	.161	1.748	1.925	.000	4.000
32-1465.5	B	41	6.269	1.731	3.570	.053	.045	.132	.000	.265	4.065	.017	.000	.174	1.670	1.861	.194	3.806
32-1465.5	B	42	6.273	1.727	3.562	.046	.036	.129	.000	.270	4.043	.016	.000	.156	1.762	1.934	.233	3.767
32-1465.5	B	43	6.224	1.776	3.598	.047	.055	.100	.000	.267	4.068	.021	.000	.157	1.696	1.873	.329	3.671
32-1465.5	A	44	6.246	1.754	3.604	.035	.025	.130	.000	.267	4.062	.020	.000	.164	1.725	1.909	.000	4.000
32-1465.5	A	45	6.254	1.746	3.580	.035	.063	.126	.000	.282	4.087	.019	.000	.166	1.654	1.840	.284	3.716
ave(8)			6.253	1.747	3.579	.051	.036	.127	.000	.272	4.066	.018	.000	.163	1.701	1.881	.187	3.813
stdev			.018	.018	.016	.018	.017	.011	.000	.006	.014	.002	.000	.006	.040	.038	.115	.115
34-799	A	48	6.003	1.997	3.816	.035	.000	.135	.000	.114	4.100	.008	.007	.448	1.431	1.895	.000	4.000
34-799	A	49	6.012	1.988	3.820	.042	.000	.136	.000	.125	4.123	.006	.000	.434	1.392	1.832	.000	4.000
34-799	A	52	5.992	2.008	3.832	.029	.000	.137	.000	.118	4.116	.007	.000	.393	1.479	1.878	.000	4.000
34-799	B	53	6.102	1.898	3.788	.040	.000	.145	.000	.112	4.085	.005	.000	.428	1.422	1.855	.000	4.000
34-799	B	54	6.023	1.977	3.846	.029	.000	.119	.000	.086	4.081	.007	.006	.463	1.423	1.899	.000	4.000
34-799	B	55	6.080	1.920	3.804	.035	.000	.131	.000	.137	4.107	.006	.000	.436	1.384	1.826	.000	4.000
ave(6)			6.035	1.965	3.818	.035	.000	.134	.000	.115	4.102	.007	.002	.434	1.422	1.864	.000	4.000
stdev			.041	.041	.019	.005	.000	.008	.000	.015	.015	.001	.003	.021	.031	.029	.000	.000
34-1028.5	A	37	6.317	1.683	3.346	.103	.000	.261	.000	.421	4.130	.011	.007	.052	1.783	1.854	.000	4.000
34-1028.5	A	40	6.360	1.640	3.406	.054	.000	.252	.000	.414	4.126	.009	.000	.054	1.804	1.867	.000	4.000
ave(2)			6.339	1.661	3.376	.078	.000	.257	.000	.417	4.128	.010	.004	.053	1.793	1.860	.000	4.000
34-1500	C	33	6.143	1.857	3.847	.000	.000	.000	.000	.239	4.086	.025	.006	.199	1.578	1.807	.000	4.000
34-1500	F	37	4.132	3.868	4.105	.007	.000	.000	.000	.049	4.162	.000	1.608	.155	.054	1.817	.000	4.000
34-1500	F	38	4.234	3.766	4.082	.008	.000	.041	.000	.115	4.247	.000	1.453	.176	.092	1.721	.000	4.000
34-1500	F	39	4.138	3.862	4.108	.006	.000	.000	.000	.051	4.166	.000	1.607	.167	.030	1.804	.000	4.000
34-1500	F	40	4.149	3.851	4.129	.010	.000	.011	.000	.048	4.198	.000	1.546	.180	.034	1.760	.000	4.000
34-1500	G	42	4.108	3.892	4.128	.007	.000	.019	.000	.066	4.220	.000	1.559	.158	.034	1.751	.000	4.000
ma, ave(4)			4.132	3.868	4.118	.007	.000	.008	.000	.054	4.186	.000	1.580	.165	.038	1.783	.000	4.000
stdev			.015	.015	.011	.002	.000	.008	.000	.007	.024	.000	.028	.010	.009	.028	.000	.000
34C-1377	A	59	6.111	1.889	3.827	.038	.000	.122	.000	.135	4.122	.000	.000	.382	1.361	1.743	.000	4.000
34C-1377	A	66	6.119	1.881	3.810	.036	.000	.130	.000	.173	4.148	.006	.000	.383	1.307	1.696	.000	4.000
34C-1377	A	67	6.114	1.886	3.808	.032	.000	.141	.000	.166	4.148	.006	.000	.350	1.357	1.712	.000	4.000
ave(3)			6.115	1.885	3.815	.035	.000	.131	.000	.158	4.139	.004	.000	.371	1.342	1.717	.000	4.000
stdev			.004	.004	.008	.002	.000	.008	.000	.016	.012	.003	.000	.015	.024	.019	.000	.000
34C-1453	C	7	6.191	1.809	3.703	.035	.000	.207	.000	.151	4.096	.000	.000	.442	1.402	1.844	.000	4.000
34C-1453	F	9	6.129	1.871	3.789	.040	.000	.177	.000	.125	4.131	.000	.000	.477	1.261	1.738	.000	4.000
34C-1453	F	10	6.132	1.868	3.748	.036	.000	.175	.000	.121	4.081	.008	.000	.506	1.365	1.878	.000	4.000
34C-1453	F	11	6.112	1.888	3.765	.039	.000	.172	.000	.122	4.097	.006	.000	.518	1.322	1.846	.000	4.000
34C-1453	F	12	6.120	1.880	3.777	.034	.000	.158	.000	.120	4.089	.000	.000	.472	1.385	1.857	.000	4.000
34C-1453	F	13	6.179	1.821	3.792	.037	.000	.181	.000	.142	4.151	.000	.000	.398	1.254	1.653	.000	4.000
34C-1453	F	14	6.117	1.883	3.747	.038	.000	.183	.000	.129	4.097	.000	.000	.514	1.352	1.867	.000	4.000
34C-1453	I	15	6.136	1.864	3.766	.038	.000	.175	.000	.135	4.114	.006	.000	.475	1.308	1.788	.000	4.000
34C-1453	I	16	6.118	1.882	3.801	.029	.000	.156	.000	.110	4.096	.000	.000	.527	1.306	1.833	.000	4.000
ave(9)			6.137	1.863	3.765	.036	.000	.176	.000	.128	4.106	.002	.000	.481	1.328	1.811	.000	4.000
stdev			.027	.027	.028	.003	.000	.014	.000	.012	.021	.003	.000	.039	.049	.069	.000	.000
34C-1747.5	D	42	6.065	1.935	3.740	.029	.000	.187	.000	.118	4.073	.000	.000	.448	1.544	1.992	.000	4.000
34C-1747.5	C	46	6.054	1.946	3.756	.027	.000	.181	.000	.130	4.094	.000	.000	.394	1.553	1.948	.000	4.000
34C-1747.5	C	48	6.053	1.947	3.745	.029	.000	.179	.000	.130	4.083	.007	.000	.423	1.541	1.972	.000	4.000
34C-1747.5	A	51	6.036	1.964	3.759	.037	.000	.197	.000	.130	4.123	.008	.000	.408	1.462	1.878	.000	4.000
34C-1747.5	A	52	6.015	1.985	3.755	.032	.000	.182	.000	.119	4.088	.000	.000	.430	1.560	1.991	.000	4.000
34C-1747.5	A	53	6.049	1.951	3.763	.034	.000	.167	.000	.129	4.093	.006	.000	.420	1.501	1.927	.000	4.000
ave(6)			6.045	1.955	3.753	.031	.000	.182	.000	.126	4.092	.004	.000	.421	1.527	1.951	.000	4.000
stdev			.016	.016	.008	.003	.000	.009	.000	.005	.015	.004	.000	.017	.035	.040	.000	.000

Table B.3. b. Biotite Mineral Chemistry.

			weight percent oxide or element (Cr_2O_3 not detected)														
Sample	area	spot	SiO_2	TiO_2	Al_2O_3	FeO	MnO	MgO	BaO	CaO	Na_2O	K_2O	ZnO	F	Total	H_2O	Total
22A-1625	C	29	37.76	0.99	19.44	10.53	0.24	17.80	0.00	0.00	0.42	8.91	0.00	1.63	97.72	3.40	100.43
22A-1625	C	30	37.92	1.04	19.16	10.66	0.23	17.42	0.00	0.00	0.42	9.84	0.00	1.53	98.22	3.45	101.02
22A-1625	A	33	37.89	1.01	19.02	10.97	0.24	17.43	0.00	0.00	0.37	8.84	0.00	1.53	97.30	3.43	100.08
22A-1625	A	34	38.43	1.10	19.25	10.77	0.23	17.42	0.00	0.00	0.43	9.67	0.00	1.72	99.02	3.39	101.69
22A-1625	A	37	37.34	0.97	19.07	10.81	0.25	17.54	0.00	0.00	0.40	8.94	0.00	1.92	97.24	3.21	99.65
ave(5)			37.87	1.02	19.19	10.75	0.24	17.52	0.00	0.00	0.41	9.24	0.00	1.67	97.90	3.37	100.57
stdev			0.35	0.05	0.15	0.15	0.01	0.15	0.00	0.00	0.02	0.43	0.00	0.15	0.66	0.08	0.72
22A-1752	B	19	38.41	1.00	18.99	9.86	0.20	19.48	na	0.00	0.36	8.19	0.00	2.75	99.24	2.92	101.00
22A-1752	B	20	38.39	0.99	18.85	9.60	0.19	19.20	na	0.04	0.40	8.95	0.00	2.91	99.52	2.83	101.13
ave(2)			38.40	1.00	18.92	9.73	0.20	19.34	na	0.02	0.38	8.57	0.00	2.83	99.38	2.88	101.06
22B-1721	B	54	36.85	1.14	19.46	16.20	0.16	13.69	0.00	0.04	0.37	9.29	0.00	1.00	98.20	3.62	101.40
22B-1721	B	55	36.66	1.23	19.42	15.96	0.15	13.69	0.00	0.00	0.24	9.30	0.00	0.89	97.54	3.65	100.82
22B-1721	B	59	35.66	1.22	18.43	19.15	0.12	13.17	0.00	0.00	0.19	8.33	0.00	0.68	96.95	3.68	100.35
22B-1721	A	60	36.93	1.26	19.46	15.98	0.12	13.48	0.00	0.06	0.34	8.99	0.00	0.91	97.53	3.65	100.80
22B-1721	A	63	37.05	1.17	19.51	15.78	0.14	13.98	0.00	0.00	0.33	9.12	0.00	0.86	97.94	3.70	101.28
ave(4)			36.87	1.20	19.46	15.98	0.14	13.71	0.00	0.03	0.32	9.18	0.00	0.92	97.80	3.66	101.07
stdev			0.14	0.05	0.03	0.15	0.01	0.18	0.00	0.03	0.05	0.13	0.00	0.05	0.28	0.03	0.27
22B-1723	B	63	37.24	1.36	18.90	14.52	0.18	15.62	0.00	0.04	0.21	8.65	0.00	1.38	98.10	3.47	100.99
22B-1723	C	66	37.18	1.17	18.69	14.35	0.17	15.44	0.00	0.00	0.33	8.90	0.00	1.64	97.87	3.32	100.50
22B-1723	C	69	36.07	1.37	18.87	14.35	0.13	16.08	0.00	0.05	0.19	8.41	0.00	1.46	96.98	3.38	99.74
22B-1723	D	70	37.30	1.22	18.89	14.34	0.17	15.42	0.00	0.04	0.31	8.62	0.00	1.47	97.78	3.41	100.57
22B-1723	D	71	37.97	1.22	18.61	14.05	0.22	15.47	0.00	0.04	0.36	9.03	0.00	1.58	98.55	3.39	101.27
ave(5)			37.15	1.27	18.79	14.32	0.17	15.61	0.00	0.03	0.28	8.72	0.00	1.51	97.86	3.39	100.62
stdev			0.61	0.08	0.12	0.15	0.03	0.25	0.00	0.02	0.07	0.22	0.00	0.09	0.51	0.05	0.52
22B-1843	B	56	36.50	1.32	18.70	11.93	0.40	16.68	0.00	0.04	0.10	9.25	0.00	0.44	95.36	3.86	99.03
22B-1843	B	57	37.84	1.18	18.80	12.17	0.46	16.51	0.00	0.00	0.09	9.34	0.00	0.51	96.90	3.90	100.58
22B-1843	A	61	37.70	1.66	18.50	11.43	0.49	16.53	0.00	0.07	0.13	9.09	0.00	0.44	96.04	3.91	99.77
22B-1843	A	62	38.04	1.77	18.57	11.23	0.45	16.42	0.00	0.08	0.10	9.44	0.00	0.49	96.59	3.91	100.30
22B-1843	A	63	38.17	1.16	18.87	11.26	0.45	16.75	0.00	0.04	0.08	9.40	0.00	0.00	96.18	4.15	100.33
ave(5)			37.65	1.42	18.69	11.60	0.45	16.58	0.00	0.05	0.10	9.30	0.00	0.38	96.21	3.95	100.00
stdev			0.60	0.25	0.14	0.38	0.03	0.12	0.00	0.03	0.02	0.12	0.00	0.19	0.52	0.10	0.55
24-1131	C	79	39.33	0.92	16.58	12.73	0.12	18.20	0.31	0.14	0.18	7.55	0.24	1.34	97.64	3.53	100.60
24-1131	C	80	38.93	1.05	17.26	12.29	0.00	18.30	0.24	0.00	0.20	8.29	0.00	1.72	98.28	3.36	100.91
24-1131	C	81	39.04	0.85	17.20	12.19	0.11	18.62	0.31	0.00	0.17	8.33	0.00	1.80	98.62	3.33	101.19
24-1131	D	82	38.37	1.21	17.04	12.69	0.00	18.20	0.31	0.00	0.17	8.17	0.00	1.49	97.65	3.43	100.46
24-1131	D	83	38.98	0.67	17.51	12.09	0.09	18.37	0.32	0.00	0.18	8.60	0.00	1.61	98.42	3.41	101.16
24-1131	D	84	38.74	0.70	17.15	12.77	0.00	18.26	0.26	0.05	0.22	7.92	0.00	1.52	97.59	3.43	100.38
24-1131	D	85	38.76	0.91	17.20	12.57	0.00	18.09	0.29	0.08	0.16	8.47	0.00	1.54	98.07	3.43	100.85
ave(7)			38.88	0.90	17.13	12.48	0.05	18.29	0.29	0.04	0.18	8.19	0.03	1.57	98.04	3.42	100.79
stdev			0.28	0.18	0.26	0.26	0.05	0.16	0.03	0.05	0.02	0.33	0.08	0.14	0.39	0.06	0.30
24-1191	F	23	38.99	0.96	17.43	14.87	0.29	16.25	na	0.00	0.24	8.40	0.00	0.94	98.37	3.72	101.69
24-1191	F	24	38.02	1.01	17.78	15.09	0.37	16.00	na	0.00	0.26	8.57	0.00	0.86	97.96	3.72	101.32
zone 6. ave(2)			38.51	0.99	17.61	14.98	0.33	16.13	na	0.00	0.25	8.49	0.00	0.90	98.17	3.72	101.51
24-1191	E	20	38.08	0.79	17.28	14.43	0.34	16.87	na	0.00	0.30	8.56	0.00	0.90	97.55	3.69	100.86
24-1191	E	21	37.83	0.91	17.18	14.78	0.40	16.77	na	0.00	0.24	8.37	0.00	0.64	97.12	3.80	100.65
24-1191	E	22	38.25	1.02	16.93	14.61	0.32	16.94	na	0.00	0.24	8.59	0.00	1.12	98.02	3.60	101.14
24-1191	G	26	38.59	1.19	16.76	13.61	0.39	17.47	na	0.00	0.25	8.39	0.00	0.00	96.65	4.14	100.79
zone 5. ave(4)			38.19	0.98	17.04	14.36	0.36	17.01	na	0.00	0.26	8.48	0.00	0.67	97.34	3.81	100.86
stdev			0.28	0.15	0.20	0.45	0.03	0.27	na	0.00	0.02	0.10	0.00	0.42	0.51	0.21	0.18
34-1028.5	A	36	37.65	1.57	18.51	13.21	0.45	15.48	0.00	0.05	0.07	10.08	0.00	0.00	97.07	4.13	101.20
34-1028.5	A	39	36.56	1.10	17.85	15.12	0.35	14.45	0.00	0.09	0.10	9.07	0.00	0.00	94.69	4.00	98.69
34-1028.5	A	41	37.24	1.10	18.92	13.04	0.40	15.79	0.00	0.09	0.09	8.98	0.00	0.00	95.65	4.10	99.75
34-1028.5	A	42	37.52	0.93	19.07	12.31	0.44	15.63	0.00	0.12	0.12	9.54	0.00	0.00	95.68	4.10	99.78
34-1028.5	A	43	37.66	1.07	19.00	12.98	0.41	15.73	0.00	0.00	0.07	9.59	0.00	0.00	96.51	4.13	100.64
ave(5)			37.33	1.15	18.67	13.33	0.41	15.42	0.00	0.07	0.09	9.45	0.00	0.00	95.92	4.09	100.01
stdev			0.41	0.22	0.45	0.95	0.04	0.49	0.00	0.04	0.02	0.40	0.00	0.00	0.81	0.05	0.86
34-1500	D	35	40.46	0.26	18.84	2.48	0.15	23.78	0.00	0.49	0.30	9.16	0.00	3.77	99.69	2.54	100.65
34-1500	G	41	41.73	0.32	17.12	1.38	0.08	25.52	0.15	0.00	0.35	9.47	0.00	3.59	99.71	2.66	100.85
34-1500	G	43	41.76	0.36	17.37	1.15	0.00	25.32	0.15	0.00	0.34	9.01	0.00	3.41	98.87	2.73	100.17
34-1500	G	44	41.44	0.35	16.81	1.33	0.08	25.15	0.16	0.00	0.33	8.55	0.00	3.38	97.58	2.69	98.85
34-1500	H	70	41.87	0.32	17.48	1.29	0.09	25.15	0.17	0.00	0.30	8.11	0.00	3.74	98.52	2.57	99.51
34-1500	H	46	41.58	0.33	17.26	1.36	0.00	25.12	0.17	0.04	0.31	8.53	0.00	3.53	98.23	2.65	99.39
ave(6)			41.68	0.34	17.21	1.30	0.05	25.25	0.16	0.01	0.33	8.73	0.00	3.53	98.58	2.66	99.76
stdev			0.15	0.02	0.23	0.08	0.04	0.15	0.01	0.02	0.02	0.47	0.00	0.13	0.71	0.05	0.69

Table B.3. b. Biotite Mineral Chemistry. (continued)

			weight percent oxide or element (Cr_2O_3 not detected)														
Sample	area	spot	SiO_2	TiO_2	Al_2O_3	FeO	MnO	MgO	BaO	CaO	Na_2O	K_2O	ZnO	F	Total	H_2O	Total
34B-759.5	A'	66	38.07	1.19	17.47	12.39	0.19	17.06	0.00	0.00	0.06	10.52	0.00	0.00	96.95	4.13	101.08
34B-759.5	A'	67	38.43	1.22	17.27	12.30	0.18	17.06	0.00	0.00	0.00	10.08	0.00	0.00	96.54	4.13	100.67
34B-759.5	A'	68	38.24	1.19	17.47	12.05	0.19	17.25	0.00	0.06	0.00	10.47	0.00	0.00	96.92	4.14	101.06
34B-759.5	B	69	37.96	0.30	18.01	10.95	0.20	18.27	0.00	0.10	0.09	9.75	0.00	0.00	95.63	4.12	99.75
34B-759.5	B	70	38.66	0.28	18.37	10.50	0.15	18.27	0.00	0.00	0.10	10.16	0.00	0.00	96.49	4.17	100.66
34B-759.5	B	71	38.66	0.27	17.70	10.51	0.17	18.43	0.12	0.00	0.00	9.74	0.00	0.51	96.11	3.89	99.79
ave(6)			38.34	0.74	17.72	11.45	0.18	17.72	0.02	0.03	0.04	10.12	0.00	0.09	96.44	4.10	100.50
stdev			0.27	0.46	0.37	0.82	0.02	0.61	0.04	0.04	0.04	0.31	0.00	0.19	0.46	0.09	0.54
34C-1453	G	18	37.61	0.92	16.94	16.89	0.00	16.32	na	0.00	0.24	8.05	0.00	3.45	100.42	2.46	101.43
34C-1377	A	56	38.42	0.24	32.16	6.92	0.26	10.13	0.00	0.00	0.93	4.57	0.00	0.00	93.63	4.33	97.96
34C-1377	A	58	39.90	0.73	18.53	9.09	0.27	19.77	0.00	0.00	0.41	8.16	0.00	2.06	98.92	3.29	101.34
34C-1377	A	64	39.74	0.71	18.39	9.01	0.31	19.76	0.00	0.00	0.41	7.90	0.00	2.44	98.67	3.09	100.73
34C-1377	A	65	39.80	0.73	18.60	9.00	0.27	19.61	0.00	0.00	0.43	8.48	0.00	2.08	99.00	3.28	101.40
34C-1377	B	69	39.84	0.70	18.47	9.04	0.26	19.84	0.00	0.00	0.39	8.18	0.00	2.14	98.86	3.25	101.21
ave(5)			39.82	0.72	18.50	9.04	0.28	19.75	0.00	0.00	0.41	8.18	0.00	2.18	98.86	3.23	101.17
stdev			0.06	0.01	0.08	0.03	0.02	0.08	0.00	0.00	0.01	0.21	0.00	0.15	0.12	0.08	0.26
34C-1747.5	C	41	37.13	1.16	18.51	13.76	0.10	15.84	0.00	0.00	0.37	8.77	0.00	1.87	97.51	3.20	99.92
34C-1747.5	C	43	37.36	1.10	19.12	13.55	0.13	15.88	0.00	0.00	0.33	9.06	0.00	1.67	98.20	3.33	100.83
34C-1747.5	D	44	37.46	1.19	18.47	13.73	0.09	15.57	0.00	0.00	0.47	8.97	0.00	1.51	97.46	3.38	100.21
34C-1747.5	D	45	37.57	1.14	18.65	13.61	0.10	15.56	0.00	0.00	0.45	8.64	0.00	1.52	97.24	3.38	99.98
34C-1747.5	A	49	36.94	1.26	18.64	13.80	0.10	15.88	0.00	0.00	0.41	8.90	0.00	1.72	97.65	3.28	100.20
34C-1747.5	A	50	37.60	1.25	18.76	14.27	0.13	15.56	0.00	0.00	0.36	9.48	0.00	1.54	98.95	3.41	101.71
ave(6)			37.34	1.18	18.69	13.79	0.11	15.72	0.00	0.00	0.40	8.97	0.00	1.64	97.84	3.33	100.48
stdev			0.24	0.06	0.21	0.23	0.02	0.15	0.00	0.00	0.05	0.27	0.00	0.13	0.58	0.07	0.63

Table B.3. b. Biotite Mineral Chemistry. (continued)

			Structural formula normalized to 44 anionic charges														F+OH=4	
Sample	area	spot	Si	Al_{iv}	Al_{vi}	Ti	Fe	Mn	Mg	Zn	site	Ba	Ca	Na	K	site	F	OH
22A-1625	C	29	5.429	2.571	.724	.107	1.266	.029	3.814	.000	5.941	.000	.000	.117	1.634	1.751	.741	3.259
22A-1625	C	30	5.451	2.549	.698	.112	1.282	.028	3.732	.000	5.852	.000	.000	.117	1.805	1.922	.696	3.304
22A-1625	A	33	5.474	2.526	.713	.110	1.325	.029	3.753	.000	5.930	.000	.000	.104	1.629	1.733	.699	3.301
22A-1625	A	34	5.479	2.521	.715	.118	1.284	.028	3.701	.000	5.846	.000	.000	.119	1.759	1.878	.776	3.224
22A-1625	A	37	5.428	2.572	.696	.106	1.314	.031	3.800	.000	5.947	.000	.000	.113	1.658	1.771	.883	3.117
ave(5)			5.452	2.548	.709	.111	1.294	.029	3.760	.000	5.903	.000	.000	.114	1.697	1.811	.759	3.241
stdev			.022	.022	.011	.004	.022	.001	.042	.000	.044	.000	.000	.006	.071	.075	.069	.069
22A-1752	B	19	5.454	2.546	.633	.107	1.171	.024	4.123	.000	6.058	.000	.000	.099	1.484	1.583	1.235	2.765
22A-1752	B	20	5.465	2.535	.628	.106	1.143	.023	4.073	.000	5.973	.000	.006	.110	1.625	1.742	1.310	2.690
ave(2)			5.460	2.540	.631	.106	1.157	.023	4.098	.000	6.016	.000	.003	.105	1.555	1.662	1.273	2.727
22B-1721	B	54	5.396	2.604	.755	.126	1.984	.020	2.988	.000	5.872	.000	.006	.105	1.736	1.847	.463	3.537
22B-1721	B	55	5.393	2.607	.761	.136	1.963	.019	3.001	.000	5.880	.000	.000	.068	1.745	1.814	.414	3.586
22B-1721	B	59	5.337	2.663	.589	.137	2.397	.015	2.938	.000	6.077	.000	.000	.055	1.591	1.646	.322	3.678
22B-1721	A	60	5.422	2.578	.790	.139	1.962	.015	2.949	.000	5.855	.000	.009	.097	1.684	1.790	.423	3.577
22B-1721	A	63	5.411	2.589	.770	.128	1.927	.017	3.043	.000	5.885	.000	.000	.093	1.699	1.793	.397	3.603
ave(4)			5.405	2.595	.769	.132	1.959	.018	2.995	.000	5.873	.000	.004	.091	1.716	1.811	.424	3.576
stdev			.012	.012	.013	.005	.020	.002	.033	.000	.011	.000	.004	.014	.025	.023	.024	.024
22B-1723	B	63	5.415	2.585	.656	.149	1.766	.022	3.385	.000	5.978	.000	.006	.059	1.605	1.670	.635	3.365
22B-1723	C	66	5.441	2.559	.666	.129	1.756	.021	3.368	.000	5.940	.000	.000	.094	1.662	1.755	.759	3.241
22B-1723	C	69	5.317	2.683	.596	.152	1.769	.016	3.532	.000	6.066	.000	.008	.054	1.582	1.644	.681	3.319
22B-1723	D	70	5.442	2.558	.691	.134	1.750	.021	3.353	.000	5.948	.000	.006	.088	1.604	1.698	.678	3.322
22B-1723	D	71	5.502	2.498	.681	.133	1.703	.027	3.341	.000	5.884	.000	.006	.101	1.669	1.777	.724	3.276
ave(5)			5.423	2.577	.658	.139	1.749	.021	3.396	.000	5.963	.000	.005	.079	1.624	1.709	.695	3.305
stdev			.060	.060	.033	.009	.024	.003	.070	.000	.060	.000	.003	.019	.035	.050	.043	.043
22B-1843	B	56	5.380	2.620	.629	.146	1.471	.050	3.664	.000	5.959	.000	.006	.029	1.739	1.774	.205	3.795
22B-1843	B	57	5.480	2.520	.689	.129	1.474	.056	3.563	.000	5.911	.000	.000	.025	1.726	1.751	.234	3.766
22B-1843	A	61	5.485	2.515	.658	.182	1.391	.060	3.584	.000	5.874	.000	.011	.037	1.687	1.735	.202	3.798
22B-1843	A	62	5.505	2.495	.673	.193	1.359	.055	3.541	.000	5.821	.000	.012	.028	1.743	1.783	.224	3.776
22B-1843	A	63	5.513	2.487	.725	.126	1.360	.055	3.605	.000	5.872	.000	.006	.022	1.732	1.761	.000	4.000
ave(5)			5.472	2.528	.675	.155	1.411	.055	3.591	.000	5.888	.000	.007	.028	1.725	1.761	.173	3.827
stdev			.048	.048	.032	.027	.051	.003	.042	.000	.046	.000	.004	.005	.020	.017	.087	.087
24-1131	C	79	5.667	2.333	.484	.100	1.534	.015	3.908	.026	6.066	.018	.022	.050	1.388	1.477	.611	3.389
24-1131	C	80	5.595	2.405	.519	.113	1.477	.000	3.919	.000	6.029	.014	.000	.056	1.520	1.589	.782	3.218
24-1131	C	81	5.598	2.402	.506	.092	1.462	.013	3.979	.000	6.053	.017	.000	.047	1.524	1.589	.816	3.184
24-1131	D	82	5.556	2.444	.465	.132	1.537	.000	3.928	.000	6.061	.018	.000	.048	1.509	1.575	.682	3.318
24-1131	D	83	5.595	2.405	.557	.072	1.451	.011	3.929	.000	6.021	.018	.000	.050	1.575	1.643	.731	3.269
24-1131	D	84	5.601	2.399	.524	.076	1.544	.000	3.934	.000	6.078	.015	.008	.062	1.461	1.545	.695	3.305
24-1131	D	85	5.590	2.410	.515	.099	1.516	.000	3.888	.000	6.018	.016	.012	.045	1.559	1.632	.702	3.298
ave(7)			5.600	2.400	.510	.098	1.503	.006	3.927	.004	6.047	.016	.006	.051	1.505	1.579	.717	3.283
stdev			.031	.031	.027	.019	.036	.007	.026	.009	.022	.002	.008	.005	.059	.052	.063	.063
24-1191	F	23	5.616	2.384	.576	.104	1.791	.035	3.488	.000	5.995	.000	.000	.067	1.544	1.611	.428	3.572
24-1191	F	24	5.521	2.479	.565	.110	1.833	.046	3.463	.000	6.016	.000	.000	.073	1.588	1.661	.395	3.605
zone 6, ave(2)			5.569	2.431	.570	.107	1.812	.040	3.475	.000	6.005	.000	.000	.070	1.566	1.636	.412	3.588
24-1191	E	20	5.542	2.458	.507	.086	1.756	.042	3.659	.000	6.052	.000	.000	.085	1.589	1.674	.414	3.586
24-1191	E	21	5.524	2.476	.481	.100	1.805	.049	3.649	.000	6.084	.000	.000	.068	1.559	1.627	.296	3.704
24-1191	E	22	5.557	2.443	.457	.111	1.775	.039	3.668	.000	6.051	.000	.000	.068	1.592	1.660	.515	3.485
24-1191	G	26	5.587	2.413	.448	.130	1.648	.048	3.770	.000	6.043	.000	.000	.070	1.550	1.620	.000	4.000
zone 5, ave(4)			5.553	2.447	.473	.107	1.746	.045	3.687	.000	6.058	.000	.000	.073	1.573	1.645	.306	3.694
stdev			.023	.023	.023	.016	.059	.004	.048	.000	.016	.000	.000	.007	.019	.022	.193	.193
34-1028.5	A	36	5.469	2.531	.639	.172	1.605	.055	3.351	.000	5.822	.000	.008	.020	1.868	1.896	.000	4.000
34-1028.5	A	39	5.479	2.521	.633	.124	1.895	.044	3.227	.000	5.924	.000	.014	.029	1.734	1.778	.000	4.000
34-1028.5	A	41	5.452	2.548	.717	.121	1.597	.050	3.445	.000	5.929	.000	.014	.026	1.677	1.717	.000	4.000
34-1028.5	A	42	5.486	2.514	.774	.102	1.505	.054	3.406	.000	5.842	.000	.019	.034	1.780	1.833	.000	4.000
34-1028.5	A	43	5.474	2.526	.730	.117	1.578	.050	3.407	.000	5.882	.000	.000	.020	1.778	1.798	.000	4.000
ave(5)			5.472	2.528	.699	.127	1.636	.051	3.367	.000	5.880	.000	.011	.026	1.768	1.804	.000	4.000
stdev			.012	.012	.054	.023	.134	.004	.076	.000	.043	.000	.007	.006	.063	.059	.000	.000
34-1500	D	35	5.601	2.399	.675	.027	.287	.018	4.906	.000	5.913	.000	.073	.081	1.618	1.771	1.650	2.350
34-1500	G	41	5.741	2.259	.518	.033	.159	.009	5.232	.000	5.952	.008	.000	.093	1.662	1.764	1.562	2.438
34-1500	G	43	5.756	2.244	.579	.037	.133	.000	5.201	.000	5.950	.008	.000	.091	1.584	1.683	1.486	2.514
34-1500	G	44	5.784	2.216	.550	.037	.155	.009	5.231	.000	5.982	.009	.000	.089	1.522	1.620	1.492	2.508
34-1500	H	70	5.782	2.218	.628	.033	.149	.011	5.176	.000	5.998	.009	.000	.080	1.429	1.518	1.634	2.366
34-1500	H	46	5.768	2.232	.590	.034	.158	.000	5.193	.000	5.975	.009	.006	.083	1.510	1.608	1.549	2.451
ave(6)			5.766	2.234	.573	.035	.151	.006	5.207	.000	5.971	.009	.001	.087	1.541	1.639	1.545	2.455
stdev			.016	.016	.037	.002	.010	.005	.022	.000	.018	.001	.002	.005	.078	.082	.054	.054

Table B.3. b. Biotite Mineral Chemistry. (continued)

			Structural formula normalized to 44 anionic charges														F+OH=4	
Sample	area	spot	Si	Al_{iv}	Al_{vi}	Ti	Fe	Mn	Mg	Zn	site	Ba	Ca	Na	K	site	F	OH
34B-759.5	A'	66	5.527	2.473	.517	.130	1.504	.023	3.691	.000	5.866	.000	.000	.017	1.948	1.965	.000	4.000
34B-759.5	A'	67	5.580	2.420	.536	.133	1.494	.022	3.691	.000	5.876	.000	.000	.000	1.867	1.867	.000	4.000
34B-759.5	A'	68	5.540	2.460	.524	.130	1.460	.023	3.725	.000	5.861	.000	.009	.000	1.935	1.945	.000	4.000
34B-759.5	B	69	5.524	2.476	.613	.033	1.333	.025	3.962	.000	5.965	.000	.016	.025	1.810	1.851	.000	4.000
34B-759.5	B	70	5.561	2.439	.676	.030	1.263	.018	3.917	.000	5.905	.000	.000	.028	1.865	1.892	.000	4.000
34B-759.5	B	71	5.607	2.393	.634	.029	1.275	.021	3.984	.000	5.942	.007	.000	.000	1.802	1.809	.234	3.766
ave(6)			5.556	2.444	.583	.081	1.388	.022	3.828	.000	5.903	.001	.004	.012	1.871	1.888	.039	3.961
stdev			.030	.030	.061	.050	.101	.002	.128	.000	.039	.003	.006	.012	.056	.054	.087	.087
34C-1453	G	18	5.502	2.498	.424	.101	2.067	.000	3.558	.000	6.150	.000	.000	.068	1.503	1.571	1.596	2.404
34C-1377	A	56	5.316	2.684	2.562	.025	.801	.030	2.089	.000	5.508	.000	.000	.250	.807	1.056	.000	4.000
34C-1377	A	58	5.607	2.393	.676	.077	1.068	.032	4.140	.000	5.994	.000	.000	.112	1.463	1.575	.915	3.085
34C-1377	A	64	5.613	2.387	.676	.075	1.064	.037	4.160	.000	6.012	.000	.000	.112	1.424	1.536	1.090	2.910
34C-1377	A	65	5.599	2.401	.683	.077	1.059	.032	4.111	.000	5.962	.000	.000	.117	1.522	1.639	.925	3.075
34C-1377	B	69	5.606	2.394	.670	.074	1.064	.031	4.161	.000	6.000	.000	.000	.106	1.469	1.575	.952	3.048
ave(5)			5.606	2.394	.676	.076	1.064	.033	4.143	.000	5.992	.000	.000	.112	1.469	1.581	.971	3.029
stdev			.005	.005	.005	.001	.003	.002	.020	.000	.018	.000	.000	.004	.035	.037	.070	.070
34C-1747.5	C	41	5.450	2.550	.653	.128	1.689	.012	3.465	.000	5.947	.000	.000	.105	1.642	1.748	.868	3.132
34C-1747.5	C	43	5.429	2.571	.705	.120	1.647	.016	3.439	.000	5.927	.000	.000	.093	1.680	1.773	.768	3.232
34C-1747.5	D	44	5.483	2.517	.670	.131	1.681	.011	3.396	.000	5.889	.000	.000	.133	1.675	1.808	.699	3.301
34C-1747.5	D	45	5.494	2.506	.710	.125	1.665	.012	3.391	.000	5.903	.000	.000	.128	1.612	1.740	.703	3.297
34C-1747.5	A	49	5.414	2.586	.635	.139	1.692	.012	3.469	.000	5.946	.000	.000	.117	1.664	1.781	.797	3.203
34C-1747.5	A	50	5.446	2.554	.650	.136	1.729	.016	3.359	.000	5.889	.000	.000	.101	1.752	1.853	.705	3.295
ave(6)			5.453	2.547	.670	.130	1.684	.013	3.420	.000	5.917	.000	.000	.113	1.671	1.784	.757	3.243
stdev			.028	.028	.028	.006	.025	.002	.041	.000	.025	.000	.000	.014	.043	.038	.062	.062

Table B.3. c. Chlorite Mineral Chemistry.

			weight percent oxide or element (Cr_2O_3 and BaO not detected)													
Sample	area	spot	SiO_2	TiO_2	Al_2O_3	FeO	MnO	MgO	CaO	Na_2O	K_2O	ZnO	F	Total	H_2O	Total
22-413	D	50	24.96	0.06	22.94	25.35	0.00	16.68	0.04	0.00	0.00	0.00	0.00	90.03	11.71	101.74
22-413	D	51	24.59	0.08	22.93	24.92	0.08	16.42	0.00	0.00	0.00	0.00	0.00	89.02	11.58	100.60
22-413	D	52	24.91	0.05	22.95	25.26	0.10	16.70	0.00	0.00	0.00	0.00	0.00	89.97	11.70	101.67
22-413	D	53	25.14	0.07	22.83	25.34	0.08	16.72	0.00	0.00	0.00	0.00	0.00	90.18	11.73	101.91
ave(4)			24.90	0.07	22.91	25.22	0.07	16.63	0.01	0.00	0.00	0.00	0.00	89.80	11.68	101.48
stdev			0.20	0.01	0.05	0.18	0.04	0.12	0.02	0.00	0.00	0.00	0.00	0.46	0.06	0.51
22-901	A	55	25.18	0.07	24.54	20.37	0.29	19.50	0.00	0.00	0.00	0.00	0.00	89.95	12.01	101.96
22-901	A	56	25.07	0.00	24.58	20.71	0.33	19.49	0.00	0.00	0.04	0.00	0.00	90.22	12.02	102.24
22-901	A	58	25.14	0.06	24.40	20.46	0.34	19.43	0.00	0.00	0.00	0.00	0.00	89.83	11.98	101.81
22-901	B	61	26.19	0.00	23.96	20.55	0.30	19.01	0.00	0.00	0.00	0.00	0.00	90.01	12.04	102.05
22-901	B	63	25.07	0.06	24.26	20.86	0.27	19.05	0.00	0.00	0.00	0.00	0.00	89.57	11.92	101.49
22-901	B	65	25.15	0.06	24.87	20.59	0.29	19.42	0.00	0.00	0.00	0.00	0.00	90.38	12.06	102.44
ave(6)			25.30	0.04	24.44	20.59	0.30	19.32	0.00	0.00	0.01	0.00	0.00	89.99	12.00	102.00
stdev			0.40	0.03	0.28	0.16	0.02	0.21	0.00	0.00	0.01	0.00	0.00	0.26	0.04	0.30
22-957	C	66	25.16	0.00	23.48	22.86	0.33	17.60	0.00	0.00	0.00	0.00	0.44	89.87	11.57	101.25
22-957	C	69	24.72	0.06	23.75	22.73	0.37	17.66	0.00	0.00	0.00	0.00	0.00	89.29	11.75	101.04
22-957	B	70	24.87	0.08	23.55	22.37	0.34	17.47	0.00	0.00	0.00	0.00	0.00	88.68	11.70	100.38
22-957	B	74	24.94	0.07	23.71	23.07	0.36	17.19	0.00	0.00	0.00	0.00	0.00	89.34	11.75	101.09
22-957	B	77	24.36	0.06	23.59	22.09	0.33	17.18	0.11	0.00	0.05	0.00	0.00	87.77	11.57	99.34
ave(5)			24.81	0.05	23.62	22.62	0.35	17.42	0.02	0.00	0.01	0.00	0.09	88.99	11.67	100.62
stdev			0.27	0.03	0.10	0.35	0.02	0.20	0.04	0.00	0.02	0.00	0.18	0.72	0.08	0.71
22-996.5	D	8	24.40	0.08	24.14	23.36	0.37	17.33	0.00	0.00	0.00	0.00	0.00	89.70	11.76	101.46
22-996.5	D	9	24.90	0.08	24.25	23.32	0.29	17.48	0.00	0.00	0.00	0.00	0.41	90.73	11.68	102.24
22-996.5	A	10	24.98	0.06	23.68	23.59	0.31	17.58	0.00	0.00	0.00	0.00	0.00	90.20	11.83	102.03
22-996.5	B	12	24.90	0.00	24.54	23.61	0.28	17.56	0.00	0.00	0.00	0.00	0.00	90.89	11.94	102.83
22-996.5	B	13	24.81	0.07	24.07	23.59	0.30	17.38	0.00	0.00	0.00	0.00	0.00	90.22	11.84	102.06
22-996.5	B	14	24.76	0.07	24.40	23.67	0.30	17.37	0.00	0.00	0.00	0.00	0.00	90.57	11.88	102.45
ave(6)			24.79	0.06	24.18	23.53	0.31	17.45	0.00	0.00	0.00	0.00	0.07	90.39	11.82	102.18
stdev			0.19	0.03	0.27	0.13	0.03	0.10	0.00	0.00	0.00	0.00	0.15	0.40	0.08	0.42
22A-1625	C	27	25.81	0.06	24.89	14.68	0.43	22.64	0.00	0.00	0.00	0.25	0.00	88.76	12.19	100.95
22A-1625	A	32	27.19	0.08	25.30	14.56	0.44	22.05	0.00	0.07	0.45	0.17	0.00	90.31	12.43	102.74
22A-1625	A	36	26.20	0.06	23.94	15.02	0.42	23.06	0.00	0.00	0.17	0.00	0.00	88.87	12.18	101.05
22A-1625	A	38	25.98	0.07	23.93	14.64	0.44	23.13	0.00	0.00	0.00	0.00	0.00	88.19	12.12	100.31
ave(4)			26.30	0.07	24.52	14.73	0.43	22.72	0.00	0.02	0.16	0.11	0.00	89.03	12.23	101.26
stdev			0.53	0.01	0.60	0.18	0.01	0.43	0.00	0.03	0.18	0.11	0.00	0.78	0.12	0.90
22A-1752	D	15	26.08	0.00	24.18	14.90	0.38	23.37	0.00	0.00	0.00	0.00	0.00	88.91	12.21	101.12
22A-1752	F	16	26.25	0.07	24.16	14.75	0.34	23.49	0.00	0.00	0.00	0.00	0.43	89.49	12.04	101.35
22A-1752	F	17	26.50	0.07	24.46	15.21	0.40	23.11	0.00	0.00	0.00	0.00	0.67	90.42	12.01	102.14
22A-1752	B	18	25.95	0.06	24.91	15.02	0.40	23.00	0.00	0.00	0.00	0.00	0.50	89.84	12.03	101.66
22A-1752	A	21	26.48	0.07	24.30	15.33	0.38	23.52	0.00	0.00	0.10	0.00	0.57	90.75	12.09	102.60
22A-1752	A	22	26.48	0.00	24.05	16.18	0.39	22.70	0.00	0.00	0.00	0.00	0.00	89.80	12.27	102.07
ave(6)			26.29	0.05	24.34	15.23	0.38	23.20	0.00	0.00	0.02	0.00	0.36	89.87	12.11	101.82
stdev			0.22	0.03	0.28	0.46	0.02	0.29	0.00	0.00	0.04	0.00	0.27	0.60	0.10	0.50
22B-1721	A	62	25.33	0.06	24.02	20.06	0.29	19.78	0.00	0.00	0.00	0.00	0.00	89.54	11.97	101.51
22B-1721	A	64	25.23	0.07	24.21	20.41	0.30	19.59	0.00	0.00	0.00	0.00	0.00	89.81	11.98	101.79
22B-1721	A	68	24.95	0.08	23.87	20.59	0.29	19.23	0.00	0.00	0.00	0.00	0.00	89.01	11.85	100.86
22B-1721	A	70	25.11	0.08	24.10	20.35	0.25	19.64	0.00	0.00	0.00	0.00	0.00	89.53	11.95	101.48
22B-1721	A	71	24.88	0.00	23.82	20.84	0.33	19.29	0.00	0.00	0.00	0.00	0.00	89.16	11.85	101.01
ave(5)			25.10	0.06	24.00	20.45	0.29	19.51	0.00	0.00	0.00	0.00	0.00	89.41	11.92	101.33
stdev			0.17	0.03	0.14	0.26	0.03	0.21	0.00	0.00	0.00	0.00	0.00	0.29	0.06	0.34
22B-1723	B	61	25.42	0.09	23.87	18.06	0.35	21.32	0.00	0.05	0.00	0.23	0.00	89.39	12.04	101.43
22B-1723	B	62	26.56	0.00	23.41	18.63	0.35	20.06	0.00	0.00	0.00	0.00	0.00	89.01	12.02	101.03
ave(2)			25.99	0.05	23.64	18.35	0.35	20.69	0.00	0.03	0.00	0.12	0.00	89.20	12.03	101.23
													*Cl			
24-1191		55	26.71	0.00	14.73	41.08	0.00	2.92	0.29	0.00	0.00	0.00	*0.60	86.33	10.00	96.19
24-1191		25	27.92	0.82	15.62	30.65	0.41	14.63	0.00	0.00	0.00	0.00	*0.88	90.93	10.93	101.49
24-1191	A	73	26.44	0.00	22.29	18.51	0.53	21.72	0.00	0.00	0.00	0.00	0.00	89.49	12.04	101.53
24-1191	A	74	25.97	0.00	22.62	18.42	0.60	21.39	0.00	0.00	0.00	0.00	0.00	89.00	11.97	100.97
24-1191	A	75	26.48	0.06	22.39	18.03	0.57	21.67	0.00	0.00	0.14	0.18	0.00	89.52	12.05	101.57
zone 5, ave(3)			26.30	0.02	22.43	18.32	0.57	21.59	0.00	0.00	0.05	0.06	0.00	89.34	12.02	101.36
stdev			0.23	0.03	0.14	0.21	0.03	0.15	0.00	0.00	0.07	0.08	0.00	0.24	0.04	0.28

Table B.3. c. Chlorite Mineral Chemistry. (continued)

weight percent oxide or element (Cr_2O_3 and BaO not detected)																
Sample	area	spot	SiO_2	TiO_2	Al_2O_3	FeO	MnO	MgO	CaO	Na_2O	K_2O	ZnO	F	Total	H_2O	Total
24-1191	B	76	25.93	0.06	22.25	19.23	0.55	20.46	0.00	0.00	0.07	0.17	0.00	88.72	11.86	100.58
24-1191	B	77	25.30	0.00	23.25	19.40	0.62	20.43	0.00	0.00	0.00	0.00	0.00	89.00	11.90	100.90
24-1191	B	78	26.85	0.00	21.97	18.95	0.56	20.85	0.00	0.00	0.09	0.00	0.00	89.27	11.99	101.26
zone 6, ave(3)			26.03	0.02	22.49	19.19	0.58	20.58	0.00	0.00	0.05	0.06	0.00	89.00	11.92	100.92
stdev			0.64	0.03	0.55	0.19	0.03	0.19	0.00	0.00	0.04	0.08	0.00	0.22	0.05	0.28
34-799	A	46	25.31	0.05	24.27	18.19	0.10	20.80	0.00	0.00	0.00	0.00	0.42	89.14	11.79	100.75
34-799	A	47	24.88	0.00	24.04	17.77	0.17	21.21	0.00	0.00	0.00	0.22	0.00	88.29	11.91	100.20
34-799	A	50	25.08	0.05	24.52	15.44	0.11	22.81	0.00	0.00	0.00	0.26	0.00	88.27	12.06	100.33
34-799	A	51	24.91	0.06	24.52	16.71	0.17	22.26	0.00	0.00	0.00	0.00	0.45	89.08	11.83	100.72
ave(4)			25.04	0.04	24.34	17.03	0.14	21.77	0.00	0.00	0.00	0.12	0.22	88.70	11.90	100.50
stdev			0.17	0.02	0.20	1.06	0.03	0.80	0.00	0.00	0.00	0.12	0.22	0.42	0.10	0.24
34-1500	C	34	28.54	0.07	22.13	4.13	0.25	30.50	0.00	0.00	0.31	0.00	1.19	87.12	11.91	98.53
34-1500	E	36	30.88	0.08	21.49	5.62	0.28	30.55	0.00	0.00	1.00	0.00	1.55	91.45	12.20	103.00
34-1500	H	45	29.99	0.07	21.97	4.83	0.30	30.70	0.00	0.00	0.56	0.00	1.43	89.85	12.11	101.36
ave(2)			30.44	0.08	21.73	5.23	0.29	30.63	0.00	0.00	0.78	0.00	1.49	90.65	12.16	102.18
stdev			0.44	0.00	0.24	0.39	0.01	0.08	0.00	0.00	0.22	0.00	0.06	0.80	0.04	0.82
34A-1484	A	44	24.60	0.06	22.67	26.91	0.08	15.31	0.04	0.00	0.00	0.00	0.00	89.67	11.55	101.22
34A-1484	A	45	24.66	0.07	22.87	26.54	0.13	15.62	0.04	0.00	0.00	0.00	0.00	89.93	11.61	101.54
34A-1484	A	46	24.72	0.06	23.02	27.33	0.11	15.81	0.00	0.00	0.00	0.00	0.00	91.05	11.71	102.76
34A-1484	B	47	24.58	0.00	22.56	27.05	0.08	15.56	0.00	0.00	0.00	0.00	0.00	89.83	11.56	101.39
34A-1484	B	48	24.83	0.09	22.70	27.12	0.07	15.55	0.00	0.00	0.00	0.00	0.00	90.36	11.64	102.00
34A-1484	B	49	24.70	0.00	22.83	26.13	0.07	16.04	0.00	0.00	0.00	0.00	0.00	89.77	11.61	101.38
ave(6)			24.68	0.05	22.78	26.85	0.09	15.65	0.01	0.00	0.00	0.00	0.00	90.10	11.61	101.72
stdev			0.08	0.03	0.15	0.40	0.02	0.23	0.02	0.00	0.00	0.00	0.00	0.48	0.05	0.53
34C-1377	B	1	26.45	0.06	24.71	12.90	0.50	24.47	0.00	0.00	0.00	0.00	0.52	89.61	12.12	101.51
34C-1377	B	2	26.29	0.06	24.66	12.88	0.51	24.33	0.00	0.00	0.00	0.00	0.00	88.73	12.31	101.04
34C-1377	B	3	26.39	0.07	24.27	12.96	0.50	24.18	0.00	0.00	0.13	0.00	0.00	88.50	12.27	100.77
34C-1377	B	4	27.17	0.08	24.49	12.94	0.49	25.15	0.00	0.00	0.00	0.00	0.48	90.80	12.32	102.92
34C-1377	D	7	26.63	0.00	24.18	13.36	0.50	24.40	0.00	0.00	0.00	0.00	0.51	89.58	12.09	101.46
ave(5)			26.59	0.05	24.46	13.01	0.50	24.51	0.00	0.00	0.03	0.00	0.30	89.44	12.22	101.54
stdev			0.31	0.03	0.21	0.18	0.01	0.34	0.00	0.00	0.05	0.00	0.25	0.81	0.10	0.74
34C-1453	A	8	24.87	0.00	24.43	20.87	0.16	19.23	0.00	0.00	0.00	0.00	0.77	90.33	11.56	101.56
34C-1453	G	17	25.17	0.00	24.53	21.66	0.13	19.17	0.00	0.00	0.00	0.00	0.00	90.66	12.04	102.70
34C-1453	J	19	25.31	0.00	24.02	21.19	0.13	19.07	0.00	0.00	0.00	0.00	0.61	90.33	11.65	101.72
ave(3)			25.12	0.00	24.33	21.24	0.14	19.16	0.00	0.00	0.00	0.00	0.46	90.44	11.75	101.99
stdev			0.18	0.00	0.22	0.32	0.01	0.07	0.00	0.00	0.00	0.00	0.33	0.16	0.21	0.50
34C-1747.5	C	47	24.94	0.07	24.00	19.70	0.17	19.60	0.00	0.00	0.00	0.00	0.00	88.48	11.84	100.32

Table B.3. c. Chlorite Mineral Chemistry. (continued)

			Structural formula normalized to 56 anionic charges												F+OH=16	
Sample	area	spot	Si	Al_{iv}	Al_{vi}	Ti	Fe	Mn	Mg	Zn	Ca	Na	K	site	F	OH
22-413	D	50	5.113	2.887	2.654	.009	4.343	.000	5.093	.000	.009	.000	.000	12.107	.000	16.000
22-413	D	51	5.091	2.909	2.689	.012	4.315	.014	5.067	.000	.000	.000	.000	12.097	.000	16.000
22-413	D	52	5.107	2.893	2.654	.008	4.331	.017	5.102	.000	.000	.000	.000	12.112	.000	16.000
22-413	D	53	5.140	2.860	2.644	.011	4.333	.014	5.095	.000	.000	.000	.000	12.097	.000	16.000
ave(4)			5.113	2.887	2.660	.010	4.331	.011	5.089	.000	.002	.000	.000	12.103	.000	16.000
stdev			.018	.018	.017	.002	.010	.007	.013	.000	.004	.000	.000	.006	.000	.000
22-901	A	55	5.029	2.971	2.806	.011	3.402	.049	5.804	.000	.000	.000	.000	12.072	.000	16.000
22-901	A	56	5.004	2.996	2.788	.000	3.457	.056	5.798	.000	.000	.000	.010	12.109	.000	16.000
22-901	A	58	5.032	2.968	2.791	.009	3.425	.058	5.797	.000	.000	.000	.000	12.079	.000	16.000
22-901	B	61	5.219	2.781	2.847	.000	3.425	.051	5.645	.000	.000	.000	.000	11.967	.000	16.000
22-901	B	63	5.043	2.957	2.796	.009	3.509	.046	5.711	.000	.000	.000	.000	12.071	.000	16.000
22-901	B	65	5.002	2.998	2.834	.009	3.425	.049	5.756	.000	.000	.000	.000	12.073	.000	16.000
ave(6)			5.055	2.945	2.810	.006	3.441	.051	5.752	.000	.000	.000	.002	12.062	.000	16.000
stdev			.075	.075	.022	.004	.035	.004	.058	.000	.000	.000	.004	.044	.000	.000
22-957	C	66	5.125	2.875	2.763	.000	3.894	.057	5.343	.000	.000	.000	.000	12.056	.283	15.717
22-957	C	69	5.046	2.954	2.761	.009	3.880	.064	5.372	.000	.000	.000	.000	12.087	.000	16.000
22-957	B	70	5.100	2.900	2.794	.012	3.837	.059	5.339	.000	.000	.000	.000	12.041	.000	16.000
22-957	B	74	5.092	2.908	2.800	.011	3.940	.062	5.231	.000	.000	.000	.000	12.043	.000	16.000
22-957	B	77	5.051	2.949	2.818	.009	3.831	.058	5.309	.000	.024	.000	.013	12.063	.000	16.000
ave(5)			5.083	2.917	2.787	.008	3.876	.060	5.319	.000	.005	.000	.003	12.058	.057	15.943
stdev			.030	.030	.022	.004	.040	.003	.048	.000	.010	.000	.005	.017	.113	.113
22-996.5	D	8	4.976	3.024	2.779	.012	3.987	.064	5.267	.000	.000	.000	.000	12.110	.000	16.000
22-996.5	D	9	5.030	2.970	2.806	.012	3.940	.050	5.263	.000	.000	.000	.000	12.070	.262	15.738
22-996.5	A	10	5.064	2.936	2.724	.009	4.000	.053	5.311	.000	.000	.000	.000	12.097	.000	16.000
22-996.5	B	12	5.003	2.997	2.816	.000	3.968	.048	5.258	.000	.000	.000	.000	12.090	.000	16.000
22-996.5	B	13	5.028	2.972	2.778	.011	3.998	.051	5.249	.000	.000	.000	.000	12.087	.000	16.000
22-996.5	B	14	4.998	3.002	2.805	.011	3.996	.051	5.226	.000	.000	.000	.000	12.088	.000	16.000
ave(6)			5.016	2.984	2.785	.009	3.981	.053	5.262	.000	.000	.000	.000	12.090	.044	15.956
stdev			.028	.028	.031	.004	.021	.005	.026	.000	.000	.000	.000	.012	.098	.098
22A-1625	C	27	5.079	2.921	2.853	.009	2.416	.072	6.639	.036	.000	.000	.000	12.025	.000	16.000
22A-1625	A	32	5.246	2.754	3.000	.012	2.349	.072	6.340	.024	.000	.026	.111	11.934	.000	16.000
22A-1625	A	36	5.158	2.842	2.715	.009	2.473	.070	6.766	.000	.000	.000	.043	12.076	.000	16.000
22A-1625	A	38	5.142	2.858	2.726	.010	2.423	.074	6.823	.000	.000	.000	.000	12.056	.000	16.000
ave(4)			5.156	2.844	2.823	.010	2.415	.072	6.642	.015	.000	.007	.038	12.023	.000	16.000
stdev			.060	.060	.116	.001	.044	.001	.187	.016	.000	.011	.045	.054	.000	.000
22A-1752	D	15	5.123	2.877	2.723	.000	2.448	.063	6.842	.000	.000	.000	.000	12.077	.000	16.000
22A-1752	F	16	5.141	2.859	2.720	.010	2.416	.056	6.857	.000	.000	.000	.000	12.059	.266	15.734
22A-1752	F	17	5.158	2.842	2.770	.010	2.476	.066	6.703	.000	.000	.000	.000	12.026	.412	15.588
22A-1752	B	18	5.073	2.927	2.815	.009	2.456	.066	6.701	.000	.000	.000	.000	12.047	.309	15.691
22A-1752	A	21	5.138	2.862	2.697	.010	2.488	.062	6.802	.000	.000	.000	.025	12.084	.350	15.650
22A-1752	A	22	5.178	2.822	2.723	.000	2.646	.065	6.616	.000	.000	.000	.000	12.049	.000	16.000
ave(6)			5.135	2.865	2.741	.007	2.488	.063	6.753	.000	.000	.000	.004	12.057	.223	15.777
stdev			.033	.033	.039	.005	.074	.003	.087	.000	.000	.000	.009	.019	.164	.164
22B-1721	A	62	5.076	2.924	2.750	.009	3.362	.049	5.907	.000	.000	.000	.000	12.078	.000	16.000
22B-1721	A	64	5.050	2.950	2.762	.011	3.416	.051	5.843	.000	.000	.000	.000	12.083	.000	16.000
22B-1721	A	68	5.049	2.951	2.744	.012	3.485	.050	5.800	.000	.000	.000	.000	12.091	.000	16.000
22B-1721	A	70	5.041	2.959	2.746	.012	3.417	.043	5.877	.000	.000	.000	.000	12.094	.000	16.000
22B-1721	A	71	5.036	2.964	2.720	.000	3.528	.057	5.819	.000	.000	.000	.000	12.122	.000	16.000
ave(5)			5.050	2.950	2.745	.009	3.442	.050	5.849	.000	.000	.000	.000	12.094	.000	16.000
stdev			.014	.014	.014	.005	.058	.004	.039	.000	.000	.000	.000	.015	.000	.000
22B-1723	B	61	5.063	2.937	2.668	.013	3.008	.059	6.329	.034	.000	.019	.000	12.131	.000	16.000
22B-1723	B	62	5.301	2.699	2.809	.000	3.110	.059	5.967	.000	.000	.000	.000	11.945	.000	16.000
ave(2)			5.182	2.818	2.739	.007	3.059	.059	6.148	.017	.000	.010	.000	12.038	.000	16.000
															*Cl	
24-1191		55	6.312	1.688	2.416	.000	8.119	.000	1.028	.000	.073	.000	.000	11.636	*.240	15.760
24-1191		25	5.901	2.099	1.793	.130	5.418	.073	4.608	.000	.000	.000	.000	12.023	*.588	15.412
24-1191	A	73	5.266	2.734	2.499	.000	3.083	.089	6.447	.000	.000	.000	.000	12.118	.000	16.000
24-1191	A	74	5.204	2.796	2.548	.000	3.087	.102	6.388	.000	.000	.000	.000	12.124	.000	16.000
24-1191	A	75	5.269	2.731	2.521	.009	3.000	.096	6.426	.026	.000	.000	.036	12.114	.000	16.000
zone 5, ave(3)			5.246	2.754	2.522	.003	3.057	.096	6.420	.009	.000	.000	.012	12.119	.000	16.000
stdev			.030	.030	.020	.004	.040	.005	.024	.012	.000	.000	.017	.004	.000	.000

Table B.3. c. Chlorite Mineral Chemistry. (continued)

			Structural formula normalized to 56 anionic charges												F+OH=16	
Sample	area	spot	Si	Al_{iv}	Al_{vi}	Ti	Fe	Mn	Mg	Zn	Ca	Na	K	site	F	OH
24-1191	B	76	5.242	2.758	2.545	.009	3.251	.094	6.164	.025	.000	.000	.018	12.107	.000	16.000
24-1191	B	77	5.100	2.900	2.625	.000	3.270	.106	6.137	.000	.000	.000	.000	12.138	.000	16.000
24-1191	B	78	5.370	2.630	2.550	.000	3.170	.095	6.214	.000	.000	.000	.023	12.052	.000	16.000
zone 6, ave(3)			5.237	2.763	2.573	.003	3.230	.098	6.172	.008	.000	.000	.014	12.099	.000	16.000
stdev			.110	.110	.037	.004	.044	.005	.032	.012	.000	.000	.010	.036	.000	.000
34-799	A	46	5.065	2.935	2.791	.008	3.045	.017	6.204	.000	.000	.000	.000	12.064	.266	15.734
34-799	A	47	5.010	2.990	2.717	.000	2.993	.029	6.365	.033	.000	.000	.000	12.136	.000	16.000
34-799	A	50	4.988	3.012	2.737	.007	2.568	.019	6.761	.038	.000	.000	.000	12.130	.000	16.000
34-799	A	51	4.962	3.038	2.720	.009	2.784	.029	6.608	.000	.000	.000	.000	12.150	.283	15.717
ave(4)			5.006	2.994	2.741	.006	2.847	.023	6.484	.018	.000	.000	.000	12.120	.137	15.863
stdev			.038	.038	.030	.004	.188	.006	.215	.018	.000	.000	.000	.033	.137	.137
34-1500	C	34	5.487	2.513	2.503	.010	.664	.041	8.739	.000	.000	.000	.076	12.033	.724	15.276
34-1500	E	36	5.727	2.273	2.425	.011	.872	.044	8.443	.000	.000	.000	.237	12.031	.909	15.091
34-1500	H	45	5.623	2.377	2.479	.010	.757	.048	8.578	.000	.000	.000	.134	12.006	.848	15.152
ave(2)			5.675	2.325	2.452	.011	.814	.046	8.511	.000	.000	.000	.185	12.019	.879	15.121
stdev			.052	.052	.027	.001	.057	.002	.068	.000	.000	.000	.051	.013	.031	.031
34A-1484	A	44	5.109	2.891	2.660	.009	4.674	.014	4.739	.000	.009	.000	.000	12.106	.000	16.000
34A-1484	A	45	5.096	2.904	2.668	.011	4.587	.023	4.811	.000	.009	.000	.000	12.107	.000	16.000
34A-1484	A	46	5.061	2.939	2.618	.009	4.680	.019	4.824	.000	.000	.000	.000	12.151	.000	16.000
34A-1484	B	47	5.101	2.899	2.620	.000	4.694	.014	4.812	.000	.000	.000	.000	12.140	.000	16.000
34A-1484	B	48	5.118	2.882	2.633	.014	4.675	.012	4.776	.000	.000	.000	.000	12.111	.000	16.000
34A-1484	B	49	5.101	2.899	2.659	.000	4.513	.012	4.936	.000	.000	.000	.000	12.120	.000	16.000
ave(6)			5.098	2.902	2.643	.007	4.637	.016	4.816	.000	.003	.000	.000	12.122	.000	16.000
stdev			.018	.018	.020	.005	.066	.004	.061	.000	.004	.000	.000	.017	.000	.000
34C-1377	B	1	5.130	2.870	2.780	.009	2.092	.082	7.073	.000	.000	.000	.000	12.036	.319	15.681
34C-1377	B	2	5.121	2.879	2.784	.009	2.098	.084	7.063	.000	.000	.000	.000	12.039	.000	16.000
34C-1377	B	3	5.161	2.839	2.756	.010	2.120	.083	7.047	.000	.000	.000	.032	12.048	.000	16.000
34C-1377	B	4	5.193	2.807	2.712	.012	2.069	.079	7.164	.000	.000	.000	.000	12.036	.290	15.710
34C-1377	D	7	5.179	2.821	2.722	.000	2.173	.082	7.072	.000	.000	.000	.000	12.049	.314	15.686
ave(5)			5.157	2.843	2.751	.008	2.110	.082	7.084	.000	.000	.000	.006	12.042	.185	15.815
stdev			.028	.028	.029	.004	.035	.002	.041	.000	.000	.000	.013	.006	.151	.151
34C-1453	A	8	5.003	2.997	2.797	.000	3.511	.027	5.765	.000	.000	.000	.000	12.100	.490	15.510
34C-1453	G	17	5.016	2.984	2.778	.000	3.610	.022	5.693	.000	.000	.000	.000	12.103	.000	16.000
34C-1453	J	19	5.086	2.914	2.776	.000	3.561	.022	5.711	.000	.000	.000	.000	12.069	.388	15.612
ave(3)			5.035	2.965	2.784	.000	3.561	.024	5.723	.000	.000	.000	.000	12.091	.293	15.707
stdev			.036	.036	.009	.000	.040	.002	.031	.000	.000	.000	.000	.015	.211	.211
34C-1747.5	C	47	5.051	2.949	2.781	.011	3.337	.029	5.916	.000	.000	.000	.000	12.073	.000	16.000

Table B.3. d. Staurolite Mineral Chemistry.

			weight percent oxide (Cr_2O_3, Na_2O, CaO not detected)										
Sample	area	spot	SiO_2	TiO_2	Al_2O_3	FeO	Fe_2O_3	MnO	MgO	ZnO	Total	H_2O	Total
22-901	A	1c	27.27	0.50	53.29	10.88	1.17	0.60	1.98	1.26	96.84	1.51	98.47
22-901	A	2r	27.43	0.51	53.62	10.23	1.18	0.66	1.89	1.16	96.56	1.76	98.43
22-901	A'	4c	27.06	0.47	54.18	10.14	1.18	0.71	1.90	1.11	96.64	1.88	98.63
22-901	A'	5r	27.25	0.42	53.67	10.19	1.18	0.62	1.82	1.07	96.10	1.88	98.10
22-901	A'	7c	27.10	0.41	53.40	10.82	1.17	0.63	2.04	1.23	96.68	1.56	98.36
22-901	A'	8r	27.25	0.53	53.47	10.46	1.17	0.59	1.95	1.13	96.44	1.67	98.23
22-901	B	10c	26.96	0.43	54.57	10.49	1.19	0.66	1.94	1.22	97.34	1.83	99.29
22-901	B	11r	27.59	0.46	52.89	9.97	1.17	0.57	1.93	1.10	95.56	1.76	97.44
core, ave(4)			27.10	0.45	53.86	10.58	1.18	0.65	1.97	1.21	96.88	1.70	98.69
stdev			0.11	0.03	0.53	0.29	0.01	0.04	0.05	0.06	0.28	0.16	0.36
rim, ave(4)			27.38	0.48	53.41	10.21	1.18	0.61	1.90	1.12	96.17	1.77	98.05
stdev			0.14	0.04	0.31	0.18	0.00	0.03	0.05	0.03	0.39	0.07	0.37
ave(8)			27.24	0.47	53.64	10.40	1.18	0.63	1.93	1.16	96.52	1.73	98.37
stdev			0.19	0.04	0.49	0.31	0.01	0.04	0.06	0.06	0.49	0.13	0.49
22-957	A	13c	26.80	0.49	53.08	10.66	1.16	0.67	1.88	1.80	96.43	1.47	98.02
22-957	A	14r	26.94	0.46	52.36	10.34	1.15	0.67	1.74	1.72	95.27	1.55	96.93
22-957	B	15c	26.67	0.53	52.70	10.60	1.16	0.69	1.84	1.72	95.79	1.46	97.36
22-957	B	16r	25.80	0.46	50.98	10.50	1.12	0.53	1.62	1.87	92.77	1.43	94.31
22-957	C	17c	26.67	0.45	52.09	10.92	1.15	0.68	1.86	1.72	95.42	1.33	96.86
22-957	C	18r	26.76	0.42	52.71	9.79	1.16	0.60	1.69	1.87	94.88	1.76	96.76
core, ave(3)			26.71	0.49	52.62	10.73	1.15	0.68	1.86	1.75	95.88	1.42	97.41
stdev			0.06	0.03	0.41	0.14	0.01	0.01	0.02	0.04	0.42	0.06	0.47
rim, ave(3)			26.50	0.45	52.02	10.21	1.14	0.60	1.68	1.82	94.31	1.58	96.00
stdev			0.50	0.02	0.75	0.31	0.02	0.06	0.05	0.07	1.10	0.14	1.20
ave(6)			26.61	0.47	52.32	10.47	1.15	0.64	1.77	1.78	95.09	1.50	96.71
stdev			0.37	0.03	0.67	0.35	0.01	0.06	0.10	0.07	1.14	0.13	1.15
22-996.5	A'	10c	27.12	0.52	54.08	12.74	1.18	0.65	1.88	0.14	98.19	1.43	99.74
22-996.5	A'	11r	27.54	0.18	53.85	12.62	1.18	0.62	1.98	0.00	97.86	1.56	99.53
22-996.5	A	12c	26.71	0.45	53.90	12.99	1.17	0.61	2.07	0.00	97.79	1.34	99.25
22-996.5	A	13r	27.00	0.47	53.45	12.73	1.17	0.57	2.07	0.00	97.34	1.34	98.80
22-996.5	A	14r	27.44	0.43	53.67	12.95	1.18	0.62	1.93	0.00	98.10	1.37	99.58
22-996.5	B	15c	27.28	0.40	53.30	13.01	1.17	0.58	2.13	0.00	97.76	1.24	99.12
ave6)			27.18	0.41	53.71	12.84	1.18	0.61	2.01	0.02	97.84	1.38	99.34
stdev			0.28	0.11	0.27	0.15	0.01	0.03	0.09	0.05	0.27	0.10	0.32
22A-1625	A	21c	26.48	0.39	54.22	6.79	1.18	0.84	2.29	5.12	97.19	1.69	98.99
22A-1625	A	22r	26.61	0.60	53.67	6.61	1.17	0.84	2.10	5.28	96.76	1.61	98.49
22A-1625	B	23	26.64	0.58	54.22	7.05	1.18	0.88	2.26	4.60	97.29	1.65	99.06
22A-1625	B	24	27.08	0.42	53.45	7.33	1.17	0.93	2.37	4.60	97.24	1.47	98.83
22A-1625	C	25	26.94	0.39	54.09	7.04	1.18	0.83	2.30	4.53	97.18	1.72	99.02
22A-1625	C	26	26.19	0.40	54.45	7.05	1.18	0.86	2.27	4.82	97.10	1.73	98.95
ave(6)			26.66	0.46	54.02	6.98	1.18	0.86	2.27	4.83	97.13	1.64	98.89
stdev			0.29	0.09	0.35	0.23	0.00	0.03	0.08	0.28	0.17	0.09	0.19
22A-1638	A	2r	27.90	0.36	53.81	5.26	1.19	0.53	2.19	6.70	97.82	2.02	99.95
22A-1638	A	3c	26.61	0.32	54.48	5.43	1.18	0.55	2.16	6.86	97.47	1.84	99.42
22A-1638	C	9	25.84	0.49	54.61	5.53	1.17	0.55	2.18	7.10	97.36	1.72	99.20
22A-1638	C	10	26.49	0.44	54.68	5.15	1.18	0.56	2.16	7.00	97.55	1.85	99.51
22A-1638	D	13	26.67	0.42	55.25	5.33	1.19	0.55	2.14	6.82	98.26	1.93	100.31
22A-1638	D	14	27.06	0.39	53.79	5.30	1.18	0.51	2.32	6.99	97.42	1.64	99.18
ave(6)			26.76	0.40	54.44	5.33	1.18	0.54	2.19	6.91	97.65	1.83	99.60
stdev			0.62	0.05	0.51	0.12	0.01	0.02	0.06	0.13	0.31	0.13	0.41
22A-1752	D	23c	26.79	0.43	53.56	6.78	1.17	0.72	2.01	4.04	95.38	1.97	97.47
22A-1752	D	24r	26.86	0.52	54.09	6.21	1.18	0.76	1.73	4.59	95.82	2.13	98.07
22A-1752	G	25c	27.00	0.40	52.93	7.11	1.16	0.71	2.11	3.75	95.06	1.83	97.01
22A-1752	G	26r	27.22	0.51	54.38	7.15	1.19	0.75	2.09	3.96	97.13	1.90	99.15
22A-1752	E	27c	27.47	0.42	53.68	7.35	1.18	0.71	2.23	3.65	96.57	1.81	98.50
22A-1752	E	28r	27.11	0.42	53.39	7.11	1.17	0.80	2.23	3.65	95.76	1.82	97.70
ave(6)			27.08	0.45	53.67	6.95	1.18	0.74	2.07	3.94	95.95	1.91	97.98
stdev			0.23	0.05	0.47	0.37	0.01	0.03	0.17	0.33	0.70	0.11	0.70
22B-1721	A	1r	27.20	0.51	52.62	9.86	1.16	0.55	1.79	2.21	95.79	1.57	97.47
22B-1721	A	2c	26.89	0.42	53.46	9.97	1.17	0.55	1.77	2.31	96.42	1.69	98.23
22B-1721	A	3c	26.88	0.51	52.72	10.67	1.16	0.52	2.15	2.28	96.77	1.22	98.11
22B-1721	B	4r	27.34	0.38	53.60	10.20	1.18	0.54	1.95	2.23	97.30	1.59	99.01
22B-1721	B	5	27.51	0.43	52.82	10.04	1.17	0.57	1.81	2.18	96.41	1.57	98.09
22B-1721	B	6	26.93	0.49	53.48	9.88	1.17	0.54	1.84	2.33	96.54	1.65	98.31

Table B.3. d. Staurolite Mineral Chemistry. (continued)

			weight percent oxide (Cr_2O_3, Na_2O, CaO not detected)										
Sample	area	spot	SiO_2	TiO_2	Al_2O_3	FeO	Fe_2O_3	MnO	MgO	ZnO	Total	H_2O	Total
22B-1721	C	7c	26.93	0.45	52.56	10.00	1.16	0.59	1.93	2.31	95.81	1.47	97.39
22B-1721	C	8r	26.86	0.46	53.82	9.76	1.18	0.57	1.86	2.46	96.85	1.69	98.66
ave(8)			27.07	0.46	53.14	10.05	1.17	0.55	1.89	2.29	96.49	1.56	98.16
stdev			0.23	0.04	0.47	0.26	0.01	0.02	0.12	0.08	0.48	0.14	0.51
22B-1723	A	20	26.94	0.40	52.68	7.09	1.16	0.57	2.09	6.10	96.91	1.33	98.36
22B-1723	B	23	26.54	0.45	53.22	6.96	1.16	0.57	2.02	6.16	96.97	1.44	98.53
22B-1723	B	24	26.66	0.38	53.99	7.04	1.18	0.62	1.98	6.31	98.04	1.52	99.68
22B-1723	C	27	26.78	0.40	53.00	7.11	1.16	0.54	2.00	6.03	96.91	1.44	98.46
22B-1723	D	28	26.56	0.44	53.57	7.28	1.17	0.62	2.14	6.11	97.77	1.36	99.25
22B-1723	D	29	26.90	0.44	53.17	7.05	1.17	0.58	2.09	6.21	97.49	1.36	98.97
ave(6)			26.73	0.42	53.27	7.09	1.17	0.58	2.05	6.15	97.35	1.41	98.87
stdev			0.16	0.03	0.42	0.10	0.01	0.03	0.06	0.09	0.45	0.07	0.47
24-1131	A	37	26.59	0.30	52.29	8.83	1.15	0.18	2.55	5.33	97.10	0.97	98.18
24-1131	B	38c	26.65	0.36	52.31	8.97	1.15	0.23	2.59	4.88	97.02	0.98	98.11
24-1131	B	39c	26.83	0.30	51.94	8.99	1.15	0.23	2.68	4.92	96.92	0.89	97.93
24-1131	C	40c	26.88	0.29	52.34	8.86	1.15	0.22	2.53	4.90	97.06	1.05	98.23
24-1131	C	42r	26.41	0.26	53.83	9.20	1.17	0.26	2.27	5.19	98.47	1.24	99.82
24-1131	D	44r	26.38	0.17	52.79	9.07	1.15	0.20	2.43	5.01	97.09	1.16	98.36
24-1131	D	45r	26.44	0.33	52.47	8.87	1.15	0.24	2.47	5.15	97.00	1.03	98.15
ave(7)			26.60	0.29	52.57	8.97	1.15	0.22	2.50	5.05	97.24	1.05	98.40
stdev			0.19	0.06	0.57	0.12	0.01	0.02	0.12	0.16	0.51	0.11	0.59
34-799	A	1c	27.16	0.37	54.10	5.70	1.18	0.27	2.21	6.93	97.81	1.71	99.63
34-799	A	2r	26.75	0.37	55.21	5.54	1.20	0.24	1.93	7.17	98.29	1.98	100.39
34-799	A	7	27.12	0.38	54.13	5.39	1.18	0.21	1.84	7.26	97.40	1.89	99.41
34-799	A	8c	26.85	0.35	54.72	5.49	1.19	0.23	1.92	7.33	97.96	1.91	99.99
34-799	A	9r	26.29	0.37	53.33	4.79	1.16	0.22	1.44	7.33	94.81	2.14	97.07
34-799	B'	12	26.86	0.45	54.14	5.89	1.18	0.23	2.06	6.91	97.60	1.72	99.44
ave(6)			26.84	0.38	54.27	5.47	1.18	0.23	1.90	7.16	97.31	1.89	99.32
stdev			0.29	0.03	0.58	0.34	0.01	0.02	0.24	0.17	1.15	0.15	1.07
34C-1377	A	1r	26.91	0.34	53.14	6.11	1.17	0.96	2.32	5.36	96.19	1.63	97.93
34C-1377	A	2c	26.75	0.33	54.02	6.04	1.18	1.00	2.62	5.22	97.04	1.66	98.81
34C-1377	A	3c	26.91	0.40	53.34	6.13	1.17	0.97	2.53	5.16	96.49	1.57	98.18
34C-1377	A	4r	26.29	0.40	52.77	6.22	1.15	1.04	2.20	5.12	95.08	1.63	96.83
34C-1377	B	7c	26.48	0.45	53.69	6.21	1.17	1.03	2.41	5.24	96.56	1.61	98.29
34C-1377	B	8r	26.82	0.38	53.96	6.20	1.18	1.09	2.16	5.21	96.88	1.77	98.76
34C-1377	B	9	26.79	0.34	53.15	6.17	1.16	0.98	2.38	5.25	96.11	1.61	97.84
core, ave(3)			26.71	0.39	53.68	6.13	1.17	1.00	2.52	5.21	96.70	1.61	98.42
stdev			0.18	0.05	0.28	0.07	0.00	0.02	0.09	0.03	0.24	0.04	0.28
rim, ave(3)			26.67	0.37	53.29	6.18	1.16	1.03	2.23	5.23	96.05	1.68	97.84
stdev			0.27	0.02	0.50	0.05	0.01	0.05	0.07	0.10	0.74	0.06	0.79
ave(7)			26.71	0.38	53.44	6.16	1.17	1.01	2.37	5.22	96.34	1.64	98.09
stdev			0.22	0.04	0.43	0.06	0.01	0.04	0.15	0.07	0.60	0.06	0.62
34C-1453	J	35	26.79	0.39	53.22	8.47	1.17	0.22	1.83	5.03	97.00	1.51	98.62
34C-1453	J	36	26.56	0.50	53.40	8.34	1.16	0.19	1.69	5.10	96.83	1.58	98.52
34C-1453	G	38	26.30	0.36	54.05	8.39	1.17	0.21	1.63	5.32	97.31	1.70	99.12
34C-1453	G	39	26.54	0.40	53.38	8.43	1.16	0.25	1.78	5.25	97.08	1.51	98.71
34C-1453	G	40	26.63	0.42	53.33	8.19	1.16	0.14	1.51	4.98	96.25	1.76	98.12
34C-1453	A	43	26.10	0.37	54.69	7.67	1.18	0.24	1.56	5.71	97.40	1.90	99.42
34C-1453	A	44	26.10	0.39	54.30	7.87	1.17	0.18	1.69	5.80	97.39	1.73	99.23
34C-1453	A	45	26.34	0.43	54.15	7.92	1.17	0.20	1.76	5.82	97.68	1.63	99.42
34C-1453	D	47	26.28	0.50	53.21	8.32	1.16	0.17	1.71	5.11	96.34	1.56	98.02
34C-1453	D	48	26.46	0.44	53.55	8.66	1.17	0.23	1.56	5.00	96.95	1.62	98.68
34C-1453	E	49c	26.74	0.42	53.06	8.22	1.16	0.22	1.81	4.99	96.51	1.55	98.18
34C-1453	E	50c	26.61	0.38	53.59	8.37	1.17	0.24	1.87	5.20	97.31	1.53	98.96
ave(12)			26.45	0.42	53.66	8.24	1.17	0.21	1.70	5.28	97.00	1.63	98.75
stdev			0.22	0.04	0.49	0.27	0.01	0.03	0.11	0.31	0.43	0.11	0.47
34C-1747.5	B	13	26.52	0.61	53.19	10.40	1.16	0.44	2.24	1.56	96.01	1.46	97.58
34C-1747.5	B	14	26.95	0.40	54.07	10.08	1.18	0.40	1.92	1.60	96.48	1.88	98.47
34C-1747.5	C	15c	26.75	0.51	53.79	9.86	1.17	0.38	2.14	1.57	96.06	1.77	97.94
34C-1747.5	C	16r	27.00	0.45	54.15	9.84	1.18	0.33	1.96	1.58	96.37	1.93	98.41
34C-1747.5	C	19	27.01	0.47	53.33	9.80	1.17	0.42	2.23	1.60	95.91	1.67	97.70
34C-1747.5	C	20	26.97	0.46	54.15	9.79	1.18	0.44	1.99	1.57	96.43	1.90	98.44
ave(6)			26.87	0.48	53.78	9.96	1.17	0.40	2.08	1.58	96.21	1.77	98.09
stdev			0.18	0.07	0.39	0.22	0.01	0.04	0.13	0.02	0.22	0.16	0.37

Table B.3. d. Staurolite Mineral Chemistry. (continued)

			Structural formula normalized to (Al+Si)=25.53 and 96 anionic charges											
			vi-site=17.78 U-site=.25											
Sample	area	spot	Si	Al_{iv}	Al_{vi}	Fe^{+3}	Mn	Fe^{+2}	Ti	Fe^{+2}	Mg	Zn	site	H
22-901	A	1c	7.727	.273	17.530	.250	.144	.106	.107	2.474	.836	.264	3.680	2.859
22-901	A	2r	7.726	.274	17.530	.250	.157	.093	.108	2.317	.793	.241	3.459	3.299
22-901	A'	4c	7.597	.403	17.530	.250	.169	.081	.099	2.301	.795	.230	3.425	3.514
22-901	A'	5r	7.685	.315	17.530	.250	.148	.102	.089	2.302	.765	.223	3.378	3.540
22-901	A'	7c	7.683	.317	17.530	.250	.151	.099	.087	2.466	.862	.257	3.672	2.958
22-901	A'	8r	7.705	.295	17.530	.250	.141	.109	.113	2.366	.822	.236	3.536	3.157
22-901	B	10c	7.539	.461	17.530	.250	.156	.094	.090	2.360	.809	.252	3.511	3.418
22-901	B	11r	7.831	.169	17.530	.250	.137	.113	.098	2.253	.816	.231	3.398	3.336
core, ave(4)			7.637	.363	17.530	.250	.155	.095	.096	2.400	.825	.251	3.572	3.187
stdev			.073	.073	.000	.000	.009	.009	.008	.073	.026	.013	.108	.283
rim, ave(4)			7.737	.263	17.530	.250	.146	.104	.102	2.309	.799	.233	3.443	3.333
stdev			.056	.056	.000	.000	.008	.008	.009	.040	.022	.007	.061	.137
ave(8)			7.687	.313	17.530	.250	.151	.099	.099	2.355	.812	.242	3.508	3.260
stdev			.082	.082	.000	.000	.010	.010	.009	.074	.028	.014	.109	.234
22-957	A	13c	7.655	.345	17.530	.250	.162	.088	.105	2.460	.800	.380	3.745	2.805
22-957	A	14r	7.757	.243	17.530	.250	.163	.087	.100	2.404	.747	.366	3.616	2.973
22-957	B	15c	7.668	.332	17.530	.250	.168	.082	.115	2.467	.788	.365	3.735	2.793
22-957	B	16r	7.668	.332	17.530	.250	.133	.117	.103	2.494	.718	.410	3.725	2.837
22-957	C	17c	7.730	.270	17.530	.250	.167	.083	.098	2.564	.803	.368	3.833	2.567
22-957	C	18r	7.685	.315	17.530	.250	.146	.104	.091	2.247	.723	.397	3.458	3.379
core, ave(3)			7.684	.316	17.530	.250	.166	.084	.106	2.497	.797	.371	3.771	2.722
stdev			.033	.033	.000	.000	.003	.003	.007	.048	.006	.006	.044	.110
rim, ave(3)			7.703	.297	17.530	.250	.148	.102	.098	2.382	.729	.391	3.599	3.063
stdev			.039	.039	.000	.000	.012	.012	.005	.102	.013	.019	.110	.230
ave(6)			7.694	.306	17.530	.250	.157	.093	.102	2.439	.763	.381	3.685	2.892
stdev			.037	.037	.000	.000	.013	.013	.007	.098	.036	.017	.120	.248
22-996.5	A'	10c	7.619	.381	17.530	.250	.155	.095	.110	2.897	.787	.029	3.823	2.675
22-996.5	A'	11r	7.724	.276	17.530	.250	.147	.103	.038	2.858	.828	.000	3.724	2.912
22-996.5	A	12c	7.555	.445	17.530	.250	.146	.104	.096	2.970	.873	.000	3.938	2.536
22-996.5	A	13r	7.658	.342	17.530	.250	.137	.113	.100	2.906	.875	.000	3.881	2.540
22-996.5	A	14r	7.723	.277	17.530	.250	.148	.102	.091	2.945	.810	.000	3.846	2.564
22-996.5	B	15c	7.728	.272	17.530	.250	.139	.111	.085	2.973	.899	.000	3.957	2.347
ave(6)			7.668	.332	17.530	.250	.145	.105	.087	2.925	.845	.005	3.862	2.596
stdev			.065	.065	.000	.000	.006	.006	.023	.041	.040	.011	.078	.171
22A-1625	A	21c	7.478	.522	17.530	.250	.201	.049	.083	1.555	.964	1.068	3.669	3.178
22A-1625	A	22r	7.558	.442	17.530	.250	.202	.048	.128	1.522	.889	1.107	3.646	3.053
22A-1625	B	23	7.510	.490	17.530	.250	.210	.040	.123	1.622	.950	.958	3.652	3.100
22A-1625	B	24	7.674	.326	17.530	.250	.223	.027	.090	1.712	1.001	.962	3.764	2.778
22A-1625	C	25	7.582	.418	17.530	.250	.198	.052	.083	1.604	.965	.941	3.593	3.226
22A-1625	C	26	7.398	.602	17.530	.250	.206	.044	.085	1.622	.956	1.005	3.667	3.257
ave(6)			7.533	.467	17.530	.250	.207	.043	.098	1.606	.954	1.007	3.665	3.099
stdev			.086	.086	.000	.000	.008	.008	.019	.060	.033	.061	.051	.159
22A-1638	A	2r	7.798	.202	17.530	.250	.125	.125	.076	1.105	.912	1.383	3.226	3.759
22A-1638	A	3c	7.479	.521	17.530	.250	.131	.119	.068	1.156	.905	1.424	3.552	3.441
22A-1638	C	9	7.312	.688	17.530	.250	.132	.118	.104	1.191	.919	1.483	3.699	3.242
22A-1638	C	10	7.436	.564	17.530	.250	.133	.117	.093	1.093	.904	1.451	3.541	3.458
22A-1638	D	13	7.417	.583	17.530	.250	.130	.120	.088	1.120	.887	1.400	3.495	3.577
22A-1638	D	14	7.636	.364	17.530	.250	.122	.128	.083	1.123	.976	1.456	3.638	3.083
ave(6)			7.513	.487	17.530	.250	.129	.121	.085	1.090	.917	1.433	3.525	3.427
stdev			.160	.160	.000	.000	.004	.004	.012	.109	.028	.034	.150	.218
22A-1752	D	23c	7.605	.395	17.530	.250	.173	.077	.092	1.532	.850	.847	3.321	3.729
22A-1752	D	24r	7.566	.434	17.530	.250	.181	.069	.110	1.394	.726	.955	3.185	4.003
22A-1752	G	25c	7.710	.290	17.530	.250	.172	.078	.086	1.621	.898	.791	3.395	3.487
22A-1752	G	26r	7.609	.391	17.530	.250	.178	.072	.107	1.599	.871	.817	3.395	3.548
22A-1752	E	27c	7.728	.272	17.530	.250	.169	.081	.089	1.648	.935	.758	3.430	3.395
22A-1752	E	28r	7.686	.314	17.530	.250	.192	.058	.090	1.627	.942	.764	3.423	3.450
ave(6)			7.651	.349	17.530	.250	.178	.072	.096	1.570	.870	.822	3.358	3.602
stdev			.060	.060	.000	.000	.008	.008	.009	.087	.072	.067	.085	.208
22B-1721	A	1r	7.782	.218	17.530	.250	.133	.117	.110	2.244	.763	.467	3.584	2.992
22B-1721	A	2c	7.635	.365	17.530	.250	.132	.118	.090	2.249	.749	.484	3.572	3.202
22B-1721	A	3c	7.708	.292	17.530	.250	.126	.124	.110	2.435	.919	.483	3.946	2.340
22B-1721	B	4r	7.710	.290	17.530	.250	.129	.121	.081	2.285	.820	.464	3.649	2.991
22B-1721	B	5	7.823	.177	17.530	.250	.137	.113	.092	2.275	.767	.458	3.591	2.971
22B-1721	B	6	7.641	.359	17.530	.250	.130	.120	.105	2.223	.778	.488	3.594	3.122

Table B.3. d. Staurolite Mineral Chemistry. (continued)

			Structural formula normalized to (Al+Si)=25.53 and 96 anionic charges											
			vi-site=17.78 U-site=.25											
Sample	area	spot	Si	Al_{iv}	Al_{vi}	Fe^{+3}	Mn	Fe^{+2}	Ti	Fe^{+2}	Mg	Zn	site	H
22B-1721	C	7c	7.734	.266	17.530	.250	.144	.106	.097	2.295	.826	.490	3.708	2.815
22B-1721	C	8r	7.593	.407	17.530	.250	.136	.114	.098	2.195	.784	.513	3.590	3.192
ave(8)			7.703	.297	17.530	.250	.133	.117	.098	2.275	.801	.481	3.654	2.953
stdev			.073	.073	.000	.000	.005	.005	.010	.068	.051	.017	.118	.261
22B-1723	A	20	7.724	.276	17.530	.250	.138	.112	.086	1.588	.893	1.291	3.858	2.547
22B-1723	B	23	7.589	.411	17.530	.250	.138	.112	.097	1.554	.861	1.301	3.812	2.754
22B-1723	B	24	7.537	.463	17.530	.250	.148	.102	.081	1.563	.834	1.317	3.796	2.871
22B-1723	C	27	7.659	.341	17.530	.250	.131	.119	.086	1.583	.852	1.273	3.795	2.739
22B-1723	D	28	7.558	.442	17.530	.250	.149	.101	.094	1.632	.908	1.284	3.917	2.579
22B-1723	D	29	7.666	.334	17.530	.250	.140	.110	.094	1.571	.888	1.307	3.859	2.587
ave(6)			7.622	.378	17.530	.250	.141	.109	.090	1.582	.873	1.296	3.840	2.679
stdev			.066	.066	.000	.000	.006	.006	.006	.025	.025	.014	.044	.117
24-1131	A	37	7.693	.307	17.530	.250	.044	.206	.065	1.930	1.100	1.139	4.234	1.869
24-1131	B	38c	7.704	.296	17.530	.250	.056	.194	.078	1.974	1.116	1.042	4.209	1.881
24-1131	B	39c	7.778	.222	17.530	.250	.056	.194	.065	1.986	1.158	1.053	4.262	1.726
24-1131	C	40c	7.747	.253	17.530	.250	.054	.196	.063	1.940	1.087	1.043	4.132	2.023
24-1131	C	42r	7.502	.498	17.530	.250	.063	.187	.056	1.998	.961	1.089	4.103	2.341
24-1131	D	44r	7.600	.400	17.530	.250	.049	.201	.037	1.985	1.043	1.066	4.131	2.225
24-1131	D	45r	7.645	.355	17.530	.250	.059	.191	.072	1.953	1.064	1.099	4.188	1.995
ave(7)			7.667	.333	17.530	.250	.054	.196	.062	1.966	1.076	1.076	4.180	2.009
stdev			.087	.087	.000	.000	.006	.006	.012	.024	.058	.033	.055	.197
34-799	A	1c	7.625	.375	17.530	.250	.064	.186	.078	1.154	.925	1.437	3.593	3.193
34-799	A	2r	7.436	.564	17.530	.250	.057	.193	.077	1.096	.800	1.472	3.444	3.681
34-799	A	7	7.614	.386	17.530	.250	.050	.200	.080	1.067	.770	1.505	3.422	3.542
34-799	A	8c	7.503	.497	17.530	.250	.054	.196	.074	1.088	.800	1.512	3.473	3.564
34-799	A	9r	7.528	.472	17.530	.250	.053	.197	.080	.949	.614	1.550	3.193	4.086
34-799	B'	12	7.562	.438	17.530	.250	.055	.195	.095	1.191	.864	1.436	3.587	3.234
ave(6)			7.545	.455	17.530	.250	.056	.194	.081	1.091	.795	1.485	3.452	3.550
stdev			.065	.065	.000	.000	.004	.004	.007	.076	.096	.041	.133	.298
34C-1377	A	1r	7.671	.329	17.530	.250	.232	.018	.073	1.439	.986	1.128	3.626	3.092
34C-1377	A	2c	7.552	.448	17.530	.250	.239	.011	.070	1.415	1.102	1.088	3.676	3.117
34C-1377	A	3c	7.651	.349	17.530	.250	.234	.016	.086	1.441	1.072	1.083	3.682	2.975
34C-1377	A	4r	7.584	.416	17.530	.250	.254	.000	.087	1.506	.946	1.091	3.629	3.145
34C-1377	B	7c	7.530	.470	17.530	.250	.248	.002	.096	1.475	1.021	1.100	3.693	3.052
34C-1377	B	8r	7.571	.429	17.530	.250	.261	.000	.081	1.475	.909	1.086	3.550	3.327
34C-1377	B	9	7.646	.354	17.530	.250	.237	.013	.073	1.460	1.012	1.106	3.652	3.064
core, ave(3)			7.578	.422	17.530	.250	.240	.010	.084	1.444	1.065	1.091	3.683	3.048
stdev			.053	.053	.000	.000	.006	.006	.011	.024	.033	.007	.007	.058
rim, ave(3)			7.609	.391	17.530	.250	.249	.001	.080	1.473	.947	1.102	3.601	3.188
stdev			.044	.044	.000	.000	.012	.012	.006	.027	.031	.019	.036	.101
ave(7)			7.601	.399	17.530	.250	.243	.007	.081	1.459	1.007	1.098	3.644	3.110
stdev			.051	.051	.000	.000	.010	.010	.009	.028	.063	.015	.045	.102
34C-1453	J	35	7.639	.361	17.530	.250	.053	.197	.084	1.823	.778	1.059	3.744	2.866
34C-1453	J	36	7.575	.425	17.530	.250	.046	.204	.107	1.786	.718	1.074	3.685	3.000
34C-1453	G	38	7.459	.541	17.530	.250	.050	.200	.077	1.789	.689	1.114	3.669	3.209
34C-1453	G	39	7.573	.427	17.530	.250	.060	.190	.086	1.823	.757	1.106	3.772	2.872
34C-1453	G	40	7.596	.404	17.530	.250	.034	.216	.090	1.738	.642	1.049	3.519	3.346
34C-1453	A	43	7.357	.643	17.530	.250	.057	.193	.078	1.615	.655	1.188	3.537	3.572
34C-1453	A	44	7.394	.606	17.530	.250	.043	.207	.083	1.659	.714	1.213	3.669	3.262
34C-1453	A	45	7.457	.543	17.530	.250	.048	.202	.092	1.674	.743	1.217	3.725	3.070
34C-1453	D	47	7.538	.462	17.530	.250	.041	.209	.108	1.787	.731	1.082	3.708	2.992
34C-1453	D	48	7.540	.460	17.530	.250	.056	.194	.094	1.870	.663	1.052	3.678	3.074
34C-1453	E	49c	7.645	.355	17.530	.250	.053	.197	.090	1.770	.771	1.053	3.685	2.964
34C-1453	E	50c	7.566	.434	17.530	.250	.058	.192	.081	1.798	.792	1.092	3.763	2.905
ave(12)			7.528	.472	17.530	.250	.050	.200	.089	1.761	.721	1.108	3.680	3.094
stdev			.088	.088	.000	.000	.008	.008	.010	.072	.048	.060	.076	.206
34C-1747.5	B	13	7.588	.412	17.530	.250	.107	.143	.131	2.347	.955	.330	3.763	2.784
34C-1747.5	B	14	7.586	.414	17.530	.250	.095	.155	.085	2.218	.805	.333	3.441	3.523
34C-1747.5	C	15c	7.574	.426	17.530	.250	.091	.159	.109	2.177	.903	.328	3.517	3.335
34C-1747.5	C	16r	7.588	.412	17.530	.250	.079	.171	.095	2.141	.821	.328	3.385	3.612
34C-1747.5	C	19	7.672	.328	17.530	.250	.101	.149	.100	2.178	.944	.336	3.558	3.171
34C-1747.5	C	20	7.582	.418	17.530	.250	.105	.145	.097	2.156	.834	.326	3.413	3.557
ave(6)			7.598	.402	17.530	.250	.096	.154	.103	2.203	.877	.330	3.513	3.330
stdev			.033	.033	.000	.000	.010	.010	.015	.069	.060	.003	.127	.286

Table B.3. e. Sphalerite Mineral Chemistry.

			weight percent element							structural formula						
Sample	area	spot	Zn	Fe	Mn	Cd	Cu	S	Total	Zn	Fe	Mn	Cd	Cu	site	S
22A-1625	H	52	57.42	7.88	0.34	0.00	0.14	34.17	99.95	0.878	0.141	0.006	0.000	0.002	1.028	1.066
22A-1625	H	53	58.34	7.64	0.47	0.47	0.00	32.12	99.04	0.892	0.137	0.009	0.004	0.000	1.042	1.002
ave(2)			57.88	7.76	0.41	0.24	0.07	33.15	99.50	0.885	0.139	0.007	0.002	0.001	1.035	1.034
22A-1638	D	1	60.39	6.69	0.09	0.00	0.00	33.45	100.62	0.924	0.120	0.002	0.000	0.000	1.045	1.043
22A-1638	D	2	60.90	6.28	0.00	0.00	0.00	33.35	100.53	0.932	0.112	0.000	0.000	0.000	1.044	1.040
22A-1638	D	3	59.83	6.71	0.00	0.00	0.00	33.03	99.57	0.915	0.120	0.000	0.000	0.000	1.035	1.030
22A-1638	D	4	60.28	6.11	0.00	0.00	0.00	33.52	99.91	0.922	0.109	0.000	0.000	0.000	1.032	1.045
22A-1638	D	5	60.49	6.44	0.00	0.00	0.00	33.19	100.12	0.925	0.115	0.000	0.000	0.000	1.041	1.035
22A-1638	A	6	62.28	4.45	0.00	0.29	0.00	32.94	99.96	0.953	0.080	0.000	0.003	0.000	1.035	1.027
22A-1638	A	7	61.16	6.46	0.11	0.00	0.00	33.30	101.03	0.936	0.116	0.002	0.000	0.000	1.053	1.038
22A-1638	C	8	61.07	5.82	0.00	0.00	0.12	33.08	100.09	0.934	0.104	0.000	0.000	0.002	1.040	1.032
22A-1638	C	9	62.11	4.86	0.00	0.00	0.00	33.25	100.22	0.950	0.087	0.000	0.000	0.000	1.037	1.037
ave(7)			60.59	6.36	0.03	0.00	0.02	33.27	100.27	0.927	0.114	0.001	0.000	0.000	1.042	1.038
stdev			0.44	0.29	0.05	0.00	0.04	0.17	0.45	0.007	0.005	0.001	0.000	0.001	0.007	0.005
22B-1723	A	51	61.47	4.02	0.00	0.00	0.41	33.41	99.31	0.940	0.072	0.000	0.000	0.006	1.019	1.042
22B-1723	A	53	57.87	8.40	0.13	0.35	0.23	33.43	100.41	0.885	0.150	0.002	0.003	0.004	1.045	1.043
22B-1723	A	54	57.28	8.32	0.16	0.59	0.17	32.30	98.82	0.876	0.149	0.003	0.005	0.003	1.036	1.007
22B-1723	C	55	60.78	5.01	0.00	0.00	0.00	33.58	99.37	0.930	0.090	0.000	0.000	0.000	1.019	1.047
ave(2)			57.58	8.36	0.15	0.47	0.20	32.87	99.62	0.881	0.150	0.003	0.004	0.003	1.040	1.025
24-1191	F	1	58.20	7.66	0.21	0.00	0.00	33.43	99.50	0.890	0.137	0.004	0.000	0.000	1.031	1.043
24-1191	F	2	58.76	7.67	0.21	0.00	0.00	33.18	99.82	0.899	0.137	0.004	0.000	0.000	1.040	1.035
24-1191	C	3	59.53	7.21	0.28	0.00	0.18	33.43	100.63	0.911	0.129	0.005	0.000	0.003	1.048	1.043
24-1191	D	4	58.79	7.07	0.20	0.00	0.00	33.12	99.18	0.899	0.127	0.004	0.000	0.000	1.030	1.033
24-1191	B	5	59.31	6.74	0.23	0.00	0.00	33.36	99.64	0.907	0.121	0.004	0.000	0.000	1.032	1.040
Zone 6, ave(2)			58.48	7.67	0.21	0.00	0.00	33.31	99.66	0.895	0.137	0.004	0.000	0.000	1.036	1.039
Zone 6, ave(5)			58.92	7.27	0.23	0.00	0.04	33.30	99.75	0.901	0.130	0.004	0.000	0.001	1.036	1.039
stdev			0.47	0.36	0.03	0.00	0.07	0.13	0.49	0.007	0.006	0.001	0.000	0.001	0.007	0.004
34-799b	D	1	60.82	5.63	0.00	0.28	0.42	31.98	99.13	0.930	0.101	0.000	0.002	0.007	1.040	0.997
34-799b	D	2	60.41	5.74	0.00	0.33	0.13	33.11	99.72	0.924	0.103	0.000	0.003	0.002	1.032	1.033
34-799b	E	3	61.59	4.44	0.00	1.07	0.00	33.20	100.30	0.942	0.080	0.000	0.010	0.000	1.031	1.035
34-799b	F	4	58.52	7.27	0.00	1.05	0.21	33.67	100.72	0.895	0.130	0.000	0.009	0.003	1.038	1.050
34-799b	F	5	58.56	7.24	0.00	1.15	0.20	33.39	100.54	0.896	0.130	0.000	0.010	0.003	1.039	1.041
ave(2)			58.54	7.26	0.00	1.10	0.21	33.53	100.63	0.896	0.130	0.000	0.010	0.003	1.038	1.046
34-799a	A	102	60.56	5.27	0.00	0.00	0.00	34.23	100.06	0.926	0.094	0.000	0.000	0.000	1.021	1.067
34-799a	A	103	67.12	0.72	0.00	0.00	0.00	33.18	101.02	1.027	0.013	0.000	0.000	0.000	1.040	1.035
34-799a	B	104	65.51	0.71	0.00	0.00	0.00	32.13	98.35	1.002	0.013	0.000	0.000	0.000	1.015	1.002
34C-1377	A	105	68.71	0.62	0.00	0.00	0.00	31.92	101.25	1.051	0.011	0.000	0.000	0.000	1.062	0.995
34C-1377	B	106	65.85	2.44	0.00	0.00	0.00	31.75	100.04	1.007	0.044	0.000	0.000	0.000	1.051	0.990
34C-1377	A	108	66.96	1.02	0.00	0.00	0.00	32.00	99.98	1.024	0.018	0.000	0.000	0.000	1.043	0.998

Table B.3. f. Gahnite Mineral Chemistry.

			weight percent oxide (TiO_2 and Cr_2O_3 not detected)							Structural formula normalized to 8 anionic charges							
Sample	area	spot	SiO_2	Al_2O_3	FeO	MnO	MgO	ZnO	Total	Al	Si	site	Fe	Mn	Mg	Zn	site
22A-1638	A	1	0.00	59.51	4.79	0.17	2.33	33.08	99.88	2.044	0.000	2.044	0.117	0.004	0.101	0.712	0.934
22A-1638	B	5c	0.00	58.43	5.06	0.15	2.50	32.47	98.61	2.035	0.000	2.035	0.125	0.004	0.110	0.708	0.947
22A-1638	B	6r	0.00	57.94	4.93	0.16	2.25	32.90	98.18	2.033	0.000	2.033	0.123	0.004	0.100	0.723	0.950
22A-1638	C	11	0.00	59.73	5.19	0.16	2.44	32.30	99.82	2.047	0.000	2.047	0.126	0.004	0.106	0.693	0.929
22A-1638	D	15	0.08	59.47	5.10	0.13	2.44	32.59	99.81	2.041	0.002	2.043	0.124	0.003	0.106	0.701	0.934
ave(5)			0.02	59.02	5.01	0.15	2.39	32.67	99.26	2.040	0.000	2.041	0.123	0.004	0.105	0.707	0.939
stdev			0.03	0.70	0.14	0.01	0.09	0.28	0.72	0.005	0.001	0.005	0.003	0.000	0.004	0.010	0.008
22B-1723	A	17	0.00	58.39	7.01	0.24	2.18	32.05	99.87	2.021	0.000	2.021	0.172	0.006	0.095	0.695	0.968
22B-1723	A	18c	0.00	58.56	7.62	0.23	2.71	30.52	99.64	2.020	0.000	2.020	0.186	0.006	0.118	0.659	0.970
22B-1723	A	19r	0.07	58.68	7.37	0.23	2.46	31.11	99.92	2.021	0.002	2.023	0.180	0.006	0.107	0.671	0.964
22B-1723	B	21	0.09	58.28	7.57	0.24	2.56	30.61	99.35	2.018	0.003	2.021	0.186	0.006	0.112	0.664	0.968
22B-1723	B	22	0.00	58.16	6.96	0.21	2.29	31.68	99.32	2.022	0.000	2.022	0.172	0.005	0.101	0.690	0.967
22B-1723	C	25c	0.07	59.38	7.49	0.25	2.67	30.30	100.16	2.029	0.002	2.032	0.182	0.006	0.115	0.649	0.952
22B-1723	C	26r	0.00	58.86	6.84	0.18	2.19	31.67	99.74	2.032	0.000	2.032	0.167	0.004	0.096	0.685	0.952
ave(7)			0.03	58.62	7.27	0.23	2.44	31.13	99.71	2.023	0.001	2.024	0.178	0.006	0.106	0.673	0.963
stdev			.04	0.38	0.30	0.02	0.20	0.63	0.28	0.005	0.001	0.005	0.007	0.001	0.009	0.016	0.007
24-1191	A'	30	1.39	57.75	5.32	0.17	1.66	33.58	99.87	1.991	0.041	2.032	0.130	0.004	0.072	0.725	0.932
24-1191	B'	31	0.08	58.50	5.84	0.23	1.66	34.14	100.45	2.023	0.002	2.025	0.143	0.006	0.073	0.739	0.961
24-1191	B'	32	0.00	57.76	5.88	0.20	1.68	33.77	99.29	2.023	0.000	2.023	0.146	0.005	0.074	0.741	0.966
24-1191	C'	33	0.08	59.10	5.95	0.22	1.83	33.58	100.76	2.029	0.002	2.031	0.145	0.005	0.079	0.722	0.952
24-1191	D'	34	0.00	58.30	5.79	0.24	1.71	33.60	99.64	2.029	0.000	2.029	0.143	0.006	0.075	0.732	0.957
24-1191	D'	35	0.09	57.79	6.13	0.20	1.75	33.44	99.40	2.019	0.003	2.022	0.152	0.005	0.077	0.732	0.966
zone 6, ave(6)			0.27	58.20	5.82	0.21	1.72	33.69	99.90	2.019	0.008	2.027	0.143	0.005	0.075	0.732	0.956
stdev			0.50	0.50	0.25	0.02	0.06	0.22	0.54	0.013	0.015	0.004	0.007	0.001	0.003	0.007	0.012
24-1131	A	36	0.00	57.84	9.72	0.08	2.86	28.99	99.49	2.003	0.000	2.003	0.239	0.002	0.125	0.629	0.995
24-1131	C	41	0.11	58.51	9.61	0.10	2.95	29.21	100.49	2.003	0.003	2.006	0.233	0.002	0.128	0.626	0.990
24-1131	C	43	0.24	57.94	9.81	0.10	3.19	28.94	100.22	1.989	0.007	1.996	0.239	0.002	0.138	0.622	1.002
24-1131	D	46	0.00	58.75	9.27	0.07	3.24	29.22	100.55	2.006	0.000	2.006	0.225	0.002	0.140	0.625	0.991
24-1131	D	47	0.13	58.07	8.47	0.07	2.89	30.23	99.86	2.003	0.004	2.007	0.207	0.002	0.126	0.653	0.988
ave(5)			0.10	58.22	9.38	0.08	3.03	29.32	100.12	2.001	0.003	2.004	0.229	0.002	0.131	0.631	0.993
stdev			0.09	0.35	0.49	0.01	0.16	0.47	0.40	0.006	0.003	0.004	0.012	0.000	0.006	0.011	0.005
34-799a	A	3c	0.00	59.89	5.77	0.00	2.37	32.40	100.43	2.044	0.000	2.044	0.140	0.000	0.102	0.692	0.934
34-799a	A	4r	0.75	58.16	5.49	0.00	1.90	32.70	99.00	2.018	0.022	2.040	0.135	0.000	0.083	0.711	0.929
34-799a	A	5c	3.24	56.91	5.35	0.00	2.01	31.66	99.17	1.945	0.094	2.039	0.130	0.000	0.087	0.678	0.894
34-799a	A	6r	0.00	59.39	5.19	0.00	2.06	32.98	99.62	2.047	0.000	2.047	0.127	0.000	0.090	0.712	0.929
34-799a	B	10c	0.00	59.10	5.70	0.09	2.44	32.11	99.44	2.039	0.000	2.039	0.139	0.002	0.106	0.694	0.942
34-799a	B	11r	0.00	58.57	5.46	0.08	2.15	32.95	99.21	2.035	0.000	2.035	0.135	0.002	0.094	0.717	0.948
core, ave(3)			1.08	58.63	5.61	0.03	2.27	32.06	99.68	2.009	0.031	2.041	0.136	0.001	0.098	0.688	0.924
stdev			1.53	1.26	0.18	0.04	0.19	0.30	0.54	0.045	0.044	0.002	0.005	0.001	0.008	0.007	0.021
rim, ave(3)			0.25	58.71	5.38	0.03	2.04	32.88	99.28	2.033	0.007	2.041	0.132	0.001	0.089	0.713	0.935
stdev			0.35	0.51	0.13	0.04	0.10	0.13	0.26	0.012	0.010	0.005	0.004	0.001	0.005	0.003	0.009
ave(6)			0.67	58.67	5.49	0.03	2.16	32.47	99.48	2.021	0.019	2.041	0.134	0.001	0.094	0.701	0.929
stdev			1.18	0.96	0.20	0.04	0.19	0.47	0.47	0.035	0.034	0.004	0.005	0.001	0.008	0.014	0.017
34-799b	E	6	0.25	58.25	5.19	0.00	2.00	33.84	99.53	2.023	0.007	2.030	0.128	0.000	0.088	0.736	0.952
34-799b	E	7	0.00	58.93	5.39	0.00	2.06	33.61	99.99	2.034	0.000	2.034	0.132	0.000	0.090	0.727	0.949
34-799b	F	8	0.11	57.97	4.99	0.00	1.92	34.59	99.58	2.020	0.003	2.024	0.123	0.000	0.085	0.755	0.963
34-799b	F	9	0.00	59.26	5.69	0.00	2.84	32.29	100.08	2.030	0.000	2.030	0.138	0.000	0.123	0.693	0.954
34-799b	D	10	0.00	57.96	4.67	0.00	1.82	34.99	99.44	2.025	0.000	2.025	0.116	0.000	0.080	0.766	0.962
34-799b	D	11	0.00	57.47	4.67	0.00	2.06	34.69	98.89	2.019	0.000	2.019	0.116	0.000	0.091	0.763	0.971
ave(6)			0.06	58.31	5.10	0.00	2.12	34.00	99.59	2.025	0.002	2.027	0.126	0.000	0.093	0.740	0.958
stdev			0.09	0.61	0.37	0.00	0.33	0.90	0.39	0.005	0.003	0.005	0.008	0.000	0.014	0.025	0.008
34C-1453	J	33	0.00	58.35	8.87	0.00	1.91	30.26	99.39	2.026	0.000	2.026	0.219	0.000	0.084	0.658	0.961
34C-1453	J	34	0.00	59.03	8.88	0.00	1.74	30.61	100.26	2.032	0.000	2.032	0.217	0.000	0.076	0.660	0.952
34C-1453	G	37	0.00	58.59	9.14	0.00	1.87	29.96	99.56	2.029	0.000	2.029	0.225	0.000	0.082	0.650	0.956
34C-1453	B	41	0.14	58.94	8.13	0.00	1.59	31.49	100.29	2.030	0.004	2.034	0.199	0.000	0.069	0.679	0.947
34C-1453	A	42	0.00	58.61	8.36	0.00	1.81	30.99	99.77	2.029	0.000	2.029	0.205	0.000	0.079	0.672	0.956
34C-1453	D	46	0.00	58.55	9.14	0.00	1.92	29.84	99.45	2.029	0.000	2.029	0.225	0.000	0.084	0.648	0.956
ave(6)			0.02	58.68	8.75	0.00	1.81	30.53	99.79	2.029	0.001	2.030	0.215	0.000	0.079	0.661	0.955
stdev			0.05	0.23	0.38	0.00	0.11	0.58	0.37	0.002	0.002	0.002	0.010	0.000	0.005	0.011	0.004

Table B.3. g. Garnet Mineral Chemistry.

			weight percent oxide or element (Cr_2O_3 not detected)								
Sample	area	spot	SiO_2	TiO_2	Al_2O_3	FeO	MnO	MgO	CaO	Na_2O	Total
22-413	D	109r	37.28	0.00	21.46	33.23	2.87	2.96	3.05	0.00	100.85
22-413	D	110	37.46	0.00	20.92	33.06	2.95	3.16	2.71	0.00	100.26
22-413	D	111	37.10	0.00	21.10	32.37	3.50	3.03	2.55	0.00	99.65
22-413	D	112c	37.21	0.00	21.20	32.76	3.42	2.94	2.76	0.00	100.29
22-413	D	113	37.41	0.00	20.94	32.70	3.52	3.02	2.86	0.00	100.45
22-413	D	114	37.17	0.00	20.49	32.52	3.12	2.96	2.83	0.00	99.09
22-413	D	115r	37.14	0.00	21.06	32.84	3.12	2.57	2.98	0.00	99.71
22A-1625	G	29r	36.78	0.14	20.87	17.53	17.86	2.93	2.94	0.00	99.05
22A-1625	G	30	36.56	0.11	20.76	15.55	20.20	2.38	2.78	0.00	98.34
22A-1625	G	31	36.88	0.13	20.65	14.57	21.64	1.92	2.71	0.00	98.50
22A-1625	G	32	36.52	0.18	20.68	14.54	22.11	1.90	2.77	0.00	98.70
22A-1625	G	33	36.74	0.13	20.60	14.27	22.52	1.84	2.38	0.00	98.48
22A-1625	G	34	36.26	0.15	20.83	14.18	22.62	1.73	2.63	0.00	98.40
22A-1625	G	35	35.95	0.17	20.76	14.46	22.80	1.71	2.42	0.07	98.34
22A-1625	G	36	36.28	0.16	20.95	14.16	22.88	1.69	2.70	0.00	98.82
22A-1625	G	37c	36.05	0.17	20.71	14.65	21.89	1.90	2.67	0.06	98.10
22A-1625	G	38	36.42	0.17	20.81	15.51	20.30	2.21	3.10	0.00	98.52
22A-1625	G	39	36.48	0.14	20.56	15.69	20.85	2.07	3.12	0.00	98.91
22A-1625	G	40	36.62	0.11	21.02	16.51	19.39	2.34	2.87	0.00	98.86
22A-1625	G	41r	36.57	0.00	21.41	19.86	15.87	3.22	2.04	0.00	98.97
22A-1625	G	42r	36.66	0.00	21.30	19.58	15.83	3.14	2.19	0.00	98.70
22A-1625	F	43r	36.49	0.00	21.17	19.56	15.99	3.13	2.23	0.00	98.57
22A-1625	F	44	36.74	0.06	21.01	18.54	16.32	3.18	2.64	0.00	98.49
22A-1625	F	45	36.59	0.12	21.06	17.04	18.37	2.66	2.83	0.00	98.67
22A-1625	F	46	36.29	0.15	20.76	15.80	20.08	2.24	2.97	0.00	98.29
22A-1625	F	47	36.28	0.13	20.83	15.13	21.39	1.96	2.88	0.00	98.60
22A-1625	F	48	36.21	0.19	20.64	15.14	21.44	1.91	2.92	0.00	98.45
22A-1625	F	49	36.51	0.19	20.80	14.61	22.17	1.81	3.04	0.00	99.13
22A-1625	F	50	36.26	0.19	20.93	14.81	21.83	1.85	3.12	0.00	98.99
22A-1625	F	51c	36.51	0.15	20.79	14.64	22.29	1.80	2.93	0.00	99.11
rim, ave(3)			36.57	0.00	21.29	19.67	15.90	3.16	2.15	0.00	98.75
stdev			0.07	0.00	0.10	0.14	0.07	0.04	0.08	0.00	0.17
22B-1721	F	12c	36.84	0.00	20.94	23.76	11.74	2.41	3.89	0.00	99.58
22B-1721	F	13	36.70	0.06	21.49	24.62	10.69	2.68	3.39	0.00	99.63
22B-1721	F	14	36.66	0.00	21.31	24.57	10.38	2.73	3.51	0.00	99.16
22B-1721	F	15r	36.51	0.00	21.54	26.03	9.79	2.78	2.67	0.00	99.32
22B-1721	F	16	36.83	0.00	21.12	23.88	11.91	2.35	3.80	0.00	99.89
22B-1721	F	17r	37.07	0.07	21.24	25.15	9.82	2.80	3.66	0.00	99.81
22B-1721	F	18	36.67	0.00	21.08	24.04	11.80	2.43	3.52	0.00	99.54
22B-1721	F	19r	36.90	0.00	21.37	25.80	9.73	2.86	2.68	0.00	99.34
22B-1721	F	20	37.27	0.00	21.18	24.28	10.86	2.69	3.64	0.00	99.92
22B-1721	F	21r	36.85	0.00	21.68	25.90	9.67	2.91	2.92	0.00	99.93
22B-1721	E	22c	36.80	0.00	21.29	25.71	9.44	3.00	3.10	0.00	99.34
22B-1721	E	23	36.94	0.00	21.42	25.33	9.25	3.03	3.26	0.00	99.23
22B-1721	E	24r	37.01	0.00	21.44	26.37	9.79	2.62	2.64	0.00	99.87
22B-1721	D	25c	36.58	0.07	21.38	23.20	11.92	2.23	4.13	0.00	99.51
22B-1721	D	26c	36.68	0.10	21.03	23.05	11.97	2.31	4.50	0.00	99.64
22B-1721	D	27	36.85	0.00	21.06	23.12	11.27	2.39	4.46	0.00	99.15
22B-1721	D	28r	36.79	0.12	20.98	23.19	11.42	2.34	4.21	0.00	99.05
22B-1721	D	29	36.76	0.09	21.13	23.54	11.69	2.35	3.92	0.00	99.48
22B-1721	D	30	36.69	0.00	21.28	25.15	9.89	2.91	3.32	0.00	99.24
22B-1721	D	31r	36.95	0.00	21.21	26.16	9.68	2.77	2.63	0.00	99.40
22B-1721	D	32	37.00	0.10	20.93	21.79	13.04	2.11	4.53	0.00	99.50
22B-1721	D	33r	37.30	0.07	21.50	25.24	9.38	2.91	3.49	0.00	99.89
22B-1721	D	34	37.08	0.12	20.96	23.12	11.50	2.46	4.54	0.00	99.78
22B-1721	D	35r	36.70	0.00	21.36	25.98	9.44	2.91	2.81	0.00	99.20
rim, ave(7)			36.90	0.02	21.41	25.75	9.64	2.85	2.98	0.00	99.56
stdev			0.23	0.03	0.16	0.37	0.16	0.06	0.39	0.00	0.29

Table B.3. g. Garnet Mineral Chemistry. (continued)

			weight percent oxide or element (Cr_2O_3 not detected)								
Sample	area	spot	SiO_2	TiO_2	Al_2O_3	FeO	MnO	MgO	CaO	Na_2O	Total
zone 5											
24-1191	E	44c	37.12	0.10	20.90	18.66	15.88	2.19	5.06	0.00	99.91
24-1191	E	45	37.18	0.12	20.86	18.10	16.19	1.92	5.36	0.00	99.73
24-1191	E	46	37.35	0.09	20.84	17.05	18.13	1.71	5.14	0.00	100.31
24-1191	E	47	37.19	0.08	21.04	18.89	15.76	2.00	4.91	0.00	99.87
24-1191	E	48r	37.20	0.07	20.79	19.03	15.46	2.07	5.26	0.00	99.88
24-1191	E	49r	37.40	0.00	20.93	19.02	15.61	1.94	5.29	0.00	100.19
24-1191	G	50r	37.22	0.00	20.78	19.26	14.37	1.94	5.98	0.00	99.55
24-1191	G	51	37.17	0.00	21.01	19.22	14.89	1.96	5.54	0.00	99.79
24-1191	G	52	37.50	0.00	20.93	18.92	15.98	1.93	5.62	0.00	100.88
24-1191	G	53	37.82	0.08	21.21	18.21	16.42	1.94	5.17	0.00	100.85
24-1191	G	54	37.31	0.06	20.78	18.24	16.95	1.93	4.90	0.00	100.17
rim, ave(3)			37.27	0.02	20.83	19.10	15.15	1.98	5.51	0.00	99.87
stdev			0.09	0.03	0.07	0.11	0.55	0.06	0.33	0.00	0.26

Table B.3. g. Garnet Mineral Chemistry. (continued)

			Structural formula normalized to 36 anionic charges									
Sample	area	spot	Si	Al_{iv}	Al_{vi}	Ti	Fe	Mn	Mg	Ca	Na	site
22-413	D	109r	5.948	0.052	3.985	0.000	4.434	0.388	0.704	0.521	0.000	6.048
22-413	D	110	6.007	0.000	3.955	0.000	4.433	0.401	0.755	0.466	0.000	6.055
22-413	D	111	5.984	0.016	3.996	0.000	4.366	0.478	0.728	0.441	0.000	6.014
22-413	D	112c	5.972	0.028	3.983	0.000	4.397	0.465	0.703	0.475	0.000	6.040
22-413	D	113	5.996	0.004	3.952	0.000	4.383	0.478	0.721	0.491	0.000	6.073
22-413	D	114	6.033	0.000	3.921	0.000	4.415	0.429	0.716	0.492	0.000	6.052
22-413	D	115r	5.996	0.004	4.005	0.000	4.434	0.427	0.618	0.516	0.000	5.995
22A-1625	G	29r	5.965	0.035	3.955	0.017	2.378	2.454	0.708	0.511	0.000	6.050
22A-1625	G	30	5.984	0.016	3.989	0.014	2.128	2.800	0.581	0.488	0.000	5.997
22A-1625	G	31	6.031	0.000	3.981	0.016	1.993	2.998	0.468	0.475	0.000	5.933
22A-1625	G	32	5.980	0.020	3.972	0.022	1.991	3.067	0.464	0.486	0.000	6.008
22A-1625	G	33	6.023	0.000	3.981	0.016	1.956	3.127	0.450	0.418	0.000	5.951
22A-1625	G	34	5.961	0.039	3.998	0.019	1.949	3.150	0.424	0.463	0.000	5.986
22A-1625	G	35	5.931	0.069	3.968	0.021	1.995	3.186	0.420	0.428	0.022	6.052
22A-1625	G	36	5.944	0.056	3.991	0.020	1.940	3.175	0.413	0.474	0.000	6.002
22A-1625	G	37c	5.945	0.055	3.972	0.021	2.021	3.058	0.467	0.472	0.019	6.037
22A-1625	G	38	5.959	0.041	3.973	0.021	2.122	2.814	0.539	0.544	0.000	6.018
22A-1625	G	39	5.966	0.034	3.931	0.017	2.146	2.889	0.505	0.547	0.000	6.086
22A-1625	G	40	5.964	0.036	3.999	0.013	2.249	2.675	0.568	0.501	0.000	5.992
22A-1625	G	41r	5.929	0.071	4.021	0.000	2.693	2.179	0.778	0.354	0.000	6.004
22A-1625	G	42r	5.953	0.047	4.031	0.000	2.659	2.177	0.760	0.381	0.000	5.977
22A-1625	F	43r	5.942	0.058	4.007	0.000	2.664	2.206	0.760	0.389	0.000	6.019
22A-1625	F	44	5.973	0.027	4.000	0.007	2.521	2.247	0.770	0.460	0.000	5.999
22A-1625	F	45	5.957	0.043	4.000	0.015	2.320	2.533	0.645	0.494	0.000	5.993
22A-1625	F	46	5.955	0.045	3.971	0.019	2.168	2.791	0.548	0.522	0.000	6.029
22A-1625	F	47	5.949	0.051	3.975	0.016	2.075	2.971	0.479	0.506	0.000	6.031
22A-1625	F	48	5.952	0.048	3.952	0.023	2.081	2.985	0.468	0.514	0.000	6.049
22A-1625	F	49	5.959	0.041	3.962	0.023	1.994	3.065	0.440	0.532	0.000	6.031
22A-1625	F	50	5.928	0.072	3.962	0.023	2.025	3.023	0.451	0.547	0.000	6.046
22A-1625	F	51c	5.963	0.037	3.965	0.018	2.000	3.083	0.438	0.513	0.000	6.034
rim, ave(3)			5.941	0.059	4.019	0.000	2.672	2.187	0.766	0.375	0.000	6.000
stdev			0.010	0.010	0.010	0.000	0.015	0.013	0.009	0.015	0.000	0.017
22B-1721	F	12c	5.963	0.037	3.958	0.000	3.216	1.610	0.581	0.675	0.000	6.082
22B-1721	F	13	5.921	0.079	4.008	0.007	3.322	1.461	0.644	0.586	0.000	6.013
22B-1721	F	14	5.938	0.062	4.007	0.000	3.328	1.424	0.659	0.609	0.000	6.021
22B-1721	F	15r	5.913	0.087	4.026	0.000	3.526	1.343	0.671	0.463	0.000	6.004
22B-1721	F	16	5.947	0.053	3.967	0.000	3.225	1.629	0.565	0.657	0.000	6.076
22B-1721	F	17r	5.961	0.039	3.987	0.008	3.382	1.338	0.671	0.631	0.000	6.021
22B-1721	F	18	5.942	0.058	3.969	0.000	3.258	1.620	0.587	0.611	0.000	6.075
22B-1721	F	19r	5.962	0.038	4.032	0.000	3.486	1.332	0.689	0.464	0.000	5.970
22B-1721	F	20	5.987	0.013	3.998	0.000	3.262	1.478	0.644	0.627	0.000	6.010
22B-1721	F	21r	5.921	0.079	4.029	0.000	3.481	1.316	0.697	0.503	0.000	5.997
22B-1721	E	22c	5.946	0.054	4.001	0.000	3.474	1.292	0.722	0.537	0.000	6.025
22B-1721	E	23	5.959	0.041	4.032	0.000	3.417	1.264	0.728	0.563	0.000	5.973
22B-1721	E	24r	5.961	0.039	4.032	0.000	3.552	1.336	0.629	0.456	0.000	5.972
22B-1721	D	25c	5.919	0.081	3.998	0.009	3.140	1.634	0.538	0.716	0.000	6.027
22B-1721	D	26c	5.933	0.067	3.943	0.012	3.118	1.640	0.557	0.780	0.000	6.095
22B-1721	D	27	5.969	0.031	3.991	0.000	3.132	1.546	0.577	0.774	0.000	6.029
22B-1721	D	28r	5.969	0.031	3.982	0.015	3.147	1.569	0.566	0.732	0.000	6.014
22B-1721	D	29	5.948	0.052	3.980	0.011	3.186	1.602	0.567	0.680	0.000	6.035
22B-1721	D	30	5.937	0.063	3.997	0.000	3.404	1.356	0.702	0.576	0.000	6.037
22B-1721	D	31r	5.974	0.026	4.018	0.000	3.538	1.326	0.667	0.456	0.000	5.986
22B-1721	D	32	5.983	0.017	3.972	0.012	2.947	1.786	0.508	0.785	0.000	6.026
22B-1721	D	33r	5.974	0.026	4.033	0.008	3.381	1.272	0.695	0.599	0.000	5.947
22B-1721	D	34	5.972	0.028	3.952	0.015	3.114	1.569	0.590	0.783	0.000	6.057
22B-1721	D	35r	5.942	0.058	4.018	0.000	3.518	1.295	0.702	0.487	0.000	6.002
rim, ave(7)			5.950	0.050	4.021	0.002	3.473	1.317	0.685	0.515	0.000	5.990
stdev			0.023	0.023	0.015	0.004	0.061	0.024	0.013	0.066	0.000	0.023

Table B.3. g. Garnet Mineral Chemistry. (continued)

			Structural formula normalized to 36 anionic charges									
Sample	area	spot	Si	Al_{iv}	Al_{vi}	Ti	Fe	Mn	Mg	Ca	Na	site
zone 5												
24-1191	E	44c	5.975	0.025	3.942	0.012	2.512	2.165	0.525	0.873	0.000	6.076
24-1191	E	45	5.993	0.007	3.958	0.015	2.440	2.211	0.461	0.926	0.000	6.038
24-1191	E	46	6.002	0.000	3.948	0.011	2.291	2.468	0.409	0.885	0.000	6.053
24-1191	E	47	5.986	0.014	3.979	0.010	2.543	2.149	0.480	0.847	0.000	6.019
24-1191	E	48r	5.992	0.008	3.940	0.008	2.564	2.109	0.497	0.908	0.000	6.078
24-1191	E	49r	6.004	0.000	3.961	0.000	2.554	2.123	0.464	0.910	0.000	6.050
24-1191	G	50r	6.005	0.000	3.952	0.000	2.599	1.964	0.466	1.034	0.000	6.062
24-1191	G	51	5.986	0.014	3.974	0.000	2.588	2.031	0.470	0.956	0.000	6.046
24-1191	G	52	5.989	0.011	3.930	0.000	2.527	2.162	0.459	0.962	0.000	6.110
24-1191	G	53	6.018	0.000	3.979	0.010	2.423	2.213	0.460	0.881	0.000	5.978
24-1191	G	54	6.002	0.000	3.941	0.007	2.454	2.310	0.463	0.845	0.000	6.071
rim, ave(3)			6.000	0.003	3.951	0.003	2.572	2.065	0.476	0.950	0.000	6.063
stdev			0.006	0.004	0.009	0.004	0.019	0.072	0.015	0.059	0.000	0.011

Table B.3. h. Calcic Amphibole Mineral Chemistry.

			weight percent oxide or element (Cr_2O_3 not detected)														
Sample	area	spot	SiO_2	TiO_2	Al_2O_3	FeO	Fe_2O_3	MnO	MgO	CaO	Na_2O	K_2O	ZnO	F	Total	H_2O	Total
22-413	B	12	40.65	0.30	15.80	10.52	11.04	0.30	6.70	9.88	1.76	0.27	0.00	0.00	96.12	2.00	99.23
22-413	B	15	39.40	0.31	15.61	12.02	8.72	0.26	6.42	10.23	1.77	0.25	0.00	0.00	94.12	1.95	96.94
22-413	C	17	40.66	0.35	16.36	8.72	12.51	0.26	6.78	9.27	1.69	0.25	0.00	0.00	95.60	2.01	98.86
ave(3)			40.24	0.32	15.92	10.42	10.76	0.27	6.63	9.79	1.74	0.26	0.00	0.00	95.28	1.99	98.34
stdev			0.59	0.02	0.32	1.35	1.56	0.02	0.15	0.40	0.04	0.01	0.00	0.00	0.85	0.03	1.00
24-1191	E	1c	44.72	0.31	13.38	5.20	7.51	1.08	12.06	11.04	1.47	0.20	0.20	0.00	96.42	2.07	99.24
24-1191	E	2r	43.98	0.32	13.97	6.22	7.69	1.04	11.22	10.99	1.47	0.20	0.00	0.00	96.33	2.06	99.16
24-1191	G	5r	43.73	0.29	14.08	6.33	7.99	1.05	10.93	10.93	1.41	0.24	0.00	0.00	96.18	2.05	99.03
24-1191	G	6r	44.40	0.37	14.08	5.62	7.10	1.00	11.80	11.02	1.47	0.25	0.00	0.00	96.40	2.07	99.18
24-1191	E	48c	43.93	0.30	13.58	3.54	9.29	1.02	12.52	10.93	1.49	0.22	0.00	0.00	95.89	2.07	98.89
24-1191	E	49r	42.07	0.23	15.59	6.31	9.56	1.04	9.74	10.60	1.53	0.31	0.00	0.00	96.02	2.04	99.02
24-1191	G	50	41.76	0.15	15.22	7.19	8.51	0.87	9.83	11.04	1.47	0.30	0.16	0.00	95.65	2.02	98.52
Zone 5, core ave(7)			43.51	0.28	14.27	5.77	8.24	1.01	11.16	10.94	1.47	0.25	0.05	0.00	96.13	2.05	99.00
stdev			1.06	0.07	0.76	1.08	0.85	0.06	0.99	0.14	0.03	0.04	0.08	0.00	0.27	0.02	0.23
24-1191	I	7r	44.36	0.38	13.62	6.73	6.96	0.88	11.66	11.34	1.43	0.26	0.00	0.00	96.93	2.07	99.69
24-1191	I	8c	44.53	0.46	13.02	7.13	6.22	0.89	11.90	11.54	1.35	0.27	0.00	0.00	96.69	2.06	99.37
24-1191	I	9r	43.17	0.32	14.88	6.77	8.66	0.99	10.42	10.98	1.48	0.32	0.00	0.00	97.12	2.06	100.05
24-1191	I	52	44.01	0.33	13.24	6.24	7.88	0.89	11.49	11.07	1.41	0.20	0.00	0.00	95.98	2.05	98.82
24-1191	I	53	44.00	0.36	13.43	4.66	9.71	0.74	11.73	10.64	1.44	0.23	0.00	0.00	95.97	2.06	99.00
Zone 4, ave(5)			44.01	0.37	13.64	6.31	7.89	0.88	11.44	11.11	1.42	0.26	0.00	0.00	96.54	2.06	99.39
stdev			0.47	0.05	0.65	0.87	1.23	0.08	0.53	0.31	0.04	0.04	0.00	0.00	0.48	0.01	0.45
24-1191	K	54	42.75	0.55	14.22	5.97	8.45	0.78	11.38	11.35	1.47	0.28	0.19	0.48	97.02	1.83	99.49
24-1191	K	55	42.71	0.43	14.45	6.40	8.78	0.81	10.78	11.10	1.40	0.29	0.00	0.00	96.27	2.05	99.19
24-1191	K	56	43.85	0.32	12.50	6.63	7.83	0.76	11.78	11.38	1.34	0.24	0.00	0.00	95.85	2.04	98.67
24-1191	J	19c	42.87	0.50	14.99	8.79	5.90	0.68	10.31	11.37	1.57	0.29	0.00	0.00	96.68	2.04	99.31
24-1191	J	20r	43.52	0.19	14.31	8.14	6.32	0.79	10.73	11.46	1.39	0.27	0.00	0.00	96.49	2.05	99.17
24-1191	J	15c	44.77	0.25	12.41	6.48	7.79	0.72	12.03	11.45	1.19	0.24	0.00	0.00	96.56	2.06	99.40
24-1191	J	16r	52.12	0.00	3.40	5.23	5.97	0.57	16.69	11.54	0.30	0.00	0.00	0.00	95.23	2.08	97.91
24-1191	H	4r	44.37	0.35	12.89	9.06	6.55	0.87	10.47	11.39	1.20	0.23	0.00	0.00	96.72	2.05	99.42
24-1191	K	25c	42.22	0.47	15.45	7.07	7.24	0.67	10.75	11.33	1.54	0.35	0.00	0.00	96.37	2.05	99.14
24-1191	K	26r	45.46	0.36	12.68	6.76	7.54	0.86	11.79	11.26	1.24	0.25	0.00	0.00	97.45	2.08	100.29
Zone 3, core ave(3)			43.29	0.41	14.28	7.45	6.98	0.69	11.03	11.38	1.43	0.29	0.00	0.00	96.54	2.05	99.29
stdev			1.08	0.11	1.34	0.98	0.79	0.02	0.73	0.05	0.17	0.04	0.00	0.00	0.13	0.01	0.11
24-1191	M	21c	51.41	0.14	5.31	5.98	5.11	0.77	15.93	11.91	0.49	0.10	0.00	0.00	96.64	2.10	99.25
24-1191	M	22r	51.49	0.15	5.25	7.56	3.47	0.71	15.72	12.39	0.50	0.08	0.00	0.00	96.98	2.09	99.42
24-1191	L	10c	54.92	0.07	2.51	6.44	2.09	0.67	18.07	12.55	0.23	0.00	0.00	0.00	97.34	2.13	99.68
24-1191	L	11r	53.17	0.10	4.00	7.31	4.11	0.66	16.25	12.07	0.36	0.06	0.00	0.00	97.68	2.12	100.21
Zone 2, ave(4)			52.75	0.12	4.27	6.83	3.69	0.70	16.49	12.23	0.40	0.06	0.00	0.00	97.16	2.11	99.64
stdev			0.47	0.05	0.65	0.87	1.23	0.08	0.53	0.31	0.04	0.04	0.00	0.00	0.48	0.01	0.45
34A-1484	C	22	42.09	0.25	14.22	9.70	12.33	0.23	7.25	9.61	1.32	0.13	0.00	0.00	95.90	2.02	99.15
34A-1484	C	25	41.73	0.28	15.06	9.09	12.77	0.23	6.85	8.77	1.27	0.20	0.00	0.00	94.98	2.01	98.27
34A-1484	C	26	42.79	0.23	14.03	9.84	11.87	0.26	7.38	9.41	1.34	0.16	0.00	0.00	96.12	2.03	99.33
34A-1484	D	28	41.53	0.25	14.95	8.29	13.32	0.30	7.16	8.89	1.29	0.13	0.00	0.00	94.78	2.01	98.12
34A-1484	D	29	42.94	0.22	13.75	6.49	16.29	0.36	7.81	7.68	1.11	0.20	0.00	0.00	95.23	2.05	98.91
ave(5)			42.22	0.25	14.40	8.68	13.32	0.28	7.29	8.87	1.27	0.16	0.00	0.00	95.40	2.02	98.76
stdev			0.56	0.02	0.52	1.22	1.56	0.05	0.31	0.67	0.08	0.03	0.00	0.00	0.52	0.01	0.48
34B-759.5		1a	53.55	0.12	3.47	8.36	0.56	0.19	17.77	13.43	0.25	0.12	0.00	0.00	97.76	2.12	99.93
34B-759.5		2a	53.08	0.09	3.86	7.80	1.78	0.23	17.44	13.15	0.26	0.22	0.00	0.00	97.73	2.12	100.02
34B-759.5		3a	55.39	0.00	2.04	6.78	0.93	0.32	19.20	13.55	0.12	0.00	0.00	0.00	98.24	2.15	100.48
34B-759.5		4a	51.37	0.17	5.22	8.51	0.51	0.30	16.87	13.34	0.38	0.35	0.00	0.00	96.97	2.09	99.11
34B-759.5		5a	52.96	0.10	3.73	7.24	1.18	0.28	18.02	13.38	0.23	0.19	0.00	0.00	97.19	2.11	99.42
34B-759.5		6a	51.42	0.12	5.29	9.08	0.47	0.24	16.61	13.35	0.37	0.41	0.00	0.00	97.31	2.09	99.45
34B-759.5		7a	52.73	0.15	4.03	8.28	0.55	0.27	17.32	13.22	0.26	0.21	0.00	0.00	96.96	2.10	99.11
34B-759.5		8a	54.30	0.00	3.42	8.00	0.01	0.20	18.40	13.60	0.25	0.18	0.00	0.00	98.36	2.14	100.50
ave(8)			53.10	0.09	3.88	8.01	0.75	0.25	17.70	13.38	0.27	0.21	0.00	0.00	97.57	2.11	99.75
stdev			1.27	0.06	0.97	0.68	0.50	0.04	0.79	0.14	0.08	0.12	0.00	0.00	0.51	0.02	0.53

Table B.3. h. Calcic Amphibole Mineral Chemistry. (continued)

			Structural formula normalized to (T+M1+M2+M3)=13 and 46 anionic charges															
							C-site=5					B-site=2					F+OH=2	
Sample	area	spot	Si	Al_{iv}	Al_{vi}	Ti	Fe^{+3}	Fe^{+2}	Mn	Mg	Zn	Ca	Na	Na	K	site	F	OH
22-413	B	12	6.084	1.916	.872	.034	1.244	1.317	.038	1.495	.000	1.585	.415	.095	.052	.147	.000	2.000
22-413	B	15	6.066	1.934	.899	.036	1.011	1.547	.034	1.473	.000	1.688	.312	.216	.049	.265	.000	2.000
22-413	C	17	6.059	1.941	.932	.039	1.403	1.087	.033	1.506	.000	1.480	.520	.000	.048	.048	.000	2.000
ave(3)			6.070	1.930	.901	.036	1.219	1.317	.035	1.491	.000	1.584	.416	.104	.049	.153	.000	2.000
stdev			.011	.011	.025	.002	.161	.188	.002	.014	.000	.085	.085	.088	.002	.089	.000	.000
24-1191	E	1c	6.476	1.524	.761	.034	.819	.629	.132	2.603	.021	1.713	.287	.126	.037	.163	.000	2.000
24-1191	E	2r	6.404	1.596	.802	.035	.843	.757	.128	2.435	.000	1.715	.285	.130	.037	.167	.000	2.000
24-1191	G	5r	6.385	1.615	.809	.032	.878	.773	.130	2.378	.000	1.710	.290	.109	.045	.154	.000	2.000
24-1191	G	6r	6.431	1.569	.835	.040	.774	.681	.123	2.547	.000	1.710	.290	.123	.046	.169	.000	2.000
24-1191	E	48c	6.371	1.629	.693	.033	1.014	.429	.125	2.706	.000	1.698	.302	.117	.041	.158	.000	2.000
24-1191	E	49r	6.181	1.819	.881	.025	1.057	.775	.129	2.133	.000	1.669	.331	.104	.058	.163	.000	2.000
24-1191	G	50	6.187	1.813	.846	.017	.949	.891	.109	2.171	.018	1.753	.247	.175	.057	.232	.000	2.000
Zone 5, ave(7)			6.348	1.652	.804	.031	.905	.705	.125	2.425	.006	1.710	.290	.126	.046	.172	.000	2.000
stdev			.108	.108	.057	.007	.097	.136	.007	.199	.009	.023	.023	.022	.008	.025	.000	.000
24-1191	I	7r	6.429	1.571	.756	.041	.760	.816	.108	2.519	.000	1.761	.239	.163	.048	.211	.000	2.000
24-1191	I	8c	6.478	1.522	.711	.050	.681	.867	.110	2.580	.000	1.799	.201	.180	.050	.230	.000	2.000
24-1191	I	9r	6.271	1.729	.819	.035	.947	.822	.122	2.256	.000	1.709	.291	.126	.059	.185	.000	2.000
24-1191	I	52	6.436	1.564	.718	.036	.868	.764	.110	2.504	.000	1.735	.265	.134	.037	.172	.000	2.000
24-1191	I	53	6.397	1.603	.699	.039	1.062	.567	.091	2.542	.000	1.657	.343	.063	.043	.106	.000	2.000
Zone 4, ave(5)			6.402	1.598	.741	.040	.864	.767	.108	2.480	.000	1.732	.268	.133	.047	.181	.000	2.000
stdev			.071	.071	.044	.005	.134	.105	.010	.115	.000	.048	.048	.040	.007	.042	.000	.000
24-1191	K	54	6.242	1.758	.689	.060	.928	.729	.096	2.476	.020	1.776	.224	.192	.052	.244	.222	1.778
24-1191	K	55	6.254	1.746	.748	.047	.968	.783	.100	2.352	.000	1.742	.258	.139	.054	.193	.000	2.000
24-1191	K	56	6.444	1.556	.609	.035	.866	.815	.095	2.580	.000	1.792	.208	.174	.045	.219	.000	2.000
24-1191	J	19c	6.287	1.713	.878	.055	.651	1.078	.084	2.253	.000	1.787	.213	.233	.054	.287	.000	2.000
24-1191	J	20r	6.374	1.626	.845	.021	.697	.997	.098	2.342	.000	1.798	.202	.193	.050	.244	.000	2.000
24-1191	J	15c	6.509	1.491	.636	.027	.853	.788	.089	2.607	.000	1.784	.216	.119	.045	.164	.000	2.000
24-1191	J	16r	7.499	.501	.075	.000	.647	.630	.069	3.579	.000	1.779	.221	.000	.000	.000	.000	2.000
24-1191	H	4r	6.505	1.495	.733	.039	.723	1.110	.108	2.288	.000	1.789	.211	.130	.043	.173	.000	2.000
24-1191	K	25c	6.185	1.815	.853	.052	.799	.866	.083	2.347	.000	1.778	.222	.216	.065	.281	.000	2.000
24-1191	K	26r	6.544	1.456	.696	.039	.817	.814	.105	2.529	.000	1.737	.263	.083	.046	.129	.000	2.000
Zone 3, core ave(3)			6.327	1.673	.789	.045	.768	.911	.085	2.402	.000	1.783	.217	.189	.055	.244	.000	2.000
stdev			.135	.135	.109	.012	.085	.122	.002	.149	.000	.003	.003	.050	.009	.057	.000	.000
24-1191	M	21c	7.343	.657	.237	.015	.549	.715	.093	3.391	.000	1.823	.177	.000	.018	.018	.000	2.000
24-1191	M	22r	7.375	.625	.262	.016	.375	.906	.086	3.356	.000	1.902	.098	.040	.015	.055	.000	2.000
24-1191	L	10c	7.728	.272	.144	.007	.221	.758	.080	3.789	.000	1.892	.108	.000	.000	.000	.000	2.000
24-1191	L	11r	7.518	.482	.184	.011	.437	.864	.079	3.424	.000	1.829	.171	.000	.011	.011	.000	2.000
Zone 2, ave(4)			7.491	.509	.207	.012	.395	.811	.085	3.490	.000	1.861	.139	.010	.011	.021	.000	2.000
stdev			.071	.071	.044	.005	.134	.105	.010	.115	.000	.048	.048	.040	.007	.042	.000	.000
34A-1484	C	22	6.258	1.742	.750	.028	1.380	1.206	.029	1.606	.000	1.531	.469	.000	.025	.025	.000	2.000
34A-1484	C	25	6.213	1.787	.856	.031	1.431	1.132	.029	1.520	.000	1.399	.601	.000	.038	.038	.000	2.000
34A-1484	C	26	6.330	1.670	.776	.026	1.321	1.217	.033	1.627	.000	1.491	.509	.000	.030	.030	.000	2.000
34A-1484	D	28	6.189	1.811	.816	.028	1.494	1.034	.038	1.590	.000	1.420	.580	.000	.025	.025	.000	2.000
34A-1484	D	29	6.275	1.725	.644	.024	1.792	.794	.045	1.701	.000	1.203	.797	.000	.037	.037	.000	2.000
ave(5)			6.253	1.747	.769	.027	1.484	1.077	.035	1.609	.000	1.409	.591	.000	.031	.031	.000	2.000
stdev			.049	.049	.072	.002	.164	.156	.006	.058	.000	.114	.114	.000	.006	.006	.000	.000
34B-759.5		1a	7.585	.415	.164	.013	.059	.990	.023	3.751	.000	2.038	.000	.069	.022	.090	.000	2.000
34B-759.5		2a	7.521	.479	.166	.010	.189	.925	.028	3.683	.000	1.997	.003	.068	.040	.108	.000	2.000
34B-759.5		3a	7.738	.262	.074	.000	.098	.792	.038	3.998	.000	2.028	.000	.033	.000	.033	.000	2.000
34B-759.5		4a	7.375	.625	.259	.018	.055	1.022	.036	3.610	.000	2.052	.000	.106	.064	.170	.000	2.000
34B-759.5		5a	7.527	.473	.152	.011	.126	.860	.034	3.817	.000	2.038	.000	.063	.034	.098	.000	2.000
34B-759.5		6a	7.374	.626	.268	.013	.051	1.089	.029	3.550	.000	2.051	.000	.103	.075	.178	.000	2.000
34B-759.5		7a	7.535	.465	.214	.016	.059	.989	.033	3.689	.000	2.024	.000	.072	.038	.110	.000	2.000
34B-759.5		8a	7.621	.379	.187	.000	.001	.940	.024	3.849	.000	2.045	.000	.068	.032	.100	.000	2.000
ave(8)			7.535	.465	.186	.010	.080	.951	.031	3.743	.000	2.034	.000	.073	.038	.111	.000	2.000
stdev			.113	.113	.059	.006	.054	.087	.005	.134	.000	.017	.001	.022	.022	.043	.000	.000

Table B.3. i. Fe-Mg Amphibole Mineral Chemistry.

			weight percent oxide or element (Cr_2O_3, K_2O and ZnO not detected)											
Sample	area	spot	SiO_2	TiO_2	Al_2O_3	FeO	MnO	MgO	CaO	Na_2O	F	Total	H_2O	Total
22-413	A	cm10	52.86	0.00	0.94	27.45	0.57	14.87	0.39	0.00	0.00	97.08	2.00	99.08
22-413	A	cm11	52.47	0.00	1.34	26.95	0.58	14.91	0.47	0.10	0.00	96.82	2.00	98.82
22-413	B	cm13	52.34	0.00	1.15	27.46	0.72	14.06	0.40	0.06	0.00	96.19	1.98	98.17
22-413	B	cm14	52.59	0.00	1.17	27.54	0.62	14.34	0.44	0.10	0.00	96.80	1.99	98.79
22-413	C	cm16	52.72	0.00	1.05	26.74	0.59	15.06	0.30	0.06	0.00	96.52	1.99	98.51
ave(5)			52.60	0.00	1.13	27.23	0.62	14.65	0.40	0.06	0.00	96.68	1.99	98.67
stdev			0.18	0.00	0.13	0.32	0.05	0.38	0.06	0.04	0.00	0.30	0.01	0.31
24-1131		an1a	54.15	0.00	2.69	19.82	0.96	19.85	0.35	0.00	0.30	98.24	1.95	100.06
24-1131		an11a	53.45	0.00	3.49	20.39	1.10	19.08	0.37	0.26	0.27	98.42	1.96	100.27
24-1131		an12a	52.78	0.00	4.36	20.16	1.10	19.00	0.41	0.29	0.20	98.31	1.99	100.22
24-1131		an10a	55.35	0.00	1.58	19.55	0.88	20.37	0.26	0.00	0.32	98.36	1.95	100.18
24-1131		an8a	52.81	0.00	3.99	20.35	1.01	18.91	0.34	0.27	0.28	97.97	1.94	99.80
24-1131		an5a	52.17	0.00	4.05	20.02	0.91	19.06	0.36	0.29	0.25	97.13	1.94	98.97
24-1131		an6a	53.56	0.00	2.44	19.84	0.94	19.84	0.31	0.00	0.22	97.29	1.96	99.16
24-1131		an7a	53.46	0.00	3.50	19.70	0.65	19.79	0.32	0.21	0.28	97.92	1.96	99.76
24-1131		an3a	52.15	0.00	5.37	20.02	0.84	19.07	0.37	0.41	0.21	98.47	1.99	100.37
24-1131		an4a	52.57	0.00	4.41	19.72	0.98	19.03	0.36	0.25	0.30	97.62	1.93	99.43
ave(10)			53.25	0.00	3.59	19.96	0.94	19.40	0.35	0.20	0.26	97.97	1.96	99.82
stdev			0.93	0.00	1.05	0.27	0.13	0.49	0.04	0.14	0.04	0.46	0.02	0.47
34A-1484	A	cm18	52.42	0.00	0.96	27.79	0.55	14.29	0.28	0.07	0.00	96.36	1.98	98.34
34A-1484	B	cm19	52.80	0.00	1.06	27.59	0.52	14.28	0.28	0.08	0.00	96.61	1.99	98.60
34A-1484	B	cm20	52.28	0.06	1.15	27.70	0.52	14.05	0.30	0.11	0.00	96.17	1.98	98.15
34A-1484	B	cm21	52.43	0.00	1.13	26.89	0.50	14.46	0.32	0.10	0.00	95.83	1.98	97.81
34A-1484	C	cm23	52.59	0.00	0.89	27.76	0.54	14.25	0.38	0.10	0.00	96.51	1.98	98.49
34A-1484	C	cm24	52.51	0.00	1.37	27.17	0.57	14.21	0.59	0.12	0.00	96.54	1.99	98.53
34A-1484	C	cm27	52.50	0.00	0.88	27.34	0.58	14.47	0.27	0.09	0.00	96.13	1.98	98.11
ave(7)			52.50	0.01	1.06	27.46	0.54	14.29	0.35	0.10	0.00	96.31	1.98	98.29
stdev			0.15	0.02	0.16	0.32	0.03	0.13	0.11	0.02	0.00	0.26	0.00	0.26

			Structural formula normalized to 46 anionic charges											F+OH=2	
Sample	area	spot	Si	Al_{iv}	Al_{vi}	Ti	Fe_t	Mn	Mg	Ca	site	Na	site	F	OH
22-413	A	cm10	7.925	0.075	0.092	0.000	3.442	0.072	3.323	0.063	6.991	0.000	0.000	0.000	2.000
22-413	A	cm11	7.879	0.121	0.117	0.000	3.385	0.074	3.337	0.076	6.987	0.029	0.029	0.000	2.000
22-413	B	cm13	7.934	0.066	0.139	0.000	3.481	0.092	3.176	0.065	6.954	0.018	0.018	0.000	2.000
22-413	B	cm14	7.919	0.081	0.127	0.000	3.468	0.079	3.218	0.071	6.963	0.029	0.029	0.000	2.000
22-413	C	cm16	7.926	0.074	0.112	0.000	3.362	0.075	3.374	0.048	6.972	0.017	0.017	0.000	2.000
ave(5)			7.917	0.083	0.117	0.000	3.428	0.079	3.286	0.065	6.974	0.019	0.019	0.000	2.000
stdev			0.019	0.019	0.016	0.000	0.047	0.007	0.075	0.009	0.014	0.011	0.011	0.000	0.000
24-1131		an1a	7.764	0.236	0.219	0.000	2.377	0.117	4.242	0.054	7.008	0.000	0.000	0.136	1.864
24-1131		an11a	7.677	0.323	0.268	0.000	2.449	0.134	4.084	0.057	6.992	0.072	0.072	0.123	1.877
24-1131		an12a	7.582	0.418	0.321	0.000	2.422	0.134	4.068	0.063	7.008	0.081	0.081	0.091	1.909
24-1131		an10a	7.896	0.104	0.162	0.000	2.332	0.106	4.331	0.040	6.971	0.000	0.000	0.144	1.856
24-1131		an8a	7.622	0.378	0.301	0.000	2.456	0.123	4.067	0.053	7.001	0.076	0.076	0.128	1.872
24-1131		an5a	7.590	0.410	0.285	0.000	2.436	0.112	4.133	0.056	7.022	0.082	0.082	0.115	1.885
24-1131		an6a	7.761	0.239	0.178	0.000	2.404	0.115	4.285	0.048	7.030	0.000	0.000	0.101	1.899
24-1131		an7a	7.676	0.324	0.269	0.000	2.366	0.079	4.235	0.049	6.998	0.058	0.058	0.127	1.873
24-1131		an3a	7.475	0.525	0.382	0.000	2.400	0.102	4.074	0.057	7.015	0.114	0.114	0.095	1.905
24-1131		an4a	7.593	0.407	0.343	0.000	2.382	0.120	4.096	0.056	6.997	0.070	0.070	0.137	1.863
ave(10)			7.664	0.336	0.273	0.000	2.402	0.114	4.161	0.053	7.004	0.055	0.055	0.120	1.880
stdev			0.113	0.113	0.067	0.000	0.037	0.015	0.096	0.006	0.016	0.039	0.039	0.018	0.018
34A-1484	A	cm18	7.937	0.063	0.108	0.000	3.519	0.071	3.224	0.045	6.967	0.021	0.021	0.000	2.000
34A-1484	B	cm19	7.956	0.044	0.144	0.000	3.477	0.066	3.207	0.045	6.939	0.023	0.023	0.000	2.000
34A-1484	B	cm20	7.929	0.071	0.134	0.007	3.513	0.067	3.176	0.049	6.946	0.032	0.032	0.000	2.000
34A-1484	B	cm21	7.946	0.054	0.148	0.000	3.408	0.064	3.266	0.052	6.938	0.029	0.029	0.000	2.000
34A-1484	C	cm23	7.949	0.051	0.107	0.000	3.509	0.069	3.210	0.062	6.957	0.029	0.029	0.000	2.000
34A-1484	C	cm24	7.916	0.084	0.159	0.000	3.425	0.073	3.192	0.095	6.945	0.035	0.035	0.000	2.000
34A-1484	C	cm27	7.952	0.048	0.109	0.000	3.463	0.074	3.266	0.044	6.957	0.026	0.026	0.000	2.000
ave(7)			7.940	0.060	0.130	0.001	3.474	0.069	3.220	0.056	6.950	0.028	0.028	0.000	2.000
stdev			0.013	0.013	0.020	0.002	0.041	0.003	0.032	0.017	0.010	0.005	0.005	0.000	0.000

Table B.3. j. Epidote Mineral Chemistry.

			weight percent oxide or element (Cr_2O_3 and F not detected)												
Sample	area	spot	SiO_2	TiO_2	Al_2O_3	Fe_2O_3	MnO	MgO	BaO	CaO	Na_2O	K_2O	Total	H_2O	Total
34-1028.5	B	30c	38.41	0.09	26.75	8.41	0.29	0.04	0.00	22.62	0.00	0.00	96.61	1.90	98.51
34-1028.5	B	31r	38.36	0.07	26.97	8.16	0.31	0.07	0.00	21.23	0.00	0.00	95.17	1.88	97.05
34-1028.5	B	32r	37.62	0.09	26.20	9.22	0.33	0.04	0.00	22.39	0.00	0.00	95.89	1.88	97.77
34-1028.5	A	34c	38.00	0.08	26.92	8.38	0.28	0.05	0.00	22.08	0.00	0.00	95.79	1.88	97.67
34-1028.5	A	35r	38.12	0.10	26.96	8.51	0.38	0.07	0.00	20.69	0.00	0.00	94.83	1.87	96.71
ave(5)			38.10	0.09	26.76	8.54	0.32	0.05	0.00	21.80	0.00	0.00	95.66	1.88	97.54
stdev			0.28	0.01	0.29	0.36	0.04	0.01	0.00	0.73	0.00	0.00	0.62	0.01	0.62
22B-1843	A	19c	36.75	1.61	25.89	8.23	0.14	0.08	0.00	22.04	0.00	0.04	94.78	1.86	96.64
22B-1843	A	20r	35.33	0.28	23.10	7.77	0.71	2.33	0.00	17.50	0.11	1.27	88.40	1.73	90.13
22B-1843	A	21	38.55	0.06	26.96	7.93	0.34	0.00	0.00	22.36	0.00	0.00	96.20	1.90	98.10
22B-1843	A	22	37.00	0.11	25.02	8.22	0.50	0.12	0.00	22.01	0.00	0.00	92.98	1.82	94.81
22B-1843	B	25c	38.67	0.05	27.57	7.91	0.18	0.06	0.00	21.88	0.00	0.00	96.32	1.90	98.23
22B-1843	B	26r	38.52	0.12	27.37	7.91	0.29	0.00	0.00	23.04	0.00	0.00	97.25	1.91	99.17
ave(5)			37.90	0.39	26.56	8.04	0.29	0.05	0.00	22.27	0.00	0.01	95.51	1.88	97.39
stdev			0.84	0.61	0.97	0.15	0.13	0.05	0.00	0.42	0.00	0.02	1.49	0.03	1.52
22B-1721	D	9	38.02	0.00	25.76	9.55	0.74	0.04	0.00	20.62	0.00	0.00	94.73	1.86	96.59
24-1191	H	3c	38.54	0.10	25.87	9.40	0.42	0.07	0.00	22.56	0.00	0.00	96.96	1.90	98.86
24-1191	L	12c	38.09	0.07	25.69	10.05	0.45	0.09	0.00	23.18	0.00	0.00	97.62	1.90	99.52
24-1191	L	13	37.99	0.00	24.86	10.85	0.32	0.00	0.00	22.81	0.00	0.00	96.83	1.88	98.71
24-1191	J	14	38.44	0.08	24.68	10.80	0.35	0.00	0.00	23.01	0.00	0.00	97.36	1.89	99.25
24-1191	J	17c	38.07	0.06	24.98	10.74	0.38	0.00	0.00	22.95	0.00	0.00	97.18	1.89	99.06
24-1191	J	18r	38.40	0.10	25.34	10.42	0.35	0.00	0.00	23.12	0.00	0.00	97.73	1.90	99.64
Zone 3, ave(6)			38.26	0.07	25.24	10.38	0.38	0.03	0.00	22.94	0.00	0.00	97.28	1.89	99.17
stdev			0.21	0.03	0.43	0.52	0.04	0.04	0.00	0.21	0.00	0.00	0.33	0.01	0.33
24-1191	M	23c	38.21	0.08	25.27	10.46	0.39	0.00	0.00	22.33	0.00	0.00	96.74	1.89	98.62
24-1191	M	24c	38.21	0.00	24.79	10.92	0.32	0.14	0.00	22.41	0.00	0.00	96.79	1.88	98.68
Zone 6, ave(2)			38.21	0.04	25.03	10.69	0.36	0.07	0.00	22.37	0.00	0.00	96.77	1.89	98.65
34B-759.5	C	11	37.65	0.09	27.42	7.38	0.00	0.00	na	24.72	0.00	0.00	96.66	1.90	99.30
34B-759.5	C	12	37.45	0.12	26.66	8.69	0.14	0.00	na	24.43	0.00	0.00	96.70	1.90	99.47
34B-759.5	A	13	38.20	0.00	27.15	7.78	0.14	0.12	na	24.39	0.00	0.00	97.07	1.91	99.76
34B-759.5	A	14	37.85	0.09	25.70	9.26	0.13	0.00	na	24.38	0.00	0.00	96.57	1.89	99.39
34B-759.5	B	15	37.86	0.00	26.82	8.60	0.00	0.00	na	24.63	0.00	0.00	97.24	1.91	100.01
34B-759.5	B	16	37.04	0.00	25.80	8.37	0.00	0.00	na	24.05	0.00	0.00	94.60	1.86	97.30
ave(6)			37.68	0.05	26.59	8.35	0.07	0.02		24.43	0.00	0.00	96.47	1.90	99.21
stdev			0.36	0.05	0.64	0.62	0.07	0.04		0.21	0.00	0.00	0.87	0.02	0.89

Table B.3. j. Epidote Mineral Chemistry. (continued)

			Structural formula normalized to 23 anionic charges, F+OH=1											
Sample	area	spot	Si	Al_{iv}	Al_{vi}	Fe^{+3}	site	Ti	Mn	Mg	Ca	Na	K	site
34-1028.5	B	30c	3.033	0.000	2.490	0.500	2.990	0.005	0.019	0.005	1.914	0.000	0.000	1.943
34-1028.5	B	31r	3.057	0.000	2.534	0.489	3.023	0.004	0.021	0.008	1.813	0.000	0.000	1.846
34-1028.5	B	32r	3.006	0.000	2.468	0.555	3.022	0.005	0.022	0.005	1.917	0.000	0.000	1.949
34-1028.5	A	34c	3.023	0.000	2.524	0.502	3.026	0.005	0.019	0.006	1.882	0.000	0.000	1.911
34-1028.5	A	35r	3.049	0.000	2.542	0.512	3.055	0.006	0.026	0.008	1.773	0.000	0.000	1.813
ave(5)			3.034	0.000	2.512	0.512	3.023	0.005	0.021	0.006	1.860	0.000	0.000	1.893
stdev			0.018	0.000	0.028	0.023	0.020	0.001	0.002	0.002	0.057	0.000	0.000	0.054
22B-1843	A	19c	2.966	0.034	2.429	0.500	2.930	0.098	0.010	0.010	1.906	0.000	0.004	2.027
22B-1843	A	20r	3.057	0.000	2.357	0.506	2.863	0.018	0.052	0.301	1.623	0.018	0.140	2.152
22B-1843	A	21	3.048	0.000	2.513	0.472	2.986	0.004	0.023	0.000	1.895	0.000	0.000	1.921
22B-1843	A	22	3.045	0.000	2.428	0.509	2.937	0.007	0.035	0.015	1.941	0.000	0.000	1.997
22B-1843	B	25c	3.044	0.000	2.559	0.469	3.027	0.003	0.012	0.007	1.846	0.000	0.000	1.868
22B-1843	B	26r	3.019	0.000	2.529	0.467	2.996	0.007	0.019	0.000	1.935	0.000	0.000	1.961
ave(5)			3.025	0.007	2.492	0.483	2.975	0.024	0.020	0.006	1.904	0.000	0.001	1.955
stdev			0.031	0.014	0.054	0.018	0.037	0.037	0.009	0.006	0.034	0.000	0.002	0.056
22B-1721	D	9	3.063	0.000	2.447	0.579	3.026	0.000	0.051	0.005	1.780	0.000	0.000	1.835
24-1191	H	3c	3.045	0.000	2.409	0.559	2.968	0.006	0.028	0.008	1.910	0.000	0.000	1.952
24-1191	L	12c	3.006	0.000	2.390	0.597	2.986	0.004	0.030	0.011	1.960	0.000	0.000	2.005
24-1191	L	13	3.027	0.000	2.335	0.650	2.985	0.000	0.022	0.000	1.947	0.000	0.000	1.969
24-1191	J	14	3.045	0.000	2.305	0.644	2.949	0.005	0.023	0.000	1.953	0.000	0.000	1.981
24-1191	J	17c	3.023	0.000	2.338	0.641	2.980	0.004	0.026	0.000	1.952	0.000	0.000	1.982
24-1191	J	18r	3.027	0.000	2.355	0.618	2.973	0.006	0.023	0.000	1.953	0.000	0.000	1.982
Zone 3, ave(6)			3.029	0.000	2.355	0.618	2.974	0.004	0.025	0.003	1.946	0.000	0.000	1.978
stdev			0.014	0.000	0.035	0.032	0.013	0.002	0.003	0.004	0.017	0.000	0.000	0.016
24-1191	M	23c	3.037	0.000	2.368	0.625	2.993	0.005	0.026	0.000	1.901	0.000	0.000	1.933
24-1191	M	24c	3.041	0.000	2.326	0.654	2.980	0.000	0.022	0.017	1.911	0.000	0.000	1.949
Zone 2, ave(2)			3.039	0.000	2.347	0.640	2.986	0.002	0.024	0.008	1.906	0.000	0.000	1.941
34B-759.5	C	11	2.965	0.035	2.510	0.437	2.947	0.005	0.000	0.000	2.086	0.000	0.000	2.091
34B-759.5	C	12	2.957	0.043	2.438	0.516	2.954	0.007	0.009	0.000	2.067	0.000	0.000	2.083
34B-759.5	A	13	2.991	0.009	2.498	0.458	2.956	0.000	0.009	0.014	2.047	0.000	0.000	2.070
34B-759.5	A	14	2.995	0.005	2.393	0.551	2.944	0.005	0.009	0.000	2.067	0.000	0.000	2.081
34B-759.5	B	15	2.972	0.028	2.454	0.508	2.962	0.000	0.000	0.000	2.072	0.000	0.000	2.072
34B-759.5	B	16	2.989	0.011	2.443	0.508	2.951	0.000	0.000	0.000	2.079	0.000	0.000	2.079
ave(6)			2.978	0.022	2.456	0.497	2.952	0.003	0.005	0.002	2.069	0.000	0.000	2.079
stdev			0.014	0.014	0.039	0.038	0.006	0.003	0.005	0.005	0.012	0.000	0.000	0.007

Table B.3. k. Kyanite Mineral Chemistry.

		weight percent oxide (Cr_2O_3, TiO_2, MnO, MgO and ZnO not detected)				Structural formula normalized to 10 anionic charges			
Sample	spot	SiO_2	Al_2O_3	Fe_2O_3	Total	Si	Al	Fe^{+3}	site
22A-1638	4	37.38	62.31	0.24	99.93	1.009	1.983	0.007	1.990
22A-1638	16	36.69	62.83	0.28	99.80	0.993	2.004	0.008	2.013
22-901	3	36.76	61.32	0.47	98.55	1.007	1.981	0.014	1.995
34C-1747.5	17	36.26	60.85	0.77	97.88	1.002	1.982	0.024	2.006
34C-1747.5	18	36.22	61.42	0.46	98.10	0.997	1.994	0.014	2.008
34C-1377	5	37.33	61.28	0.27	98.88	1.018	1.970	0.008	1.979
34-1500	16	36.23	61.61	0.00	97.84	0.999	2.002	0.000	2.002
34-1500	17	36.41	61.36	0.00	97.77	1.004	1.995	0.000	1.995
34-1500	18	36.38	61.65	0.00	98.03	1.001	1.999	0.000	1.999
22A-1752	19	36.40	62.38	0.30	99.08	0.992	2.004	0.009	2.014
22A-1752	20	36.89	62.64	0.34	99.87	0.997	1.997	0.011	2.007
22A-1752	21	36.44	63.24	0.40	100.08	0.984	2.013	0.012	2.025

Table B.3. l. Tourmaline Mineral Chemistry.

		weight percent oxide or element (Cr_2O_3, BaO, K_2O and ZnO not detected)												
Sample	spot	SiO_2	TiO_2	Al_2O_3	FeO	MnO	MgO	CaO	Na_2O	F	Total	H_2O	B_2O_3	Total
22A-1638	1c	37.15	0.27	32.53	2.60	0.00	9.61	1.15	1.87	0.72	85.90	3.37	10.77	99.74
22A-1638	2r	35.45	0.33	33.25	3.34	0.00	9.14	1.00	2.04	0.63	85.18	3.36	10.62	98.90
34C-1377	22c	35.95	0.33	32.64	3.42	0.00	9.48	1.13	1.86	0.74	85.55	3.32	10.65	99.21
34C-1377	23r	36.56	0.33	33.26	3.01	0.00	9.60	1.04	1.92	0.74	86.46	3.38	10.80	100.33
34C-1377	24c	36.93	0.12	34.37	3.46	0.08	8.50	0.35	1.76	0.57	86.14	3.46	10.82	100.19
34C-1377	25r	35.95	0.38	33.60	3.21	0.00	9.41	1.06	1.92	0.75	86.28	3.35	10.76	100.08
34C-1377	26c	37.31	0.15	34.22	3.47	0.00	8.48	0.37	1.76	0.00	85.76	3.74	10.86	100.36
34C-1377	27r	36.67	0.33	33.09	2.90	0.00	9.60	1.02	1.91	0.67	86.19	3.40	10.79	100.10

		Structural formula normalized to 49 anionic charges												F+OH=4		B=3
Sample	spot	Si	Al_{iv}	Al_z	Al_y	Ti	Fe	Mn	Mg	site	Ca	Na	site	F	OH	B
22A-1638	1c	5.997	0.003	6.000	0.188	0.033	0.351	0.000	2.312	2.883	0.199	0.585	0.784	0.368	3.632	3.000
22A-1638	2r	5.803	0.197	6.000	0.220	0.041	0.457	0.000	2.230	2.948	0.175	0.648	0.823	0.326	3.674	3.000
34C-1377	22c	5.867	0.133	6.000	0.147	0.041	0.467	0.000	2.306	2.960	0.198	0.589	0.786	0.382	3.618	3.000
34C-1377	23r	5.884	0.116	6.000	0.194	0.040	0.405	0.000	2.303	2.942	0.179	0.599	0.778	0.377	3.623	3.000
34C-1377	24c	5.932	0.068	6.000	0.440	0.014	0.465	0.011	2.035	2.965	0.060	0.548	0.608	0.290	3.710	3.000
34C-1377	25r	5.810	0.190	6.000	0.212	0.046	0.434	0.000	2.266	2.958	0.184	0.602	0.785	0.383	3.617	3.000
34C-1377	26c	5.974	0.026	6.000	0.434	0.018	0.465	0.000	2.024	2.941	0.063	0.546	0.610	0.000	4.000	3.000
34C-1377	27r	5.909	0.091	6.000	0.196	0.040	0.391	0.000	2.306	2.933	0.176	0.597	0.773	0.341	3.659	3.000

Table B.3. m. Plagioclase Mineral Chemistry.

			weight percent oxide						
Sample	area	spot	SiO_2	Al_2O_3	FeO	CaO	Na_2O	K_2O	Total
22-413	D	1	63.18	23.60	na	5.57	8.67	0.01	101.02
22-413	D	2	60.33	24.08	na	6.21	8.11	0.02	98.74
22-413	D	3	60.64	24.40	na	6.10	8.17	0.02	99.33
22-413	C	4	59.48	23.50	na	5.99	8.31	0.13	97.41
22-413	C	4a	62.63	23.07	na	4.79	8.94	0.03	99.45
22-413	C	6	63.35	22.55	0.00	4.64	9.31	0.04	99.92
22-413	C	7	60.99	23.93	0.00	5.71	8.40	0.04	99.10
22-413	C	8	60.16	24.07	0.36	5.85	8.34	0.05	98.83
22A-1752	H	1	61.87	23.59	0.00	5.65	8.44	0.04	99.60
22A-1752	H	2	63.80	23.25	0.00	5.04	8.97	0.06	101.12
22A-1752	H	3	64.88	22.17	0.00	5.10	8.50	0.06	100.70
22A-1752	H	4	64.41	22.90	0.00	4.72	9.04	0.07	101.19
22A-1752	H	4r	63.39	23.23	0.00	4.78	9.20	0.06	100.66
22A-1752	E	5	63.03	24.81	0.00	6.17	8.16	0.01	102.18
22A-1752	E	5r	62.26	24.31	0.00	6.56	8.07	0.03	101.31
22B-1721	D	1	56.26	26.49	0.44	8.07	6.61	0.09	97.96
22B-1721	D	1r	58.68	25.11	0.00	7.90	7.30	0.04	99.06
22B-1721	D	1e	62.48	24.06	0.00	7.92	6.31	0.04	100.80
22B-1721	D	1a	54.71	29.07	0.00	11.98	4.96	0.03	100.77
22B-1721	D	2	54.40	28.80	0.00	11.73	5.13	0.04	100.11
22B-1721	D	2e	53.84	29.42	0.00	12.41	5.01	0.04	100.77
22B-1721	D	2a	57.73	26.32	0.00	8.88	6.84	0.05	99.86
22B-1721	D	3	58.66	25.26	0.00	7.76	7.41	0.05	99.17
22B-1721	D	3e	58.54	26.50	0.00	8.38	7.09	0.06	100.59
22B-1721	D	3a	55.39	28.44	0.00	11.04	5.52	0.04	100.49
22B-1721	D	3b	56.74	27.19	0.13	10.21	6.03	0.06	100.36
22B-1721	E	4	59.25	25.62	0.00	8.44	7.03	0.06	100.43
22B-1721	E	4a	59.50	25.48	0.00	7.82	7.43	0.04	100.28
22B-1721	E	4b	57.52	26.23	0.00	8.60	6.97	0.04	99.41
22B-1721	E	4c	50.23	30.28	0.00	13.58	3.88	0.02	98.00
22B-1721	E	4d	52.46	28.18	0.00	11.57	5.11	0.04	97.36
22B-1721	E	4e	50.54	29.68	0.00	13.47	4.11	0.04	97.90
22B-1721	E	5	54.80	28.10	0.00	11.56	5.29	0.04	99.84
24-1131	A	1	45.12	35.31	0.00	19.74	0.36	0.01	100.61
24-1131	A	2	44.96	35.56	0.13	20.29	0.33	0.00	101.26
24-1131	A	3	45.13	35.42	0.15	19.97	0.35	0.00	101.02
zone 6									
24-1191	D	39c	55.61	29.60	0.00	10.76	5.04	0.05	101.06
24-1191	D	40r	58.18	27.60	0.00	8.61	6.30	0.00	100.69
24-1191	D	41c	61.36	25.39	0.00	6.25	7.70	0.06	100.76
24-1191	D	42r	60.12	25.97	0.00	6.89	7.25	0.05	100.28
24-1191	A	1	61.08	23.92	0.00	5.70	8.41	0.06	99.27
24-1191	A	2c	57.46	26.04	0.00	9.18	6.54	0.05	99.35
24-1191	A	2r	54.77	25.81	1.66	8.47	6.39	0.04	97.13
24-1191	C	3c	57.31	26.57	0.00	9.15	6.50	0.05	99.65
24-1191	C	3	61.49	23.84	0.00	5.83	8.34	0.05	99.54
24-1191	C	3r	56.79	26.07	0.00	8.98	6.66	0.05	98.63
24-1191	D	4c	56.87	25.95	0.00	8.72	6.67	0.06	98.36
24-1191	D	4r	57.92	25.87	0.18	8.50	6.81	0.05	99.33
zone 5									
24-1191	E	36c	61.42	24.90	0.00	5.70	7.85	0.00	99.87
24-1191	E	37	61.49	24.81	0.00	5.82	7.83	0.00	99.95
24-1191	E	38r	60.37	26.16	0.00	6.83	7.25	0.06	100.67
24-1191	G	5c	57.34	26.66	0.13	9.60	6.33	0.04	100.10
24-1191	G	5r	57.45	26.20	0.23	8.60	6.86	0.05	99.39
24-1191	G	6	52.21	29.65	0.47	12.78	4.33	0.03	99.46
24-1191	G	7	51.46	30.30	0.40	13.87	3.78	0.02	99.83
24-1191	G	8r	56.87	26.18	0.23	8.86	6.76	0.04	98.94
zone 4									
24-1191	I	33c	47.28	34.72	0.17	16.74	1.63	0.00	100.54
24-1191	I	34	47.82	33.89	0.00	15.91	2.12	0.00	99.74
24-1191	I	35r	47.13	35.03	0.11	16.84	1.52	0.00	100.63
24-1191	I	9	49.89	31.12	0.23	14.85	3.25	0.02	99.37
24-1191	I	9a	45.85	33.64	0.27	16.89	1.70	0.02	98.37
24-1191	I	9b	45.75	32.66	0.23	16.85	1.95	0.02	97.47
24-1191	I	9r	46.39	32.57	0.14	16.59	1.99	0.00	97.68

Table B.3. m. Plagioclase Mineral Chemistry. (continued)

			weight percent oxide						
Sample	area	spot	SiO_2	Al_2O_3	FeO	CaO	Na_2O	K_2O	Total
zone 3									
24-1191	H	27	47.24	34.55	0.00	16.48	1.64	0.00	99.91
24-1191	H	28	47.37	34.90	0.00	16.60	1.65	0.00	100.52
24-1191	H	29	48.21	34.68	0.00	16.07	1.92	0.00	100.88
24-1191	K	30	45.95	35.60	0.00	17.74	1.09	0.00	100.38
24-1191	K	31	46.18	35.30	0.00	17.66	1.08	0.00	100.22
24-1191	K	32	46.83	35.22	0.00	16.95	1.47	0.00	100.47
24-1191	K	10	45.31	34.11	0.11	18.49	1.01	0.00	99.03
24-1191	K	10a	46.71	33.89	0.00	18.24	1.24	0.00	100.18
24-1191	K	10b	44.83	33.44	0.54	17.46	1.34	0.00	97.59
24-1191	K	10d	45.43	34.08	0.13	18.55	1.09	0.00	99.27
34C-1377	I	1	59.28	24.84	0.00	7.35	7.61	0.05	99.14
34C-1377	I	1a	60.17	25.01	0.00	7.17	7.62	0.04	100.04
34C-1377	I	1b	60.76	25.43	0.00	7.07	7.64	0.04	100.95
34C-1377	I	2	59.11	25.05	0.00	7.16	7.64	0.03	99.00
34C-1377	I	3	59.75	25.02	0.00	7.14	7.64	0.19	99.74
34C-1377	E	5	61.17	25.14	0.00	5.78	8.08	0.07	100.24
34C-1377	E	6	60.82	26.08	0.18	4.24	8.30	0.18	99.80

Table B.3. m. Plagioclase Mineral Chemistry. (continued)

			Structural formula normalized to 64 anionic charges											
Sample	area	spot	Si	Al_{iv}	Fe	site	Ca	Na	K	site	Ab	An	Or	Comment
22-413	D	1	11.080	4.879	na	15.959	1.047	2.948	0.002	3.997	73.76	26.19	0.06	
22-413	D	2	10.860	5.110	na	15.970	1.198	2.831	0.005	4.033	70.19	29.70	0.11	
22-413	D	3	10.847	5.145	na	15.992	1.169	2.834	0.005	4.007	70.71	29.18	0.11	
22-413	C	4	10.872	5.064	na	15.936	1.173	2.945	0.030	4.149	70.99	28.28	0.73	
22-413	C	4a	11.142	4.839	na	15.980	0.913	3.084	0.007	4.004	77.02	22.81	0.17	
22-413	C	6	11.225	4.710	0.000	15.935	0.881	3.199	0.009	4.088	78.23	21.55	0.22	
22-413	C	7	10.929	5.055	0.000	15.984	1.096	2.918	0.009	4.024	72.53	27.25	0.23	
22-413	C	8	10.841	5.114	0.054	16.009	1.130	2.914	0.011	4.055	71.86	27.86	0.28	
22A-1752	H	1	11.016	4.952	0.000	15.968	1.078	2.914	0.009	4.001	72.83	26.94	0.23	within clast
22A-1752	H	2	11.165	4.797	0.000	15.962	0.945	3.044	0.013	4.002	76.05	23.61	0.33	within clast
22A-1752	H	3	11.363	4.578	0.000	15.941	0.957	2.887	0.013	3.857	74.84	24.81	0.35	within clast
22A-1752	H	4	11.252	4.716	0.000	15.968	0.883	3.062	0.016	3.961	77.30	22.30	0.39	within clast
22A-1752	H	4r	11.149	4.817	0.000	15.966	0.901	3.137	0.013	4.052	77.43	22.23	0.33	within clast
22A-1752	E	5	10.934	5.074	0.000	16.008	1.147	2.745	0.002	3.894	70.49	29.45	0.06	matrix
22A-1752	E	5r	10.924	5.029	0.000	15.952	1.233	2.745	0.007	3.985	68.89	30.95	0.17	matrix
22B-1721	D	1	10.297	5.716	0.067	16.080	1.583	2.346	0.021	3.949	59.40	40.07	0.53	grain 1: core
22B-1721	D	1r	10.589	5.342	0.000	15.931	1.528	2.554	0.009	4.091	62.44	37.34	0.23	grain 1: core
22B-1721	D	1e	10.977	4.984	0.000	15.961	1.491	2.150	0.009	3.649	58.90	40.85	0.25	grain 1: core
22B-1721	D	1a	9.808	6.144	0.000	15.953	2.301	1.724	0.007	4.032	42.76	57.07	0.17	grain 1: internal contact
22B-1721	D	2	9.819	6.128	0.000	15.947	2.269	1.795	0.009	4.073	44.08	55.70	0.23	grain 1: mantle
22B-1721	D	2e	9.685	6.239	0.000	15.925	2.392	1.747	0.009	4.149	42.12	57.66	0.22	grain 1: mantle
22B-1721	D	2a	10.368	5.573	0.000	15.940	1.709	2.382	0.011	4.102	58.06	41.66	0.28	grain 1: rim
22B-1721	D	3	10.574	5.368	0.000	15.942	1.499	2.590	0.011	4.100	63.16	36.55	0.28	grain 2: core
22B-1721	D	3e	10.417	5.559	0.000	15.976	1.598	2.446	0.014	4.058	60.29	39.38	0.34	grain 2: core
22B-1721	D	3a	9.942	6.018	0.000	15.960	2.123	1.921	0.009	4.054	47.39	52.38	0.23	grain 2: internal contact
22B-1721	D	3b	10.172	5.747	0.019	15.938	1.961	2.096	0.014	4.071	51.49	48.18	0.34	grain 2: rim
22B-1721	E	4	10.551	5.378	0.000	15.929	1.610	2.427	0.014	4.051	59.91	39.75	0.34	grain 3: core
22B-1721	E	4a	10.597	5.350	0.000	15.948	1.492	2.566	0.009	4.067	63.08	36.69	0.22	grain 3: core
22B-1721	E	4b	10.374	5.577	0.000	15.952	1.662	2.437	0.009	4.109	59.32	40.45	0.22	grain 3: core
22B-1721	E	4c	9.327	6.629	0.000	15.956	2.702	1.397	0.005	4.104	34.04	65.84	0.12	grain 3: internal contact
22B-1721	E	4d	9.753	6.176	0.000	15.929	2.305	1.842	0.009	4.156	44.32	55.45	0.23	grain 3: mantle
22B-1721	E	4e	9.402	6.510	0.000	15.912	2.685	1.483	0.009	4.177	35.49	64.28	0.23	grain 3: mantle
22B-1721	E	5	9.917	5.995	0.000	15.912	2.242	1.856	0.009	4.107	45.20	54.58	0.22	grain 3: mantle
24-1131	A	1	8.289	7.647	0.000	15.936	3.886	0.128	0.002	4.016	3.19	96.75	0.06	
24-1131	A	2	8.223	7.667	0.020	15.909	3.976	0.117	0.000	4.093	2.86	97.14	0.00	
24-1131	A	3	8.264	7.646	0.023	15.933	3.918	0.124	0.000	4.042	3.07	96.93	0.00	
zone 6														
24-1191	D	39c	9.886	6.203	0.000	16.089	2.050	1.737	0.011	3.798	45.74	53.96	0.30	gahnite inclusions
24-1191	D	40r	10.314	5.769	0.000	16.083	1.636	2.166	0.000	3.801	56.97	43.03	0.00	gahnite inclusions
24-1191	D	41c	10.799	5.268	0.000	16.067	1.179	2.628	0.013	3.820	68.79	30.86	0.35	relict with rutile trails
24-1191	D	42r	10.652	5.425	0.000	16.077	1.308	2.491	0.011	3.810	65.37	34.33	0.30	relict with rutile trails
24-1191	A	1	10.934	5.048	0.000	15.982	1.093	2.919	0.014	4.026	72.50	27.16	0.34	
24-1191	A	2c	10.378	5.545	0.000	15.922	1.777	2.290	0.012	4.078	56.16	43.56	0.28	gahnite inclusions
24-1191	A	2r	10.198	5.665	0.258	16.122	1.690	2.307	0.010	4.006	57.58	42.18	0.24	gahnite inclusions
24-1191	C	3c	10.318	5.639	0.000	15.957	1.765	2.269	0.011	4.046	56.09	43.63	0.28	gahnite inclusions
24-1191	C	3	10.962	5.010	0.000	15.972	1.114	2.883	0.011	4.008	71.93	27.79	0.28	gahnite inclusions
24-1191	C	3r	10.338	5.595	0.000	15.932	1.752	2.351	0.012	4.114	57.14	42.58	0.28	gahnite inclusions
24-1191	D	4c	10.371	5.579	0.000	15.950	1.704	2.358	0.014	4.076	57.86	41.80	0.34	gahnite inclusions
24-1191	D	4r	10.443	5.499	0.027	15.969	1.642	2.381	0.012	4.034	59.01	40.70	0.29	gahnite inclusions
zone 5														
24-1191	E	36c	10.883	5.202	0.000	16.085	1.082	2.697	0.000	3.779	71.36	28.64	0.00	relict with rutile trails
24-1191	E	37	10.890	5.180	0.000	16.071	1.104	2.689	0.000	3.793	70.88	29.12	0.00	relict with rutile trails
24-1191	E	38r	10.650	5.441	0.000	16.091	1.291	2.480	0.014	3.785	65.53	34.11	0.36	relict with rutile trails
24-1191	G	5c	10.286	5.638	0.020	15.944	1.845	2.202	0.009	4.056	54.28	45.49	0.23	symplectite with pyrrhotite
24-1191	G	5r	10.368	5.574	0.035	15.976	1.663	2.400	0.012	4.075	58.91	40.81	0.28	symplectite with pyrrhotite
24-1191	G	6	9.538	6.386	0.072	15.996	2.502	1.534	0.007	4.043	37.94	61.89	0.17	contact to po inclusion
24-1191	G	7	9.390	6.518	0.061	15.969	2.712	1.337	0.005	4.054	32.99	66.90	0.11	contact to po inclusion
24-1191	G	8r	10.322	5.602	0.035	15.959	1.723	2.379	0.009	4.111	57.86	41.91	0.23	symplectite with pyrrhotite
zone 4														
24-1191	I	33c	8.622	7.464	0.026	16.087	3.271	0.576	0.000	3.847	14.98	85.02	0.00	symplectite with pyrrhotite
24-1191	I	34	8.761	7.319	0.000	16.080	3.123	0.753	0.000	3.876	19.43	80.57	0.00	symplectite with pyrrhotite
24-1191	I	35r	8.583	7.520	0.017	16.103	3.286	0.537	0.000	3.823	14.04	85.96	0.00	symplectite with pyrrhotite
24-1191	I	9	9.171	6.744	0.035	15.950	2.925	1.158	0.005	4.088	28.34	71.55	0.11	symplectite with pyrrhotite
24-1191	I	9a	8.571	7.414	0.042	16.028	3.383	0.616	0.005	4.004	15.39	84.49	0.12	symplectite with pyrrhotite
24-1191	I	9b	8.642	7.273	0.036	15.951	3.410	0.714	0.005	4.129	17.30	82.59	0.12	symplectite with pyrrhotite
24-1191	I	9r	8.722	7.219	0.022	15.963	3.342	0.725	0.000	4.068	17.83	82.17	0.00	symplectite with pyrrhotite

Table B.3. m. Plagioclase Mineral Chemistry. (continued)

			Structural formula normalized to 64 anionic charges											
Sample	area	spot	Si	Al_{iv}	Fe	site	Ca	Na	K	site	Ab	An	Or	Comment
zone 3														
24-1191	H	27	8.647	7.456	0.000	16.102	3.232	0.582	0.000	3.814	15.26	84.74	0.00	
24-1191	H	28	8.620	7.487	0.000	16.108	3.237	0.582	0.000	3.819	15.24	84.76	0.00	
24-1191	H	29	8.724	7.399	0.000	16.123	3.116	0.674	0.000	3.790	17.78	82.22	0.00	
24-1191	K	30	8.406	7.678	0.000	16.084	3.477	0.387	0.000	3.864	10.01	89.99	0.00	
24-1191	K	31	8.456	7.621	0.000	16.077	3.465	0.383	0.000	3.848	9.96	90.04	0.00	
24-1191	K	32	8.537	7.570	0.000	16.107	3.311	0.520	0.000	3.831	13.56	86.44	0.00	
24-1191	K	10	8.438	7.489	0.017	15.945	3.690	0.365	0.000	4.054	9.00	91.00	0.00	
24-1191	K	10a	8.586	7.344	0.000	15.929	3.592	0.442	0.000	4.034	10.95	89.05	0.00	
24-1191	K	10b	8.476	7.454	0.085	16.015	3.537	0.491	0.000	4.028	12.19	87.81	0.00	
24-1191	K	10d	8.444	7.468	0.020	15.932	3.694	0.393	0.000	4.087	9.61	90.39	0.00	
34C-1377	I	1	10.671	5.271	0.000	15.942	1.418	2.656	0.011	4.085	65.02	34.70	0.28	
34C-1377	I	1a	10.717	5.252	0.000	15.969	1.368	2.632	0.009	4.009	65.64	34.13	0.23	
34C-1377	I	1b	10.713	5.286	0.000	15.998	1.336	2.612	0.009	3.956	66.01	33.76	0.23	
34C-1377	I	2	10.649	5.321	0.000	15.970	1.382	2.669	0.007	4.058	65.77	34.06	0.17	
34C-1377	I	3	10.686	5.275	0.000	15.962	1.368	2.649	0.043	4.061	65.24	33.69	1.07	
34C-1377	E	5	10.822	5.244	0.000	16.066	1.096	2.772	0.016	3.883	71.38	28.22	0.41	in pressure shadow
34C-1377	E	6	10.785	5.452	0.027	16.237	0.806	2.854	0.041	3.700	77.13	21.77	1.10	in pressure shadow

Appendix C

Whole-rock Geochemical Analysis.

A suite of 303 samples, representative of the lithologies and alteration types (*see* Table A.1) was selected for whole-rock geochemical analysis. The samples were mainly splits of drill core, supplemented by outcrop samples. The samples varied in weight from a few grams (not less than 12 g) for microcrystalline cherty rocks, to more than 400 grams for coarsely porphyroblastic rocks. Some small-scale heterogeneities were represented by separating clasts and matrix in breccias, beds in metasediments, and different intensities or types of alteration in cases in which there appeared to be a variation in the hand sample. Separates extracted from the same hand sample have the same drill-hole and footage designation in their sample number, and are numbered from 1–N in the last designator. They are linked by tie lines in the figures (*ie.* in Chapter 11).

A rock saw was used to split drill core and to extract clasts, *etc.* from hand samples. Saw marks and metallic smears were removed on a diamond lap. The specific gravity (ρ) was determined by weighing the samples in air and in water, and calculating the ratio: $\rho = weight_{air}/(weight_{air} - weight_{water})$. The samples were passed through a jaw crusher and, in the case of relatively large samples, the resulting sand was coned-and-quartered and an aliquot was taken. Samples of at least 50 ml were pulverized to a fine powder within 25–60 seconds in a tungsten carbide swing mill. Smaller samples were pulverized in a mechanical agate mortar-and-pestle.

The sample powders were submitted to G.Lachance of the Analytical Chemistry Section, Mineral Resources Division, Geological Survey of Canada for geochemical analysis of major and trace elements, and ferrous iron. The major oxides, SiO_2, TiO_2, Al_2O_3, Cr_2O_3, Fe_2O_{3t}, MnO, MgO, CaO, Na_2O, K_2O and P_2O_5, were determined by X-ray fluorescence (XRF) wavelength dispersive analysis on fused disks. The trace elements, Ba, Nb, Rb, Sr, Y and Zr, were determined semi-quantitatively by the same method on the same fused disks. FeO, H_2O, CO_{2t} and S were analysed by rapid chemical methods. Due to limitations inherent in the methods, H_2O and FeO were determined only in samples containing less than 1% S. Quantitative analyses of the trace elements, Be, Co, Cr, Cu, La, Ni, V, Yb and Zn, were obtained

by inductively-coupled plasma (ICP) emission spectrometry. One gram of sample was dissolved in HF and then fused with any remaining residue. The fused bead was subsequently dissolved in 10% HCl and diluted to 100 ml. In some samples, the additional trace elements, Ag and Pb, were determined by atomic absorption (AA) spectroscopy.

Calibration ranges, error estimates and detection limits supplied by the laboratory are listed in Table C.1. As an independent check on accuracy and precision, blind standards (Table C.2), sample duplicates (Table C.3, a) and sample replicates (Table C.4) were interspersed in the sample suite. In general, the precision and reproducibility were very good; however one significant and disturbing exception occurred among the replicates (Table C.4). The ICP trace element analysis of one replicate of sample 27-484-1 reported values 1–3 orders of magnitude higher than that of the 5 other replicates. As this problem appears only in ICP analyses, it is a laboratory error incurred during preparation or analysis by this particular technique. (Recall that Pb was analysed by AA.) The most likely explanation is that one of the spiked standards used to maintain the calibration during on-line analysis, was mistakenly read as a sample analysis (G.Lachance, *pers. comm.*, 1988). As the spiked standards have elevated values for all the elements, including some which were typically low in samples from the Linda suite (*ie.* Be, Ni, Cr), a mistake of this nature should be identifiable and appears to have been an isolated instance.

Table C.5 lists the analyses of the sample suite. All major elements are reported, excepting Cr_2O_3 which was generally below the detection limit and is therefore reported as Cr determined by ICP. Among the semi-quantitative trace-element analyses, Y and Nb occurred at low levels, near the detection limits, without significant variation at the 2σ confidence limits; they are not reported. Likewise, Be and Ag showed values near or below detection limits for quantitative analysis. Co was not considered to be significant in view of probable contamination contributed by tungsten carbide crushing surfaces. In summary, in addition to major elements, the analyses of the following trace elements are tabulated in Table C.5: Ba, Rb, Sr, Zr, Cr, Cu, La, Ni, Pb, V, Yb and Zn.

Table C.1. Calibration Ranges, Estimated Errors and Detection Limits of Whole-rock Geochemical Analyses.

(as reported by Analytical Chemistry Section, Geological Survey of Canada)

Major Oxides and Elements					Trace Elements			
oxide or element	calibration range (%)	error estimate absolute+relative%		detection limit(%)	element	error estimate absolute+relative%		detection limit (ppm)
SiO_2	0–100	0.40	1	0.40	Ba	20	2	20
TiO_2	0–3	0.02	1	0.02	Rb	20	2	20
Al_2O_3	0–60	0.40	1	0.40	Sr	20	10	20
Fe_2O_3t	0–90	0.10	1	0.10	Zr	20	10	20
FeO	0–30	0.20	2	0.20	Cr	10	5	10
MnO	0–1	0.01	2	0.01	Cu	10	5	10
MgO	0–50	0.10	1	0.10	La	10	5	10
CaO	0–35	0.10	1	0.10	Ni	10	5	10
Na_2O	0–10	0.50	1	0.50	Pb	20	10	20
K_2O	0–15	0.05	1	0.05	V	5	5	5
H_2O	0–5	0.10	5	0.10	Yb	0.5	5	0.5
CO_2t	0–20	0.05	3	0.05	Zn	5	5	5
P_2O_5	0–1	0.02	1	0.02				
S	0–3	0.04	5	0.04				

Table C.2. Whole-rock Standards.

a. Major Element Analyses (weight percent oxide or element)

Sample	SiO_2	TiO_2	Al_2O_3	Fe_2O_3t	Fe_2O_3	FeO	MnO	MgO	CaO	Na_2O	K_2O	H_2Ot	CO_2t	P_2O_5	S	Total
32-1700-2	52.30	1.10	17.30	9.60	3.80	5.20	0.22	4.26	6.95	2.90	1.71	2.50	0.20	0.23	0.04	98.70
DR-N*	52.85	1.09	17.52	9.70	3.70	5.40	0.22	4.40	7.05	2.99	1.70	2.47	0.10	0.25	0.04	99.77
34B-1200-2	67.40	0.03	17.80	0.40	0.00	0.50	0.04	0.01	0.65	5.90	3.23	0.90	0.20	1.42	0.01	98.09
MA-N*	66.60	0.01	17.62	0.47	0.13	0.31	0.04	0.04	0.59	5.84	3.18	1.29	0.13	1.39	0.01	97.18
22B-2100-2	38.70	2.65	10.00	12.80	5.50	6.60	0.20	13.20	13.98	3.10	1.41	2.00	1.00	1.06	0.02	99.42
BE-N*	38.20	2.61	10.07	12.84	5.34	6.74	0.20	13.15	13.87	3.18	1.39	2.74	0.74	1.05	0.03	99.30
19B-1000-2	59.30	0.16	11.60	6.50	2.50	3.60	0.32	2.57	8.28	4.10	4.15	0.60	0.40	0.55	0.05	98.17
SY-3*	59.68	0.15	11.80	6.42	2.44	3.58	0.32	2.67	8.26	4.15	4.20	0.42	0.38	0.54	0.01	98.59
27-1000-2	47.90	1.18	17.30	10.10	2.30	7.00	0.16	8.41	11.97	2.10	0.21	0.40	0.10	0.13	0.01	99.17
NBS688*	48.40	1.17	17.36	10.35	1.86	7.64	0.17	8.40	12.17	2.15	0.19	-	0.05	0.13	-	99.69
29-700-2	39.00	3.73	8.40	17.60	8.50	8.20	0.17	13.47	14.50	0.70	0.21	1.10	1.10	0.06	0.07	99.19
MGR-1*	39.32	3.69	8.50	17.82	8.26	8.63	0.17	13.49	14.77	0.71	0.18	0.98	1.00	0.06	0.06	99.81
80-1400-2	49.40	1.40	27.30	13.80	10.60	2.90	0.02	0.82	1.62	0.20	2.27	0.50	9.90	0.39	0.19	107.46
NBS1633a*	48.80	1.30	26.00	13.40			0.03	0.75	1.55	0.23	2.26					94.32
I6-6-1	60.10	0.16	11.50	6.40	2.20	3.80	0.32	2.59	8.32	4.10	4.21	0.60	0.40	0.31	0.06	98.66
SY-3*	59.68	0.15	11.80	6.42	2.44	3.58	0.32	2.67	8.26	4.15	4.20	0.42	0.38	0.54	0.01	98.59

b. Trace Element Analyses (ppm)

Sample	Ba	Nb	Rb	Sr	Y	Zr	Ag	Be	Co	Cr	Cu	La	Ni	Pb	V	Yb	Zn
32-1700-2	396	0	63	393	13	132		1.7	37	42	55	20	24		190	2.2	140
DR-N*	385		70	400	30	125		1.8	35	42	50	21	16		225	2.8	145
34B-1200-2	98	224	3915	120	0	24		340.0	2	5	140	1	9		0	0.0	230
MA-N*	42	173	3600	84	1	27		280.0	1	3	140	1	3		5		220
22B-2100-2	1024	99	76	1334	22	248		1.9	56	310	85	71	230		200	1.5	130
BE-N*	1025	100	47	1370	30	265			61	360	72	82	267		235	1.8	120
19B-1000-2	424	222	212	290	692	360	0	20.0	12	15	40	1200	16	150	48	53.0	240
SY-3*	430	130	208	306	740	320		22.0	12	10	16	1350	11	130	51	65.0	240
27-1000-2	184	0	0	151	0	44	0	0.6	51	290	100	4	160	10	230	1.8	89
NBS688*	200		2	169					50	330	96		150	3	250	2.1	58
29-700-2	113	1	0	216	0	86	0	0.8	79	400	140	3	180	21	480	0.3	210
MGR-1*	50	20	8	260	16	105	0	0.6	86	450	135	10	195	10	520	1.0	190
80-1400-2	1267	21	111	778	68	240	0	13.0	44	170	110	76	120	63	260	6.3	240
NBS1633a*	1500		131	830				12.0	46	196	118		127	72	300		220
I6-6-1	464	218	195	290	642	335		22.0	14	20	67	1300	19		57	58.0	250
SY-3*	430	130	208	306	740	320		22.0	12	10	16	1350	11	130	51	65.0	240

* values from Govindaraju (1984).

Table C.3. Whole-rock Duplicate Analyses.

a. Blind Duplicates—Major Element Analyses (weight percent oxide or element)

Sample	SiO_2	TiO_2	Al_2O_3	Fe_2O_3t	Fe_2O_3	FeO	MnO	MgO	CaO	Na_2O	K_2O	H_2Ot	CO_2t	P_2O_5	S	Total
32-657-1	72.80	0.36	11.80	3.30	1.00	2.00	0.09	2.15	3.12	1.10	3.67	1.10	0.20	0.07	0.03	98.48
32-1657.5-1	72.70	0.34	11.70	3.30	1.10	2.00	0.09	2.15	3.13	1.10	3.67	1.00	0.20	0.06	0.02	98.16
34-1275-1	66.60	0.36	15.80	5.40			0.09	1.90	2.68	1.50	2.90		0.00	0.08	1.26	98.26
34-2275.5-1	66.20	0.34	15.70	5.20			0.10	1.89	2.66	1.50	2.87		0.10	0.07	1.22	97.55
34A-1463.5-1	49.90	0.47	18.20	12.70	3.10	8.60	0.17	5.93	8.61	4.40	0.10	1.20	0.10	0.06	0.01	97.75
34A-2463-1	49.80	0.46	18.10	12.80	3.50	8.40	0.17	5.91	8.63	4.40	0.11	1.10	0.00	0.06	0.01	97.15
34C-1453-1	48.40	0.52	24.80	12.90			0.04	0.69	0.14	1.10	3.61		0.00	0.06	8.30	98.49
34C-2453.5-1	48.60	0.50	25.10	13.10			0.04	0.69	0.13	1.10	3.64		0.10	0.06	8.14	99.17
22A-1515-1	71.00	0.31	13.10	6.80	1.80	4.50	0.08	2.39	1.42	1.50	1.89	1.60	0.00	0.07	0.30	98.09
22A-2515.5-1	70.70	0.29	13.00	6.90	2.00	4.40	0.08	2.38	1.42	1.50	1.93	1.60	0.10	0.08	0.30	97.71
19-440-1	72.80	0.30	12.50	5.00	0.80	3.80	0.14	1.51	1.64	2.80	2.34	1.00	0.10	0.06	0.06	99.04
19-1440.5-1	73.00	0.26	12.60	5.20	1.10	3.70	0.15	1.53	1.64	2.70	2.37	1.00	0.10	0.06	0.05	99.15
24-277.5-1	52.40	0.40	19.20	10.20			0.10	10.20	0.15	0.30	0.86		0.00	0.08	1.02	94.66
24-1277-1	52.10	0.48	19.20	9.70			0.09	10.14	0.15	0.30	0.89		0.10	0.08	1.23	94.15
24-1082-1	65.50	0.32	13.30	7.80			0.07	4.62	0.95	0.50	1.63		0.10	0.10	3.91	97.82
24-2082.5-1	65.90	0.35	13.30	7.80			0.07	4.63	0.95	0.50	1.66		0.10	0.10	3.74	98.17
27-1324.5-1	71.80	0.27	12.70	4.90			0.11	1.84	2.32	1.40	1.17		0.00	0.07	2.05	98.12
27-2324-1	72.50	0.27	12.80	5.00			0.11	1.86	2.34	1.40	1.18		0.00	0.07	2.09	99.10
29-478.5-1	49.10	0.50	17.30	13.80	3.20	9.60	0.18	6.54	8.82	2.00	0.18	2.30	0.10	0.08	0.01	96.71
29-1478-1	49.00	0.54	17.30	13.50	2.70	9.70	0.18	6.49	8.78	1.90	0.19	2.40	0.30	0.07	0.01	96.86
29-1099-1	68.20	0.34	13.40	6.90			0.02	0.97	1.70	1.20	2.23		0.00	0.10	4.92	98.75
29-2099.5-1	68.40	0.33	13.50	7.00			0.02	0.98	1.70	1.10	2.24		0.10	0.10	4.85	99.11
31-970.5-1	53.00	0.48	17.10	11.80	1.80	9.00	0.15	6.25	6.54	1.60	1.75	2.20	0.10	0.07	0.08	98.30
31-1970-1	53.30	0.47	17.10	11.90	1.60	9.30	0.15	6.29	6.57	1.60	1.77	2.20	0.20	0.07	0.07	99.07
73-1170.5-2	76.10	0.19	10.80	4.80	0.70	3.70	0.03	2.70	0.00	0.20	1.96	2.70	0.00	0.02	0.04	98.43
73-2170-2	76.00	0.18	10.80	4.80	0.70	3.70	0.03	2.72	0.00	0.30	1.94	2.70	0.00	0.02	0.05	98.43
80-1138-1	74.00	0.14	14.30	0.90	0.00	1.00	0.01	0.36	1.86	5.70	0.91	0.40	0.10	0.00	0.01	98.79
80-2138.5-1	74.50	0.15	14.50	0.90	0.00	0.90	0.01	0.35	1.88	5.80	0.91	0.50	0.10	0.00	0.00	99.60
I8-27-1	70.60	0.26	14.40	4.90	0.70	3.80	0.08	1.75	3.58	2.70	1.60	1.00	0.20	0.04	0.05	100.05
D4-1-1	70.40	0.25	14.40	4.90	0.50	4.00	0.08	1.74	3.59	2.70	1.59	1.00	0.20	0.04	0.04	100.02
22B-1044-1	76.60	0.22	11.50	6.30	2.00	3.90	0.09	2.15	0.15	0.20	1.44	2.40	0.10	0.03	0.08	98.84
33-1044-1	76.20	0.22	11.50	6.30	1.80	4.00	0.09	2.19	0.15	0.20	1.43	2.40	0.10	0.03	0.08	98.57

Table C.3. Whole-rock Duplicate Analyses. (continued)

b. Blind Duplicates—Trace Element Analyses (ppm)

Sample	Ba	Nb	Rb	Sr	Y	Zr	Ag	Be	Co	Cr	Cu	La	Ni	Pb	V	Yb	Zn
32-657-1	540	0	64	72	8	65		0.6	5	16	9	6	9		4	2.7	84
32-1657.5-1	605	0	51	77	16	72		0.6	5	11	10	7	6		4	2.7	85
34-1275-1	714	0	52	169	31	101		0.6	8	11	63	7	6		12	3.7	150
34-2275.5-1	697	0	52	171	37	103		0.6	8	9	63	7	5		11	3.4	150
34A-1463.5-1	79	0	0	284	0	22		0.4	49	23	100	2	26		300	0.5	55
34A-2463-1	70	0	0	280	0	13		0.4	49	24	100	2	28		310	0.5	60
34C-1453-1	422	0	64	50	70	164		0.6	32	5	180	14	8		3	5.3	7100
34C-2453.5-1	427	0	57	47	29	162		0.5	32	13	180	15	12		3	5.5	6400
22A-1515-1	356	0	39	45	26	84		0.6	27	9	22	7	7		11	2.8	92
22A-2515.5-1	337	0	29	45	31	80		0.6	27	10	22	6	8		10	2.7	90
19-440-1	625	0	55	71	0	83	0.0	0.6	21	11	15	7	5	15	5	2.7	60
19-1440.5-1	620	37	60	61	37	82	0.0	0.6	21	7	9	6	3	18	5	2.7	58
24-277.5-1	123	0	7	42	0	115	0.0	0.2	15	4	8	5	7	7	0	3.0	240
24-1277-1	99	44	0	75	33	104	0.0	0.3	16	9	15	6	11	7	1	3.5	280
24-1082-1	232	0	16	35	0	62	2.0	0.4	46	11	680	3	23	120	55	2.2	280
24-2082.5-1	238	29	21	37	32	56	0.0	0.4	45	12	690	3	24	110	56	2.7	290
27-1324.5-1	191	0	17	83	0	91	0.0	0.5	30	9	22	6	6	23	7	3.0	84
27-2324-1	190	34	16	83	29	85	0.0	0.6	31	11	23	8	9	27	10	3.0	130
29-478.5-1	74	0	0	304	0	51	0.0	0.5	60	33	120	3	35	10	310	0.6	110
29-1478-1	79	0	0	300	0	33	0.0	0.5	60	37	110	2	36	6	330	0.6	100
29-1099-1	218	0	41	71	0	59	0.0	0.5	45	64	20	5	21	18	80	1.8	63
29-2099.5-1	262	0	49	66	0	56	0.0	0.5	42	59	22	5	19	16	79	1.8	63
31-970.5-1	276	0	30	80	0	31	0.0	0.5	49	46	100	3	36	0	250	0.7	95
31-1970-1	300	0	41	77	0	45	0.0	0.5	49	63	110	4	39	0	250	0.8	93
73-1170.5-2	829	0	37	63	0	80	0.0	0.2	23	10	32	1	4	0	5	2.0	14
73-2170-2	804	0	36	62	0	75	0.0	0.2	23	8	31	1	4	5	5	1.9	16
80-1138-1	684	0	21	415	0	46	0.0	0.6	31	6	2	0	4	25	9	0.1	18
80-2138.5-1	696	0	0	411	0	37	0.0	0.6	31	7	2	0	3	11	8	0.1	19
I8-27-1	298	0	19	133	0	61		0.5	33	15	51	7	10		48	1.8	57
D4-1-1	267	0	23	134	0	59		0.5	32	14	48	7	11		48	1.7	58
22B-1044-1	474	0	0	43	17	65		0.4	41	12	14	7	6		7	2.5	51
33-1044-1	451	0	0	46	0	65		0.4	39	10	13	6	3		4	2.3	50

Table C.4. Whole-rock Replicate Analyses.

a. Major Element Analyses (weight percent oxide or element)

Sample	SiO_2	TiO_2	Al_2O_3	Fe_2O_3t	Fe_2O_3	FeO	MnO	MgO	CaO	Na_2O	K_2O	H_2Ot	CO_2t	P_2O_5	S	Total
27-484-1	77.10	0.27	11.40	3.90			0.02	1.07	0.11	0.60	2.16		0.10	0.04	2.05	98.31
19-1003-2	75.30	0.42	11.00	3.50			0.02	1.04	0.11	0.50	2.04		0.00	0.04	1.91	95.40
24-1003-2	77.10	0.21	11.30	4.00			0.03	1.08	0.11	0.60	2.11		0.10	0.04	2.01	98.19
29-1003-2	77.80	0.22	11.40	4.00			0.02	1.08	0.11	0.60	2.15		0.10	0.04	2.01	99.03
70-1003-2	77.60	0.21	11.40	4.00			0.03	1.09	0.11	0.60	2.13		0.00	0.04	1.95	98.67
73-1003-2	77.70	0.20	11.30	4.20			0.02	1.08	0.11	0.60	2.13		0.00	0.04	2.10	98.96
Ave(6)	77.10	0.26	11.30	3.93			0.02	1.07	0.11	0.58	2.12		0.05	0.04	2.01	98.09
Stdev	0.85	0.08	0.14	0.21			0.00	0.02	0.00	0.04	0.04		0.05	0.00	0.06	1.24
70-462-1	70.80	0.28	11.60	5.40	1.40	3.60	0.08	2.77	3.23	1.30	3.30	1.10	0.00	0.06	0.07	99.57
24-502-2	70.50	0.28	11.50	5.40	1.40	3.60	0.08	2.75	3.21	1.30	3.27	1.20	0.10	0.06	0.07	99.30
27-502-2	71.10	0.24	11.80	5.60	1.70	3.50	0.08	2.78	3.21	1.30	3.29	1.10	0.10	0.06	0.07	100.31
28-502-2	70.60	0.28	11.60	5.50	1.70	3.40	0.08	2.76	3.22	1.30	3.28	1.10	0.10	0.06	0.07	99.53
31-502-2	70.10	0.34	11.60	5.20	1.20	3.60	0.08	2.74	3.17	1.30	3.26	1.00	0.20	0.06	0.07	98.70
80-502-2	70.40	0.24	11.60	5.60	1.60	3.60	0.08	2.77	3.21	1.30	3.30	1.10	0.10	0.06	0.06	99.41
Ave(6)	70.58	0.28	11.62	5.45	1.50	3.55	0.08	2.76	3.21	1.30	3.28	1.10	0.10	0.06	0.07	99.47
Stdev	0.31	0.03	0.09	0.14	0.18	0.08	0.00	0.01	0.02	0.00	0.01	0.06	0.06	0.00	0.00	0.47
22B-2036-1	70.70	0.34	12.80	4.50			0.09	1.51	2.52	1.20	1.86		0.60	0.09	2.68	98.22
32-1001-2	71.00	0.31	13.00	4.60			0.09	1.55	2.53	1.20	1.86		0.10	0.09	2.75	98.39
34-1001-2	72.20	0.33	13.10	4.80			0.09	1.54	2.57	1.20	1.94		0.10	0.09	2.79	100.05
34A-1001-2	71.80	0.30	13.00	4.80			0.09	1.54	2.56	1.20	1.91		0.10	0.09	2.13	98.99
34B-1001-2	71.40	0.33	13.00	4.60			0.09	1.53	2.55	1.20	1.94		0.10	0.09	2.69	98.85
22-1001-2	70.00	0.30	12.90	4.60			0.09	1.52	2.54	1.20	1.92		0.20	0.09	2.74	97.42
Ave(6)	71.18	0.32	12.97	4.65			0.09	1.53	2.55	1.20	1.91		0.20	0.09	2.63	98.65
Stdev	0.72	0.02	0.09	0.11			0.00	0.01	0.02	0.00	0.03		0.18	0.00	0.23	0.81

b. Trace Element Analyses (ppm)

Sample	Ba	Nb	Rb	Sr	Y	Zr	Ag	Be	Co	Cr	Cu	La	Ni	Pb	V	Yb	Zn
27-484-1	310	0	36	58	23	68	0.0	0.4	21	7	29	4	6	39	2	2.6	900
19-1003-2	261	0	22	70	21	61	0.0	0.4	20	15	25	3	6	33	2	2.4	930
24-1003-2	313	0	39	51	14	71	0.0	0.4	21	5	27	5	4	29	2	2.4	890
29-1003-2	326	0	36	53	27	73	0.0	0.4	22	8	27	6	5	37	3	2.3	880
70-1003-2*	320	0	35	55	17	74	0.0	1.0	95	2800	84	14	1600	20	30	5.5	1900
73-1003-2	311	0	42	50	19	76	0.0	0.4	22	6	29	6	6	23	4	2.4	900
Ave(5)	304	0	35	56	21	70	0.0	0.4	21	8	27	5	5	32	3	2.4	900
Stdev	22	0	7	7	4	5	0.0	0.0	1	4	1	1	1	6	1	0.1	17
70-462-1	1133	0	56	49	14	72	0.0	0.4	25	11	37	7	4	0	10	2.7	85
24-502-2	1118	0	40	50	17	77	0.0	0.4	28	9	38	5	5	8	8	2.6	110
27-502-2	1118	0	60	47	18	76	0.0	0.4	27	8	39	5	5	11	8	2.7	76
28-502-2	1126	0	53	48	25	75	0.0	0.4	26	9	37	6	5	5	9	2.6	77
31-502-2	1096	0	44	54	13	72	0.0	0.4	27	10	36	5	5	0	9	2.6	74
80-502-2	1099	0	60	48	28	76	0.0	0.4	28	10	35	7	5	17	10	2.7	78
Ave(6)	1115	0	52	49	19	75	0.0	0.4	27	10	37	6	5	7	9	2.7	83
Stdev	13	0	8	2	6	2	0.0	0.0	1	1	1	1	0	6	1	0.1	12
22B-2036-1	243	0	40	65	12	58		0.5	36	23	48	6	13		56	2.3	140
32-1001-2	249	0	57	54	16	63		0.5	40	24	48	9	12		55	2.3	150
34-1001-2	243	0	49	61	11	63		0.5	37	23	47	7	12		55	2.3	140
34A-1001-2	249	0	39	62	23	61		0.5	37	22	48	7	11		54	2.2	140
34B-1001-2	259	0	42	64	8	61		0.5	39	25	48	7	13		57	2.2	150
22-1001-2	247	0	60	58	10	63		0.5	51	24	50	7	13		56	2.2	130
Ave(6)	248	0	48	61	13	62		0.5	40	24	48	7	12		56	2.3	142
Stdev	5	0	8	4	5	2		0.0	5	1	1	1	1		1	0.0	7

* laboratory error in ICP analysis, see text for explanation.

Table C.5. Whole-rock Geochemical Analyses.

The totals are adjusted for S and for Fe_2O_3 where analysed.

a. Major Element Analyses (weight percent oxide or element)

Sample	Unit	Code	SiO_2	TiO_2	Al_2O_3	FeOt	Fe_2O_3	FeO	MnO	MgO	CaO	Na_2O	K_2O	H_2Ot	CO_2t	P_2O_5	S	Total
24-097-1	1	epy	72.40	0.25	12.20	5.04	0.80	4.30	0.11	1.75	2.18	2.80	1.87	1.00	0.10	0.04	0.17	99.93
24-657-1	1	epm	70.10	0.34	13.30	4.23			0.09	1.36	1.45	2.60	3.40		0.10	0.06	1.11	97.86
27-830-1	1	mvpy	72.80	0.28	12.20	5.13	1.40	3.80	0.16	1.92	1.78	0.00	2.17	2.00	0.20	0.05	0.33	99.01
29-1146-1	1	cepvx	62.90	0.61	16.10	6.12	1.60	4.70	0.09	2.30	3.22	4.10	1.38	1.30	0.10	0.12	0.08	98.58
29-336b-1	1	cpmi	61.90	0.36	18.10	5.58	1.40	4.30	0.07	3.07	1.23	2.30	4.74	2.20	0.20	0.08	0.04	99.98
29-711.5-1	1	pxv	61.70	0.50	14.80	9.54	5.10	4.90	0.07	2.33	1.24	5.80	0.88	1.30	0.00	0.13	0.90	99.43
31-705-1	1	cdhnx	65.60	0.47	13.60	8.01	3.50	4.90	0.08	2.06	3.76	4.30	0.17	0.70	0.10	0.17	0.11	99.49
32-426-1	1	epx	72.90	0.26	11.70	6.21	1.60	4.70	0.06	1.59	2.42	2.60	1.68	0.80	0.20	0.05	0.00	100.56
34C-1315-1	1	pxi	74.90	0.28	12.90	3.60	1.60	2.20	0.06	0.92	1.85	4.80	0.56	0.50	0.10	0.07	0.50	101.12
34-1130-1	1	epyxi	73.30	0.29	12.50	4.41	1.10	3.40	0.11	1.11	1.46	4.70	1.15	0.50	0.10	0.07	0.30	100.02
34-757.5-1	1	ep	70.70	0.34	10.90	5.67	0.70	5.00	0.09	3.62	2.69	0.00	2.76	1.30	0.00	0.06	0.18	98.30
H9-63-1	1	pl	73.00	0.19	11.90	3.96	0.60	3.50	0.08	1.11	1.92	3.10	2.83	0.90	0.90	0.02	0.00	100.05
H9-64-1	1	ply	78.50	0.16	10.70	1.89	0.20	1.70	0.13	0.52	2.99	2.50	1.34	0.90	1.10	0.02	0.00	100.76
34-1753.5-1	1	gvpqu	60.60	0.47	15.20	8.55	2.30	6.50	0.10	5.75	3.07	1.60	0.76	3.40	0.10	0.05	0.70	100.43
24-097-2	1	fhlpv	64.00	0.20	10.50	7.29	1.80	5.70	0.38	3.05	7.80	1.70	0.76	1.20	3.20	0.04	0.00	100.33
29-1146-2	1	chfp	63.60	0.46	15.10	7.02	2.00	5.20	0.18	2.58	4.89	3.40	0.84	1.10	0.40	0.11	0.07	99.91
32-426-2	1	fphx	70.10	0.22	10.80	7.74	2.20	5.70	0.13	1.99	5.04	2.10	0.61	0.90	0.50	0.06	0.00	100.35
34C-1315-2	1	fhyxi	68.70	0.31	14.50	5.58	2.90	3.00	0.20	1.06	4.00	3.80	0.24	0.70	0.10	0.06	0.83	100.19
34C-1385-1	1	fh	61.50	0.58	18.20	3.78			0.06	1.26	6.65	3.10	0.58		0.10	0.04	3.11	98.18
29-336a-1	1a	c	79.00	0.24	12.20	0.18			0.01	0.00	0.75	6.30	0.27	0.30	0.20	0.06	0.00	99.51
29-501-1	1a	dn	73.00	0.35	11.80	4.59	0.60	4.00	0.06	2.04	2.12	4.70	0.26	0.60	0.10	0.09	0.06	99.77
31-259.5-1	1a	cd	78.70	0.27	12.20	0.36	0.00	0.40	0.00	0.14	0.49	6.60	0.28	0.20	0.20	0.07	0.00	99.55
32-1374.5-1	1a	vpxi	65.90	0.36	13.80	8.73	3.70	5.40	0.06	2.27	1.12	5.20	0.27	1.70	0.20	0.10	0.27	100.28
34A-1292.5-1	1a	dx	83.60	0.18	9.40	0.36	0.00	0.60	0.01	0.00	0.70	4.90	0.10	0.20	0.10	0.03	0.10	99.90
34C-1385-2	1a	ph	74.40	0.28	12.70	2.07			0.18	0.64	4.66	2.30	0.28		0.20	0.05	1.49	98.88
H8-14-1	1a	my	76.70	0.25	12.00	1.62			0.26	0.97	4.56	0.90	1.28	0.80	0.30	0.03	0.43	99.99
I8-42-5	1a	pml	74.00	0.21	12.80	2.79	0.40	2.50	0.06	1.24	2.52	2.20	2.79	1.00	0.50	0.02	0.00	100.24
19-688-1	1a/10p	cd	79.80	0.22	10.40	1.35			0.01	0.10	0.48	5.60	0.13		0.00	0.05	1.08	98.95
34-1397.5-1	1a/10p	dyvmx	77.40	0.28	10.30	4.05	1.50	2.70	0.07	0.96	0.91	3.60	0.24	1.00	0.10	0.06	0.14	99.23
I8-13-1	1a/10c	pqlx	74.80	0.21	11.20	3.60	1.30	2.40	0.09	1.03	3.05	3.20	1.24	0.60	0.60	0.03	0.00	99.75
19-744.5-1	1c	acd	79.30	0.19	11.70	1.44			0.01	0.00	0.62	6.00	0.23		0.10	0.05	1.15	100.50
27-1228-1	1c	p	77.50	0.26	11.20	2.34	0.10	2.20	0.05	0.33	1.89	3.90	0.80	0.40	0.40	0.06	0.07	99.14
34A-1360-1	1c	du	80.00	0.20	9.70	2.61			0.00	0.00	0.39	5.40	0.12		0.10	0.03	2.48	100.41
34-1306.5-1	1c	d	81.80	0.22	10.10	1.08	0.10	1.00	0.00	0.00	0.56	5.60	0.10	0.10	0.10	0.05	0.84	100.36
34-1443.5-1	1c	acd	82.20	0.19	9.80	0.90	0.00	1.00	0.00	0.10	0.34	5.40	0.15	0.20	0.00	0.03	0.69	99.93
34-1443.5-2	1c	cdum	72.40	0.19	9.60	7.20			0.00	0.00	0.31	4.80	0.35		0.10	0.03	6.33	99.73
19-440-1	1b	cp	72.80	0.30	12.50	4.50	0.80	3.80	0.14	1.51	1.64	2.80	2.34	1.00	0.10	0.06	0.06	99.84
19-543-1	1b	p	61.80	0.43	16.40	4.77			0.03	1.22	2.83	3.40	2.25		0.00	0.05	3.14	95.54
19-629-1	1b	a	82.30	0.26	10.30	0.63	0.40	0.30	0.01	0.14	1.67	2.40	1.05	0.60	0.00	0.06	0.15	99.60
22A-1479-1	1b	p	67.90	0.45	16.10	4.86	0.70	4.20	0.07	1.05	3.08	4.60	1.83	0.60	0.10	0.10	0.07	100.83
22B-1509.5-1	1b	cpi	73.60	0.34	12.60	3.96	0.60	3.50	0.09	1.58	2.20	3.70	1.55	0.80	0.10	0.08	0.13	100.84
27-1165-1	1b	cpmi	73.30	0.27	12.50	4.32	0.70	3.70	0.06	1.37	1.63	3.20	2.01	1.00	0.20	0.06	0.02	100.02
28-288-1	1b	cphv	61.80	0.38	15.00	6.84	0.90	6.00	0.11	5.43	3.75	1.90	2.20	2.20	0.20	0.08	0.02	99.97
28-329.5-1	1b	cmp	66.10	0.39	16.30	3.78	1.80	2.20	0.06	2.44	2.40	3.10	2.92	1.30	0.10	0.10	0.69	99.73
29-301.5-1	1b	a	81.30	0.20	10.70	0.36	0.00	0.40	0.01	0.14	1.82	3.60	0.63	0.30	0.10	0.06	0.00	99.26
29-362-1	1b	cdemp	76.40	0.20	12.00	2.88	0.80	2.10	0.04	1.27	1.27	2.10	2.50	1.10	0.20	0.04	0.12	100.11
32-1093.5-1	1b	a	86.90	0.20	7.40	0.54	0.00	0.60	0.05	0.00	1.51	2.70	0.15	0.20	0.10	0.04	0.10	99.93
32-1118.5-1	1b	cpy	77.40	0.22	12.10	2.70	0.40	2.30	0.05	0.73	1.63	3.90	1.17	0.50	0.00	0.04	0.11	100.52
32-828.5-1	1b	cpui	74.80	0.31	11.60	3.42	0.20	3.20	0.09	1.25	2.26	3.50	1.22	0.60	0.10	0.08	0.66	99.71
32-950-1	1b	cep	73.40	0.31	12.00	4.41	0.50	3.90	0.09	1.15	1.57	3.10	2.64	0.70	0.10	0.06	0.23	99.69
34A-1268-1	1b	ay	84.80	0.21	8.40	0.72	0.10	0.60	0.03	0.15	1.38	3.40	0.22	0.10	0.10	0.07	0.05	99.60
34C-1185-1	1b	pm	72.90	0.31	12.40	4.41	0.90	3.60	0.17	1.32	2.05	1.90	2.61	1.10	0.30	0.05	0.00	99.61
73-617-1	1b	cph	67.10	0.38	12.00	7.20	1.90	5.50	0.09	3.70	2.66	2.70	1.78	1.30	0.10	0.07	0.35	99.54
80-1084.5-1	1b	cpnx	67.60	0.77	13.70	5.85	2.20	3.80	0.07	1.62	2.48	4.80	0.76	0.70	0.10	0.12	0.12	98.81
22-413-1	1d	nhx	57.90	1.12	15.20	11.25	2.60	8.90	0.21	3.66	4.44	4.50	0.07	0.60	0.10	0.11	0.25	99.60
22-550-1	1d	h	54.80	0.31	11.90	9.36	2.80	6.80	0.16	8.99	7.74	4.00	0.24	1.20	0.10	0.02	0.29	99.28
70-397-1	1d	h	54.00	0.24	15.20	7.83	2.60	5.50	0.15	7.66	7.76	4.90	0.29	1.20	0.10	0.00	0.15	99.71
29-1197-1	4	mu	66.10	0.27	14.30	6.39			0.03	1.23	1.75	1.80	2.25		0.00	0.07	4.90	97.87
29-464.5-1	4	dmpu	59.30	0.39	19.40	4.95			0.02	1.64	2.29	2.50	4.26		0.00	0.12	2.39	96.66
29-774-1	4	dpm	68.50	0.40	16.00	2.52	1.10	1.50	0.04	1.40	2.06	4.00	2.31	1.10	0.10	0.11	0.40	98.92
29-804-1	4		78.20	0.28	11.30	0.90	0.00	0.90	0.05	0.70	4.53	1.20	0.57	0.60	0.50	0.08	0.08	98.97
31-767-1	4	dmv	68.60	0.39	17.20	1.98	0.40	1.60	0.02	1.54	1.74	3.20	2.63	1.70	0.20	0.11	0.06	99.38
31-989.5-1	4	mp	76.30	0.24	11.50	2.61	0.10	2.50	0.04	1.32	2.20	1.50	1.16	1.40	0.10	0.03	0.33	98.64
32-1169.5-1	4	dmp	72.20	0.37	15.40	1.89	0.20	1.70	0.03	1.27	3.45	2.60	2.05	0.80	0.10	0.11	0.21	100.44
32-1388-1	4	dpx	68.80	0.34	13.60	6.57	2.60	4.20	0.09	1.64	2.83	3.10	1.70	0.80	0.10	0.06	0.87	100.51

Table C.5. Whole-rock Geochemical Analyses. (continued)

a. Major Element Analyses (weight percent oxide or element)

Sample	Unit	Code	SiO_2	TiO_2	Al_2O_3	FeOt	Fe_2O_3	FeO	MnO	MgO	CaO	Na_2O	K_2O	H_2Ot	CO_2t	P_2O_5	S	Total
32-1434.5-1	4	dmp	71.20	0.34	14.40	2.70	0.00	2.80	0.03	1.40	2.43	2.40	2.69	1.20	0.10	0.06	0.88	99.71
32-1565-1	4	vp	62.90	0.47	15.60	6.30	0.80	5.60	0.12	4.71	2.54	3.10	1.25	2.60	0.10	0.12	0.16	100.03
34-1834.5-1	4	pmi	78.20	0.19	11.70	2.70	0.50	2.20	0.06	1.08	2.71	1.70	1.27	0.80	0.10	0.04	0.10	100.63
80-1138-1	4	p	74.00	0.14	14.30	0.81	0.00	1.00	0.01	0.36	1.86	5.70	0.91	0.40	0.10	0.00	0.00	98.78
H8-1-1	4	pmlx	73.90	0.24	11.90	3.78			0.05	1.01	2.65	2.40	2.24	1.00	1.00	0.04	0.00	100.21
I7-29-1	4	pmli	72.40	0.24	11.80	3.96	0.90	3.10	0.06	1.57	4.57	0.50	2.09	1.50	1.30	0.04	0.08	100.13
I7-32-1	4	pm	74.00	0.24	11.90	4.14	0.90	3.30	0.04	1.71	2.60	1.30	2.77	1.50	0.50	0.04	0.00	100.80
19-1233-1	4	gp	68.60	0.34	14.10	4.05	1.60	2.60	0.09	3.29	4.34	1.20	2.19	1.10	0.10	0.09	0.87	100.29
24-1200-1	4	gp	68.50	0.41	13.50	4.86	1.70	3.30	0.07	3.61	2.22	1.00	1.94	2.20	0.00	0.10	0.98	99.29
34A-1644.5-1	4	gaui	78.20	0.33	11.50	1.53			0.01	0.44	3.77	2.60	0.35		0.20	0.08	1.05	99.80
34A-1644.5-2	4	bgpui	51.20	0.32	11.80	9.54			0.14	2.01	11.00	1.20	0.93		5.60	0.04	6.71	98.82
34C-1878-1	4	gmvu	67.90	0.29	13.80	4.23			0.10	4.53	0.80	0.70	2.11		0.20	0.08	1.45	95.83
I8-6-1	4	ph	68.90	0.25	14.50	3.96	0.50	3.50	0.09	1.63	4.77	2.90	1.29	0.90	0.80	0.04	0.00	100.07
I8-27-1	4	pyhti	70.60	0.26	14.40	4.41	0.70	3.80	0.08	1.75	3.58	2.70	1.60	1.00	0.20	0.04	0.05	100.75
22A-1191-1	1/10d	pvym	71.30	0.33	13.10	5.58	1.30	4.40	0.28	2.76	1.91	0.06	2.45	1.80	0.10	0.07	0.22	100.03
24-463.5-1	1/10d	m	73.30	0.28	12.20	4.86			0.05	1.21	1.62	1.30	2.04		0.00	0.06	1.50	98.05
70-1037.5-1	1/10d	vpy	73.00	0.22	11.20	5.04	0.50	4.60	0.29	2.97	3.36	0.40	1.22	1.50	0.10	0.05	0.00	99.41
70-1153-1	1/10d	pmvyi	72.60	0.26	12.40	4.95	1.10	3.90	0.13	1.23	1.54	3.50	1.36	1.00	0.10	0.06	0.15	99.29
80-1416-1	1/10d	pmv	72.10	0.30	12.10	3.78	0.50	3.30	0.04	2.98	1.47	2.80	1.92	1.30	0.20	0.12	0.00	99.13
31-312.5-1	1b/10d	cdmpv	59.60	0.34	21.00	4.41	1.30	3.30	0.05	2.60	0.62	2.60	5.56	2.60	0.10	0.05	0.00	99.72
80-1680.5-1	1b/10d	mvp	71.40	0.29	12.30	5.04	0.50	4.60	0.04	3.71	0.68	1.20	2.21	2.60	0.10	0.05	0.11	99.76
19-1041.5b-1	1/10p	pv	55.70	0.67	18.70	8.91			0.06	4.05	4.15	3.30	1.04		0.20	0.09	1.67	98.12
22B-1783.5-1	1/10p	py	67.50	0.31	15.10	4.50	1.10	3.50	0.21	2.34	5.46	1.00	1.65	1.10	0.10	0.05	0.71	99.95
19-986-1	1/10p	gpv	72.70	0.27	13.20	4.50	0.80	3.80	0.10	1.54	3.38	1.60	1.20	1.20	0.10	0.07	0.13	100.06
24-1044-1	1/10p	gvpu	52.30	0.37	14.00	13.86			0.12	8.40	2.37	0.00	0.29		0.10	0.03	4.81	95.45
24-981a-1	1/10p	gv	73.60	0.24	11.80	3.96	0.80	3.30	0.06	2.89	2.58	1.80	0.34	2.00	0.10	0.06	0.26	99.77
27-1324.5-1	1/10p	gmvur	71.80	0.27	12.70	4.41			0.11	1.84	2.32	1.40	1.17		0.00	0.07	2.05	97.63
27-1343-1	1/10p	gvp	68.40	0.27	12.70	4.41	0.70	3.80	0.04	6.15	3.19	0.50	1.15	2.60	0.10	0.07	0.12	99.76
29-1092-1	1/10p	cgmpu	64.90	0.46	15.50	6.12			0.08	1.97	3.42	1.70	2.53		0.10	0.11	2.57	98.82
34A-1679-1	1/10p	gmuy	70.00	0.35	13.30	5.13			0.03	0.89	2.42	1.50	1.92		0.10	0.09	3.86	98.63
19B-872-1	1b/10p	mupvi	66.40	0.30	13.90	8.10			0.02	0.87	0.15	0.50	3.58		0.10	0.07	4.80	97.59
19-1237-1	1b/10p	cpmv	66.50	0.40	13.90	6.84			0.18	3.26	3.02	1.30	2.12		0.00	0.08	1.89	99.02
19-662-1	1b/10p	mui	64.70	0.22	9.50	12.42			0.00	0.39	0.29	0.70	1.90		0.10	0.05	10.90	98.45
22A-1515-1	1b/10p	cpvsi	71.00	0.31	13.10	6.12	1.80	4.50	0.08	2.39	1.42	1.50	1.89	1.60	0.00	0.07	0.30	99.89
22A-1551.5-1	1b/10p	cpvi	73.80	0.26	12.10	4.14	0.60	3.60	0.04	2.37	2.13	2.40	1.20	1.30	0.10	0.06	0.09	100.03
22A-1752-1	1b/10p	muk	65.00	0.24	11.60	11.61			0.02	0.76	0.48	1.00	1.08		0.10	0.07	9.90	99.39
22A-1752-2	1b/10p	am	83.00	0.16	8.30	3.15			0.01	0.52	0.18	0.60	1.68		0.10	0.05	2.38	99.54
34-1275-1	1b/10p	mp	66.60	0.36	15.80	4.86			0.09	1.90	2.68	1.50	2.90		0.00	0.08	1.26	97.72
19-1100-1	4/10p	mvupi	62.30	0.25	9.30	13.95			0.02	1.12	0.26	0.50	2.07		0.20	0.07	10.10	97.62
19-1250-1	4/10p	mi	71.10	0.26	12.00	5.31			0.06	0.84	1.91	1.00	2.33		0.80	0.07	3.69	98.45
22A-1885-1	4/10p	mkpui	46.40	0.72	26.90	6.75			0.02	5.57	0.26	0.80	4.41		0.00	0.07	4.04	94.93
22A-1975.5-1	4/10p	puqy	61.40	0.45	15.10	8.10			0.18	2.30	6.05	0.90	1.47		0.10	0.06	2.03	97.63
22A-1979-1	4/10p	mvusi	68.40	0.26	11.40	8.91			0.02	2.36	0.22	0.00	1.74		0.00	0.04	4.94	97.06
22A-2004-1	4/10p	omvus	65.90	0.30	13.30	8.82			0.07	2.96	0.20	0.00	2.60		0.10	0.09	4.82	97.96
22B-2036-1	4/10p	mvupi	70.70	0.34	12.80	4.05			0.09	1.51	2.52	1.20	1.86		0.60	0.09	2.68	97.77
24-1082-1	4/10p	rmvu	65.50	0.32	13.30	7.02			0.07	4.62	0.95	0.50	1.63		0.10	0.10	3.91	97.05
24-1228-1	4/10p	pvm	70.90	0.36	13.70	3.15			0.03	1.29	1.62	4.10	1.32		0.10	0.09	1.32	97.65
28-343-1	4/10p	om	70.10	0.37	18.70	1.62			0.00	0.38	0.19	1.20	4.20		0.00	0.10	1.21	97.77
29-1057-1	4/10p	cmrpu	61.30	0.51	14.80	8.55			0.05	4.10	1.40	0.80	0.20		0.10	0.11	4.58	95.36
29-1099-1	4/10p	mu	68.20	0.34	13.40	6.21			0.02	0.97	1.70	1.20	2.23		0.00	0.10	4.92	98.06
29-876-1	4/10p	mvui	59.50	0.37	12.80	12.60			0.02	2.45	0.28	0.00	2.78		0.10	0.07	8.35	97.24
31-869.5-1	4/10p	py	66.40	0.54	15.50	3.96	0.30	3.70	0.11	2.41	2.58	4.30	1.80	1.10	0.30	0.12	0.09	99.23
34A-1565-1	4/10p	dmp	72.70	0.33	14.30	1.89	0.30	1.60	0.04	2.15	2.79	0.80	2.81	1.40	0.10	0.10	0.14	99.53
34C-1747.5-1	4/10p	omukp	67.80	0.27	11.00	10.35			0.01	1.23	0.17	0.00	2.43		0.00	0.08	7.34	98.85
34-1666-1	4/10p	mpki	74.80	0.34	13.80	2.97			0.01	1.17	0.35	0.80	2.75		0.10	2.09		99.18
22A-1788-1	4/10p	gvpu	71.40	0.28	12.00	3.78	1.00	2.90	0.11	4.07	4.03	0.80	1.47	1.30	0.10	0.07	0.99	100.27
24-1044-2	4/10p	cgvp	74.00	0.23	9.40	6.21			0.04	1.96	3.77	0.00	0.38		0.00	0.07	2.68	98.07
34C-1831-1	4/10p	gmup	68.50	0.28	12.70	5.40			0.06	1.29	2.38	1.50	2.03		0.00	0.05	3.94	97.15
34-1728-1	4/10p	gmpv	72.10	0.33	13.00	3.24	0.70	2.60	0.05	2.43	2.04	0.80	2.50	1.70	0.10	0.09	0.95	99.15
22B-1044-1	10d	ovmsi	76.60	0.22	11.50	5.67	2.00	3.90	0.09	2.15	0.15	0.00	1.44	2.40	0.10	0.03	0.08	100.64
22-901-1	10d	omvks	75.80	0.21	12.20	4.59			0.03	1.48	0.10	0.00	2.09		0.10	0.04	2.52	98.53
22-957-1	10d	ovmsr	73.30	0.31	13.20	3.69	0.90	2.90	0.08	2.26	0.62	0.00	1.86	2.40	0.10	0.04	0.31	98.20
22-996.5-1	10d	ovmsx	71.20	0.28	11.60	9.18	4.20	5.40	0.11	3.31	0.15	0.00	0.96	2.60	0.10	0.06	0.14	100.08
24-444.5-1	10d	omuvi	68.60	0.22	11.80	9.18			0.08	0.93	0.16	0.00	3.14		0.10	0.06	4.32	97.51
27-593.5-1	10d	ovsmx	74.50	0.23	11.90	7.11	3.00	4.40	0.10	2.24	0.13	0.00	1.27	2.30	0.10	0.07	0.14	100.35

Table C.5. Whole-rock Geochemical Analyses. (continued)

a. Major Element Analyses (weight percent oxide or element)

Sample	Unit	Code	SiO_2	TiO_2	Al_2O_3	FeOt	Fe_2O_3	FeO	MnO	MgO	CaO	Na_2O	K_2O	H_2Ot	CO_2t	P_2O_5	S	Total
27-733-1	10d	omvr	71.40	0.33	12.80	4.77			0.05	3.05	0.82	0.00	1.82		0.10	0.05	1.21	96.10
34B-930-1	10d	vmski	70.40	0.23	12.70	6.48			0.06	4.89	0.18	0.00	1.15		0.10	0.06	1.70	97.53
34B-967-1	10d	vmsi	70.30	0.37	12.80	5.04	1.00	4.10	0.10	3.87	1.04	1.10	0.71	2.80	0.10	0.07	0.83	98.98
34-863.5-1	10d	vmki	73.00	0.24	12.30	4.05	0.90	3.30	0.02	4.31	0.18	0.00	1.34	3.20	0.10	0.03	0.69	99.44
34-937-1	10d	vmysi	70.20	0.36	13.20	4.77	0.50	4.30	0.13	3.84	1.71	1.60	0.68	2.80	0.10	0.07	0.24	99.67
70-664-1	10d	ovsmx	74.40	0.22	11.20	7.47	3.90	4.00	0.04	2.09	0.11	0.00	0.87	1.80	0.10	0.06	0.00	98.79
70-687-1	10d	ovsmp	72.00	0.25	11.80	7.65	2.20	5.70	0.05	3.20	0.12	0.00	1.29	2.80	0.00	0.06	0.00	99.47
70-822.5-1	10d	omvsx	73.50	0.23	11.70	5.94	1.90	4.20	0.04	2.24	0.14	0.00	2.14	2.70	0.10	0.06	0.08	99.01
70-876.5-1	10d	omvki	74.30	0.27	11.20	5.13	0.50	4.70	0.02	3.12	0.10	0.00	1.52	2.70	0.00	0.05	0.04	98.51
70-934-1	10d	omvy	69.90	0.23	12.70	5.94	1.10	4.90	0.20	4.54	0.29	0.00	1.99	3.60	0.10	0.05	0.54	100.01
73-1107.5-1	10d	omvs	77.00	0.17	11.10	4.23	0.70	3.60	0.04	2.73	0.00	0.00	1.96	2.70	0.00	0.02	0.00	100.02
73-1170.5-1	10d	omvks	67.90	0.24	13.50	8.64			0.05	3.98	0.00	0.00	1.21		0.10	0.02	1.41	96.70
73-1170.5-2	10d	omvi	76.10	0.19	10.80	4.32	0.70	3.70	0.03	2.70	0.00	0.00	1.96	2.70	0.00	0.02	0.04	98.93
73-1224-1	10d	omvsx	75.40	0.27	11.30	4.68	1.20	3.60	0.03	2.35	0.14	0.00	2.01	2.60	0.00	0.08	0.08	99.04
73-1257-1	10d	omv	75.10	0.32	10.80	3.60	0.40	3.30	0.02	3.31	0.14	0.00	1.95	2.80	0.10	0.08	0.00	98.32
73-1316-1	10d	omkst	70.60	0.24	11.50	6.66			0.04	4.04	0.12	0.00	1.41		0.00	0.06	1.61	95.88
73-949-1	10d	omv	78.30	0.24	11.50	2.70	0.40	2.40	0.02	2.21	0.12	0.00	2.33	2.30	0.00	0.06	0.00	99.88
80-1176-1	10d	pvmi	67.80	0.57	14.00	5.22	0.07	4.60	0.09	2.58	1.80	2.90	2.05	1.50	0.00	0.14	0.04	98.13
80-1382-1	10d	omv	76.00	0.23	11.90	2.25	0.20	2.00	0.02	2.69	0.58	0.70	2.22	2.40	0.40	0.04	0.00	99.38
80-1639.5-1	10d	ovm	71.60	0.25	12.30	4.68	0.80	4.00	0.06	4.59	0.12	0.00	1.87	3.30	0.00	0.05	0.00	98.94
24-277.5-1	10d	wovmk	52.40	0.40	19.20	9.18			0.10	10.20	0.15	0.00	0.86		0.00	0.08	1.02	93.34
80-1571.5-1	10d	wovkm	31.90	0.52	39.70	10.89	2.20	8.90	0.07	7.64	0.41	0.00	1.28	5.70	0.10	0.27	0.40	98.99
27-484-1	10da	ot	77.10	0.27	11.40	3.51			0.02	1.07	0.11	0.60	2.16		0.10	0.04	2.05	97.92
27-504-1	10da	oki	82.10	0.17	9.90	2.70			0.02	0.25	0.10	0.60	1.79		0.00	0.03	1.84	99.04
34-799-1	10da	ou	81.60	0.26	10.60	1.08	0.50	0.60	0.00	0.24	0.12	0.50	2.38	1.30	0.00	0.05	0.61	98.61
19B-785-1	10p	ckru	74.00	0.27	12.90	3.33			0.02	0.72	2.50	2.40	0.67		0.00	0.04	2.16	98.47
19-801-1	10p	omrku	51.10	0.43	19.60	13.23			0.00	0.44	0.48	0.50	3.10		0.20	0.03	11.60	97.82
19-950-1	10p	ckmup	68.00	0.25	16.60	5.40			0.01	1.06	0.53	1.20	1.70		0.10	0.03	4.41	98.19
22A-1625-1	10p	omvsy	69.80	0.29	13.30	5.49			0.12	3.15	0.18	0.50	2.44		0.10	0.08	2.47	97.30
22B-1703-1	10p	pmysx	74.50	0.26	12.40	4.50	1.30	3.40	0.12	1.37	2.89	0.90	1.53	1.30	0.20	0.04	0.06	100.26
22B-1721-1	10p	mpysu	72.10	0.25	12.30	6.12			0.17	2.31	1.20	0.70	2.34		0.10	0.07	1.48	98.77
22B-1721-2	10p	omspy	71.50	0.32	12.20	6.03			0.09	1.87	0.54	0.00	2.06		0.10	0.07	2.41	96.59
24-812-1	10p	kmup	45.50	0.65	30.00	8.64			0.01	0.93	1.58	3.30	1.32		0.10	0.07	6.92	97.29
24-812-2	10p	mkut	53.50	0.51	27.10	5.40			0.01	0.75	1.41	4.20	1.66		0.10	0.06	4.11	97.79
24-812-3	10p	muk	42.90	0.62	27.60	11.16			0.01	0.96	0.58	3.50	2.01		0.00	0.07	9.21	96.32
24-991-1	10p	cmsk	75.80	0.32	14.70	2.07			0.00	0.27	0.58	1.80	1.24		0.10	0.07	1.71	98.23
32-1465.5-1	10p	dmu	59.50	0.51	15.70	9.27			0.01	0.55	1.76	1.00	3.47		0.10	0.08	8.94	98.66
34A-1614-1	10p	mui	67.80	0.38	14.20	5.94			0.01	0.75	1.04	0.90	3.35		0.20	0.10	4.51	98.06
34C-1377-1	10p	mskut	55.80	0.45	22.10	8.55			0.05	0.75	0.87	1.50	3.49		0.10	0.06	6.92	98.91
34-1347-1	10p	mvuk	70.70	0.30	15.10	4.86			0.07	1.98	0.79	1.60	1.62		0.10	0.07	2.91	99.37
34-1477-1	10p	muj	71.50	0.23	10.90	8.28			0.01	0.30	0.28	0.00	2.79		0.20	0.00	7.05	99.78
34-1551-1	10p	cmui	74.00	0.24	12.10	6.48			0.01	0.42	0.34	0.90	2.41		0.10	0.03	3.53	99.68
34-1607.5-1	10p	gmk	70.30	0.30	16.10	4.86			0.01	0.56	1.40	1.30	1.38		0.10	0.06	3.74	99.18
34C-1626-1	10p	gvup	63.00	0.43	12.70	11.52			0.04	4.14	1.87	2.20	0.24		0.10	0.09	3.76	99.15
34C-1710-1	10p	gv	57.40	0.66	16.70	8.28			0.09	5.56	3.48	2.00	0.14		0.20	0.09	3.22	97.02
19B-663.5-1	10pa		72.80	0.26	11.20	5.76			0.01	0.96	0.28	1.00	2.11		0.00	0.06	4.39	97.74
22A-1638-1	10pa	ouk	77.10	0.25	11.30	3.51			0.01	0.24	0.10	0.90	2.09		0.10	0.03	2.96	97.85
22A-1650-1	10pa	ui	76.20	0.25	12.20	3.51			0.02	0.32	0.23	0.70	2.15		0.00	0.04	2.67	97.62
22A-1650-2	10pa	opui	74.70	0.27	12.50	3.96			0.02	1.04	0.18	0.60	2.53		0.10	0.04	2.56	97.86
22B-1723-1	10pa	outi	72.10	0.34	13.60	3.87			0.02	0.58	0.69	0.60	2.52		0.10	0.07	2.67	96.49
27-1295.5-1	10pa	cpu	71.80	0.26	11.80	7.11			0.05	1.63	0.30	0.50	2.55		0.10	0.06	2.97	98.39
34C-1435-1	10pa	uk	62.40	0.24	12.00	12.42			0.00	0.17	0.40	1.50	0.82		0.00	0.00	10.60	97.91
34C-1453-1	10pa	ou	48.40	0.52	24.80	11.61			0.04	0.69	0.14	1.10	3.61		0.00	0.06	8.30	97.20
34-1539-1	10pa	ui	68.30	0.23	12.20	9.27			0.00	0.27	0.16	1.30	1.76		0.10	0.00	6.94	98.80
19-848-1	10p/5	orumk	33.80	0.32	20.90	23.67			0.01	1.82	1.39	0.00	1.59		0.10	0.02	18.05	97.17
24-1131a-1	10p/5	zsu	57.40	0.29	10.00	19.53			0.19	3.45	1.52	0.00	0.09		0.50	0.02	6.10	97.57
34-1525.5-1	10p/5	mupj	36.80	0.33	15.70	26.73			0.02	1.19	5.66	0.90	1.08		0.10	0.00	14.30	99.24
24-1190.5-1	4/5	upv	52.10	0.21	7.70	20.97			0.05	2.64	1.22	1.30	0.89		0.00	0.04	15.90	99.06
29-1019-1	4/5a	clu	42.80	0.07	1.60	9.90			0.16	0.32	20.07	0.00	0.21		16.50	0.00	8.43	97.96
34-1498.5-1	3	ourpi	15.50	0.31	6.00	36.90			0.01	0.54	1.18	0.00	0.43		17.60	0.05	34.60	*91.69
H8-10-1	4/10	kpu	67.90	0.28	14.40	3.87			0.05	2.36	3.12	1.40	1.37		0.00	0.05	1.60	96.00
H9-13-1	4/10	pusk	68.60	0.27	14.10	4.68			0.08	3.52	3.24	0.90	1.75		0.20	0.04	1.27	98.33
H9-30-1	4a/10	pm	69.60	0.25	14.30	4.59	0.70	4.00	0.07	1.71	4.36	1.40	2.34	1.20	0.60	0.04	0.06	100.62
H9-30-2	4a/10	psmy	74.80	0.25	13.50	3.15	0.80	2.50	0.06	1.51	1.88	1.70	1.92	1.30	0.00	0.04	0.00	100.26
H9-30-3	4a/10	hv	73.90	0.24	13.40	3.24	0.20	3.00	0.11	1.38	3.84	1.80	1.15	0.90	0.10	0.04	0.00	100.06

* The total assumes C_t rather than CO_2 as this sample is graphitic.

Table C.5. Whole-rock Geochemical Analyses. (continued)

a. Major Element Analyses (weight percent oxide or element)

Sample	Unit	Code	SiO_2	TiO_2	Al_2O_3	FeOt	Fe_2O_3	FeO	MnO	MgO	CaO	Na_2O	K_2O	H_2Ot	CO_2t	P_2O_5	S	Total
H9-54-5	1/10	psk	68.90	0.25	15.00	4.77	0.40	4.40	0.05	3.77	1.84	1.50	2.50	1.50	0.00	0.04	0.00	100.15
H9-60-2	4/10	ms	55.90	0.64	28.10	2.61	1.80	1.00	0.05	0.76	2.77	3.20	3.66	2.10	0.10	0.03	0.00	100.11
H9-6-2	4/10	skpm	58.70	0.57	25.50	3.24	1.30	2.10	0.07	1.04	3.46	3.40	2.28	1.50	0.10	0.03	0.00	100.05
31-814-1	10m	vpy	62.40	0.59	15.40	8.64	2.90	6.00	0.16	2.97	3.75	1.80	1.04	2.10	0.10	0.09	0.90	99.98
73-834-1	10m	vhpqi	53.30	0.22	14.40	8.82	2.00	7.00	0.15	11.40	4.55	0.70	0.84	4.60	0.10	0.02	0.24	99.46
80-1265-1	10m	ovhyi	50.40	0.22	14.30	15.21	3.60	12.00	0.78	10.94	0.97	0.00	0.06	6.20	0.20	0.02	0.10	99.77
80-1286.5-1	10m	ohv	46.50	0.21	11.00	16.65	5.90	11.30	0.40	10.14	9.30	1.10	0.19	1.90	0.40	0.00	0.22	98.51
80-1316-1	10m	pv	57.70	0.29	21.70	3.33	0.40	3.00	0.05	2.76	5.82	4.50	1.30	1.30	0.10	0.00	0.12	99.01
19-157-1	1/10c	vpy	67.40	0.31	13.20	6.66	1.40	5.40	0.15	4.22	1.30	0.50	1.91	3.20	0.00	0.07	0.53	99.46
19-274.5-1	1/10c	lm	60.10	0.24	9.80	3.33	0.90	2.60	0.09	1.15	11.45	1.90	1.99	0.90	8.20	0.05	0.81	99.98
22A-1350.5-1	1/10c	qpm	71.40	0.31	12.60	3.96	1.00	3.00	0.11	1.63	4.34	0.50	3.15	1.00	0.20	0.06	0.15	99.41
22B-1347-1	1/10c	pmq	71.90	0.34	12.80	4.32	1.60	2.90	0.07	1.71	2.30	1.00	3.19	1.40	0.10	0.07	0.48	99.74
22B-1843-1	1/10c	pmqu	66.40	0.28	11.40	3.78			0.13	2.66	5.56	0.00	1.99		1.20	0.07	1.46	94.57
22-685.5-1	1/10c	cpm	72.30	0.25	12.00	3.96	0.80	3.20	0.10	1.07	3.52	1.90	2.64	1.00	1.50	0.05	0.00	100.33
22-789-1	1/10c	pqm	71.30	0.34	10.80	4.05	1.90	2.40	0.12	2.55	5.13	0.00	3.11	1.00	0.10	0.07	0.16	98.94
24-668-1	1/10c	mpq	68.30	0.39	15.70	3.24	1.50	1.90	0.04	1.68	0.72	0.00	5.42	2.30	0.40	0.06	0.23	98.58
27-328-1	1/10c	pmq	72.80	0.23	11.50	4.23	1.50	2.90	0.09	1.67	2.95	0.60	4.19	1.20	0.30	0.07	0.05	100.04
27-763-1	1/10c	mpvui	68.50	0.27	12.40	7.20			0.09	3.20	1.24	0.00	2.76		0.10	0.07	1.75	97.14
29-183.5-1	1/10c	p	72.80	0.25	11.90	3.33	0.60	2.80	0.09	0.87	3.32	3.10	1.90	0.90	1.40	0.06	0.04	100.02
29-716-1	1/10c	mpq	55.90	0.44	22.40	5.49			0.04	1.56	2.30	1.60	5.75		0.10	0.08	1.90	97.09
31-716-1	1/10c	cmpq	56.10	0.38	20.30	7.56	2.30	5.50	0.11	2.36	3.89	2.90	3.78	1.70	0.20	0.05	0.35	99.83
32-657-1	1/10c	qp	72.80	0.36	11.80	2.97	1.00	2.00	0.09	2.15	3.12	1.10	3.67	1.10	0.20	0.07	0.03	99.48
34A-1252-1	1/10c	qpl	67.80	0.28	11.70	3.96	2.60	1.60	0.12	2.00	8.67	0.00	2.09	1.10	1.60	0.05	0.04	99.64
34A-992-1	1/10c	pqm	71.40	0.29	11.80	3.78	1.10	2.80	0.16	2.86	3.87	0.00	2.63	1.20	0.10	0.07	0.29	98.50
34B-1032.5-1	1/10c	pvmy	71.80	0.28	12.10	5.49	0.70	4.80	0.06	2.86	2.63	0.00	2.45	1.60	0.10	0.07	0.07	99.50
34-1028.5-1	1/10c	pql	71.90	0.25	11.30	3.69	1.40	2.40	0.12	2.41	4.72	0.00	2.39	0.90	0.10	0.07	0.50	98.34
34-697.5-1	1/10c	pql	66.50	0.28	9.90	6.30	2.00	4.50	0.15	3.30	4.88	0.00	3.37	1.40	2.30	0.06	0.56	99.06
70-462-1	1/10c	pq	70.80	0.28	11.60	4.86	1.40	3.60	0.08	2.77	3.23	1.30	3.30	1.10	0.00	0.06	0.07	99.57
70-560-1	1/10c	pq	45.80	0.51	17.70	13.68	6.30	8.00	0.12	4.44	6.99	0.60	6.56	2.20	0.40	0.06	0.38	99.97
70-566.5-1	1/10c	cmqp	73.70	0.25	11.40	3.24	1.30	2.10	0.04	1.86	2.20	0.00	4.28	1.60	0.70	0.06	0.04	99.52
73-1380.5-1	1/10c	pmyu	71.30	0.32	11.70	5.49	1.10	4.50	0.08	2.49	2.26	1.10	2.76	1.20	0.10	0.07	0.30	99.21
80-1738-1	1/10c	pmq	71.90	0.26	12.40	4.05	0.80	3.40	0.03	2.00	1.67	1.30	3.68	1.30	0.20	0.05	0.00	98.99
80-1795-1	1/10c	pql	61.60	0.25	12.00	8.28	2.70	5.90	0.14	3.73	5.80	0.00	3.97	1.80	1.10	0.05	0.07	99.09
22B-1911-1	1b/10c	plu	70.30	0.22	10.60	2.79			0.04	3.74	5.12	0.50	1.85		1.40	0.03	1.07	97.39
24-624.5-1	1b/10c	apq	77.00	0.20	10.00	3.15	1.10	2.10	0.18	0.96	4.23	1.40	1.46	0.80	1.00	0.05	0.23	100.65
24-624.5-2	1b/10c	mpq	69.60	0.35	13.60	4.50	1.40	3.20	0.19	1.69	2.35	0.90	3.64	1.60	0.40	0.07	0.19	99.13
27-963.5-1	1b/10c	pmqy	70.00	0.32	13.30	5.13	1.10	4.10	0.13	1.75	2.26	1.00	3.49	1.40	0.40	0.07	0.08	99.38
D4-37-1	1b/10c	hqpy	64.10	0.31	14.30	7.83	2.60	5.50	0.21	1.67	7.96	1.20	0.94	1.30	0.10	0.07	0.25	100.45
22B-1950-1	4/10c	hvp	62.40	0.35	12.20	5.85			0.09	9.60	2.55	0.00	1.49		0.10	0.09	1.15	95.58
24-1252.5-1	4/10c	pq	57.80	0.45	14.50	6.75			0.13	2.23	3.98	2.30	2.19		0.10	0.11	1.10	91.37
27-1486-1	4/10c	p	66.80	0.36	13.50	4.95	0.80	4.20	0.05	3.95	4.68	0.00	2.75	1.30	0.00	0.09	0.21	98.64
27-1486-2	4/10c	pqh	66.30	0.33	13.10	4.59	1.00	3.70	0.07	3.93	7.07	0.00	2.02	1.00	0.80	0.09	0.39	99.70
28-393.5-1	4/10c	pl	70.70	0.25	13.80	4.14	0.70	3.50	0.06	1.42	3.65	2.90	1.76	0.80	0.50	0.07	0.09	100.18
29-739-1	4/10c	mpu	68.40	0.30	13.40	7.56			0.03	0.96	1.51	2.00	2.64		0.10	0.06	2.82	99.08
32-1426-1	4/10c	dqpm	64.50	0.41	18.00	4.14	2.60	1.80	0.07	1.74	3.49	0.00	4.47	2.10	0.10	0.11	0.39	99.68
73-602-1	4/10c	pq	70.70	0.25	11.30	4.68	1.50	3.30	0.08	1.76	4.92	1.80	1.91	1.00	1.00	0.06	0.10	99.66
D4-9-1	4/10c	lhq	48.60	0.38	12.70	7.11	0.80	6.40	0.14	6.60	11.38	1.00	0.58	2.10	9.00	0.06	0.32	99.98
D4-9-2	4/10c	lyhp	56.70	0.39	13.20	5.40	1.30	4.20	0.15	2.76	12.14	1.20	0.71	1.30	5.30	0.05	0.51	99.78
H9-10-1	4/10c	pqlx	67.40	0.28	14.00	5.22	1.80	3.60	0.11	1.74	3.80	2.70	3.23	1.00	0.50	0.04	0.00	100.20
19-1023.5-1	10i	cl	52.70	0.49	12.30	7.11	1.60	5.70	0.14	4.15	14.51	0.70	0.39	1.10	5.70	0.07	0.19	99.69
22A-1262-1	10i	qhp	70.90	0.26	10.60	4.05	1.90	2.30	1.50	3.85	6.56	0.00	1.66	1.10	0.10	0.04	0.00	100.77
22A-1262-2	10i	ohp	62.80	0.24	10.90	5.22	2.60	2.90	0.27	5.99	11.77	0.00	0.39	1.30	0.20	0.06	0.00	99.42
24-1053-1	10i	h	58.80	0.60	15.30	6.84	2.10	4.90	0.16	4.49	9.26	1.30	0.42	1.10	0.10	0.10	0.80	99.23
24-471-1	10i	ohlq	44.40	0.11	5.00	6.39	0.90	5.50	0.54	10.42	22.01	0.00	0.07	1.50	9.20	0.02	0.00	99.67
27-1557-1	10i	hq	48.70	0.40	13.00	10.35	3.90	6.90	0.23	10.79	12.05	0.80	0.20	1.70	0.10	0.08	0.53	99.25
27-703.5-1	10i	h	48.00	0.18	8.70	11.88	4.30	8.00	0.48	14.67	11.52	0.80	0.15	2.40	0.40	0.12	0.21	99.88
29-858-1	10i	lhq	56.50	0.44	13.50	6.66			0.17	3.80	11.17	0.00	0.17		3.40	0.05	3.40	98.41
31-790-1	10i	hu	48.50	0.35	9.50	10.35			0.12	13.74	11.12	1.00	0.21		0.10	0.03	3.22	97.44
34B-759.5-1	10i	ohqpl	50.30	0.06	4.70	6.21	1.70	4.70	0.27	13.26	21.91	0.00	0.06	1.00	2.60	0.04	0.00	100.60
34C-1841.5-1	10i	ohql	56.40	0.22	9.80	11.25			0.24	6.76	11.71	0.00	0.08		0.20	0.03	2.27	98.39
34-697.5-2	10i	oplhq	44.00	0.17	6.80	7.38	1.30	6.20	0.38	7.20	16.19	0.00	3.81	1.60	12.10	0.04	0.19	99.93
34-876.5-1	10i	hql	55.00	0.16	10.40	5.76	2.50	3.50	0.17	11.99	14.30	0.00	0.07	1.60	0.20	0.16	0.00	100.05
73-677.5-1	10i	hq	55.60	0.14	12.50	6.48	3.70	3.10	0.20	7.54	13.65	0.50	0.18	1.70	0.20	0.02	0.00	99.03
73-677.5-2	10i	phq	48.80	0.25	15.00	9.27	3.10	6.50	0.15	10.07	6.60	1.00	4.00	2.50	0.30	0.00	0.58	98.71
28-199-1	2	hnvx	52.00	0.47	17.10	12.24	2.90	9.60	0.17	6.68	4.50	4.20	0.22	2.60	0.10	0.05	0.00	100.59

Table C.5. Whole-rock Geochemical Analyses. (continued)

a. Major Element Analyses (weight percent oxide or element)

Sample	Unit	Code	SiO_2	TiO_2	Al_2O_3	FeOt	Fe_2O_3	FeO	MnO	MgO	CaO	Na_2O	K_2O	H_2Ot	CO_2t	P_2O_5	S	Total
29-669-1	2	hv	50.40	0.47	16.90	12.33	2.90	9.70	0.18	5.95	7.77	3.30	0.11	2.00	0.20	0.05	0.09	100.00
29-757.5-1	2	hpvy	49.40	0.44	19.50	11.97	2.90	9.30	0.23	5.55	3.97	3.60	1.88	2.70	0.10	0.08	0.20	99.80
31-272.5-1	2	dhx	46.70	0.50	18.20	12.51	3.10	9.70	0.23	6.38	9.81	3.20	0.26	1.60	0.10	0.05	0.00	99.83
31-361-1	2	phv	47.80	0.52	18.70	13.23	1.90	11.50	0.12	6.55	3.52	2.20	2.96	3.40	0.10	0.06	0.00	99.33
31-399.5-1	2	h	51.30	0.48	16.30	12.06	3.40	9.00	0.18	5.96	9.12	1.90	0.17	1.90	0.10	0.05	0.07	99.91
31-473-1	2	h	52.20	0.48	16.60	11.43	3.00	8.70	0.21	5.32	10.13	1.60	0.21	1.20	0.10	0.05	0.00	99.80
31-521.5-1	2	h	50.60	0.45	17.00	11.88	2.70	9.50	0.18	6.12	8.91	2.50	0.24	1.80	0.20	0.05	0.00	100.25
31-558-1	2	hq	53.10	0.49	16.20	10.98	2.80	8.50	0.20	5.16	10.40	1.30	0.16	1.40	0.20	0.06	0.00	99.97
32-1323.5-1	2	h	51.30	0.47	17.40	12.15	2.90	9.50	0.19	5.59	8.63	3.10	0.10	1.50	0.00	0.06	0.00	100.74
34A-1459b-1	2	h	53.90	0.45	16.60	9.27	2.40	7.10	0.17	5.31	8.63	4.50	0.05	1.10	0.00	0.00	0.00	100.21
34A-1463.5-1	2	h	49.90	0.47	18.20	11.43	3.10	8.60	0.17	5.93	8.61	4.40	0.10	1.20	0.10	0.06	0.00	100.84
29-478.5-1	2a	hv	49.10	0.50	17.30	12.42	3.20	9.60	0.18	6.54	8.82	2.00	0.18	2.30	0.10	0.08	0.00	99.90
29-580.5-1	2a	h	50.70	0.47	16.80	10.98	2.30	8.90	0.19	6.02	10.35	1.80	0.16	1.40	0.00	0.05	0.06	99.19
29-633.5b-1	2a	h	50.60	0.43	16.80	11.07	2.70	8.70	0.17	6.49	8.36	4.10	0.12	1.50	0.00	0.04	0.00	100.01
D4-38-1	2a	hv	49.10	0.45	17.30	12.60	2.60	10.30	0.22	6.50	7.41	3.20	0.27	2.60	0.40	0.02	0.00	100.37
J8-2-1	2a	hx	51.70	0.44	17.00	11.34	3.60	8.10	0.18	5.73	7.56	2.90	0.73	2.10	0.50	0.03	0.00	100.57
28-272.5-1	2e	hvnx	51.10	0.49	17.20	12.33	2.50	10.10	0.16	6.37	5.67	4.40	0.13	2.30	0.10	0.05	0.00	100.57
29-685.5-2	2/10s	hn	63.90	0.40	13.90	8.91	2.40	6.70	0.12	3.49	3.43	4.40	0.07	1.20	0.00	0.15	0.08	100.22
34A-1484-1	2/10s	hnx	70.10	0.37	12.20	6.66	1.50	5.30	0.08	1.86	4.65	3.10	0.08	0.70	0.10	0.09	0.00	100.13
34A-1484-2	2/10s	nvx	68.90	0.40	13.10	7.83	2.70	5.40	0.06	2.17	2.88	4.00	0.00	1.20	0.00	0.09	0.04	100.93
H9-52-1	2b/10s	nypx	71.20	0.47	12.10	7.38	1.50	6.00	0.16	1.18	1.93	5.00	0.36	0.60	0.10	0.11	0.00	100.71
H9-61-5	2c/10s	ahy	69.80	0.69	14.20	3.87	0.40	3.50	0.02	1.79	5.06	3.30	0.31	0.70	0.10	0.18	0.00	100.05
29-633.5a-1	2/10e	oqhl	44.10	0.40	16.40	8.73	5.30	4.00	0.16	3.52	19.99	0.00	0.07	1.40	3.60	0.04	0.00	98.98
29-685.5-1	2/10e	hl	59.80	0.43	11.70	6.39	2.20	4.40	0.20	2.59	10.46	2.50	0.09	0.80	3.40	0.17	0.30	98.97
29-820a-1	2/10e	hqylu	59.00	0.18	9.60	13.86			0.73	2.74	8.60	0.30	0.12		1.80	0.05	2.72	99.02
34A-1459b-2	2/10e	oqlh	39.30	0.36	16.20	7.83	5.50	2.90	0.19	2.87	23.85	0.00	0.00	1.60	6.60	0.02	0.00	99.39
I8-20-1	2/10	hyp	52.90	0.77	14.30	17.73	4.40	13.80	0.51	2.43	7.81	0.00	1.22	1.40	0.20	0.16	0.04	99.93
24-1294-1	6a	bhv	45.70	0.54	18.20	13.14	2.90	10.50	0.22	7.44	8.04	2.90	0.20	2.80	0.10	0.05	0.22	99.76
24-1294-2	6a	ah	58.90	0.43	15.00	7.56	1.50	6.20	0.18	4.28	8.19	3.20	0.15	1.00	0.90	0.07	0.07	100.05
27-1611.5-1	6a	bhv	48.90	0.55	17.00	12.42	2.80	9.90	0.17	7.56	7.22	2.70	0.14	2.70	0.10	0.07	0.12	99.90
27-1611.5-2	6a	ahl	53.40	0.48	13.90	9.27	2.10	7.40	0.19	5.57	10.43	2.20	0.15	1.20	1.70	0.08	0.00	98.80
29-1223.5-1	6a	chv	53.70	0.42	14.70	9.90	2.20	7.90	0.17	7.28	8.72	1.80	0.28	2.00	1.00	0.07	0.07	100.29
32-1610-1	6a	hlv	52.10	0.51	16.70	10.80	2.10	8.90	0.18	6.62	6.93	3.20	0.53	2.20	0.40	0.06	0.04	100.46
34A-1760.5-1	6a	dhvn	50.00	0.50	17.30	11.43	2.70	9.00	0.18	6.33	7.18	3.60	0.12	2.50	0.70	0.08	0.11	100.27
34D-2010-1	6a	bhvn	51.40	0.42	15.50	11.25	1.90	9.50	0.18	8.60	7.72	2.90	0.10	2.10	0.10	0.03	0.00	100.45
34D-2010-2	6a	anhv	57.20	0.40	16.00	9.00	0.60	8.40	0.15	7.13	4.64	4.50	0.06	1.40	0.00	0.03	0.00	100.51
22A-2075.5-1	6	hl	52.50	0.46	15.10	10.62	2.30	8.50	0.19	7.34	8.79	2.90	0.09	1.50	0.10	0.05	0.05	99.86
24-1285-1	6	hp	60.10	0.54	15.30	8.64	1.50	7.30	0.11	3.01	5.25	3.20	1.13	1.40	0.40	0.14	0.04	99.41
28-453.4-1	6	ph	46.00	0.50	20.80	13.41			0.26	4.75	5.35	1.60	3.70		0.10	0.08	1.28	97.51
31-970.5-1	6	hpv	53.00	0.48	17.10	10.62	1.80	9.00	0.15	6.25	6.54	1.60	1.75	2.20	0.10	0.07	0.08	100.10
34-1851-1	6	hp	49.50	0.43	15.30	9.72	1.60	8.30	0.23	7.83	11.99	0.60	0.43	1.60	0.60	0.05	0.05	98.50
34C-1888-1	6/10e	hqpl	51.00	0.44	15.00	9.90	4.00	6.30	0.19	6.34	13.05	0.40	0.70	1.80	0.20	0.06	0.00	99.48
J8-23-1	7	dp	74.50	0.26	12.20	3.42	0.10	3.30	0.04	1.30	0.83	4.30	2.18	0.90	0.10	0.03	0.00	100.04

Table C.5. Whole-rock Geochemical Analyses. (continued)

b. Trace Element Analyses (ppm), Derived Values and Specific Gravity (ρ)

			Semi-quantitative									Quantitative			Derived values			
Sample	Unit	Code	Ba	Rb	Sr	Zr	Cr	Cu	La	Ni	Pb	V	Yb	Zn	Total% alkalis	$iv(FeOt)$	log Zr/TiO_2	ρ
24-097-1	1	epy	213	39	74	63	0	11	0	0	0	0	1.9	150	4.67	4.85	-1.60	2.74
24-657-1	1	epm	1028	59	86	83	0	90	0	0	0	0	2.7	560	6.00	2.99	-1.61	2.73
27-830-1	1	mvpy	735	25	73	74	10	85	0	0	0	0	2.5	140	2.17	4.76	-1.58	2.77
29-1146-1	1	cepvx	285	19	145	36	17	59	0	16	0	190	1.2	100	5.48	6.03	-2.23	2.76
29-336b-1	1	cpmi	1022	57	71	123	0	15	0	0	0	6	3.8	130	7.04	5.54	-1.47	2.76
29-711.5-1	1	pxv	191	0	39	27	13	390	0	19	0	61	1.9	67	6.68	8.53	-2.27	2.78
31-705-1	1	cdhnx	72	0	67	33	10	160	0	10	0	26	1.7	42	4.47	7.89	-2.15	2.80
32-426-1	1	epx	184	35	67	75	0	0	0	0		0	2.5	64	4.28	6.21	-1.54	2.73
34C-1315-1	1	pxi	180	22	195	83	0	37	0	0		7	1.8	86	5.36	3.04	-1.53	2.70
34-1130-1	1	epyxi	304	0	90	72	10	27	0	0		0	2.2	75	5.85	4.07	-1.61	2.71
34-757.5-1	1	ep	251	49	43	63	12	28	0	0		0	2.2	150	2.76	5.47	-1.73	2.77
H9-63-1	1	pl	602	62	112	52	14	0	11	0		5	3.0	82	5.93	3.96	-1.56	2.70
H9-64-1	1	ply	379	27	102	45	11	40	10	0		7	2.5	140	3.84	1.89	-1.55	2.73
34-1753.5-1	1	gvpqu	156	0	80	66	41	51	0	21		180	2.2	120	2.36	7.77	-1.85	2.78
24-097-2	1	fhlpv	78	0	48	53	0	0	0	0	0	0	3.0	180	2.46	7.29	-1.58	2.83
29-1146-2	1	chfp	177	0	113	38	18	55	0	18	0	180	1.5	110	4.24	6.94	-2.08	2.81
32-426-2	1	fphx	102	0	61	71	12	10	0	10		0	4.9	77	2.71	7.74	-1.49	2.83
34C-1315-2	1	fhyxi	79	0	268	89	11	55	0	10		11	4.1	110	4.04	4.65	-1.54	2.75
34C-1385-1	1	fh	150	0	255	169	10	15	0	11		8	2.1	98	3.68	0.30	-1.54	2.78
29-336a-1	1a	c	36	0	121	71	10	0	0	0	0	0	1.7	130	6.57	0.18	-1.53	2.64
29-501-1	1a	dn	149	0	99	84	20	67	0	11	0	41	2.4	50	4.96	4.52	-1.62	2.73
31-259.5-1	1a	cd	85	0	77	91	0	33	0	0	0	0	1.9	19	6.88	0.36	-1.47	2.65
32-1374.5-1	1a	vpxi	118	0	48	30	12	68	0	10		50	1.6	180	5.47	8.43	-2.08	2.74
34A-1292.5-1	1a	dx	71	0	83	53	0	41	0	0		0	1.5	0	5.00	0.25	-1.53	2.65
34C-1385-2	1a	ph	87	0	164	81	12	55	0	0		7	2.3	56	2.58	0.40	-1.54	2.74
H8-14-1	1a	my	263	0	117	44	10	57	0	9		0	2.5	110	2.18	1.14	-1.75	2.75
I8-42-5	1a	pml	408	27	97	79	11	0	0	0		8	2.0	58	4.99	2.79	-1.42	2.74
19-688-1	1a/10p	cd	80	0	65	78	11	13	0	0	0	6	1.5	23	5.73	0.14	-1.45	2.66
34-1397.5-1	1a/10p	dyvmx	61	0	66	86	11	35	0	0		5	2.4	82	3.84	3.89	-1.51	2.70
I8-13-1	1a/10c	pqlx	209	0	109	85	13	0	0	0		6	3.5	70	4.44	3.60	-1.39	2.76
19-744.5-1	1c	acd	88	0	61	62	0	0	0	0	0	0	1.1	46	6.23	0.15	-1.49	2.67
27-1228-1	1c	p	121	0	67	69	10	0	0	0	0	8	1.8	57	4.70	2.26	-1.58	2.69
34A-1360-1	1c	du	39	0	79	59	0	15	0	0		8	1.1	27	5.52	-0.17	-1.53	2.70
34-1306.5-1	1c	d	43	0	76	68	0	0	0	0		0	1.0	0	5.70	0.14	-1.51	2.64
34-1443.5-1	1c	acd	77	0	54	54	0	20	0	0		0	1.3	16	5.55	0.13	-1.55	2.67
34-1443.5-2	1c	cdum	76	0	31	55	0	13	0	0		8	1.2	64	5.15	0.11	-1.54	2.80
19-440-1	1b	cp	625	55	71	83	11	15	0	0	0	5	2.7	60	5.14	4.43	-1.56	2.74
19-543-1	1b	p	556	35	144	109	12	18	0	12	0	9	3.4	75	5.65	1.25	-1.60	2.78
19-629-1	1b	a	252	8	126	60	0	28	0	0	0	0	1.3	12	3.45	0.46	-1.64	2.67
22A-1479-1	1b	p	633	25	179	90	0	33	10	0		7	4.7	94	6.43	4.78	-1.70	2.75
22B-1509.5-1	1b	cpi	365	30	70	68	0	24	0	0		5	2.4	82	5.25	3.81	-1.70	2.72
27-1165-1	1b	cpmi	269	26	69	87	11	30	0	0	0	7	3.0	49	5.21	4.30	-1.49	2.72
28-288-1	1b	cphv	828	63	77	40	28	59	0	21	0	140	1.3	79	4.10	6.82	-1.98	2.80
28-329.5-1	1b	cmp	325	44	89	83	240	57	0	51	24	87	1.4	110	6.02	3.01	-1.67	2.72
29-301.5-1	1b	a	98	0	206	61	0	20	0	0	0	0	1.4	17	4.23	0.36	-1.52	2.67
29-362-1	1b	cdemp	583	32	80	98	12	29	10	0	0	5	3.4	100	4.60	2.75	-1.31	2.72
32-1093.5-1	1b	a	80	0	107	35	0	42	0	0		0	0.9	8	2.85	0.43	-1.76	2.65
32-1118.5-1	1b	cpy	622	46	140	94	10	33	0	11		0	2.7	89	5.07	2.58	-1.37	2.69
32-828.5-1	1b	epui	321	0	79	64	11	18	0	0		0	2.2	180	4.72	2.68	-1.69	2.72
32-950-1	1b	cep	712	50	71	79	11	22	0	0		7	2.3	220	5.74	4.15	-1.59	2.71
34A-1268-1	1b	ay	139	0	151	57	0	21	0	0		0	1.6	19	3.62	0.66	-1.57	2.65
34C-1185-1	1b	pm	541	52	64	78	13	12	0	0		0	3.2	52	4.51	4.41	-1.60	2.75
73-617-1	1b	cph	262	35	85	64	65	150	0	28	0	69	1.9	76	4.48	6.81	-1.77	2.79
80-1084.5-1	1b	cpnx	234	0	83	76	10	50	0	0	28	28	3.7	100	5.56	5.72	-2.01	2.74
22-413-1	1d	nhx	82	0	214	42	11	67	0	12		100	2.9	150	4.57	10.97	-2.43	2.90
22-550-1	1d	h	57	0	81	0	970	75	0	160		210	0.2	180	4.24	9.04		2.95
70-397-1	1d	h	158	0	145	0	860	140	0	140	0	240	0.0	94	5.19	7.66		2.91
29-1197-1	4	mu	345	43	112	65	12	56	0	20	21	52	1.4	58	4.05	0.90	-1.62	2.81
29-464.5-1	4	dmpu	1077	43	122	96	36	47	0	14	0	70	1.4	220	6.76	2.27	-1.61	2.80
29-774-1	4	dpm	197	75	116	80	12	40	0	0	0	56	2.1	100	6.31	2.07	-1.70	2.71
29-804-1	4		176	0	187	57	0	26	0	0	0	36	1.7	38	1.77	0.81	-1.69	2.69
31-767-1	4	dmv	568	33	185	86	20	24	0	13	0	72	2.0	100	5.83	1.91	-1.66	2.72
31-989.5-1	4	mp	244	0	100	109	15	10	11	10	0	6	3.5	44	2.66	2.24	-1.34	2.71
32-1169.5-1	4	dmp	497	68	224	83	12	29	0	17		46	2.0	84	4.65	1.65	-1.65	2.72
32-1388-1	4	dpx	653	40	77	45	14	370	0	10		62	1.9	29	4.80	5.60	-1.88	2.76

Table C.5. Whole-rock Geochemical Analyses. (continued)

b. Trace Element Analyses (ppm), Derived Values and Specific Gravity (ρ)

			Semi-quantitative					Quantitative							Derived values			
Sample	Unit	Code	Ba	Rb	Sr	Zr	Cr	Cu	La	Ni	Pb	V	Yb	Zn	Total% alkalis	$iv(FeOt)$	log Zr/TiO_2	ρ
32-1434.5-1	4	dmp	486	57	83	69	12	37	0	0		51	2.0	73	5.09	1.71	-1.69	2.73
32-1565-1	4	vp	203	28	91	49	15	37	0	19		190	1.1	97	4.35	6.12	-1.98	2.69
34-1834.5-1	4	pmi	215	23	129	120	0	16	12	0		4	3.1	55	2.97	2.59	-1.20	2.71
80-1138-1	4	p	684	21	415	46	0	0	0	0	25	9	0.1	18	6.61	0.81	-1.48	2.65
H8-1-1	4	pmlx	304	33	81	54	19	12	0	12		31	2.0	56	4.64	3.78	-1.65	2.75
I7-29-1	4	pmli	297	0	53	51	19	100	0	10		30	1.6	63	2.59	3.87	-1.67	2.79
I7-32-1	4	pm	279	23	70	52	15	0	0	12		27	1.8	25	4.07	4.14	-1.66	2.77
19-1233-1	4	gp	405	42	49	62	14	40	0	11	20	63	1.6	200	3.39	3.08	-1.74	2.76
24-1200-1	4	gp	359	37	49	59	10	45	0	0	0	62	1.7	56	2.94	3.76	-1.84	2.76
34A-1644.5-1	4	gaui	256	0	138	41	21	73	0	14		53	1.4	57	2.95	0.35	-1.91	2.70
34A-1644.5-2	4	bgpui	709	0	63	47	250	230	0	40		110	2.6	540	2.13	2.03	-1.83	2.88
34C-1878-1	4	gmvu	294	25	49	69	11	63	0	0		41	1.7	310	2.81	2.61	-1.62	2.72
I8-6-1	4	ph	231	0	142	64	13	30	0	11		43	1.8	49	4.19	3.96	-1.59	2.75
I8-27-1	4	pyhti	298	19	133	61	15	51	0	10		48	1.8	57	4.30	4.35	-1.63	2.79
22A-1191-1	1/10d	pvym	538	55	34	74	13	41	0	0		0	2.8	220	2.51	5.33	-1.65	2.78
24-463.5-1	1/10d	m	260	24	65	75	0	43	0	0	28	0	2.4	76	3.34	3.18	-1.57	2.75
70-1037.5-1	1/10d	vpy	165	37	44	73	18	0	0	10	0	5	2.7	120	1.62	5.04	-1.48	2.77
70-1153-1	1/10d	pmvyi	516	12	78	76	210	10	0	120	0	0	2.6	39	4.86	4.78	-1.53	2.73
80-1416-1	1/10d	pmv	245	82	101	74	10	0	13	0	0	5	2.3	30	4.72	3.78	-1.61	2.71
31-312.5-1	1b/10d	cdmpv	1209	63	79	205	18	10	0	0	0	0	4.9	160	8.16	4.41	-1.22	2.76
80-1680.5-1	1b/10d	mvp	165	33	70	73	11	0	0	0	0	5	2.1	87	3.41	4.92	-1.60	2.74
19-1041.5b-1	1/10p	pv	220	0	86	72	0	24	0	17	0	210	2.3	110	4.34	7.04	-1.97	2.79
22B-1783.5-1	1/10p	py	202	28	89	91	13	76	13	10		11	3.4	93	2.65	3.71	-1.53	2.77
19-986-1	1/10p	gpv	618	30	126	92	24	39	0	11	0	5	3.3	90	2.80	4.35	-1.47	2.75
24-1044-1	1/10p	gvpu	78	0	0	48	790	160	0	89	0	310	0.0	340	0.29	8.47	-1.89	2.83
24-981a-1	1/10p	gv	92	0	94	78	0	33	0	10	0	0	2.5	92	2.14	3.67	-1.49	2.71
27-1324.5-1	1/10p	gmvur	191	0	83	91	0	22	0	0	23	7	3.0	84	2.57	2.11	-1.47	2.76
27-1343-1	1/10p	gvp	343	59	37	79	31	0	0	11	0	14	2.7	110	1.65	4.28	-1.53	2.73
29-1092-1	1/10p	cgmpu	288	49	84	72	18	39	0	11	31	72	2.7	76	4.23	3.24	-1.81	2.80
34A-1679-1	1/10p	gmuy	313	30	88	61	50	30	0	20		71	1.6	38	3.42	0.81	-1.76	2.79
19B-872-1	1b/10p	mupvi	471	35	36	92	0	140	0	0	21	0	3.1	55	4.08	2.72	-1.51	2.84
19-1237-1	1b/10p	cpmv	276	37	48	65	18	31	0	13	20	49	2.8	190	3.42	4.72	-1.79	2.79
19-662-1	1b/10p	mui	201	22	74	55	0	160	0	0	54	6	1.7	95	2.60	0.21	-1.60	2.96
22A-1515-1	1b/10p	cpvsi	356	39	45	84	0	22	0	0		11	2.8	92	3.39	5.78	-1.57	2.77
22A-1551.5-1	1b/10p	cpvi	254	18	78	84	0	11	0	0		8	3.0	22	3.60	4.04	-1.49	2.72
22A-1752-1	1b/10p	muk	184	0	40	70	0	180	0	0		6	2.1	310	2.08	0.52	-1.54	2.98
22A-1752-2	1b/10p	am	280	32	62	52	0	13	0	0		9	1.2	21	2.28	0.48	-1.49	2.75
34-1275-1	1b/10p	mp	714	52	169	101	11	63	0	0		12	3.7	150	4.40	3.45	-1.55	2.77
19-1100-1	4/10p	mvupi	205	0	0	40	0	2200	0	15	1100	36	1.1	120	2.57	2.64	-1.80	2.97
19-1250-1	4/10p	mi	356	47	52	67	10	49	0	13	21	40	2.2	82	3.33	1.18	-1.59	2.78
22A-1885-1	4/10p	mkpui	451	44	58	124	19	160	19	26		140	5.2	160	5.21	2.23	-1.76	2.99
22A-1975.5-1	4/10p	puqy	210	0	89	39	16	77	0	25		190	1.8	110	2.37	5.83	-2.06	2.82
22A-1979-1	4/10p	mvusi	230	0	35	50	53	590	0	23		64	1.8	1100	1.74	3.38	-1.72	2.86
22A-2004-1	4/10p	omvus	371	40	36	66	10	89	0	12		69	1.7	630	2.60	3.42	-1.66	2.84
22B-2036-1	4/10p	mvupi	243	40	65	58	23	48	0	13		56	2.3	140	3.06	1.05	-1.77	2.77
24-1082-1	4/10p	rmvu	232	0	35	62	11	680	0	23	120	55	2.2	280	2.13	2.64	-1.71	2.81
24-1228-1	4/10p	pvm	254	0	139	66	10	26	0	0	0	55	1.9	71	5.42	1.67	-1.74	2.71
28-343-1	4/10p	om	395	31	180	84	0	490	11	0	120	54	1.8	1700	5.40	0.26	-1.64	2.77
29-1057-1	4/10p	cmrpu	418	0	72	65	0	240	0	0	51	60	2.8	71	1.00	3.42	-1.89	2.85
29-1099-1	4/10p	mu	218	41	71	59	64	20	0	21	0	80	1.8	63	3.43	0.70	-1.76	2.83
29-876-1	4/10p	mvui	206	40	25	51	21	1400	0	30	61	73	1.6	490	2.78	3.25	-1.86	2.92
31-869.5-1	4/10p	py	403	44	175	45	16	48	0	16	0	160	1.3	91	6.10	3.86	-2.08	2.73
34A-1565-1	4/10p	dmp	329	33	110	73	11	33	0	0		53	1.9	89	3.61	1.73	-1.66	2.72
34C-1747.5-1	4/10p	omukp	301	21	68	48	12	500	0	0		42	2.0	50	2.43	2.13	-1.75	2.91
34-1666-1	4/10p	mpki	291	54	57	69	0	33	0	0		55	1.1	390	3.55	2.97	-1.69	2.78
22A-1788-1	4/10p	gvpu	136	35	62	72	20	29	0	15		27	2.4	97	2.27	2.67	-1.59	2.75
24-1044-2	4/10p	cgvp	120	0	32	25	450	92	0	61	0	130	0.0	110	0.38	3.21	-1.96	2.77
34C-1831-1	4/10p	gmup	262	20	62	52	37	26	0	16		66	1.8	59	3.53	0.99	-1.73	2.79
34-1728-1	4/10p	gmpv	361	56	35	59	10	23	0	0		54	2.1	85	3.30	2.18	-1.75	2.74
22B-1044-1	10d	ovmsi	474	0	43	65	12	14	0	0		7	2.5	51	1.44	5.58	-1.53	2.77
22-901-1	10d	omvks	436	25	43	76	0	110	0	0		5	2.5	140	2.09	1.77	-1.44	2.79
22-957-1	10d	ovmsr	458	39	41	78	25	0	0	12		5	2.4	350	1.86	3.34	-1.60	2.76
22-996.5-1	10d	ovmsx	245	0	0	71	12	34	0	11		8	2.4	93	0.96	9.02	-1.60	2.84
24-444.5-1	10d	omuvi	557	29	0	72	0	230	0	0	0	0	2.7	160	3.14	4.34	-1.49	2.85
27-593.5-1	10d	ovsmx	253	22	20	77	0	41	0	0	0	5	2.2	160	1.27	6.95	-1.48	2.81

Table C.5. Whole-rock Geochemical Analyses. (continued)

b. Trace Element Analyses (ppm), Derived Values and Specific Gravity (ρ)

			Semi-quantitative					Quantitative							Derived values			
Sample	Unit	Code	Ba	Rb	Sr	Zr	Cr	Cu	La	Ni	Pb	V	Yb	Zn	Total% alkalis	$iv(FeOt)$	log Zr/TiO_2	ρ
27-733-1	10d	omvr	452	28	34	73	0	110	0	0	0	0	2.9	41	1.82	3.42	-1.66	2.77
34B-930-1	10d	vmski	208	0	29	79	0	19	0	0		0	3.2	260	1.15	4.58	-1.46	2.79
34B-967-1	10d	vmsi	108	0	58	72	11	26	0	10		0	2.8	450	1.81	4.11	-1.71	2.75
34-863.5-1	10d	vmki	143	0	55	83	10	0	0	0		0	2.3	74	1.34	3.28	-1.46	2.74
34-937-1	10d	vmysi	141	0	78	82	12	19	0	10		0	3.1	230	2.28	4.50	-1.64	2.73
70-664-1	10d	ovsmx	569	10	0	78	19	12	0	11	0	7	2.6	25	0.87	7.47	-1.45	2.83
70-687-1	10d	ovsmp	446	0	32	76	10	0	0	0	0	7	2.7	28	1.29	7.65	-1.52	2.80
70-822.5-1	10d	omvsx	879	31	80	70	0	35	12	0	0	0	2.1	30	2.14	5.85	-1.52	2.77
70-876.5-1	10d	omvki	500	22	64	67	860	61	0	490	0	23	5.1	87	1.52	5.09	-1.61	2.75
70-934-1	10d	omvy	585	27	45	79	22	100	0	11	0	6	4.5	70	1.99	5.34	-1.46	2.76
73-1107.5-1	10d	omvs	767	36	61	71	0	0	0	0	0	0	1.3	31	1.96	4.23	-1.38	2.73
73-1170.5-1	10d	omvks	530	0	0	94	0	650	0	0	0	0	4.0	56	1.21	7.06	-1.41	2.83
73-1170.5-2	10d	omvi	829	37	63	80	10	32	0	0	0	5	2.0	14	1.96	4.28	-1.38	2.73
73-1224-1	10d	omvsx	764	24	77	74	10	30	0	0	0	9	2.4	170	2.01	4.59	-1.56	2.75
73-1257-1	10d	omv	464	24	35	62	0	0	0	0	0	0	2.3	48	1.95	3.60	-1.71	2.73
73-1316-1	10d	omkst	346	0	51	75	0	180	0	0	0	8	2.6	210	1.41	4.86	-1.51	2.77
73-949-1	10d	omv	862	40	39	73	0	0	0	0	0	7	1.9	17	2.33	2.70	-1.52	2.72
80-1176-1	10d	pvmi	348	37	128	95	14	11	0	0	0	0	5.1	150	4.95	5.18	-1.78	2.75
80-1382-1	10d	omv	476	33	60	82	12	0	0	0	0	0	2.9	45	2.92	2.25	-1.45	2.70
80-1639.5-1	10d	ovm	306	26	69	80	11	0	0	0	0	0	2.5	44	1.87	4.68	-1.49	2.73
24-277.5-1	10d	wovmk	123	0	42	115	0	0	0	0	0	0	3.0	240	0.86	8.04	-1.54	2.84
80-1571.5-1	10d	wovkm	409	0	20	135	10	84	17	16	0	0	6.8	120	1.28	10.44	-1.59	3.17
27-484-1	10da	ot	310	36	58	68	0	29	0	0	39	0	2.6	900	2.76	1.21	-1.60	2.73
27-504-1	10da	oki	287	0	47	62	0	0	0	0	32	0	1.9	2300	2.39	0.64	-1.44	2.77
34-799-1	10da	ou	328	49	48	67	0	0	0	0		5	2.1	990	2.88	0.40	-1.59	2.72
19B-785-1	10p	ckru	134	33	141	84	0	52	0	13	35	13	1.6	200	3.07	0.91	-1.51	2.75
19-801-1	10p	omrku	314	42	97	130	0	250	10	10	22	11	2.9	780	3.60	0.24	-1.52	3.10
19-950-1	10p	ckmup	228	39	106	162	0	110	14	10	87	0	4.1	300	2.90	0.46	-1.19	2.89
22A-1625-1	10p	omvsy	338	59	36	87	10	65	0	0		10	2.3	720	2.94	2.72	-1.52	2.80
22B-1703-1	10p	pmysx	525	0	107	77	14	36	20	0		15	3.1	73	2.43	4.43	-1.53	2.68
22B-1721-1	10p	mpysu	260	34	33	78	11	110	0	0		10	3.1	580	3.04	4.46	-1.51	2.79
22B-1721-2	10p	omspy	243	67	80	76	11	120	0	10		10	2.8	3000	2.06	3.33	-1.62	2.85
24-812-1	10p	kmup	210	0	306	191	0	36	14	0	130	0	4.1	97	4.62	0.89	-1.53	3.10
24-812-2	10p	mkut	272	0	478	166	0	14	0	0	180	7	3.6	44	5.86	0.80	-1.49	2.90
24-812-3	10p	muk	345	0	440	204	0	22	0	0	180	9	3.9	56	5.51	0.85	-1.48	3.10
24-991-1	10p	cmsk	279	0	167	97	0	0	0	0	22	7	2.1	140	3.04	0.16	-1.52	2.78
32-1465.5-1	10p	dmu	1048	37	66	79	810	210	0	210		140	0.8	110	4.47	-0.74	-1.81	2.94
34A-1614-1	10p	mui	1105	37	55	90	500	130	0	140		120	0.9	110	4.25	0.89	-1.63	2.83
34C-1377-1	10p	mskut	141	119	75	341	0	64	10	0		10	4.5	2000	4.99	0.80	-1.12	2.98
34-1347-1	10p	mvuk	251	47	136	94	0	42	0	0		10	3.4	370	3.22	1.60	-1.50	2.80
34-1477-1	10p	muj	346	63	37	69	0	460	0	10		7	1.8	3200	2.79	0.38	-1.52	2.91
34-1551-1	10p	cmui	382	55	55	82	0	250	0	0		5	2.8	52	3.31	2.53	-1.47	2.79
34-1607.5-1	10p	gmk	356	0	88	115	0	100	0	0		6	3.5	180	2.68	0.67	-1.42	2.86
34C-1626-1	10p	gvup	69	0	56	54	0	130	0	11		60	1.6	76	2.44	7.31	-1.90	2.82
34C-1710-1	10p	gv	70	0	55	68	0	49	0	15		100	3.8	160	2.14	4.67	-1.99	2.79
19B-663.5-1	10pa		274	47	124	71	0	58	0	0	56	7	2.1	1800	3.11	0.84	-1.56	2.82
22A-1638-1	10pa	ouk	308	45	47	76	0	280	0	0		10	2.3	*10000	2.99	0.20	-1.52	2.80
22A-1650-1	10pa	ui	244	44	60	75	0	12	0	0		13	2.9	2200	2.85	0.52	-1.52	2.80
22A-1650-2	10pa	opui	285	55	59	75	0	150	0	0		14	3.0	1600	3.13	1.09	-1.56	2.80
22B-1723-1	10pa	outi	366	54	39	88	0	24	0	0		9	3.7	8000	3.12	0.88	-1.59	2.81
27-1295.5-1	10pa	cpu	290	76	43	74	13	100	0	13	21	7	2.5	4800	3.05	3.78	-1.55	2.84
34C-1435-1	10pa	uk	144	0	77	68	0	43	0	11		11	1.9	8000	2.32	0.55	-1.55	3.03
34C-1453-1	10pa	ou	422	64	50	164	0	180	14	0		0	5.3	7100	4.71	2.32	-1.50	3.11
34-1539-1	10pa	ui	216	0	109	72	0	200	0	0		6	1.9	3400	3.06	1.50	-1.50	2.91
19-848-1	10p/5	orumk	321	21	46	149	0	990	15	36	96	46	3.4	230	1.59	3.46	-1.33	3.46
24-1131a-1	10p/5	zsu	54	0	0	63	0	1600	0	15	73	22	0.6	*10000	0.09	12.70	-1.66	3.14
34-1525.5-1	10p/5	mupj	336	0	61	38	230	6200	0	50		280	0.0	6500	1.98	10.72	-1.94	3.19
24-1190.5-1	4/5	upv	73	0	0	36	0	2400	0	18	75	38	0.8	2100	2.19	3.16	-1.77	3.12
29-1019-1	4/5a	clu	55	0	0	0	17	410	0	27	93	26	0.5	330	0.21	0.46		2.90
34-1498.5-1	3	ourpi	167	0	0	48	41	1200	0	270		260	2.2	6600	0.43	-1.85	-1.81	3.88
H8-10-1	4/10	kpu	364	0	109	63	15	61	16	14		84	1.5	56	2.77	2.08	-1.65	2.82
H9-13-1	4/10	pusk	323	25	83	64	16	69	0	14		82	1.7	150	2.65	3.26	-1.63	2.76
H9-30-1	4a/10	pm	226	51	121	58	12	16	0	10		45	1.7	100	3.74	4.52	-1.63	2.80
H9-30-2	4a/10	psmy	178	28	96	58	13	73	0	0		34	1.8	81	3.62	3.15	-1.63	2.77
H9-30-3	4a/10	hv	188	0	98	56	16	13	0	10		47	1.9	70	2.95	3.24	-1.63	2.76

* upper detection limit.

Table C.5. Whole-rock Geochemical Analyses. (continued)

b. Trace Element Analyses (ppm), Derived Values and Specific Gravity (ρ)

			Semi-quantitative									Quantitative			Derived values			
Sample	Unit	Code	Ba	Rb	Sr	Zr	Cr	Cu	La	Ni	Pb	V	Yb	Zn	Total% alkalis	$iv(FeOt)$	log Zr/TiO_2	ρ
H9-54-5	1/10	psk	361	65	167	82	11	0	10	0		35	2.5	68	4.00	4.77	-1.48	2.80
H9-60-2	4/10	ms	470	64	173	29	17	100	0	0		280	1.4	24	6.86	2.61	-2.34	2.88
H9-6-2	4/10	skpm	433	31	176	39	31	120	0	0		250	1.2	48	5.68	3.24	-2.16	2.83
31-814-1	10m	vpy	164	28	77	55	10	21	0	11	0	120	2.3	170	2.84	7.63	-2.03	2.79
73-834-1	10m	vhpqi	95	0	82	0	590	110	0	140	0	230	0.0	130	1.54	8.55		2.85
80-1265-1	10m	ovhyi	54	0	0	0	690	39	0	140	0	220	0.0	560	0.06	15.10		2.89
80-1286.5-1	10m	ohv	42	0	0	0	920	27	0	180	0	200	0.0	150	1.29	16.41		3.15
80-1316-1	10m	pv	257	34	223	103	17	43	0	23	140	86	3.3	190	5.80	3.20	-1.45	2.73
19-157-1	1/10c	vpy	313	23	68	73	0	59	0	0	0	0	2.4	920	2.41	6.07	-1.63	2.77
19-274.5-1	1/10c	lm	290	26	110	59	12	29	0	11	0	9	2.7	32	3.89	2.42	-1.61	2.74
22A-1350.5-1	1/10c	qpm	260	46	57	75	10	16	0	10		0	2.7	39	3.65	3.79	-1.62	2.76
22B-1347-1	1/10c	pmq	258	45	38	81	11	22	0	0		0	2.8	130	4.19	3.78	-1.62	2.77
22B-1843-1	1/10c	pmqu	217	33	37	71	11	43	0	11		10	3.0	110	1.99	2.15	-1.60	2.80
22-685.5-1	1/10c	cpm	484	41	76	81	10	0	0	0		6	2.8	47	4.54	3.96	-1.49	2.74
22-789-1	1/10c	pqm	597	78	79	58	11	19	0	0		6	2.2	51	3.11	3.87	-1.77	2.83
24-668-1	1/10c	mpq	873	49	31	96	0	78	0	0	0	6	2.5	98	5.42	2.98	-1.61	2.76
27-328-1	1/10c	pmq	605	34	76	76	0	77	0	0	0	8	2.4	94	4.79	4.17	-1.48	2.76
27-763-1	1/10c	mpvui	725	68	47	80	0	220	0	0	0	7	2.5	100	2.76	5.24	-1.53	2.80
29-183.5-1	1/10c	p	383	44	85	87	10	31	0	0	0	7	3.0	67	5.00	3.29	-1.46	2.71
29-716-1	1/10c	mpq	2317	40	65	96	15	92	0	0	0	210	1.9	69	7.35	3.36	-1.66	2.84
31-716-1	1/10c	cmpq	1034	39	90	26	16	510	0	12	0	160	0.5	35	6.68	7.14	-1.96	2.83
32-657-1	1/10c	qp	540	64	72	65	16	0	0	0		0	2.7	84	4.77	2.94	-1.74	2.75
34A-1252-1	1/10c	qpl	709	77	90	82	10	37	0	0		8	3.1	82	2.09	3.92	-1.53	2.87
34A-992-1	1/10c	pqm	228	46	32	70	10	13	0	0		0	2.8	58	2.63	3.46	-1.62	2.74
34B-1032.5-1	1/10c	pvmy	203	46	69	74	11	19	0	10		0	2.4	77	2.45	5.41	-1.58	2.75
34-1028.5-1	1/10c	pql	270	46	45	69	10	24	0	0		0	3.0	65	2.39	3.13	-1.56	2.78
34-697.5-1	1/10c	pql	386	64	77	56	13	47	0	10		5	2.4	370	3.37	5.67	-1.70	2.81
70-462-1	1/10c	pq	1133	56	49	72	11	37	0	0	0	10	2.7	85	4.60	4.78	-1.59	2.78
70-560-1	1/10c	pq	766	56	103	0	21	170	0	21	0	340	0.0	140	7.16	13.26		3.02
70-566.5-1	1/10c	cmqp	661	82	61	74	19	17	0	11	0	8	2.4	54	4.28	3.20	-1.53	2.76
73-1380.5-1	1/10c	pmyu	152	37	37	70	11	11	0	0	0	5	2.4	95	3.86	5.15	-1.66	2.77
80-1738-1	1/10c	pmq	632	62	42	82	0	0	0	0	0	6	2.3	80	4.98	4.05	-1.50	2.74
80-1795-1	1/10c	pql	536	91	64	74	11	12	0	0	0	0	3.0	130	3.97	8.20	-1.53	2.89
22B-1911-1	1b/10c	plu	211	49	54	64	11	16	0	10		10	2.2	22	2.35	1.59	-1.54	2.74
24-624.5-1	1b/10c	apq	395	25	72	60	0	33	0	0	0	0	2.5	160	2.86	2.89	-1.52	2.74
24-624.5-2	1b/10c	mpq	1211	62	66	79	10	26	0	0	0	0	2.9	290	4.54	4.29	-1.65	2.78
27-963.5-1	1b/10c	pmqy	750	61	44	80	13	14	0	0	0	0	3.0	120	4.49	5.04	-1.60	2.77
D4-37-1	1b/10c	hqpy	399	0	131	32	14	61	0	17		32	1.9	120	2.14	7.55	-1.99	2.93
22B-1950-1	4/10c	hvp	144	22	75	47	38	130	0	20		76	1.7	1400	1.49	4.56	-1.87	2.80
24-1252.5-1	4/10c	pq	363	40	110	44	15	52	0	30	0	180	1.7	120	4.49	5.52	-2.01	2.81
27-1486-1	4/10c	p	289	52	83	63	10	14	0	10	0	47	2.3	75	2.75	4.72	-1.76	2.79
27-1486-2	4/10c	pqh	229	35	79	61	11	20	0	10	0	44	1.9	67	2.02	4.15	-1.73	2.82
28-393.5-1	4/10c	pl	339	61	82	61	13	16	0	0	0	37	1.7	56	4.66	4.04	-1.61	2.73
29-739-1	4/10c	mpu	804	52	79	55	15	76	0	33	0	73	1.7	38	4.64	4.40	-1.74	2.79
32-1426-1	4/10c	dqpm	1173	45	54	71	28	37	0	0		69	1.6	93	4.47	3.70	-1.76	2.83
73-602-1	4/10c	pq	360	52	114	56	26	390	0	17	0	55	2.3	59	3.71	4.57	-1.65	2.78
D4-9-1	4/10c	lhq	176	0	113	30	15	69	0	26		150	1.4	78	1.58	6.75	-2.10	2.84
D4-9-2	4/10c	lyhp	286	0	77	31	16	61	0	22		150	1.5	65	1.91	4.83	-2.10	2.84
H9-10-1	4/10c	pqlx	716	39	139	60	15	27	0	0		81	1.7	72	5.93	5.22	-1.67	2.76
19-1023.5-1	10i	cl	104	0	44	41	10	14	0	18	0	100	1.8	100	1.09	6.90	-2.08	2.89
22A-1262-1	10i	qhp	538	33	60	78	12	19	0	0		9	2.4	94	1.66	4.05	-1.52	2.86
22A-1262-2	10i	ohp	218	0	60	70	13	14	0	14		10	2.6	97	0.39	5.22	-1.54	2.99
24-1053-1	10i	h	92	0	64	58	18	15	0	19	0	110	2.7	150	1.72	5.94	-2.01	2.89
24-471-1	10i	ohlq	35	0	42	71	15	0	0	16	0	6	1.8	180	0.07	6.39	-1.19	3.00
27-1557-1	10i	hq	51	0	0	0	650	120	0	110	0	220	0.8	190	1.00	9.76		3.09
27-703.5-1	10i	h	65	0	0	42	13	76	0	15	0	5	1.9	240	0.95	11.65	-1.63	3.10
29-858-1	10i	lhq	64	0	72	43	51	320	0	52	28	170	1.8	230	0.17	2.85	-2.01	2.84
31-790-1	10i	hu	74	0	0	53	33	78	0	34	24	150	0.5	1200	1.21	6.74	-1.82	3.11
34B-759.5-1	10i	ohqpl	72	0	35	0	14	12	0	17		10	1.1	110	0.06	6.21		3.17
34C-1841.5-1	10i	ohql	53	0	0	24	770	72	0	87		220	0.0	85	0.08	8.71	-1.96	3.10
34-697.5-2	10i	oplhq	143	40	64	39	16	21	0	14		7	1.9	500	3.81	7.17	-1.64	2.81
34-876.5-1	10i	hql	54	0	37	28	13	10	0	15		7	1.9	130	0.07	5.76	-1.76	3.03
73-677.5-1	10i	hq	82	0	190	0	510	10	0	93	0	220	0.5	59	0.68	6.48		3.06
73-677.5-2	10i	phq	710	46	114	0	680	120	0	130	0	240	0.0	110	5.00	8.62		2.96
28-199-1	2	hnvx	85	0	136	20	23	260	0	22	0	290	0.0	83	4.42	12.24	-2.37	2.88

Table C.5. Whole-rock Geochemical Analyses. (continued)

b. Trace Element Analyses (ppm), Derived Values and Specific Gravity (ρ)

			Semi-quantitative					Quantitative							Derived values			
Sample	Unit	Code	Ba	Rb	Sr	Zr	Cr	Cu	La	Ni	Pb	V	Yb	Zn	Total% alkalis	$iv(FeOt)$	log Zr/TiO_2	ρ
29-669-1	2	hv	85	0	159	25	22	650	0	25	0	310	0.0	79	3.41	12.23	-2.27	2.98
29-757.5-1	2	hpvy	1556	37	118	48	29	100	0	11	0	240	0.0	120	5.48	11.75	-1.96	2.88
31-272.5-1	2	dhx	126	0	506	31	20	240	0	26	0	320	0.5	92	3.46	12.51	-2.21	3.07
31-361-1	2	phv	899	72	67	21	14	200	0	23	0	330	0.0	150	5.16	13.23	-2.39	2.90
31-399.5-1	2	h	64	0	161	23	16	280	0	24	0	300	0.5	85	2.07	11.98	-2.32	3.03
31-473-1	2	h	67	0	212	0	18	140	0	24	0	310	0.0	90	1.81	11.43		3.03
31-521.5-1	2	h	134	0	215	23	21	180	0	23	0	290	0.0	84	2.74	11.88	-2.29	3.02
31-558-1	2	hq	80	0	263	26	21	210	0	25	0	300	0.5	84	1.46	10.98	-2.28	3.03
32-1323.5-1	2	h	73	0	278	0	21	190	0	23		300	0.0	67	3.20	12.15		3.01
34A-1459b-1	2	h	84	0	235	0	22	87	0	24		260	0.5	49	4.55	9.27		2.92
34A-1463.5-1	2	h	79	0	284	22	23	100	0	26		300	0.5	55	4.50	11.43	-2.33	2.95
29-478.5-1	2a	hv	74	0	304	51	33	120	0	35	0	310	0.6	110	2.18	12.42	-1.99	3.01
29-580.5-1	2a	h	161	0	224	0	27	260	0	34	0	280	0.5	87	1.96	10.91		3.04
29-633.5b-1	2a	h	62	0	209	27	26	31	0	27	0	280	0.0	60	4.22	11.07	-2.20	2.98
D4-38-1	2a	hv	91	0	153	0	21	100	0	27		380	0.7	73	3.47	12.60		2.96
J8-2-1	2a	hx	356	0	214	0	27	72	0	27		310	0.7	61	3.63	11.34		2.98
28-272.5-1	2c	hvnx	97	0	157	24	20	30	0	22	0	320	0.0	98	4.53	12.33	-2.31	2.92
29-685.5-2	2/10s	hn	78	0	89	30	0	530	0	12	0	39	1.1	120	4.47	8.82	-2.12	2.82
34A-1484-1	2/10s	hnx	78	0	45	29	13	54	0	13		36	1.6	61	3.18	6.66	-2.11	2.80
34A-1484-2	2/10s	nvx	87	0	69	30	10	90	0	11		40	1.3	58	4.00	7.79	-2.12	2.78
H9-52-1	2b/10s	nypx	568	0	86	29	12	0	0	0		55	1.9	96	5.36	7.38	-2.21	2.76
H9-61-5	2e/10s	ahy	95	0	577	31	20	91	0	21		230	1.5	45	3.61	3.87	-2.35	2.75
29-633.5a-1	2/10e	oqhl	83	0	377	20	23	23	0	24	0	260	0.0	36	0.07	8.73	-2.30	3.18
29-685.5-1	2/10e	hl	59	0	88	58	16	1400	0	23	0	70	1.8	90	2.59	6.05	-1.87	2.86
29-820a-1	2/10e	hqylu	63	0	0	33	28	65	0	16	0	15	2.2	210	0.42	10.81	-1.74	3.06
34A-1459b-2	2/10e	oqlh	66	0	332	0	23	110	11	26		330	0.6	24	0.00	7.83		3.17
I8-20-1	2/10	hyp	220	26	144	58	13	66	15	17		54	2.6	140	1.22	17.69	-2.12	3.21
24-1294-1	6a	bhv	64	0	129	56	52	110	0	40	0	320	0.6	110	3.10	12.89	-1.98	3.01
24-1294-2	6a	ah	82	0	159	25	50	35	0	36	0	200	1.0	66	3.35	7.48	-2.24	2.69
27-1611.5-1	6a	bhv	151	0	187	32	120	110	0	47	0	290	0.6	99	2.84	12.29	-2.24	2.97
27-1611.5-2	6a	ahl	121	0	176	0	95	31	0	39	0	190	0.8	85	2.35	9.27		2.96
29-1223.5-1	6a	chv	105	0	57	42	130	100	0	47	0	230	0.8	80	2.08	9.82	-2.00	2.95
32-1610-1	6a	hlv	298	0	98	26	71	160	0	35		250	0.5	83	3.73	10.76	-2.29	2.93
34A-1760.5-1	6a	dhvn	84	0	178	51	47	110	0	36		270	0.9	98	3.72	11.31	-1.99	2.93
34D-2010-1	6a	bhvn	65	0	41	20	97	100	0	44		290	1.1	88	3.00	11.25	-2.32	2.96
34D-2010-2	6a	anhv	82	0	81	24	110	27	0	48		230	0.6	77	4.56	9.00	-2.22	2.87
22A-2075.5-1	6	hl	70	0	119	43	130	77	0	59		240	0.9	88	2.99	10.57	-2.03	2.99
24-1285-1	6	hp	322	21	98	37	31	21	0	16	0	130	1.3	110	4.33	8.60	-2.16	2.85
28-453.4-1	6	ph	661	51	90	60	18	200	0	16	0	220	1.5	140	5.30	11.98	-1.92	2.93
31-970.5-1	6	hpv	276	30	80	31	46	100	0	36	0	250	0.7	95	3.35	10.53	-2.19	2.92
34-1851-1	6	hp	169	0	80	0	470	55	0	110		220	0.4	100	1.03	9.66		3.01
34C-1888-1	6/10e	hqpl	159	0	70	37	120	45	0	44		220	0.7	79	1.10	9.90	-2.08	3.05
J8-23-1	7	dp	332	36	74	66	10	23	0	0		42	2.6	39	6.48	3.42	-1.60	2.72

W

LEGEND FOR THE LINDA AREA

Unit 11. Not intersected.

Unit 10. Altered rocks.

10d. Distal alteration zone—chlorite-muscovite schists containing staurolite±biotite±kyanite.

10da. Muscovite-gahnite-staurolite schist.

10p. Proximal alteration zone—muscovite-chlorite schists containing staurolite ±biotite±kyanite.

10pa. Muscovite-gahnite-staurolite schists.

10m. Mafic schists containing chlorite±hornblende.

10s. Silicified/feldspathized rock—'cherty' rocks commonly containing cummingtonite-hornblende-magnetite.

10v. Quartz veins.

10c. Concordant calc-silicate alteration—epidote-muscovite±biotite±calcite defining S_1 layering.

10i. Static calc-silicate alteration—localized intense, statically crystallized ca

NW

A

70

Overburden

1b

40%

1d

1a

1

1d

1

1a

73

1

limjts
of
logging

NW

A´

70

Overburden

1b

40%

1d

1a

1

1a

1a

1d

1

1/10c

5

1/10c

73

1

limjts
of
logging

31 29

19

24

27

1

1↘

4

10m

1d

1a

1b

1/10c

1b

1a

1/10c

183.5

1b

1a

1a

2

259.5

272.5

1a

1a

2

301.5

2/10s

312.5

361

1c

336

1

1↘

lost core

10i

157

10%

274.5

1b

1b/10c

1/10c

97

10d

277.5

50%

1/10c

10m

1d

10m

1d

60%

20%

SE

A

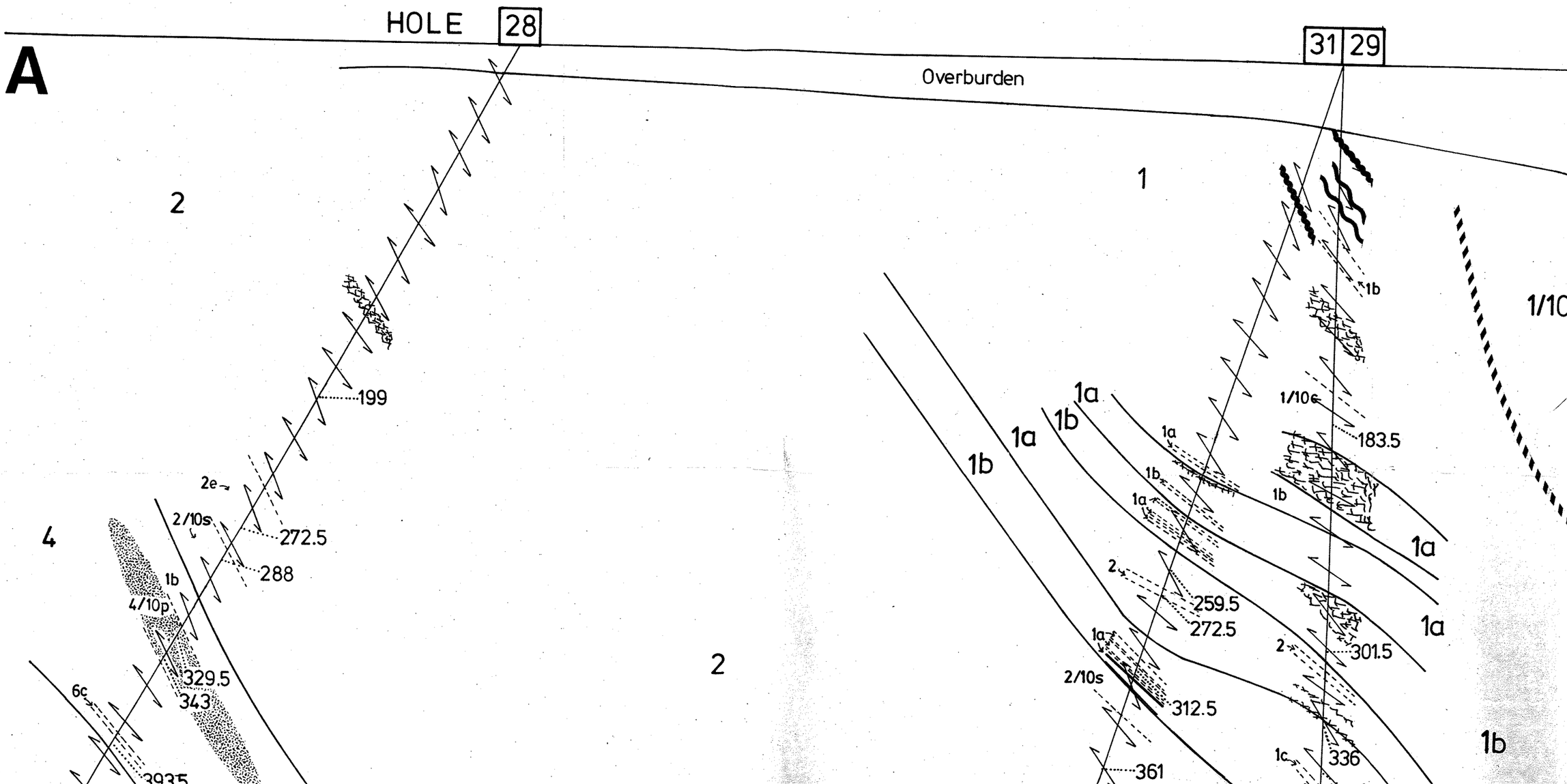
HOLE 28
31 29
Overburden
1
2
4
6
199
2e
2/10s
272.5
288
1b
4/10p
329.5
343
6c
3935
1a
1b
1/10e
183.5
259.5
272.5
301.5
2/10s
312.5
361
1c
336
1/10
1b

biotite±kyanite.

10da. Muscovite-gahnite-staurolite schist.

10p. Proximal alteration zone—muscovite-chlorite schists containing staur-
lite ±biotite±kyanite.

10pa. Muscovite-gahnite-staurolite schists.

10m. Mafic schists containing chlorite±hornblende.

10s. Silicified/feldspathized rock—'cherty' rocks commonly containing cum-
mingtonite-hornblende-magnetite.

10v. Quartz veins.

10c. Concordant calc-silicate alteration—epidote-muscovite±biotite±calc-
defining S_1 layering.

10i. Static calc-silicate alteration—localized intense, statically crystallized ac-
tinolite-epidote-calcite±sphene.

10e. Epidotized-carbonatized mafic rocks—epidote-hornblende±calcite asso-
ciated with mafic volcanic rocks.

Units 7–9. Not intersected.

Unit 6. Mafic to intermediate, mainly volcaniclastic rocks.

6a. Heterolithic breccia—containing clasts of unit 4.

6b. Breccia, lapillstone and tuffs.

6c. Layered amphibolite—containing coarsely recrystallized amphibole.

Unit 5. Massive and semi-massive sulfide mineralization.

5a. Pyrite-calcite rocks.

Unit 4. Quartz-megaphyric felsic volcanic rocks.

Unit 3. Graphitic metasedimentary rocks.

Unit 2. Mafic volcanic rocks, with minor intermediate rocks.

2a. Homogeneous, commonly with epidote knots.

2b. Pillowed flows.

2c. Homogeneous and massive, except for hornblende lineation.

2d. Undifferentiated pillowed flows, breccias, lapillistones and tuffs, common
plagioclase-hornblende (after pyroxene) phyric.

2e. Breccias, lapillistones and tuffs.

Unit 1. Felsic volcanic rocks, with minor intermediate to mafic rocks.

1a. 'Cherty' felsic rocks—silicic/feldspathic alteration or possible rhyolite
flows.

1b. Volcaniclastic rocks.

1c. Mineralized 'cherty' breccia.

1

1a

1a

1/10c

5

1/10c

10m+10i

10m

1a

1a

397

1d

1/10c

1d

10m→

462

1d

1/10d

1d

1/10d

560

566.5

15%

1/10c

10d

664

687

50%

70%

1d

1

limjts of logging

1a

4

1a

1d

73

1

10m+10i %

1a

1b

4

10m+10i

4/10c

1d/10c

4/10c

1b/10c

602

10m

617

1b/10c

10m+10i

1a

677.5

1a

1

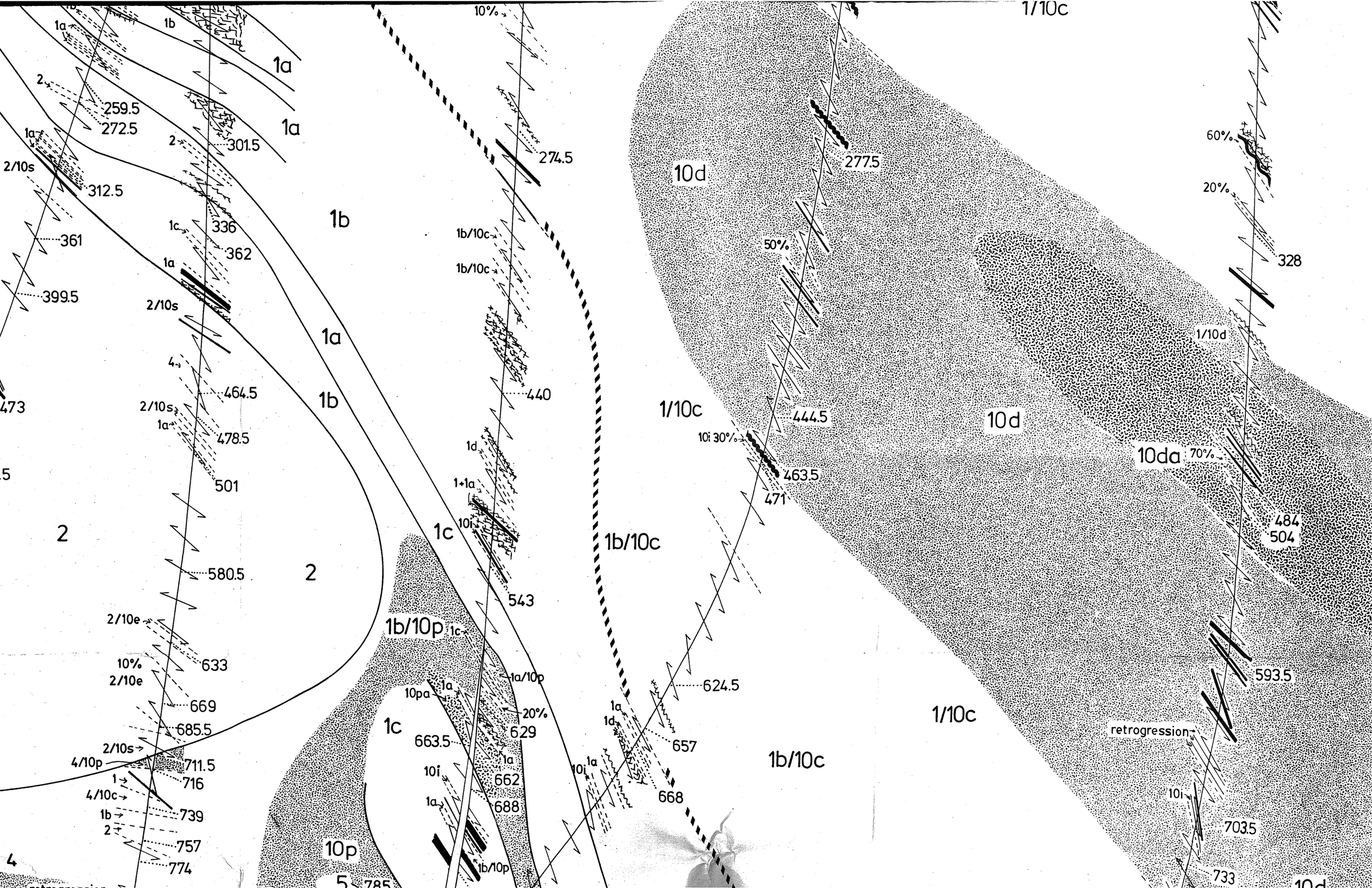
1a
1b
2
259.5
272.5
1a
301.5
2/10s
312.5
1b
1c
336
361
362
1a
399.5
2/10s
1a
1b
4
464.5
473
2/10s
1a
478.5
501
2
580.5
2
2/10e
633
10%
2/10e
669
685.5
2/10s
4/10p
711.5
716
1
4/10c
739
1b
2
757
774
4
10%
274.5
1b/10c
1b/10c
440
1d
1+1a
10i
543
1c
1b/10p
1c
1a/10p
10pa
1a
20%
629
1c
663.5
1a
10i
662
688
1a
1b/10p
10p
5
785
1/10c
10d
277.5
50%
444.5
10i 30%
463.5
471
1b/10c
624.5
1a
1d
657
10i
1a
668
1/10c
1b/10c
1/10c
60%
20%
328
1/10d
10d
10da
70%
484
504
593.5
retrogression
10i
703.5
733
10d

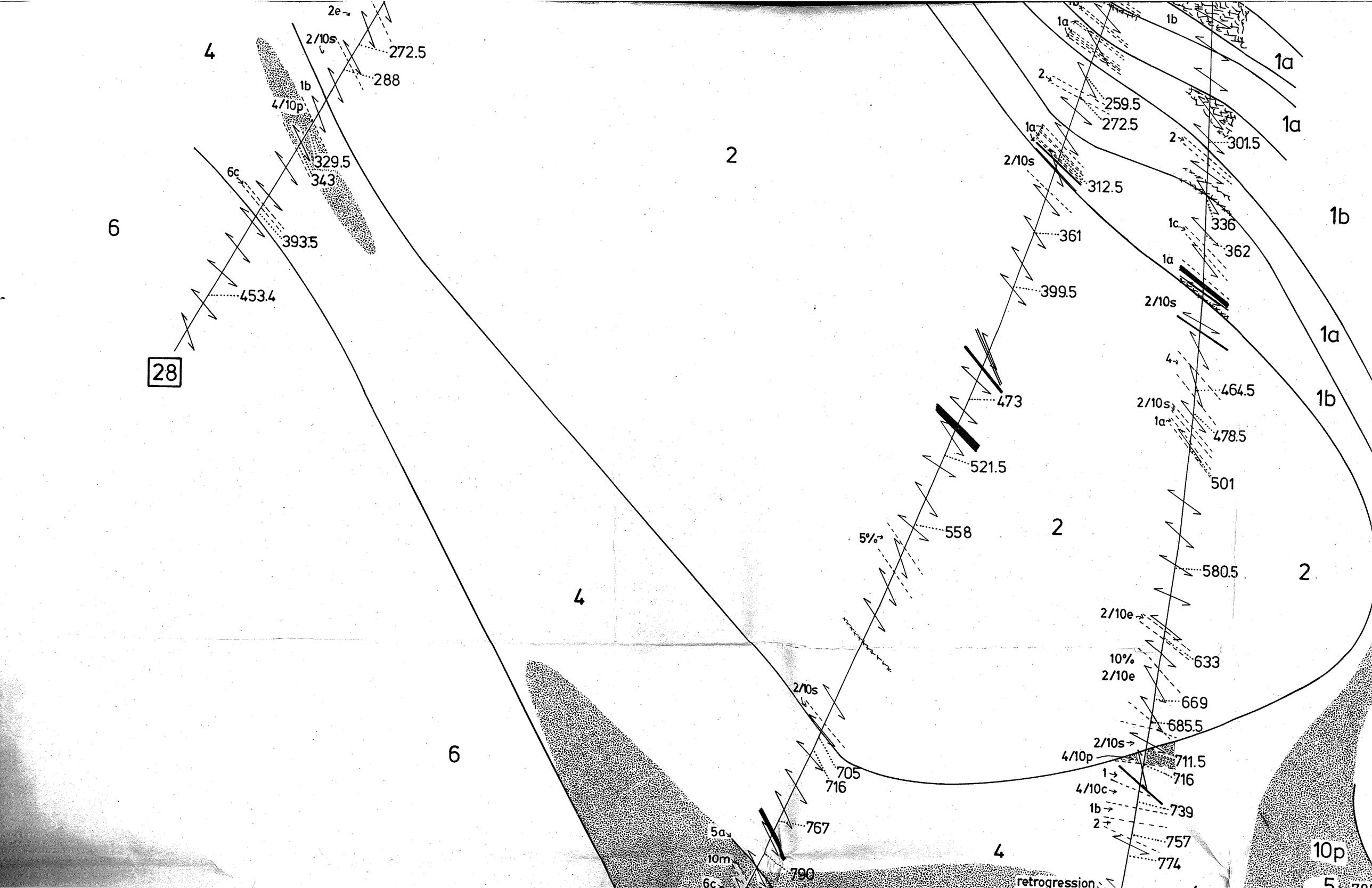
4
2e
2/10s
272.5
288
1b
4/10p
329.5
343
6c
393.5
453.4
28
6
2
1a
1b
2
259.5
272.5
1a
2
301.5
2/10s
312.5
1b
1c
336
361
362
1a
399.5
2/10s
1a
1b
4
464.5
2/10s
1a
478.5
473
521.5
501
558
2
5%
580.5
2
2/10e
10%
2/10e
633
669
685.5
2/10s
4/10p
711.5
716
1
4/10c
1b
2
739
757
774
2/10s
705
716
767
5a
10m
6c
790
4
6
10p
5
retrogression

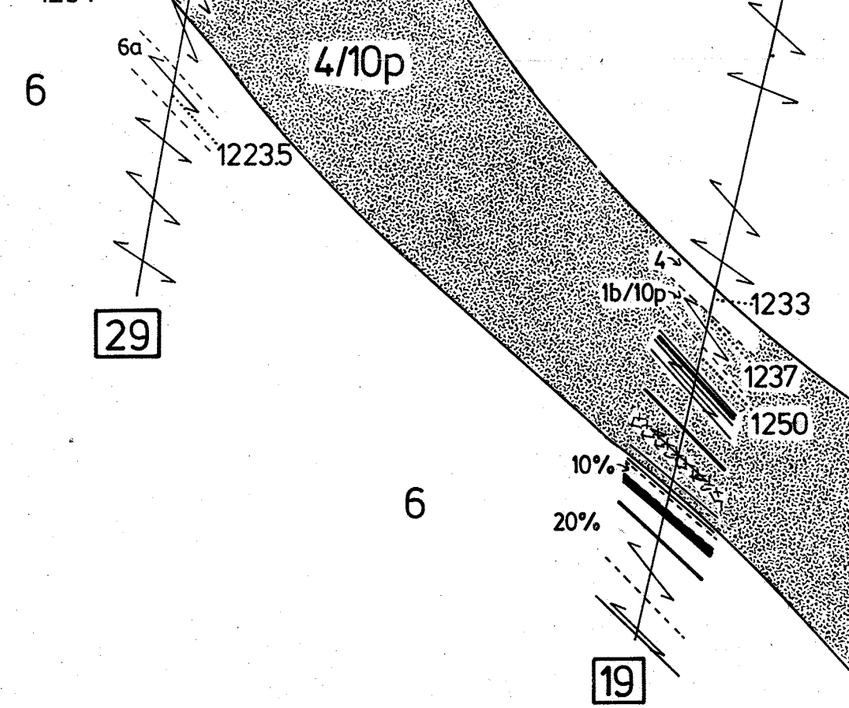

KEY

Dip of dominant layering or schistosity, measured to core axis.

Quartz veins, drawn to scale.

20% Percentage of quartz veins in indicated interval.

S-C structure.

Clay gouge zone.

Fracture network, hematite-carbonate alteration.

Contact between major units.

Contact between subunits, or boundaries of interval.

Outer limits of calc-silicate alteration zone.

....1099 Geochemical sample location. Numbers refer to drill-hole footage. All numbers are prefixed by the drill-hole number.

29 Drill-hole number.

10p

5a

4/10p

4/10p

6

10pa

10p

1a+1c

retrogression

1165

1228

10m

1295.5

1324.5

1343

10i

1486

1/10c

4/10c+10i

4/10c

1557

1611.5

27

1153

70

0 50 100 metres

0 100 200 300 feet

10d

1/10c

1170.5

1224

1257

10d

1316

1/10d

1380.5

73

1/10c

1/10c

80

1795

10d

1176

10m

1265

1286.5

1316

1382

1416

10d

1571.5

1/10d

1639.5

1680.5

1/10c

1738

80

1795

6

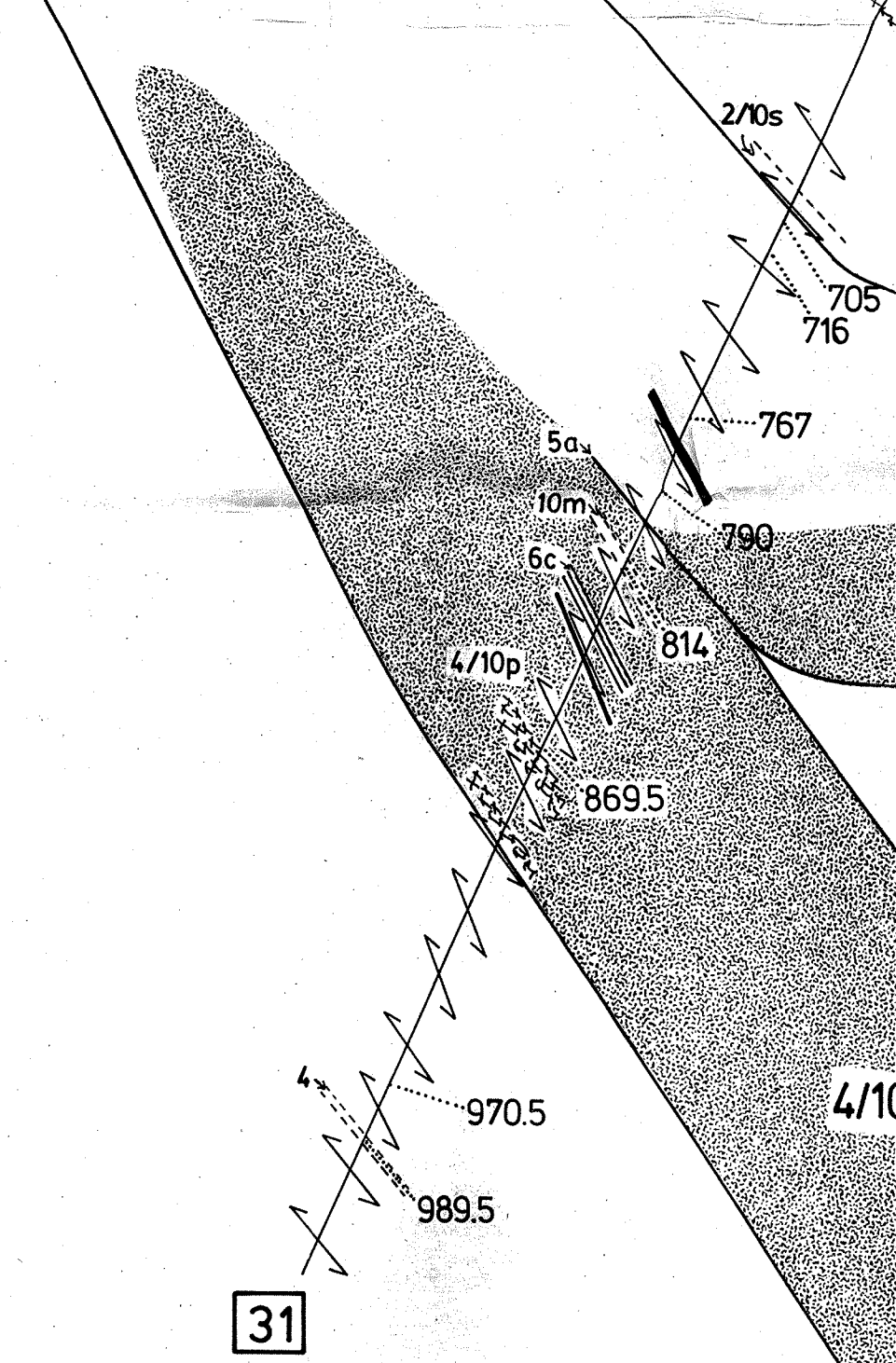

6

KEY

Dip of dominant layering or schistosity, measured to core axis.

Quartz veins, drawn to scale.

20% Percentage of quartz veins in indicated interval.

S-C structure.

Clay gouge zone.

Fracture network, hematite-carbonate alteration.

Contact between major units.

Contact between subunits, or boundaries of interval.

Outer limits of calc-silicate alteration zone.

....1099 Geochemical sample location. Numbers refer to drill-hole footage. All numbers prefixed by the drill-hole number.

29 Drill-hole number.

2

543

1b/10p

1c

1a/10p

10pa

1a

20%

629

663.5

1c

1a

662

10i

1a

688

10p

1b/10p

5

785

744.5

3

10p

801

812

5+

10p

10p

872

848

1c

10p

19B

981

991

950

10pa

missing
core

1044

053

1b/10p

10p

1a/10c

986

5

5a

1b/10c

1023.5

1041.5

1/10c

lost
core

10i

1100

5a

4/10p

10p

4

1b/10p

1233

1237

1250

5a

4/10p

19

1b/10c

624.5

1a

1d

657

1/10c

1a

10i

668

1b/10c

1b

1b/10c

10i

963

70%

1165

retrogression

1a+1c

1228

10pa

10p

10m

1295.5

1324.5

1343

10i

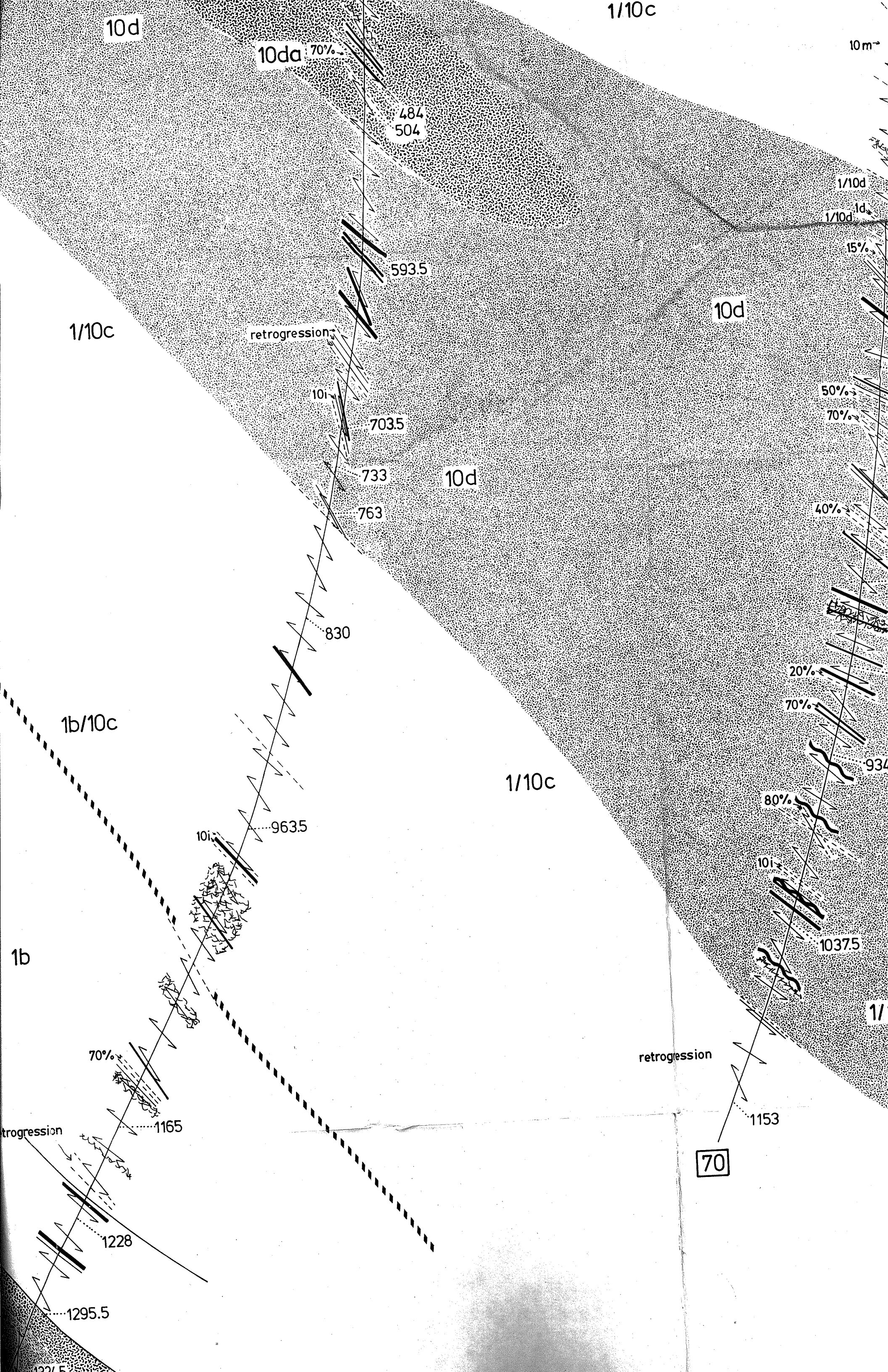
10d
10da
70%
484
504
593.5
1/10c
retrogression
10i
703.5
733
763
830
963.5
1b/10c
1b
70%
1165
retrogression
1228
1295.5
1/10c
10d
10m
1/10d
1d
1/10d
15%
10d
50%
70%
40%
20%
70%
934
80%
10i
1037.5
1/
retrogression
1153
70

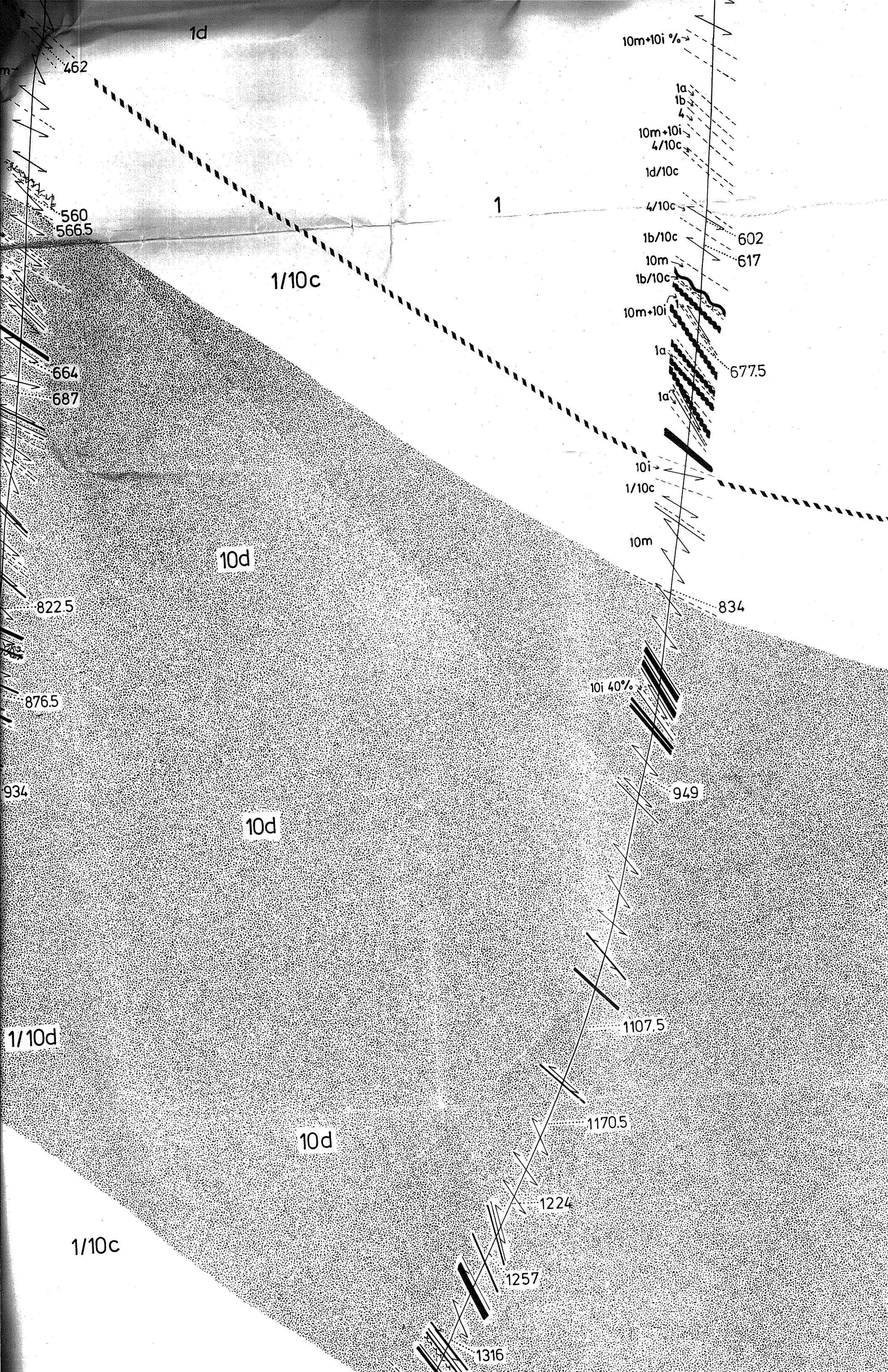
1d
462
560
566.5
1
1/10c
664
687
10d
822.5
876.5
934
10d
1/10d
10d
1/10c
10m+10i %
1a
1b
4
10m+10i
4/10c
1d/10c
4/10c
602
1b/10c
617
10m
1b/10c
10m+10i
1a
677.5
1a
10i
1/10c
10m
834
10i 40%
949
1107.5
1170.5
1224
1257
1316

Unit 6. Mafic to intermediate, mainly volcaniclastic rocks.

6a. Heterolithic breccia—containing clasts of unit 4.

6b. Breccia, lapillstone and tuffs.

6c. Layered amphibolite—containing coarsely recrystallized amphibole.

Unit 5. Massive and semi-massive sulfide mineralization.

5a. Pyrite-calcite rocks.

Unit 4. Quartz-megaphyric felsic volcanic rocks.

Unit 3. Graphitic metasedimentary rocks.

Unit 2. Mafic volcanic rocks, with minor intermediate rocks.

2a. Homogeneous, commonly with epidote knots.

2b. Pillowed flows.

2c. Homogeneous and massive, except for hornblende lineation.

2d. Undifferentiated pillowed flows, breccias, lapillistones and tuffs, common plagioclase-hornblende (after pyroxene) phyric.

2e. Breccias, lapillistones and tuffs.

Unit 1. Felsic volcanic rocks, with minor intermediate to mafic rocks.

1a. 'Cherty' felsic rocks—silicic/feldspathic alteration or possible rhyolite flows.

1b. Volcaniclastic rocks.

1c. Mineralized 'cherty' breccia.

1d. Intermediate to mafic rocks—mainly volcaniclastic, locally heterolithic, minor amphibolite.

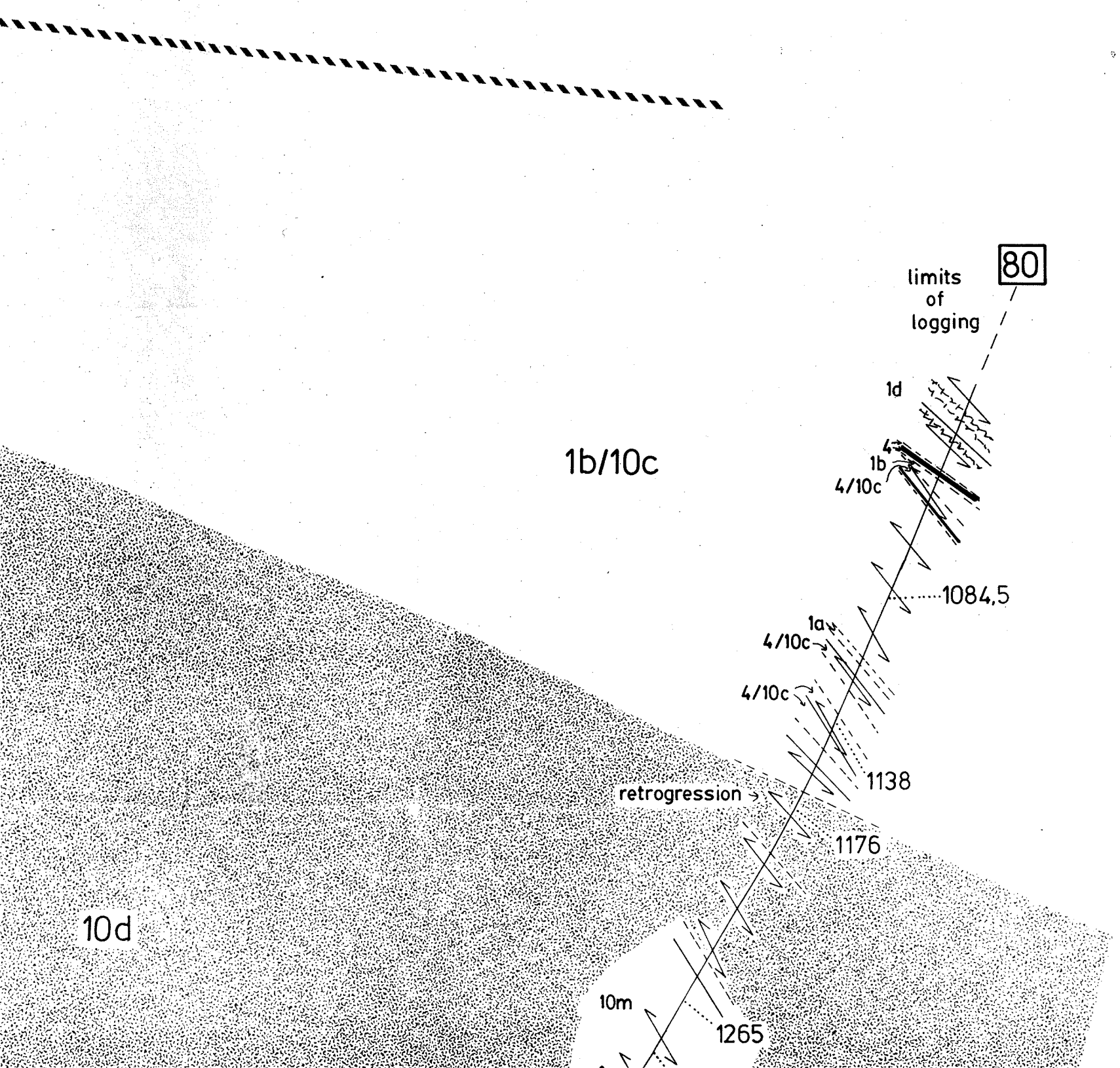

1b
4
10m+10i
4/10c
1d/10c
4/10c
1b/10c
602
10m
617
1b/10c
10m+10i
1a
677.5
1a
10i
1/10c
10m
834
40%
949
1107.5
5
10d
10d
10d
Unit
Unit

1d/10c

1

4/10c

602

1b/10c

617

10m

1b/10c

1/10c

10m+10i

1a

677.5

1a

10i

1/10c

10m

834

10i 40%

949

10d

10d

10d

1107.5

1170.5

10d

1224

1257

10d

1316

1/10d

1380.5

73

1/10c

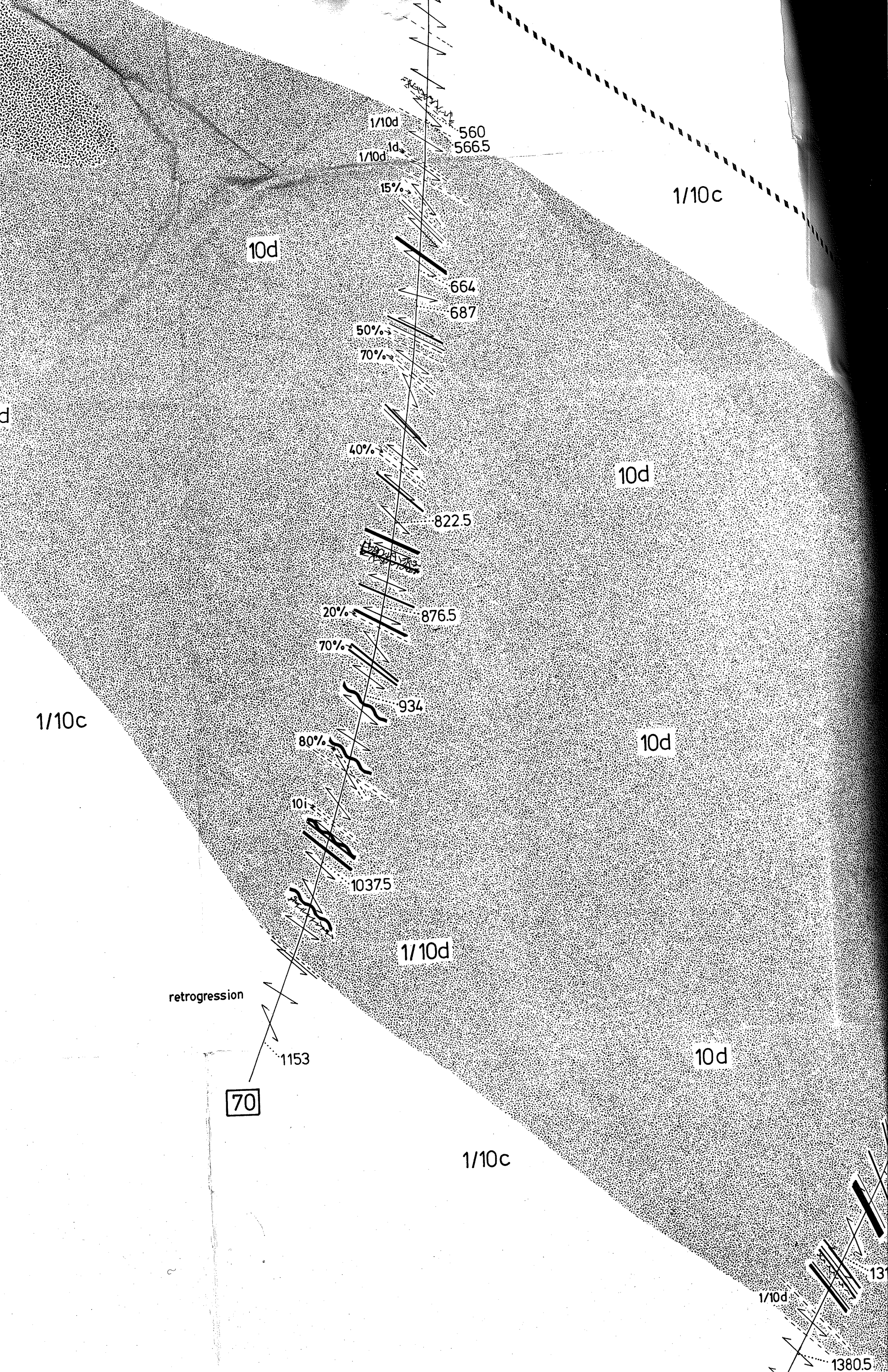
1/10d
1d
1/10d
15%
560
566.5
1/10c
10d
664
687
50%
70%
d
40%
10d
822.5
20%
876.5
70%
934
1/10c
80%
10d
10i
1037.5
1/10d
retrogression
1153
70
10d
1/10c
1/10d
1380.5

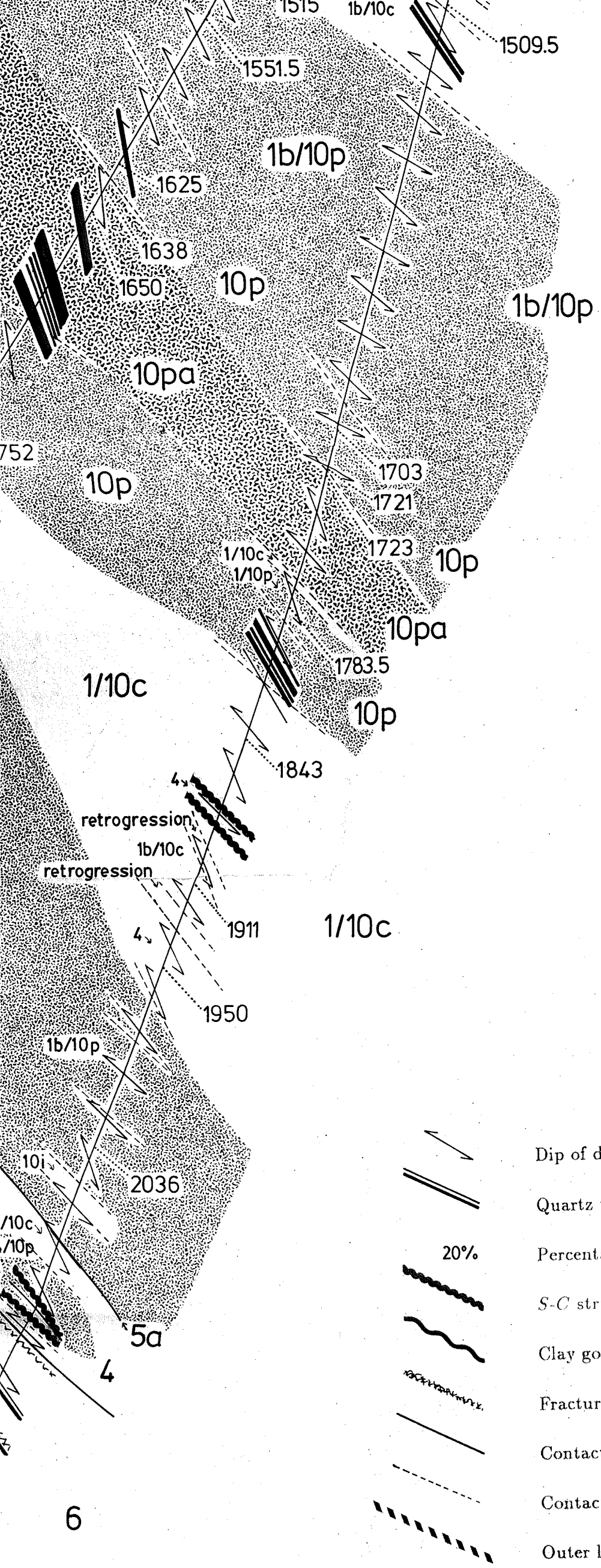

KEY

Dip of dominant layering or schistosity, measured to core axis.

Quartz veins, drawn to scale.

20% Percentage of quartz veins in indicated interval

S-C structure.

Clay gouge zone.

Fracture network, hematite-carbonate alteration.

Contact between major units.

Contact between subunits, or boundaries of interval.

Outer limits of calc-silicate alteration zone.

.....799 Geochemical sample location. Numbers refer to drill-hole footage. All numbers are prefixed by the drill-hole number.

22 Drill-hole number

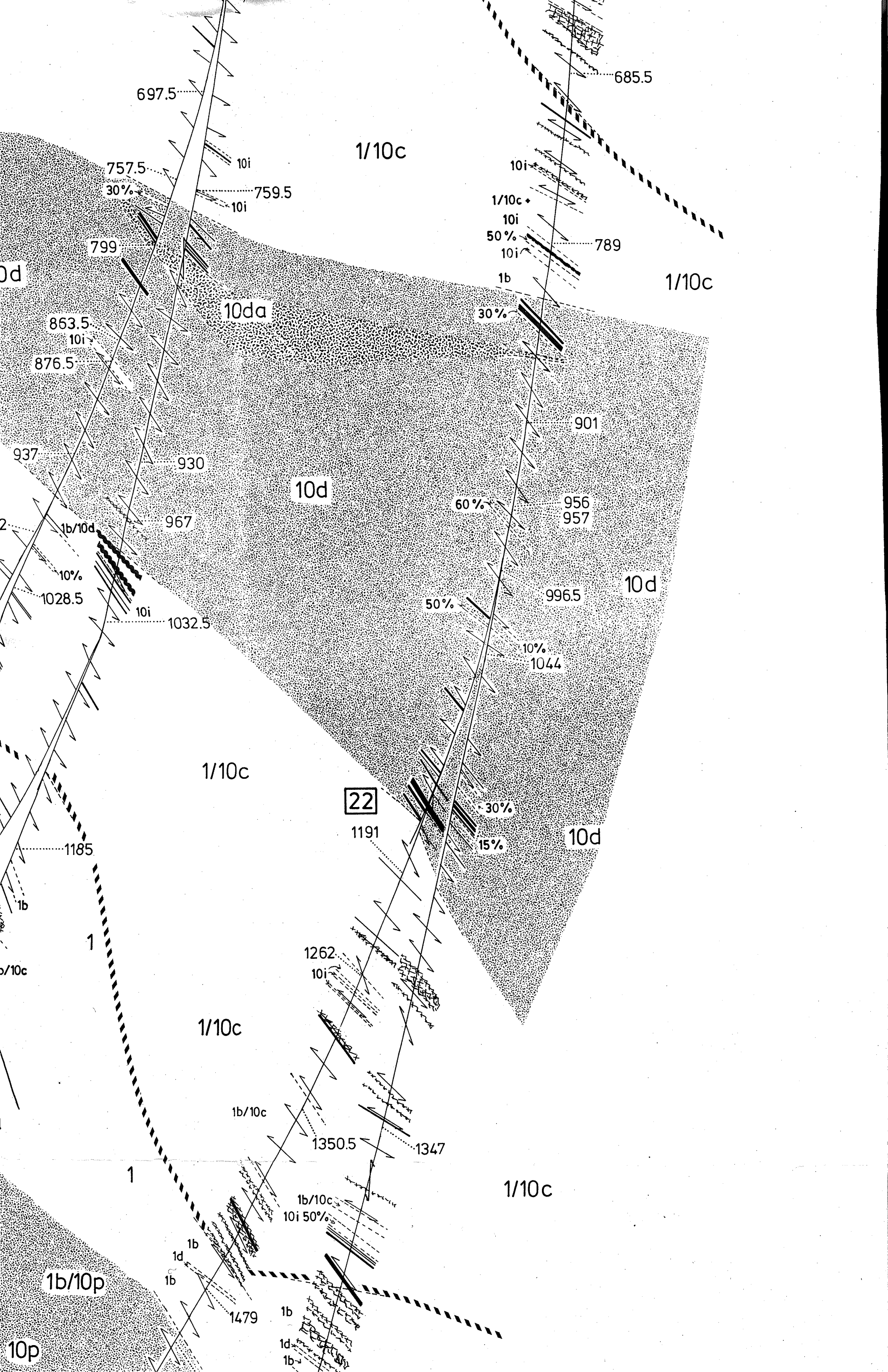
697.5
757.5
30%
759.5
10i
10i
1/10c
685.5
10i
1/10c
10i
50%
789
10i
1b
1/10c
799
10da
863.5
10i
876.5
30%
901
937
930
10d
60%
956
957
967
1b/10d
10%
1028.5
10i
1032.5
996.5
10d
50%
10%
1044
1/10c
22
1191
30%
15%
10d
1185
1b
1
1262
10i
1/10c
1b/10c
1350.5
1347
1
1/10c
1b/10c
10i 50%
1b
1d
1b
1b/10p
1479
1b
1d
1b
10p

NW

C´

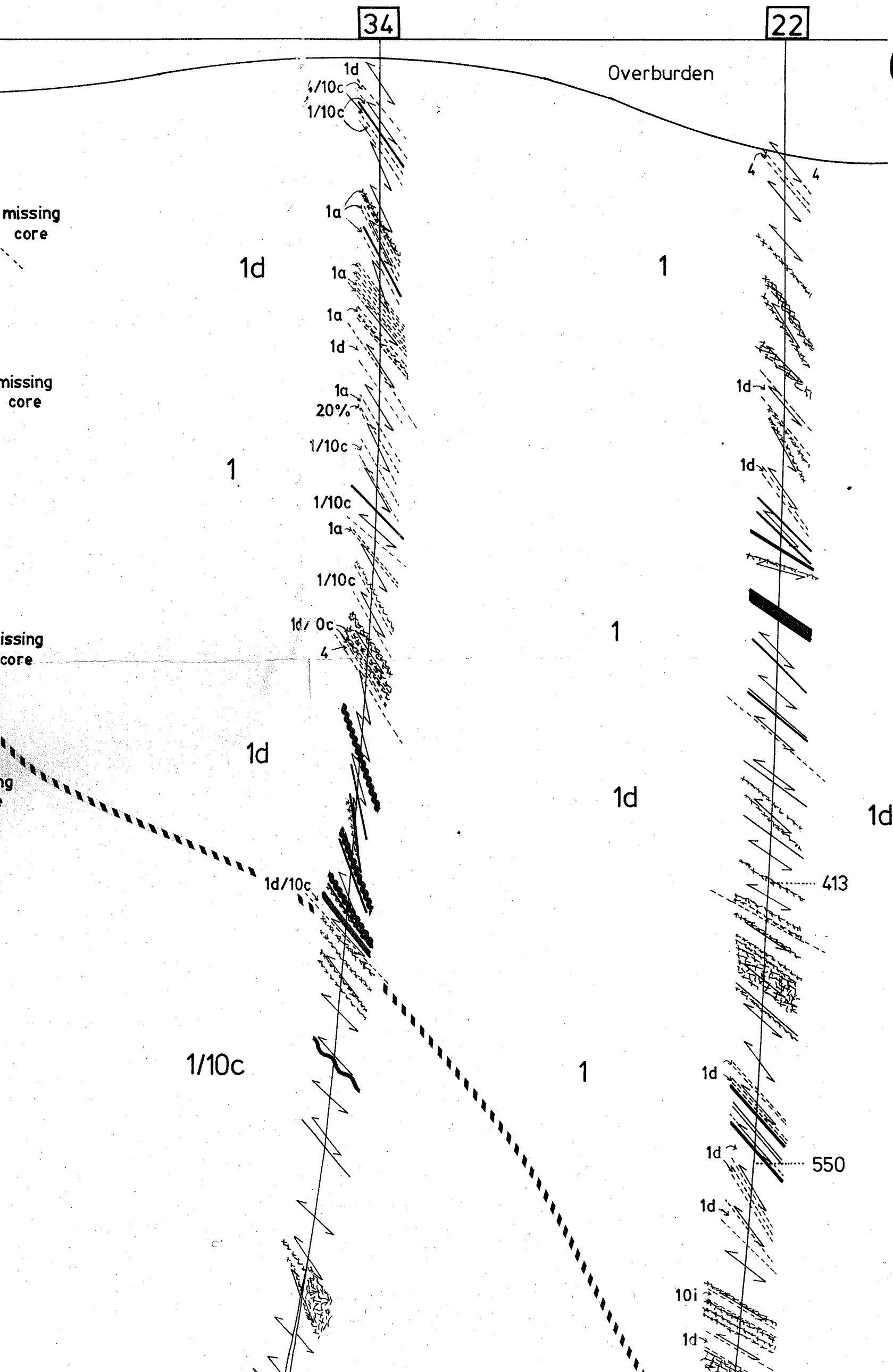
34
22
Overburden
1d
4/10c
1/10c
missing core
1d
1a
1a
1a
1d
missing core
1a
20%
1/10c
1
1/10c
1a
1/10c
1d/10c
issing core
4
1d
1d/10c
1/10c
1
1
1
1d
1d
1d
1d
1d
413
1d
1d
550
1d
1
10i
1d

LEGEND FOR THE LINDA AREA

Unit 11. Not intersected.

Unit 10. Altered rocks.

10d. Distal alteration zone—chlorite-muscovite schists containing staurolite± biotite±kyanite.

10da. Muscovite-gahnite-staurolite schist.

10p. Proximal alteration zone—muscovite-chlorite schists containing staurolite ±biotite±kyanite.

10pa. Muscovite-gahnite-staurolite schists.

10m. Mafic schists containing chlorite±hornblende.

10s. Silicified/feldspathized rock—'cherty' rocks commonly containing cummingtonite-hornblende-magnetite.

10v. Quartz veins.

10c. Concordant calc-silicate alteration—epidote-muscovite±biotite±calcite defining S_1 layering.

10i. Static calc-silicate alteration—localized intense, statically crystallized actinolite-epidote-calcite±sphene.

10e. Epidotized-carbonatized mafic rocks—epidote-hornblende±calcite associated with mafic volcanic rocks.

Units 7–9. Not intersected.

Unit 6. Mafic to intermediate, mainly volcaniclastic rocks.

6a. Heterolithic breccia—containing clasts of unit 4.

6b. Breccia, lapillstone and tuffs.

6c. Layered amphibolite—containing coarsely recrystallized amphibole.

Unit 5. Massive and semi-massive sulfide mineralization.

5a. Pyrite-calcite rocks.

Unit 4. Quartz-megaphyric felsic volcanic rocks.

Unit 3. Graphitic metasedimentary rocks.

Unit 2. Mafic volcanic rocks, with minor intermediate rocks.

2a. Homogeneous, commonly with epidote knots.

2b. Pillowed flows.

2c. Homogeneous and massive, except for hornblende lineation.

2d. Undifferentiated pillowed flows, breccias, lapillistones and tuffs, commonly plagioclase-hornblende (after pyroxene) phyric.

2e. Breccias, lapillistones and tuffs.

Unit 1. Felsic volcanic rocks, with minor intermediate to mafic rocks.

1a. 'Cherty' felsic rocks—silicic/feldspathic alteration or possible rhyolite flows.

1b. Volcaniclastic rocks.

1c. Mineralized 'cherty' breccia.

1d. Intermediate to mafic rocks—mainly volcaniclastic, locally heterolithic, minor amphibolite.

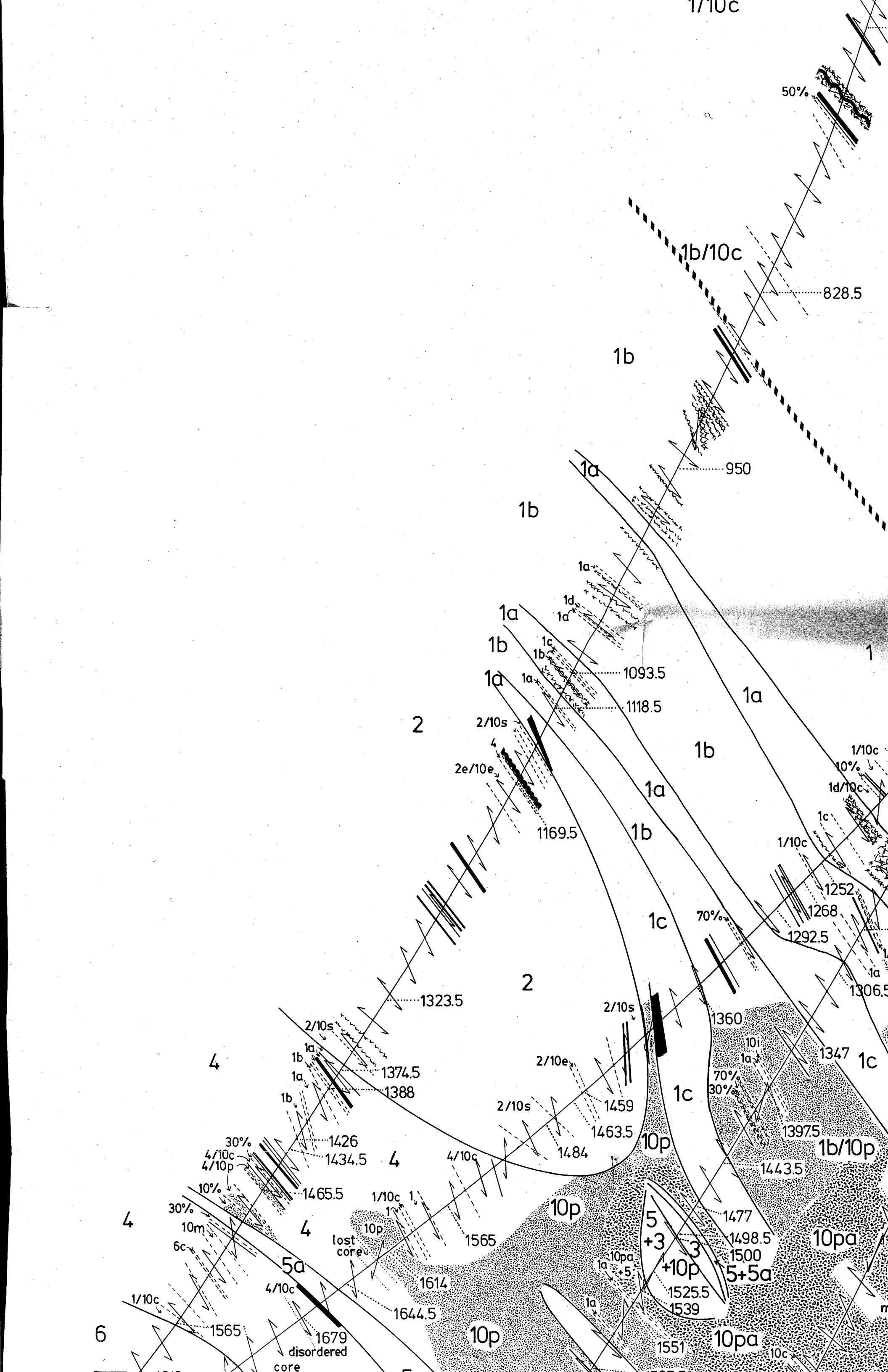
1/10c
50%
1b/10c
828.5
1b
950
1a
1b
1a
1d
1a
1c
1b
1b
1a
1093.5
1a
1118.5
1a
2
2/10s
4
2e/10e
1169.5
1b
1a
1b
1/10c
10%
1d/10c
1c
1/10c
1252
1268
1292.5
70%
1a
1306.5
1323.5
2
2/10s
1360
2/10s
10i
1a
1347
1c
4
2/10s
1a
1b
1a
1374.5
1388
1b
2/10e
1459
1463.5
2/10s
1484
1c
70%
30%
1397.5
1b/10p
1426
1434.5
30%
4/10c
4/10p
4
4/10c
10p
1443.5
10%
1465.5
1/10c
1
1565
10p
4
4
30%
10m
6c
lost
core
10p
5
+3
1477
1498.5
1500
3
+10p
10pa
5+5a
10pa
+5
1a
1525.5
1539
1614
5a
4/10c
1644.5
1/10c
1565
6
1679
disordered
core
10p
1551
10pa
10c
1a

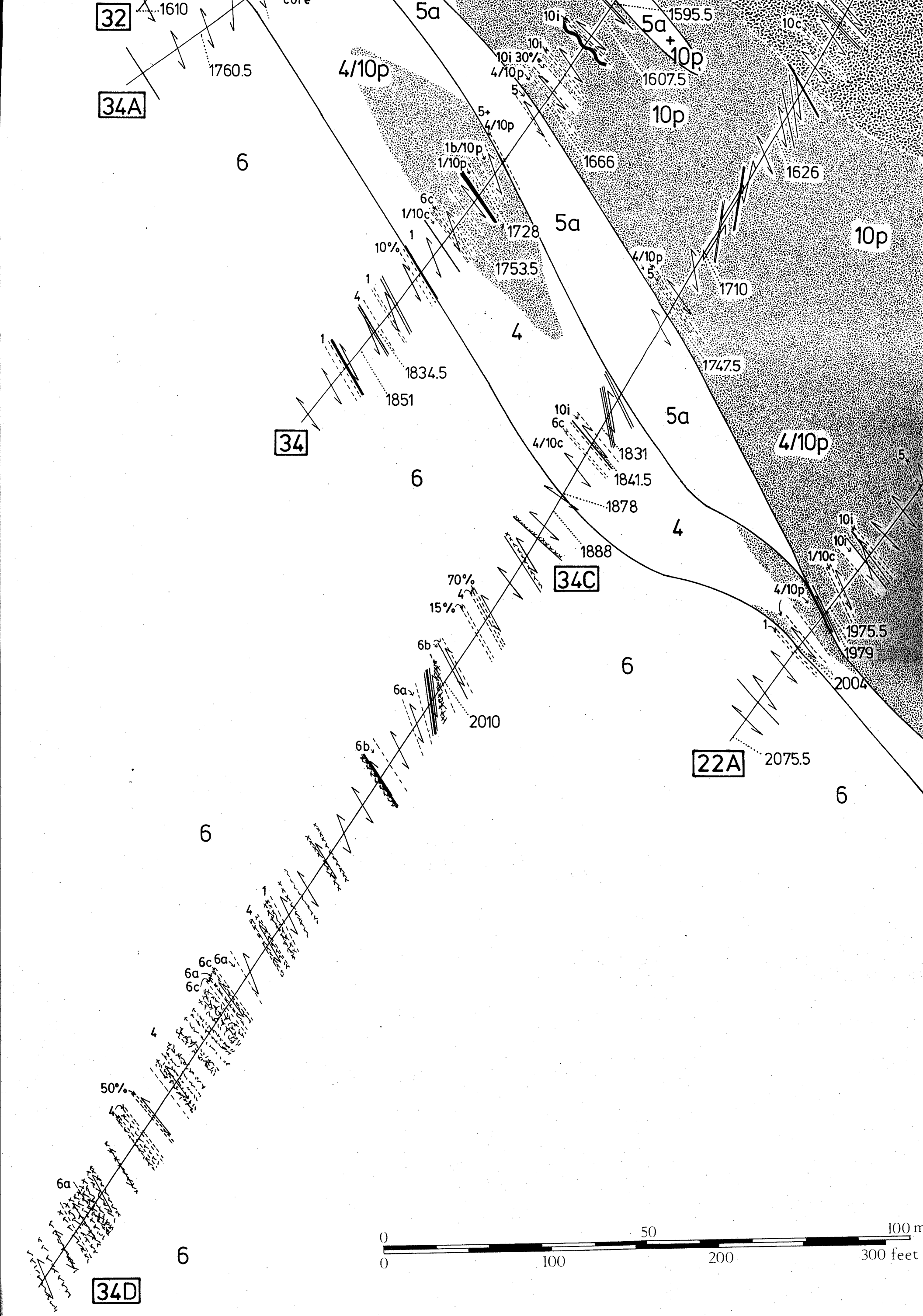
32
1610
core
5a
10i
1595.5
5a + 10p
10c
10i
10i 30%
4/10p
5
1760.5
4/10p
1607.5
34A
10p
5+
4/10p
1b/10p
1/10p
6
1666
1626
6c
1/10c
1728
5a
10p
1
10%
2
1753.5
4/10p
5
1710
1
4
4
1747.5
1834.5
1851
10i
6c
4/10c
5a
4/10p
34
1831
6
1841.5
1878
4
5
10i
10i
1/10c
1888
34C
70%
4
15%
4/10p
1
1975.5
1979
6b
6
2004
6a
2010
6b
22A
2075.5
6
6
1
4
6c
6a
6a
6c
4
50%
4
6a
6
34D
0
50
100 m
0
100
200
300 feet

99°55'

99°54'

Key

Outcrop

66 — S_0 strike and dip, facing direction unknown

78 — S_1 strike and dip

65 35 — S_1 strike and dip with trend and plunge of lineation

80 — S_2 strike and dip

30 30 — F_2 minor fold axis, with fold asymmetry

70 20 — F_2 minor fold axial plane strike and dip with fold axis trend and plunge

F_2 minor fold asymmetry

Facing direction

Known contact

Contact inferred or projected from drill hole data

Contact approximate or assumed

● H9·32·1 — Geochemical sample location

gt-cm-hb — Mineral assemblage: bi-biotite, ch-chlorite, cm-cummingtonite, cl-calcite, ep-epidote, gt-garnet, hb-hornblende, ky-kyanite, mg-magnetite, mu-muscovite, po-pyrrhotite, py-pyrite, si-sillimanite, st-staurolite

N

Rod 2 minesite

4

1

2

2b

4a

hb-gt-cm-bi

bi-hb-gt-py

H9·10·1 ● *bi-ep-cl-mg*

54°51'

99°56'

Stall
Lake

1

4

2d

2

bi-hb-py-gt

I7·32·1

cm-hb-gt-bi

cm-hb-gt

I7·29·1

bi-st-gt-ch

bi-hb-gt

hb-ep-po-gt

ch-st-bi-mg

bi-mu-cl-ep

H8·1·1

Rod 1
minesite

bi-mu-ep-cl-mg

A'

B'

C'

bi-ch-ky-

bi-ky-st-py

H8·10·1

H8·14·1

LEGEND FOR THE LINDA AREA

11. Gabbro.

10. Altered rocks.

9. Metaturbidite and metagreywacke.

8. Mafic volcanic rocks.

7. Quartz-megaphyric felsic volcanic rocks.

6. Mafic to intermediate, mainly volcaniclastic rocks.

6a. Heterolithic breccia—containing clasts of unit 4.

6b. Breccia, lapillstone and tuffs.

6c. Layered amphibolite—containing coarsely recrystallized amphibole.

5. Massive and semi-massive sulfide mineralization. Not exposed.

4. Quartz-megaphyric felsic volcanic rocks.

4a. Breccia.

3. Graphitic metasedimentary rocks. Not exposed.

2. Mafic volcanic rocks, with minor intermediate rocks.

2a. Homogeneous, commonly with epidote knots.

2b. Pillowed flows.

2c. Homogeneous and massive, except for hornblende lineation.

2d. Undifferentiated pillowed flows, breccias, lapillistones and tuffs, commonly plagioclase-hornblende (after pyroxene) phyric.

2e. Breccias, lapillistones and tuffs.

1. Felsic volcanic rocks, with minor intermediate to mafic rocks.

1a. 'Cherty' felsic rocks—silicic/feldspathic alteration or possible rhyolite flows.

1b. Volcaniclastic rocks. Not exposed.

1c. Mineralized 'cherty' breccia. Not exposed.

1d. Intermediate to mafic rocks—mainly volcaniclastic locally heterolithic, minor amphibolite. Not exposed.

Anderson

LEGEND FOR THE LINDA AREA

Unit 11. Gabbro.

Unit 10. Altered rocks.

Unit 9. Metaturbidite and metagreywacke.

Unit 8. Mafic volcanic rocks.

Unit 7. Quartz-megaphyric felsic volcanic rocks.

Unit 6. Mafic to intermediate, mainly volcaniclastic rocks.

6a. Heterolithic breccia—containing clasts of unit 4.

6b. Breccia, lapillstone and tuffs.

6c. Layered amphibolite—containing coarsely recrystallized amphibole.

Unit 5. Massive and semi-massive sulfide mineralization. Not exposed.

Unit 4. Quartz-megaphyric felsic volcanic rocks.

4a. Breccia.

Unit 3. Graphitic metasedimentary rocks. Not exposed.

Unit 2. Mafic volcanic rocks, with minor intermediate rocks.

2a. Homogeneous, commonly with epidote knots.

2b. Pillowed flows.

2c. Homogeneous and massive, except for hornblende lineation.

2d. Undifferentiated pillowed flows, breccias, lapillistones and tuffs, commonly plagioclase-hornblende (after pyroxene) phyric.

2e. Breccias, lapillistones and tuffs.

Unit 1. Felsic volcanic rocks, with minor intermediate to mafic rocks.

1a. 'Cherty' felsic rocks—silicic/feldspathic alteration or possible rhyolite flows.

1b. Volcaniclastic rocks. Not exposed.

1c. Mineralized 'cherty' breccia. Not exposed.

1d. Intermediate to mafic rocks—mainly volcaniclastic, locally heterolithic, minor amphibolite. Not exposed.

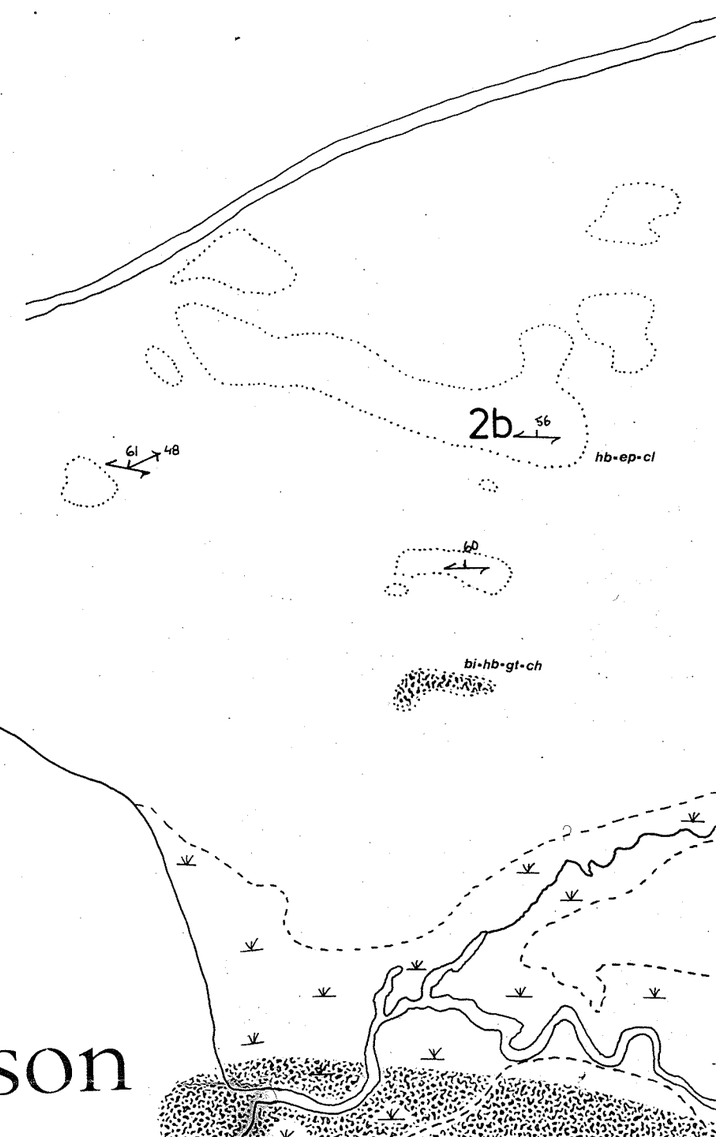

Anderson

Anderson Bay

D4·9·1
D4·9·2
cl·hb·ep·bi·po·pl

1
2
4
6b
11
6a
4a
7
8

99°56'

Distal alteration zone (projected)

Proximal alteration zone (projected)

A

B

C

C'

D4·37·1

D4·38·1

J8·2·1

J8·23·1

I8·13·1

I8·20·1

I8·27·1

I8·6·1

bi-st-gt-mu

bi-mu-cl

bi-ep-cl

bi-hb-ep-cl

hb-gt-bi-ep

bi-hb

99°55'

54°50'

Wekusko Lake

H8·10·1
H8·14·1
H9·10·1 bi-ep-cl-mg
bi-hb-gt-py
bi-st-ky
silicified pillows
hb-cm-gt-bi-mg
H9·52·1
bi-st-ky-py
H9·13·1
hb-cm-gt-bi
bi-st-ky
hb-cm-gt-bi-ch
H9·61·5
hb-cm-gt-bi-ch-mg
bi-gt-hb-cm-ch-mg
st-bi-ch-gt
hb-bi-ch
H9·30·1
H9·30·2
H9·30·3
H9·38·1
bi-hb-gt-py
H9·60·2
gt-bi-st-mu-ch
st-ky-bi-mu
H9·6·2
bi-st-gt-mu-gr
Road marks
northeastern limit of
grid control on mapping

0 500
0 1000

99°54'
54°51'

H9·10·1 bi·ep·cl·mg

bi·hb·gt·py

silicified pillows
hb·cm·gt·bi·mg

H9·52·1

bi·st·ky

bi·st·ky·py

H9·13·1

hb·cm·gt·bi

hb·cm·gt·bi·ch

H9·61·5

hb·cm·gt·bi·ch·mg

st·bi·ch·gt
hb·bi·ch

H9·30·1
H9·30·2
H9·30·3

H9·38·1

bi·hb·gt·py

H9·60·2

gt·bi·st·mu·ch
st·ky·bi·mu

H9·6·2

bi·st·gt·mu·gr

st·gt·bi·mu

Korman's Lake

bi·st·gt

Road marks
northeastern limit of
grid control on mapping

0 500 1000 metres
0 1000 2000 3000 feet

54°51'